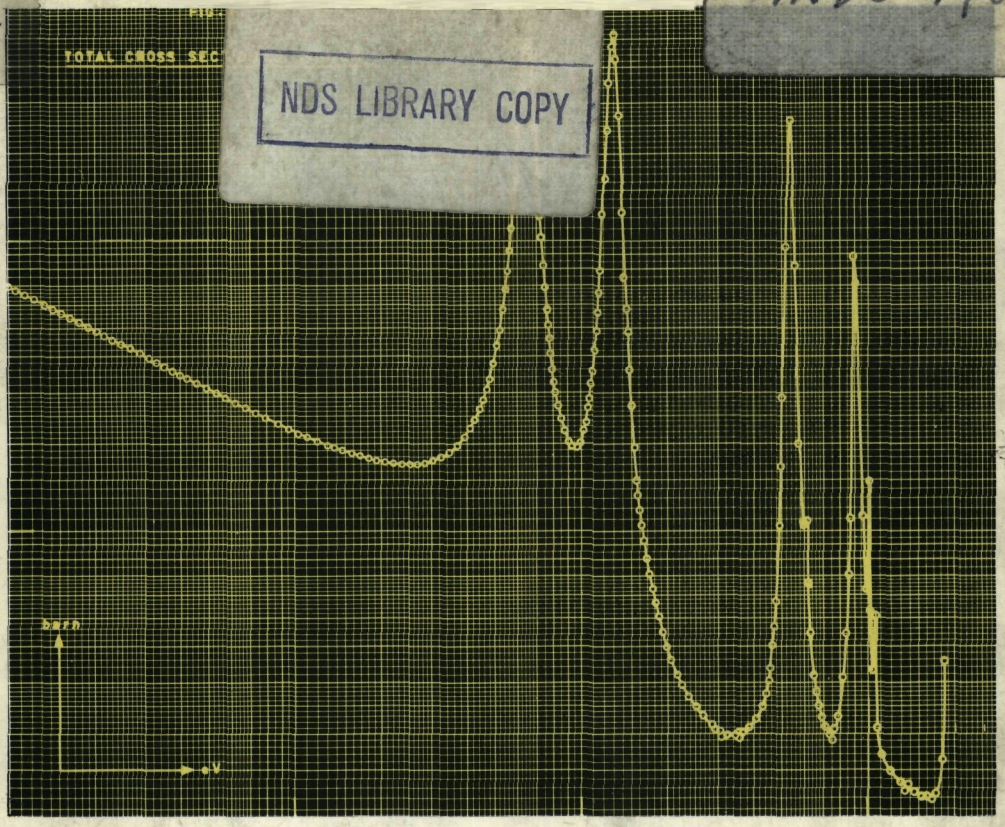

CONFERENCE PROCEEDINGS, PARIS, 17–21 OCTOBER 1966

NUCLEAR DATA FOR REACTORS

VOL. I

INTERNATIONAL ATOMIC ENERGY AGENCY, VIENNA, 1967

NUCLEAR DATA FOR REACTORS

VOL. I

The following States are Members of the International Atomic Energy Agency:

AFGHANISTAN
ALBANIA
ALGERIA
ARGENTINA
AUSTRALIA
AUSTRIA
BELGIUM
BOLIVIA
BRAZIL
BULGARIA
BURMA
BYELORUSSIAN SOVIET SOCIALIST REPUBLIC
CAMBODIA
CAMEROON
CANADA
CEYLON
CHILE
CHINA
COLOMBIA
CONGO, DEMOCRATIC REPUBLIC OF
COSTA RICA
CUBA
CYPRUS
CZECHOSLOVAK SOCIALIST REPUBLIC
DENMARK
DOMINICAN REPUBLIC
ECUADOR
EL SALVADOR
ETHIOPIA
FINLAND
FRANCE
GABON
GERMANY, FEDERAL REPUBLIC OF
GHANA
GREECE
GUATEMALA
HAITI
HOLY SEE
HONDURAS
HUNGARY
ICELAND
INDIA
INDONESIA
IRAN
IRAQ
ISRAEL
ITALY
IVORY COAST
JAMAICA
JAPAN
JORDAN
KENYA
KOREA, REPUBLIC OF
KUWAIT
LEBANON
LIBERIA
LIBYA
LUXEMBOURG
MADAGASCAR
MALI
MEXICO
MONACO
MOROCCO
NETHERLANDS
NEW ZEALAND
NICARAGUA
NIGERIA
NORWAY
PAKISTAN
PANAMA
PARAGUAY
PERU
PHILIPPINES
POLAND
PORTUGAL
ROMANIA
SAUDI ARABIA
SENEGAL
SINGAPORE
SOUTH AFRICA
SPAIN
SUDAN
SWEDEN
SWITZERLAND
SYRIAN ARAB REPUBLIC
THAILAND
TUNISIA
TURKEY
UKRAINIAN SOVIET SOCIALIST REPUBLIC
UNION OF SOVIET SOCIALIST REPUBLICS
UNITED ARAB REPUBLIC
UNITED KINGDOM OF GREAT BRITAIN AND NORTHERN IRELAND
UNITED STATES OF AMERICA
URUGUAY
VENEZUELA
VIET-NAM
YUGOSLAVIA

The Agency's Statute was approved on 26 October 1956 by the Conference on the Statute of the IAEA held at United Nations Headquarters, New York; it entered into force on 29 July 1957. The Headquarters of the Agency are situated in Vienna. Its principal objective is "to accelerate and enlarge the contribution of atomic energy to peace, health and prosperity throughout the world".

Printed by the IAEA in Austria
April 1967

PROCEEDINGS SERIES

NUCLEAR DATA FOR REACTORS

PROCEEDINGS OF A CONFERENCE ON
NUCLEAR DATA - MICROSCOPIC CROSS-SECTIONS
AND OTHER DATA BASIC FOR REACTORS
HELD BY THE
INTERNATIONAL ATOMIC ENERGY AGENCY
IN PARIS, 17-21 OCTOBER 1966

In two volumes

VOL. I

INTERNATIONAL ATOMIC ENERGY AGENCY
VIENNA, 1967

NUCLEAR DATA FOR REACTORS
(*Proceedings Series*)

ABSTRACT. Proceedings of a Conference organized by the IAEA and held in Paris, 17-21 October 1966, at the invitation of the French Government and the French Atomic Energy Commission. The meeting was attended by 213 participants from 24 countries and 4 international organizations.

The main theme of the Conference was the discussion of neutron cross-sections and other neutron data with regard to their use for nuclear reactor calculations, emphasizing the roles of the compiler and the evaluator in this connection.

Contents: (Vol.I) Keynote address; Nuclear data requirements (4 papers); Cross-section and resonance parameters of non-fissile nuclides in the resonance energy region (13 papers); Statistical properties of resonance parameters (8 papers); (n,p), (n,α), (n,2n)-reactions, etc. and inverse reactions (5 papers); Cross-sections and constants used as standards (7 papers); Neutron cross-sections above the resonance energy region (13 papers); Neutron radiative capture (16 papers); (Vol.II) Cross-sections and parameters of fissile nuclides (23 papers); Comparison of fission cross-sections in the resonance energy region (3 papers); Neutron data evaluation (12 papers); International co-operation in the field of nuclear data (1 paper); Panel discussion.

Of the 106 papers contained in these Proceedings, 83 are published in full with abstracts and 23 are presented by title and abstract only. Each paper is in its original language (69 English, 19 French and 18 Russian), the abstracts being in English and the original language if this is not English. Discussions are in English.

(Vol.I: 576 pp., Vol.II: 437 pp., 16 x 24 cm, paper-bound, 320 figures)
(1967)

Vol.I: US $12.00; £4.4.8
Vol.II: US $ 9.00; £3.3.6

NUCLEAR DATA FOR REACTORS, IAEA, VIENNA, 1967
STI/PUB/140

FOREWORD

A Conference on Nuclear Data for Reactors, held in Paris at the invitation of the French Government, was convened by the International Atomic Energy Agency on 17-21 October 1966. The meeting was held as a result of recommendations made by the International Nuclear Data Scientific Working Group. Over 200 delegates attended, representing 24 countries and four international organizations, and 106 papers were submitted. Of the 106 papers, 23 are given here by title and abstract only, since they were not presented at the Conference; copies of these papers, however, can be obtained on request from the Nuclear Data Unit of IAEA, Vienna.

The main purpose of the Conference was to provide an opportunity for reviewing results from recent basic neutron physics investigations against a background of need for basic information, especially as it applies to reactors.

After a keynote address, the meeting proceeded with three papers dealing with reactor and shielding needs. These were followed by sessions on basic neutron physics, which included the following topics: thermal and resonance fission cross-sections; cross-sections of non-fissile nuclides in and above the resonance region; neutron-induced particle reactions (and their inverse); radiative capture; the interpretation of fission cross-sections and the application of the optical and statistical models to the calculation of neutron cross-sections beyond the resonance region.

In his keynote address Dr. Usachev of the USSR gave special emphasis to the widening gulf of communication between data measurers and data users. Several sessions had been designed to try to bridge this gap. These consisted of: a session on standards, which was concerned with cross-sections and constants suitable for use as standards and which included a paper summarizing the precision of present standards in relation to need; a session on the critical comparison of the cross-sections of fissile nuclides; a session on neutron data evaluation; and a session on the international exchange of neutron data.

A summary discussion by a panel of experts concluded the Conference. Their opinion was that there now exists essentially adequate information for thermal reactor calculations, that gaps and discrepancies in information for present needs will almost certainly be resolved as techniques improve, but that unforeseen needs and benefits justify a continued long-term search for fundamental understanding. The benefits from international co-operation were stressed throughout.

An assessment of the Conference in retrospect should take note of the interest shown in the sessions on standards, cross-sections of fissile nuclides, neutron data evaluations and international data exchange. Of these,

the session on data evaluation was especially noteworthy, not only because the need to include it as a session was due to the number and quality of the papers submitted by the evaluators, but also because of the recognition of the importance of the professional evaluator as the indispensable middleman between the physicist concerned with basic measurements and the physicist concerned with reactor applications. The growth in size and importance of this professional group of evaluators should give great impetus to the organizing of future conferences on the lines of the one held in Paris.

EDITORIAL NOTE

The papers and discussions incorporated in the proceedings published by the International Atomic Energy Agency are edited by the Agency's editorial staff to the extent considered necessary for the reader's assistance. The views expressed and the general style adopted remain, however, the responsibility of the named authors or participants.

For the sake of speed of publication the present Proceedings have been printed by composition typing and photo-offset lithography. Within the limitations imposed by this method, every effort has been made to maintain a high editorial standard; in particular, the units and symbols employed are to the fullest practicable extent those standardized or recommended by the competent international scientific bodies.

The affiliations of authors are those given at the time of nomination.

The use in these Proceedings of particular designations of countries or territories does not imply any judgement by the Agency as to the legal status of such countries or territories, of their authorities and institutions or of the delimitation of their boundaries.

The mention of specific companies or of their products or brand-names does not imply any endorsement or recommendation on the part of the International Atomic Energy Agency.

CONTENTS

KEYNOTE ADDRESS

Могут ли понять друг друга экспериментаторы, оценщики-компиляторы и потребители ядерных данных? (CN-23/130) 3
Л.Н.Усачев

NUCLEAR DATA REQUIREMENTS (Session I)

Nuclear data requirements for thermal reactor design and operation (CN-23/117) 13
G.H. Kinchin

Nuclear data requirements for fast reactor design and operation (CN-23/52) 27
R.D. Smith

Discussion 37

Basic nuclear data for fast reactor calculations (CN-23/14*) 38
M. Segev, S. Yiftah and L. Gitter

Cross-section requirements for neutron shielding (CN-23/118) 39
H. Goldstein

Discussion 48

CROSS-SECTIONS AND RESONANCE PARAMETERS OF NON-FISSILE NUCLIDES IN THE RESONANCE ENERGY REGION (Session II)

Neutron cross-sections of Pr, Yb, Lu, Er, Ho and Tm (CN-23/129) 53
R.L. Zimmerman, L.Q. Amaral, R. Fulfaro, M.C. Mattos, M. Abreu and R. Stasiulevicius

Total cross-section of dysprosium, lutetium and iridium for neutrons of energy between 0.01 and 10 eV (CN-23/20) 61
J. Brunner and F. Widder

Полные нейтронные сечения изотопа торий-230 в области энергий (0,02 – 50) эв (CN-23/104) 71
С.М.Калебин, Р.Н.Иванов, П.Н.Палей, З.К.Каралова, Г.М.Кукавадзе, В.И.Пыжова, Н.П.Шибаева, Г.В.Руколайне

Нейтроноспектроскопические исследования разделенных изотопов серебра (CN-23/107) 79
Г.В.Мурадян, Ю.В.Адамчук

Нейтроноспектроскопическое исследование разделенных изотопов кадмия (CN-23/108) 93
Ю.Г.Щепкин, Ю.В.Адамчук, Л.С.Данелян, Г.В.Мурадян,

Полные нейтронные сечения тяжелых четно-четных изотопов олова в области энергий до 10 кэв (CN-23/109) 101
Ю.В.Адамчук, С.С.Москалев, Г.В.Мурадян
Discussion on papers CN-23/107, 108 and 109 105
Dispositifs et programmes pour l'acquisition et le traitement des informations de temps de vol (CN-23/71) 107
P. Ribon, B. Cauvin, H. Derrien, A. Michaudon et M. Sanche
Etude de quelques sections efficaces neutroniques totale et de diffusion dans le domaine des résonances (CN-23/72) 119
P. Ribon, B. Cauvin, H. Derrien, A. Michaudon, E. Silver et J. Trochon
Discussion on papers CN-23/71 and 72 128
Low-energy neutron cross-sections of sodium (CN-23/27) 129
M. C. Moxon and N. J. Pattenden
Discussion 136
High-resolution cross-section measurements for some fast reactor structural materials in the keV energy range (CN-23/9) 137
G. Rohr, E. Friedland and J. Nebe
Discussion 146
Obtention des paramètres caractérisant les résonances de neutrons par combinaison de différentes méthodes (CN-23/61*) 146
P. L. Chevillon, J. Julien, J. Morgenstern, F. Netter et C. Samour
Processing and analysis of neutron transmission data and considerations of the accuracy (CN-23/17) 147
T. Fuketa, A. Asami, M. Ohkubo, Y. Nakajima, Y. Kawarasaki and H. Takekoshi
The influence of chemical binding on neutron cross-sections at higher energies (CN-23/80*) 155
K. Drittler

STATISTICAL PROPERTIES OF RESONANCE PARAMETERS
(Session III)

Параметры структуры нейтронной силовой функции средних и тяжелых ядер (CN-23/105) 159
С.И.Сухоручкин
Discussion 163
Плотность уровней и структура атомных ядер (CN-23/106*) 163
Ю.Н.Шубин, А.В.Малышев, В.С.Ставинский
Neutron strength function measurements in the medium and heavy nuclei (CN-23/36) 165
C. A. Uttley, C. M. Newstead and K. M. Diment
Discussion 174
Etude de la distribution des largeurs radiatives partielles de ^{195}Pt à l'aide d'un détecteur au Ge-Li (CN-23/60) 175
C. Samour, H. E. Jackson, P. L. Chevillon, J. Julien et J. Morgenstern
Discussion 181

Valeur de la fonction densité S_0 et du rayon de diffusion R' en fonction du nombre de masse et fluctuation de S_0 en fonction de l'énergie dans le domaine d'énergie compris entre 0 et 300 keV (CN-13/65) 183
J. Morgenstern, S. de Barros, P. L. Chevillon, M. J. Gauthier, H. Jackson, J. Julien et C. Samour
Discussion 191
Distributions des espacements des résonances et valeurs des coefficients de corrélation entre les différents paramètres (CN-23/63) 193
S. de Barros, P. L. Chevillon, H. Jackson, J. Julien, J. Morgenstern et C. Samour
Discussion 203
Dépendance de la fonction densité S_0 suivant la valeur du spin (CN-23/64*) 205
J. Julien, S. de Barros, P. L. Chevillon, V. D. Huynh, J. Morgenstern, F. Netter et C. Samour
Discussion 205

(n, p), (n, α), (n, 2n) REACTIONS, ETC. AND INVERSE REACTIONS (Session IV)

The (n, 2n) cross-sections of ^{9}Be and D in the threshold regions (CN-23/18*) 209
M. Holmberg and J. Hansén
Discussion 209
Etude de la réaction ^{9}Be(n, 2n) à 14 MeV (CN-23/76) 211
R. Bouchez, J. C. Gondrand, P. Perrin, C. Perrin, A. Giorni, R. Darves-Blanc et P. Quivy
Measurements of 14-MeV neutron-induced reaction cross-sections on enriched isotopes of calcium (CN-23/12*) 216
P. N. Tiwari and E. Kondaiah
Cross-sections for some (n, p) reactions near threshold (CN-23/90) 217
A. Paulsen and H. Liskien
Discussion 224
Cross-sections of some (n, p), (n, t), and (n, α) reactions in the neutron energy region 13-19 MeV (CN-23/81) 225
M. Bormann, F. Dreyer, H. Neuert, I. Riehle and U. Zielinski
^{16}O(n, α) ^{13}C reaction cross-sections from the ^{13}C(α, n)^{16}O reaction (CN-23/13) 233
A. S. Divatia, K. K. Sekharan and M. K. Mehta

CROSS-SECTIONS AND CONSTANTS USED AS STANDARDS (Session V)

Primary standard data and standard samples (CN-23/119) 241
J. Spaepen
Discussion 263

Mesure de la section efficace de la réaction $^{6}Li(n, \alpha)T$ par la méthode de la particule associée (CN-23/67) 267
E. Fort et J. L. Leroy
Discussion 275
An absolute (n, γ) cross-section measurement for gold at 30 keV and its application in the normalization of other data (CN-23/6) .. 277
W. P. Pönitz
Discussion 294
Fission cross-sections of some plutonium isotopes in the neutron energy range 5-150 keV (CN-23/7*) 295
W. B. Gilboy and G. F. Knoll
Direct and absolute measurements of average fission neutron yield from uranium-235 and californium-252 (CN-23/40) 297
A. De Volpi and K. G. Porges
Confirmatory experimental data on the Harwell boron pile $\bar{\nu}$ values (CN-23/33) 307
D. W. Colvin, M. G. Sowerby and R. I. Macdonald
Discussion on papers CN-23/40 and 33 317
Measurement of average cross-section ratios in fundamental fast-neutron spectra (CN-23/46) 321
J. A. Grundl and G. E. Hansen
Discussion 335

NEUTRON CROSS-SECTIONS ABOVE THE RESONANCE ENERGY REGION (Session VI)

The calculation of nuclear cross-sections by the optical model (CN-23/45) 339
D. T. Goldman
Discussion 365
Gamma rays from neutron inelastic scattering in germanium (CN-23/59*)..... 365
J. F. Barry
Inelastic scattering of fast neutrons from ^{58}Ni and ^{60}Ni (CN-23/35) 367
J. H. Towle, R. Batchelor and W. B. Gilboy
Neutron inelastic scattering from ^{56}Fe (CN-23/86) 373
E. Barnard, J. A. M. de Villiers and D. Reitmann
Discussion 381
Inelastic scattering of fast neutrons by ^{235}U (CN-23/22) 383
B. H. Armitage, A. T. G. Ferguson, J. H. Montague and N. Starfelt
Discussion 392
Etude de la diffusion élastique et inélastique des neutrons de 14 MeV par les noyaux ^{6}Li, ^{7}Li et ^{9}Be (CN-23/75) 393
F. Merchez, V. Regis, Nguyen van Sen, R. Darves-Blanc, Pham Dinh Lien et R. Bouchez
Discussion 397

Microscopic neutron scattering cross-sections for reactor design (CN-23/49) 399
A. B. Smith and D. Lister
Discussion 407
An optical model study of neutrons elastically scattered by iron, nickel, cobalt and copper in the energy region 1.5 to 4.6 MeV (CN-23/85) 409
B. Holmquist and T. Wiedling
Pulsed fast neutron research at the Los Alamos Van de Graaff accelerator (CN-23/84) 419
The Neutron Time-of-Flight Group
Discussion 428
Evaluation of heavy even-even nuclide elastic and inelastic cross-sections by means of a non-spherical optical model (CN-23/41) .. 429
C. L. Dunford
Discussion 442
Elastic and inelastic neutron cross-sections (CN-23/37*) 443
D. Wilmore
A novel method for very high resolution cross-section measurements (CN-23/11*) 444
S. Cierjacks, P. Forti, D. Kopsch, L. Kropp and H. Unseld
A new method for the measurement of neutron cross-sections (CN-23/116) 445
M. J. Ohanian, R. B. Perez and R. E. Uhrig
Discussion 451

NEUTRON RADIATIVE CAPTURE (Session VII)

Измерение сечений поглощения нейтронов с энергией 24 кэв в сферической геометрии (CN-23/96) 455
Т.С.Беланова, А.А.Ваньков, Ф.Ф.Михайлус, Ю.Я.Стависский
Радиационный захват быстрых нейтронов (CN-23/98) 459
А.И.Абрамов, А.А.Ваньков, В.Н.Кононов, А.В.Малышев, Ю.Я.Стависский, В.А.Толстиков, А.В.Шапарь
Сечения радиационного захвата быстрых нейтронов для изотопов Ag, Dy, W, Ta и Re (CN-23/99) 469
В.Н.Кононов, Ю.Я.Стависский, С.Р.Чистозвонов, В.С.Шорин
Радиационный захват быстрых нейтронов ядрами иттрия-89 и иридия-193 (CN-23/103) 473
В.П.Королева, В.А.Толстиков, В.Е.Колесов, А.Г.Довбенко
Discussion on papers CN-23/96, 98, 99 and 103 477
Mesures des sections efficaces et des intégrales de résonance par la méthode d'oscillation (CN-23/74) 479
J. C. Carré et R. Vidal
Discussion 494

Pile neutron capture cross-sections of rare earth isotopes (CN-23/82) 495
R. Dobrozemsky, E. Formann, G. Lugmair, F. Pichlmayer, F. P. Viehböck and H. Wotke
Discussion 501
Measurements of effective (resonance-shielded) neutron cross-sections in the keV region (CN-23/8*) 502
H. Miessner and E. Arai
An improved analysis of sphere transmission experiments for average capture cross-sections (CN-23/83) 503
D. Bogart
Discussion 511
Capture cross-section measurements for some medium- and heavy-weight nuclei using a large liquid scintillator (CN-23/10) 513
D. Kompe
Discussion 519
Neutron capture between 5 keV and 3 MeV (CN-23/51*) 520
D. C. Stupegia, C. R. Keedy, M. Schmidt and A. A. Madson
Fission-product absorption in thermal reactors (CN-23/1) 521
W. H. Walker
Discussion 536
Fission-product neutron-capture cross-sections in the energy range 1 keV - 10 MeV (CN-23/115) 537
V. Benzi and M. V. Bortolani
Statistical calculations of fission-product cross-sections (CN-23/78) 549
J. L. Cook
Valeur des largeurs radiatives totales Γ_γ en fonction du nombre de masse A (CN-23/62) 559
V.-D. Huynh, S. de Barros, P. L. Chevillon, J. Julien, G. le Poittevin, J. Morgenstern et C. Samour
Discussion 563
Etude des spectres de rayonnement gamma de capture, à l'aide de détecteurs au germanium (CN-23/66*) 564
H. Jackson, C. Samour, A. Bloch, J. Julien, C. Lopata et J. Morgenstern
Neutron radiative capture measurements at the Rensselaer Polytechnic Institute's electron linac (CN-23/126) 565
R. C. Block, R. W. Hockenbury, Z. Bartolome and R. R. Fullwood

Chairmen of Sessions 577
Secretariat of the Conference 578

* This paper is presented by title and abstract only, since it was not read at the Conference.

KEYNOTE ADDRESS

МОГУТ ЛИ ПОНЯТЬ ДРУГ ДРУГА ЭКСПЕРИМЕНТАТОРЫ, ОЦЕНЩИКИ-КОМПИЛЯТОРЫ И ПОТРЕБИТЕЛИ ЯДЕРНЫХ ДАННЫХ?

Л.Н.УСАЧЕВ
ФИЗИКО-ЭНЕРГЕТИЧЕСКИЙ ИНСТИТУТ, ОБНИНСК
СССР

Международное агентство по атомной энергии созывает конференции, посвященные разнообразным научным вопросам. Каждый из этих вопросов имеет существенное значение для развития ядерной энергетики. Это и вопросы технологии тепловыделяющих элементов, их стойкости в нейтронных полях и их химической переработки, это и вопросы физики реакторов, математических методов расчета, вопросы защиты и дозиметрии. Вопрос микроскопических ядерных данных, существенных для реакторов, с этой точки зрения является одним из многих. Но мне хотелось бы напомнить, что сама принципиальная возможность высвобождения ядерной энергии была выяснена в результате получения ядерных данных о существовании процесса деления ядра урана после захвата нейтрона и о вылете 2 – 3-х вторичных нейтронов деления. В годы зарождения ядерной энергетики знание ядерных данных было чрезвычайно существенным или даже решающим. Так, например, знание баланса нейтронов в быстрых реакторах определяло их способность к расширенному воспроизводству, ради которой и стоило начинать их разработку. Правда, о знании ядерных данных применительно к тому времени трудно говорить, скорее надо говорить об их понимании и ощущении, которые вытекали из имевшихся физических представлений о делении ядер, о радиационном захвате и рассеянии нейтронов. Экспериментальная информация была очень скудной, но именно по этому она была особенно ценной.

По сравнению с теми временами теперь положение с ядерными данными коренным образом изменились, количество информации чрезвычайно возросло. Однако положение еще далеко не удовлетворительно. Состояние знаний ядерных данных не обеспечивает достаточной надежности расчетов реакторов. И это в то время, когда в различных странах мира разрабатываются и осуществляются широкие планы развития ядерной энергетики!

Для обеспечения развития атомной энергетики заданной мощности планируется добыча урана, обогатительное производство, химическая переработка и другие отрасли промышленности, составляющие заметную долю в общем экономическом балансе страны.

Надежность расчетов указанных объемов производств существенно лимитируется в настоящее время неопределенностями в ядерных данных. Таким образом, развитие ядерной энергетики вызывает с настоятельной необходимостью стремление к получению максимальной точности ядерных данных.

Деятельность по уточнению ядерных данных складывается из трех этапов: из их измерения, из сбора, оценки и выработки значений, рекомендуемых для расчета реакторов, и проверки их на расчетах макроскопических реакторных экспериментов. Это весьма широкое поле деятель-

ности, которое требует разделения труда и специализации. Успех такой комплексной работы определяется как достижениями в каждой из специализированных областей, так и эффективной взаимосвязью между ними. Однако, эти два условия противоречивы. Специализация, кроме все больших и больших достижений в каждой из областей, ведет к тому, что специалисты утрачивают понимание работы соседа, проблем, которые перед ним стоят, утрачивают общий язык. Эффективная взаимосвязь при этом становится затруднительной.

К сожалению, мы часто являемся свидетелями того, что экспериментаторы не извлекают из своего эксперимента информации, которая чрезвычайно полезна для потребителей. Например, физики, работающие на селекторах, обычно прекращают свои измерения как только их аппаратура перестает разрешать отдельные резонансы. Потребители теряют весьма нужную информацию о средних сечениях в районе от одного килоэлектронвольта до нескольких десятков килоэлектронвольт. Но в этом виноваты и сами потребители, которые, не понимая возможностей эксперимента, не ставят соответствующих задач.

Не задумываясь о том, где и как будут использованы получаемые ими данные, экспериментаторы часто не указывают в своих статьях некоторых деталей проведения эксперимента и его обработки. Но без этих деталей оценщик-компилятор не может сравнить результаты разных работ.

Цель, ради которой все присутствующие собрались в этом зале, по мысли инициаторов и организаторов конференции, состоит в улучшении взаимопонимания физиков-ядерщиков, измеряющих микроскопические ядерные данные, физиков, оценивающих эти данные и вырабатывающих рекомендуемые для расчета реакторов значения этих величин, и физиков-реакторщиков и проектировщиков, которые используют рекомендованные значения для расчета реакторов, а также ведут макроскопические эксперименты с критическими сборками и реакторами.

Работа этих трех групп ученых имеет единую конечную цель — обеспечение все большей надежности и точности ядерно-физических расчетов реакторов. Но общность конечной цели сама по себе еще далеко не обеспечивает взаимопонимания, поскольку у указанных групп ученых объективно разное положение и отношение к точности ядерных данных. Если реакторщики справедливо требуют точности в пределах процента для расчетов характеристик реакторов, что ведет к требованиям примерно такой же точности для основных микроскопических ядерных данных, то ядерщики-экспериментаторы справедливо сетуют на чрезмерность этих требований, скептически относясь к возможностям современного эксперимента в отношении достижения такой точности. Дело в том, что, несмотря на большие усилия и успехи физиков-экспериментаторов в развитии экспериментальных методик, часто значения одной и той же величины, полученные наиболее совершенными методами и наиболее компетентными авторами, отличаются одно от другого значительно больше указанных авторами ошибок. Это свидетельствует о наличии каких-то систематических ошибок, природа которых пока не понята. Поэтому истинную точность результатов характеризует не ошибка, указываемая самими авторами, а разброс между результатами различных авторов.

Неудовлетворительное положение с микроскопическими ядерными данными уже отмечались на Конференции по технологии нейтронных сечений в Вашингтоне в марте этого года, на Лондонской конференции по

быстрым реакторам в мае этого года. Чтобы еще раз наглядно убедиться в неудовлетворительности положения, возьмем для примера некоторые ядерные данные, важные для реакторов на быстрых нейтронах. Так, например, если воспользоваться последней компиляцией BNL-325 [1], то можно убедиться, что для сечения захвата урана-238 имеет место разброс точек относительно рекомендованной кривой на 20% вверх и вниз (на рисунке представлено сечение деления плутония-239). В области ниже 150 кэв имеется разброс того же порядка. Интересно отметить, что последние данные Уайта и других [2], помеченные на рисунке косыми крестами в кружке, отличаются от других особенно резко.

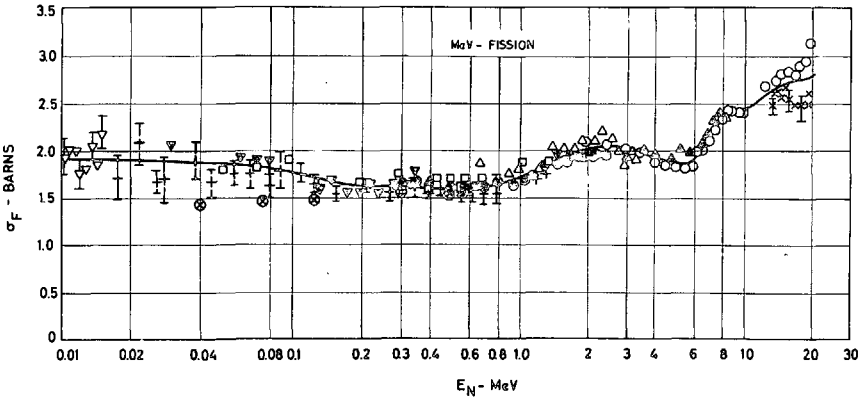

Разброс в сечении деления урана-235 составляет ~5% в районе 500 кэв и увеличивается до 15% в области ниже 100 кэв.

До недавнего времени существовало убеждение, что значения $\bar{\nu}$ в тепловой области известны с точностью 0,5%. В недавней работе Колвина и Соурби [3] измеренное значение среднего числа вторичных нейтронов при спонтанном делении калифорния-252 оказалось ниже примерно на 2% использовавшегося ранее средне-взвешенного значения. Такое же двухпроцентное изменение относится и ко всем другим делящимся изотопам, поскольку $\bar{\nu}$ калифорния используется в качестве стандарта. Если при этом иметь в виду большой разброс значений, даваемых разными авторами в относительном ходе кривой $\bar{\nu}(E)$ в зависимости от энергии падающих нейтронов, то оценка неопределенности ~2% весьма оптимистична.

Поговорим теперь об ученых, оценивающих ядерные данные с точки зрения использования этих данных при расчетах реакторов. Они должны рекомендовать реакторщикам совершенно определенные значения всех величин, несмотря на весьма большие неопределенности в экспериментальных данных. И самое интересное то, что в ряде случаев это удается весьма успешно делать. Так, удивительно хороша точность расчетов реакторов на быстрых нейтронах, состоящих, в основном, из урана-238 и урана-235, если пользоваться 26-групповой системой констант, разработанной еще в 1962 – 1963 годах в СССР под руководством покойного профессора И.И.Бондаренко [4]. В то время не было еще возможности проверить эту систему констант на больших критических сборках. Тем не менее широкий набор сборок ZPR-III [5] и сборок

БФС [6] описывается этой системой констант с завышением k_{ef} в среднем на 1,5%, но не более 3% [7]. И это несмотря на то, что отмеченные выше неопределенности в микроскопических ядерных данных, существующие в настоящее время, не говоря уже о неопределенностях, имевшихся в 1962 году, должны были бы приводить к неточности в k_{ef} не менее 10 – 15%. С первого взгляда это явление представляется случайной удачей. Однако причину столь удовлетворительного согласия можно понять, если вспомнить, что выбираемые значения сечений проверялись на ряде макроскопических опытов. Это были специально проведенные с большой точностью опыты по распределению чисел захвата и деления в блоках обедненного урана. Таким образом, относительные величины сечений, которые, в основном, и определяют баланс нейтронов и, следовательно, эффективный коэффициент размножения, оказались выбранными правильно. Из этого примера видна очень большая роль разумно поставленных макроскопических экспериментов и учета их результатов при выборе величин, рекомендуемых для расчета ядерных реакторов. Это яркий пример так называемой обратной связи результатов макроскопических опытов с микроскопическими сечениями

Вместе с тем надо отметить, что использование указанной системы констант для расчета некоторых других реакторных параметров не дает столь точного согласия. Например, расчет времени жизни мгновенных нейтронов меньше экспериментального в среднем на 20%. В этом, по моему мнению, повинно то обстоятельство, что до измерения времени жизни не было проведено какого-либо макроскопического эксперимента, результаты которого сильно зависели бы от абсолютных значений урана-238 и урана-235. Поэтому абсолютные значения этих сечений, выбранные на основе неточных микроскопических данных, могли оказаться отличающимися от действительных.

Какой же вклад могут внести реакторщики в дело взаимопонимания, в дело выбора таких значений констант, которые будут описывать все процессы в реакторах с достаточной точностью? Конечно, во-первых, они должны продолжать предъявлять свои суровые требования к точности микроэксперимента. Но наряду с этим они должны вместе с оценщиками обеспечить постоянную обратную связь между результатами реакторных и других макроскопических экспериментов с микроконстантами.

Реакторщики получают информацию об интегральных экспериментах, которые могут быть сделаны с хорошей статистической точностью. Конечно, в каждом реакторном эксперименте есть свои специфические особенности, неправильная интерпретация которых может привести к систематической ошибке. При анализе экспериментов требуется введение ряда поправок, например на изломанный характер поверхности сборки, гетерогенность, несферичность формы и т.д. Только после введения этих поправок может быть проведено сравнение с расчетом, обычно идеализированным. Для того чтобы результаты таких экспериментов могли непосредственно влиять на выбор рекомендованных значений ядерных данных, результаты расчета этого эксперимента надо представить в таком виде, чтобы можно было просто оценить, как влияет то или иное изменение констант на значения измеренных величин.

Такую возможность дает, например, теория возмущений, развиваемая нами с 1963 года [8]. В соответствии с этой теорией относительное изменение любого измеряемого параметра, например отношения

чисел процессов, реактивностей образцов, времени жизни мгновенных нейтронов, может быть линейно выражено через относительные изменения констант. Вычислив однажды коэффициенты линейной связи для каждой сборки и для всех измеренных на ней характеристик, можно проводить эффективную и целенаправленную работу по улучшению рекомендованных значений констант, добиваясь наилучшего согласия экспериментальных и расчетных характеристик всех имеющихся сборок.

Пример такого рода работ представлен нами на данную конференцию [9], и там показано, как результаты макроскопического эксперимента по времени жизни мгновенных нейтронов и по критичности реактора, выступают в поддержку наметившейся тенденции изменения микроскопических данных.

С использованием техники теории возмущений "обратная связь" станет регулярно действующей, и сложный язык этой связи будет переведен самими реакторщиками на общепонятный и простой язык линейного соотношения, в коэффициентах которого учтены все реакторные тонкости.

Уже отмечалось, что состояние сведений о микроскопических ядерных данных сейчас таково, что использование обратной связи может существенно повлиять на выбор рекомендуемых значений. Но нашей целью должно являться достижение такого положения, когда обратная связь уже не будет требовать изменения тех величин, которые получены из микроэксперимента. Но для этого мы должны будем научиться измерять микроскопические сечения с точностью в несколько процентов, а иногда и с более высокой. Необходимым условием будет являться полное согласие результатов измерений одной и той же величины, выполненных разными методиками и авторами. Иными словами, надо добиться отсутствия систематических ошибок в экспериментах. Предполагается, конечно, соответствующая точность и со стороны реакторщиков.

Окончательный результат этой деятельности должен состоять в избавлении от дорогостоящей необходимости собирать модели реакторов, а также в избавлении от еще более дорогостоящих ошибок в расчете времени кампании, изотопного состава и других характеристик реактора, самым решающим образом влияющих на его экономические показатели. Определять время кампании каждого нового типа или модификации реактора лишь после того, как эта кампания действительно будет отработана — это слишком дорогая плата за неточность ядерных данных. Надежность рассмотрения вопросов динамики реактора, тесно связанных с его безопасностью, также определяется надежностью и точностью ядерных данных. Конечно, надо еще раз подчеркнуть, что в этих рассуждениях предполагается одновременный прогресс и в методах и в теории расчета реакторов, учитывающих реальную геометрию и различные другие реакторные эффекты, например эффект резонансной блокировки. В уточнении ядерных данных заинтересована и ядерная физика.

Уточнение всей совокупности сечений каждого элемента несомненно уточнит и физические представления о природе ядерных реакций, происходящих под действием нейтронов, и о структуре ядра вообще. Хорошо известны примеры в науке, когда уточнение данных приводило не только к лишним знакам после запятой, но и к качественно новым результатам. У нас нет основания отбросить такую надежду в отношении обсуждаемой области науки. В то же время, несомненно, что интерес к прецизионным и надежным измерениям со стороны ядерной физики

существенно повысит энтузиазм и тщательность работы физиков-экспериментаторов, измеряющих ядерные данные для реакторов.

Мне хотелось бы привести пример, в котором интерес со стороны исследования механизма явления стимулировал проведение особо тщательных измерений, давших свои результаты в первую очередь для потребителей-реакторщиков.

Это – работа, выполняемая в Обнинске по измерению энергетического хода числа вторичных нейтронов для урана-235 и урана-233 в зависимости от энергии нейтрона, вызывающего деление. Благодаря тому, что эта зависимость была поставлена в связь с каналовыми эффектами деления, она исследовалась со всевозможной скурпулезностью.

Наряду с измерениями $\bar{\nu}$ измерялась средняя кинетическая энергия осколков, их массовые и энергетические распределения. Такая комплексность исследования, направленная на выяснение механизма явления, повышает надежность результатов [11, 12].

Существенную роль в развитии интереса к комплексному изучению явления могут сыграть теоретики-ядерщики. По-моему, надо преодолеть имеющийся скептицизм в отношении возможностей теории. Конечно не все согласятся с тем, что теория может дать количественные предсказания. Однако все должны согласиться с тем, что в тесном содружестве с экспериментом, стимулируя его, она может дать весьма ценные результаты. Хотя здесь надо предостеречь от гипнотизирующего влияния теоретических представлений на экспериментатора и через него на результаты эксперимента. Такое влияние – это главная и единственная опасность, могущая проистечь от указанного сотрудничества. В этом отношении у экспериментаторов должен сохраняться скептицизм. Но я думаю, что эта опасность не очень велика, поскольку, как гласит известная шутка, теоретик отличается от экспериментатора тем, что никто не верит результатам теоретика, кроме него самого, в то время как результатам экспериментатора верят все, за исключением самого автора.

Несмотря ни на что, оценщики все же пользуются услугами теоретиков. Использование оптической модели для интерполяций и экстраполяций в неисследованные области энергий и масс полных сечений и угловых распределений упруго рассеянных нейтронов хорошо известно. Можно констатировать также прогресс в развитии систематики плотности уровней [13], который позволяет надеяться, в частности, на увеличение точности предсказаний сечений радиационного захвата. Возможность такого предсказания особенно ценна в отношении сечений захвата нейтронов осколками деления, так как непосредственные измерения с ними весьма затруднены.

Одна из основных причин выделения промежуточной специализации оценщиков-компиляторов – это быстрое возрастание объемов экспериментальной информации, необходимость ее осмысливания и переработки. Проблема обработки больших объемов информации сейчас начинает успешно решаться применением электронных вычислителей для хранения и переработки данных. В настоящее время известны две системы хранения и переработки данных. Одна из них, разработанная в Брукхэвенском Σ-центре система СЦИСРС, обращена лицом к микроскопическому эксперименту, она хранит и перерабатывает первоначальные экспериментальные данные. Другая известная система, разработанная в

Англии, обращена лицом к реакторным расчетам и содержит рекомендуемые для расчета кривые. В промежутке между этими двумя системами лежит труд оценщика, еще не механизированный.

Доктор Паркер на Вашингтонской конференции по технологии нейтронных сечений [14] выразил убеждение, что этот труд можно механизировать, так как если процедура выбора рекомендованных сечений логична, то она поддается программированию, а если нелогична, то ее и не стоит проводить. Кроме того преимущества, что каждая новая информация о сечениях может быть оперативно учтена, имеется еще одно — полное избавление от субъективизма при выборе рекомендованных значений, поскольку алгоритм выбора может быть предварительно широко обсужден. Замечу, что, по-моему, этот будущий алгоритм должен включать как составную часть использование описанной выше техники теории возмущений. В процессе создания и обсуждения такого алгоритма, который надо будет объяснить электронному вычислителю, и поэтому он должен быть ясным и логичным, его создатели, среди которых должны быть представители всех специализаций, вынуждены будут найти общий язык

Я надеюсь, что из всего сказанного видна реальная база взаимопонимания между физиками-экспериментаторами, оценщиками и потребителями-реакторщиками. Ясно также и то, что для реального его достижения надо много поработать как на этой конференции, так и в течение длительного периода после нее.

ЛИТЕРАТУРА

[1] Neutron Cross Sections, BNL-325, Suppl. No. 2, Vol. III., 1965.

[2] WHITE, P.H., HODGKINSON, I.G., WALL, G.I., Physics and Chemistry of Fission, Proc. Symp. Salzburg, 22-26 March 1965. IAEA, Vienna 1 (1965) 219.

[3] COLVIN, D.W., SOWERBY, M.G., Physics and Chemistry of Fission, Proc. Symp. Salzburg, 22-26 March 1965. IAEA, Vienna 2 (1965) 25.

[4] АБАГЯН Л.П., БАЗАЗЯНЦ Н.О., БОНДАРЕНКО И.И., НИКОЛАЕВ М.Н., Групповые константы для расчета ядерных реакторов. Атомиздат, 1964.

[5] DAVEY, W.G., Nucl. Sci. and Engng. 19 (1964) 259.

[6] ЛЕЙПУНСКИЙ А.И. и др., Доклад на III Женевской конференции. Proc. 3d UN Int. Conf. PUAE 4 (1965) 377.

[7] БАЗАЗЯНЦ Н.О., ЗАРИЦКИЙ С.М., ТРОЯНОВ М.Ф., Бюллетень Информационного центра по ядерным данным, вып. II, стр. 247, Атомиздат, 1965.

[8] УСАЧЕВ Л.Н., "Атомная энергия", декабрь (1963).
АБАГЯН А.А., ДРУЖИНИНА Г.И., ДУБИНИН А.А., ЗАРИЦКИЙ С.М., ОРЛОВ В.В., ПУПКО В.Я., СУВОРОВ А.П., УСАЧЕВ Л.Н., ФЕДОРЕНКО Р.П., Proc. 3d UN Int. Conf. PUAE 4 (1965) 359.
УСАЧЕВ Л.Н., ЗАРИЦКИЙ С.М., Бюллетень Информационного центра по ядерным данным, вып. II, стр. 242, Атомиздат, 1965.
ЛЕЙПУНСКИЙ А.И. и др., Экспериментальные и теоретические исследования по физике быстрых реакторов. Доклад на Конференции по быстрым реакторам-размножителям. Лондон, 17 – 19 мая 1966 г.

[9] УСАЧЕВ Л.Н., ЗАРИЦКИЙ С.М., Точность расчета характеристик реакторов в зависимости от точности элементарных констант. См. это изд. т.2, CN-23/94.

[10] БЕЛАНОВА Т.С., ВАНЬКОВ А.А., МИХАЙЛУС Ф.Ф., СТАВИССКИЙ Ю.Я. См. это изд. т.2, CN-23/96.

[11] BLYUMKINA, Yu.A., BONDARENKO, I.I., KUZNETSOV, V.F., NESTEROV, V.G., OKOLOVITCH, V.N., SMIRENKIN, G.N., USACHEV, L.N., Nucl. Phys. 52 (1964) 648.
ПРОХОРОВА Л.И., СМИРЕНКИН Г.Н., Каналовые эффекты в энергетической зависимости $\bar{\nu}$ для U-235 и Th-232. См. это изд. т.2, CN-23/95.
КУЗНЕЦОВ В.Ф., СМИРЕНКИН Г.Н., Тонкая структура в энергетической зависимости $\bar{\nu}$ для U-233 и U-235 при делении нейтронами ниже 1 Мэв. См. это изд. т.2, CN-23/97.

[12] КУЗЬМИНОВ Б.Д., СЕРГАЧЕВ А.И., ДЬЯЧЕНКО П.П., ВОРОБЬЕВА В.Г., СЕНЧЕНКО В.И., ТАРАСКО М.З., О влиянии вариаций энергетических и массовых распределений осколков деления на энергетическую зависимость $\bar{\nu}$. См. это изд. т.2, CN-23/110.

[13] ШУБИН Ю.Н., МАЛЫШЕВ А.В., СТАВИНСКИЙ В.С. Плотность уровней и структура атомных ядер. CN-23/106 (Не опубликовано).

[14] PARKER, K., Mechanised Evaluation of Neutron Cross Sections, Conf. on Neutron Cross Section Technology, March 22-24 1966, Wash. D.C.

Session I

NUCLEAR DATA REQUIREMENTS

NUCLEAR DATA REQUIREMENTS FOR THERMAL REACTOR DESIGN AND OPERATION

G. H. KINCHIN
ATOMIC ENERGY ESTABLISHMENT WINFRITH,
DORCHESTER, DORSET, UNITED KINGDOM

Abstract

NUCLEAR DATA REQUIREMENTS FOR THERMAL REACTOR DESIGN AND OPERATION. The accuracy required in calculations of the properties of thermal reactors, in all stages from initial assessment to final operation, is a matter of judgement. The factors to be considered in making this judgement are outlined, and it is suggested that a common basis of accuracy requirements for reactor properties be used. Even if this common basis for properties, such as reactivity, is assumed, there are many ways of meeting the desired objectives for a particular reactor system, ranging from large-scale experiments on a range of lattices to a more theoretical approach relying on sophisticated methods of calculation and accurate nuclear data. Nuclear data requirements should be determined on the basis of the latter approach.

A variety of thermal reactors must be considered in arriving at the required accuracy of nuclear data, because materials differ from one reactor system to another, and even for the most common fissile isotopes, such as ^{235}U and ^{239}Pu, the concentrations and neutron spectrum will vary over a wide range. Finally, there are many ways in which the errors in nuclear data may be compounded, but the accuracy requirements at different neutron energies may be arranged to be consistent with the known difficulties of cross-section measurements at different energies. The nuclear data needs for thermal reactors are on the way to being met. The status of available data is briefly reviewed in the light of required accuracies, and outstanding requirements are considered, bearing in mind the contribution which integral measurements can make.

1. INTRODUCTION

The accuracy requirements for nuclear data for thermal reactors are related to the accuracy demanded in predicting various reactor properties. There is no clear-cut rule for specifying the accuracy needed for predictions of reactivity, temperature coefficients and other important reactor properties, but it is unlikely that there will be a very large spread in opinion. The first part of this paper considers the accuracies for predictions of thermal reactor properties and these are then related to nuclear data accuracies. Finally the status of available data is briefly reviewed.

2. PREDICTION OF REACTOR PROPERTIES

The primary requirements for reactor design are sufficiently accurate predictions of reactivity and power distribution. In addition it is convenient to identify some reactivity changes, such as the changes due to variations of composition as burn-up proceeds, leading to a reactivity lifetime of the fuel, changes of reactivity with the temperature of various reactor components and changes of reactivity with the insertion of control absorbers. The designer will wish to know the critical size or critical enrichment for the reactor, whether he can obtain the expected power output (which may be reduced if the power distribution is less uniform than anticipated), whether the temperature coefficients of reactivity and

the control design will lead to a safe kinetic behaviour of the reactor, and whether he can achieve the expected fuel lifetime.

Before considering these reactor properties further it is worthwhile noting that there are some general considerations which will put limits on the accuracies which are useful. The first of these is a knowledge of the composition of the reactor, not only in terms of weight and disposition of fuel, moderator and canning material but also of fuel enrichment and the presence of small amounts of high cross-section impurities. Whilst all of these factors can be taken into account in experimental assemblies using a high level of testing and inspection, even in this case the information is sometimes inadequate and in a power reactor it becomes impracticable to test each component in detail. For the four almost identical Calder reactors, after taking considerable care with material inventory and cross-sections, a spread in reactivity of $\frac{1}{4}\%$ was observed, which gives some idea of the minimum reactivity uncertainty which must arise even when experiments on full-scale identical reactors are available. In enriched reactors a larger uncertainty must be expected because of a spread in enrichment. The second general consideration which must be kept in mind is the uncertainty in other aspects of a reactor design than the reactor physics; in magnox reactors a 5% error in heat transfer coefficient has a comparable effect on generating cost to an error of a few °C in measuring the maximum can temperature, and there is little incentive to reduce the reactor physics uncertainties to a very much lower level than the other uncertainties inherent in the design.

There are differences between natural and enriched uranium reactors which make it desirable to consider the requirements separately.

2.1. Natural uranium reactors

2.1.1. Reactivity

The restriction to natural uranium reduces design flexibility and demands a higher degree of precision in predictions of reactivity. Taking the graphite-moderated magnox reactors as an example, it is possible to determine the economic consequences of uncertainties in some of the reactor properties, in somewhat artificial conditions which assume that there are no compensating errors in other parts of the design. Even in this case the conclusions must depend on the detailed plant design, and in practice the margins on temperatures, blower power, turbine capacity and so on must determine what remedial measures may be taken to correct errors.

Let us suppose that a 275-MW(e) magnox reactor when built turns out to have a reactivity 0.5% lower than expected. It would be possible, if no reactivity margin were built in, to down-rate the whole reactor, to reduce the flattened radius of the reactor, to reduce the fuel irradiation level or, though we shall not consider it further here because we are confining our attention to natural uranium reactors, to enrich the un-flattened region [1]. Down-rating the whole reactor is an unattractive and expensive alternative. Reduction of flattened radius may cause a reduction in thermal output due to an impaired radial averaging factor and a reduction in outlet temperature; the effect of 1°C change in outlet temperature is dependent on detailed turbine design and may give anything

between 0.12% and 1.2% change of electrical output. If no regagging of the coolant channels is possible the increase in generating cost would be from 3.5 to 12.5%; if regagging is possible the increase would be from 1.5 to 2.5%. Finally reduction of fuel lifetime would increase generating cost by about 5%.

Had the reactor been optimized to take account of the low reactivity at the design stage, the generating cost would have increased by 0.5%, so that the net effect of being unaware of the error is 1 to 2% on generating cost if regagging is possible. If the reactivity turns out to be 0.5% greater than expected, it is assumed that on the one hand the reactivity can be taken up in absorbers without impairing the radial averaging factor but that on the other no profitable use is made of the excess reactivity. The unnecessarily large capital cost of the reactor will then increase generating costs by 0.5%.

It is clear, therefore, that for magnox reactors some reactivity margin should be built in, that $\pm 1\%$ on reactivity may well be acceptable and that it is difficult to justify a requirement more stringent than $\pm 0.5\%$. Note that these arguments refer to equilibrium reactivity.

Similar arguments apply to heavy-water-moderated reactors of the CANDU type, although the ways in which reactivity errors could be taken up are different in detail. With a bi-directional fuelling scheme, changes in the refuelling rate can, for instance, be used to adjust reactivity, with consequent effect on fuel lifetime and power distribution. Nevertheless, the acceptable reactivity uncertainties are likely to be very much the same as those for the graphite-moderated reactors.

2.1.2. Power distribution

In the magnox reactors already considered, an error of $\pm 4\%$ in radial peak-mean channel power ratio corresponds to a $\pm 0.5\%$ reactivity error and precisely the same arguments apply when regagging is possible. If regagging is not possible, the penalties are liable to be greater since temperature conditions in each individual channel must be maintained below some limiting operational level and limiting temperatures may be achieved in channels which are not operating at the maximum channel power. It therefore seems appropriate to seek an error of $\pm 4\%$ in the individual channel powers rather than on the peak-mean channel power ratio.

2.1.3. Temperature coefficients

From the point of view of safety and stability an error of about $\pm 20\%$ on fuel and moderator temperature coefficients is acceptable, and where appropriate a similar accuracy should be sought on the void coefficient due to the production of steam or loss of coolant in water-cooled reactors. Of course, both moderator coefficient and void coefficient may change sign during irradiation and the accuracy requirement of $\pm 20\%$ must be taken with a pinch of salt when the coefficient approaches zero. Nevertheless this figure gives a general impression of the requirements, and the point illustrates the difficulty of giving precise limits.

2.1.4. Control

Bearing in mind that some control margin must be built in, an accuracy of ± 10% in control rod worth appears to be adequate for predicting the necessary control rod investment at the design stage.

2.2. Enriched uranium reactors

2.2.1. Reactivity

It may be argued that any reactivity error detected in the initial loading of an enriched uranium reactor can be taken into account by adjusting the equilibrium feed enrichment so that by the time equilibrium is reached no penalty will be incurred. Also, since metallurgical lifetime or the endurance limit of fuel is not usually a very well defined quantity, and fuel costs are not particularly sensitive to fuel lifetime near the design point, the economic consequences are not likely to be severe even if the error is not corrected.

However, it may take some years to reach equilibrium and if the initial loading is chosen to be just critical, penalties can accrue from an error in initial reactivity. As in the case of the magnox reactors, the more difficult situation is the one in which reactivity is lower than expected, and the remedial measures such as the removal of flattening absorbers, increasing the fraction of more highly enriched fuel with probable adverse effects on form factor, reducing fuel lifetime or even sacrificing some measure of xenon override capability, will all lead to economic loss. A quantitative assessment is difficult, but an error of ± 2% in reactivity may be judged to be acceptable in this case, and this is not inconsistent with the increased background uncertainty due to inadequate knowledge of the uranium enrichment.

2.2.2. Other factors

The target for power distribution uncertainties will be similar to that for the natural uranium reactors, as will be those on control and reactivity coefficients.

2.3. Other fuel cycles

Although in natural and enriched uranium reactors significant quantities of plutonium are built up, it is appropriate to enquire whether for a thermal reactor fuelled by plutonium or ^{233}U, and possibly using thorium as a fertile material, any difference is to be expected in the requirements for accuracy in predicting reactor properties. The question may quickly be answered. The characteristics of these reactors are sufficiently similar to those of the ^{235}U reactors that no additional consideration is needed, and the requirements will be the same as those for enriched uranium reactors.

In summary, therefore, the designer and operator would like an accuracy of ± 0.5% in reactivity for a natural uranium reactor but could accept ± 1%, especially if attention is given to design flexibility. Similarly they would like ± 1% in reactivity but could accept ± 2% for an

enriched reactor. The remaining thermal reactor accuracy requirements are ± 4% in power distribution, ± 20% in reactivity coefficients and ± 10% in control.

3. RELATION TO NUCLEAR DATA

In a reactor calculation, errors may be due either to the method of calculation or to the nuclear data. In the early days of reactor design, neither were satisfactory and it was therefore necessary to carry out integral experiments, i.e. experiments on exponential or low power critical assemblies. These experiments covered a range of reactor lattices in the region of interest, with varying fuel element size, pitch, channel diameter, etc., and the results were correlated using relatively crude theoretical models to give sets of adjusted nuclear data which would reproduce the observed reactivities, fine structure, etc. It was realized that any departure from the range covered by experiment led to gross uncertainties and called for further experiments, but the range of interest for natural uranium fuels was relatively small, and the procedure was generally satisfactory. With the advent of improved nuclear data, the greatly increased capability for sophisticated calculations provided by digital computers, and the greater variety of reactor designs possible with enriched fuel, more attention is focussed on using methods of calculation which virtually eliminate the approximations formerly used, and on using basic nuclear data. Integral experiments will still be required, but may be regarded as checks of theory and data, rather than the closest possible simulation of a real reactor. It should, therefore, be possible to assume that there is no error inherent in the methods of calculation and that the nuclear data should be sufficiently accurate to meet the sort of requirements outlined above. This does not, of course, mean that every designer will use the most sophisticated method available for all his calculations, but rather that the design methods of calculation can be checked at critical points by the more sophisticated methods.

We have seen that for reactivity, the most important reactor parameter from the point of view of nuclear data, a range of uncertainties from ± 0.5% to ± 2% can be justified. I would like to suggest that for thermal reactors one should accept ± 1% as the right reactivity uncertainty to use in deducing the required accuracies for nuclear data, for two reasons.

The first is that history cannot be ignored. Whilst it is undeniably true that natural uranium reactors are more sensitive to reactivity uncertainty than enriched reactors, there are many integral experiments such as those mentioned in Refs. [2] and [3] which are available for making fine data adjustments in conjunction with the preferred method of calculation for graphite or heavy-water reactors fuelled with natural uranium. We thus eliminate the ± 0.5%.

The second reason is that whilst some typical cases will be considered, it is difficult to be exhaustive. A somewhat higher accuracy in initial reactivity may be needed in initial enrichment if ± 2% is to be achieved in the equilibrium reactor, and a better accuracy may be called for if there is to be, as anticipated above, considerable extrapolation from relatively few integral experiments.

Thus for the purpose of determining nuclear data accuracies it is suggested that the following accuracies for thermal reactor parameters be assumed:

Reactivity	± 1%
Power distribution	± 4%
Reactivity coefficients	± 20%
Control	± 10%

3.1. Relation to reactor cross-sections

It is convenient to enquire first into the accuracy needed in cross-sections averaged over a reactor spectrum, and then to consider how this is related to the data accuracies at different neutron energies.

From the simple expression for k_{eff}

$$k_{eff} = \frac{\eta \epsilon p f}{1 + \text{leakage}}$$

an error of about $\pm \frac{1}{2}\%$ may be allowed on each factor, leading to the overall uncertainty of ± 1%. (If an error of ± 1% were allowed on any individual factor, the remainder would have to be determined with no error). To arrive at accuracies of reactor cross-sections, it is necessary to consider a range of thermal reactors, and whilst the arguments put forward here will cover the most important data for fissile and fertile nuclides, it is clear that it is not possible to comment on all materials which might be used in the construction of power or zero-energy reactors. The approach outlined here should, however, be generally applicable.

It is entirely possible for virtually all of the fissions in a thermal reactor to occur in ^{235}U, in ^{233}U or in ^{239}Pu and it is therefore reasonable to seek to know the eta values for these isotopes to ± 0.5%. It is difficult, however, to envisage a thermal reactor in which, whatever the initial fuel, significantly more than half the fissions occur in ^{241}Pu at any stage of irradiation. The accuracy on eta may therefore be relaxed for this isotope to ± 0.9%.

The fast fission factor ϵ is high in undermoderated water reactors and with an upper limit of about 1.1 for ϵ, errors of ± 3% in the fission and total cross-sections of ^{238}U above 1 MeV are acceptable, with a corresponding error in the neutron yield for ^{238}U fast fission. Thorium has a much smaller fast fission effect and the acceptable errors are consequently greater.

The product pf of the resonance-escape probability and thermal utilization is a measure of absorption in non-fissile isotopes, and since η is approximately 2 this product cannot be less than 0.5. It follows, therefore, that absorptions in fissile and other materials should be determined with an accuracy of ± 0.7%.

Similar arguments apply to leakage, which requires a knowledge of absorption and scattering cross-sections, but it is clear that all of these arguments lead to lower numerical limits for the uncertainties since a given reactor cannot at the same time have, for instance, large non-fissile absorption and large leakage.

This sort of consideration leads to a firm basis for the required effective reactor cross-sections, and it is worthwhile pointing out that it is necessary to use a broad brush; more detailed study of the acceptable accuracies for a particular reactor is of little value in arriving at nuclear data requirements because the measurements requested must suffice for a range of reactors for a significant period of time.

3.2. Relation to required differential nuclear data

The European American Nuclear Data Committee has produced a compilation of EANDC requests for nuclear data [4]. The previous discussion outlines the basis, which hopefully is generally acceptable, for arriving at the U.K. requests, but there are still further points to be kept in mind in making the final conversion to requests for some differential data.

Resonance effects are further considered in section 3.3, but for the moment it is convenient to assume that cross-sections vary slowly with energy and that reactors are homogeneous, when a reactor effective cross-section may be defined as

$$\frac{\int \phi(E)\,\sigma(E)\,dE}{\int \phi(E)\,dE}$$

where the integration over the reactor neutron spectrum is carried out over all energies. If all cross-sections had the same energy dependence, the neutron spectrum would not be very important, but especially in plutonium-fuelled reactors this is far from being the case. As a minimum, therefore, additional requirements must be placed on those cross-sections, especially the moderator scattering cross-sections, which are important in determining neutron spectrum in the reactor, so that this additional uncertainty can be removed.

Permissible errors in neutron yield per absorption and in the absorption cross-section for fissile materials were deduced above, but it must be remembered that other parameters, such as the neutron yield per fission, fission and absorption cross-sections, could have been used. In fact there is a large set of inter-related nuclear data for the fissile materials, and when such a set of data is considered as a whole, as in the survey by Westcott et al. [5] of the 2200 m/s constants for ^{233}U, ^{235}U, ^{239}Pu and ^{241}Pu, there may be significant improvements in the accuracy of several of the parameters. For the fissile nuclides, therefore, this allows some relaxation in the accuracy requirements for direct measurements of the separate parameters.

Given an accuracy for a reactor-averaged cross-section or reaction rate, it is necessary to determine how accuracies may be assigned to cross-sections at different energies so that the objective is met. Except in the rather special case of 2200 m/s values, nuclear constants are used in the form of averages over small intervals of energy. For a

particular energy group with lower energy boundary E_i and upper energy boundary E_{i+1}

$$\sigma_i = \frac{\int_{E_i}^{E_{i+1}} \phi(E)\,\sigma(E)\,dE}{\int_{E_i}^{E_{i+1}} \phi(E)\,dE}$$

and if

$$\int_{E_i}^{E_{i+1}} \phi(E)\,dE = \phi_i$$

then the total reaction rate is simply

$$\phi_1\sigma_1 + \phi_2\sigma_2 + \ldots = \Sigma_i \phi_i \sigma_i$$

It seems reasonable to make the highest demands for accuracy in the energy regions where the majority of the reactions occur, and one way of doing this is to divide the total permitted variance equally between a number of different energy groups, so that where the number of events is small a large percentage error in cross-section is allowable. For thermal reactors this procedure has the advantage of widening the permissible error band at higher energies, where accurate measurement becomes more difficult.

If all of the errors were truly random, there would appear to be advantages in choosing an extremely large number of energy groups and ascribing correspondingly large percentage errors to the average in each group. It is clear that this procedure is ridiculous in the limit, and that there must be correlation between the errors in adjacent groups; or, to put it in another way, there must be systematic cross-section errors common to many narrow closely-spaced energy groups. On the other hand, it is equally unlikely that a given cross-section will be systematically in error by the same amount over the whole energy range from a fraction of an electron volt to several million electron volts.

Some sort of intermediate assumption must be made, and one which at least appears plausible from an examination of independent sets of measurements is that errors may be considered to be uncorrelated between about eight different energy groups, four below and four above 1 eV. Required accuracies may then be allocated to each of these groups so that each shall contribute about equally to the variance of the total reaction rate. By taking into account a range of different reactors one finds that it is not worth specifying any variation of permitted accuracy within such energy groups, and it remains to define a little more

clearly what is meant by "an accuracy of ± x% between energies E_1 and E_2". A convenient choice is to request that the averages over relatively fine energy intervals, corresponding to 0.25 or 0.5 lethargy units, shall be determined to ± x% over the energy range from E_1 to E_2 .

Calculations may be made for a number of reactors, perturbing cross-sections in different energy ranges to study the energy-dependent sensitivities. Hellens [6] has carried out this exercise with a range of water-moderated reactors using three broad energy groups, whilst Figs. 1 and 2 illustrate in more detail the sensitivity in the range of graphite-moderated lattices defined in Table I [7]. In these figures the reactivity changes caused by 1% changes in nuclear data at different energies are illustrated.

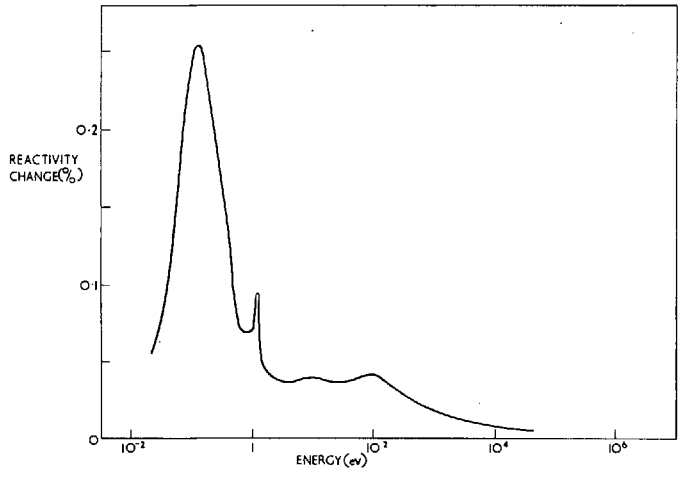

FIG.1. Reactivity change due to 1% change of η over unit lethargy (8% ^{235}U)

3.3. Resonance parameters and reactivity changes

It was stated at the outset that reactivity uncertainty is the most important criterion for determining the accuracies of nuclear data. It is worthwhile reviewing some of the other criteria and examining the resonance region more closely to justify the statement.

3.3.1. Resonance parameters

The discussion so far has been oriented in terms of relatively smoothly varying nuclear constants, especially in the thermal region. Even the simple expression for reactivity, quoted earlier, contains a resonance-escape probability however, and resonance absorption in ^{238} U and thorium is significant and important. Because of the strong self-shielding, the resonance integral of a dilute sample of ^{238}U is not of great relevance in a reactor calculation and more importance may be attached to cross-sections in the wings of resonances than to those at the resonance peaks. Resonance parameters are often used both to

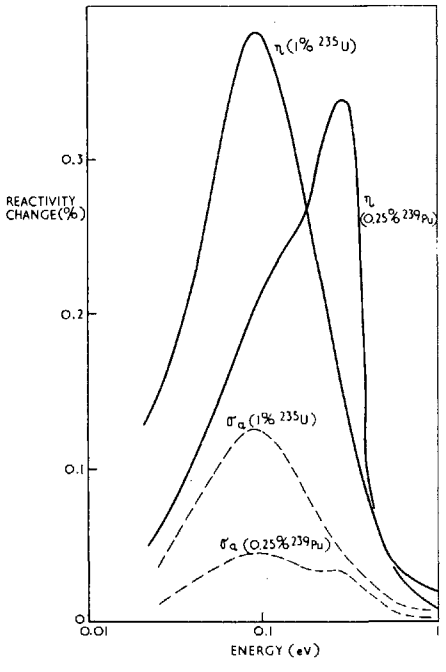

FIG.2. Reactivity changes due to 1% change of η and σ_a over unit lethargy

TABLE I. CELL COMPOSITIONS

Cell	Fuel compositions (%)			Fuel radius (cm)	Cell radius (cm)	k_∞
	^{235}U	^{239}Pu	^{238}U			
8% ^{235}U	8	-	92	1.25	7.0	1.43
1% ^{235}U	1	-	99	1.25	7.0	1.06
0.5% ^{239}Pu	0.5	0.5	99	1.25	7.0	1.17

summarize experimental results and for reactor calculations, and permissible accuracies for resonance parameters can be assessed from the point of view of both reactivity and the temperature coefficient arising from the Doppler effect. It turns out that resonance data for fertile and fissile materials which will give the requisite reactivity accuracy are more than adequate for determining Doppler coefficients.

3.3.2. Reactivity coefficients, control and power distribution

Evidently there are no additional restrictions arising from the resonance structure of cross-sections and their contributions to fuel

temperature coefficients. For the moderator temperature coefficient, the work of Griggs and Sumner [8] suggests that if the data are sufficiently accurate for reactivity purposes it is unlikely that there will be significant errors in temperature coefficients. These conclusions should apply generally to thermal reactors since the cases studied were chosen to be sensitive to changes of plutonium data.

The fuel and moderator cross-sections required for determining reactivity are more than sufficiently precise for determining power distributions. The prime problem for the reactor designer here is in the method of calculation to be employed. The same situation applies to control absorbers and although data will be needed for different control materials the requirements are not very stringent.

3.3.3. Burn-up

It has been implied that a satisfactory way of accounting for composition changes due to burn-up is to take the nominal fuel composition at various stages of irradiation and assign nuclear data accuracies which will lead to a reactivity uncertainty of ± 1% in all cases. Let us be specific and consider an enriched uranium reactor building up plutonium during irradiation, and let us further suppose that the arguments put forward above in favour of considering plutonium-enriched reactors (which would lead to more stringent requirements on the plutonium data) have no appeal for a particular designer, who is determined to save all his plutonium for fast reactors. It is of interest then to enquire whether the data errors needed to determine reactivity to ± 1% on each of the nominal fuel compositions would not lead to much larger reactivity errors if carried right through the burn-up calculation, giving changes in composition as well. The answer is suggested by the work of Hellens [6] who has studied the effect of cross-section changes on reactivity throughout the life of water-moderated reactors. If the absorption cross-section of ^{239}Pu or ^{241}Pu is increased, the increased absorption is at least partially compensated by a reduction in the quantities of those isotopes. For an increase in η for ^{239}Pu, with constant absorption, there is a reduction in ^{239}Pu capture which leads to a reduction in ^{240}Pu production. This will give a further increase in reactivity, but the effect appears to be small and to be cancelled by a reduction in ^{241}Pu production. Thus it seems that the reactivity changes introduced by changes in cross-section which persist during burn-up are no worse than those caused by cross-section changes at the end of life, and in many cases are much less. Where the change in reactivity during lifetime is about 10%, a reactivity uncertainty of ± 1% will lead to an uncertainty of about ± 15% in reactivity lifetime.

3.4. Summary

In summarizing the stages in the specification of accuracy requirements for nuclear data measurements for thermal reactors, it appears that reactivity is the most important criterion. Taking into account available integral data, an accuracy of ± 1% in reactivity seems a reasonable aim. Considering a range of reactor compositions, including the changes due to irradiation, the accuracy required of reaction rates

in different materials may be assessed. Bearing in mind the impact of related cross-sections, especially for the fissile nuclides, the accuracy of measurement in different energy ranges may then be determined.

4. STATUS OF THERMAL REACTOR DATA

It is hardly surprising, in view of the semi-quantitative nature of the procedures outlined above, that there is a spread in the accuracies requested by different users in such compilations of requests as Ref. [4], and it is to be expected that different users will attach different importance to each request.

Nevertheless some useful general remarks may be made on the status of the data required for thermal reactors, the first being that above about 100 eV the far more stringent requests originating from fast reactors rapidly reduce the thermal reactor requests to a role of academic interest. Also, whilst data for new materials may from time to time be needed, it is unlikely that existing requests based on the general arguments presented above will be succeeded by further requests demanding ever higher accuracy.

4.1. Moderator scattering laws

It is difficult to specify in detail the accuracies needed for moderator scattering properties, but such comparisons as have been made between alternative scattering models based on experimental data indicate that data errors are unlikely to contribute significantly to reactivity uncertainty [9].

4.2. Fertile materials

The general agreement on resonance parameters and the satisfactory comparison of the measured infinitely dilute resonance integral with that calculated from resonance parameters seem to indicate that for both ^{238}U and ^{232}Th there is no major uncertainty. It has been suggested, however, that there may be discrepancies between observed and calculated ^{238}U data [2], and since the effect is most pronounced in cases where there is substantial self-shielding, the accuracy of ^{238}U and ^{232}Th data between resonances may repay further study.

4.3. Fissile materials

The current discrepancies in ν values are disconcerting, although the final accuracies [5] ranging from ± 0.3 to $\pm 0.8\%$ are satisfactory. Harris [10] has emphasized the possibility of significant variations in fission yield below 10 eV, where it is often assumed constant. Although no change in ν greater than 0.5% is observed between 0.025 eV and the important 0.3-eV resonance of ^{239}Pu, the possibility of variation in other resonances of the fissile nuclides must be kept in mind.

The absorption cross-sections of the fissile nuclides are determined quite accurately below 1 eV except in energy ranges (above 0.5 eV for ^{239}Pu for instance) where the cross-sections are low and accuracy not

very important. The accuracies of about ±1%, or a little more, are likely to meet most requirements. At higher energies the absorption cross-sections are less well determined but in general meet the relaxed requirements proposed above.

Further discussion will be restricted to the eta values, although it is clear that fission and capture cross-sections and capture-fission ratios are relevant, and should be used to check for systematic errors and reduce the uncertainties in direct measurements wherever possible. Below 1 eV data are available to the required sort of accuracy, or within reach, for ^{233}U, ^{235}U and ^{239}Pu. However, even though the demands are less onerous, they are not met for ^{241}Pu, largely because of the absence of direct measurements of $\eta(E)$. There is more uncertainty in η values for all the fissile nuclides above 1 eV, but a number of measurements which may be expected to achieve sufficient accuracy for thermal reactors are in progress. In this area it is interesting to note the contribution which integral measurements (for example, measurements of the epithermal capture-to-fission ratio for ^{235}U) can make to the checking and refinement of errors in differential measurements.

4.4. Other non-fissile heavy nuclides

Apart from ^{238}U and ^{232}Th, the most important nuclide from the point of view of thermal reactors is ^{240}Pu. The existence of sub-threshold fission may be significant in fast reactors but is of trivial importance in thermal reactors, for which the data are adequately known. Similarly the data for ^{234}U, ^{236}U and ^{242}Pu are sufficiently good.

4.5. Fission products

Fission-product absorption is made up of a large number of separate contributions. For the non-saturating (relatively low absorption cross-section) fission products, the product of yield and cross-section is important. There are few fission products which are of sufficient individual importance and for which the cross-sections are so inaccurately known as to justify separate measurements, but some improvements are desirable.

The broad picture for thermal reactors, then, is one in which the needs for nuclear data can be met with the required precision by differential measurements. Great strides have been made towards meeting the objectives, and the torch which has been carried in the quest for precise nuclear data can almost be handed over from the thermal to the fast reactor field.

REFERENCES

[1] SYRETT, J.J., O'DELL, F.P., private communication.
[2] BARCLAY, F.R., UKAEA Rep. AEEW-R 473 (1966).
[3] HONECK, H.C., CRANDALL, J.L., USAEC Rep. BNL-8253 (1964).
[4] Compilation of EANDC Requests, EANDC 55 U.

[5] WESTCOTT, C. H., EKBERG, K., HANNA, G. C., PATTENDEN, N. J., SANATANI, S., ATTREE, P.M., Atomic Energy Review 3 2 (1965).
[6] HELLENS, R. L., USAEC Rep. BNL-10058 (1966).
[7] MACDOUGALL, J. D., private communication.
[8] GRIGGS, C. F., SUMNER, H. M., UKAEA Rep. AEEW-M 221
[9] Proc. of Brookhaven Conf. on neutron thermalisation, USAEC Rep. BNL-719 (C-32) (1962).
[10] HARRIS, D. R., Paper presented at Am. Phys. Soc. meeting, Washington, March 1966.

NUCLEAR DATA REQUIREMENTS FOR FAST REACTOR DESIGN AND OPERATION

R. D. SMITH
ATOMIC ENERGY ESTABLISHMENT WINFRITH,
DORCHESTER, DORSET, UNITED KINGDOM

Abstract

NUCLEAR DATA REQUIREMENTS FOR FAST REACTOR DESIGN AND OPERATION. Calculation of the neutron physics behaviour of a reactor requires accurate nuclear data which must be supplied by nuclear physics measurements supplemented by integral measurements on zero-power reactors. The nuclear physics parameters of a power reactor are needed for three main purposes: (a) design, (b) safety studies and (c) operations. The accuracy required increases as the reactor progresses from the design-concept stage through detailed design to construction and operation.

The main parameters needed for fast reactors are discussed together with an indication of the accuracy required. The methods by which the accuracy of the data needed to meet these requirements can be deduced are then considered. It is shown that precise independent definitions of the required accuracy for all cross-sections cannot be obtained but that the published data request list forms a good working guide for data measurers. Some of the more important data requests are high-lighted and it is pointed out that a limit to the accuracy needed is set by limits in our knowledge of the composition of actual reactors.

1. INTRODUCTION

Up to the present time zero-power reactor experiments have played a large part in determining the design of power producing reactors. In particular every large-power fast reactor has been preceded by a mock-up critical assembly on a zero-power fast reactor. These mock-ups are, as far as possible, of the same dimensions and of the same atomic composition as the power reactor and contain the same amount of fuel, but operate at 100 W or less. Measurements of critical enrichment, reaction rates and similar properties are then directly applicable to the power reactor. The latest examples of these mock-ups are the Sefor mock-up on ZPR III, the British prototype fast reactor mock-up in Zebra and the Russian BN 350 mock-up on B. F. S. These experiments have been needed because theoretical calculations were insufficiently accurate or insufficiently reliable to supply the necessary data for the design or operation of the reactors. Considerable improvements have been made and are continuing to be made in these calculations and there is a possibility that future experimental work can be limited to relatively few assemblies. Indeed in the thermal reactor field this situation already exists, at least partially, and for many types of thermal reactors accurate predictions can be made on the basis of existing knowledge.

It is therefore appropriate to enquire what accuracy is needed for fast reactor calculations, and since this conference is concerned with nuclear data, to enquire what additional nuclear data are required.

2. REACTOR REQUIREMENTS

Before it is possible to determine the data needed we must first enquire what neutron physics properties of a power reactor we need to know and to what accuracy we need to know them. There are three fairly distinct demands for reactor physics knowledge. Firstly the designer needs to be able to calculate and optimize the behaviour of his projected design and later needs sufficient information to complete the detailed design of the reactor. Secondly since he will be concerned in ensuring that his design is a safe one he will also need physics information pertinent to accident conditions. Ultimately this physics information will form part of a complete safety assessment for the reactor. Since this will involve physics data additional to that required for the normal optimization of the reactor it is convenient to consider safety requirements separately. Finally when construction of the reactor is complete the operator will require a detailed understanding of the reactor in order that he may operate it as efficiently as possible. In general the more detailed and accurate the data on the reactor are the more accurately safety margins can be determined, thus enabling the reactor to be run at higher powers, to higher burn-ups or with greater reliability.

The accuracy with which the data are needed to satisfy these requirements tends to become steadily more exacting as the design proceeds from a conceptual study through engineering design and development to reactor operation.

Consider the first stage of conceptual design. At this stage two considerations are paramount, feasibility and economics. The designer will wish to know that the reactor is safe and stable and that it will work; he will not, for example, be interested in precise values of the temperature coefficients, nor of control rod worths. He will need to know sufficient about the performance of the reactor, including the critical enrichment and breeding gain, to enable him to make sufficiently good cost estimates to compare with other reactors. In general existing data will be adequate to do this, with perhaps some reservations on the accuracy to which breeding gains and temperature coefficients can at present be calculated. For example the accuracy of calculation of breeding is no better than $\pm$ 0.1, which for a typical large sodium-cooled, oxide-fuelled, fast reactor might result in a range of fuel doubling time from 10 to 20 yr. The effect of this variation on the estimated unit cost depends on many assumptions including particularly those on plutonium value, but may well result in a variation over 10% in the cost of electricity generation.

As the more detailed design proceeds more accurate data will be needed. The enrichment of the fuel will need to be specified when manufacture of the fuel starts, possibly over a year before the completion of the reactor. The accuracy of the specification of the enrichment of this fuel is important, both for fast and thermal reactors. In both reactor designs the factors to be considered are the total investment of reactivity necessary to overcome temperature and burn-up effects and the method of adjustment of errors in the initial predictions. The larger the installed reactivity control, the less important a small error in initial reactivity will be. Fast reactors usually show a small variation of reactivity with burn-up and require no compensation for xenon poisoning. In consequence

the installed reactivity control is usually smaller and may be much smaller than that for highly rated enriched thermal reactors. Natural uranium-fuelled reactors, on the other hand, may also have a small reactivity change, at least up to the irradiation levels normally achieved, but compensation of any error in initial loading by variation of enrichment is, of course, impossible. Adjustment by addition or subtraction of absorbers intended for power flattening may, however, provide a range of adjustment without a large effect on the reactor output. In a fast reactor, if too low a value is specified, at worst the reactor will fail to reach criticality or at best some of the absorbers intended to compensate for fuel burn-up may have to be withdrawn. To keep the reactor critical, fresh fuel will have to be supplied at an earlier date than would otherwise be necessary, thus incurring extra expenditure. Alternatively, if the enrichment specified is too high the reactor will operate with fewer fuel elements in its core and a loss of power output will result. This problem is accentuated in large reactors, since compensation of an error in enrichment by additional fuel elements at the periphery of the core may require the addition of an impractical number of fuel elements. For a 1000-MW(e) reactor in fact an error of 1% in the reactivity, corresponding to 2% in enrichment, would require the addition of about 8% of fuel elements to the outer edge of the core to compensate. If the core has more than one enrichment zone adjustment of reactivity is, of course, possible by altering the relative sizes of the zone. As before, fairly large numbers of fuel elements will be required and a loss of power output will result. It may therefore be concluded that it is desirable to be able to calculate the core reactivity to 1% or better.

It was pointed out earlier that the value of the breeding gain of a fast reactor plays a significant part in determining its economic performance. In the first instance, the overall breeding gain in conjunction with the fissile materials inventory determines the doubling time of the system and hence the rate at which fast reactors can be installed in a power system. Secondly, the breeding gain of the core itself affects the loss of reactivity with burn-up. Good breeding in the core reduces the reactivity changes and reduces the need for burn-up compensating absorbers, which further improves the breeding gain. The designer must therefore know the internal or core breeding gain so as to estimate his control rod requirements. An absolute accuracy of better than $\pm$ 0.05 in the breeding gain is desirable. The accurate calculation of breeding gain involves both the loss of fissile isotopes by fission and capture and their gain by capture in fertile isotopes. The calculation presents considerable difficulties, even for an idealized cold clean core containing no fission products and no control rods. These difficulties are even greater for an actual reactor, particularly if the fuel contains a high proportion of higher plutonium isotopes. A power reactor under average operating conditions will be fuelled with a mixture of plutonium isotopes and will contain both fission products and partially inserted control rods. The major data deficiencies in these calculations are the values for the capture cross-sections, particularly of the plutonium isotopes.

The data required for sufficiently accurate calculation of reactivity and breeding gain is sufficient for most other calculations for the reactor, with the exception of some of the temperature coefficients. For example,

although the calculation of control rod worths presents difficulties, these are more associated with methods of calculation rather than the data. Nevertheless, the capture cross-sections of the absorbers commonly used for control rods are still in need of some improvement.

On the other hand, the sodium temperature coefficient and more particularly the Doppler coefficient depend heavily on low energy neutrons. The Doppler coefficient of a typical power reactor depends almost solely on the neutron population below 10 keV, although these neutrons make only a minor contribution to the overall reactivity of the reactor.

For a detailed calculation of the Doppler effect, resonance data for the appropriate isotopes, namely ^{239}Pu and ^{238}U, are required up to an energy of about 10 keV. At this energy experimental evaluation of resonances is difficult though the use of resonance parameters enables approximate extrapolations to be made on the basis of measurements at lower energies.

The sodium temperature or density coefficient of reactivity is sensitive to the variation of neutron effectiveness with energy and this neutron effectiveness is dependent on the cross-sections of all the reactor constituents over a wide energy range. In particular it is affected by the fissile material fission cross-sections and it is noteworthy that there is much uncertainty in the ^{239}Pu fission cross-section from 100 eV to 100 keV.

In the early design stages only approximate values for the sodium and Doppler coefficients are needed, but as the design progresses and detailed safety studies are carried out more accurate values will be asked for. In particular reactivity changes resulting from the loss of sodium from particular parts of the core will be required. This calculation is more difficult than isothermal whole core coefficients and may place added demands on the data. In addition to the safety requirements, design of the temperature compensating control rods requires an accurate knowledge of the temperature coefficients. Errors in predictions of reactivity worth necessitate the provision of reserve control absorbers. Over and above the expense of extra rods and mechanisms it is particularly difficult in fast reactors to find room for the extra control rods and the voids made in the core to accommodate them. As mentioned earlier, the rods also have a deleterious effect on the performance of the reactor. An accuracy in prediction of $\pm$ 20% or better is therefore needed.

There are additional requirements for data needed when the reactor is operating. In most power reactors direct measurements inside the core and reflector are difficult and very expensive since they take up appreciable time on the reactor. There is therefore a strong incentive to cut measurements to the minimum necessary to give some spot checks on the theoretical calculations of the reactor behaviour. Although the operator will usually be able to measure the overall kinetic behaviour of the reactor more accurately than it can be calculated, he will need to make accurate calculations of all the separate components to understand the behaviour of the reactor, and particularly to help in the unravelling of any anomalous features. Similarly, he will be able to measure the overall reactivity loss with burn-up more accurately than calculation, but may require to compare his results with accurate calculations to identify unexpected phenomena such as fuel migration within the fuel

elements. One of the operator's main concerns will, however, be the calculation of temperatures, particularly the temperatures at 'hot spots' in the core and blanket. For this he must have accurate values for reaction rates, particularly in the fissile materials. He will also require data on γ-heating which is more difficult to predict and involves further cross-section data. For his neutron damage calculations he will require data on reaction rates for damage caused by transmutation and on the high energy neutron spectrum for damage caused by displacement. Thus there are data requirements similar to those for the detailed design, with the additional incentive that in many cases the more accurate the data the more power can be obtained from the reactor.

In addition to data required directly for the design and operation of the reactor additional data may be needed for measuring instruments used in the power reactor itself, or more important for zero-power reactor experiments. At the present time zero-power reactor measurements are essential, and therefore data for their operation is also essential. This data may differ from that required for power reactors for several reasons. First the zero-power reactors contain materials not present in power reactors. For example, the fuel clad may be different and aluminium is frequently used as a convenient substitute for sodium. Secondly, data are required for materials which though not actually used in either zero-power or power reactors, are used in measuring techniques. These include materials used in fission chambers, e.g. ^{234}U, activation materials (e.g. gold) and materials used in counters or spectrometers (e.g. ^{6}Li). The possible range of these materials is large, but an accurate knowledge of their cross-sections is necessary before much useful information can be obtained from measurements made with them. To cut down the data requirements as much as possible attention has been focussed on a few materials. Experience has shown, however, that it is dangerous to prune this list too severely since errors have arisen in these measurements in the past due to the presence of contaminants, often unsuspected. Even if their presence is known, however, impurities may make measurements difficult,in particular the presence of a small quantity of a thermally fissile material in a threshold fission chamber may upset measurements of fast flux. For example, it is often wise to make measurements both with ^{238}U and ^{232}Th fission chambers, even though the response of both these chambers in a fast reactor flux should be almost identical. The final choice, therefore, represents a compromise in the number of isotopes for which data is requested.

Similar studies of the accuracy required in the prediction of power reactor parameters have been made in other countries concerned with fast reactor development. At the present time there seems to be a reluctance to publish precise values but where numbers have been given these are not greatly different from the target accuracies suggested here. For example, Greebler [1] has also suggested an overall accuracy of about 1% in reactivity, whilst Cecchini et al. [2] suggested 2% in reactivity and 4% in breeding ratio.

In summary, therefore, we require data in sufficient accuracy to calculate the reactivity to $\pm$ 1%; reactivity coefficients to $\pm$ 20%, breeding gains to $\pm$ 0.05 or better, and reactivity worths of control rods to $\pm$ 10%. Additional data will be required to enable fission rates to be calculated to good accuracy (5% or better) and for supporting measurements in zero

power reactors. The data needs for the latter categories are relatively easy to specify, but we shall consider in the next section how the data needs for reactivity, breeding gains and temperature coefficients may be deduced.

3. DATA ACCURACY NEEDED

When the quantities needed have been determined it is at least theoretically possible to establish the accuracy of data needed. In practice difficulties arise. Firstly, it is not possible to set an independent limit on the accuracy of each piece of data required: for example, if ν, the number of neutrons per fission, can be measured to a very high accuracy it may be possible to allow some relaxation in the value of σ_f. Secondly, the data needed for different reactor designs will be different since different reactors have widely different spectra and contain different elements in different proportions. Thirdly, many microscopic data are measured relative to one another, so that hidden correlations exist in the present data. In many cases these relative measurements can be made more accurately than absolute measurements, but the specification of accuracies in a way which will take full account of the actual measurements made in the nuclear physics experiments is an impossible task.

In the end, therefore, a rigorous approach is impossible and some rule of thumb method has to be adopted.

The approach adopted in the U.K. has been first to determine the effect of inaccuracies in the data on calculations of the critical size and breeding gain of a typical large sodium-cooled power reactor by independently varying the individual group cross-sections in a multigroup calculation. The results were first published by Moorhead [3]. It is then necessary to consider additional requirements for different types of reactors and different reactor quantities, particularly the temperature and power coefficients. Other requirements such as those for shielding and zero-power reactor experiments are then added. Although this is a somewhat arbitrary procedure it has proved satisfactory as a guide to data measurers and forms the basis of the U.K. fast reactor data request list.

Similar studies have been made in other countries. For example, a paper by Greebler and Hutchins [4] examined user requirements for cross-sections in the energy range from 100 eV to 100 keV.

It is worthwhile comparing the results of this study with the U.K. study, since this illustrates some of the difficulties I have mentioned in arriving at a data request list.

Greebler and Hutchins considered five different fast reactors, including a hard spectrum oxide-fuelled reactor, a large oxide reactor with a ^{238}U-^{239}Pu ratio of 8, a similar reactor using thorium as a fertile material, a steam-cooled reactor and a carbide-fuelled reactor using V-20% Ti fuel cans. He then computed the changes of the physics parameters resulting from 25% changes in the fission and capture cross-sections in the range 100 eV to 100 keV. Independent changes were made in two energy intervals, 100 eV to 10 keV and 10 keV to 100 keV. In addition he considered the effect of a 10% change in elastic scattering cross-sections for all these reactors.

TABLE I. COMPARISON OF REACTOR MODELS

Composition	Moorhead	Greebler (Reactor 2)
Sodium coolant	35%	50%
Steel clad	20%	20%
Fuel	45%	30%
	(Pu-U carbide)	(Pu-U oxide)
Isotopic ratios		
N 238/N 239	8	8
Pu 239/240/241/242	100/25/0/0	100/41/7/3

TABLE II. PERCENTAGE CHANGE IN CRITICAL ENRICHMENT FOR A 25% CHANGE IN CROSS-SECTION

	Energy (keV)	Moorhead	Greebler (No. 2)
^{239}Pu σ_f	10 - 100	-8.0	-6.1
	0.1 - 10	-3.1	-4.0
σ_c	10 - 100	0.9	0.6
	0.1 - 10	0.7	0.9
σ_a	10 - 100	-7.1	-5.5
	0.1 - 10	-2.4	-3.1
^{238}U σ_c	10 - 100	4.9	4.0
	0.1 - 10	2.3	2.0
^{240}Pu σ_c	10 - 100	0.22	0.4
	0.1 - 10	0.12	0.5

Using a 60-group code Greebler worked out the effects on critical size, core breeding ratio, Doppler coefficient and coolant void reactivity effect for each reactor.

The sensitivity of the reactor parameters to the cross-section variations obtained by Greebler is similar to that obtained by Moorhead. This can be illustrated by comparing the results for critical enrichment variations for Moorhead's reactor and Greebler's Reactor 2. Table I shows the composition of these reactors.

The ratio of moderator-to-fuel is higher in the Greebler reactor model and the plutonium contains a higher proportion of higher isotopes.

The percentage change in critical enrichment caused by a 25% change in a cross-section is given in Table II.

(For the Moorhead column the figure for the range 10-100 keV has been obtained by taking 0.2 × Group 3 (67 - 300 keV) plus Group 4 (9.1 to 67 keV) and, for the range 0.1 - 10 keV, Group 5 (below 9.1 keV)).

The differences between the two sets of results are no greater than would be expected from the differences between the models and differences in cross-section data. It is clear that if we are seeking for accuracies applicable to a range of fast reactors, variations of a factor of two in the data accuracy required are to be expected.

As explained above the next step in converting the sensitivities into accuracy requirements is a subjective one. Greebler assigned probable accuracies to data in the 0.1 to 100 keV range and then worked out the maximum uncertainties that could arise in the reactor parameters from the variations specified. The resulting uncertainties do not include errors caused by data errors above 100 keV nor those from other nuclear parameters such as $\bar{\nu}$ and the fission spectrum. Also in the cases where the sensitivity to data varies with energy, the magnitude of the effect will depend on the number of energy groups and the positions of the group boundaries.

In this way he was able to specify accuracies and Table III is deduced from his results.

The difficulty of how to add up the various contributions is apparent. The maximum error takes no account of the probability that some errors

TABLE III. CONTRIBUTION OF INDIVIDUAL CROSS-SECTION ERRORS TO OVERALL REACTIVITY ERROR

Cross-section		Accuracy specified (%)	Resulting error	
			Critical enrichment (%)	Reactivity
^{239}Pu σ_f (α-constant)	0.1 - 100 keV	± 3	1.03	0.56
^{238}U σ_c	0.1- 10 keV	± 5	0.4	0.22
^{238}U σ_c	10 - 100 keV	± 3	0.48	0.26
^{239}Pu σ_c	0.1- 10 keV	± 5	0.18	0.10
^{239}Pu σ_c	10 - 100 keV	± 10	0.24	0.13
^{240}Pu σ_c	0.1 - 10 keV	± 5	0.2	0.11
^{241}Pu σ_f	0.1 - 100 keV	± 5	0.36	0.19
Maximum error			2.89	1.57
Square root of sum of squares			1.3	0.7

will cancel, whilst the standard deviation takes no account of the correlation of errors.

The approach originally adopted in the U.K. study was to limit the uncertainty contributed by any cross-section in any of the five energy groups used to 0.1% in reactivity. When one allows for the fact that the number of constituents times cross-sections times groups was of the order of 100, an r.m.s. error of 1% in reactivity is obtained. The accuracy requirement for ^{239}Pu σ_f in the range 0.1 → 100 keV would give an uncertainty in reactivity of 0.22%. This is equivalent to an average requirement of ± 0.9% on σ_f for the full range to 100 keV and we have chosen to make this ± 0.5% above 40 keV relaxing to ± 3% at 1 keV, corresponding with the decrease in flux per unit lethargy. An alternative approach is to let each of the dominant macroscopic cross-sections in the core and blanket $\bar{\nu}$, Σ_f, Σ_c, χ (fission spectrum), Σ_{in}, $\Sigma_{el,tr}$ (elastic transport) and $\Sigma_{el\,mod}$ (elastic moderation) each contribute about $\frac{1}{3}$% in reactivity. Elastic transport and elastic moderation are considered separately because they arise predominantly from different elements. Dominant cross-sections, such as ^{239}Pu fission, are limited to making a contribution of about 0.33%, or a little more, and a contribution of about 0.22% from ^{239}Pu σ_f, from energies below 100 keV is therefore also consistent with this approach.

The accuracies thus deduced for the individual cross-sections were then incorporated in the overall U.K. data request list, which in turn forms part of the E.A.N.D.C. "Compilation of E.A.N.D.C. Requests" [5].

4. DISCUSSION

I do not wish to review in any detail the particular requests that have emerged from this procedure, but I would like to draw attention to one or two key cross-sections. It is obvious that $\bar{\nu}$ and σ_f play a dominant part in determining many of the reactor characteristics and that errors in these cross-sections will swamp much larger errors in the other nuclear data used in fast reactor calculations. In particular it appears that to achieve our objectives we shall need to know the fission cross-sections to about $\frac{1}{2}$% over a wide energy range and it is disappointing to the reactor physicists that differences between different laboratory measurements are still measured in tens of per cent rather than tenths of per cent. One of the most abundant materials in large fast reactors is ^{238}U and its cross-sections also are therefore important. In this instance the inelastic scattering cross-sections play a large part in determining the neutron spectrum in the reactor. During the last few years new measurements have greatly improved our knowledge of these cross-sections but again increased accuracy would be desirable. Another cross-section of particular importance which, together with the cross-sections of other plutonium isotopes, plays a large part in determining the breeding gain is the capture cross-section of ^{239}Pu, and there is still much uncertainty in this cross-section in the range 100 eV to 15 keV.

It is worth noting that the requests for accurate data are not likely to go on increasing in stringency as the years roll by. Even if good reason were found for trying to increase the accuracies of calculation of reactor physics parameters such as critical enrichment beyond those suggested earlier as targets, a limit to the accuracy achievable would

be set by our knowledge of the actual composition of any real reactor. After carrying out survey calculations with four or five figure accuracy it is always a salutory experience to attempt to assemble the input data for a calculation on an actual reactor. Specifications for the fuel and structural materials allow for considerable variations in chemical composition and density, and dimensional tolerances of fuel elements and structure are often large and the isotopic composition of the fuel will be variable and will probably only have been carried out in a limited number of samples.

When difficulties of determining the actual geometry of the structure have been included (and it is an almost universal experience that for some reason or another the actual structure is not identical with the drawings) the error becomes even larger. The actual composition (usually specified as atoms per cubic centimetre) is therefore uncertain, to at least 0.1%, and possibly 1%. Even if all the complex geometrical and heterogeneity problems could be completely calculated (which they cannot) there is no point in asking for measurements of the cross-section of any element to much greater precision than that with which the number of atoms present can be determined. At present this limit is just about being reached in the case of the cross-sections for the fissile materials. Thus even if the error in the cross-sections of these materials could be reduced to zero the error resulting from the determination of their concentration in the reactor would swamp the error from the cross-sections of many materials of low importance, and therefore these cross-sections will never be needed to accuracies better than 10% or so.

We believe that the accuracies asked for in the present data request list represent the best guide that can at present be given to those who measure nuclear data. In particular it is valuable in showing the rough relative importance of the various cross-sections involved. We do not believe it is possible to specify data requirements rigorously, since the errors in the various data interact in such a complex manner. Some refinement of the requests could be achieved by considering only a particular reactor design, but this was thought to be an unnecessary restriction at present.

In summary, therefore, there is a limit of accuracy desirable in nuclear cross-section measurements. This limit has not yet been reached by the nuclear data measurers for many important cross-sections, but it is not far beyond the accuracy attainable using present-day methods. Whether in the long run it will be an economic proposition to measure the microscopic data directly or whether some form of data adjustment from integral measurements will provide the necessary reactor calculational accuracy, remains to be seen.

REFERENCES

[1] GREEBLER, P., private communication.

[2] CECCHINI, G., FARINELLI, U., GONDINI, A., SALVATORES, M., Proc. 3rd UN Int. Conf. PUAE 2 (1965) 388.

[3] MOORHEAD, T.P., Physics of Fast and Intermediate Reactors II, IAEA, Vienna (1962) 111.

[4] GREEBLER, P., HUTCHINS, B.A., "User requirements for cross-sections in the energy range from 100 eV to 100 keV", Conf. on Neutron Cross-section Technology, Washington, 22-24 March 1966.

[5] Compilation of E.A.N.D.C. Requests, EANDC 55 "U". O.E.C.D. European Nuclear Energy Agency (March 1966).

DISCUSSION

(on papers CN-23/117 and CN-23/52)

N. STARFELT: Reactivity coefficients and breeding ratios have been discussed in detail in the papers just presented, but the cross-sections needed for calculation of radiation damage have not been mentioned. For instance, (n, p) and (n, α) reactions in construction materials like steel lead to the production of hydrogen and helium, which may influence the strength of the material and thus the reactor economy. These cross-sections are often not known with good accuracy. Are problems of this kind not considered to be of importance?

R. D. SMITH: Data on (n, p) and (n, α) reactions are indeed needed for the understanding of problems of neutron damage. Similar data are also needed for all structural materials for calculations of reactivity, breeding gain and temperature coefficients. The accuracy required for metallurgical calculations is usually lower than that required for other purposes.

R. VIDAL: I should like to address my question to the authors of both papers. How far is uncertainty, as regards the reactivity, due to errors in the nuclear constants and how far is it due to imperfect methods of calculation? Also, in the same connection, should our efforts be concentrated mainly on differential measurements or on integral measurements (critical and exponential experiments, oscillation or activation measurements)?

G. H. KINCHIN: My presentation assumed that the errors due to methods of calculation are small compared with those due to nuclear data, and I believe this to be true for thermal reactors. Integral measurements can, however, be very valuable, for example integral measurements of epithermal capture-to-fission ratio have been useful in resolving apparent discrepancies in the microscopic data.

R. D. SMITH: At present, errors due to methods of calculating the reactivity of fast reactors are much lower than errors due to data. This is likely to remain true for simple geometrical systems even when the data errors have been greatly reduced compared with their present level. In an actual power reactor the complex geometrical shapes introduce further difficulties in calculation but, at present, data errors are still predominant for nearly all situations.

D. GOLDMAN: How accurate are the present reactivity calculations with the inexact cross-sections available?

G. H. KINCHIN: The answer for thermal reactors must depend on whether data from integral experiments are included. If this information is included (and it is difficult to eliminate), I should think, say ± 0.5% for natural uranium reactors and ± $1\frac{1}{2}$% or ± 2% for enriched reactors.

R. D. SMITH: My estimate would be that the reactivities of those systems which lie within the range of types that have been measured on zero-power reactors can probably be calculated to better than 1% by what are essentially interpolation methods. For systems which have not been measured directly, including systems containing large proportions of the higher isotopes of plutonium or fission products, the reactivity cannot be calculated to better than 5%.

J. CHERNICK: Is not accuracy to 1% also likely to be unobtainable with the complicated, fast-reactor assemblies, such as those with complete loss of sodium, or pancake power reactors of the modular type?

R. D. SMITH: Calculations for assemblies without sodium can be made to a similar accuracy as for those with sodium. The sodium void coefficient, which depends on the difference in the reactivity of the two systems, cannot yet be calculated with acceptable accuracy. Modular systems, or systems with very low 1/d ratios (0.1 or less), fall into the category of systems that have not been extensively studied on zero-power assemblies and may give rise to inaccuracies in reactivity calculations.

BASIC NUCLEAR DATA FOR FAST REACTOR CALCULATIONS

M. SEGEV, S. YIFTAH AND L. GITTER
ISRAEL ATOMIC ENERGY COMMISSION,
SOREQ NUCLEAR RESEARCH CENTRE,
YAVNE, ISRAEL

Abstract

BASIC NUCLEAR DATA FOR FAST REACTOR CALCULATIONS. Despite the concerted efforts over the last twenty years to refine the experimental nuclear data used in reactor calculations, uncertainties still exist and presumably will continue to exist for some time to come. A fast reactor physicist thus finds that the basic nuclear data which he requires for his calculations must be obtained in part from theoretical considerations, systematics and sometimes crude "guesstimates".

Three aspects of this problem are discussed: (1) The criticality factor, and the coolant loss and Doppler effects are examined. Given a certain specified accuracy needed in the calculated values of these reactor quantities, what is the corresponding required accuracy in the basic nuclear data used as input? The answer is obtained by using a group-diffusion code to get the corresponding accuracies in group parameters. The latter are interpreted in terms of accuracies in basic nuclear data. (2) The required and available accuracies are compared, and it is found that both average cross-sections and resonance parameters for a PuO_2-UO_2 core are insufficiently known. (3) What are the nuclear parameters introduced into the fast reactor equations and how are these parameters obtained from the nuclear physicist's data? Due to a persistent theoretical difficulty in describing neutron energy spectra in various reactor mixtures, other quantities besides cross-sections should be considered as basic and accordingly measured.

CROSS-SECTION REQUIREMENTS FOR NEUTRON SHIELDING

H. GOLDSTEIN
COLUMBIA UNIVERSITY,
NEW YORK, NEW YORK,
UNITED STATES OF AMERICA

Abstract

CROSS-SECTION REQUIREMENTS FOR NEUTRON SHIELDING. The role that microscopic neutron cross-sections play in reactor shielding is in several respects similar to their role in core physics. The need for such cross-sections arises in both situations primarily in detailed calculations starting from first principles. With shields as with reactors, a large body of input cross-section data is needed to arrive at relatively few parameters, e. g., for shielding, fast neutron dose, secondary gamma-ray dose, heating density, albedo etc. The effect of changes in the cross-section data therefore becomes difficult to isolate.

The differences in cross-section needs between reactors and shields are however often more striking, appearing in the energy regions of interest, the types of cross-sections involved and the varieties of materials dealt with. In many instances of deep penetration, especially for hydrogenous shields, the high-energy behaviour of the neutron interactions is the dominating property, focussing interest on the region above 6 MeV to as high as 14 MeV, where, at present, the greatest technical difficulties in measurement exist. When hydrogen is present in a shield in significant proportions the most significant cross-sections are the total and the elastic, especially the shape of the scattered angular distribution. In heavy-element shields the details of the inelastic scattering become highly significant. With all shields the values of the cross-sections resulting in secondary gamma production, and the spectrum of such gamma rays, are of great interest. These details of the epithermal radiative capture process become important in high-efficiency shields. Finally the common core materials are rarely of great concern for shielding (although those in the reflector often are). The most frequent shield materials typically involve light elements such as H, C, N, O through Si and Ca, the structural elements such as Fe and Ni and (rarely) the heavier elements such as Pb. Occasionally more exotic nuclei such as Li or Nb occur. Detailed illustrations of these aspects of shielding needs for microscopic neutron data are given.

I INTRODUCTION

From the earliest days of the development of nuclear energy, shielders have considered as their goal the calculation of deep penetration of radiation from first principles using microscopic cross-sections of the interactions with the shield materials. For awhile the goal seemed to be receding rapidly as more was learned of the complexity of the cross-section behavior and of the difficulty of carrying out rigorous transport calculations. As with reactors, recourse was therefore necessary to approximate models with "cross-sections" determined empirically or "adjusted" to make the model fit integral experiments. The ability to perform useful and rigorous penetration calculations was, for various reasons, achieved first for gamma rays. In recent years, it has become clear that even for neutrons the original goal is, if not here already, at least well

within sight. One reason for the improvement is our growing knowledge of the numerical mathematics involved in solving the rigorous linear Boltzmann transport equation. The theoretician now has available a sizable collection of sophisticated techniques for calculation of radiation penetration, of which Monte Carlo and anisotropic S_n lead the list. They can be applied to reasonably complicated geometries (this is particularly true of Monte Carlo) and their problems and pitfalls have by now been learned — usually the hard way. Another reason, of course, is the rapid development of computer facilities, both hardware and software, so that one can talk of actually performing these lengthy and sophisticated calculations. Extensive, accurate calculations of realistic shields are in principle feasible with computers now coming on the line. They will unquestionably be practical with the next generation of computers — if the necessary microscopic cross-sections are available to the requisite accuracy.

What quantities do we seek to calculate? One can imagine wanting to know a great deal of detail, of course, about what goes on inside and outside a shield. But in practice a relatively small amount of information suffices. First of all there is the biological dose from neutrons and photons at various points outside and inside the shield, or along and inside ducts. A secondary need, but by no means unimportant, may be for energy deposition relating to heating or radiation damage in certain parts of the shield. Time dependence enters in a crude way, when one distinguishes between what happens when the primary radiation source, e.g. a reactor, is in operation or at various times after shutdown. The overall shielding problem may be broken down into several component parts, and there is then need for intermediate information, such as thermal and epithermal collision densities to find sources of secondary radiation, or details of the angular distribution of shield exit fluxes as they affect the subsequent air or structure scattering. But even with these complications the volume of numbers desired as output from the calculations is often quite small compared to the volume of cross-section data required as input. As a result of this imbalance between size of input and output, and because of the complicated calculations that go in between, it is very difficult to say in what manner and to what extent the result of the calculation depends upon some particular input cross-section. Far too little has yet been

done by way of cross-section "sensitivity" calculations in shielding. Much of what can now be said, particularly on accuracy requirements, must therefore be fuzzy and based on plausibility arguments.

We can use a rough mathematical analogy in discussing shielding involvement in cross-sections. We can speak of a neutron "cross-section interest" function for shielding which exists over a multidimensional domain (the 'region of interest') described by some such set of coordinates as follows:

1. element or nucleus
2. incident neutron energy
3. cross-section type
4. spread of incident energy (resolution)
5. accuracy of the cross-section

Perhaps there should be an additional coordinate characteristic of the particular shielding application, for the region of interest will shift a good deal depending upon whether it's a ground-based power-reactor shield, or shielding for a reactor in a space vehicle. But all we can hope to do here, in order to avoid time consuming detail, is to consider a sort of range of average or typical shielding situations and describe the corresponding region of interest in the space of the other coordinates, i.e. give the ranges of the variables where shielding interest is high.

Most of the previous discussion in outline applies equally well to shielding or reactor applications. But from now on we shall see that the specifications of the region of interest for shielding are often markedly different from those for considerations of the core.

II VARIABLES DEFINING CROSS-SECTION REQUIREMENTS

1. Materials or Nuclei

First on the list for most shielding applications are the very light elements including almost everything from hydrogen through oxygen. For example, lithium is a fascinating element for the shielder. In its own right it is a moderately good neutron moderator by elastic scattering. For fast neutrons there is an additional important moderation through nonelastic processes. And it has a high thermal cross-section for absorption by a mechanism which does not produce any secondary gamma rays. The combination of Li with H, as LiH, therefore makes

one of the best neutron shielding materials known. It is far too expensive, of course, for most situations, but there are applications, in the laboratory and for the space effort, where cost is not the overruling factor. For these we need to know more about Li cross-sections. At the other economic extreme is oxygen, an almost ubiquitous component of shielding materials. For the scattering and penetration in air of neutrons from reactors and other sources the properties of oxygen and nitrogen are all important. These light nuclei are of course in the region of the periodic table where theory is most difficult to apply — too complicated for direct many-nucleon calculations, but having too few nucleons for continuous or statistical models such as the optical model. It is true that the optical model has been used with surprising success in recent years even for nuclei as light as carbon, but the applications have been of an ad-hoc nature, essentially interpolating experimental data, rather than based on fundamental considerations. So, in the last analysis experimental measurement is the primary need with these nuclei.

Above oxygen the nuclei of general interest are usually well separated. There is Na — common coolant in fast reactors. Silicon and calcium show up as constituents of concretes. The common structural materials, particularly iron and the elements which alloy with it, form a cluster of great interest. Iron is far from the best gamma ray shielding material one can think of, but it has the great virtue of relative low cost, so it often appears in shields primarily in that role. Past iron and neighboring materials shielding interest drops markedly in general. For some applications such "exotic" materials as Zr, Nb or W sometimes are mentioned, and of course Pb appears fairly frequently, but that's all. The fissionable and fissile elements, so all important for the core, practically do not figure at all for shielding except as they affect the source. Depleted uranium has some obvious advantages as a gamma-ray shield, but it is too expensive normally to warrant consideration.

It must be emphasized that we have only described here the usual or general range of interest. Particular applications may have burning interest in nuclei not mentioned. For example, potassium is a possible coolant in space reactors. Again, for measurement of shields, fast neutron activation reactions are often used, bringing in a new set of cross-sections.

2. Incident Neutron Energy

Here too the contrast with reactor concerns is marked. Thermal and epithermal cross-sections are of interest principally for radiative capture, producing secondary gamma rays. But most of the cross-sections here are well enough known for shielding purposes (but this is not always true for the spectra of the resultant gamma rays). The energies of interest for fast neutron penetration and slowing down are quite high, in the MeV range. For example, when hydrogen is present in a shield, a 1-MeV neutron has a very much smaller chance of penetrating deeply than a 10-MeV neutron. Numerous studies (1) have shown that with a fission source the penetrating neutrons through a thick H_2O or LiH shield start out from the source in the 6-10 MeV region. Even in shields where moderation is chiefly by inelastic scattering, the dominant energy is also often quite high, although cross-section "windows" occasionally spotlight regions in the low MeV or even keV range. It hardly needs underlining here that 6-10 MeV is just the region where existing monoenergetic sources peter out. For most fast reactors, measurements up to 2.5 MeV cover a large portion of the region of interest. For shielding they do not begin to tell the story.

3. Type of Cross-Section

Probably the single most important cross-section — although often overlooked — is the total cross-section. A large fraction of all collisions greatly reduces the chance of a neutron penetrating much further in the shield, hence the total cross-section remains the strongest factor determining the overall relaxation length. Often we assume the total cross-section is well known. But surprisingly large discrepancies show up in many nuclei of interest. Thus most of the nitrogen data are quite old, going back to the 1950's. Recent measurements of Glasgow et al. at Battelle-Northwest show large qualitative differences in the 5-6 MeV range. Semi-integral measurements of neutron penetration in liquid nitrogen at ORNL by C. E. Clifford and collaborators (2) tend to confirm Glasgow's data (see Fig. 1). They point out that this is undoubtedly the largest uncertainty in calculating neutron penetration in air. Again, although Be has been measured frequently in recent years, its fast total cross-section is still uncertain to about 10%, especially in the interesting regions of low cross-sections. It should be remembered that the total cross-section in effect appears in the exponent,

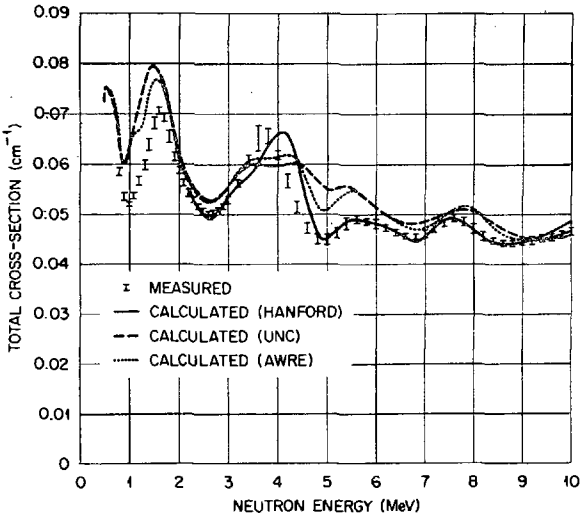

FIG.1. Macroscopic total cross-section of nitrogen, smoothed with a resolution function approximately 20%-15% full width at half maximum. (Clifford and Straker, ORNL)

so that deep in a thick shield even a small uncertainty becomes greatly magnified.

After the total cross-section, the next most sensitive cross-section is the angular distribution of elastically scattered neutrons. Rarely is this known well enough to satisfy shielding requirements. The various sets of oxygen data used in shielding calculations differ mainly in the shape of the assumed angular distribution, and at 120 cm in water with a fission source, this uncertainty alone probably accounts for a factor of two spread in the fast dose. It is not at all clear what features of the angular distribution are of interest, or how to characterize them. Numerous failures have shown that the assumption of linear anisotropy, i.e. P_1 approximation to the scattering kernel, is completely inadequate. But there is some recent evidence that a Legendre polynomial expansion through P_3 or P_4 may be sufficient. Thus Shure (3) has had remarkable success with a P_3 code in shielding calculations, and Norwood et al. (4) have found in S_n calculations for LiH that P_3 is almost as good as P_9. Tentatively we can say therefore that structure in the angular distribution wiggling faster than $\cos^4\theta$ is not terribly interesting. But a lot more work must be done before we are on firm ground here.

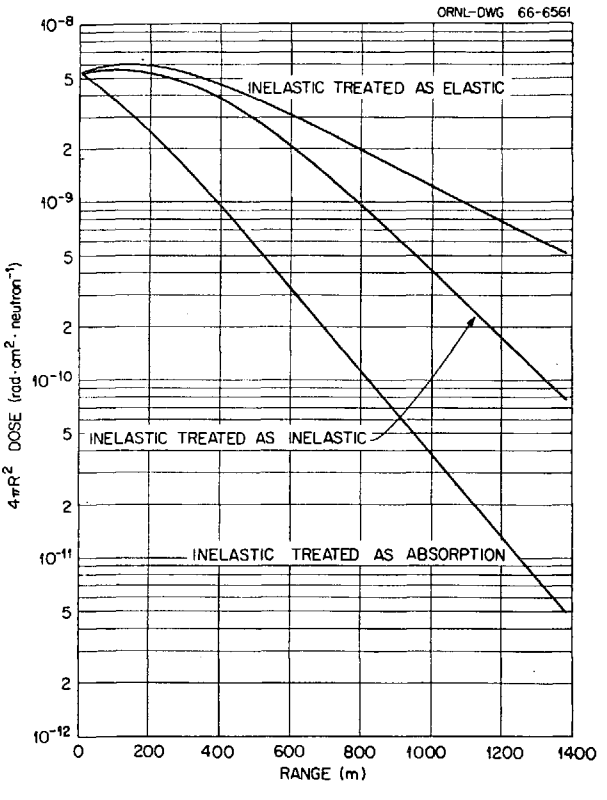

FIG.2. Calculations of first-collision dose in air from a 14-MeV source under various cross-section assumptions. (Straker, ORNL)

In certain cases inelastic scattering cross-sections can be as important or more so than elastic scattering. Thus in thick layers of iron elastic scattering does little to the neutrons except have them bounce around a bit; the primary slowing down process is inelastic scattering. Shure (3) has shown that a 10% change in the inelastic scattering in an Fe shield had a marked effect on the relaxation length of the neutrons emerging into a subsequent water shield, amounting to a 50% change after 40 cm of water. Again for a 14-MeV neutron source in air, Straker (5) has shown that treating the inelastic scattering as elastic increased the asymptotic dose relaxation length by 80%, while treating it as absorption decreased the same length by 60% (see Fig. 2). These are, however, extreme situations. On the other hand, in hydrogenous shields inelastically scattered neutrons usually have too little energy to penetrate much further, so that the slope of the dose curve is relatively insensitive to assumptions

about the inelastic spectrum. In a LiH shield for example, the magnitude of the fast nonelastic processes is important; the energy and angle spectrum of the resulting neutrons is much less so.

One class of cross-sections unique to shielding requirements is that involving secondary gamma production. In many shields the emergent gamma dose is not from primary source photons, but mainly from secondary gammas resulting from neutron interactions in the shield. Usually radiative capture is the culprit. In the past it has been often assumed that the photon spectrum for thermal capture could be used for all energies of interest. It now seems that this is not always the case, and so there are instances where not only is the radiative capture cross-section needed at epithermal energies, but also the energy and possibly angular distribution of the hard gamma rays as a function of incident neutron energy.

Inelastic scattering is another possible source of gamma rays. But these are almost always softer than the capture spectrum and obviously have a lower multiplicity. With the present generation of power reactors they are not a very large fraction of the secondary gamma dose. But one can think of possible cases where this source becomes important, e.g. a fast reactor with a highly poisoned shield (so thermal absorption is non-radiative) and close-in location of the heavy gamma ray shielding material. On the whole however, gamma-ray production by inelastic scattering is given lower priority than in past years.

4. Spread of Incident Energy

We know very little yet about how much detail of the cross-section structure has to be included in the calculations. The presumption is that the resolution does not have to be as fine, in terms of the resonance structure, as for reactor calculations. But one point can be made emphatically. Where the cross-section shows considerable structure, as for O and N in the MeV region, poor resolution is preferable to good resolution if the energy points are widely spaced. 50 keV resolution with points 1 MeV apart (as has been done) is of less use than 500-keV resolution with the same spacing.

5. Cross-Section Accuracy

The little that can be said here has already been discussed in connection with cross-section types, for these two "coordinates"

are really not independent in their effect on the "interest" function. Before any honest specifications can be written for the desired accuracy much more work must be done on 'sensitivity' calculations. It would be highly desirable to develop perturbation techniques for this purpose similar to those recently introduced by our reactor colleagues. But one general point can be reiterated. The highest accuracy will be needed for cross-sections which effect the slope of the spatial variation, i.e. the relaxation length, because here the uncertainty in the resulting dose becomes magnified after several mean free paths. This class usually includes among others the total cross-section and the differential elastic cross-section. It does not seem unjustifiable to ask for 2% accuracy in the total cross-section in some cases, especially in broad valleys in the curve. On the other hand less accuracy is needed for cross-sections which affect only the local density of scattered neutrons or the source strength of secondary photons. The uncertainty resulting here does not grow with increasing shield thickness. Thus, generally speaking, we can relax considerably our accuracy requirements when it comes to the spectrum of neutrons or photons emerging from inelastic scattering.

III CONCLUSION

In the past reactor needs for cross-sections have claimed the lion's share of attention among the cross-section measurers. That's as it should and undoubtedly will continue to be. But we hope that the cross-section experimenters working with fast neutrons will give a thought to shielding needs when they seek new worlds to conquer with their tandems, variable-energy cyclotrons and linear accelerators. Given a monoenergetic neutron source the cross-sections desired for shielding are almost all well within the range of modern measuring techniques. The demands for neither detail nor accuracy are excessive. The major problem, of course, is that monoenergetic sources are increasingly difficult to come by as the energy rises, especially in the 6 to 12 MeV region. If one is forced to use sources that are not monoenergetic then many of the measurements are good tests of the experimenters' skill and ingenuity. Difficult techniques, such as double time-of-flight, may have to be mastered.

A broad survey such as this cannot hope to justify in detail the expenditure of time and effort that may be required by some specific difficult measurement. But the experimenter, perhaps wavering on the brink of plunging into a long and tricky measurement, can be provided

by the shielding community with a detailed discussion of the reasons behind the request for any specific cross-section of high "interest". You have only to call on us.

REFERENCES

1. Goldstein, H., "Fundamental Aspects of Reactor Shielding", Adderson-Wesley, Reading 1959, Sect. 6-6.

2. Clifford, C. E., Private communication, Sept. 1966.

3. Shure, K., Nucl. Sci. and Eng. 19, 310 (1964).

4. Norwood, J. M., et al., "Investigation of Analytical Methods, Solution Sensitivity, and Structural Scattering in Neutron Transport", AFWL-TR-65-209, March 1966.

5. Straker, E. A., "Calculations of the Transport of Neutrons from Fission and 14-MeV Point Sources in an Infinite Medium of Air", ORNL-TM-1547, Aug. 1966.

DISCUSSION

D. BOGART: Is it a feasible proposition to embark on calculations for heterogeneous shields of "expensive" materials such as W and LiH with the cross-section data and calculational techniques at present available? What we are interested in getting is shields of minimum weight for specified doses.

H. GOLDSTEIN: The cross-section values available are not entirely adequate, but they are now sufficiently complete to give reasonable first approximations of the attenuation if modern, sophisticated computation techniques are used.

A. B. SMITH: Taking the case of a 1000-MW fast reactor, what sum in dollars would be saved through improving the accuracy at shielding cross-sections by a factor of two?

H. GOLDSTEIN: It is very difficult to give a specific answer to such a question without considering the given reactor design in detail; moreover, there are other types of reactor applications where the economic advantage is much more evident. As a general answer, there is evidence that improving the cross-section accuracy by a factor of 2 would bring a worthwhile benefit amounting to several million dollars in the course of a decade.

CHAIRMAN'S SUMMARY

P. W. MUMMERY: We have heard, in Session I, of the factors governing reactor needs for nuclear data. In particular, we have heard of

the uncertainties in nuclear data which can be accepted, with allowance for the flexibility of reactor designs in accommodating them. This provides an essential background to the sessions which follow. I hope that you will allow me a few personal and perhaps provocative comments on these issues.

As one speaker said, the torch of high-precision measurement is passing from the thermal-reactor objectives to the fast-reactor objectives. There is a challenge here which I am sure will be accepted, but we must not forget that the torch will not burn for ever, even for fast reactors; this must be clear when we consider that the participants in this Conference are probably spending between 5 and 10 million dollars a year on nuclear data collection. I would suggest that against this background it is important to decide which nuclear data should receive priority, and it seems to me that the choice should fall on data relevant to the computation of reactor situations which cannot easily be simulated in integral experiments and data for the systematic interpretation of integral experiments.

I believe that the requirements for thermal reactors are well on the way to being met and that the next few years will determine the appropriat balance for meeting the fast-reactor and shielding requirements by a combination of differential and integral measurements. There is certainly still much to be done, as the remaining sessions will clearly show.

Session II

CROSS-SECTIONS AND RESONANCE PARAMETERS OF NON-FISSILE NUCLIDES IN THE RESONANCE ENERGY REGION

NEUTRON CROSS-SECTIONS OF Pr, Yb, Lu, Er, Ho AND Tm

R. L. ZIMMERMAN, L. Q. AMARAL, R. FULFARO,
M. C. MATTOS, M. ABREU AND R. STASIULEVICIUS
NUCLEAR PHYSICS DIVISION,
INSTITUTO DE ENERGIA ATOMICA,
SAO PAULO, BRAZIL

Abstract

NEUTRON CROSS-SECTIONS OF Pr, Yb, Lu, Er, Ho AND Tm. The total neutron cross-sections of praseodymium, ytterbium, lutetium, erbium, holmium, and thulium have been measured by transmission within the neutron energy range 0.001 to 1.0 eV, with special attention given to obtaining values at the thermal energy 0.025 eV. A crystal spectrometer coupled with a mechanical monochromator, and a slow chopper, were used at the swimming-pool research reactor of the Instituto de Energia Atômica. Powder samples of the oxides were supplied in high purity, with particular care to eliminate contamination by the rare earths of high neutron cross-section. The data were analysed to determine the nuclear absorption and the nuclear scattering cross-sections. Effects of nuclear resonances and of the atomic paramagnetic scattering were properly considered. In the case of lutetium, the parameters of the first resonance are presented.

INTRODUCTION

The interpretation of the total interaction between slow neutrons and rare earth atoms involves both the high density of nuclear resonances and the magnetic forces between the neutrons and unpaired orbital electrons. Previous measurements of rare earth neutron cross-sections have often not been over a neutron energy range appropriate for the analysis of these interactions. Consequently, current nuclear data tables often contain nuclear partial cross-sections based on too limited experimental data or on an incomplete analysis of the experimental data.

This work describes an effort to measure and to analyse the total cross-sections of Pr, Yb, Lu, Er, Ho and Tm over an appropriate energy interval (0.001 to 1 eV) such that it is possible to determine the various nuclear interactions and the paramagnetic interaction owing to their different energy dependences. Some of the results in this work have been published previously [1-3].

Powder samples of the oxides were supplied in high purity, with particular care to eliminate contamination by the rare earths of high neutron cross-section. A crystal spectrometer coupled with a mechanical velocity monochromator that eliminates order contamination [4, 5] was used for most measurements; part of the lutetium results were obtained with a slow chopper time-of-flight equipment [6].

THULIUM

Thulium is a typical example of the means of analysing the experimental data and Fig. 1 shows its total cross-section versus energy. The

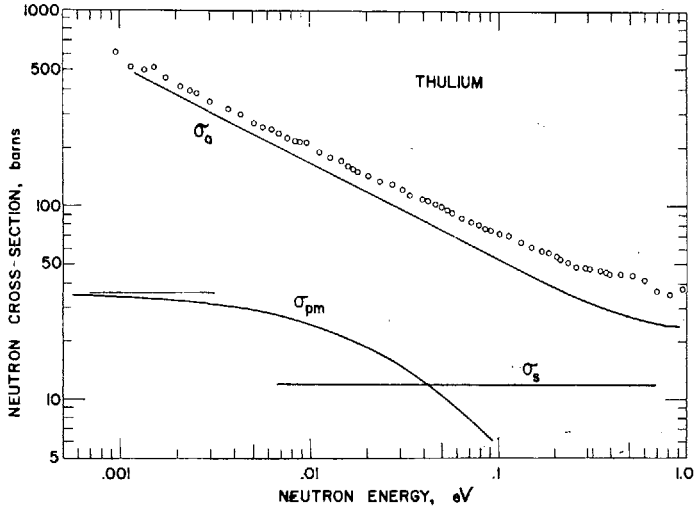

FIG.1. Total cross-section of thulium. The observed data shown as open circles were analysed as a sum of the nuclear absorption, paramagnetic scattering and nuclear scattering; σ_a, σ_{pm}, σ_s, respectively, shown by the solid curves. The functional form σ_{pm} is shown for reference only and, except for the asymptotic value shown here at 35.4 b, is not used to determine the nuclear partial cross-sections.

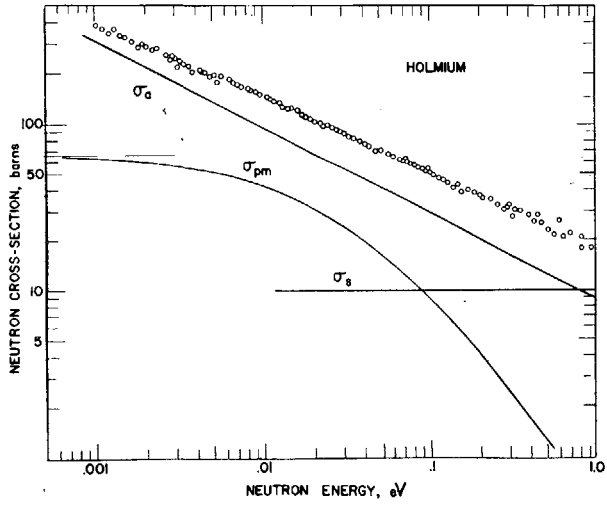

FIG.2 Total cross-section of holmium. The observed data were analysed similarly to those of thulium.

absorption cross-section dominates at very low energy, where it has a 1/v behaviour. Over this region the nuclear scattering cross-section gives a comparatively small contribution of little influence and the asymptotic value of the paramagnetic cross-section is well known, its value 35.4 b being given by the interaction between the magnetic moment of the neutron and the one from the ion of thulium. In this region of energy the absorption cross-section was determined and afterwards extrapolated to higher energies, taking into account the deviation from 1/v

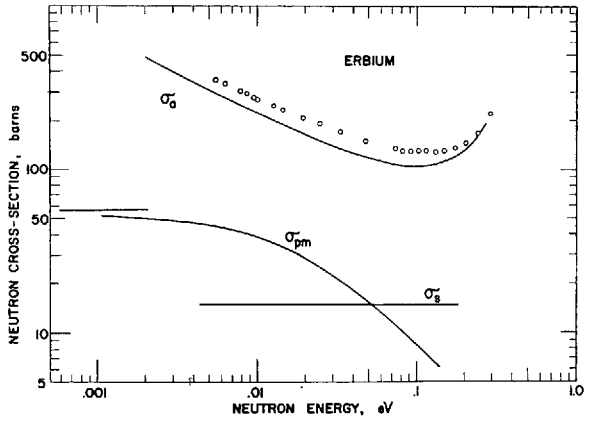

FIG.3. Total cross-section of praseodymium

due to the first resonance at 3.92 eV. At the thermal energy 0.025 eV the total cross-section has the value 134 ± 2 b and we determined the absorption cross-section as 106 ± 3 b.

The contribution of all known resonances was calculated using the published [7] resonance parameter values that have a certain experimental error. This contribution is 73 ± 10 b. So there are still 33 ± 10 b that are attributed to bound states, or energy levels below the binding energy of the neutron.

The curve of absorption cross-section that appears in this figure is composed of the contribution of both positive resonances and bound states, the latter giving a small deviation from 1/v for higher energies, depending on the parameters assumed for the bound state.

The value and the limits of variation of the scattering cross-section necessary to explain the observed values near 1 eV, where the influence of the paramagnetic cross-section is known to be negligible, was determined analysing the uncertainties of these two contributions (bound and virtual states). A value of 12 ± 2 b was found for the nuclear scattering cross-section taken as constant over the considered energy range.

The curve of paramagnetic cross-section appearing in the figure was calculated [8] using the paramagnetic form factors calculated with Hartree-Fock wave functions for isolated ions of rare earths tabulated by Blume, Freeman and Watson [9].

HOLMIUM

Figure 2 shows the results obtained for holmium. The analysis of the data has followed the same lines, using the asymptotic paramagnetic cross-section of 65.2 b. At thermal energy an absorption cross-section of 61 ± 3 b was determined, the total cross-section being 98 ± 2 b. The contribution of positive resonances has been calculated and is 23 ± 2 b and so 38 ± 2 b are attributed to contributions from bound states that cause a small deviation from 1/v in the region near 1 eV. The limits of this deviation and its most probable value were calculated to determine

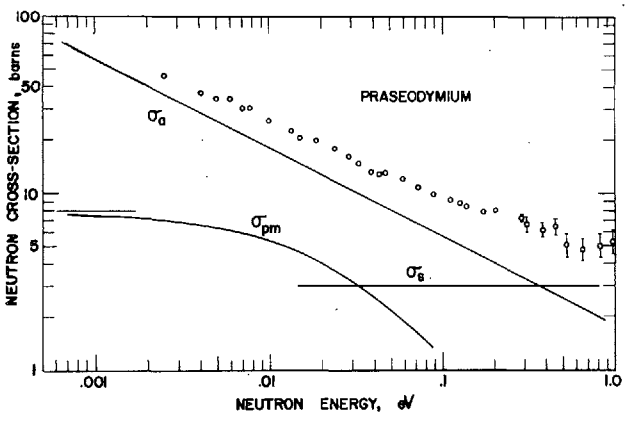

FIG. 4. Total cross-section of erbium

the value and probable error of the scattering cross-section, which is determined in this energy region. A value of 10 ± 2 b for the nuclear scattering cross-section was found.

PRASEODYMIUM

Figure 3 shows the results obtained for praseodymium. The total cross-section at thermal energy is 17.6 ± 0.5 b, and the same line of analysis gave for the thermal absorption the value 11.5 ± 1.0 b using the asymptotic paramagnetic cross-section of 7.8 b. The absorption in this case is probably 1/v because of the large level spacing, although about 10 b of the thermal absorption are due to bound states. Near 1 eV the total cross-section was used to determine the nuclear scattering as 3 ± 1 b.

ERBIUM

Figure 4 shows the total cross-section of erbium. The total cross-section at 0.025 eV is 192 ± 6 b and the absorption value determined at this energy was 150 ± 8 b, using the asymptotic paramagnetic cross-section of 56.2 b. Practically all absorption comes from the first resonances at 0.46 and 0.584 eV. Within the experimental errors of the resonance parameters published, no contribution due to bound states can be detected. A nuclear scattering of 15 ± 5 b was used in our analysis. Because of the absorption being dominant over the whole energy region considered, our data do not well determine the nuclear scattering. Our value is consistent with current tabulations [10] of scattering cross-sections.

YTTERBIUM

Figure 5 shows our ytterbium results. The total cross-section at the thermal energy is 64 ± 2 b and a similar analysis gave a thermal

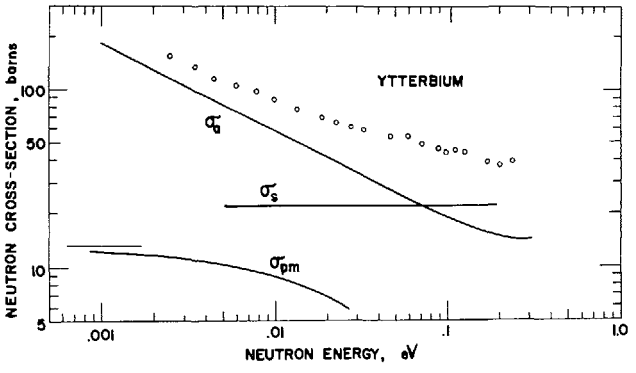

FIG. 5. Total cross-section of ytterbium.

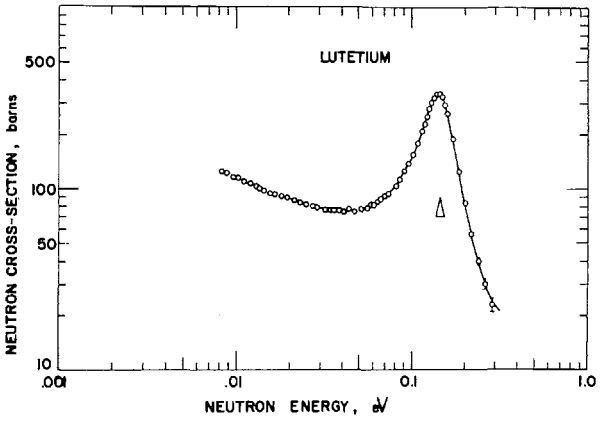

FIG. 6. Total cross-section of lutetium. The experimental points below 0.4 eV were taken with a slow chopper. The rest were taken with a crystal spectrometer as with all the other elements. The solid curve shows the Breit-Wigner fit.

absorption of 37 ± 5 b and a nuclear scattering of 22 ± 5 b, using the asymptotic value of the paramagnetic cross-section 12.3 b. To this thermal absorption, only about 5 b are contributed by the first resonance at 0.597 eV. No other parameters have been published, but the level spacing appears [7] to be large enough so that the rest of the absorption has a 1/v dependence.

LUTETIUM

The experimental results shown in Fig. 6 of the total lutetium cross-section versus neutron energy were obtained with the crystal spectrometer for energies higher than 0.04 eV and with the slow chopper for energies below this value. In this case there is no paramagnetic cross-section, because the magnetic moment of the Lu ion is zero. In the energy

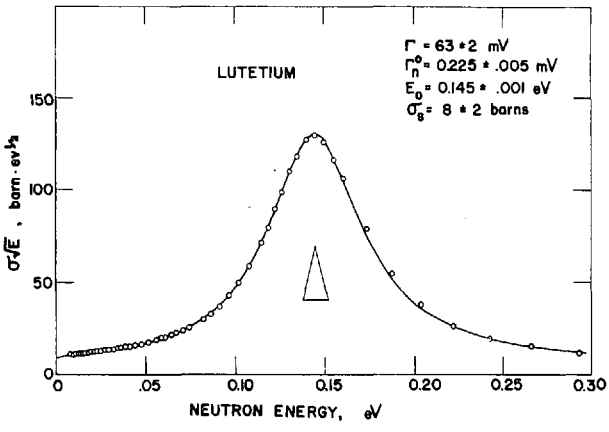

FIG.7. $\sigma\sqrt{E}$ for lutetium. The experimental points and the Breit-Wigner fit are the same as in Fig.6. The triangle shows the resolution of the crystal spectrometer.

TABLE I. THERMAL CROSS-SECTIONS SHOWING THE MEASURED TOTAL CROSS-SECTION AND THE DERIVED PARTIAL NUCLEAR CROSS-SECTIONS OF SCATTERING (σ_s) AND ABSORPTION (σ_a).

	σ_{total} (barns)	$\sigma_{absorption}$	$\sigma_{scattering}$
Pr	17.6 ± 0.5	11.5 ± 1.0	3 ± 1
Yb	64 ± 2	37 ± 5	22 ± 5
Lu	82 ± 3	74 ± 3	8 ± 2
Er	192 ± 6	150 ± 8	(15 ± 5)
Ho	98 ± 2	61 ± 3	10 ± 2
Tm	134 ± 2	106 ± 3	12 ± 2

region measured the isotope ^{176}Lu presents a resonance, due mostly to absorption.

The total cross-section was studied in detail, and the Breit-Wigner parameters were determined by adjusting the theoretical curve to the experimental results. The effect of finite resolution has been taken into account. No corrections were needed for the Doppler effect.

In Fig. 7 a plot of $\sigma\sqrt{E}$ versus the neutron energy with the curve obtained is shown. In this energy region there is predominance of the S-wave interaction, and the usual Breit-Wigner formula can be used for the resonance cross-section. The effect of interference between potential

and resonance scattering is negligible. The potential scattering is considered constant over the considered energy region. The influence of absorption peaks at other energies gives a practically 1/v contribution. Small deviations at the higher energies occur because part of this contribution comes from bound states.

The following resonance parameters have been obtained:

$E_0 = 0.145 \pm 0.001$ eV

$\Gamma_\gamma = 63 \pm 2$ MeV

$\Gamma_n^\circ = 0.225 \pm 0.005$ MeV

From the analysis made it was possible also to separate the absorption and scattering partial cross-sections at thermal energy, the total cross-section being 82 ± 3 b. A value 8 ± 2 b was obtained for the nuclear scattering, and a thermal absorption of 74 ± 3 b was found, out of which about 11 b are contributions of bound states.

CONCLUSION

Table I shows a tabulation of the measured total cross-sections and the derived partial cross-sections at thermal energy for the six elements. The partial cross-sections have greater errors due to uncertainties in the analysis. The nuclear scattering cross-sections listed here are not to be interpreted necessarily as the potential scattering. Interference with resonance scattering may give scattering at thermal energy larger or smaller than the potential scattering by an amount depending on the resonance parameters, which are now insufficiently well known.

ACKNOWLEDGEMENTS

The authors would like to express their gratitude to the many colleagues who helped with the experiments, especially the reactor staff and Dr. Brill, Dr. Alcidio Abrao and Dr. Ludmilla Federghun, who purified and analysed the samples.

REFERENCES

[1] ZIMMERMAN, R. L., MARTINS, O. W., ABREU, M., MATTOS, M. C., Proc. 4th Inter-Am. Symp. on the Peaceful Applications of Nuclear Energy, Mexico (1962); Report IEA 75.

[2] AMARAL, L. Q., ABREU, M., BIANCHINI, F. G., MATTOS, M. C., Utilization of Research Reactors II (Meeting held in Sao Paulo) IAEA, Vienna (1965) 133;Report IEA 86.

[3] FULFARO, R., MATTOS, M. C., STASIULEVICIUS, R., Proc. XVIII Meeting of the Brazilian Society for the Progress of Sciences SBPC (1966); Report IEA 124.

[4] BRENNER, R., ZIMMERMAN, R. L., Utilization of Research Reactors II (Meeting held in Sao Paulo) IAEA, Vienna (1965) 123; Report IEA 76.

[5] BIANCHINI, F. G., ABREU, M., AMARAL, L. Q., MARTINS, O. W., Utilization of Research Reactors II (Meeting held in Sao Paulo) IAEA, Vienna (1965) 107; Report IEA 78.

[6] HERDADE, S. B., AMARAL, L. Q., VINHAS, L. A., RODRIGUES, C., Proc. XVIII Meeting of the Brazilian Society for the Progress of Sciences SBPC (1966).

[7] HUGHES, D. J., SCHWARTZ, R. B., Neutron Cross Sections, Rep. BNL 325, U. S. Government Printing Office (1958).

[8] MATTOS, M. C., Proc. 5th Rare Earth Research Conference, Ames, Iowa, USA (1965).

[9] BLUME, M., FREEMAN, A. J., WATSON, R. E., J. chem. Phys. 37 (1962) 1245.

[10] BACON, G. E., Neutron Diffraction, 2nd ed., Oxford University Press (1962).

TOTAL CROSS-SECTION OF DYSPROSIUM, LUTETIUM AND IRIDIUM FOR NEUTRONS OF ENERGY BETWEEN 0.01 AND 10 eV

J. BRUNNER AND F. WIDDER
FEDERAL INSTITUTE FOR REACTOR RESEARCH,
WÜRENLINGEN, SWITZERLAND

Abstract

TOTAL CROSS-SECTION OF DYSPROSIUM, LUTETIUM AND IRIDIUM FOR NEUTRONS OF ENERGY BETWEEN 0.01 AND 10 eV. The measurements described in this paper have been started in order to improve the basic data for the thermal neutron detector dysprosium and the "neutron thermometer" lutetium. For iridium more accurate cross-sections have been requested for the two resonances around 1 eV which can be used for the measurement of resonance absorption in the 1.06-eV resonance in ^{240}Pu. The total neutron cross-section of dysprosium, lutetium and iridium has been measured in the energy range between 0.01 eV and 10 eV with the EIR mechanical chopper installation at the reactor DIORIT. The resolution obtained is 0.5 μs/m including the time analyser channel width.

For the dysprosium measurements samples of metal and oxide were used, for lutetium the oxide, and for iridium the metal only. The purity of the samples was 99.9%, the main impurities being Ho and Y in the dysprosium samples and Yb and Tm in the lutetium samples, with negligible influence on the accuracy of the measurements. Corrections to the measurements are applied for dead time, oxygen content and time-dependent background. The results are given in the form of curves. For some well-resolved resonances, the resonance parameters which were calculated with the computer programme of Atta and Harvey are indicated. All data accessible in the literature for the energy range considered are collected. A careful discussion of the results is given and best values are proposed.

1. INTRODUCTION

Thermal neutron activation detectors are an important tool in the determination of spatial and spectral variation of neutron fluxes in reactors. Due to their small size and high sensitivity they are particularly well suited in cases where high spatial resolution is required. The accuracy of these measurements depends on the accuracy of the nuclear data of the activation detectors.

Dysprosium has found a widespread application as a detector for the thermal neutron flux since its cross-section obeys nearly the 1/v-law and the resonance integral is small. It is also considered as burnable poison and control rod material. Lutetium is a convenient detector for the determination of the neutron temperature because through the resonance at 0.14 eV in ^{176}Lu the activation of a given lutetium foil becomes strongly temperature dependent. Since iridium contains two isotopes, ^{191}Ir having a resonance at 0.65 eV and ^{193}Ir having a resonance at 1.3 eV, it appears to be an ideal detector for the absorption of neutrons in the ^{240}Pu resonance at 1.06 eV and thus for the resonance escape in this resonance [1]. The measurements described in this paper have been undertaken to improve the basic data for the three detectors mentioned above.

The total neutron cross-section has been measured in the energy range between 0.01 eV and 10 eV with the EIR mechanical chopper installation at the reactor DIORIT. A neutron beam is extracted from the centre

of the reactor. The chopper consists of a K-Monel rotor of 145-mm diameter with 4 straight slits of 1-mm height. The resolution obtained at 18 000 rpm and a flight path of 15 m is 0.5 μs/m including the time analyser channel width. The rotating speed of the chopper can be varied between 1'500 rpm and 18'000 rpm.

2. SAMPLE DESCRIPTION

2.1. Dysprosium

For the measurements of the cross-section of dysprosium, samples of metal and oxide have been used. The purity of the samples was 99.9%, the main impurities being Ho and Y with negligible influence on the accuracy of the measurements. The important characteristics of the samples used are given in Table I. Each sample was only used in an energy range where the transmission did not deviate too much from 0.5.

TABLE I. CHARACTERISTICS OF THE DYSPROSIUM SAMPLES

Sample No.	Sample	Thickness (g/cm^2)	barns/atom
1	oxide	1.987	155.8
2	oxide	0.991	312.5
3	metal plate	0.780	346.0
4	oxide + sulphur	0.217 (0.158)	1426

The oxide powder was pressed into pellets of 1-in. diameter. The pellets were protected on both sides by thin aluminium foils. Similar foils were mounted on empty sample holders in the sample-out measurements to avoid the application of corrections for the protecting foils.

Sample No. 4 in Table I has been prepared from a homogeneous mixture of dysprosium oxide powder and 99.99% pure sulphur powder. This mixture was pressed into a pellet like samples 1 and 2. The additional weight of the sulphur is given in parentheses.

All values listed in Table I have been determined with a precision of 1‰ or better.

2.2. Lutetium

The measurements on lutetium were performed on oxide samples only. The purity of the material was again 99.9%, the main impurities being Yb and Tm with negligible influence on the accuracy of the measurements.

The main characteristics of the lutetium samples are given in Table II. The oxide powder was pressed into pellets similar to the dysprosium samples.

TABLE II. CHARACTERISTICS OF THE LUTETIUM SAMPLES

Sample No.	Sample	Thickness (g/cm^2)	barns/atom
1	oxide	9.82 ± 0.05	33.67
2	oxide	1.244 ± 0.001	265.3
3	oxide	0.967 ± 0.001	341.3

TABLE III. CHARACTERISTICS OF THE IRIDIUM SAMPLES

Sample No.	Sample	Thickness (g/cm^2)	barns /atom
1	metal	10.09	31.65
2	metal	1.120	284.9
3	chloride + sulphur	0.0908 (0.197)	5458
4	chloride + sulphur	0.0355 (0.197)	13970

2.3. Iridium

The measurements on iridium outside the resonances have been made with samples consisting of metal plates with a purity of 99.9%, the main impurities being Pt, Pd and Rh. The Rh content is less than 0.05% and can be neglected even in the energy range around its resonance at 1.26 eV. The other impurities are unimportant.

The samples for the measurements in the resonances have been prepared from a homogeneous mixture of specifically pure $IrCl_3$ with sulphur which was pressed into pellets of 1-in. diameter.

The characteristics of the Ir samples used are given in Table III. The values listed for the thickness have been determined with a precision of 1‰ or better. The additional weight of the sulphur is given in parentheses.

3. ANALYSIS OF THE MEASUREMENTS

For the transformation of the time-of-flight data into cross-sections, standard methods have been applied. The cross-sections of oxygen, chlorine and sulphur contained in the samples are well known and small compared to the cross-sections to be measured. The whole energy range was covered by several runs with different rotating speeds. The time-dependent background was determined by a method similar to that described by Simpson et al. [2], using different absorbers of boron carbide.

The resonance parameters of some well-resolved resonances have been calculated with the AREA and SHAPE programmes of Atta and Harvey [3]. The programmes have been transformed to a full FORTRAN version for a CDC 1604A computer. The resolution function of the time-of-flight installation is approximated by a gaussian distribution.

4. EXPERIMENTAL RESULTS

4.1. Dysprosium

Our results for the total cross-section of dysprosium are represented in the curve of Fig. 1. The energy range where improvements have been obtained extends from 0.01 to 2.5 eV. Below 0.1 eV our curve is considerably lower than the BNL-325 curve. A measurement by Okamoto [11] with a neutron velocity selector is a continuation of our measurements towards lower energies and is apparently in favour of our results. The resonance at 1.71 eV in ^{163}Dy was measured with improved resolution.

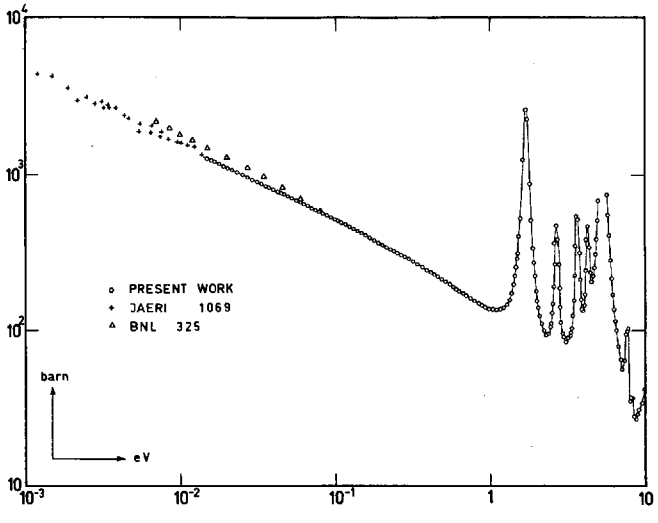

FIG. 1. Total cross-section of dysprosium

Table IV gives all significant cross-section data for the element Dy at 0.0253 eV available in the literature.

Only one measurement of the scattering cross-section by Brockhouse [6] exists for dysprosium with no stated error. The error given in Table IV is taken from BNL-325. Only two of the five values of the absorption cross-section are measured on natural dysprosium, three values being composed from measurements on separated isotopes. The curve for the total cross-section in BNL-325 is evidently too high. The value for σ_{tot} of Okamoto is calculated with a linear function in 1/v given in Ref. [11]. If one compares the cross-section curve in the same reference it seems that this linear function gives too high a value at

TABLE IV. CROSS-SECTION OF DYSPROSIUM AT 0.0253 eV IN BARNS

σ_{tot}	σ_{abs}	σ_{sc}	Method	Ref. Year	
1150			chopper	[4] 1947	BNL 325
	925		pile osc.	[5] 1951	σ Au = 98.7 b
		100 (± 20)	cryst. sp.	[6] 1954	
	953 ± 120		pile osc.	[7] 1958	comp. from sep. isotope values
	936 ± 20		pulsed s.	[8] 1961	
	920 ± 30		cryst. sp. t. o. f.	[9] 1961 [10] 1964	comp. from sep. isotope values
1051 ± 30			vel. sel.	[11] 1964	
	910 ± 120		pile osc.	[12] 1966	comp. from sep. isotope values
1015 ± 5				present work	

TABLE V. RESONANCE PARAMETERS OF A RESONANCE IN ^{163}Dy

E_0 (eV)	σ_0 (b)	$2g\Gamma_n^0$ (MeV)	Γ_γ (MeV)	Ref. Year
1.71		1.13 ± 0.08	103 ± 10	[13] 1957
1.713 ± 0.004	12200 ± 110	1.281 ± 0.005	102.6 ± 0.8	present work

0.0253 eV. Our value for σ_{tot} of 1015 ± 5 b lies within the error limits of Ref. [11] and is not in disagreement with the best values given for σ_{abs} and σ_{sc}.

Our results for the resonance parameters of the 1.71-eV resonance in ^{163}Dy together with an earlier reference is given in Table V.

Data about the experimental conditions of the measurements in Ref. [13] are not available. Our measurements were made with greatly improved accuracy.

4.2. Lutetium

Recently Sokolowski et al. [16] pointed out that there exist meaningful discrepancies in the existing cross-section data of lutetium. Our measurements are a contribution to the improvement of this situation. Figure 2 gives the result of our total cross-section measurement.

Our measurement improves the data in the energy region between 0.01 and 4 eV where good resolution and very good statistical accuracy is achieved.

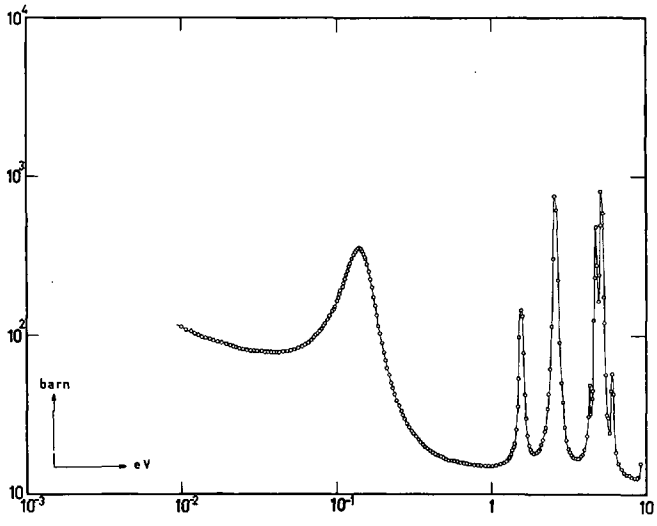

FIG. 2. Total cross-section of lutetium

TABLE VI. CROSS-SECTION OF LUTETIUM AT 0.0253 eV IN BARNS

σ_{tot}	σ_{abs}	Method	Ref. Year	
	108 ± 5	pile osc.	[5] 1951	res. at 0.14 eV not yet known
82.5 ± 5	(77)	chopper	[14] 1960	σ_{pot} = 5.5 b
	89.8 ± 1.1	pile osc.	[16] 1964	g + rs = 1.9886 for ^{176}Lu
82 ± 3	74 ± 3	chopper	[15] 1966	
34.7 ± 0.5		chopper	present work	

Table VI shows all significant cross-section data for the element lutetium at 0.0253 eV.

Sokolowski et al. give too high a value for σ_{abs}, since the contribution from the resonance integral cannot be corrected accurately in this integral measurement [16]. Our result for the total cross-section which improves the accuracy considerably is in agreement with the value of Baston [14] composed from measurements on separated isotopes and with Zimmerman [15] within the error limits.

In Table VII the resonance parameters of two resonances in ^{176}Lu and of one resonance in ^{175}Lu which can be found in the literature are collected together with our results.

The accuracy of the resonance parameters resulting from our analysis is similar or better than that stated in Refs. [17] and [18]. An unsolved

discrepancy exists in Γ_γ of the 2.6-eV resonance where our analysis gives a width considerably larger than indicated by Landon [17].

TABLE VII. RESONANCE PARAMETERS OF RESONANCES IN LUTETIUM

Isotope	E_0 (eV)	σ_0 (b)	$2g\Gamma_n^0$ (MeV)	Γ_γ (MeV)	Ref. Year
176	0.143	13860	0.24	61 ± 2	[17] 1955
	0.142		0.234 ± 0.013	60 ± 2	[14] 1960
	0.1420 ± 0.0004	13630 ± 70	0.2320 ± 0.0009	58.8 ± 0.2	[18] 1960
	0.145 ± 0.001		0.225 ± 0.005	63 ± 3	[15] 1966
	0.1413 ± 0.0003	13520 ± 60	0.2311 ± 0.0009	59.2 ± 0.2	present work
176	1.574	7990 ± 80	0.41 ± 0.05	55 ± 5	[17] 1955
	1.57		0.32 ± 0.05	(60)	[19] 1959
	1.563 ± 0.004	7500 ± 150	0.399 ± 0.002	55.0 ± 1.1	present work
175	2.604 ± 0.010	2010 ± 40		50 ± 1	[17] 1955
	2.61		0.14 ± 0.02	(60)	[19] 1959
	2.576 ± 0.006	1520 ± 55	0.132 ± 0.003	70.7 ± 2.1	present work

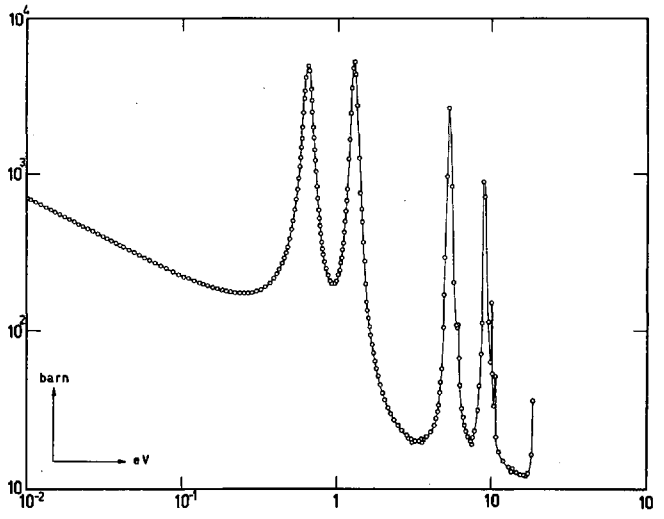

FIG.3. Total cross-section of iridium

TABLE VIII. CROSS-SECTION OF IRIDIUM AT 0.0253 eV IN BARNS

σ_{tot}	σ_{abs}	σ_{sc}	Method	Ref. Year
417 ± 20			T.o.f.	[20] 1947
	440 ± 25		pile osc.	[5] 1951
	436 ± 40		act.	[21] 1963
		14	diffr.	[22] 1964
439.5 ± 2				present work

TABLE IX. RESONANCE PARAMETERS OF RESONANCES IN IRIDIUM

Isotope	E_0 (eV)	σ_0 (b)	$2g\Gamma_n^0$ (MeV)	Γ_γ (MeV)	Reference
191	0.654 ± 0.002	14200 ± 300	0.62 ± 0.03	73.5 ± 1	[17] 1955
	0.6551 ± 0.0014	15100 ± 240	0.668 ± 0.006	70.8 ± 0.9	present work
193	1.303 ± 0.005	10200 ± 200	0.81 ± 0.02	86.5 ± 1	[17] 1955
	1.301 ± 0.003	10200 ± 320	0.783 ± 0.015	87.0 ± 2.2	present work

4.3. Iridium

Our results for the total cross-section of iridium are represented in Fig. 3. An improvement of the data in the thermal region and around the resonances at 1 eV could be achieved. In Table VIII are shown all significant cross-section data for the element Ir at 0.0253 eV.

The value of Rainwater [20] corresponds to the curve in BNL-325. The measurements of σ_{abs} and σ_{sc} are in favour of our measurements but are not in disagreement with Rainwater's value. A measurement of the total cross-section made by Seppi [23] in the energy range between 0.00253 and 0.00473 eV gives an extrapolated value of 439.3 ± 2 b at 0.0253 eV, in perfect agreement with our result.

Our results for the resonance parameters of the low-energy resonances in Ir together with earlier references are given in Table IX.

5. ERRORS

5.1. Errors in energy scale

The uncertainties of the different components and their influence on the accuracy of the energy scale, the cross-sections and the resonance

TABLE X. ERROR COMPONENTS

Energy scale

Component	Error on: component	energy (‰)
Flight path length	1 ‰	2
Frequency of analyser	< 0.005 ‰	< 0.01
Analyser start time	± 0.5 μs	≤1.5
Energy scale total (energy range below 2.6 eV)		≤2.5

Cross-sections

Component	Error on: component (‰)	cross-section (‰)
Absorber thickness	≤1	≤1
Transmission:		
(a) statistical errors	3.5	5
(b) dead-time corr.	< 0.15	< 0.2
Impurities and content of O, Cl and S resp.	< 1	≤1
Effect of grain size in powder samples		< 1
Relative uncertainty in a single measurement of a cross-section		5.3

Resonance parameters

Component	Error on: component (%)	Γ_γ (%)	$2g\Gamma_n^\circ$ (%)
Absorber thickness	≤ 0.1	no influence	≤ 0.1
Isotope abundance	≤ 0.4	no influence	≤ 0.4
Resolution	≤ 5	≤ 2.3	≤ 1.3
Doppler width	≤ 3	≤ 1.5	≤ 0.65
Cross-section of potential scattering	11 - 25	not considered	not considered
Standard deviation (programme SHAPE)	-	≤ 2.5	≤ 1.9

TABLE XI. ISOTOPIC ABUNDANCES USED IN THE CALCULATIONS

Isotope	(%)	Isotope	(%)	Isotope	(%)
^{160}Dy	2.29	^{175}Lu	97.41	^{191}Ir	37.3
^{161}Dy	18.9	^{176}Lu	2.59	^{193}Ir	62.7
^{162}Dy	25.53				
^{163}Dy	24.97				
^{164}Dy	28.18				

parameters are listed in Table X. The isotopic abundances given in Table XI have been used in the calculations.

6. CONCLUSIONS

We succeeded in improving the total cross-section data in different energy intervals in the thermal region of the elements dysprosium, lutetium and iridium. Several resonance parameters in the same energy range could be improved while some discrepancies in the resonance parameters remain unsolved.

REFERENCES

[1] MAUNDERS, E.J., UKAEA Rep. AEEW-M 661 (1966).
[2] SIMPSON, O.D. et al., Nucl. Instrum. Meth. 30 (1964) 293.
[3] ATTA, S.E., HARVEY, J.A., USAEC Rep. ORNL 3205 (1961).
[4] BRILL, T., LICHTENBERGER, H.V., Phys. Rev. 72 (1947) 585.
[5] POMERANCE, H., Phys. Rev. 83 (1951) 641.
[6] BROCKHOUSE, B.N., Can. J. Phys. 31 (1953) 432.
[7] HOUSE, L.L., FROST, R.T., Bull. Am. phys. Soc. Ser. II, 3 (1958) 337.
[8] MEADOWS, J.W., WHALEN, J.F., Nucl. Sci. Engng 9 (1961) 132.
[9] SHER, R. et al., Nucl. Sci. Engng 11 (1961) 369.
[10] DANELJAN, L.S. et al., Atomnaja Energija 16 (1964) 56.
[11] OKAMOTO, K., Rep. JAERI 1069 (1964).
[12] SCOVILLE, J.J. et al., Nucl. Sci. Engng 25 (1966) 12.
[13] ZIMMERMAN, R.L., Bull. Am. phys. Soc. Ser. II, 2 (1957) 42.
[14] BASTON, A.H. et al., J. nucl. Energy Part A, 13 (1960) 35.
[15] ZIMMERMAN, R. L. et al., Paper CN-23/129, these proceedings I.
[16] SOKOLOWSKI, E. et al., Nukleonik 6 (1964) 245.
[17] LANDON, H.H., Phys. Rev. 100 (1955) 1414.
[18] ROBERGE, J.P., SAILOR, V.L., Nucl. Sci. Engng 7 (1960) 502.
[19] BLOCK, R.C. et al., USAEC Rep. ORNL 2718 (1959) 26.
[20] RAINWATER, L.J. et al., Phys. Rev. 71 (1947) 65.
[21] KEISCH, B., Phys. Rev. 129 (1963) 769.
[22] MUELLER, M.H. et al., Bull. Am. phys. Soc. Ser. II, 9 (1964) 179.
[23] SEPPI, E.J. et al., USAEC Rep. HW 55879 (1958).

ПОЛНЫЕ НЕЙТРОННЫЕ СЕЧЕНИЯ ИЗОТОПА ТОРИЙ-230 В ОБЛАСТИ ЭНЕРГИЙ (0,02 – 50) эв

С.М.КАЛЕБИН, Р.Н.ИВАНОВ, П.Н.ПАЛЕЙ,
З.К.КАРАЛОВА, Г.М.КУКАВАДЗЕ, В.И.ПЫЖОВА,
Н.П.ШИБАЕВА, Г.В.РУКОЛАЙНЕ
(Доклад представил С.И.Сухоручкин)
ГОСУДАРСТВЕННЫЙ КОМИТЕТ ПО ИСПОЛЬЗОВАНИЮ
АТОМНОЙ ЭНЕРГИИ, МОСКВА
СССР

Abstract — Аннотация

TOTAL NEUTRON CROSS-SECTION OF THORIUM-230 AT (0.02-50) eV. One hundred and five milligrams of purified ^{230}Th have been chemically educed for measurement of total cross-sections. The purity of the prepared sample was controlled by the mass spectrometer analysis. The measurement of neutron cross-sections was performed with the help of a fast chopper suspended in a magnetic field. Resonances were found at 1.107, 1.431, 2.39, 7.80, 17.40, 24.0, 31.9, 39.2 and 47.5 eV.

With the level parameters obtained, the average value of the level spacing D = 7.67 eV and the strength function $S_0 = 0.74 \times 10^{-4}$ were calculated. The total cross-section at the thermal point (0.025 eV) is 70 b. The potential scattering cross-section is 13 b. A good coincidence of location of ^{230}Th energy levels with levels of Hf is emphasized.

ПОЛНЫЕ НЕЙТРОННЫЕ СЕЧЕНИЯ ИЗОТОПА ТОРИЙ-230 В ОБЛАСТИ ЭНЕРГИЙ (0,02 ÷ 50) эв. Для исследования полных нейтронных сечений химическим путем выделен и очищен от примесей изотоп торий-230 в количестве 105 мг. Чистота приготовленного образца установлена с помощью масс-спектроскопического анализа. Измерения нейтронных сечений выполнены на механическом прерывателе, подвешенном в магнитном поле. В исследуемой области энергий обнаружены уровни с энергией: 1,107; 1,431; 2,39; 7,80; 17,40; 24,0; 31,9; 39,2 и 47,5 эв.

В статье приведены параметры этих уровней и вычислено по ним среднее расстояние между уровнями $\bar{D} = 7{,}67$ эв и силовая функция $S_0 = 0{,}74 \cdot 10^{-4}$. В статье приводится полное нейтронное сечение в тепловой точке для тория-230, равное 70 барнам, и сечение потенциального рассеяния, равное 13 барнам. Отмечается хорошее совпадение энергий уровней изотопа тория-230 с положением нейтронных уровней у гафния.

На тяжеловодном реакторе ИТЭФ проводятся измерения полных нейтронных сечений изотопа торий $_{90}Th^{230}$. Пульсирующий поток нейтронов получали с помощью механического прерывателя, подвешенного в магнитном поле [1, 2]. Пролетная база для нейтронов равна 50 м, при исследовании полных нейтронных сечений она обеспечивает разрешение, равное 0,03 мксек/м. Минимальный размер образца, применяемый при измерениях, равен 0,096 см^2, максимальный – 1,248 см^2. Система подвеса механического прерывателя в магнитном поле легко позволяет осуществлять его вращение, синхронное с частотой кварца в широком диапазоне скоростей ($\sim 0 \div 25 \cdot 10^3$ об/мин). Исследуемый изотоп торий-230 стоит в ряду изотопов с массовыми числами $\sim 210 \div 230$, нейтронные резонансы которых исследованы мало. Для проведения измерений торий-230 был выделен химическим путем в количестве 105 мг. Исходным сырьем для получения ториевого образца послужил протактиний-ониевый концентрат, выделенный из урановой руды путем сочета-

ния приемов выщелачивания, осаждения и концентрации алкилфосфатными кислотами [3].

Последующая очистка тория-230 осуществлялась как с помощью ионного обмена в среде минеральных кислот на отечественных сорбентах АВ-17 и КУ-2, так и путем использования приемов соосаждения. Многократные операции по анионному обмену в концентрированной солянокислой среде обеспечили отделение изотопов тория от элементов: Zr; Hf; Ti; U; Pa; Po. Катионный обмен в солянокислой и азотнокислой средах способствовал отделению изотопов тория от редкоземельных элементов, марганца и частично от урана, железа и протактиния. С помощью ионного обмена в сернокислых средах выполнена дополнительная очистка ториевого образца от марганца, редкоземельных элементов и следов других примесей. Окончательно образец был приготовлен в виде окиси ThO_2, и масс-спектроскопическим путем установлен его изотопный состав и состав примесей. Данные масс-спектроскопического анализа сведены в табл.1.

ТАБЛИЦА 1. ХИМИЧЕСКИЙ СОСТАВ ОБРАЗЦА

№	Состав образца	% содержания относительно общего веса тория
1	Th^{230}	55,0 ±0,2
2	Th^{232}	41,0 ±0,2
3	Nd	0,07 ±0,015
4	La	≤0,014
5	Ce	≤0,5
6	Pr	<0,004
7	Sm	<0,04
8	Eu	<0,01
9	Gd	<0,02
10	Hf	<0,06*
11	Zr	<3,00

* При масс-спектроскопическом анализе гафний не был обнаружен. Данная верхняя граница его содержания в образце определена по цирконию, считая, что примесь гафния в цирконии не превышает 2%. Если считать, что резонансы с энергиями 1,108 эв; 2,39 эв; 7,80 эв принадлежат гафнию, то содержание последнего в образце должно быть не менее ~0,5%.

Для определения нейтронного сечения изотопа торий-230 в тепловой области использовался образец, площадь которого была равна 0,096 $см^2$ и толщина $n = 1{,}93 \cdot 10^{21}$ $ат/см^2$. При измерениях "без образца" в нейтронный пучок помещался образец окиси изотопа торий-230 в количестве, определяемом процентным содержанием этого изотопа в исследуемом ториевом препарате (табл.1). При таком измерении полученное сечение изотопа торий-230 исправлялось только на сечение кислорода, который непосредственно соединен с изотопом торий-230. Поправки на сечение редкоземельных элементов, обладающих высоким нейтронным сечением в тепловой области, как, например, самарий, европий и др., не делались.

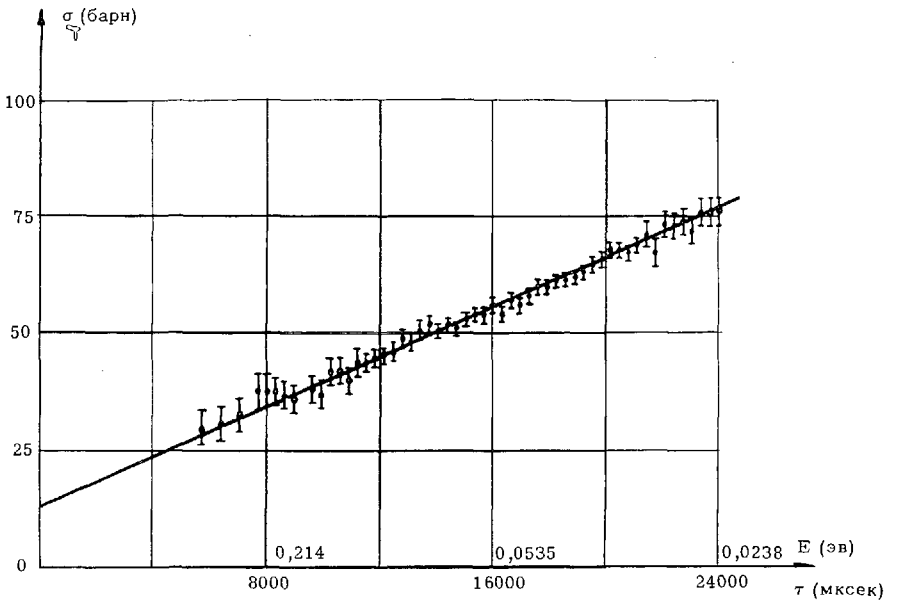

Рис. 1. Полное нейтронное сечение тория-230 в тепловой области энергий.

Масс-спектроскопический анализ естественного тория, который ставился в пучок нейтронов при измерениях "без образца", указал, что примесей редкоземельных элементов в нем меньше, чем в образце тория-230, данные по которому представлены в табл.1. Экспериментально полученное полное нейтронное сечение изотопа торий-230 в тепловой области представлено во временной шкале на рис.1. Ход сечения экстраполирован прямой линией:

$$\sigma_T(E) = (13 + 0{,}97\, E^{-1/2}) \text{ барн}$$

Эта прямая при $t = 0$ определяет потенциальное сечение рассеяния и в данном случае для тория-230 дает следующую его величину:

$$\sigma_p = 13 \pm 3 \text{ барн}$$ pot. scat

Данное сечение в дальнейшем было использовано для определения параметров в резонансной области. Полное нейтронное сечение в тепловой точке ($E_0 = 0{,}025$ эв), которое следует из представленной кривой на рис.1, для тория-230 равно 70 ± 3 барна. Одновременно с измерением полного нейтронного сечения с помощью временных анализаторов, измерялось независимо от них усредненное по спектру пропускания механического прерывателя полное нейтронное сечение в области, выделенной кадмиевым фильтром. Измеренное таким способом усредненное полное нейтронное сечение в тепловой области оказалось равным:

$$\bar{\sigma}_T = 55 \pm 1 \text{ барн}$$ total avg. thr

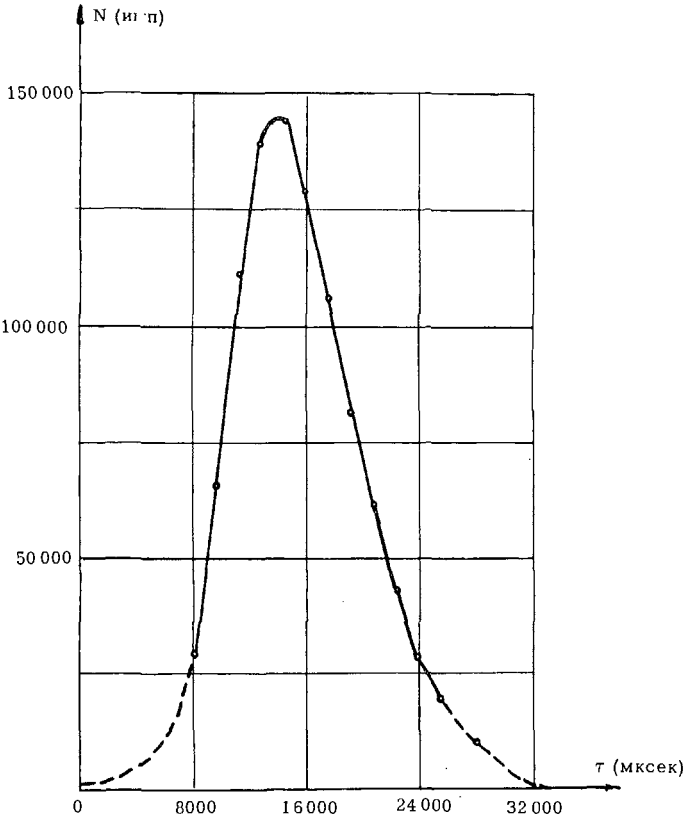

Рис. 2. Функция пропускания Ф(E) механического прерывателя в тепловой области энергий.

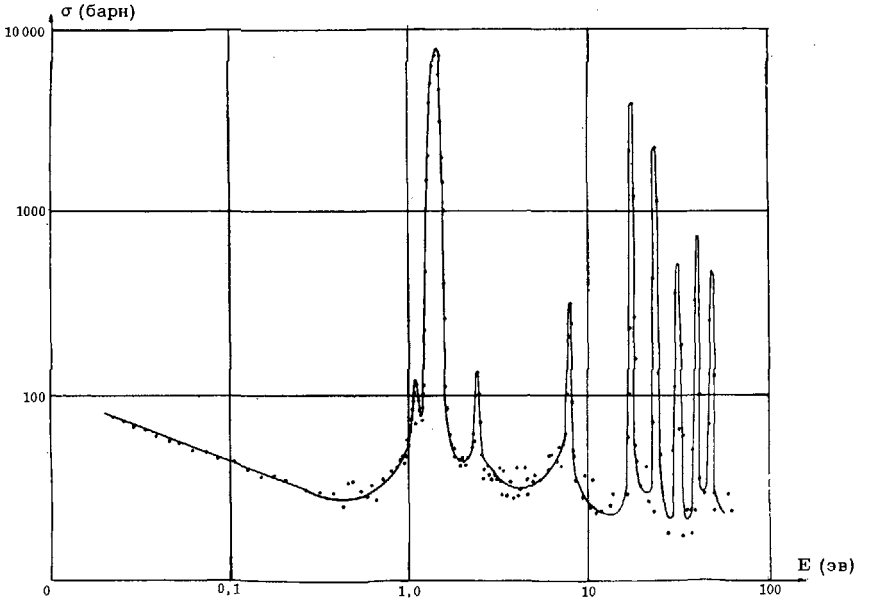

Рис. 3. Полные нейтронные сечения тория-230 в области энергий (0,02 ÷ 50) эв. Толщина образца $n = 1{,}72 \cdot 10^{21}$ ат/см^2.

Эту величину нейтронного сечения можно связать с полученным на анализаторе результатом, показанном на рис.1. Действительно, представим измеренное усредненное сечение в виде формулы:

$$\bar{\sigma}_T = \frac{1}{n} \ln \frac{1}{T},$$

где T – пропускание исследуемого образца, n – его толщина, выраженная в атомах на квадратный сантиметр. Учитывая, что пропускание для образца близко к единице, указанную формулу можно переписать в виде:

$$\bar{\sigma}_T \approx \frac{1-T}{n} = \frac{N_0 - N}{nN_0}, \qquad (1)$$

где N_0 – число пропущенных нейтронов механическим прерывателем при измерениях без образца, а N – число нейтронов при измерениях с образцом. Обозначим функцию пропускания механического прерывателя в исследуемой области энергий через $\Phi_{(E)}$. Тогда можно записать:

$$N_0 = \int \Phi(E)\, dE$$

$$N = \int e^{-n\sigma_T(E)} \Phi(E)\, dE \approx \int [1 - n\sigma_T(E)]\, \Phi(E)\, dE.$$

В этом случае из равенства (1) следует:

$$\bar{\sigma}_T = \frac{\int \sigma_T(E)\, \Phi(E)\, dE}{\int \Phi(E)\, dE} \qquad (2)$$

Указанное выражение связывает независимо измеренное усредненное сечение $\bar{\sigma}_T$ с сечением $\sigma_T(E)$, полученным с помощью анализатора. Функция $\Phi(E)$ экспериментально измерена тем же нейтронным детектором, который применялся при всех измерениях, и эта функция представлена на рис.2. Полученная величина для $\bar{\sigma}_T$ хорошо согласуется с результатом ее вычисления по формуле (2). Результат такого вычисления равен:

$$\bar{\sigma} = \frac{\int (13 + 0{,}97\, E^{-1/2})\, \Phi(E)\, dE}{\int \Phi(E)\, dE} = 56{,}5 \text{ барн} \approx \bar{\sigma}_T.$$

Полученное равенство говорит в пользу указанной выше измеренной для тория-230 зависимости его полного нейтронного сечения от энергии в тепловой области.

Однако полученную величину сечения тория в тепловой точке трудно согласовать с данными, опубликованными в работе [7]. По-видимому, это связано с тем, что в расчете этого сечения не был учтен вклад примесей, а потому результат $\sigma = 70$ барн следует считать предварительным.

Измерение полных нейтронных сечений в области выше тепловой проводилось на образцах толщиной $n = 1{,}72 \cdot 10^{21}$ ат/см^2 и $n = 1{,}83 \cdot 10^{20}$ ат/см^2. Измерения, полученные с образцом $n = 1{,}72 \cdot 10^{21}$ ат/см^2, представлены на рисунке 3. Обработка уровне велась методом площадей [4, 5], поправка площади уровня на "крылья

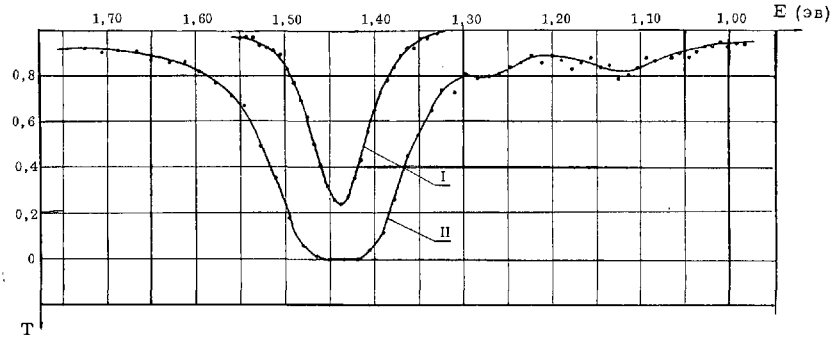

Рис. 4. Кривые пропускания для уровня 1,431 эв: кривая I — пропускание образца толщиной $n = 1{,}83 \cdot 10^{20}$ ат/см^2; кривая II — пропускание образца толщиной $n = 1{,}72 \cdot 10^{21}$ ат/см^2.

ТАБЛИЦА 2. ПАРАМЕТРЫ РЕЗОНАНСНЫХ УРОВНЕЙ*

№	E_0 (эв)	Γ_γ (mv)	Γ_γ (mv)	$\Gamma_n^0 \cdot 10^{-4}$	Примечание
1	1,107 ± 0,006	–	–	–	Возможный уровень гафния
2	1,431 ± 0,007	27,8 ± 2	0,19 ± 0,01	1,59 ± 0,1	
3	2,39 ± 0,008	–	–	–	– " –
4	7,80 ± 0,05	–	–	–	– " –
5	17,40 ± 0,08	23,1 ± 4	5,1 ± 0,6	12,2 ± 0,5	
6	24,0 ± 0,12	26,8 ± 8	4,60 ± 0,8	9,4 ± 1,6	
7	31,9 ± 0,2	21,0 ± 8	1,40 ± 0,25	2,50 ± 0,4	
8	39,2 ± 0,3	27 ± 10	3,2 ± 0,8	5,1 ± 1,2	
9	47,5 ± 0,35	26 ± 11	2,2 ± 0,8	3,2 ± 1,2	

* В таблице приведены только статистические ошибки.

резонанса вычислялась по формуле:

$$\Delta A = \frac{n\sigma_0\Gamma^2}{4}\left(\frac{1}{\eta_1}+\frac{1}{\eta_2}\right),$$

где η_1, η_2 – значения энергий, при которых ограничивалась площадь резонанса.

Кривые пропускания для уровня с энергией 1,431 эв показаны на рис.4. Параметры измеренных уровней сведены в табл.2.

При рассмотрении табл.2 следует заметить, что энергии уровней тория-230 совпадают с положением нейтронных уровней у гафния [6]. Указанное обстоятельство не могло не вызвать подозрения, что в исследуемом образце тория имеется примесь гафния. Такое подозрение усиливалось тем, что слабые уровни тория-230 с энергией 1,107 эв, 2,39 эв и уровень 7,8 эв не только совпадали по энергии с сильными уровнями гафния 1,1 эв, 2,38 эв, 7,80 эв, но и качественно повторяли интенсивность указанных уровней гафния. Хотя химический процесс выделения образца тория и методы его последующей очистки, указанные в нача-

ле статьи, давали мало повода к указанному сомнению, все же для окончательного выяснения был проведен дополнительный масс-спектроскопический анализ на выявление примеси гафния в исследуемом образце тория. Такой анализ дал отрицательный результат, гафний не был обнаружен.

Указанное совпадение уровней гафния и тория-230 следует отметить как экспериментальный факт, который требует дополнительного исследования.

Если считать, что уровни 1,1 эв, 2,38 эв, 7,8 эв все же принадлежат гафнию, то среднее расстояние между уровнями тория-230 будет 9,5 эв, а оценочное значение силовой функции составит величину $0{,}6 \cdot 10^{-4}$.

Авторы признательны Ю.Г.Абову, С.И.Сухоручкину, В.Н.Андрееву и И.В.Кирпичникову за ряд критических замечаний, сделанных в ходе измерений, и сотрудникам: В.С.Артамонову, А.Н.Полозову, В.Савинову, О.М.Гудкову, А.С.Алпееву, принимавшим непосредственное участие в проведении измерений.

ЛИТЕРАТУРА

[1] КАЛЕБИН С.М., ВЛАДИМИРСКИЙ В.В., ПТЭ, №3, 36 (1962).
[2] КАЛЕБИН С.М., РУКОЛАЙНЕ Г.В., СОКОЛОВСКИЙ В.В., ПТЭ, №4, 48 (1963).
[3] ПАЛЕЙ П.Н., КАРАЛОВА З.К., ШИБАЕВА Н.П., ПЫЖОВА З.И. Журнал аналитической химии, 21, вып. 1, (1966) 126; 21, вып. 7, (1966) 874; 21, вып. 8 (1966) 950.
[4] LYNN J.E., RAE E.R. J. Nuclear Energy 4, 418 (1957).
[5] ЕФИМОВ В.Н., ШЕЛОНЦЕВ И.И. "Расчет графиков для определения параметров нейтронных резонансов по методу пропускания образца". Дубна, 1961 (Препринт).
[6] ГОРДЕЕВ И.В., КАРДАШЕВ Д.А., МАЛЫШЕВ А.В. "Ядерно-физические константы". М. Атомиздат, 1963.
[7] Neutron cross sections BNL–325 V.III, 1965.

НЕЙТРОНОСПЕКТРОСКОПИЧЕСКИЕ ИССЛЕДОВАНИЯ РАЗДЕЛЕННЫХ ИЗОТОПОВ СЕРЕБРА

Г.В.МУРАДЯН, Ю.В.АДАМЧУК
ИНСТИТУТ АТОМНОЙ ЭНЕРГИИ им. И.В.КУРЧАТОВА,
МОСКВА
СССР

Abstract — Аннотация

NEUTRON-SPECTROSCOPIC INVESTIGATION OF SEPARATED SILVER ISOTOPES. The paper gives the results of measurements on radiative capture of neutrons in the separated silver isotopes ^{107}Ag and ^{109}Ag in an energy range up to 1000 eV. A number of new levels are found. It is shown that the marked discrepancy between the level-spacing distribution for Ag and the Wigner distribution for various superposed level systems is only apparent. It is also shown that there is no correlation between ^{107}Ag and ^{109}Ag levels within the limits of statistical accuracy obtained.

The values of the strength functions S_0 for ^{107}Ag and ^{109}Ag are found equal to $(0.43 \pm \frac{0.17}{0.12}) \times 10^{-4}$ and $(0.83 \pm \frac{0.23}{0.19}) \times 10^{-4}$, respectively. This marked difference in the values of the strength function of nuclei of almost the same atomic weight is not consistent with the optical model of the nucleus and can probably be explained on the hypothesis of compound-nucleus formation through three quasi-particle interactions.

НЕЙТРОНОСПЕКТРОСКОПИЧЕСКИЕ ИССЛЕДОВАНИЯ РАЗДЕЛЕННЫХ ИЗОТОПОВ СЕРЕБРА. Приводятся результаты измерений радиационного захвата нейтронов разделенных изотопов серебро-107 и серебро-109 в области энергий до ~1000 эв. Выявлен ряд новых уровней. Показано, что обнаруженное сильное отклонение распределения расстояний между уровнями для серебра от распределения Вигнера для нескольких наложенных друг на друга систем уровней является кажущимся. Показано также, что корреляция между уровнями серебра-107 и серебра-109 в пределах достигнутой статистической точности отсутствует.

Значения S_0-силовых функций серебра-107 и серебра-109 оказались равными $\left(0{,}43^{+0{,}17}_{-0{,}12}\right) \cdot 10^{-4}$ и $\left(0{,}83^{+0{,}23}_{-0{,}19}\right) \cdot 10^{-4}$ соответственно. Столь сильное расхождение значений силовых функций близких по атомному весу ядер не укладывается в рамки оптической модели ядра и, по-видимому, может быть объяснено с помощью представления образования составного ядра через трехквазичастичные взаимодействия.

В работе рассмотрены результаты изучения радиационного захвата изотопов серебра – серебро-107 и серебро-109. Эти исследования, в отличие от проводившихся ранее исследований естественной смеси изотопов серебра [1], дают возможность более точно сопоставить выводы теории с данными эксперимента. Помимо всего прочего, интерес к измерениям разделенных изотопов серебра (серебро-107 и серебро-109) был вызван тем, что проведенные недавно измерения полных нейтронных сечений естественной смеси серебра на колумбийском синхроциклотроне (США) с наилучшим в настоящее время разрешением (0,5 нсек/м) [1] привели к неожиданному результату: малые расстояния между уровнями серебра встречаются реже, чем это следует из распределения Вигнера в случае наложения нескольких систем уровней (в данном случае более, чем четырех систем). Этот вывод приводит к следствиям, требующим коренного пересмотра современной теории ядра.

Данные, полученные в публикуемой работе, показали, что наблюдаемое отсутствие малых расстояний между уровнями является кажущимся и объясняется слиянием уровней разных изотопов.

Измерения радиационного захвата изотопов серебро-107 и серебро-109 проводились по методу времени пролета на нейтронном спектрометре ИАЭ [2]. Длина пролетного расстояния составляла 37 м, длительность нейтронного импульса – 0,2 мксек, ширина канала 2048-канального временного анализатора – 0,25 мксек, разрешение ~10 нсек/м.

Образцы разделенных изотопов серебро-107 и серебро-109 представляли собой металлические диски диаметром 70 мм. Число атомов на барн для серебра-107 составляло 0,0186 и 0,00475, для серебра-109 – 0,0156 и 0,00276. Содержание основного изотопа в образцах было ~99%.

РЕЗУЛЬТАТЫ И ОБСУЖДЕНИЯ

На рис.1, 2 и 3 приведены результаты измерений радиационного захвата толстых образцов серебра-107 и серебра-109 в интервале энергий до 1 кэв. Измерения разделенных изотопов дали нам возможность идентифицировать уровни по изотопам.

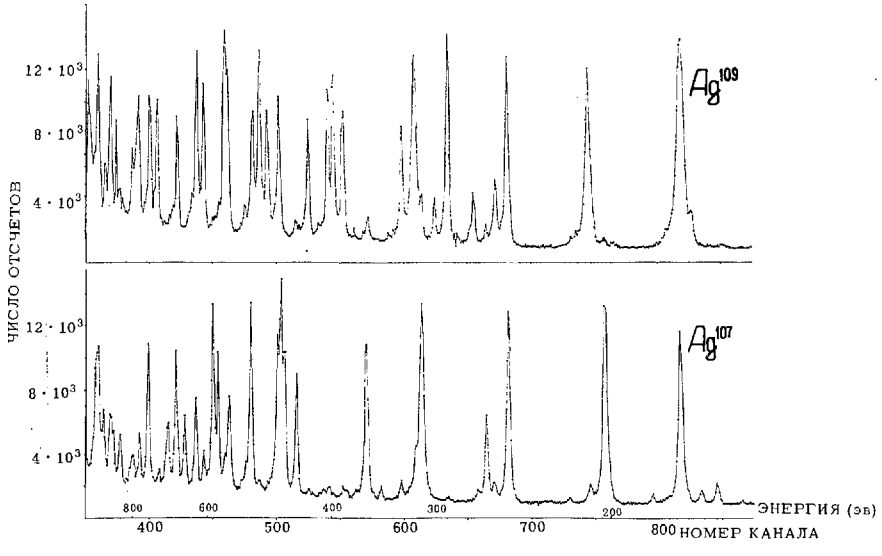

Рис. 1. Измерение радиационного захвата изотопов серебра в области энергий 1000 ÷ 150 эв.

В таблице приведена изотопная идентификация уровней серебра. Там же приведены параметры уровней серебра-107 и серебра-109, взятые в основном из работы [1]. Звездочкой помечены уровни, впервые обнаруженные в данной работе, и уровни, для которых уточнены значения $2g\Gamma_n^0$. Значение параметра $2g\Gamma_n^0$ для вновь найденных уровней серебра-107 и серебра-109 определялось в предположении $\Gamma_\gamma = 140$ мэв.

На рисунках 4 и 5 приведены зависимости числа уровней от энергии. Из этих рисунков видно, что до энергий ~ 650 эв уровни не пропускаются.

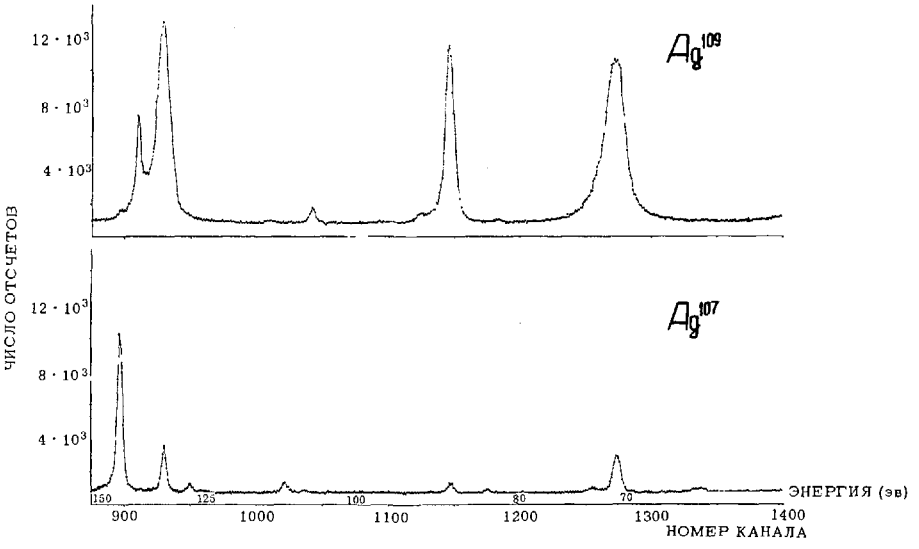

Рис. 2. Измерение радиационного захвата изотопов серебра в области энергий 150 ÷ 60 эв.

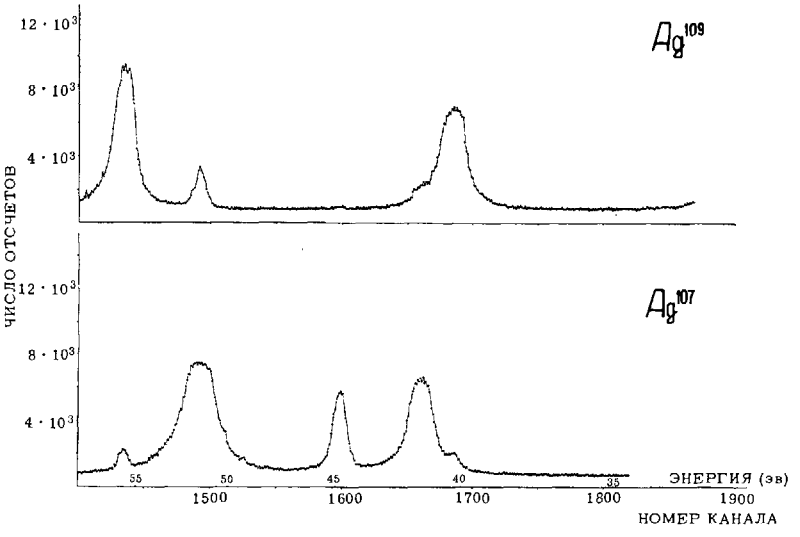

Рис. 3. Измерение радиационного захвата изотопов серебра в области энергий 60 ÷ 33 эв.

Определенные в этой области значения средних расстояний между уровнями оказались равными:

для серебра-107 – $\langle D \rangle = 13{,}5$ эв,
для серебра-109 – $\langle D \rangle = 12{,}8$ эв,
для серебра-107 + серебро-109 – $\langle D \rangle = 6{,}6$ эв.

Заметим, что в работе [1] для естественной смеси изотопов серебра приводится значение $\langle D \rangle = 8{,}75$ эв.

Несмотря на то, что разрешение нейтронного спектрометра, использованного в работе [1], на порядок лучше, чем в настоящей работе, измерение разделенных изотопов дало нам возможность выявить ~20 новых

уровней. Дело в том, что уровни серебра-107 и серебра-109 в ряде случаев совпадали в пределах своих ширин и разрешения и поэтому измерение естественной смеси не давало возможности идентифицировать эти случаи, как случаи двойных уровней.

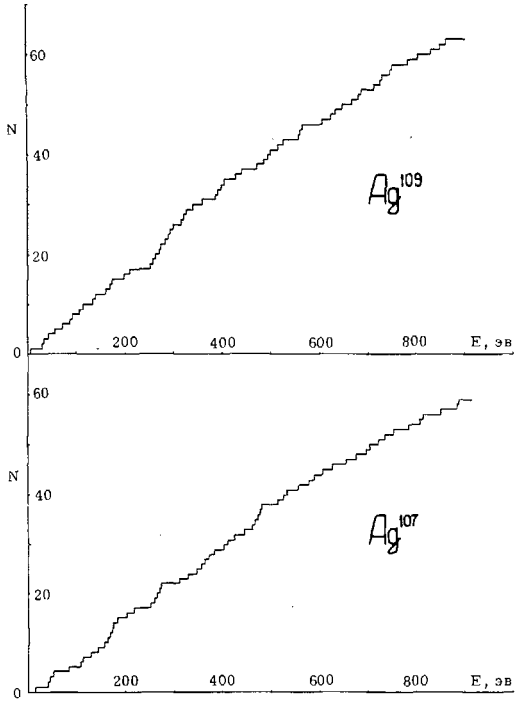

Рис. 4. Зависимость числа уровней серебра-107 и серебра-109 от энергии нейтронов.

Именно это обстоятельство привело авторов работы [1] к распределению расстояний между уровнями, в котором малые расстояния встречаются аномально редко (рис. 6А). Из этого распределения можно сделать следующие выводы:

1) Либо проявляется одна из четырех систем уровней (в естественной смеси серебра должны проявиться, по крайней мере, 4 системы уровней – у каждого изотопа две системы s-уровней, соответствующие двум спиновым состояниям, плюс p-уровни).

2) Либо существует довольно сильная корреляция между положениями уровней, соответствующими разным изотопам, спинам и орбитальному моменту.

Из ранних измерений серебра в области до 100 эв [3] было известно, что в указанной области энергии проявляется 4 системы уровней, так что первое заключение не имеет места. Вторая альтернатива – существование сильной корреляции между уровнями различных систем уровней – противоречит существующим теориям. Положение усугубляется еще тем, что серебро не единственное ядро, на котором обнаружен указанный тип распределения уровней. Аналогичные результаты получены для I и Cs [1] и урана-235 [4, 5]. Серебро является наиболее ярким представителем из этого ряда ядер, поскольку число независимых систем уровней у серебра в 2 раза больше.

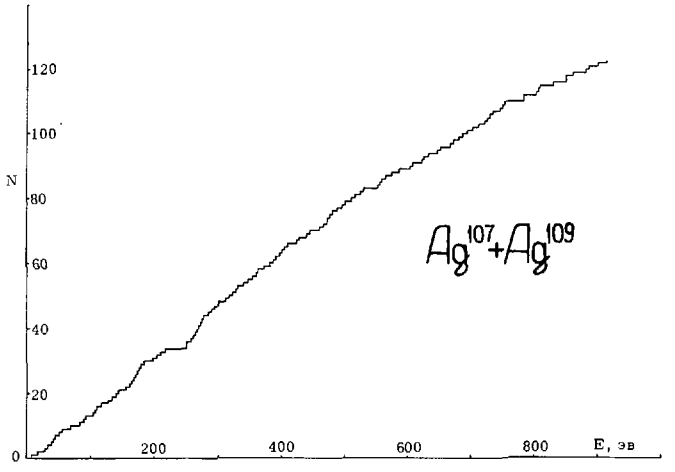

Рис. 5. Зависимость числа уровней серебра-107 и серебра-109 от энергии нейтронов.

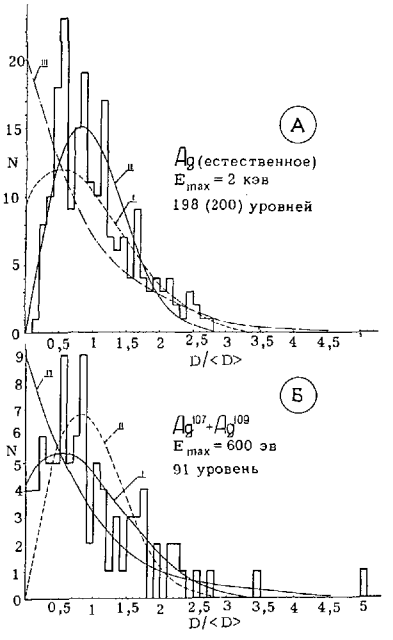

Рис. 6. А) Распределение расстояний между уровнями естественной смеси изотопов серебра из работы [1]. Б) Распределение расстояний между уровнями серебра-107 + серебро-109 по результатам настоящей работы. Кривая I – распределение Вигнера для двух систем уровней; кривая II – распределение Вигнера для одной системы уровней; кривая III – случайное распределение.

На рис.6Б и 7 приведены распределения расстояний между уровнями для серебра-107, серебра-109 и серебра-107+серебро-109, построенные по данным настоящей работы.

При построении рис.6Б и 7 мы ограничились областью до ~650 эв, где, с одной стороны, отсутствует пропуск уровней, а с другой – разре-

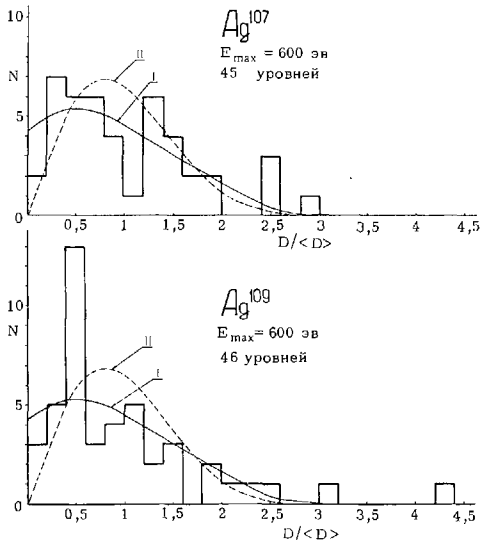

Рис. 7. Распределение расстояний между уровнями для изотопов серебра. Кривая I – распределение Вигнера для двух систем уровней; кривая II – распределение Вигнера для одной системы уровней.

шение и допплеровская ширина существенно меньше $\langle D \rangle$. Поэтому изучение разделенных изотопов в этой области энергий дало нам возможность обнаружить слившиеся уровни и несколько слабых уровней, выявленных в работе [1]. Эти обстоятельства привели к появлению малых расстояний между уровнями для каждого изотопа серебра в отдельности (рис.7).

Приведенные рисунки показывают, что экспериментальные распределения хорошо согласуются с распределением Вигнера в случае наложения нескольких систем уровней, особенно если учесть возможные потери уровней из-за наложения разных спиновых систем уровней в пределах одного изотопа.

Таким образом, не имеет места полученное в работе [1] несоответствие экспериментального распределения уровней серебра теоретическому распределению, получаемому из наложения нескольких независимых систем уровней.

Заметное количество выявленных случаев совпадения уровней серебра-107 и серебра-109 наводит на мысль о возможной корреляции между положениями уровней этих изотопов. Для проверки этого предположения был проведен приближенный корреляционный анализ.

Рассмотрим две системы уровней $\{A_i\}$ и $\{B_j\}$ (например, системы уровней серебра-107 и серебра-109). Пусть D_i^A – расстояния между уровнями системы A. Если в системе A между уровнями A_i и A_{i+1} случайно бросить уровень B_j, то возникнут два новых расстояния D_{ij} и $D_{i+1,\,j}$. Если всегда выбирать из этих двух расстояний наикратчайшее, то вероятность того, что либо D_{ij}, либо $D_{i+1,\,j}$ окажется в пределах $D_{ij} \div D_{ij} + \Delta D\left(D_{ij} \le \frac{D_i^A}{2}\right)$, то есть $2\Delta D / D_i^A$. Когда в промежуток $A_i \div A_{i+1}$ попадают K_i уровней системы B, то для вероятности получения D_{ij} в пределах $D_{ij} \div D_{ij} + \Delta D$ получим выражение:

$$P_i = \frac{2K_i \cdot \Delta D}{D_i^A} \qquad (1)$$

Теперь видно, что математическое ожидание числа случаев D_{ij} в пределах $D_{ij} \div D_{ij} + \Delta D$ дается формулой:

$$f(D_{ij}) \cdot \Delta D = P_i \cdot m_{ij} \cdot \Delta D = \left(\frac{2K_i}{D_i^A}\right) \cdot m_{ij} \cdot \Delta D, \qquad (2)$$

где m_{ij} – число промежутков системы A, для которых $D_i^A \geq 2 \cdot D_{ij}$. При построении распределения $f(D_{ij})$ значения K_i, m_{ij} и D_i^A берутся из экспериментальных данных. (Заметим, что распределение $f(D_{ij})$ можно построить также по известным распределениям расстояний между уровнями в системах A и B – например, по распределению Вигнера).

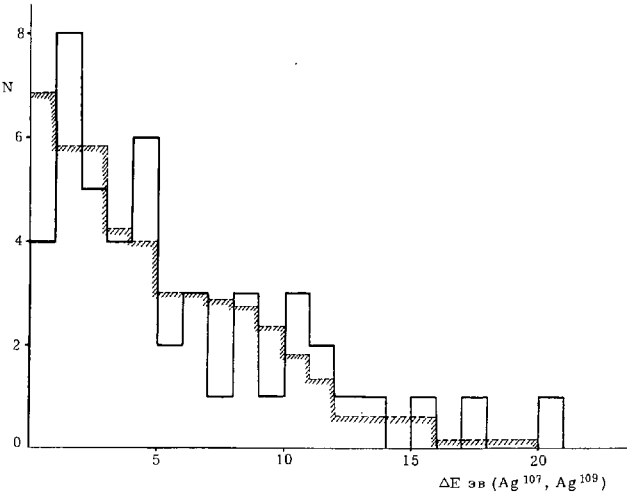

Рис. 8. Гистограммы распределения расстояний между парой ближайших уровней серебра-107 и серебра-109. Сплошная кривая построена по экспериментальным данным, заштрихованная – соответствует теоретически ожидаемому распределению.

На рис.8 приведено распределение расстояний между парой ближайших уровней серебра-107 и серебра-109 (сплошная кривая). Там же приводится теоретически ожидаемая гистограмма (заштрихованная кривая), которая получается, если на данную конкретную сетку уровней серебра-107 случайно наложить столько уровней, сколько их у серебра-109, т.е. распределение (2).

Из приведенного рисунка можно сделать следующие выводы:

1) В пределах достигнутой статистической точности отсутствует корреляция между уровнями серебра-107 и серебра-109. (Построение аналогичных графиков с отбрасыванием слабых уровней приводит к аналогичному выводу).

2) Вероятность случайного наложения уровней серебра-107 и серебра-109 составляет заметную величину. При этом доля слившихся уровней зависит от расстояния между уровнями, энергетического разрешения, эффекта Допплера и ширины уровня. Так, например, в области энергий, где разрешение, эффект Допплера и ширина уровня дают неоп-

ределенность ~2 эв, доля необнаруженных уровней составляет ~10%: Исходя из графиков, аналогичных рис.8, можно в области малых расстояний вводить соответствующие поправки при построении гистограмм распределений расстояний между уровнями в случае наложения нескольких систем уровней.

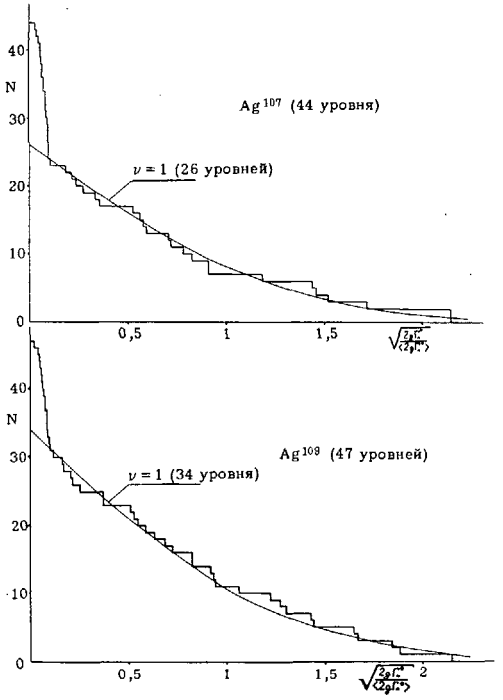

Рис. 9. Гистограмма интегрального распределения приведенных нейтронных ширин $2g\Gamma_n^\circ$ для серебра-107 и серебра-109. Сплошная кривая соответствует распределению Портера-Томаса с $\nu = 1$.

Заметим, что учет эффекта случайного наложения двух уровней, принадлежащих различным системам (наряду с учетом других эффектов в случае урана-235 [6]), возможно, изменит вывод об "аномальности" распределений расстояний между уровнями для I, Cs и урана-235.

На рис.9 приведены интегральные распределения приведенных нейтронных ширин. Сплошные кривые соответствуют распределению Портера-Томаса с $\nu = 1$. В случае серебра-107 эти кривые были отнормированы к числу уровней N = 26 со средним $\langle 2g\Gamma_n^\circ \rangle = 2{,}15$ эв, а в случае серебра-109 к N = 34 со средним $\langle 2g\Gamma_n^\circ \rangle = 2{,}96$ эв. Эти значения N и $\langle 2g\Gamma_n^\circ \rangle$ обеспечивают наилучшее согласие экспериментальных гистограмм с распределением Портера-Томаса в области $2g\Gamma_n^\circ > 0{,}02$ мэв. Как видно из рисунков, в области $2g\Gamma_n^\circ \leq 0{,}02$ мэв число уровней заметно отклоняется от приведенных теоретических кривых, что объясняется примесью p-уровней.

Вычисления S_0 – силовых функций изотопов серебра проводились по формуле:

$$S_0 = \frac{\sum_{i=1}^{n} 2g\Gamma_{ni}^\circ}{2E_{max}} \qquad (3)$$

и при $E_{max} \sim 800$ эв оказались равными:

$$S_0 = \left(0{,}43^{+0{,}17}_{-0{,}12}\right) \cdot 10^{-4} \quad \text{для } Ag^{107},$$

$$S_0 = \left(0{,}83^{+0{,}23}_{-0{,}19}\right) \cdot 10^{-4} \quad \text{для } Ag^{109},$$

Значение S_0 для серебра-107 хорошо согласуется с величиной $S_0 = (0{,}80 \pm 0{,}24) \cdot 10^{-4}$, приведенной в работе [14].

Ошибки в значениях S_0 для серебра-107 и серебра-109 вычислены с учетом флюктуации, приведенных нейтронных ширин и расстояний между уровнями, исходя из распределения силовых функций $\omega(S)$ [7]. Хотя распределение $\omega(S)$ выведено в предположении одинаковости спинов рассматриваемых уровней, тем не менее им можно пользоваться и в случае наложения нескольких спиновых систем уровней для оценки величины ошибок в S_0. Действительно дисперсия S_0 в основном определяется флюктуацией нейтронной ширины. В распределении $\omega(S)$ использовано в качестве меры флюктуации нейтронной ширины распределение Портера-Томаса. В рассматриваемом случае нейтронные ширины с достаточной степенью точности распределены по Портеру-Томасу (рис.9). В качестве распределения расстояний между уровнями в $\omega(S)$ взято распределение Вигнера для одной системы уровней. Замена этого распределения на распределение для двух систем уровней не приводит к существенному изменению полуширины функции $\omega(S)$ и поэтому оценка ошибки в силовой функции для нескольких систем уровней по распределению $\omega(S)$ является вполне корректной.

Для определения величины дисперсии S_0 по графикам [7] (исходя из числа уровней n) находится величина $q^{*}{}^{+\Delta q^{+}}_{-\Delta q^{-}}$, пропорциональная S_0. Зная S_0 и q^*, определяем коэффициент пропорциональности $k = S_0/q^*$, а затем из соотношения $\Delta S^{\pm} = k \cdot \Delta q^{\pm}$ – дисперсию S_0.

При вычислении значений силовых функций и их ошибок мы отбрасывали часть слабых уровней, которые в соответствии с рис.9, по-видимому, принадлежат взаимодействию с нейтронной p-волной. Отбрасывание этих уровней практически не повлияло на величину силовой функции, однако увеличило значение ошибок, что дало возможность относиться к последним более уверенно.

На рис.10 построены вероятности различных значений силовых функций $\omega(S)$ для серебра-107 и серебра-109, вытекающие из наших экспериментальных данных [7]. По распределениям $\omega(S)$ мы определили меру случайного расхождения значений силовых функций серебра-107 и серебра-109 (η), то есть вероятность того, что значение силовой функции серебра-107 не меньше значения силовой функции серебра-109:

$$\eta = \int_0^S \omega_{107}(S) \int_0^S \omega_{109}(S')\,dS' \cdot dS \qquad (4)$$

Эта вероятность оказалась равной $\eta \approx 3\%$, что указывает на несовместимость S_0 (серебро-107) и S_0 (серебро-109). S_0 (серебро-109) примерно на два раза больше S_0 (серебро-107). Столь сильное расхождение значений силовых функций близких по атомному весу ядер не может быть объяснено в рамках оптической модели.

ТАБЛИЦА. ИЗОТОПНАЯ ИДЕНТИФИКАЦИЯ И ПАРАМЕТРЫ РЕЗОНАНСНЫХ УРОВНЕЙ СЕРЕБРА

№ п/п	Ag^{107}			Ag^{109}		
	E_0, эв	$2g\Gamma_n^0$, мэв	Примечание	E_0, эв	$2g\Gamma_n^0$, мэв	Примечание
1	16,30	1,48 ±0,06		5,20	8,16 ±0,06	
2	41,50	1,32 ±0,16		30,50	2,00 ±0,18	
3	44,80	0,27 ±0,04		32,63	0,0019 ±0,0004	*
4	51,40	4,48 ±0,40		40,20	1,36 ±0,16	
5	83,50	0,0030 ±0,0007		55,70	2,56 ±0,20	
6	107,6	0,0019 ±0,0004	*	70,80	4,76 ±0,44	
7	110,88	0,008 ±0,001		87,67	1,00 ±0,08	
8	128,04	0,008 ±0,004		91,50	0,005 ±0,001	
9	144,20	0,76 ±0,08		106,29	0,012 ±0,004	
10	154,7	0,0045 ±0,0009	*	113,5	0,0054 ±0,0011	*
11	162,40	0,02 ±0,01		133,90	10,40 ±0,80	
12	167,10	0,016 ±0,004		139,70	0,18 ±0,02	
13	171,2	0,0065 ±0,0013	*	160	0,0079 ±0,0016	*
14	173,10	5,00 ±0,40		169,80	0,028 ±0,008	
15	183,60	0,012 ±0,004		172,8	6,1 ±0,9	*
16	202,50	1,12 ±0,12		198,4	0,011 ±0,02	*
17	218,20	0,012 ±0,012		209,60	2,48 ±0,20	
18	251,29	0,60 ±0,16	*	251,29	0,80 ±0,12	*
19	260	0,0168 ±0,0034	*	258,89	0,125 ±0,019	*
20	264,47	0,24 ±0,02		264,47	0,022 ±0,004	*
21	270,5	0,0076 ± 0,0015	*	272,5	0,12 ±0,01	
22	310,92	10,0 ±2,0		274,90	0,020 ±0,008	
23	329	0,018 ±0,004	*	283,90	0,016 ±0,008	
24	347,34	0,020 ±0,008		290,86	0,76 ±0,08	
25	356,20	0,020 ±0,008		293,00	0,020 ±0,008	
26	361,83	1,80 ±0,08		300,64	0,08 ±0,02	
27	372	0,0145 ±0,0030	*	316,40	14,0 ±2,0	
28	382,10	0,020 ±0,008		322,10	0,020 ±0,008	
29	401,70	0,024 ±0,012		327,80	0,40 ±0,06	
30	410,01	0,016 ±0,008		340,4	0,010 ±0,002	*
31	424	0,0073 ±0,0015	*	360	0,074 ±0,015	*
32	444,60	1,80 ±0,20		387,00	3,32 ±0,12	
33	461,40	1,08 ±0,12		391,60	0,016 ±0,004	
34	466,80	4,60 ±1,20		398,00	1,52 ±0,08	
35	472,2	0,72 ±0,08		404,40	5,0 ±0,2	
36	476,10	0,16 ±0,02		428,40	0,88 ±0,08	
37	479,54	0,12 ±0,02		441,0	0,009 ±0,002	*
38	512,27	0,68 ±0,08		469,61	2,0 ±0,8	
39	524,90	0,020 ±0,008		487,72	1,16 ±0,08	

№ п/п	Ag^{107}			Ag^{109}		
	E_0, эв	$2g\Gamma_n^\circ$, мэв	Примечание	E_0, эв	$2g\Gamma_n^\circ$, мэв	Примечание
40	532,20	0,07 ±0,02		495,20	0,04 ±0,02	
41	554,51	10,00 ±1,00		500,60	10,0 ±1,0	
42	576,67	3,04 ±0,40		515,47	4,4 ±0,4	
43	587,47	6,40 ±0,60		526,60	0,04 ±0,02	
44	605,06	0,10 ±0,02		558	0,26 ±0,05	*
45	625,59	0,64 ±0,08		560,66	6,0 ±0,8	
46	653,50	1,00 ±0,08		565,43	8,0 ±0,8	
47	674,50	3,00 ±0,28		607,93	2,6 ±0,2	
48	695,89	1,08 ±0,12		622,17	5,6 ±1,2	
49	703,51	0,26 ±0,02		634,27	0,04 ±0,02	
50	721,26	0,04 ±0,01		648,21	0,04 ±0,02	
51	734,70	0,04 ±0,01		669,45	1,68 ±0,20	
52	752,57	2,00 ±0,50	*	681,50	0,16 ±0,04	
53	784	0,21 ±0,04	*	687,40	0,08 ±0,02	
54	806	0,215 ±0,040	*	713,87	0,07 ±0,02	
55	813,0	0,24 ±0,06		726,08	1,04 ±0,12	
56	849	0,30 ±0,05	*	730,39	0,07 ±0,01	
57	882,33	4,00 ±0,60		747,49	5,20 ±0,40	
58	886,67	0,40 ±0,12		752,6	2,0 ±0,5	*
59	914,87	0,24 ±0,04		784,7	11,6 ±1,2	
60				803,80	1,8 ±0,4	
61				831,39	0,20 ±0,08	
62				849	0,090 ±0,014	*
63				861,83	0,52 ±0,08	
64				902,84	0,60 ±0,12	

В настоящее время в теории ядра проверяется и уточняется концепция образования составного ядра через последовательность переходов из начального одноквазичастичного (1q) состояния во все трехквазичастичные (3q) состояния, отвечающие принципам Пауди, с учетом закона сохранения энергии [8, 9]. Поскольку свойства входных трехквазичастичных состояний связаны с оболочечной структурой ядер и энергией возбуждения, то можно ожидать нерегулярную зависимость силовой функции от атомного номера. Поэтому указанное расхождение силовых функций серебра-107 и серебра-109 говорит в пользу применимости к этим ядрам концепции образования составного ядра через 3q возбуждения.

Следует отметить, что аналогичный эффект наблюдается в случае четно-четных изотопов Sn [10, 11], где наличие протонной магики дает дополнительное основание для сопоставления экспериментально найденных силовых функций изотопов олова с вычисленными на основании трехквазичастичных взаимодействий.

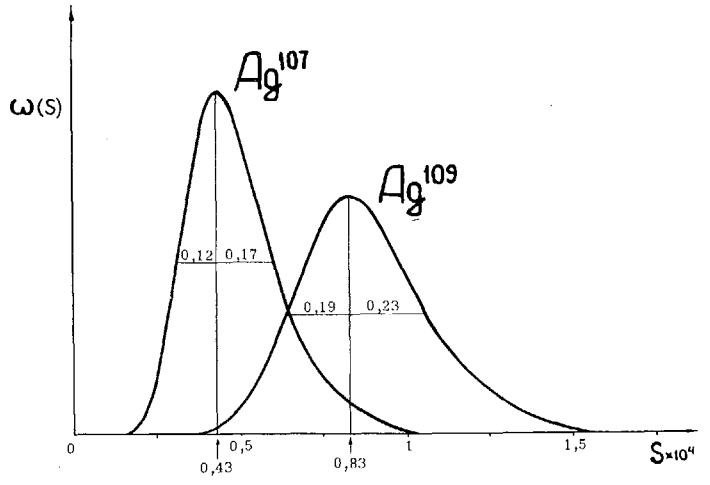

Рис. 10. Распределение силовых функций серебра-107 и серебра-109.

Как уже указывалось, отбрасывание 18 уровней серебра-107 и 13 уровней серебра-109 с $2g\Gamma_n^0 \leq 0{,}02$ мэв в области, где нет пропуска уровней, приводит к наилучшему согласию экспериментальных данных с распределением Портера-Томаса. Приписывая этим уровням орбитальный момент $l = 1$, оценим значения силовых функций серебра-107 и серебра-109 для нейтронной p-волны:

$$S_1 = \frac{1}{2l+1} \cdot \frac{\sum_{i=1}^{n} g\Gamma_{ni}^{l}}{E_{max}}, \qquad (5)$$

где $g\Gamma_n^l = (g\Gamma_n) \cdot E_0^{-2/3} \cdot E_R$. Здесь E_R – энергия, при которой $kR = 1$, k – волновой вектор нейтрона, а R – радиус ядра.

Значения S_1 при $E_{max} = 450$ эв и $E_R \simeq 500$ кэв оказались равными:

$$S_1 = \left(1{,}9\ ^{+1{,}3}_{-0{,}6}\right) \cdot 10^{-4} \qquad \text{для } Ag^{107},$$

$$S_1 = \left(1{,}4\ ^{+1{,}1}_{-0{,}5}\right) \cdot 10^{-4} \qquad \text{для } Ag^{109}.$$

Дисперсия S_1 найдена аналогично дисперсии S_0. Полученные значения S_1 хорошо согласуются с предсказаниями оптической модели ядра [12, 13].

В заключение авторы считают своим приятным долгом поблагодарить Певзнера М.И. и Мостового В.И. за интерес, проявленный к данной работе, а также Стрельникова Е.М. и Марухина В.И. за помощь в измерениях и обработке данных.

ЛИТЕРАТУРА

[1] GARG, J.B., RAINWATER J., HAVENS W.W., Phys. Rev. 137, B547 (1965).
[2] МУРАДЯН Г.В., АДАМЧУК Ю.В., МОСКАЛЕВ С.С., ПТЭ (1966).
[3] HUGHES D.J., SCHWARTZ R.B., BNL-325, 1958.

[4] ГУРЕВИЧ И.И., ПЕВЗНЕР М.И. ЖЭТФ 31, 162 (1956); см. также Nucl. Physics 2, 575 (1956/57).
[5] MICHAUDON A., BERGERE R., COIN A., JOLY R., J. Phys. Rad. 21, 429 (1960).
[6] LYNN J.E., Phys. Rev. Letters 13, 412 (1964).
[7] MURADYAN H.V., ADAMCHUK Yu.V., Nucl. Phys. 68, 549 (1965).
[8] WEISSKOPF V.F., Phys. Today 14, 18 (1961).
[9] BLOCK B., FESHBACH H., Ann. Phys. (N.Y.) 23, 47 (1963).
[10] FUKETA, T., KHAN F.A., HARVEY J.A., ORNL-3425, 1963.
[11] АДАМЧУК Ю.В., МОСКАЛЕВ С.С., МУРАДЯН Г.В. Ядерная физика (1966).
[12] BUCK B., PEREY F., Phys. Rev. Letters 8, 444 (1962).
[13] FIEDELDEY H., FRAHN W., Ann. Phys. (N.Y.) 19, 428 (1962).
[14] PATTENDEN N.J., Доклад на международной конференции по изучению структуры ядра нейтронами. Бельгия, 19 – 23 июля 1965 г. "Nuclear Structure Study with Neutrons", Amsterdam, 1966, p. 533.

НЕЙТРОНОСПЕКТРОСКОПИЧЕСКОЕ ИССЛЕДОВАНИЕ РАЗДЕЛЕННЫХ ИЗОТОПОВ КАДМИЯ

Ю.Г.ЩЕПКИН, Ю.В.АДАМЧУК, Л.С.ДАНЕЛЯН, Г.В.МУРАДЯН
ОРДЕНА ЛЕНИНА ИНСТИТУТ АТОМНОЙ ЭНЕРГИИ им. И.В.КУРЧАТОВА, МОСКВА СССР

Abstract — Аннотация

NEUTRON SPECTROSCOPIC STUDY OF SEPARATED CADMIUM ISOTOPES. A time-of-flight method was used with the neutron spectrometers of the I. V. Kurchatov Institute of Atomic Energy to measure total neutron cross-sections, radiative capture cross-sections and self-indication of separated cadmium isotopes in the incident-neutron energy range up to 1.5 keV. The resolution in the total cross-section measurements was ~ 10 ns/m and in the radiative capture and self-indication measurements it was ~ 25 ns/m.

Level parameters were determined; strength function values, S_0, and average spacing between levels were calculated. The spin value was determined for a number of even-odd isotope levels.

НЕЙТРОНОСПЕКТРОСКОПИЧЕСКОЕ ИССЛЕДОВАНИЕ РАЗДЕЛЕННЫХ ИЗОТОПОВ КАДМИЯ. На нейтронных спектрометрах ИАЭ им. И.В.Курчатова методом времени пролета проведены измерения полного нейтронного сечения, сечения радиационного захвата и самоиндикации разделенных изотопов кадмия в области энергии падающих нейтронов до ~1,5 кэв. Разрешающая способность в измерениях полных сечений составила ~10 нсек/м, в измерениях радиационного захвата и самоиндикации ~25 нсек/м.

Определены параметры уровней, вычислены значения S_0-силовых функций и средние расстояния между уровнями. Для ряда уровней четно-нечетных изотопов определено значение спина.

Изучение разделенных изотопов кадмия проводилось на нейтронных спектрометрах ИАЭ с использованием линейного ускорителя электронов в качестве пульсирующего источника нейтронов. Длительность нейтронного импульса составила 0,25 мксек, частота следования импульсов – 122 гц, ширина канала 2048-канального анализатора – 0,25 мксек.

Измерения полных нейтронных сечений велись на спектрометре с пролетным расстоянием 37 м и разрешением ~10 нсек/м [1], в измерении радиационного захвата и самоиндикации – 15 м и соответственно ~25 нсек/м [2]. Регистрация нейтронов в измерениях полных сечений осуществлялась сцинтилляционным детектором с двумя кристаллами NaJ (Tl) диаметром 150 мм по реакции $B^{10}(n, \gamma)$. Образцы изотопов кадмия были выполнены в виде металлических дисков диаметром 50 мм. Вес и изотопный состав исследуемого кадмия приведены в табл.1.

Измерения полных сечений проводились для образцов кадмия-111 и кадмия-113. Образец кадмия-111 содержал $n = 0{,}00415$ атомов/барн основного изотопа, а кадмия-113 – $n = 0{,}0143$ атомов/барн. Обработка результатов проводилась методом площадей с учетом интерференции между потенциальным и резонансным рассеянием [3]. При этом использовались различные комбинации толщин образцов, помещенных на пути нейтронного пучка (n_T) и в детекторе (n_D): для кадмия-111 $n_T = 2n_D = 0{,}00105$ атомов/барн, $n_T = n_D = 0{,}0021$ атомов/барн; для кадмия-113

ТАБЛИЦА 1. ВЕС И ИЗОТОПНЫЙ СОСТАВ КАДМИЯ

Основной изотоп	Вес вещества, г	Содержание изотопов кадмия, %							
		106	108	110	111	112	113	114	116
Cd^{110}	2,34	0,4	2,7	65	14,5	7,6	3,0	5,8	1,0
Cd^{111}	12,43	0,3	0,5	13,6	61,3	16,4	3,2	4,0	0,7
	11,09	6,2	0,3	11,5	66,7	14,4	2,5	3,9	0,5
Cd^{112}	13,1	0,2	0,4	2,1	13,1	69,6	4,8	8,7	1,1
Cd^{113}	53,36	0,1	0,2	3,2	7,0	11,7	53,6	21,9	2,3
	43,73	0,1	0,2	3,2	7,4	11,8	55,5	19,4	2,4
Cd^{114}	10,31	0,1	0,1	0,5	0,6	1,9	6,4	88,5	1,9
	16,87	0,7	0,6	0,9	1,4	1,3	2,0	91,6	1,5
Cd^{116}	42,71	0,2	0,2	2,6	3,1	6,5	3,2	11,8	72,4

$n_T = n_D = 0{,}000812$ атомов/барн, $n_T = 2n_D = 0{,}00162$ атомов/барн, $n_T = 4n_D = 0{,}0032$ атомов/барн, $n_T = n_D = 0{,}0032$ атомов/барн.

Измерения сечения радиационного захвата проведены с набором различных толщин образцов для кадмия-110, кадмия-111, кадмия-112, кадмия-113, кадмия-114 и кадмия-116. Площадь под кривой резонансного захвата нейтронов A_γ определялась, исходя из суммы $\sum_i N_i$ в области резонанса, где N_i – число отсчетов в i-том канале анализатора. Коэффициенты пропорциональности между A_γ и $\sum_i N_i$ вычислялись по резонансам с известными параметрами (эти калибровочные резонансы для каждого изотопа отмечены в табл.2 звездочкой).

Основная ошибка в измерениях сечений радиационного захвата связана с изменением эффективности детектора к регистрации акта захвата от резонанса к резонансу и составляет ~15%. Вклад в сумму $\sum_i N_i$, вносимый нейтронами, захваченными в образец после рассеяния, составляет величину не более 2% и нами не учитывался. На рисунках 1, 2 и 3 приведены зависимости $g\Gamma_n$ от Γ, вычисленные из измерений полного нейтронного сечения, сечения радиационного захвата и измерений самоиндикации для уровней кадмия-113 при 193,5 эв, 415,8 эв и 512 эв. При помощи таких же графиков находились параметры остальных уровней – нейтронная, радиационная ширины и спин уровня. Возможность определения радиационной ширины уровня Γ_γ и спина уровня I зависит от соотношения нейтронной Γ_n и радиационной Γ_γ ширин и от точности измерения.

Для кадмия-113 значения спинов определены для тринадцати уровней, из которых два уровня имеют спин I = 0 и 11 уровней имеют спин I = 1. Величины спинов для уровней кадмия-113 при энергиях 84,9 эв, 108,4 эв, 193,5 эв, 216,0 эв и кадмия-111 при энергии 164,2 эв согласуются с ранее полученными значениями [4].

Всего идентифицирован 61 уровень в области энергий до ~1500 эв. На рис.4 приведена зависимость суммарного числа уровней кадмия, определенная из измерений отдельных изотопов. Параметры найденных уровней приведены в таблице 2. В эту таблицу включены также значения спинов уровней кадмия-113 при энергиях 0,178 эв, 18,35 эв и 63,7 эв,

ТАБЛИЦА 2. ПАРАМЕТРЫ НАЙДЕННЫХ УРОВНЕЙ КАДМИЯ

Изотопы	E_0, эв	ΔE_0, эв	I	Γ_n, мэв	$\Delta\Gamma_n$, мэв	Γ_n^0, мэв	Γ_γ, мэв	$\Delta\Gamma_\gamma$, мэв
Cd^{110}	89,6	0,3		120	20,7	12,7		
$j_0=0$	372	3						
Cd^{111}	27,5*	0,2		7,70	0,24	1,47		
$j_0=1/2$	69,5	0,5		0,136	0,016	0,016		
	86,3	0,3		4,0	1,0	0,43		
	99,6	0,3	(1)	13,0	1,0	1,30	72	26
	103,2	1,0		1,44	0,14	0,14		
	115,0	1,0		0,66	0,20	0,061		
	138,2	0,5		14,0	1,4	1,19		
	164,2	0,5	1	59,0	4,0	4,6	104	12
	225,5	0,6		50,0	12,0	3,34		
	233,8	0,7	0	230	20	15,0	160	30
	275,8	0,8		34	6	2,05		
	314	3		5,4	0,8	0,305		
	332,2	1,2		12,0	3,0	0,66		
	356,5	1,3	(1)	49,0	6,0	2,60	93	36
	389,5	1,5	(0)	124	16	6,28	90	25
	439,0	1,7		24	10	1,14		
	480	6		14	6	0,64		
	541,0	2,4		126	30	5,41		
	578,0	2,7	(0)	296	20	12,3	150	30
	606,0	2,8		90	30	3,65		
	625,0	3,0		104	40	4,16		
Cd^{112}	66,7*	0,1		10	2	1,23		
$j_0=0$	83,3	0,6		0,76	0,2	0,083		
	226,6	0,6		25	8	1,66		
	444,3	1,7		60	15	2,85		
	743	10		180	70	6,6		
	935	15		220	70	7,2		
	1125	20		600	200	17,9		
	1450	40						
Cd^{113}	0,178	0,002	1	0,65	0,02	1,5	113	5
$j_0=1/2$	18,35*	0,10	1	0,200	0,012	0,0467		
	56,3	0,3		0,106	0,016	0,014		
	63,7	0,1	1	3,1	0,4	0,39	110	50
	84,90	0,15	1	29	2	3,15	121	17
	108,4	0,2	(1)	12	3	1,15	128	40
	144,5	1,5		6,8	1,6	0,56		
	158,9	0,4		19	5	1,51		
	193,5	0,5	0	224	8	15,50	112	18
	216,0	0,6	1	33	3	2,24	114	20
	261,5	0,8	1	45	5	2,78	106	16
	270,0	0,9	0	64	8	3,89	124	20
	292,2	1,0		11,4	2,4	0,66		
	415,8	1,6	1	140	10	6,85	116	18
	433,8	1,7	1	36	7	1,73	110	27
	503,0	2,0	(1)	80	20	3,55	95	30
	527,0	2,3	1	44	9	1,91	100	30
	552,0	2,6	1	137	8	5,83	110	20
	625,0	3,0		80	16	3,2		
	675,0	3,3		190	50	7,3		
	724	10	(1)	53	13	1,97		
	858	5	(1)	660	130	22,5		

Таблица 2 (продолжение)

Изотопы	E_0, эв	ΔE_0, эв	I	Γ_n, мэв	$\Delta\Gamma_n$, мэв	Γ_n°, мэв	Γ_γ, мэв	$\Delta\Gamma_\gamma$, мэв
Cd^{114} $j_0=0$	120,0*	0,2		60	6	5,47		
	226	2		1,8	0,6	0,12		
	394,1	1,5		760	60	38,3		
	673	12		220	170	8,5		
	756	10		140	60	5,1		
	970	15						
	1107	22		1500	800	45		
Cd^{116} $j_0=0$	29,3	0,2		0,042	0,01	0,0078		

определенных в исследованиях спектра гамма-лучей захвата методом сложения совпадений [5]. Из-за недостаточного количества вещества значение спина для кадмия-111 определено только для 6 уровней. Величина радиационной ширины определялась по известным графикам зависимости $A_\gamma/\Gamma_\gamma = f(n\sigma_0, \Gamma/\Delta)$ [6] или по разности Γ и Γ_n.

Для четно-четных изотопов параметры уровней определялись в предположении $\Gamma_\gamma = 100 \div 50$ мэв.

Полученные значения параметров уровней использовались для вычисления наиболее вероятных значений силовых функций S* и наиболее вероятных значений средних расстояний между уровнями D* [7]. Для нахождения среднего расстояния между уровнями $D_{прив.}$, приведенного к одной энергии возбуждения U = 6,5 Мэв, использовалась статистическая формула плотности уровней [8]. Значения S*, D* и $D_{прив.}$ приведены в табл.3. Там же представлены значения средних расстояний между уровнями $\overline{D} = \Delta E/n$ и значения $\overline{S} = \Sigma 2g\Gamma_n^\circ/2\Delta E$. Для кадмия-111 и кадмия-113 величины $\overline{D}$ находились независимо от спина с учетом всех уровней, входящих в энергетический интервал.

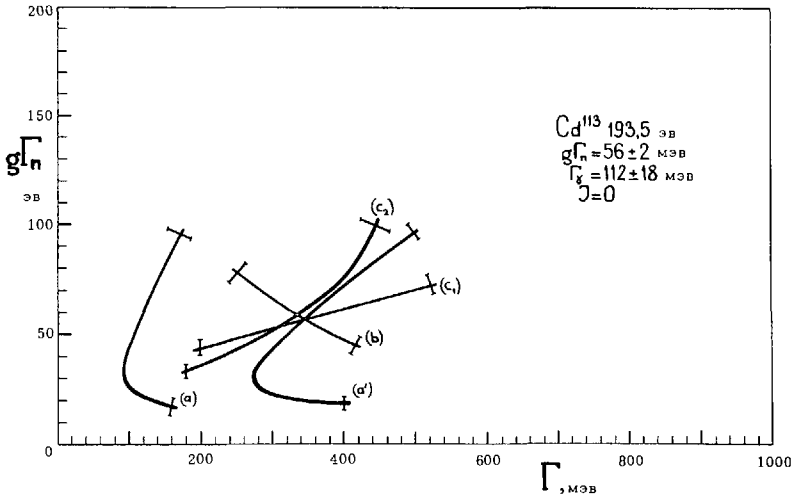

Рис. 1. Зависимость $g\Gamma_n$ от Γ для уровня кадмия-113 при $E_0 = 193,5$ эв: (a) – радиационный захват нейтронов с образцом n = 0,00122 ат/барн в предположении I = 1; (a') – тоже в предположении I = 0; (b) – измерение полного сечения с образцом n = 0,0143 ат/барн; (c_1) – самоиндикация с образцами $n_T = n_D = 0,00082$ ат/барн; (c_2) – самоиндикация с образцами $n_T = n_D = 0,0032$ ат/барн.

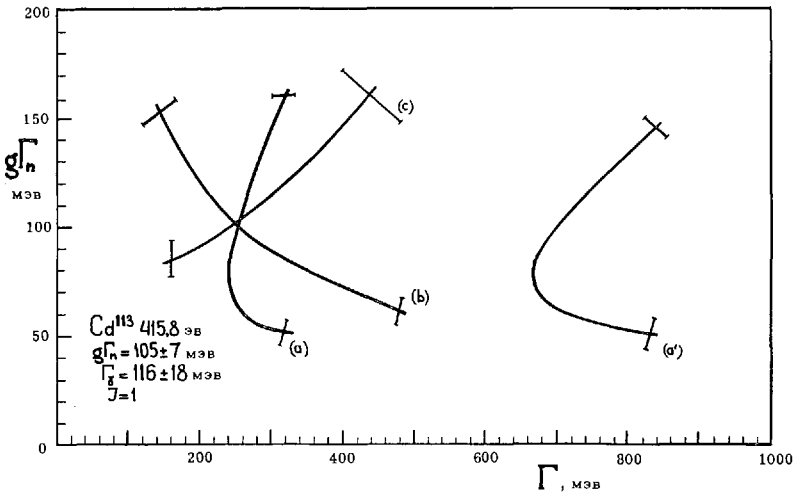

Рис. 2. Зависимость $g\Gamma_n$ от Γ для уровней кадмия-113 при $E_0 = 415{,}8$ эв: (a) – радиационный захват нейтронов с образцом $V_n = 0{,}00122$ ат/барн в предположении $I = 1$; (a') – тоже в предположении $I = 0$; (b) – измерение полного сечения с образцом $n = 0{,}0143$ ат/барн; (c) – самоиндикация с образцами $n_T = n_D = 0{,}0032$ ат/барн.

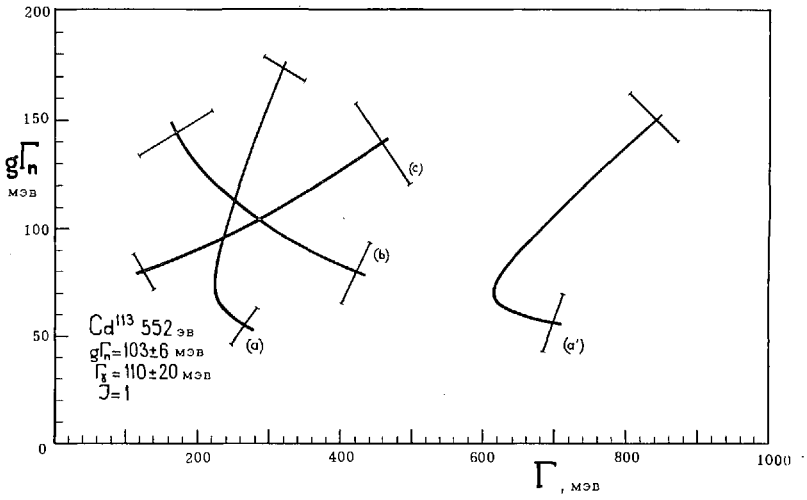

Рис. 3. Зависимость $g\Gamma_n$ от Γ для уровней кадмия-113 при $E_0 = 552$ эв: (a) – радиационный захват нейтронов с образцом $n = 0{,}00122$ ат/барн в предположении $I = 1$; (a') – тоже в предположении $I = 0$; (b) – измерение полного сечения с образцом $n = 0{,}0143$ ат/барн; (c) – самоиндикация с образцами $n_T = n_D = 0{,}0032$ ат/барн.

Определение S* для кадмия-114 приводилось без исключения значений Γ_n° для двух последних уровней, так как они получены с большой неопределенностью. По этой же причине при вычислении S* и $\overline{S}$ для кадмия-113 не учитывался уровень при энергии 858 эв.

Кроме данных, которые включены в таблицу 2, для ряда резонансов определены значения полной ширины уровней Γ для кадмия-111 при 27,5 эв и 138,2 эв, кадмия-112 при 66,7 эв, кадмия-113 при 63,7 эв и

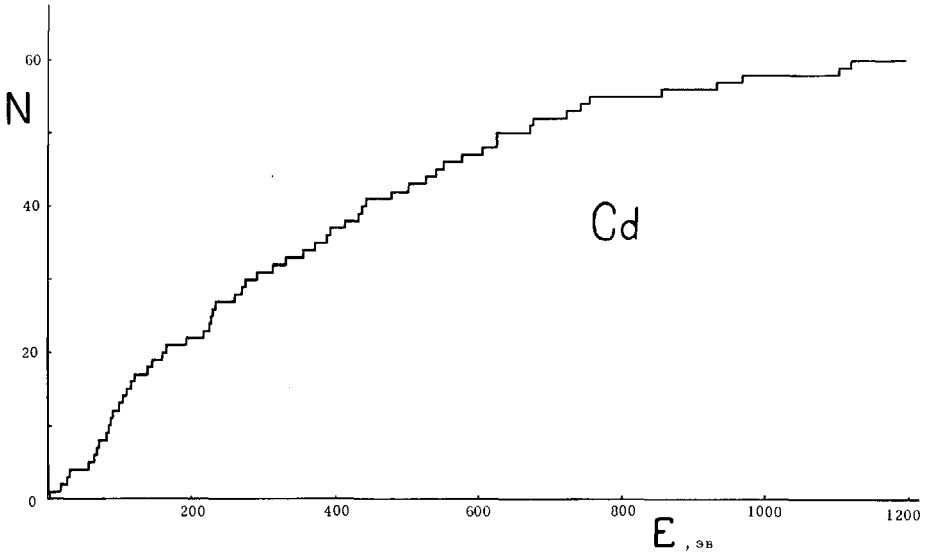

Рис. 4. Зависимость суммарного числа уровней изотопного кадмия от энергетического интервала.

кадмия-114 при 120,1 эв, равные соответственно 110 ± 10 мэв, 110 ± 40 мэв, 110 ± 30 мэв, 115 ± 50 мэв и 110 ± 20 мэв.

Значения силовых функций кадмия-111, кадмия-113 и кадмия-114 в пределах ошибок согласуются с предсказаниями оптической модели. Обращает на себя внимание довольно низкое значение силовой функции кадмия-112, равное $S^* = 0{,}26 \cdot 10^{-4}$, что, по-видимому, можно объяснить, исходя из трехквазичастичного взаимодействия [9].

В заключение авторы выражают благодарность Е.М.Стрельникову и Лунину А.Я. за помощь в измерениях и обработке данных.

ТАБЛИЦА 3. ЗНАЧЕНИЯ S*, D* И D.

Изотоп	D*, эв	$D_{прив}$, эв	$\overline{D}$, эв	$S^* \cdot 10^4$	$\overline{S} \cdot 10^4$
Cd^{111}	–	600	26 (E = 400 эв)	–	$0{,}46^{+0{,}29}_{-0{,}15}$
Cd^{112}	198 (E = 1460 эв)	2,8		$0{,}26^{+0{,}27}_{-0{,}12}$	$0{,}35^{+0{,}38}_{-0{,}16}$
Cd^{113}	25,8 (E = 300 эв) I = 1	380	24,5 (E = 300 эв)	$0{,}75^{+0{,}5}_{-0{,}28}$ I = 1	$0{,}50^{+0{,}26}_{-0{,}16}$
Cd^{114}	157 (E = 1110 эв)	1,0		$0{,}66^{+0{,}93}_{-0{,}34}$	$0{,}91^{+1{,}25}_{-0{,}47}$

Примечание: В скобках указан энергетический интервал, в котором определялась приводимая величина.

ЛИТЕРАТУРА

[1] МУРАДЯН Г.В., АДАМЧУК Ю.В., МОСКАЛЕВ С.С., ПТЭ (1966).
[2] ДАНЕЛЯН Л.С., ЕФИМОВ Б.В. "Атомная энергия", 14, 264 (1963).
[3] МУРАДЯН Г.В. Материалы рабочего совещания по взаимодействию нейтронов с ядрами (9 – 12 июня 1964 г.) Препринт ОИЯИ 1845, Дубна, 1965, стр. 45.
[4] HUGHES, D., J. Nucl. Energy 1 (1955) 237.
[5] BOLLINGER, L., COTE, R., Bull. Am. Phys. Soc. 5 (1960) 294.
[6] HUGHES, D., MAGURNO, B., BRUSSEL, M., BNL-325, Suppl. 1., 1960.
[7] MURADYAN, H.V., ADAMCHUK, Yu.V., Nucl. Phys. 68 (1965) 549.
[8] АДАМЧУК Ю.В., СТРУТИНСКИЙ В.М. Доклад на конференции по структуре ядер, Кингстон, Канада, 1960; Препринт №94, ИАЭ, 1960.
[9] BLOCK, B., FESHBACH, H., Ann. Phys. (N.Y.) 23 (1963) 47.

ПОЛНЫЕ НЕЙТРОННЫЕ СЕЧЕНИЯ ТЯЖЕЛЫХ ЧЕТНО-ЧЕТНЫХ ИЗОТОПОВ ОЛОВА В ОБЛАСТИ ЭНЕРГИЙ ДО 10 кэв

Ю.В.АДАМЧУК, С.С.МОСКАЛЕВ,
Г.В.МУРАДЯН
ОРДЕНА ЛЕНИНА ИНСТИТУТ АТОМНОЙ ЭНЕРГИИ им.И.В.КУРЧАТОВА, МОСКВА СССР

Abstract — Аннотация

TOTAL NEUTRON CROSS-SECTIONS OF HEAVY EVEN-EVEN ISOTOPES OF TIN IN THE ENERGY REGION UP TO 10 keV. A study was made of the total neutron cross-sections of heavy, even-even isotopes of tin. Level parameters were determined, taking into account the interference between resonance and potential scattering. The most likely values of the strength functions of ^{116}Sn, ^{118}Sn, ^{120}Sn, ^{122}Sn and ^{124}Sn are $0.46^{+0.41}_{-0.19}$, $0.36^{+0.29}_{-0.15}$, $0.12^{+0.09}_{-0.045}$, $0.49^{+0.62}_{-0.22}$ and $0.13^{+0.22}_{-0.08}$ respectively (10^4). These values are higher than the previously published experimental data.

ПОЛНЫЕ НЕЙТРОННЫЕ СЕЧЕНИЯ ТЯЖЕЛЫХ ЧЕТНО-ЧЕТНЫХ ИЗОТОПОВ ОЛОВА В ОБЛАСТИ ЭНЕРГИЙ ДО 10 кэв. Исследованы полные нейтронные сечения тяжелых четно-четных изотопов олова. Определены параметры уровней с учетом интерференции между резонансным и потенциальным рассеянием. Наиболее вероятные значения силовых функций Sn^{116}, Sn^{118}, Sn^{120}, Sn^{122} и Sn^{124} равны соответственно (10^4): $0{,}46^{+0{,}41}_{-0{,}19}$, $0{,}36^{+0{,}29}_{-0{,}15}$, $0{,}12^{+0{,}09}_{-0{,}045}$, $0{,}49^{+0{,}62}_{-0{,}22}$, $0{,}13^{+0{,}22}_{-0{,}08}$. Эти величины лежат выше опубликованных ранее экспериментальных данных.

Интерес к изучению полных нейтронных сечений и силовых функций изотопов олова вызван тем, что для этих изотопов значения силовых функций, найденные экспериментально, расходятся со значениями, вычисленными по оптической модели ядра. Так, по данным работы [2] силовые функции олова-120, олова-122 и олова-124 соответственно равны (10^4): $0{,}09 \pm 0{,}04$; $0{,}20 \pm 0{,}10$; $0{,}04 \pm 0{,}02$. Для объяснения столь малых значений силовых функций Фешбах [3] включил в рассмотрение трехчастичное взаимодействие, т.е. взаимодействие "две частицы дырка", как поправку к оптическому потенциалу. Варьируя параметр теории Δ, можно получить различные значения силовых функций. В случае изотопов Sn наилучшее согласие теории с экспериментом получается при $\Delta = 3$ Мэв [2, 4]. Однако следует отметить, что в [2] экспериментально определенные значения силовых функций имеют большие ошибки. Кроме того, при определении Γ_{ni}, исходя из которых находятся силовые функции, не принималась во внимание интерференция между резонансным и потенциальным рассеянием.

В измерениях настоящей работы в отличие от [2]:

а) расширен измеряемый энергетический интервал, благодаря чему уменьшена статистическая ошибка в значении силовой функции;

б) параметры уровней определены с учетом интерференции между резонансным и потенциальным рассеянием;

в) найдены наиболее вероятные значения силовых функций [5].

ТАБЛИЦА 1. ИЗОТОПНЫЙ СОСТАВ ОБРАЗЦОВ И ЧИСЛО АТОМОВ ТЯЖЕЛЫХ ЧЕТНО-ЧЕТНЫХ ИЗОТОПОВ ОЛОВА НА 1 см^2

Осн. изотоп	Вес образца, г	Процентное содержание изотопов олова в образцах									
		112	114	115	116	117	118	119	120	122	124
Sn^{116}	8,15	<0,1	<0,1	0,20	92,23	3,06	3,90	0,14	0,47	<0,1	<0,1
Sn^{116}	18,21	0,2	0,4	0,7	66,9	12,2	11,3	1,4	6,0	0,4	0,5
Sn^{118}	28,65	0,24	0,20	0,14	2,46	2,98	82,29	4,12	6,43	0,64	0,50
Sn^{120}	11,02	<0,05	<0,05	<0,05	<0,05	0,4	0,6	2,5	96,5	<0,1	<0,1
Sn^{120}	246,56	0,09	0,09	0,08	0,59	0,55	6,18	2,70	86,52	2,20	1,00
Sn^{122}	21,51	<0,1	<0,1	<0,1	0,68	0,99	1,48	1,14	18,71	70,30	6,70
Sn^{124}	19,41	0,3	0,2	0,2	0,7	0,6	3,2	1,0	3,5	2,5	87,8
Sn^{124}	62,62	0,10	0,16	0,15	2,42	1,56	3,81	2,25	5,59	4,63	79,33

Первое и последнее обстоятельство уточняют силовые функции. Учет интерференции приводит к росту силовой функции.

Измерения полных нейтронных сечений проводились на нейтронном спектрометре по времени пролета, на базе линейного ускорителя электронов ИАЭ. Пролетное расстояние составляло 108 м. Разрешение спектрометра было порядка 6 нсек/м. Более подробно аппаратура описана в работах [6]. Помимо полных сечений в некоторых случаях дополнительно проводились измерения радиационного захвата.

В качестве образцов использовались металлические диски изотопов олова диаметром 50 и 70 мм. Изотопный состав образцов и число атомов тяжелых четно-четных изотопов олова на 1 см^2 приведены в табл.1.

В целях проведения правильной идентификации изотопной принадлежности уровней были измерены полные нейтронные сечения всех изотопов олова.

Параметры обнаруженных уровней определялись по методу площадей. Для учета интерференции использовалась процедура симметризации [1]. Значение параметров резонансных уровней тяжелых четно-четных изотопов олова приведено в табл.2. Звездочкой помечены уровни, параметры которых взяты из работы [2]. Из данных по параметрам уровней найдены наиболее вероятные значения силовых функций S*, наиболее вероятные значения средних расстояний между уровнями D* [5]. Для нахождения среднего расстояния между уровнями $D^*_{прив}$, приведенного к одной энергии возбуждения U = 6,5 Мэв, использовалась статистическая формула плотностей уровней [7]. В табл.3 приведены S*, D*, $D^*_{прив}$, а также значения силовой функции, определенные в работе [2] – S' и теоретическое значени $S_{теор}$ по вычислениям с учетом трехчастичного взаимодействия при $\Delta = 3$ Мэв [4].

В этой же таблице приведены значения числа уровней n и числа промежутков между уровнями m, которые использовались при вычислении S* и D*.

Для сравнения в таблице приведены также значения силовых функций, вычисленные по методу гистограмм, исходя из наших данных $S_{гист}$.

Анализируя полученные данные, можно сделать следующие выводы:

1. Полученные нами значения силовых функций лежат систематически выше ранее известных значений S'. Частично это расхождение можно

ТАБЛИЦА 2. ЗНАЧЕНИЕ ПАРАМЕТРОВ РЕЗОНАНСНЫХ УРОВНЕЙ ТЯЖЕЛЫХ ЧЕТНО-ЧЕТНЫХ ИЗОТОПОВ ОЛОВА

E_0, эв	Γ_n, мэв	Γ_n^0, мэв
	Sn^{116}	
111,2*	66 ± 5%	6,26
148,2*	3 ± 12%	0,25
652*	30 ± 20%	1,17
750*	4,3 ± 20%	0,16
981*	16 ± 35%	0,51
1337*	300 ± 25%	8,20
1557 ± 8	3200 ± 300	81,01
1802 ± 10	240 ± 100	5,65
3380 ± 15	3900 ± 1000	67,01
3460 ± 15	1400 ± 500	23,77
4640 ± 20	4000 ± 1000	58,74
	Sn^{118}	
45,75*	0,72 ± 5%	0,106
289*	0,50 ± 30%	0,029
307,5*	0,80 ± 10%	0,046
343,9*	2,3 ± 10%	0,124
360 ± 2	300 ± 20	15,79
773 ± 5	900 ± 100	32,37
1589 ± 7	330 ± 60	8,28
1710*	33 ± 40%	0,80
2984 ± 16	1000 ± 300	18,32
3470 ± 20	1700 ± 300	28,81
3960 ± 25	1100 ± 500	17,40
4725 ± 30	6300 ± 2000	91,65
	Sn^{120}	
364,8*	2,2 ± 12%	0,115
426,9*	26 ± 15%	1,26
922*	23 ± 50%	0,76
953*	90 ± 30%	2,92
1289*	39 ± 80%	1,09
1428*	140 ± 70%	3,70
1718 ± 10	100 ± 50	2,41
2850 ± 10	250 ± 80	4,70
3135 ± 20	500 ± 200	8,93
3445 ± 20	850 ± 250	14,45
3855 ± 25	1000 ± 300	16,10
5290 ± 30	1500 ± 300	20,60
9000 ± 80	6000 ± 2500	63,20
9520 ± 90	4500 ± 1500	46,00
12670 ± 110	6000 ± 3000	53,30

Таблица 2 (продолжение)

E_0, эв	Γ_n, мэв	Γ_n^0, мэв
	Sn^{122}	
106,9%	0,77 ± 10%	0,074
259,9*	1,75 ± 7%	0,108
1760 ± ?	4100 ± 500	97,61
3450 ± 25*	120 ± 80%	2,04
5400 ± 80	5000 ± 2000	68,03
6880 ± 30	23000 ± 4000	277,11
	Sn^{124}	
61,95*	11,0 ± 5%	1,40
579*	1,5 ± 30%	0,062
950*	6 ± 50%	0,19
2380 ± 20	2700 ± 100	55,32
3390 ± 40	1400 ± 600	24,01
5360 ± 40*	700 ± 100%	9,52
9960 ± 120	8600 ± 400	86,01

ТАБЛИЦА 3. ЗНАЧЕНИЯ СИЛОВЫХ ФУНКЦИЙ

Изотоп	$\overline{\Gamma_n^0}$, Мэв	D*, эв	$D^*_{прив}$, эв; U = 6,5 Мэв	n	m	$S^* \cdot 10^4$	$S_{гист} \cdot 10^4$	$S' \cdot 10^4$	$S_{теор} \cdot 10^4$
Sn^{116}	12,9	249	395	8	7	$0{,}46^{+0{,}41}_{-0{,}19}$	0,58	0,37 ± 0,14	0,41
Sn^{118}	17,9	562	247	12	11	$0{,}36^{+0{,}29}_{-0{,}15}$	0,42	0,32 ± 0,12	0,38
Sn^{120}	5,2	406	100	11	10	$0{,}12^{+0{,}09}_{-0{,}045}$	0,20	0,09 ± 0,04	0,095
Sn^{122}	74,2	1320	108	6	5	$0{,}49^{+0{,}62}_{-0{,}22}$	0,54	0,20 ± 0,10	0,081
Sn^{124}	22,8	1360	94	4	3	$0{,}13^{+0{,}22}_{-0{,}08}$	0,15	0,04 ± 0,02	0,086

объяснить учетом интерференции между резонансным потенциальным рассеянием, а также увеличением рассматриваемого энергетического интервала, вследствие чего уменьшена статистическая ошибка.

2. Значение S^* хорошо согласуется с $S_{теор}$ для олова-116, олова-118, олова-120 и олова-124. Для олова-122 наши измерения дают сильное расхождение с $S_{теор}$ при $\Delta = 1$, 2 и 3 Мэв [4].

3. Приведенное расстояние между уровнями $D^*_{прив}$ монотонно убывает с ростом атомного веса. Это связано с удалением от замкнутой оболочки (с числом нейтронов N = 50) по мере роста A.

Отметим, что в нашей работе, как и в работе [2], не проведена идентификация уровней по орбитальному моменту налетающих нейтронов. Не

исключено, что такая идентификация может существенно изменить наши выводы относительно силовых функций.

В заключение авторам приятно поблагодарить Е.М.Стрельникова и В.Е.Чарнко за помощь в измерениях и обработке данных.

ЛИТЕРАТУРА

[1] МУРАДЯН Г.В., Материалы рабочего совещания по взаимодействию нейтронов с ядрами (9 – 12 июня 1964 г.). Препринт ОИЯИ-1845, 1965, стр.45.
[2] FUKETA, T., KHAN, F.A., HARVEY, J.A., ORNL-3425, 1963.
[3] FESHBACH, H., Annal of Physics 5, 357 (1958) and Annal of Physics 19, 287 (1962).
[4] SHAKIN, C., Annal of Physics 22, 54 and 373 (1963).
[5] MURADYAN, H.V., ADAMCHUK, Yu.V., Nucl. Phys. 68, 549 (1965).
[6] MOSKALEV, S.S., MURADYAN, H.V., ADAMCHUK, Yu., Nucl. Phys. 53, 667 (1964). ПЕВЗНЕР М.И., АДАМЧУК Ю.В., ДАНЕЛЯН Л.С., ЕФИМОВ Б.В., МОСКАЛЕВ С.С., МУРАДЯН Г.В., ЖЭТФ 44, 1187 (1963).
[7] АДАМЧУК Ю.В., СТРУТИНСКИЙ В.М., Доклад на международной конференции по структуре ядер в г.Кингстоне. Канада, 1960 г. Препринт ИАЭ-94, 1960.

DISCUSSION

(on papers CN-23/107, CN-23/108 and CN-23/109)

C.H. WESTCOTT: Are the curves of cross-section as a function of energy available for Sn and Cd as well as for Ag, and will the corresponding detailed numerical results be communicated to one of the data centres at Brookhaven, Saclay, Vienna or Obninsk?

G. V. MURADYAN: Data for Sn, Cd and Ag will be sent to Obninsk.

J. JULIEN: We have studied silver in the energy range 300-750 eV and determined the spin for certain resonances. The resolution used was of the order of 0.5 ns/m and the sample employed was natural silver. The values of $g\Gamma_n$ are in agreement with yours. We can detect more levels, because our sample is thicker than yours and our resolution is better. By using the resonance-to-isotope allocation of Harwell and Kurchatov, we found that the strength functions differed somewhat depending on the spin states. The S_0 value for ^{109}Ag and $S = 0$ is about 1.4 times greater than for $S = 1$. The number of resonances analysed, even including those analysed below 300 eV, is not sufficient for us to assume that the strength function varies according to the spin value.

The average spacing $<D>$ for combinations of the two isotopes is of the order of 5.5 eV, and the step curve representing the number of levels as a function of the energy tends towards a parabola for neutron energies above 400 eV. This is probably due to p-resonances, but we were not able to identify them. The distribution of $g\Gamma_n^0$ values does not conform to the Porter-Thomas law, but we cannot give a value S_1 (density function $l = 1$) as it is difficult to distinguish a weak level $l = 0$ from a strong level $l = 1$.

M. MOXON: I would like to confirm the overlapping of levels in ^{107}Ag and ^{109}Ag in the energy region 200 to 600 eV. Also, transmission measurements on natural Sn indicate $\Gamma_n \sim 6$ meV and $\Gamma_\gamma \sim 250$ meV for the resonance at 61.95 eV in ^{124}Sn.

M. NEVE DE MEVERGNIES: Is the identification of p-levels based on statistical considerations, or on some detailed study of individual levels?

G. V. MURADYAN: We identified the p-levels by the relatively small neutron width. We are now planning to identify s and p levels using a moving sample method.

DISPOSITIFS ET PROGRAMMES POUR L'ACQUISITION ET LE TRAITEMENT DES INFORMATIONS DE TEMPS DE VOL

P. RIBON, B. CAUVIN, H. DERRIEN, A. MICHAUDON
ET M. SANCHE
CEA, CENTRE D'ETUDES NUCLEAIRES DE SACLAY, FRANCE

Abstract — Résumé

EQUIPMENT AND PROGRAMMES FOR OBTAINING AND PROCESSING TIME-OF-FLIGHT DATA.
The paper briefly describes the equipment and programmes used for carrying out and interpreting time-of-flight experiments with the Saclay linear accelerator.

- The data can be collected by means of 16-track magnetic tapes, 4096-channel memory blocks or by an on-line CAE-510 computer (maximum of 16364 channels). The CAE-510 computer can also read (on-line) the 4096-channel memory blocks and (out-of-line) the 16-track magnetic tapes. It can also keep a check on whether the experiments are proceeding properly.

- Preliminary data reduction (simple calculations which utilize large amounts of data) can be performed on this computer or on the IBM-7094 computer at the computation centre. The support of the data and the experimental series is strictly admissible by the two computers at both the input and the output sides, which permits some degree of flexibility. For example, the "big" computer can perform certain preliminary data reduction tasks if the "small" one is temporarily overloaded.

- Resonances can be analysed by means of a shape analysis programme based on a least-squares method, which has been in operation for four years. With this programme, which is based on a sum of Breit and Wigner single-level formulas, we can deal with as many as 30 resonances and 1600 experimental points.

- With a multilevel programme for fissionable nuclei, which has just been developed, we can calculate the capture, fission, total and transmission cross-sections for different thicknesses, making allowance for the Doppler effect and the experimental resolution. The programme can deal with 30 resonances and 1700 experimental points. A subsequent refinement, which is now being worked out, will permit us to compare these results with experimental findings.

The paper includes various examples illustrating the application of these programmes.

DISPOSITIFS ET PROGRAMMES POUR L'ACQUISITION ET LE TRAITEMENT DES INFORMATIONS DE TEMPS DE VOL. Les auteurs décrivent succinctement les dispositifs et programmes destinés à faciliter l'exécution et l'interprétation des expériences de temps de vol effectuées auprès de l'accélérateur linéaire de Saclay.

- L'acquisition des informations peut être effectuée par bandes magnétiques à 16 pistes, par blocs mémoires de 4096 canaux, par un calculateur CAE 510 en ligne (16 364 canaux au maximum). Ce dernier peut également lire, en ligne, les blocs mémoires à 4096 canaux et, hors ligne, les bandes magnétiques à 16 pistes. Il peut également contrôler la bonne marche des expériences.

- Le prédépouillement (calculs simples mettant en œuvre un grand nombre d'informations) peut être effectué sur ce calculateur ou sur le calculateur IBM 7094 du centre de calculs. Le support des données et des séries expérimentales est rigoureusement admissible par les deux calculateurs aussi bien en entrée qu'en sortie, ce qui permet une certaine souplesse: le « grand » calculateur peut effectuer, par exemple, certaines opérations du prédépouillement si le « petit » calculateur est momentanément surchargé.

- Un programme d'analyse de forme par une méthode de moindres carrés, en service depuis quatre ans, permet l'analyse des résonances. Fondé sur une somme de formules de Breit et Wigner à un niveau, il permet de traiter jusqu'à 30 résonances et 1600 points expérimentaux.

- Un programme multiniveaux, pour les noyaux fissiles, vient d'être mis au point; il permet de calculer les sections efficaces de capture, de fission, totale et la transmission pour différentes épaisseurs, en tenant compte de l'effet Doppler et de la résolution expérimentale. Il peut traiter jusqu'à 30 résonances et 1700 points expérimentaux. Un développement ultérieur, en cours de mise au point, permettra la comparaison de ces résultats avec l'expérience.

Les auteurs donnent différents exemples d'application de ces programmes.

INTRODUCTION

Un des principaux problèmes qui se posent aux physiciens faisant des expériences par la méthode du temps de vol avec des neutrons d'énergie «intermédiaire» (quelques eV à quelques centaines de keV) est celui de l'acquisition des données et de leur traitement. En effet, l'amélioration des résolutions obtenues par temps de vol a pour conséquence l'augmentation du nombre de «canaux», celle du nombre de résonances pouvant être résolues, et rend possible des expériences qui ne l'étaient pas il y a quelques années.

A titre d'exemple, l'étude de la section efficace totale du ^{239}Pu jusqu'à 700 eV, récemment effectuée à Saclay, a exigé l'acquisition et le traitement de plus de 500 000 points. Pour la section efficace de fission jusqu'à 300 eV, le nombre d'informations accumulées peut être estimé à plus de 60 000. Enfin, le nombre de résonances que nous avons pu analyser est de 290 en section efficace totale (transmission), et de 100 en fission. En dehors des problèmes de recouvrement des résonances, il ne saurait être question de déterminer leurs paramètres par des méthodes manuelles.

Dans ce mémoire, nous décrivons d'abord les méthodes utilisées pour l'acquisition des informations, puis leur réduction (traitement préliminaire pour condenser toutes ces données en un résultat normalisé). Nous décrivons ensuite quelques programmes utilisés pour l'analyse des résultats.

1. ACQUISITION DES INFORMATIONS

Les moyens dont nous disposons correspondent en fait à des besoins différents. Ils utilisent tous les mêmes types de codeur de temps de vol, à savoir:

- Codeur HC25 (Intertechnique) [1 à 3], à largeur de canal variable par programme, par bonds d'un facteur 2, de 50 à 3200 ns. Le nombre de canaux est égal à 2^n, n étant compris entre 9 (512 canaux) et 16 (65 536 canaux).
- Codeur HC50 [4], également à largeur de canal variable s'il est associé aux programmateurs H52 et H55. Dans un même programme, la largeur d'un canal peut être égale à 1, 2, 4 ou 8 fois la largeur de base, celle-ci pouvant être égale à 10, 20, 40, 80, 160, 320, 640 ou 1280 ns. Le nombre maximal de canaux est de 65 536.
- Codeur HC51, variante du HC50 [5], dont nous disposerons d'ici un an. Ce codeur a le même nombre de canaux que le HC50, la largeur de base variant de 1 à 128 ns, mais il n'est possible d'obtenir une largeur de canal variable dans un même programme (avec programmateur H52 et H55) que pour les largeurs de base supérieures à 8 ns.

Ces différents codeurs sont connectés, soit directement, soit par l'intermédiaire de mémoires tampons, types BM10, temps mort 1,5 μs, ou BM11, temps mort 0,1 μs, [6, 7] aux mémoires d'acquisition dont les types sont décrits dans les paragraphes suivants.

1.1. Bandes magnétiques à 16 pistes (temps pur)

Elles sont toujours commandées par l'intermédiaire d'une mémoire tampon. L'enregistrement est du type NRZ avec une piste pour le contrôle de parité. Les 15 pistes utiles permettent d'accumuler 32 768 canaux en temps de vol au plus avec plusieurs détecteurs (par exemple quatre détecteurs et 8192 canaux). La longueur des bandes magnétiques est de 2200 m, et elles peuvent comporter 80 digits par cm (200 par in.), soit au total, si elles sont remplies à leur densité maximale, $\simeq 17 \cdot 10^6$ informations par bande. Afin d'éviter les pertes, très difficiles à corriger, nous limitons la densité à l'enregistrement à moins de la moitié de la densité maximale. Pour qu'une même bande dure près de 24 h, ou plus, il faut que le taux de comptage soit inférieur à 100 coups/s. Enfin il est possible, en inscrivant des «titres» sur la bande, d'enregistrer des informations correspondant à différentes phases d'une expérience et de les distinguer à la lecture. Cela peut être utile pour des expériences automatisées.

La lecture de bandes magnétiques peut être ensuite effectuée soit sur des blocs mémoires BM96 (voir 1.2), soit sur le calculateur CAE 510 (voir 1.4).

En résumé, la bande magnétique est utilisée pour des expériences à faible taux de comptage pouvant mettre en œuvre un grand nombre de canaux. Mais la lecture des bandes magnétiques est une sujétion.

1.2. Bandes magnétiques à 16 pistes (multiparamétrique) [8, 9]

L'enregistrement est également du type NRZ avec piste de contrôle de parité. Il est séquentiel, c'est-à-dire que l'information peut occuper plusieurs lignes sur la bande magnétique. Le nombre de digits utiles est le suivant:

Nombre de lignes	Nombre de digits d'identification	Nombre de digits utiles
1	0	15
2	1	$14 \times 2 = 28$
4	2	$13 \times 4 = 52$

La lecture peut être effectuée soit sur des blocs mémoires BM96 en passant par des «conditionneurs» (AP22 et AP25), soit sur le calculateur CAE510 avec conditionnement programmé. Plusieurs lectures peuvent être nécessaires pour exploiter toute l'information.

1.3. Blocs mémoire à 4096 canaux [10]

Ces blocs sont utilisés depuis 1962. Ils permettent essentiellement:
- l'acquisition des résultats avec ou sans mémoire tampon (temps mort de 16 μs dans ce dernier cas),
- la visualisation des 4096 canaux,
- la sortie des résultats sur bande perforée (environ 15 min pour 4096 canaux),
- le transfert des résultats vers un calculateur (environ 1 s).

La capacité maximale de chaque canal est de 100 000. Deux ou plusieurs blocs peuvent être associés en parallèle pour des expériences avec 8192 canaux ou plus.

Ils conviennent très bien aux expériences à fort taux de comptage, mais il est difficile de les utiliser pour l'acquisition d'expériences à plusieurs séquences (spectre, bruits de fond, en plus de l'expérience elle-même) car il faudrait autant de blocs ou de groupes de blocs qu'il y a de séquences, et cela nécessiterait une trop grande immobilisation de matériel. Enfin, la sortie électromécanique des résultats est lente et rarement exempte d'erreurs.

1.4. Calculateur CAE 510 «en ligne»

Dans un rapport à paraître, nous exposerons les raisons motivant l'emploi d'un calculateur et décrirons son installation [11, 12].

Avec une mémoire de 24 576 mots de 18 bits, ce calculateur est équipé de deux unités de ruban magnétique (une troisième sera installée prochainement), d'une unité de visualisation, d'une imprimante rapide, d'un lecteur et d'un perforateur de cartes, et d'un traceur de courbes.

La figure 1 représente les différentes liaisons réalisées. Le calculateur peut recevoir les informations:

- Directement d'une mémoire tampon pour une seule expérience (exp. 1); le temps d'accès est de 30 μs, le taux de comptage moyen ne peut dépasser 6000 coups/s (le classement de chaque information dans les mémoires d'accumulation durant environ 180 μs); le programme occupant 8192 mots environ, l'accumulation en ligne est possible dans 16 384 canaux au plus;
- Venant des blocs mémoires BM96 à travers une unité de multiplexage;
- Il peut également recevoir le contenu d'échelles de comptage.

Ce calculateur permet une automatisation des expériences:

a) L'accumulation a lieu dans le calculateur (exp. 1: 16 384 canaux au plus) et sur des blocs mémoires BM96 (exp. 2, 3 et 4: 12 288 canaux ou moins pour chacune).

b) La fin du temps d'accumulation est donnée par une horloge qui déclenche l'arrêt de l'acquisition, les changements d'écrans et la lecture des échelles par le calculateur.

c) Le calculateur transfère le contenu de sa mémoire rapide sur bande magnétique, lit les blocs mémoires et transfère également leur contenu sur bande magnétique. Il est possible, par intervention de l'opérateur, d'effectuer certaines opérations pour chaque expérience (visualisation par exemple).

d) La séquence d'acquisition suivante commence lorsque toutes les opérations de décodage et de mouvements mécaniques sont terminées.

Des commandes secondaires permettent d'interdire le décodage pour toutes les expériences où pour certains blocs mémoire et de commander l'effacement ou le non-effacement de chaque bloc après son décodage. Différents dispositifs permettent de contrôler le bon fonctionnement de l'ensemble, notamment la nuit (système d'alerte).

L'installation et la programmation en ligne ont été terminées en avril dernier; le calculateur a fonctionné en ligne en mai et juin, et l'expérience de ces deux mois nous a permis d'apporter les dernières retouches.

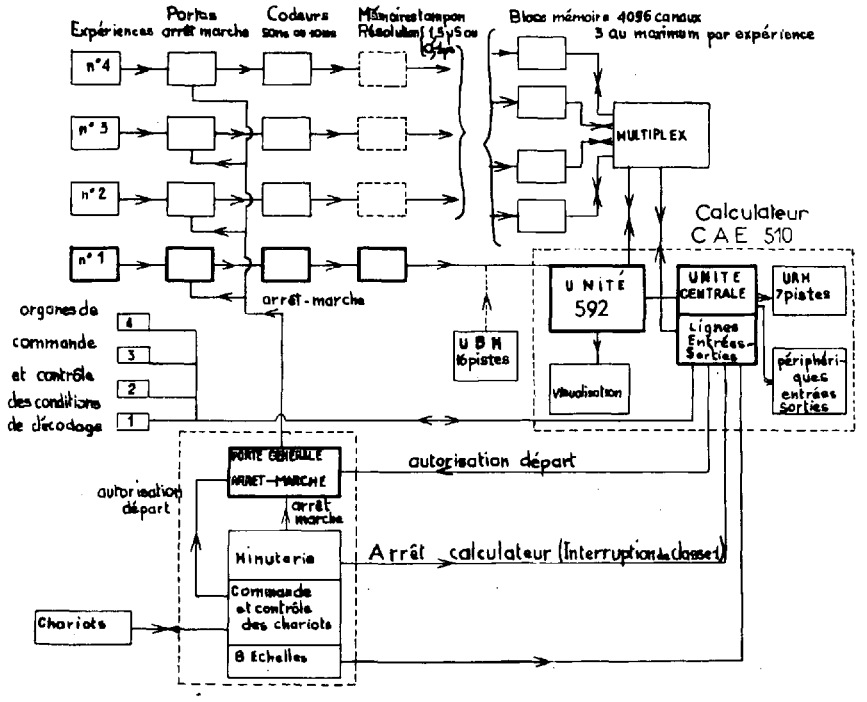

FIG.1. Organigramme de l'acquisition avec le calculateur CAE 510 en ligne

1.5. Calculateur CAE 510 «hors ligne»

Il permet la lecture des bandes magnétiques à 16 pistes (voir 1.1 et 1.2). Le fonctionnement en temps différé est en réalité identique à celui de l'acquisition en ligne avec une mémoire tampon.

2. DEPOUILLEMENTS PRELIMINAIRES

Par ce terme, nous entendons les calculs simples mettant en œuvre un grand nombre de données expérimentales et ayant pour but:
- d'additionner les résultats de plusieurs expériences,
- de corriger des effets expérimentaux (correction de temps mort, évaluation et soustraction de bruit de fond, normalisation),
- de réduire les effets de fluctuations statistiques (lissage de spectres),
- éventuellement, de corriger certaines fautes de l'appareillage (correction de points aberrants).

Ces opérations peuvent être effectuées soit sur un grand calculateur (IBM 7094), soit sur CAE510. Pour cela, tous les programmes sont écrits à la fois en Fortran (pour 7094) et en «logrammes» pour CAE 510. Les calculs sont effectués sur l'un ou sur l'autre des deux calculateurs selon les disponibilités et les urgences. En particulier, l'unité de visualisation du petit calculateur permettra de vérifier les résultats en évitant de les tracer.

Les bandes magnétiques, support commun des résultats, peuvent être lues par les deux calculateurs; elles sont écrites en mode CAE, qui est interprété et restitué par l'IBM 7094 lors de la lecture et de l'écriture sur la bande.

Chaque expérience inscrite sur la bande magnétique comporte, outre les résultats proprement dits, un certain nombre de données définissant l'expérience (numéro, nombre de canaux, programme de temps de vol, longueur de vol, comptage des échelles moniteurs, etc.). Les calculs sont effectués à partir de ces données et il sera possible d'effectuer des dépouillements quasi automatiquement (c'est-à-dire sans intervention du physicien) tout au moins pour les expériences les plus simples.

3. ANALYSE DES RESONANCES

La détermination des paramètres des résonances par analyse de forme est certainement la méthode la plus précise: elle est la seule à permettre l'utilisation de toute l'information donnée par l'expérience. Un programme de moindres carrés permet d'effectuer cette analyse.

3.1. Formulation de la section efficace

Une bonne approximation de la section efficace valable pour $<\Gamma_{\lambda\alpha}> \ll \bar{D}$ est donnée [13, 14], pour des ondes s, par

$$\sigma_{n,n} = \pi \lambda^2 \left| e^{-i\,2KR} - 1 + i \Sigma_\lambda \frac{\Gamma_{\lambda n}}{E - E_\lambda + i \frac{\Gamma_\lambda}{2}} \right|^2$$

$$\sigma_{n,\alpha \neq n} = \pi \lambda^2 \left| \Sigma_\lambda \frac{\sqrt{\Gamma_{\lambda n}} \sqrt{\Gamma_{\lambda \alpha}}}{E - E_\lambda + i \frac{\Gamma_\lambda}{2}} \right|^2$$

d'où l'on peut déduire, en admettant que $\Sigma_{\alpha \neq n} \sqrt{\Gamma_{\lambda\alpha}} \simeq 0$,

avec $\sigma_t = \sigma_p + \sigma_R + \sigma_{iP} + \sigma_{iR}$

$$\sigma_p = 4\pi\lambda^2 \sin^2 KR$$

$$\sigma_R = 4\pi\lambda^2 \cos 2KR \; \Sigma_\lambda \frac{\Gamma_{n\lambda}}{\Gamma_\lambda} \cdot \frac{1}{1+X^2}$$

$$\sigma_{iP} = 4\pi\lambda^2 \sin 2KR \; \Sigma_\lambda \frac{\Gamma_{n\lambda}}{\Gamma_\lambda} \cdot \frac{X}{1+X^2}$$

$$\sigma_{iR} = 4\pi\lambda^2 \Sigma_\lambda \Sigma_{\lambda' \neq \lambda} \frac{\Gamma_{n\lambda}}{\Gamma_\lambda} \cdot \frac{\Gamma_{n\lambda'}}{\Gamma_{\lambda'}} \cdot \frac{1 + X_\lambda X'_{\lambda'}}{(1+X^2_\lambda)(1+X'^2_{\lambda'})}$$

Dans cette formule, $\Gamma_n = \Gamma_n^0 \sqrt{E}$. Le dernier terme représente l'interférence entre résonances. On peut se demander dans quelle mesure ce terme constitue une bonne approximation d'une formule multi-niveaux. Cette formule peut être établie autrement, en partant de la formulation proposée par Vogt [15] (voir paragraphe 4). On peut calculer σ_{iR} lorsque $\sqrt{\Gamma_{n\lambda}/\Gamma_\lambda} \cdot \sqrt{\Gamma_{n'\lambda'}/\Gamma_{\lambda'}} \ll 1$. On retrouve alors exactement l'expression de la section efficace totale, sauf pour le terme d'interférence entre résonances

$$\sigma'_{iR} = 4\pi\lambda^2 \Sigma_\lambda \Sigma_{\lambda' \neq \lambda} \frac{\Gamma_{n\lambda}}{\Gamma_\lambda} \cdot \frac{\Gamma_{n\lambda'}}{\Gamma_{\lambda'}} \cdot \frac{X_\lambda X'_{\lambda'} - 1}{(1+X^2_\lambda)(1+X'^2_{\lambda'})}$$

cette formule constitue en fait une bonne approximation lorsque $\sqrt{\Gamma_{n\lambda} \cdot \Gamma_{n\lambda'}}/\Gamma_\lambda \cdot \Gamma_{\lambda'}$ est faible. La qualité de cette approximation peut être vérifiée numériquement.

La figure 2 représente un cas de deux résonances hypothétiques, sans voie de fission, mais avec des valeurs assez grandes pour Γ_n/Γ_t: $\Gamma_{n_1}/\Gamma_1 = 1/3$, $\Gamma_{n_2}/\Gamma_2 = 3/5$, et, par conséquent, $\sqrt{\Gamma_{n_1}\Gamma_{n_2}}/\Gamma_1\Gamma_2 = 0,45$. Les points « exacts » ont été calculés par le programme Muffle [16]. L'accord est très bon.

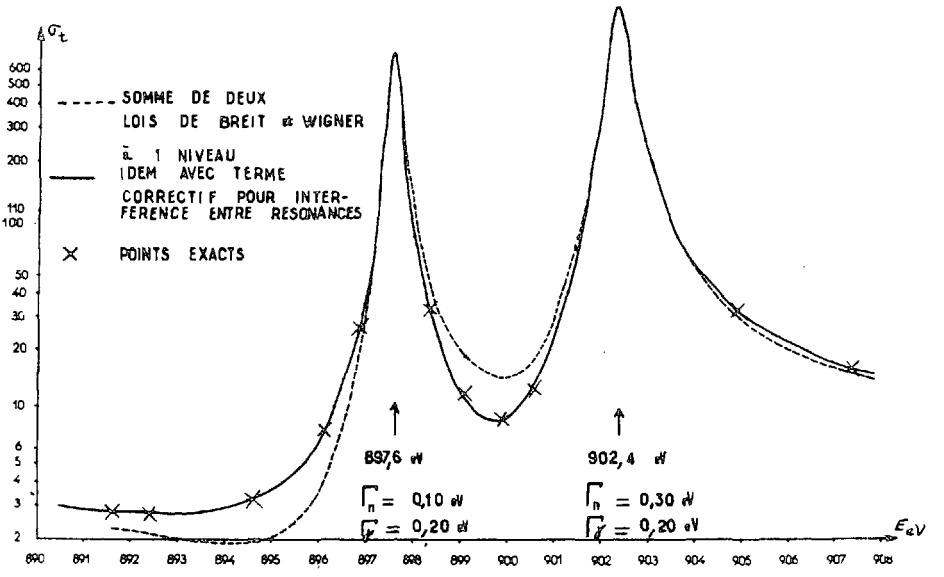

FIG.2. Comparaison d'un calcul approché de l'interférence entre résonances (formule 2) avec les points exacts (obtenus par le programme multiniveaux Muffle [16])

3.2. Effets expérimentaux

a) L'effet Doppler est introduit par la convolution des fonctions $1/(1+X^2)$ et $X/(1+X^2)$ par la gaussienne $(1/\beta\sqrt{\pi})e^{-X^2/\beta^2}$, avec $\beta = 2\Delta/\Gamma_t$,

$\Delta = K\sqrt{T_{eff} \cdot E/M}$. Les fonctions de X, β résultats de cette convolution sont respectivement appelées Ψ et Φ.

L'effet Doppler n'intervient évidemment pas sur le terme potentiel et est négligé sur le terme d'interférence entre résonances.

b) La résolution expérimentale est définie par 61 points ou moins. Elle peut être:

- calculée point par point par le programme, elle est alors supposée gaussienne, et son écart quadratique moyen est de la forme

$$\sigma_R^2 = \frac{R_1^2}{2} E^2 + \frac{R_2^2}{2} E^3$$

R_1 inclut les composantes de la résolution expérimentale affectant la résolution en énergie suivant une loi en E^1 (temps de ralentissement, différences de longueur en vol); R_2 celles qui affectent la résolution suivant une loi en $E^{3/2}$ (fluctuations de temps: largeur de canal sélecteur, etc.);
- définie point par point, elle peut alors avoir n'importe quelle forme.

Dans le cas des mesures de sections efficaces partielles (fission, diffusion, ...), une résolution de forme gaussienne et l'effet Doppler peuvent être réunis. Dans le cas de la transmission, la résolution expérimentale est appliquée à la transmission.

c) Il est également possible de corriger le bruit de fond (coefficients a et b) et la normalisation (coefficient c), et de tenir compte d'un certain décalage en énergie (coefficient δE). La formule résultante est, en transmission,

$$T_{exp} = a + b\sqrt{E} + c \cdot \mathscr{R} * E^{-n[\mathscr{D} * \sigma_{(E+\delta E)}]}$$

et, pour les sections efficaces partielles (fission, diffusion),

$$\sigma_{exp} = a + b\sqrt{E} + c \cdot (\mathscr{R} * \mathscr{D}) * \sigma_{(E+\delta E)}$$

$\mathscr{R}$ représentant la résolution expérimentale, $\mathscr{D}$ l'effet Doppler.

3.3. Possibilités du programme

Le programme existe en deux versions, A et B. La seconde version admet davantage de données que la première (2200 points expérimentaux) et offre davantage de possibilités d'entrée et de sortie; mais tout le programme et les données ne peuvent être simultanément en mémoire rapide du calculateur IBM 7094: il est nécessaire d'utiliser des suites. Le calcul est plus long, et cette version est peu utilisée.

Nous ne parlerons que de la version A. Elle admet:

- 1600 points expérimentaux contenus par une à six séries expérimentales distinctes (représentant chacune, par exemple, une transmission avec une épaisseur différente, ou éventuellement une résolution différente);

- 32 à 38 résonances pouvant être classées en familles; seules interfèrent entre elles (terme σ_{iR}) les résonances d'une même famille; une valeur du coefficient statistique g est donnée pour chaque famille.

Il est possible de faire varier simultanément jusqu'à 50 paramètres. Ces derniers peuvent être:

- communs à toutes les séries et toutes les résonances (rayon et coefficient effet Doppler: R et $\eta = \Delta/\sqrt{E}$)
- communs à chaque série (termes correctifs a, b, c, δE)
- pour chaque résonance:

$$E, \Gamma, \begin{cases} 2g\,\Gamma_n & \text{(transmission)} \\ 2g\,\dfrac{\Gamma_n \Gamma_f}{\Gamma_t} & \text{ou (fission)} \end{cases}$$

Les séries expérimentales peuvent être lues sur bandes magnétiques ou cartes perforées. Les résultats sont, outre les paramètres et les erreurs sur ces paramètres, la somme des carrés des écarts entre les points expérimentaux et les points théoriques (χ^2) et les tracés superposés des courbes expérimentales et théoriques (fig. 3).

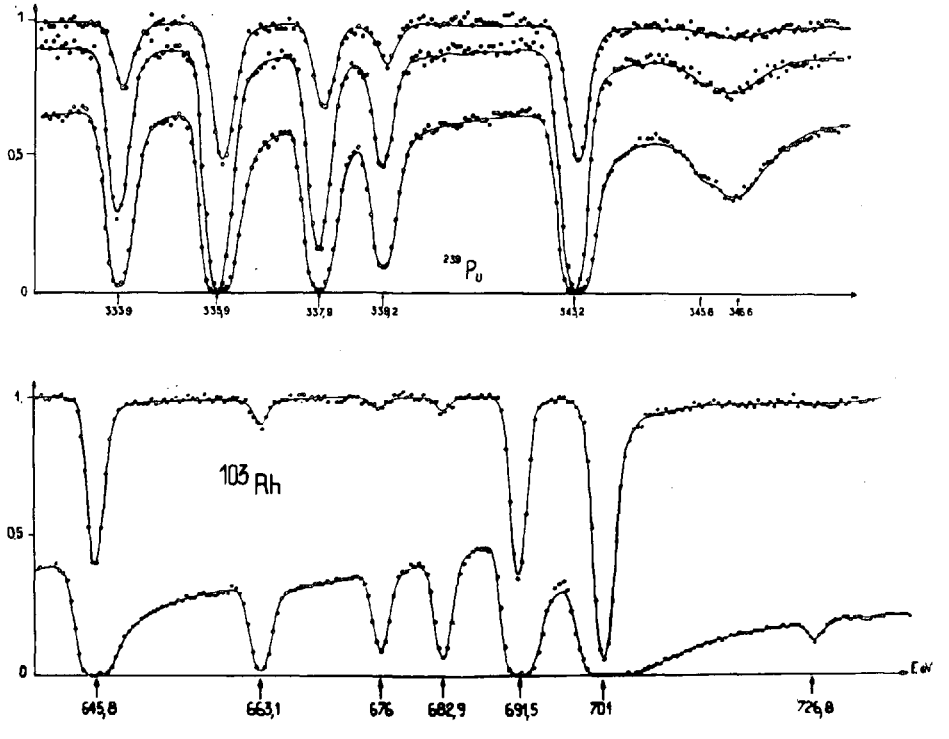

FIG. 3. Exemples de cas d'analyse de forme par moindres carrés

Le calcul effectue des itérations, jusqu'à ce que la somme des carrés varie moins qu'une quantité définie en donnée, ou augmente (pas d'amélioration, ou calcul divergent).

3.4. Programme

Ce programme a été écrit au Service de calcul électronique de Saclay, une première version en 1961 par Mme Guillot, les versions actuelles en 1963 par M. Solal [17].

Ce programme utilise une présentation sans modèle imposé des données (sous-programme PSLD [18]). Certaines parties sont écrites en FAP (sous-programmes de calcul des fonctions Ψ et Φ, calcul de la fonction de résolution, etc.). Il en résulte que ces programmes doivent être adaptés pour pouvoir être utilisés sur d'autres calculateurs.

Le temps de calcul dépend beaucoup du nombre de points expérimentaux, de résonances, du pas de calcul ΔE.

Chaque valeur expérimentale est donnée avec son énergie et son erreur: celle-ci (écart quadratique moyen) résulte des calculs appelés «dépouillements préliminaires». Si les erreurs sont correctement évaluées, si la courbe expérimentale peut être correctement décrite par la formule théorique utilisée, le X^2 résultant doit être de l'ordre de grandeur du nombre de points expérimentaux (en toute rigueur égal au nombre de points moins le nombre de paramètres variables).

Il n'est pas toujours possible de définir en une seule fois tous les paramètres des résonances étudiées, à moins que celles-ci soient isolées les unes des autres et déterminées chacune par un grand nombre de points. Dans les autres cas, il est nécessaire de procéder par étapes en ajustant les paramètres les uns après les autres, ajoutant au besoin des corrections manuelles entre les passages.

A titre d'exemple la figure 3 représente deux cas d'analyse de transmission.

Le premier concerne le ^{239}Pu. Il y a trois épaisseurs (n = 0, 002462, 0, 009832, 0, 03449 at/b) avec 201 points chacune. Le nombre de résonances prises en compte par le programme est de 19, dont sept seulement sont situées dans la zone étudiée (les autres intervenant comme des corrections). Il y a 23 paramètres variables et le X^2 final est de 830.

Le second exemple représente une partie d'un calcul sur le rhodium. Les épaisseurs sont de 0, 00608 et 0, 2385 at/b, le nombre total des points pour chaque épaisseur étant de 381. Le nombre total de résonances est de 27, dont 13 dans la zone étudiée; il y a 36 paramètres variables, et le X^2 final est de 1900: il y a un désaccord systématique entre les deux résonances à 691 et 701 eV (dû en partie à l'existence d'une petite résonance vers 698 eV).

4. PROGRAMME MULTINIVEAUX

Il est prévu pour l'analyse des corps fissiles; il utilise la méthode de Vogt [15] et ne prend en compte, dans les éléments non diagonaux de la matrice A^{-1}, que les termes de fission de la forme

$$-\frac{i}{2}\vec{g}_{\lambda}^{f}\vec{g}_{\lambda'}^{f} = -\frac{i}{2}\sqrt{\Gamma_{\lambda}^{f}\Gamma_{\lambda'}^{f}}\left[\cos\varphi_{\lambda}\cos\varphi_{\lambda'}\cos(\theta_{\lambda}-\theta_{\lambda'})+\sin\varphi_{\lambda}\cdot\sin\varphi_{\lambda'}\right]$$

les termes diagonaux étant égaux à $(E_{\lambda}-E)-i\Gamma_{\lambda}/2$. Le nombre de voies de sortie est limité à 3. La position de chaque vecteur $\vec{g}_{\lambda}^{f}$ dans l'espace des voies de sortie est donnée par les deux angles φ_{λ} et θ_{λ}.

Il permet de calculer les sections efficaces de fission, de capture, de diffusion et totale. Il permet de relier ces résultats par l'effet Doppler, puis par la résolution expérimentale (appliquée à exp $[-n(\mathscr{D}*\sigma)]$ dans le cas de la transmission).

Les résonances peuvent être

- soit calculées par une formule à un niveau (sans aucune interférence entre résonances)
- soit calculées à partir de l'inversion de la matrice A^{-1}
- soit calculées par une approximation des interférences de fission:

$$\sigma_{iR} = 4\pi \lambda^2 \Sigma_\lambda \Sigma_{\lambda' \neq \lambda} \frac{\sqrt{\Gamma_n \Gamma'_n}}{\Gamma_\lambda \Gamma'_\lambda} \cdot \frac{X_\lambda X'_{\lambda'} \vec{g}^f_\lambda \vec{g}^f_{\lambda'}}{(1+X^2_\lambda)(1+X'^2_{\lambda'})}$$

Les résultats sont tracés et tabulés. La mise au point de ce programme est presque terminée.

Dans une phase ultérieure il sera possible de comparer ces résultats de calcul avec des données expérimentales (tracés superposés et valeur de X^2, somme des carrés des écarts).

5. INTERPRETATION DES PARAMETRES

L'augmentation du nombre de résonances étudiées nous a conduit à écrire un programme pour aider l'interprétation des paramètres. Il permet des opérations simples telles que

- Calcul de différents paramètres à partir de données élémentaires (énergie à partir du temps, Γ_f d'après l'aire de la résonance en fission, etc.) et les erreurs résultantes;
- Calcul de valeurs moyennes (moyenne pondérée d'un paramètre, fonction densité);
- Tracés des distributions des différents paramètres pouvant être comparés directement avec les lois de probabilité théoriques;
- Calcul des coefficients de corrélations entre les paramètres;
- Reconstitution d'une courbe de section efficace à partir de paramètres.

CONCLUSION

Pour assurer l'enchaînement direct des différentes étapes de l'acquisition et du dépouillement, nous avons dû établir des modèles bien définis pour les résultats: mode d'écriture sur bandes magnétiques, modèles de perforation des cartes.

Les programmes nécessaires pour cela représentent un ensemble important, nécessitant le travail permanent de deux personnes, une troisième étant chargée d'assurer la préparation des cas de calcul. L'expérience nous a prouvé qu'il était nécessaire que le programmeur travaille en liaison très étroite avec les physiciens: c'est grâce à des contacts très fréquents que le programme de moindres carrés a pu être mené à bon terme.

Bien que nous cherchions à rendre nos programmes suffisamment généraux, l'évolution des dispositifs expérimentaux et des expériences réalisées conduit à renouveler les programmes tous les cinq ans. Actuellement, le programme de moindres carrés, défini dans sa version actuelle en 1961, doit être entièrement revu.

REFERENCES

[1] OLLIVIER, B., POUSSOT, R., THENARD, J., «Horloge à 20 MHz à transistors», Nuclear Electronics II, IAEA, Vienna (1962) 81.

[2] THENARD, J., «Codage en temps par échelle binaire», Nuclear Electronics II, IAEA, Vienna (1962) 101.

[3] THENARD, J., VICTOR, G., «Changement de pas programmé de trains d'impulsions; application à la mesure des temps de vol de neutrons», Electronique nucléaire 1963, ENEA, Paris (1964) 333.

[4] DURAND, P., GIRAUD, P. «Codeur de temps transistorisé à 10 nanosecondes par canal», Electronique nucléaire 1963, ENEA, Paris (1964) 643.

[5] DURAND, P. et al., "Transistorized time coder with several thousand channels of one nanosecond width", Electronique nucléaire 1963, ENEA, Paris (1964) 651.

[6] BOUCHERIE, A., «Mémoire-tampon à transistors», Electronique nucléaire 1963, ENEA, Paris (1964) 409.

[7] BOUCHERIE, A., Etude d'une mémoire à faible capacité, Thèse CNAM (1964).

[8] AMRAM, Y. «Analyseur bidimensionnel 2X3», Nuclear Electronics II, IAEA, Vienna (1962) 73.

[9] HUGO, Ch., MALAVAL, P., «Ensemble transistorisé d'enregistrement et de lecture sur bande magnétique», Electronique nucléaire 1963, ENEA, Paris (1964) 401.

[10] TISSIER, J.M., «Sélecteurs multidimensionnels à mémoire magnétique», Nuclear Electronics II, IAEA, Vienna (1962) 155.

[11] GAUVIN, B. et al., Utilisation d'un petit calculateur pour des expériences de physique auprès d'un accélérateur linéaire, Rapport CEA à paraître.

[12] CAUVIN, B. et al., Utilisation en ligne d'un calculateur CAE 510 pour des expériences de temps de vol, Journées d'études de la SFER, 25-26 octobre 1966.

[13] THOMAS, R.G., Phys. Rev. 97 (1955) 224.

[14] CHASE, P.M. et al. Rpt WADC (1958) 58-79.

[15] VOGT, E., Phys. Rev. 112 1 (1958) 203.

[16] PRESSKITT, C.A., Muffle, ORNL TM 1180.

[17] SOLAL, R., Note CEA n° 592.

[18] Spécification SCE (CEN Saclay) SN 1100.

ETUDE DE QUELQUES SECTIONS EFFICACES NEUTRONIQUES TOTALE ET DE DIFFUSION DANS LE DOMAINE DES RESONANCES

R. RIBON, B. CAUVIN, H. DERRIEN, A. MICHAUDON,
E. SILVER* ET J. TROCHON
CEA, CENTRE D'ETUDES NUCLEAIRES DE SACLAY,
FRANCE

Abstract — Résumé

INVESTIGATION OF SOME SCATTERING AND TOTAL NEUTRON CROSS-SECTIONS IN THE RESONANCE RANGE. The authors present some recent work on non-fissionable elements (sodium, xenon, gadolinium).

Xenon and gadolinium were studied to determine the spin of a sufficient number of resonances to enable the strength functions for each spin state to be obtained. For xenon, the optimum resolution was 1.5 ns/m at 900 eV (in transmission) and 45 ns/m at 100 eV (in scattering). Several samples of varying thickness were used, the thickest being 100 g of XeF_2.

Gadolinium has been studied earlier in transmission. The scattering measurements, made with the same resolution as for Xe, are difficult to interpret owing to the large number of resonances due to different isotopes. To improve their results, the authors used separated isotopes: a sample containing 2 g of ^{155}Gd enriched to 94% and another containing 2 g of ^{157}Gd, also enriched to 94%.

These isotopic assignments, in the case of the Gd and Xe in transmission, were made using a short flight path (17 m) and small sample surfaces (1 to 2 cm^2). Sodium was studied up to several hundred keV in order to detect very small resonances, one of which – at 35 keV – had been found earlier by an activation method. The resolution was of the order of 0.25 ns/m and the thickness of the sample was 17 g/cm^2.

The authors present some resonance parameters and discuss the statistical distributions of these parameters.

ETUDE DE QUELQUES SECTIONS EFFICACES NEUTRONIQUES TOTALE ET DE DIFFUSION DANS LE DOMAINE DES RESONANCES. Les auteurs présentent quelques travaux récents concernant des éléments non fissiles (sodium, xénon, gadolinium).

Pour ces deux derniers éléments, leur but a été de déterminer le spin d'un nombre de résonances suffisant pour obtenir les fonctions densité pour chaque état du spin. Dans le cas de Xe, la résolution optimale est de 1,5 ns/m à 900 eV en transmission et de 45 ns/m à 100 eV en diffusion. Plusieurs échantillons, d'épaisseurs différentes, sont utilisés - l'échantillon le plus épais étant constitué de 100 g de XeF_2.

Le gadolinium a déjà été étudié en transmission; les mesures de diffusion, faites avec la même résolution que pour Xe, sont difficiles à interpréter par suite du grand nombre de résonances dues aux différents isotopes. Pour améliorer les résultats, les auteurs utilisent des isotopes séparés – un échantillon contenant 2 g de ^{155}Gd enrichi à 94% et un autre de 2 g de ^{157}Gd également à 94%.

Ces attributions isotopiques sont faites, pour Gd et Xe en transmission, en utilisant une base de vol courte (17 m) et de petites surfaces d'échantillon (1 à 2 cm^2). Le sodium est étudié jusqu'à plusieurs centaines de keV. Le but des auteurs est de mettre en évidence de très petites résonances, dont une à 35 keV, précédemment trouvée par une méthode d'activation. La résolution est de l'ordre de 0,25 ns/m, l'échantillon ayant une épaisseur de 17 g/cm^2.

Les auteurs donnent des paramètres de résonances, et étudient les distributions statistiques de ces paramètres.

---

* Détaché au CEN de Saclay par l'ORNL.

Nous présentons dans ce mémoire quelques travaux récemment effectués et dont l'exploitation n'est pas terminée. Il s'agit donc de résultats préliminaires obtenus en transmission et en diffusion.

1. XÉNON

Depuis quelques années, plusieurs auteurs ont signalé une dépendance possible de la fonction densité du spin du noyau composé [1-3]. Mais la plupart des résultats concernent des noyaux de nombres de masse compris entre 60 et 110 d'une part et voisins de 200 d'autre part, correspondant à des régions où S_0 décroît pour A croissant. Nous voulons essayer de déterminer si une telle variation - de même sens - existe dans les régions de nombre de masse croissant, et ce pour des noyaux de spin 1/2 et 3/2. Pour cela nous avons entrepris l'étude du Xe, qui comporte les isotopes 129 (26,4% dans le Xe naturel - I = 1/2) et 131 (21,2% - I = 3/2).

Echantillons

a) Pour la diffusion, nous avons utilisé deux échantillons de Xe gazeux naturel de 10 cm d'épaisseur - un à la pression de 1 kg/cm^2 (n = 0,000 268 at/b), l'autre à la pression de 2,5 kg/cm^2 (n = 0,000 669 at/b).

b) les échantillons utilisés en transmission ont été:
- Xe gazeux - 0,03 g/cm^2 n = 0,000 124 at/b } pour les résonances à
- Xe gazeux - 0,23 g/cm^2 n = 0,00 105 at/b } 14 et 9 eV seulement
- Xe gazeux - 0,556 g/cm^2 n = 0,00 251 at/b
- Xe solide - sous forme de XeF_2 - épaisseur 4,95 g/cm^2 de XeF_2 sur une surface de 23,8 cm^2 - n = 0,01760 at/b.

c) Nous avons disposé, pour une première expérience d'attribution isotopique, d'un échantillon de Xe lourd [4]. La composition isotopique en est donnée par le tableau I. L'épaisseur de l'échantillon était de 0,013 g/cm^2 (n = 0,0027 at/b).

TABLEAU I. COMPOSITION ISOTOPIQUE DE L'ECHANTILLON DE Xe LOURD UTILISE

Nombre de masse	124	126	128	129	130	131	132	134	136
Teneur (%) Xe lourd	0,011	0,026	1,14	20	3,73	21,6	29,6	12,7	11,2
Xe naturel	0,094	0,092	1,92	26,4	4,1	21,2	26,9	10,4	8,9

Conditions expérimentales

Le tableau II résume les conditions expérimentales

Les dispositifs expérimentaux ont été décrits ailleurs [5-7]. Nous rappelons que les compteurs à BF_3 utilisés comme détecteurs ont une fluctuation du temps de réponse de 0,55 μs.

TABLEAU II. CONDITIONS EXPERIMENTALES

Expérience	Energie (eV)	Echantillon (at/b)	Longueur de vol (m)	Largeur de l'impulsion de l'accélérateur (ns)	Largeur de canal du sélecteur (ns)	Résolution nominale (ns/m)
Transmission	1 à 20	Xe naturel n = 0, 000124 n = 0, 00105	17, 7	200	100	12
Transmission	20 à 300	Xe naturel n = 0, 00251 n = 0, 0176	53, 7	100	50	2, 5 à 300 eV
Transmission	300 à 900	Xe naturel n = 0, 0176	53, 1	60	40 et 20	1, 2 à 900 eV
Identification isotopique (transmission)	< 450 (avec trou vers 330)	Xe naturel n = 0, 00283 Xe lourd n = 0, 00273	17, 1	100	50	12 à 100 eV
Diffusion	400	Xe naturel n = 0, 00027 n = 0, 00067	12, 5	100	200	100 à 100 eV 130 à 300 eV

Résultats

a) Attribution isotopique. Les résultats sont résumés dans le tableau II. La figure 1 représente les rapports des teneurs isotopiques ($a_{Xe\ lourd}/a_{Xe\ naturel}$) déterminés expérimentalement pour chaque résonance et comparés aux données de l'analyse par spectrométrie de masse. L'erreur est souvent telle que l'attribution isotopique est ambiguë. Cette ambiguïté a parfois pu être levée par les résultats de diffusion. Nos résultats sont toujours en accord avec les mesures précédentes [8]; des mesures avec des échantillons plus épais de Xe lourd et Xe léger avec une meilleure résolution nous permettront de déterminer l'attribution isotopique au-delà de 200 eV.

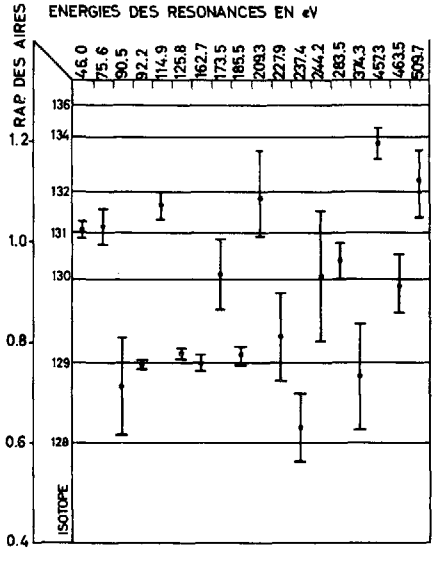

FIG.1. Attribution isotopique des résonances du Xe

b) Transmission. Les paramètres des résonances ont été déterminés par analyse de forme avec une méthode de moindres carrés. Ils sont donnés dans le tableau III. Il a été possible de déterminer le spin de quelques résonances d'après les valeurs possibles de Γ_γ.

La valeur du rayon R a été déterminée par l'analyse du terme d'interférence potentiel pour quelques résonances. La figure 2 représente la somme des moindres carrés en fonction de la valeur du rayon pour la résonance à 14 eV ainsi que l'influence de ce rayon sur les valeurs de Γ et $2\,g\Gamma_n$. Le meilleur accord est pour $R = 0{,}625 \cdot 10^{-12}$ cm. Le même calcul pour la résonance à 9,4 eV a donné $R = 0{,}63 \cdot 10^{-12}$ cm.

c) Diffusion. La surface mesurée pour une résonance est proportionnelle à $(2\,ag\Gamma_n)^2/ag\Gamma$, g étant le facteur statistique, et à la proportion isotopique. (Les quantités $2\,ag\Gamma_n$ et Γ sont obtenues par l'analyse de la transmission.) La méthode de dépouillement – en particulier en ce qui

concerne la correction de l'autoabsorption - a été exposée ailleurs [6, 7]. La figure 3 représente un exemple de résultat expérimental pour l'échantillon de $0,67 \cdot 10^{-3}$ at/b.

Il a été possible de confirmer ou de préciser certaines attributions isotopiques et d'affecter quelques spins. Les résultats sont portés dans le tableau III.

Actuellement, le nombre de niveaux étudiés est trop faible pour pouvoir déterminer les valeurs des fonctions densité.

2. GADOLINIUM

L'étude du Gd a été entreprise en diffusion pour compléter des mesures faites en transmission [9]. Le Gd comporte deux isotopes impairs de spin 3/2: le 155 (proportion isotopique dans le Gd naturel:14,7%) et le 157 (15,7%). L'espacement moyen des résonances est faible - moins de 1,5 eV pour le Gd naturel - et il est difficile à étudier en diffusion (expérience ayant une mauvaise résolution). Nous avons pu néanmoins faire cette étude sur des isotopes séparés prêtés par l'USAEC.

Echantillons

Nous disposions de 2 g de Gd_2O_3 enrichi à 94,3% en ^{155}Gd, et de 2 g enrichis à 93,7% en ^{157}Gd.

a) Transmission. Outre des échantillons de Gd_2O_3 naturel, nous avons utilisé les isotopes séparés pour effectuer une attribution isotopique. Dans cette mesure, la longueur de vol était de 17 m et la surface des échantillons était de 1 cm^2 (l'épaisseur de 2 g/cm^2 correspond à n = 0,00658 at/b pour le ^{155}Gd, et à n = 0,00686 at/b pour le ^{157}Gd.

b) Diffusion. La surface des échantillons constitués par les 2 g d'oxyde était de 8 cm^2 (diamètre: 32 mm), l'épaisseur de 0,25 g/cm^2 (soit n = 0,00085 at/b). La poudre pressée était enfermée entre deux minces feuilles d'aluminium (e = 15 mm).

Résultats

La figure 4 représente les transmissions superposées pour les deux isotopes de Gd; du fait de la petite surface du faisceau utile, le bruit de fond était relativement élevé: de l'ordre de 30% vers 60 eV. Mais le taux de comptage était encore très important: la durée d'accumulation a été de 8 h pour chaque échantillon. Les dépouillements sont en cours. L'espacement moyen est de 2,35 eV pour le ^{155}Gd, de 4,9 pour le ^{157}Gd. Les espacements moyens D_0 corrigés du spin - $D_0 = 2(2I+1)D$, D étant l'espacement moyen pour les deux états de spins - sont respectivement égaux à 18,8 et 39,5 eV - soit dans un rapport 2,1.

Cela est en bon accord avec les estimations théoriques [10, 11] en tenant compte de la différence d'énergie de liaison dans les deux isotopes (A+I) (respectivement 8,45 MeV et 7,92 MeV pour le ^{156}Gd et le ^{158}Gd).

TABLEAU III. PARAMETRES DES RESONANCES

Energie	Isotope	Γ	$2ag\Gamma_n$	J	Γ_n	Γ_γ	Γ_n^0
9,57	129	120 ± 4	2,34 ± 0,03	(1)	6	112	1,91
9,88		128 ± 70	0,074 ± 0,025				
14,41	131	309 ± 5	57,3 ± 0,6	2	216	93	57,8
46,01	131	124 ± 5	2,89 ± 0,03	(2)	(11)	113	(1,8)
75,57	131	134 ± 7	2,91 ± 0,03	2	11	123	1,3
90,53	(129)	144 ± 16	1,27 ± 0,03				
92,25	129	199 ± 6	32,0 ± 0,5	1	81	108	8,42
114,9	(131)[a]	145 ± 8	8,32 ± 0,9	(2)	(31)	(114)	(2,9)
125,8	129	413 ± 15	42,6 ± 0,5	0	323	90	28,9
162,7	129	201 ± 8	26,4 ± 0,3	1	66,6	134	5,23
173,5	(131)[a]	174 ± 15	5,71 ± 0,08	(1)	(36)	(137)	(2,74)
185,5	129	221 ± 11	30,1 ± 0,4	1	76	145	5,60
209,3	(131)[a]	211 ± 10	19,9 ± 0,24	(2)	(75)	(136)	(5,20)
227,9	129 / 130 ?	209 ± 12	16,5 ± 0,20				
237,4	128 / 129 ?	393 ± 22	11,5 ± 0,16				
244,2	(130)[a]	194 ± 30	8,3 ± 0,20	(1/2)	(102)	(92)	
283,2	131[a]	450 ± 25	48,3 ± 0,8	1	304	146	18
374,3	(129)	336 ± 40	32,4 ± 0,9	(0)	(245)	(91)	12,7
451,3	134	1142 ± 70	178,4 ± 5	1/2	854	288	
509,7	(132)	358 ± 80	16,9 ± 0,8	(1/2)	(31,4)	(326)	

[a] Attribution isotopique précisée par la mesure de diffusion.

3. SODIUM

L'étude du Na a été entreprise à la suite des résultats obtenus en capture [12, 13], qui montrent une résonance de capture importante vers 35 keV. Pour réaliser cette expérience, nous avons dû éliminer tout aluminium sur le parcours des neutrons: les bases de vol ont été fermées par des fenêtres minces de mylar et remplies d'hélium.

L'épaisseur de l'échantillon de Na est de 17,5 g/cm^2 – soit n = 0,457 at/b. Les parois sont en acier inoxydable, de 0,05 mm d'épaisseur. Le détecteur utilisé est toujours celui du type dit à rayon gamma de capture de bore-10 [5]. Un échantillon de Li naturel de 6 g/cm^2 – soit n = 0,53 at/b – en permanence dans le faisceau donne un point de bruit de fond à 250 keV.

La longueur de vol était de 103,7 m; le tableau IV donne une évaluation de plusieurs facteurs qui entrent dans la fonction de résolution.

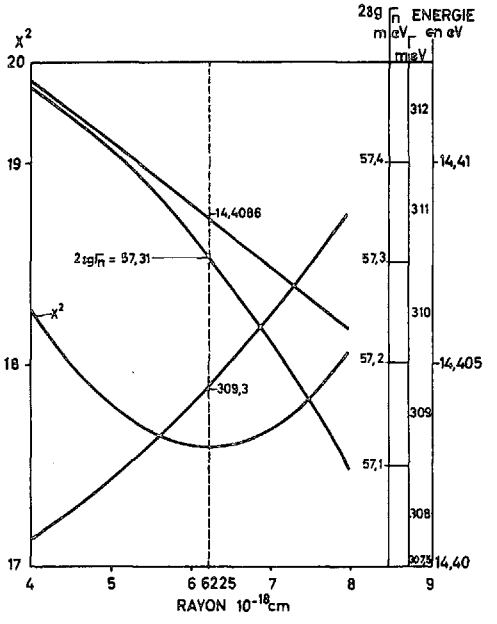

FIG.2. Influence du rayon sur les valeurs de X^2 (somme des carrés des écarts entre les points expérimentaux et les points théoriques), de l'énergie E_0, des largeurs Γ et $(2g\,\Gamma_n)$

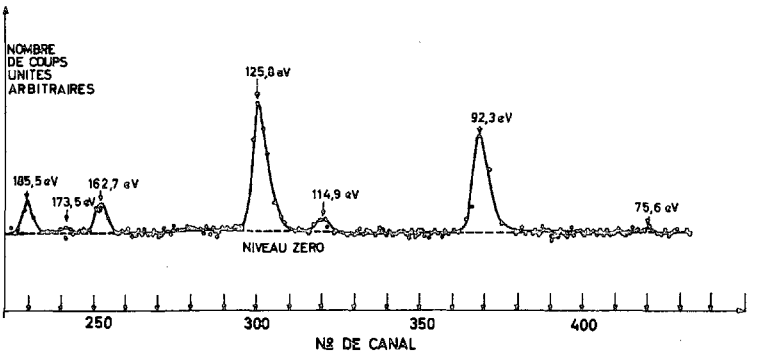

FIG.3. Exemple de résultat obtenu en diffusion avec l'échantillon de Xe

L'incertitude due au temps de ralentissement est faible: elle est équivalente à un écart quadratique moyen de 7 ns² vers 40 keV. Mais il est d'autres causes mal connues qui affectent la résolution:

- les diffusions multiples dans la cible d'uranium, entre les deux ralentisseurs et dans la chambre des cibles,
- les diffusions multiples et les captures radiatives qui en résultent dans le détecteur.

Cette expérience n'a duré que 14 h au total, la fréquence de répétition de l'accélérateur étant de 500 Hz; elle devait permettre de vérifier si les conditions expérimentales étaient satisfaisantes. La statistique est faible:

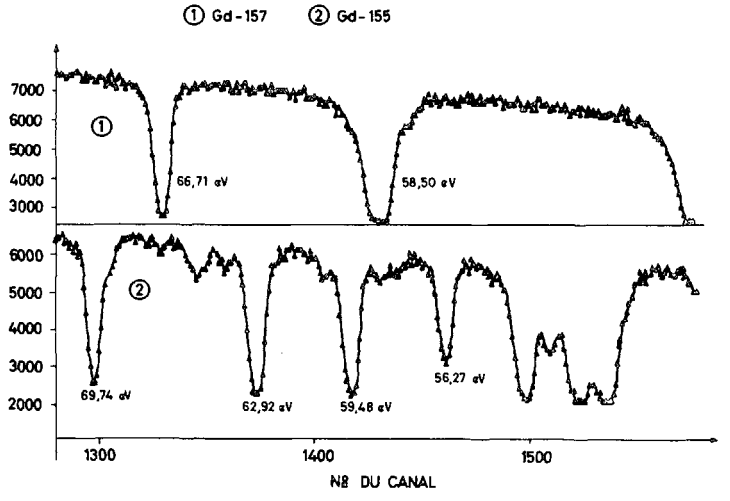

FIG.4. Exemples de résultats obtenus en transmission avec 2 g d'oxyde de gadolinium (isotopes séparés 155 et 157)

TABLEAU IV. FACTEURS ENTRANT DANS LA FONCTION DE RESOLUTION

	Forme	Largeur (ns)	Ecart quadratique moyen (ns^2)
Largeur de l'impulsion de l'accélérateur	~ Gaussienne	15	42
Largeur de canal du sélecteur	Carrée	10	8,5
Mise en phase du peigne du sélecteur	Carrée	10	8,5
Fluctuations du T_0 par rapport au déclenchement de l'accélérateur	~ Gaussienne	~ 3	2
Fluctuation des retards électroniques		~3	2
Total			63 ns^2

elle atteint 1000 coups par canal pour le spectre et la transmission à 200 keV.

Nous avons pu mettre en évidence la résonance à 35 keV ainsi qu'une autre à 117 keV (fig. 5). Cette dernière correspond probablement à l'augmentation de la section efficace de capture observée par Le Rigoleur vers 110 keV [12, 13].

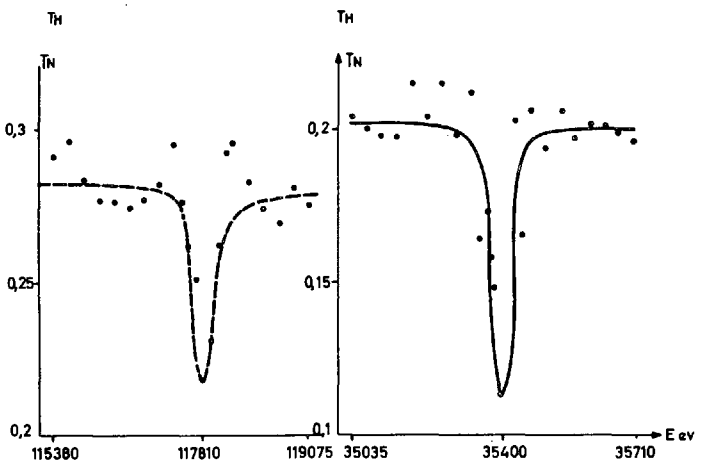

FIG.5. Résonances à 35 et à 117 keV du ^{23}Na observées en transmission avec un échantillon de 17,5 g/cm^2.

Malgré la très faible statistique, nous avons pu déterminer les surfaces approchées de ces deux résonances (tableau IV).

E = 117 610 eV	S = 170 b·eV
E = 35 390 eV	S = 60 b·eV

En supposant que la résonance à 35 keV soit due à une onde p et que Γ_γ = 0,3 eV, on obtient un très bon accord avec les résultats de Le Rigoleur (g = 7/8, Γ_n = 0,55 eV). Cependant, cette résonance n'est peut-être pas p, mais plutôt d, ou même d'un ordre supérieur [12, 13].

Cette mesure doit être reprise pour être réalisée dans les mêmes conditions mais avec une meilleure statistique. Il est à noter que le détecteur est utilisé à peu près au maximum de ses possibilités: la diffusion par le bore est supérieure à la capture au-delà de 40 keV. Nous avons néanmoins obtenu des résultats cohérents jusque vers 1,2 MeV.

REFERENCES

[1] JULIEN, J. et al., Int. Conf. on the Study of Nuclear Structure with Neutrons, Antwerp (July 1965) No. 80.
[2] ASGHAR, M. et al., Int. Conf. on the Study of Nuclear Structure with Neutrons, Antwerp (July 1965) No. 65.
[3] RIBON, P. et al., Int. Conf. on the Study of Nuclear Structure with Neutrons, Antwerp (July 1965) No. 165.
[4] MOLINARI, P., TANIEL, G., Bulletin d'informations scientifiques et techniques du CEA 103 (1966) 99.
[5] RIBON, P. et al., Time of Flight Methods, CEN Saclay (1961) 97.
[6] TROCHON, J. et al., C.r. hebd. Séanc. Acad. Sci. 262 (1966) 507.
[7] TROCHON, J., Rapport CEA (à paraître).
[8] MANN, D. P. et al., CHRIEN, R. E. et al., Phys. Rev. 116 6 (1959) 1516
[9] SAMOUR, C. et al., communication privée.
[10] NEWSON, H. W., GIBBONS, J. H., Fast Neutron Physics, p. 1601.
[11] HARVEY, J. A., Neutron Time of Flight Methods, CEN Saclay (1961) 32.
[12] LE RIGOLEUR, C. et al., Int. Conf. on the Study of Nuclear Structure with Neutrons, Antwerp (July 1965) No. 167.
[13] LE RIGOLEUR, C. et al., J. nucl. Energy, Parts A and B 20 (1966) 67.

DISCUSSION

(on papers CN-23/71 and CN-23/72)

J. JULIEN: Do you think it was necessary to operate the linear accelerator with a 15-ns neutron pulse in the sodium experiment?

P. RIBON: We tried to improve the resolution by increasing as much as possible the speed of our electronics and we used a relatively thin boron screen to avoid multiple scattering. We shall check with the true experimental resolution obtained from the 35-keV sodium resonance.

R. C. BLOCK: You measured the transmission of sodium with thick samples. Did you observe the 7.6-keV resonance that we observed in capture at the Rensselaer Polytechnic Institute?

P. RIBON: In this preliminary work we did not try to measure the cross-section below 25 keV.

LOW-ENERGY NEUTRON CROSS-SECTIONS OF SODIUM

M. C. MOXON AND N. J. PATTENDEN
ATOMIC ENERGY RESEARCH ESTABLISHMENT,
HARWELL, DIDCOT, BERKS,
UNITED KINGDOM

Abstract

LOW-ENERGY NEUTRON CROSS-SECTIONS OF SODIUM. The Harwell 45-MeV electron linear accelerator pulsed-neutron source has been used to measure the total and capture cross-sections of sodium over the energy range from 200 eV to 100 keV. Flight paths of 94 m and 32 m were used for the total and capture measurements, respectively, giving best resolutions of 2.6 and 10 nA/m, respectively. Samples of pure sodium metal and sodium chloride solution in heavy water were used in the measurements, having thicknesses between 0.003 and 0.025 Na atom/b.

Shape and area analysis methods were used to obtain parameters of resonances at 2.8 and 54 keV. The radiative capture cross-section as a function of energy was obtained from the observed γ-ray yield data by correcting for the neutron capture following multiple scattering in the sample with a Monte Carlo calculation programmed for an IBM-7030 computer.

1. INTRODUCTION

Sodium is a possible coolant material for fast power reactors. In these reactors, the fission neutron spectrum is degraded by collisions with cooling and structural materials, and a significant fraction of the neutrons have energies below 10 keV. Consequently, an accurate knowledge of the variation with energy of the sodium cross-sections, especially the capture cross-section, is of great importance in design considerations.

Numerous measurements have been made of the cross-section in the 2.9-keV region, and the data have been interpreted in a variety of ways [1 - 6]. It is generally concluded that the resonance is s-wave, but there is conflicting evidence on whether the total angular momentum, J, is 1 or 2, on the value of neutron width, and on the scattering amplitude. Almost no information has been available hitherto on the value of radiation width.

In this paper we present measurements of the total and capture cross-sections in the region of the 2.9-keV resonance, and measurements of the total cross-section over the 54-keV resonance. The derivation from these data of parameters of the 2.9- and 54-keV resonances is discussed.

2. EXPERIMENTAL PROCEDURE

The measurements were carried out on the Harwell 45-MeV electron linac, using the booster target as the pulsed neutron source. For the capture measurements, a 32-m flight path was used with a neutron pulse of about 200 ns before moderation. For the total cross-section measurements, a 94-m flight path was used with a neutron pulse of about 250 ns

before moderation. In both types of measurement, 125-ns time channels were used, the individual neutron flight times were recorded in 16-bit binary form on magnetic tape, and the counts per channel were subsequently summed by playing back into a D. E. C. PDP-4 computer. This gave a maximum of 16384 channels per pass of the tape. The contents of the PDP-4 memory were written onto IBM-compatible magnetic tape for reading into an IBM-7030 computer in which further processing was carried out.

2.1. Samples

Three metallic samples of sodium were prepared by pressing freshly cut sodium between 0.25-mm aluminium foils, the thickness and uniformity being determined by steel shims. The thickness of the sodium calculated from the weight of the samples minus the calculated weight of the aluminium foils was in good agreement with the thickness of the steel shims used in the preparation. The thickest sample was sealed in a 1.5-mm thick aluminium can after weighing. The uniformity and absence of holes was checked by taking X-ray photographs of the samples. The n values calculated from the weight of the samples are given below

(1) 2.446×10^{-2} atom/b
(2) 2.14×10^{-3} atom/b
(3) 8.75×10^{-4} atom/b

with estimated uncertainties of 0.5% on (1) and 5% on (2) and (3). The sample purity is discussed below in section 3.1.

In addition, some total cross-section measurements have been made with a sample consisting of a solution of NaCl in heavy water, contained in a silica cell of dimensions $5.0 \times 5.0 \times 3.0$ cm. The NaCl concentration was 0.1 g/ml, giving 3.09×10^{-3} Na atom/b. This sample was compared with an identical container of NaCl-free heavy water.

2.2. Capture cross-section measurements

The neutron capture rate from the three samples of metallic sodium was measured as a function of neutron time-of-flight using a Moxon-Rae [7] neutron-capture gamma-ray detector.

The gamma-ray detector has an efficiency proportional to the gamma-ray energy emitted on neutron capture. Using this fact the detector was calibrated with "black" resonances, i.e. having zero transmission in the resonance energy region, so that ideally all the incident neutrons of resonance energy were captured (for a more detailed description see Ref. [7]). The elements used for calibration were Ag, Au and U, all having some neutron resonances below 100 eV where the radiation width is nearly equal to the total width. To obtain the neutron-capture cross-section from the observed counts, the incident neutron spectrum and the background must be determined as a function of neutron time-of-flight. The shape of the neutron spectrum in the keV region was measured by counting the 480-keV gamma ray from the $^{10}B\ (n, \alpha)^{7*}Li$ reaction with the capture detector. The following assumptions were made in calculating the neutron spectrum from the observed counts:

(i) the $^{10}B(n, \alpha)^{7*}Li$ reaction cross-section is inversely proportional to the neutron velocity in the neutron energy region 1 eV to 10 keV.

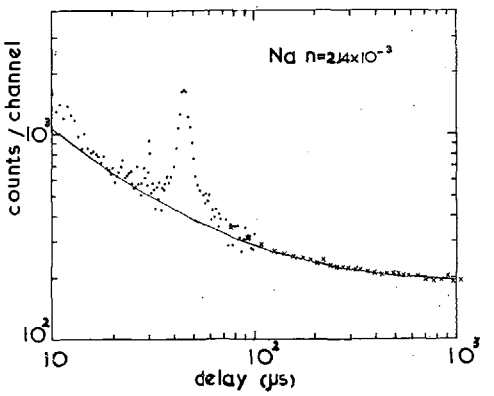

FIG.1. Normalized counts from the sodium sample ($n = 2.14 \times 10^{-3}$) versus neutron time-of-flight
. single channels
× average of 16 channels
The smooth curve is the fitted background obtained from the runs with resonance filters in the neutron beam.

(ii) the ratio of the alphas going to the ground state to those going to the first excited state in ^{7}Li remains constant over the same energy region.

The spectrum shape calculated from the ^{10}B counts was normalized to the neutron flux multiplied by the detector efficiency which was measured at low neutron energies.

Because of the low-capture cross-section of sodium, the accurate determination of the background was very important. The background for each sample was measured by placing resonance filters in the neutron beam between the capture sample and the source. The counts per channel in the bottom of the resonance dips, after subtraction of the machine-independent background and correction for the attenuation of the background by the filters, were fitted to the form

$$B(n) = (a + b/t_n^c)\ \Delta t$$

where B(n) is the background in channel n of width Δt and delay t_n. a, b and c are constants determined from the data.

The unexpectedly high count rate on the low energy side of the 2.9-keV resonance (Fig. 1) required an additional investigation of the background in that region. Selenium was selected as the resonance filter as it has large resonances on either side of the 2.9-keV sodium resonance. The transmission runs on selenium confirmed that the background fitted the form given above and that in the neutron energy region below the 2.9-keV resonance no anomalies occurred in the background. A further check to see if the high count rate was due to scattered neutrons was carried out by looking for a change in shape of the resonance when the neutron beam at all energies was scattered into the detector. A 3.8-cm thick sample of reactor-grade graphite was placed behind the sodium sample in the neutron beam, which scattered ~90% of the incident neutron beam at all energies into the detector. Within statistical accuracy the shape of the resonance did not change and it could only be assumed that the high count rate on the

low energy side of the 2.9-keV resonance came from the sample; its significance will be discussed later.

In the neutron energy region below 500 eV for the two thin samples, no statistical difference between the counts in the bottom of the resonance dips and the regions between them could be detected. In the thick sample only a small difference could be detected, which gave a very inaccurate determination of the capture cross-section.

2.3. Total cross-section measurements

As the 94-m flight path transmission detector has not been described before a brief description will be given here.

The neutron detector consisted of a disc of ^{10}B 8.9-cm diameter and containing ~ 1 g/cm^2 of ^{10}B, mounted in the neutron beam. Four sodium iodide crystals (~ 12 cm diameter and 3.8 cm thick) mounted on 9530 EMI photomultipliers, were used to observe the 480-keV γ-ray from the $^{10}B(n, \alpha)^7Li$ reaction. The detecting system was surrounded by about 10 cm of lead and 30 cm of paraffin wax loaded with boric acid.

The transmission sample was mounted on an automatic sample changer, about 2 m in front of the detector. Another automatic sample changer enabled a filter of materials with "black" resonances at convenient neutron energies to be inserted in the neutron beam to determine the energy dependence of the background. A permanent filter of sulphur was used to provide a normalization point at ~ 110 keV and a boron filter was used to remove neutrons with energies less than 5 eV and to provide a normalization point for the background below this energy. The sequence of sample changer conditions (1 sample in, filters out – 2 sample out, filters out – 3 sample in, filters in – 4 sample out, filters in) was repeated continuously to minimize the effects of electronic drifting and unknown changes in experimental conditions.

To calculate the transmission as a function of time-of-flight, the computer summed together similar runs on a given sample, fitted polynomial relations to the "black" resonances in the filters-in conditions to obtain background curves, normalized these to the filters-out condition, subtracted the background and calculated the transmission per channel. This could then be converted to total cross-section as a function of neutron energy.

3. RESULTS AND ANALYSIS

3.1. Capture cross-section

The capture yield of the metallic sodium sample of thickness 2.14×10^{-3} atom/b is shown in Fig. 2. It is dominated by the capture peak associated with the 2.9-keV resonance. The smooth curve is a Monte Carlo calculation of the capture yield from this sample assuming $J = 1$, $\Gamma_n = 410$ eV and $\Gamma_\gamma = 0.5$ eV. As can be observed, the curve is not a good fit to the data. Several checks were carried out on the high yield region below the 2.9-keV resonance (see section 2.2), and the conclusion was that the high yield was produced by the sample, and must have been due to

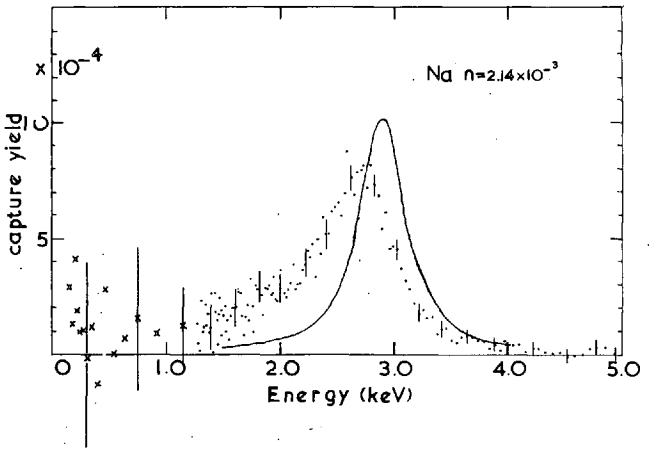

FIG.2 The capture yield from the sodium sample ($n = 2.14 \times 10^{-3}$) versus neutron energy. The smooth curve was obtained from a Monte Carlo calculation assuming J = 1, $\Gamma_n = 410$ eV and $\Gamma_\gamma = 0.5$ eV.

either a genuine high sodium capture cross-section or to impurities in the sample.

Capture runs on the thickest sample ($n = 2.446 \times 10^{-2}$ atom/b) showed five additional peaks below 50 keV. Two at 5.9 and 35 keV, were associated with the aluminium can. Two others, at 340 and 1080 eV, could be attributed to manganese, and the fifth, at 580 eV, to copper. No other elements with resonances at neutron energies below 2 keV, appeared to be present. Assuming radiation widths of 0.6 eV for both Mn and Cu, the amount of each element present in the sample was estimated to be (100 ± 30) ppm and (25 ± 20) ppm respectively and a calculation showed that these impurities would contribute only a few per cent to the capture yield in the energy region below 2.5 keV.

The area of the capture peak after correction for multiple scattering (assuming J = 1) and impurities indicates a radiation width of 0.6 eV for the 2.9-keV sodium resonance. The shape of the capture yield suggests some form of interference in the capture cross-section. Calculations using known resonances and assuming that all the capture amplitudes interfere constructively below the 2.9-keV resonance still give a cross-section a factor of two below that observed.

3.2. Total cross-section

3.2.1. 2.9-keV resonance

The transmission of the metallic sample of thickness $n = 2.446 \times 10^{-2}$ Na atom/b was measured across the resonance. Approximately 35 channels showed zero transmission. An area analysis was performed on the data, using the Atta-Harvey programme [8], which gave a $g\Gamma_n$ value of 159 ± 5 meV for an assumed Γ-value of 410 meV. Since for this resonance $\Gamma_n \doteqdot \Gamma$, this shows that g = 3/8 and the resonance J-value is 1. An attempt was made to analyse the data with the shape analysis programme of Atta-Harvey [8], which was unsuccessful due to the sensitivity of the parameters obtained to the value of scattering amplitude assumed. In

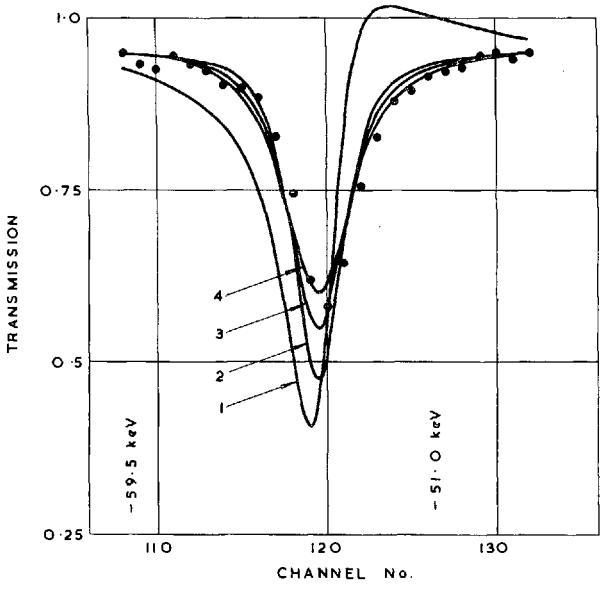

FIG.3. Na 54-keV resonance. Transmission of sample of $n = 2.446 \times 10^{-2}$ atom/b. Points are experimental. Curves are calculated by the Atta-Harvey area analysis programme [8], with the following fixed parameters:

1. Γ = 800 eV, a = 4.9 f
2. Γ = 800 eV, a = 0.0
3. Γ = 1200 eV, a = 0.0
4. Γ = 1600 eV, a = 0.0

these measurements, the sample thickness was not large enough to obtain accurate total cross-section measurements far from the resonance energy. A general conclusion was drawn from the shape analysis that satisfactory fits to the data could be obtained assuming that the resonance was s-wave. The resonance energy was 2860 ± 15 eV.

The transmission of the NaCl solution sample of thickness $n = 3.09 \times 10^{-3}$ Na atom/b was also measured across the resonance. The cells containing the solution and the blank heavy water were first checked by comparing their transmissions when filled with light water, which were the same to within 0.3%. The minimum transmission at the sodium resonance peak was 0.34 ± 0.02, corresponding to an observed total cross-section of 350 ± 25 b. Since the Doppler width is about 3.7 eV and the resolution width (full width at half maximum) is about 11 eV, the observed peak cross-section should correspond closely to the true peak value σ_0. This also indicates a value for g of 3/8, from the relation

$$\sigma_0 = 4\pi \lambda\!\!\!^{-2} g \Gamma_n / \Gamma$$

and confirms the value obtained from the thick sample area analysis.

3.2.2. 54-keV resonance

The transmission of the metallic sample of thickness $n = 2.446 \times 10^{-2}$ Na atom/b was measured across the resonance, and an area analysis was performed on the data using the Atta-Harvey programme [8]. The

programme is not strictly applicable to this energy range, since it assumes an energy-independent scattering amplitude, but the assumption is not important in this case, as will be apparent in the following discussion.

The experimental data, together with the transmissions calculated by the programme for different assumed parameters, are shown in Fig. 3. Curve 1 is for an assumed Γ of 800 eV and a scattering amplitude of 4.9 f. The curve shows clearly the characteristic shape of interference between an s-wave level and potential scattering, which is not observed in the data. The other three curves are for Γ-values of 800, 1200 and 1600 eV with the scattering amplitude set to zero. This simulates the shape of a p-wave resonance, and shows that the data can be fitted satisfactorily in this way, with a Γ-value of 1400 ± 200 eV. The calculated curves are corrected for resolution and Doppler broadening, but since the resolution width is about 900 eV at resonance energy, the observed minimum transmission is sensitive to the exact resolution value used. We consider that the resolution uncertainty does not affect significantly the error on Γ shown above.

The area analysis programme gives a $g\Gamma_n$ value of 750 ± 40 eV for an assumed Γ of 1400 eV. In this case, the $g\Gamma_n$ value derived is rather insensitive to the Γ-value assumed. Hence this analysis tends to favour a g-value of 5/8, corresponding to a value of J = 2 for the resonance, although the results are not conclusive. We estimate the resonance energy to be 54 ± 1 keV.

4. DISCUSSION

Our measurements indicate that the resonance at 2860 ± 15 eV has $l = 0$, $J = 1$ and $\Gamma_n = 424 \pm 13$ eV, and the resonance at 54 ± 1 keV has $l = 1$, $g\Gamma_n = 750 \pm 40$ eV and $J = 2$ (although the last value is not conclusive). In the case of the 2.9-keV resonance, we are in complete agreement with Lynn et al. [2] and Good et al. [4], but disagree with Hibdon [1] ($l = 0$, $J = 2$, $\Gamma_n = 220$ eV) and Garg et al. [5] ($l = 0$, $J = 2$, $\Gamma_n = 380 \pm 20$ eV). The disagreement with Hibdon is largely one of angular momentum assignment from the σ_0 value, and we feel that his method of obtaining σ_0 by linear extrapolation to zero resolution width may be in error. We cannot account for our disagreement with Garg et al., and we propose to make further measurements over a wider range of energy and sample thickness to investigate this further. The area of the capture yield peak at 2.9 keV (including the high low energy wing) gives a Γ_γ value of 0.6 eV. There appears to be no plausible explanation for the shape of the low energy side of the capture yield curve, and further measurements will be performed, using both thicker and thinner samples, especially in the 1-eV to 2-keV region.

In the case of the 54-keV resonance, the main disagreement amongst authors concerns the angular momentum assignment, with Hibdon [1] giving $J = 3$, and Garg et al. [5] $J = 1$. Further measurements with improved resolution must be performed to attempt to remove these discrepancies.

REFERENCES

[1] HIBDON, C. T., Phys. Rev. 118 (1960) 514.
[2] LYNN, J. E., FIRK, F. W. K., MOXON, M. C., Nucl. Phys. 5 (1958) 926.
[3] BLOCK, R. C., Phys. Rev. 109 (1958) 1217.

[4] GOOD, W. M. et al., Phys. Rev. 109 (1958) 926.
[5] GARG, J. B. et al., Int. Conf. on the study of nuclear structure with neutrons, Antwerp (1965) paper 74.
[6] STEPHENSON, T. E., USAEC Rep. BNL 961 (T-401) (1965) (unpublished).
[7] MOXON, M. C., RAE, E. R., Nucl. Instrum. Meth. 24 (1963) 445.
[8] ATTA, S. E., HARVEY, J. A., USAEC Rep. ORNL-3205 (1961) (unpublished).

DISCUSSION

J. J. SCHMIDT: Can you say anything further about the reasons for the disagreement between your transmission measurements in the vicinity of the 2.9-keV resonance and those of Garg et al. from Columbia University? The latter group get an experimental maximum σ_T of 600 b, corresponding to J = 2, for this resonance with a resolution of only 2 eV.

M. C. MOXON: To check the equivalence of the cells containing the solution and plain heavy water, we repeated the measurement with their roles reversed, i.e. with the solution in the cell which had previously contained plain heavy water. The result was the same to within the experimental errors. Unfortunately, the Columbia group give so few details in their Antwerp Conference paper that no serious evaluation of their work can be made.

J. J. SCHMIDT: I would like to make a comment regarding σ_γ in the vicinity of the 3-keV resonance in Na. With the Columbia values of the g-factor, Γ_n and the thermal capture cross-section of Na one can calculate a Γ_γ and a σ_γ (E) which, when integrated with 1/E weighting, give very good agreement with the best known direct measurement of the non-1/v part of the Na infinite dilution capture resonance integral, viz. about 0.07 b.

M. C. MOXON: If we use the Columbia data for the capture calculation, a lower value of Γ_γ is required to obtain the same capture cross-section. Integrating our observed capture cross-section with a 1/E factor, we obtain a resonance integral over the energy range 1.0 to 5.0 keV of $\sim$ 0.2 b, in contrast to the value of 0.07 b which is obtained by subtracting a 1/v component from an integral measurement in a well-moderated reactor.

R. C. BLOCK: At the Rensselaer Polytechnic Institute too, we have measured thin sample sodium capture and I should like to confirm Mr. Moxon's findings. We observe too much capture at energies below 2.9 keV, compared with what is to be expected from the transmission data presented by the Columbia group.

HIGH-RESOLUTION CROSS-SECTION MEASUREMENTS FOR SOME FAST REACTOR STRUCTURAL MATERIALS IN THE keV ENERGY RANGE*

G. ROHR, E. FRIEDLAND AND J. NEBE
KERNFORSCHUNGSZENTRUM KARLSRUHE,
KARLSRUHE, FEDERAL REPUBLIC OF GERMANY

Abstract

HIGH-RESOLUTION CROSS-SECTION MEASUREMENTS FOR SOME FAST REACTOR STRUCTURAL MATERIALS IN THE keV ENERGY RANGE. Total neutron cross-sections with high resolution were measured in the energy region of about 18-220 keV with two kinds of detectors, together with a 1-ns pulsed Van de Graaff generator and a thick ^{7}Li target. For the lower energy region up to 50 keV the boron slab detector was used in the following manner. Around the boron slab four well-shielded NaI(Tl) detectors were mounted perpendicular to the neutron beam. With this arrangement the background is not time-correlated and can be measured in a very simple and accurate manner. The instrumental time resolution for the four parallel-connected NaI(Tl) detectors was measured as 2.8 ns with the 478-keV γ-ray from the lithium target. The overall time resolution was determined by the above-mentioned instrumental uncertainty, the channel width, and the transit time spread of the detected neutrons in the boron slab.

Above 50 keV the proton recoil detector with two photomultipliers in coincidence was used. The overall time resolution of the spectrometer was determined in a similar way as for the boron slab. With the correct information for the background and the energy resolution of the spectrometer a new technique in determining the resonance parameters was used. Measured cross-sections were compared with the cross-sections of the R-matrix multilevel formula taking into account the finite energy resolution. In this manner one can assign resonance parameters even for resonances which are not completely resolved.

The total neutron cross-section with a resolution of 0.39 ns/m (for 220 keV) was measured for ^{51}V, ^{55}Mn, ^{57}Fe and natural iron. Some new resonances were detected. With the new technique for analysing resonance parameters the spin of more resonances than hitherto known could be determined.

1. INTRODUCTION

In the past high-resolution measurements of total neutron cross-sections in the resonance region were in general analysed by the one-level formula or, in the case of not completely resolved resonances, by the total area method. Both methods have the disadvantage that the influence of neighbouring resonances is difficult to judge. Multilevel formulas have been used only in a few cases, and there usually only the nearest levels have been considered, whilst the more distant resonances, which also might change the shape of the cross-section curve, have been neglected.

It was the intention of this work to analyse the total neutron cross-sections by a multilevel formula, taking into account as many resonances as possible over a wide energy range. To get reliable parameters for not completely resolved resonances, this multilevel formula should also include resolution effects. A precise knowledge of the spectrometer resolution is thus important.

* This work was performed for the Fast Reactor Project within the Framework of the Association Euratom-Gesellschaft für Kernforschung m. b. H., Karlsruhe.

TABLE I. RESONANCE PARAMETERS OF ^{51}V

E(keV)	Γ_n(keV)	J	E(keV)	Γ_n(keV)	J
4.17[a] ±	0.508 ± 0.006	4	68.1	4.70 ± 0.10	4
6.89[a] ±	1.28 ± 0.014	3	83.0	1.20 ± 0.05	4
11.81[a]	5.5 ± 0.05	3	87.6	3.20 ± 0.08	4
16.60[a]	0.35 ± 0.04	4	110.8	0.25 ± 0.03	3
17.40[a]	0.35 ± 0.04	4	113.5	0.11 ± 0.01	4
21.65[a]	0.79 ± 0.05	3	114.8	0.08 ± 0.01	3
29.45	0.191 ± 0.02	4	116.6	2.40 ± 0.08	4
39.3	0.57 ± 0.04	3	118.7	20.5 ± 1.0	4
48.15	0.15 ± 0.02	4	118.7	0.13 ± 0.02	3
49.55	0.63 ± 0.04	3	134.7	3.20 ± 0.15	4
51.95	0.115 ± 0.02	4	141.3	3.60 ± 0.15	3
53.0	0.98 ± 0.04	3	145.7	1.50 ± 0.10	3
62.9	3.80 ± 0.10	3	152.9	3.50 ± 0.15	4

[a] Determined by Firk et al. [3].

2. EXPERIMENTAL METHOD

Transmission measurements on ^{51}V, ^{55}Mn, ^{57}Fe and natural iron were performed in the energy range of 20 to 220 keV by the time-of-flight method with a pulsed 3-MeV Van de Graaff accelerator with a pulse duration of 1 ns. The neutrons were generated in a thick lithium target by means of the (p,n) reaction.

For energies up to about 50 keV a boron slab detector was used. In our detector the boron slab was surrounded by four heavily shielded NaI(Tl)-scintillation detectors connected in parallel, and mounted perpendicular to the neutron beam. This resulted in a background which was virtually time-uncorrelated and furthermore much lower than in the conventional setup, where the scintillator is placed directly behind the boron slab [1].

At higher energies it was advantageous to use a proton recoil detector. In this detector two multipliers in coincidence were coupled to the plastic scintillators to discriminate against multiplier noise.

The resolution of both spectrometers was determined from the measured time-width of the 478-keV γ-line originated in the target, and by furthermore taking into account the transit time spread of the neutrons through the detecting material and the channel width of the time analyser. The first mentioned time uncertainty was found as 2.8 ns for the boron slab detector, which is about 30% higher than for the detector with a single scintillator. In the case of the proton recoil detector this uncertainty was slightly energy dependent, changing from 3.9 to 3 ns between 50 and

TABLE II. RESONANCE PARAMETERS OF ^{55}Mn

E(keV)	Γ_n(keV)	J	E(keV)	Γ_n(keV)	J
53.4	0.09 ± 0.01	2	123.5	0.51 ± 0.05	2
57.45	0.81 ± 0.03	3	127.0	2.03 ± 0.20	3
58.0	0.06 ± 0.01	2	128.1	1.51 ± 0.15	2
59.5	0.27 ± 0.02	3	129.5	1.21 ± 0.15	2
59.95	0.10 ± 0.01	2	131.0	0.22 ± 0.03	3
64.1	1.01 ± 0.05	3	142.1	0.55 ± 0.06	3
66.6	0.16 ± 0.02	2	151.3	0.41 ± 0.08	2
69.55	0.14 ± 0.02	3	155.8	1.02 ± 0.10	2
70.07	0.32 ± 0.02	2	158.7	0.92 ± 0.05	3
73.9	0.71 ± 0.04	3	166.9	0.31 ± 0.05	2
81.3	0.44 ± 0.03	2	172.2	1.72 ± 0.15	3
84.35	1.31 ± 0.05	3	176.9	0.32 ± 0.03	3
96.05	0.21 ± 0.02	2	179.9	0.35 ±. 0.05	2
98.2	0.45 ± 0.04	3	181.0	0.25 ± 0.05	3
103.7	0.27 ± 0.02	2	184.4	1.00 ± 0.15	2
104.9	1.51 ± 0.06	2	186.2	2.20 ± 0.20	3
107.0	0.41 ± 0.04	2	188.5	0.81 ± 0.10	3
109.4	1.32 ± 0.13	2	193.9	0.30 ± 0.03	3
110.9	1.83 ± 0.15	3	197.6	0.62 ± 0.05	2
116.1	0.47 ± 0.03	3	203.4	2.70 ± 0.30	3
118.4	0.71 ± 0.04	3	207.7	2.80 ± 0.30	2

250 keV. The overall resolution was 0.39 ns/m at 220 keV for a flight path of 10 m.

3. ANALYSING TECHNIQUE

For analysis of the data the multilevel formula which results from the R-matrix formalism [2] was programmed for the IBM 7074 computer. An energy-dependent correction term for the phase shift was assumed in order to approximate the influence of the unknown resonances outside the measured range [3]. This term was found to change only slowly over the greatest part of the range, but was strongly energy dependent near the energy limits of the measured spectrum, showing the importance of outside resonances. The finite resolution of the spectrometer was accounted for by folding the multilevel formula with the experimental resolution function. This resolution function could be very well approximated by assuming a gaussian form.

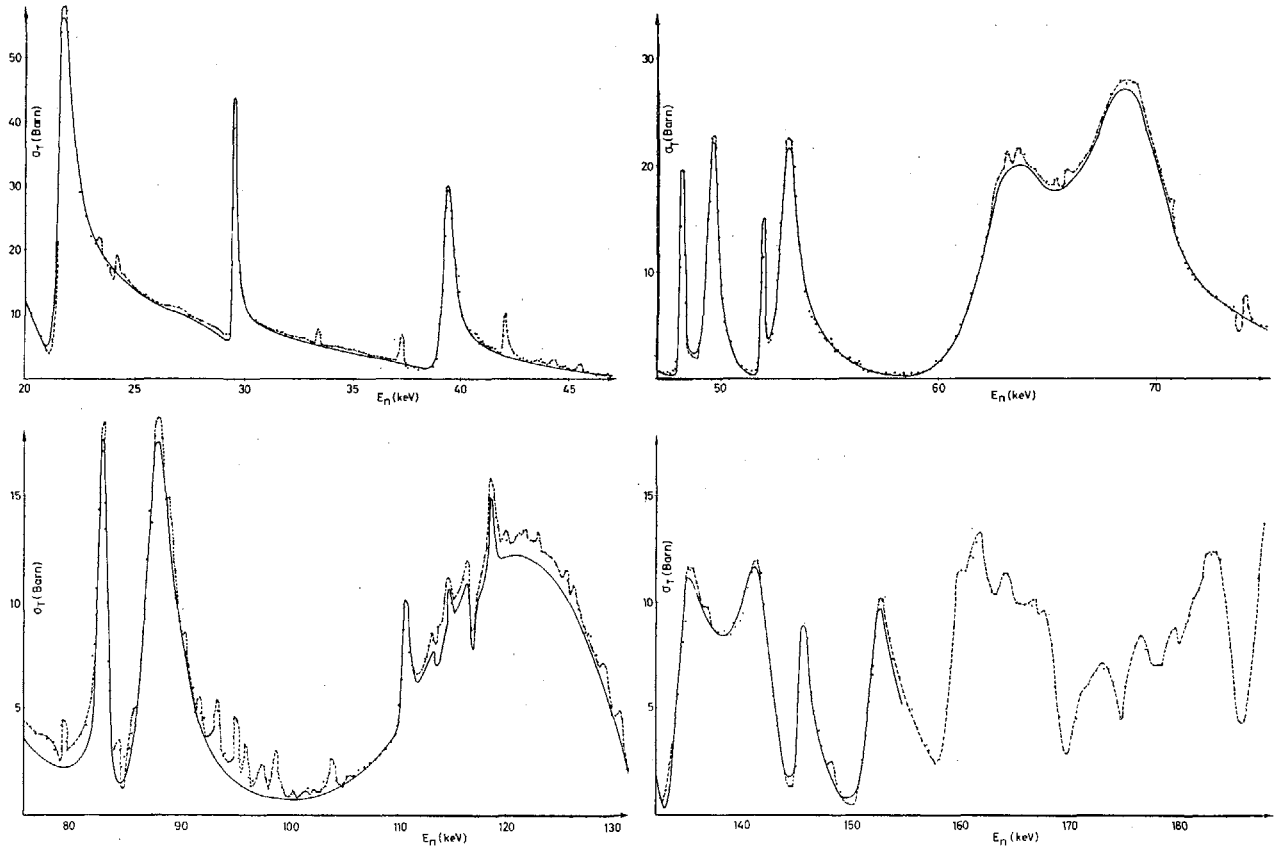

FIG.1. Total neutron cross-section curve for ^{51}V. The solid line represents the multilevel fit.

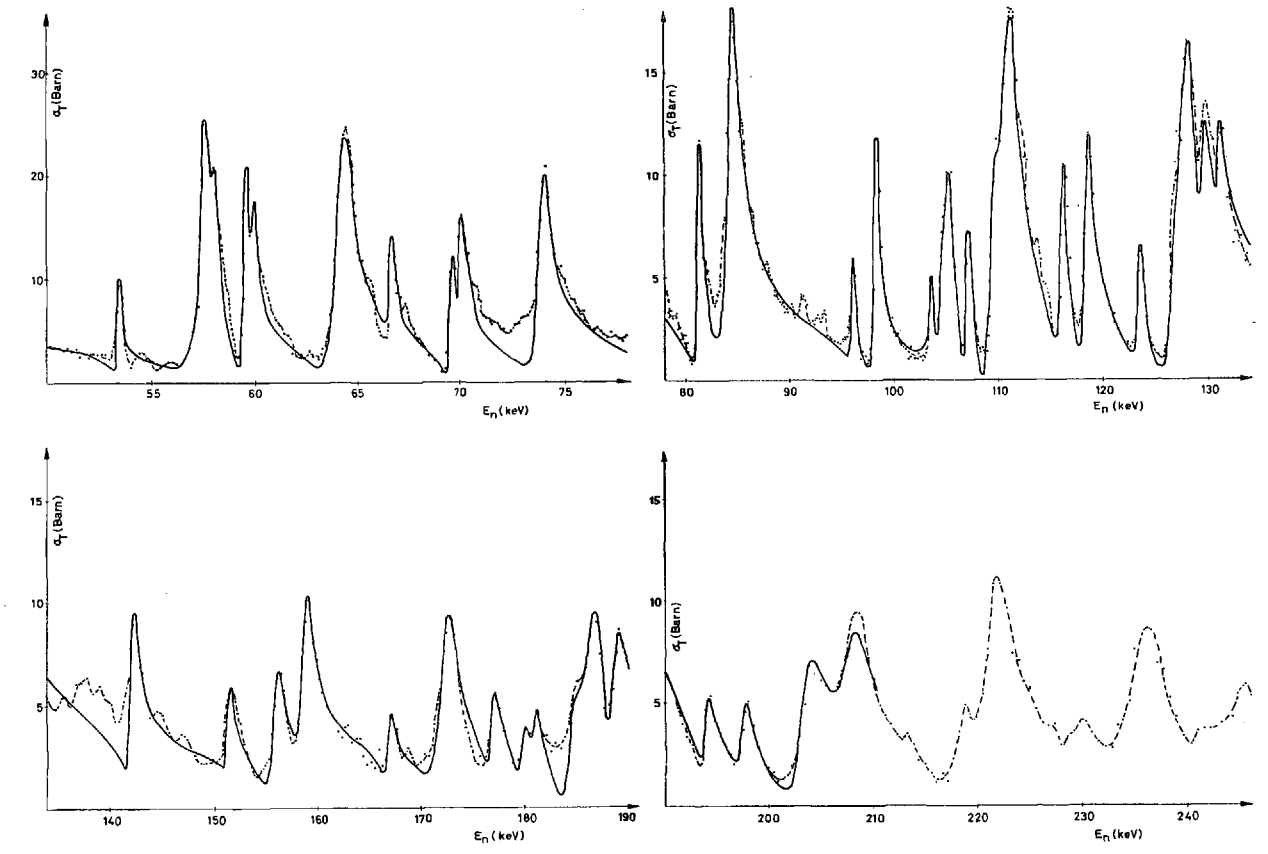

FIG. 2. Total neutron cross-section curve for ^{55}Mn. The solid line represents the multilevel fit.

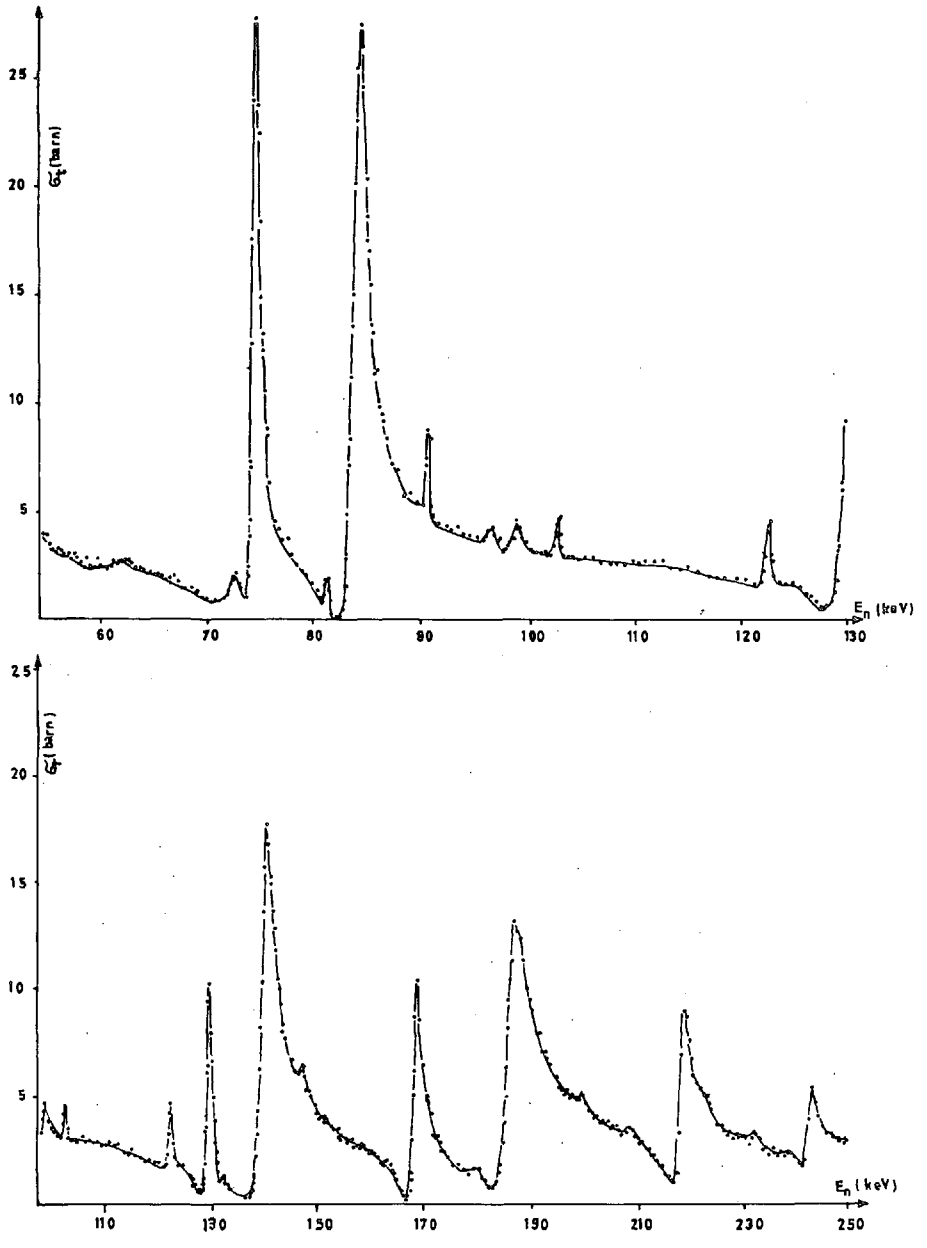

FIG.3. Total neutron cross-section curve for natural iron

TABLE III. RESONANCE PARAMETERS OF ^{56}Fe

E(keV)	Γ_n(keV)	J	E(keV)	Γ_n(keV)	J
74.0	0.539 ± 0.042	1/2	139.9	2.460 ± 0.110	1/2
83.5	0.912 ± 0.085	1/2	168.4	0.874 ± 0.074	1/2
90.2	<0.050	1/2	186.3	3.425 ± 0.267	1/2
122.4	0.125 ± 0.023	1/2	219.2	1.470 ± 0.085	1/2
129.5	0.479 ± 0.038	1/2	242.7	0.630 ± 0.042	1/2

The programme is able to accomodate a maximum of 50 resonances for each spin system for a mixture of three different isotopes, considering s- and p-waves only. The computing time is about 10 min for 100 points of the cross-section curve.

To extract the resonance parameters from the experimental cross-sections, tentative parameters were assigned to each peak for a first trial. The calculated cross-section curve was then compared with the experimental data and the parameters were adjusted until a satisfactory agreement was obtained.

4. RESULTS

For the interpretation of our data only s-waves were considered, as the p-wave strength function is a minimum in this mass region. By the above-mentioned method, it was thus possible to find parameters for all major resonances from 20 to 160 keV for ^{51}V and from 50 to 210 keV for ^{55}Mn. As the influence of neighbouring levels is strongly dependent on the spin state, it was in some cases even possible to assign unambiguous spin values to resonances which were far from resolved.

In Table I all known parameters are given for ^{51}V. For ^{55}Mn the parameters of 42 resonances are tabulated in Table II. The parameters for resonances up to 80 keV were determined before by Morgenstern et al. [4]; their results do not agree in all cases with ours.

The multilevel fit with our parameters is shown in Figs. 1 and 2. The solid line is the calculated cross-section curve and the broken line represents the experimental values. The two curves show generally good agreement.

Figure 3 shows the neutron cross-section for natural iron. No multilevel analysis has been made yet. The parameters in Table III are found by area analysis.

Since our spectrometer needs only small amounts of sample material, it is suited for the investigation of separated isotopes. Up to now only ^{57}Fe, enriched to 90%, has been measured. The cross-section is given in Fig. 4. Analysis of these data is still in progress.

For ^{55}Mn and ^{51}V enough resonance widths have been measured to study the statistical behaviour of them. One must keep in mind, however, that an appreciable number of small resonances are missed. In this

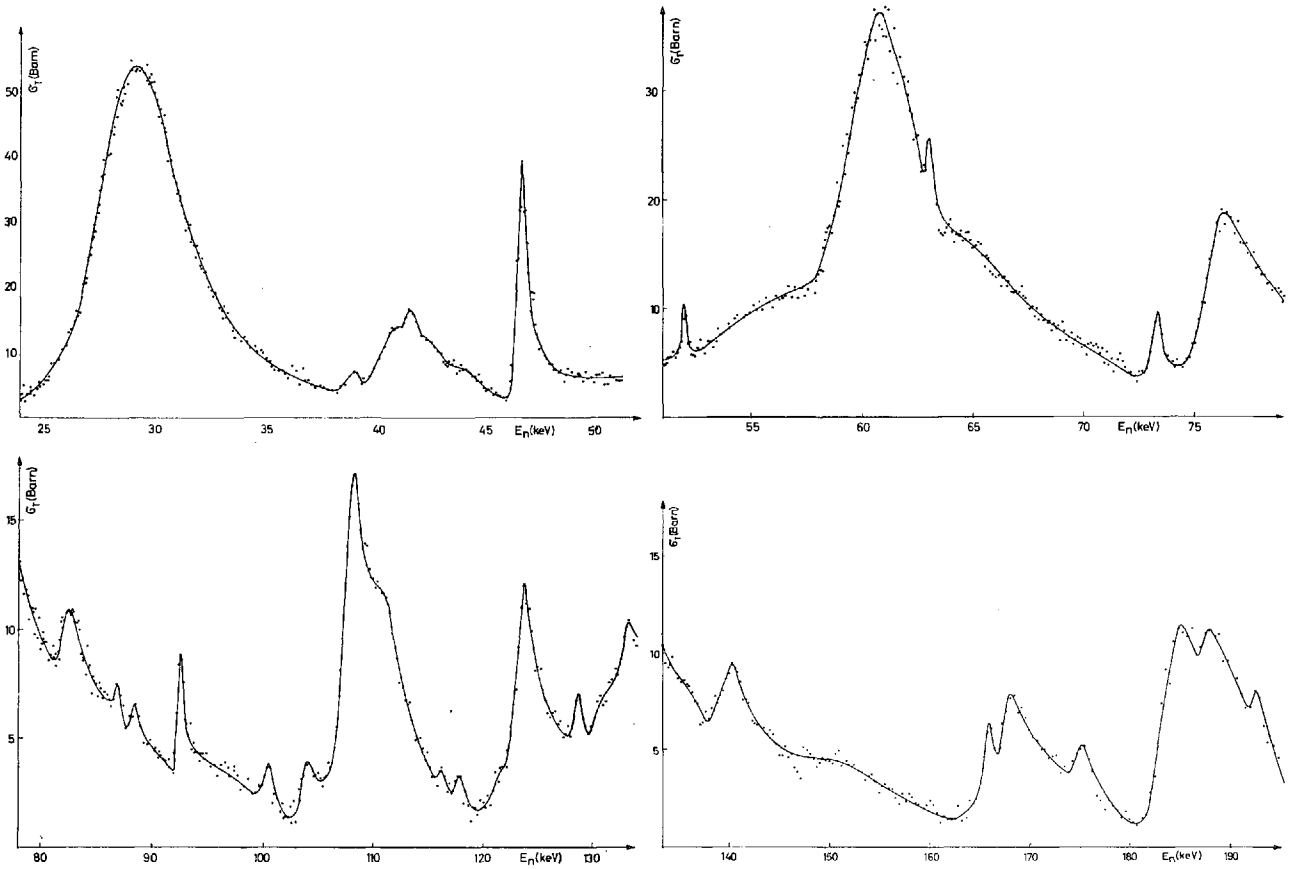

FIG.4. Total neutron cross-section curve for ^{57}Fe

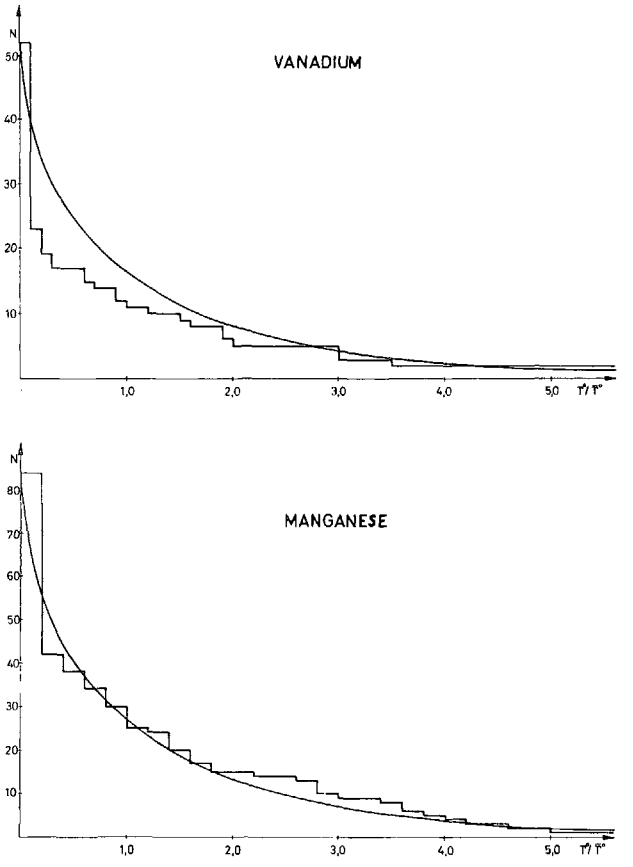

FIG. 5. Number of levels N with a normalized reduced width larger than $\Gamma^0/\bar{\Gamma}$. The smooth curve shows the Porter-Thomas distribution.

sense a resonance is regarded as missed, if the width is too small for determining all the resonance parameters. If the resolution of the spectrometer is known, this number can be estimated under the assumption that their widths obey a Porter-Thomas distribution. With the method of Fuketa and Harvey [5] we found for ^{55}Mn that approximately 42 resonances with a reduced width smaller than 1/5 of the average value were missed. The resulting distribution function is shown in the lower diagram of Fig. 5. Good agreement is found with the expected Porter-Thomas distribution.

In the case of ^{51}V the same method yielded an unrealistic small number of about 5 missed resonances. Therefore the missed levels were estimated by counting every meaningful peak in the cross-section curve, giving a lower limit of 27 missed levels. The upper histogram in Fig. 5 shows the result. It is obvious from this diagram that ^{51}V does not obey a Porter-Thomas distribution. The reason for this might be the existence of broad doorway state resonances, which tend to shift the average width at too high values. This question, together with a discussion on the influence of doorway-state resonances on other average nuclear properties, will be treated in more detail in a future publication.

REFERENCES

[1] GOOD, W. M., NEILER, J. H., GIBBONS, J. H., Phys. Rev. 109 (1958) 926.
[2] BOWMAN, C. D., BILPUCH, E. G., NEWSON, H. W., Ann. Phys. 13 (1962) 319.
[3] FIRK, F. W. K., LYNN, J. E., MOXON, M. C., Proc. phys. Soc. 82 (1963) 477.
[4] MORGENSTERN, J., DE BARROS, S., BIANCHI, G., CORGE, C., HUYNH, V. D., JULIEN, J., LE POITTEVIN, G., NETTER, F., SAMOUR, C., Int. Conf. on the Study of Nucl. Struct. with Neutrons, Antwerpen (1965) Paper 86.
[5] FUKETA, T., HARVEY, J. A., Nucl. Instrum. Meth. 33 (1965) 107.

DISCUSSION

M. F. JAMES: I was interested to note that the paper mentions an energy-dependent term representing the effect of distant resonances. Are the parameters describing this term available?

G. ROHR: The energy-dependent correction term for the phase shift, taking approximate account of the influence of the unknown resonances outside the measured range, is given by the following expression:

$$R^{\infty} = A + B\,(E - E_M) + C\,(E - E_M)^2$$

In the case of ^{55}Mn the constants have the following values:

$$A = 0,\ B = 1.0 \times 10^{-3},\ C = -4.0 \times 10^{-5},\ \text{and}\ E_M = 150\ \text{keV}.$$

OBTENTION DES PARAMETRES CARACTERISANT LES RESONANCES DE NEUTRONS PAR COMBINAISON DE DIFFERENTES METHODES

P. L. CHEVILLON, J. JULIEN, J. MORGENSTERN,
F. NETTER ET C. SAMOUR
CEA, CENTRE D'ETUDES NUCLEAIRES DE SACLAY,
FRANCE

Abstract — Resumen

COMBINED METHOD FOR OBTAINING NEUTRON RESONANCE PARAMETERS. The resonance parameters published by different laboratories are sometimes incompatible, especially those for the total width Γ. Moreover, the value of the spin J is rarely given. The authors describe the different experimental analytical methods they used for the accurate determination of these parameters, in particular of the value J. The paper gives examples of samples of 60 or more resonances, the spin value being given for at least half of the resonances.

OBTENTION DES PARAMETRES CARACTERISANT LES RESONANCES DE NEUTRONS PAR COMBINAISON DE DIFFERENTES METHODES. Les valeurs des paramètres des résonances publiées par les différents laboratoires sont parfois incompatibles, en particulier celles qui sont relatives à la valeur de la largeur totale Γ. De plus, la valeur du spin J est rarement donnée. Les auteurs décrivent les différentes méthodes expérimentales et d'analyse qu'ils ont utilisées pour l'obtention précise des paramètres, en particulier la valeur J. Ils donnent des exemples d'échantillons de 60 résonances ou plus, la valeur du spin étant attribuée au moins à la moitié des résonances.

PROCESSING AND ANALYSIS OF NEUTRON TRANSMISSION DATA AND CONSIDERATIONS OF THE ACCURACY

T. FUKETA, A. ASAMI, M. OHKUBO, Y. NAKAJIMA,
Y. KAWARASAKI AND H. TAKEKOSHI
JAPAN ATOMIC ENERGY RESEARCH INSTITUTE,
TOKAI-MURA, IBARAKI-KEN, JAPAN

Abstract

PROCESSING AND ANALYSIS OF NEUTRON TRANSMISSION DATA AND CONSIDERATIONS OF THE ACCURACY. The main features of the computer programmes which are being used in processing and analysing the neutron transmission data from JAERI (Japan Atomic Energy Research Institute) Linac Time-of-Flight Spectrometer are described, and the related accuracies are discussed. In these programmes, the background is formulated to a channel-dependent expression by making least-squares fitting to the raw data of the background, and the statistical error of the transmission is computed at every individual channel. Some modification of the area-analysis programme which was originally written by S. E. Atta and J. A. Harvey of ORNL is made to expand its functions. That is, in the present programme, computations are iterated semi-automatically until the values of Γ and Γ_n satisfy the condition of self-consistency, $\Gamma = \Gamma_n + \Gamma_\gamma$, for an assumed value of Γ_γ and of the g-factor; and, in estimating the error of the $g\Gamma_n$-value, the statistical error of the transmission at individual channels and the error of the baseline under which the resonance area is defined are taken into account.

The accuracy of the final result of $g\Gamma_n$ depends not only on the statistical errors in the transmission data but also on their systematic errors and on the adequacy of the choice of input parameters for the analysis. Some semi-empirical examinations were made on the influences of these errors upon the value of $g\Gamma_n$. A 20% systematic error in the background, whose amount was about 1% of the open-beam counting rate, gave rise to an error of more than 4% in the computed $g\Gamma_n$-value of a resonance chosen for the test.

1. INTRODUCTION

The development of a technique for automatic data-acquisition and -reduction is progressing rapidly. Many new systems which have recently been developed for these purposes have been reported in recent conferences [1]. Although analysis is generally made after an accumulation of data, the actual procedure of analysis is related closely to the data-acquisition and -reduction system, and as the efficiency of data-acquisition is increased, the method for data-analysis should also be improved. However, one would probably feel that the progress in the soft-ware is not so clear as in the hard-ware. In this connection, investigations of the elements of the individual systems in actual operation and computer-analysis programme of experimental data, for example, are important for further development.

In sections 2 and 3 of this paper, the main features of the computer programmes which are being used in processing and analysing the neutron transmission data from JAERI (Japan Atomic Energy Research Institute) Linac Time-of-Flight Spectrometers [2] are described. To find ways of improving accuracy both in measurement and analysis, some trials were made to investigate the relations between the errors in the input data and the accuracies of the results of analyses. The results of the numerical tests on these relations are exemplified in section 4.

In Fig. 1 the scheme of processing is shown. Although the scheme which we finally reached might be an ordinary one, only a few modifications were needed before the scheme was put into routine execution, but these are beyond the scope of this Conference. As far as the present

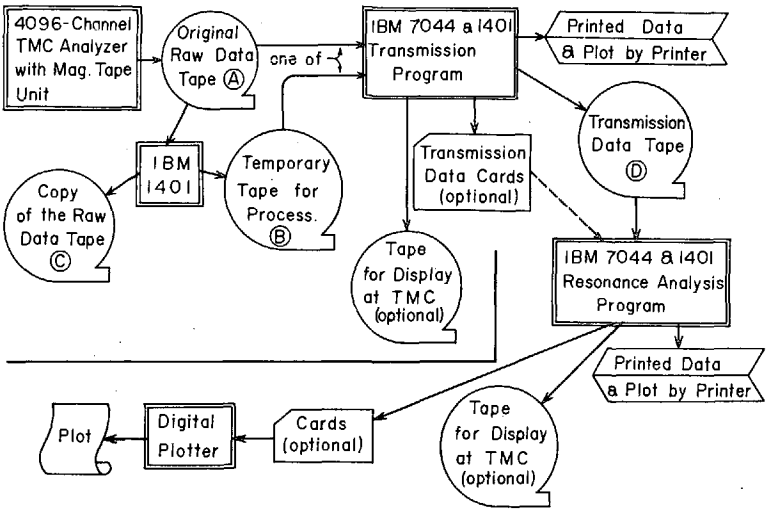

FIG. 1. A schematic flow diagram of processing of neutron-transmission data from the JAERI Linac Time-of-Flight Spectrometer.

transmission-type experiment is concerned, use of an on-line computer of, for example, 4K or 8K words and 2-μs memory-cycle time, will not have a definite advantage over a 4096-channel analyser with 2-μs dead-time and a magnetic tape unit for read-out, unless the computer is also on-line with a large computer. But when the partial cross-section measurements are involved in addition to the total cross-section measurement, it is desirable to set up an on-line computer system with our present equipment.

2. PROGRAMME FOR COMPUTING TRANSMISSION

The first step of the data processing in the total cross-section measurement is calculation of the transmission. The transmission T(i) is defined by the following formula:

$$T(i) = \frac{Z_I(i)/M_I - B_I(i)/M_{BI}}{Z_O(i)/M_O - B_O(i)/M_{BO}} \qquad (1)$$

where, i = a channel number of the time-of-flight,
Z(i) = detector count at the channel i during the time in which the monitor count reaches M, and
B(i) = background count at the channel i during the time in which the monitor count reaches M_B.
The suffixes I and O indicate that those symbols Z, B, M, and M_B are

measured under the condition of sample-in and sample-out (open-beam), respectively.

An effort was made, in the programming, to provide the programme with a comprehensive function of input varieties of the raw data. Initial delay, channel width, and total number of channels can be different for the Z- and B-data. The raw data of each run is identified by a run number of four figures which are tagged with the data in the input magnetic tape. The raw data of more than one experimental run can be read for the computation of one set of the transmission data. Then, each term in Eq.(1) consists of a sum of the counts of those different runs.

From the viewpoint of accuracy, it is preferable to measure the four terms in the above formula cyclically. But in some cases, the background measurements are made separately depending upon the number of channels necessary and/or other experimental circumstances. When the raw data of more than one experimental run are used in the computation, an inter-calibration among the sets of monitor counts can be made, if it is judged necessary, by use of ratios among the off-resonance counts in different runs, although precautions are taken in the measurements so that this sort of calibration may not be needed.

The measurement of backgrounds is made by the standard method; that is, the backgrounds are measured by inserting a lamination of materials containing elements such as tungsten, cobalt, and manganese into the neutron beam. Each element in the lamination has a thickness sufficient to black-out the neutron beam at prominent resonances of the elements. The channel regions, where the resonance dips are clearly saturated, are specified at the input of-the computation. The expressions of the background for the whole energy range, $B_I(i)$ and $B_O(i)$ are then determined by fitting either of the following expressions to the above-mentioned background counts by the use of the least-squares method:

$$B(i) = b_0 + \frac{b_1}{i} + \frac{b_2}{i^2} + \text{---} \qquad (2)$$

or

$$B(i) = b_0 + b_1 e^{-b_2 i} + b_3 e^{-b_4 i} \qquad (3)$$

where b_0, b_1, etc. are parameters, and suffixes I and O are omitted for the sake of simplicity. The number of terms of the expression to be fitted is specified at the input. The fitting to the measured backgrounds is weighted in accordance with the statistical accuracies of the background counts. Expression (2) is satisfactory in the energy region below about 1 keV, while expression (3) is more reasonable in the higher energy region where the background increases rapidly with the increase of the neutron energy. On the other hand, the computation of parameters in expression (2) is simpler and faster than in (3). In case the sample to be measured is thick enough to black-out the neutron beam at its strong resonance, the backgrounds, $B_I(i)/M_{BI}$ and $B_O(i)/M_{BO}$, can be adjusted, if necessary, so that there the computed transmission may become zero precisely. The programme can deal with the case where no measurement for the background for sample-in, B_I, exists. $B_I(i)/M_{BI}$ is then taken to be the same as that for sample-out $B_O(i)/M_{BO}$. It is also possible to make a computation of transmissions with pre-fixed values of b's instead of computing them in the programme.

The statistical error $\Delta T(i)$ of the transmission T(i) is computed at every individual channel from the statistical errors of the counts concerned. When the sample contains material other than the element to be measured, oxygen in oxide sample for example, a corrected transmission can be computed by the following formula before the computation of the cross-section from the transmission:

$$T_{cor}(i) = T(i) \Big/ \left(P_0 + \frac{P_1}{\sqrt{E(i)}} + \frac{P_2}{E(i)} \right)$$

where E(i) is the neutron energy at channel i and P_0, P_1, and P_2 are parameters given at the input by evaluating the contribution of the foreign material. The programme is also provided with conventional functions such as correction for the deadtime of the time analyser, reduction of statistical fluctuations in the open-beam spectrum by averaging the counts in neighbouring channels consecutively, correction for erroneous counts in the raw data due to misfunction of the analyser, and the computation of the cross-section and its error.

The output of the programme consists of a print-out of the input parameters and the computed data, a plot of the transmission by a line-printer, and transmission and its error recorded in a magnetic tape to be used as an input of the succeeding computation. Integers made by truncation of T(i) times 80 000 can be optionally recorded in another magnetic tape for the purpose of displaying the transmission curve on the CRT screen of the time analyser, whose ordinate is (10^5-1) at the maximum.

On an average, five minutes are needed by an IBM-7044 computer for processing a 1024-channel transmission datum including the background fitting with expression (2). A detailed description of this programme with its FORTRAN list will be published in a JAERI Report (3).

3. PROGRAMME FOR ANALYSIS OF NEUTRON RESONANCES [1]

The next step after the computation of transmission is analysis of resonance dips in the transmission. The methods for this analysis are generally classified according to two types, so-called shape-analysis and area-analysis. While the former is applied when experimental resolution width is narrower than the width of resonance and the Doppler effect, the latter is applied in a wide range of energy where the resonances are resolved. Atta and Harvey [4] wrote computer programmes for these two types of methods, and their programmes have since been used quite successfully for the analysis of experimental data from the ORNL Fast-Chopper and the RPI Linac Time-of-Flight Spectrometers. We have made, however, some modifications of their area-analysis programme as are outlined in the following.

In the Harvey-Atta Area-Analysis Code, the computation of $fg\Gamma_n^0$-value of a resonance is made first by using an assumed input value of the total width Γ with other input parameters, such as channel number where the resonance peak occurs, channel region where the resonance area should be computed, and so on; where f is the fractional abundance of the isotope

[1] The computer programming work was supported by the Japanese Nuclear Data Committee.

in sample, g the statistical weight factor, and $\Gamma_n^0 = \Gamma_n/\sqrt{E_0}$ the reduced value of the neutron width Γ_n of the resonance at energy E_0. After the output, including graphical plots of the experimental and computed transmissions, has been examined, a run with a corrected input value of Γ is computed. Adjustable input parameters other than the Γ-value are also corrected in this second run, if necessary.

In our programme, the computations are iterated automatically in the following manner. The first run starts with an assumed value of the total width $\Gamma(1)$. Then the second run starts with the value of the total width, $\Gamma(2)$, which is evaluated by the following equation:

$$\Gamma(2) = \Gamma(1) + K(1)\{\Gamma_\gamma^{as} - [\Gamma(1) - \Gamma_n(1)]\},$$

where Γ_γ^{as} represents an assumed value of the radiation width, K(1) a factor of convergence, and $\Gamma_n(1)$ the neutron width obtained by the first run. The j-th run starts with the value of the total width, $\Gamma(j)$, which is given by

$$\Gamma(j) = \Gamma(j-1) + K(j-1)\{\Gamma_\gamma^{as} - [\Gamma(j-1) - \Gamma_n(j-1)]\},$$

where $\Gamma_n(j-1)$ is the value of neutron width computed in the (j-1)-th run. The values of K(1), K(2), --- K(J) are given at the input arbitrarily, where J is the maximum number of iteration which is specified at the input, and if J is larger than 6, K(7), --- K(J) are all taken to be equal to K(6). When the following condition is satisfied, the iteration stops even before it reaches the maximum:

$$\frac{\left|\Gamma_\gamma^{as} - \{\Gamma(j) - \Gamma_n(j)\}\right|}{\Gamma_\gamma^{as}} < \epsilon$$

where ϵ is a limit specified at the input. The values of $\Gamma(j)$ and $\Gamma_n(j)$ are included in the print-out of the final output. In many cases of well-resolved resonances, the input parameters other than the value of Γ are generally determined quite properly at the beginning, and the modification mentioned above would be justified.

When more than one resonance is analysed simultaneously, the iteration stops if the above condition is satisfied for a given number of the resonances. This provision is made to prevent inadequate continuation of the computation, since an intermediate check on the input parameters and the computed result may be appropriate when the analysis is relatively complicated because of the number of resonances included and/or the overlapping of the resonances.

In the Harvey-Atta Code, the error of the computed value of $fg\Gamma_n^0$ is evaluated on the assumption that the statistical accuracy of the count is equal to a constant throughout the entire range of channels. This constant value of accuracy is estimated from statistical error of the off-resonance transmission. The open-beam counting-rate per channel of equal time-of-flight interval is nearly constant for a wide energy range in the reactor-chopper time-of-flight spectrometer with a 1/v detector; but in our Linac Time-of-Flight Spectrometer, it is approximately in inverse proportion to the square root of the neutron time-of-flight. Therefore, in our case,

the statistical accuracies of the off-resonance transmissions cannot be represented by a single value. Furthermore, the statistical accuracy of the count at a channel in a resonance dip is naturally different from the one at an off-resonance channel. Our output of the transmission programme contains channel-by-channel errors of the transmission as mentioned before, and these errors are used in computing the error of $fg\Gamma_n^0$-value.

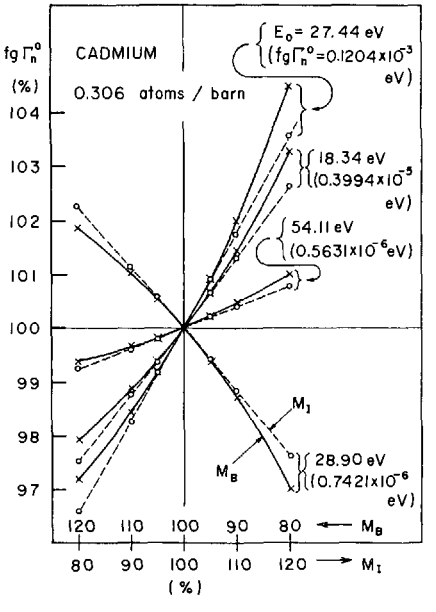

FIG.2. An example of influence which a systematic error of transmission data reflects on the value of $fg\Gamma_n^0$.

Besides the statistical errors, there are some other factors which entail additional errors on the computed $fg\Gamma_n^0$-value. One such error is in the computation of position and shape of the baseline. The resonance area is defined by the transmission curve and the baseline, which is an interpolation between portions of the transmission curve at the off-resonance regions. In our programme, the error of the baseline which is due to the statistical errors of the off-resonance transmissions is also taken into account in the estimation of the error of $fg\Gamma_n^0$-value.

If a resonance is well isolated, the baseline can be determined definitely, but in a region where the resonances are closely spaced, the determination of the baseline becomes ambiguous. Where the off-resonance regions are hardly chosen, there is no definite method to estimate the error of the computed baseline, but a rough estimation of its maximum possible error can be made by inspecting a superposition of the experimental transmissions and the computed curves of transmission and baseline; and this estimated value of the baseline error can be put in our programme to estimate an upper-limit of the error in $fg\Gamma_n^0$-value due to the ambiguity in baseline.

The modifications we have made so far do not change the essential part of the Harvey-Atta Code. The computation time depends upon various conditions of the data and input specifications, but is, on the average,

roughly a half minute or less by IBM-7044 for the analysis of one resonance with J = 1. A detailed description including a FORTRAN list will be published in a JAERI Report [5].

4. EMPIRICAL TESTS OF RELATIONS BETWEEN THE ERRORS OF THE INPUT DATA AND THE RESULTANT ERROR OF THE OUTPUT

From errors in the input data, the statistical error is rigorously treated in our area analysis programme. However, since the accuracy of measurements is improving steadily and the accuracy requested is becoming higher, it is now considered important to estimate the role of errors in the transmission data, other than the statistical error, and in the input parameters.

It is desirable to relate analytically the influence of these errors on the value of $fg\Gamma_n^0$ obtained by the area analysis. But the relations would be complicated because of variations in the conditions, such as size of resonance dip and overlapping of resonances. In this chapter the results of some numerical tests, not analytical but experimental, are presented.

It might have been generally accepted that the value of $fg\Gamma_n^0$ resulting from the area analysis of the transmission dip is not too sensitive to systematic error of the transmission data, because the $fg\Gamma_n^0$ value is, in principle, not affected by the kind of error that can be corrected by multiplication of a constant factor, and any systematic error is, to some extent, of such a character. But this will not hold rigorously.

The test on the role of a systematic error was made by the use of a series of imaginary transmission data, which were computed with artificially varied values of the monitor counts, M_I or M_B. Throughout the computations, all input data other than the monitor count were kept unchanged, and the background counting rates for the sample-in and -out counting were taken to be equal to each other. Then, the area-analysis computations were made with the sets of imaginary transmissions, all the input parameters being kept unchanged. The results of this test on the transmission data of natural cadmium at four of its resonances is shown in Fig. 2. The abscissa indicates the variation of monitor counts M_I or M_B, and the ordinate that of the value of $fg\Gamma_n^0$, each in percentage. The solid and broken curves correspond to the change of M_B and M_I, respectively. The resonance energies and the $fg\Gamma_n^0$-values which are derived from the original data are given in the figure. But the numerical values themselves are preliminary.

The influence is larger in percentage for resonances with larger $fg\Gamma_n^0$-values. It should be noted that a percentage error of $fg\Gamma_n^0$-value evaluated from the counting statistics is generally smaller for a larger resonance. The small resonance dip at 28.9 eV was on the slope of a big dip at 27.4 eV, and these two dips were analysed simultaneously. In Fig. 2, the behaviour of the curves for this 28.9-eV dip is different from others both in direction and amount. This is considered to be due to the effect of overlapping.

The range of the abscissa, 20% change in M_I or M_B, might be unlikely to happen in actual cases. However, 20% error, not in the monitor count M_B itself but in the background measurement, happens sometimes, because there are technical difficulties in making really adequate measurement of

the background. In the black-resonance method of background measurement, the black-resonance sample itself perturbs the experimental condition for which the background should be determined, and situations are similar in other methods of background measurement. In the data, on which the above-mentioned test was made, the background counting rate was about 1% of the open-beam counting rate. It is noteworthy that a 20% change of this relatively low background could cause a change of more than 4% in the value of $fg\Gamma_n^0$.

Results of the test for influences of errors in the input parameters upon the area analysis are discussed now; only the case of the 18.3-eV resonance is included for simplicity of explanation. In the tests all input data, other than one which was specified in each test in accordance with the purpose of the test, were kept unchanged. Two-percent shift of the baseline position up and downwards gave rise to about ± 6.5% change in the $fg\Gamma_n^0$ value. When the change in the position of the baseline exceeds 2%, fit of the computed transmission curve to the experimental one could easily be judged unlikely. A change of the input value for the Doppler width equivalent to ± 20°C change of the sample temperature from 20°C resulted in -1.7 and + 1.9% change of $fg\Gamma_n^0$-value, respectively. For a variation of the input value of the resolution width between 0.5 and 4 channels, where 2 channels was the actual resolution width, the resulting $fg\Gamma_n^0$-value changed within only 0.5%, as it should be in the area analysis. For the case of overlapped resonances, the relation between input parameters and the computed result is more complicated than the example tested here. The case of 28.9-eV resonance in the test for systematic errors of transmission was only one instance of complication.

5. CONCLUDING REMARKS

The first half of this paper describes the functional features of our computer programmes for computation of the transmission and for the area analysis. These might be understood as an example of computer programmes that are always subject to modifications, extensions, and/or improvements. There are miscellaneous functions such as an automatic identification[6] of resonance dips in the transmission data, which it would be better to include in the neutron-data processing.

The tests on the relations among errors in the latter half of this paper are far from a systematic investigation, but they have been done to achieve a basis for further improvements. One of the results of the tests is summarized as follows: if the estimation of background is in error by an amount equivalent to 0.2% of the open-beam counting rate, the $fg\Gamma_n^0$-value of a resonance can be in error of more than 4% at a measurement of relatively low background of 1%. Thus, we place emphasis on the importance of background measurement even in an experiment with relatively low background rate. It would be important to deal with the discrepancies among data of different sources not only by remeasurements but also by improving estimation of errors.

In this paper only the area-analysis method has been dealt with, but, the shape-analysis method is, needless to say, another important one to be used frequently, and also, necessity of the use of the multi-level analysis in which interference among levels are taken into account will increase in the near future.

ACKNOWLEDGEMENTS

The authors would like to thank Dr. J. A. Harvey for his support by sending us the detailed information on their computer programmes, Miss E. Kimura and Mr. A. Tachibana for their efforts in writing the computer programmes, and Dr. T. Momota for reading the manuscript and for his interest and encouragement. Valuable assistance and discussions with the members of the JAERI Computer Center and the Japanese Nuclear Data Committee are gratefully acknowledged.

REFERENCES

[1] Proc. Conf. on the Utilization of Multiparameter Analysers in Nuclear Physics, Nov. 1962, CU(PNPL)-227, or EANDC (U. S.)-37U, and Proc. of Conference on the Automatic Acquisition and Reduction of Nuclear Data, July 1964, INDSWG-66.

[2] The instrumentation and performances of the Spectrometer are to be published in JAERI Report.

[3] KIMURA, E., ASAMI, A., NAKAJIMA, Y., FUKETA, T., to be published in JAERI Report.

[4] ATTA, S. E., HARVEY, J. A., Rep. ORNL-3205 (1961) and its Addendum (1963).

[5] TACHIBANA, A., IWAKI, T., ASAMI, A., KIMURA, E., NAKAJIMA, Y., FUKETA, T., to be published in JAERI Report.

[6] MENZEL, J. H., private communication.

THE INFLUENCE OF CHEMICAL BINDING ON NEUTRON CROSS-SECTIONS AT HIGHER ENERGIES

K. DRITTLER
REAKTORSTATION GEESTHACHT,
FEDERAL REPUBLIC OF GERMANY

Abstract

THE INFLUENCE OF CHEMICAL BINDING ON NEUTRON CROSS-SECTIONS AT HIGHER ENERGIES. From the formalism of Van Hove, a formula is derived from which the influence of chemical binding on neutron cross-sections at higher energies can be calculated. The cross-section is equal to that of free atoms only if strongly inharmonic binding forces are not present. But strongly inharmonic binding forces are to be expected in crystals. Therefore, crystals with atoms of middle and high mass numbers should still show effects of the crystal binding on the cross-section up to a few thousand eV. Since these effects are comparatively small and nearly temperature-independent, it is difficult to measure them. Therefore, with the anisotropic properties of the chemical binding in crystals, the transmissions of copper single crystals for two different crystallographic orientations were measured from 9 to 3000 eV. From a comparison of these results for the two it is obvious that with great probability there is an influence of the chemical binding. The significance of these effects for reactor calculations is briefly discussed.

Session III

STATISTICAL PROPERTIES OF RESONANCE PARAMETERS

ПАРАМЕТРЫ СТРУКТУРЫ НЕЙТРОННОЙ СИЛОВОЙ ФУНКЦИИ СРЕДНИХ И ТЯЖЕЛЫХ ЯДЕР

С.И.СУХОРУЧКИН
ИНСТИТУТ ТЕОРЕТИЧЕСКОЙ И ЭКСПЕРИМЕНТАЛЬНОЙ

Abstract — Аннотация

PARAMETERS OF THE STRUCTURE OF THE NEUTRON STRENGTH FUNCTION OF MEDIUM AND HEAVY NUCLEI. To obtain reliable values of strength functions when averaging the neutron widths of individual resonances it is necessary to fulfil the condition that the averaging interval exceed the characteristic energy period of modulation of the neutron widths, which is related to single-particle effects in the entrance channel (nuclear). The author presents the results of his analysis of the experimental data with a view to determining the parameters of the single-particle structure of the neutron strength function.

ПАРАМЕТРЫ СТРУКТУРЫ НЕЙТРОННОЙ СИЛОВОЙ ФУНКЦИИ СРЕДНИХ И ТЯЖЕЛЫХ ЯДЕР. Для получения достоверных значений силовых функций при усреднении нейтронных ширин индивидуальных резонансов необходимо соблюдение условия, чтобы интервал усреднения превосходил характерный энергетический период модуляции нейтронных ширин, связанный с одночастичными эффектами во входном ядерном канале. В работе приводятся результаты анализа экспериментальных данных с целью определения параметров одночастичной структуры нейтронной силовой функции.

Нейтронная силовая функция является параметром, необходимым для расчета реакторов, и так как современные теоретические модели ядер не дают возможности заранее рассчитывать ее для каждого конкретного ядра, возникает необходимость в проведении многочисленных измерений, в том числе и на нейтронных спектрометрах по времени пролета. Среди способов получения величин силовой функции одним из основных является метод усреднения параметров нейтронных резонансов, главным образом, первых резонансов, где разрешение спектрометров оказывается оптимальным. Метод усреднения нейтронных ширин предполагает отсутствие корреляций между положением нейтронных уровней и их свойствами, во всяком случае в масштабе нескольких килоэлектроновольт. Ниже будет показано, что экспериментальные данные, по-видимому, противоречат предположению о некоррелированном распределении положений нейтронных резонансов, так что к вопросу об ошибках в величинах силовых функций, полученных усреднением параметров небольшого числа первых нейтронных уровней, следует подходить с определенной осторожностью.

Обратимся сначала к области энергий нейтронов до ~ 100 кэв. Здесь мы можем ожидать проявления неслучайной модуляции нейтронных сечений (и тонкую структуру силовой функции) из-за одночастичных эффектов во входном нейтронном канале. Характерными энергетическими параметрами такой модуляции сечения должны быть интервалы, проявляющиеся и в положениях нижних возбужденных уровней ядер. Рассмотрение у всех ядер положений уровней, отличающихся от основного состояния на величину полного момента $\Delta J = 1^+$ и 2^+ (рис.1) приводит к выводу, что интервальность характеризуется периодом 30 кэв (для

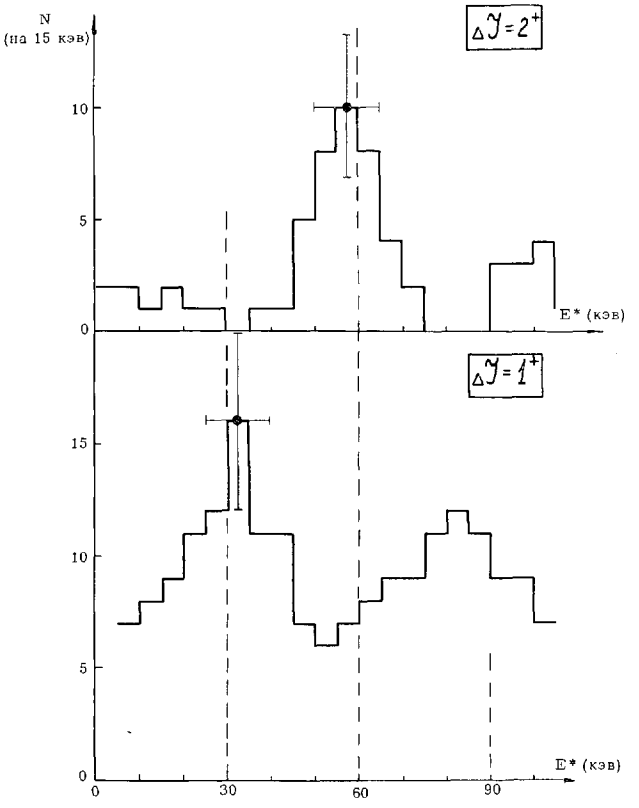

Рис. 1. Распределение энергий (E*) возбужденных уровней (всех ядер) с моментами, отличающимися от момента основного состояния на $\Delta I = 1^+$ и 2^+.

гистограммы рис.1 – числа уровней, попадающих в интервал ±7,5 кэв – были взяты известные к настоящему времени с точностью не хуже, чем 10 кэв, положения всех возбужденных состояний ядер, не имеющие ротационной природы). Распределение положений нейтронных уровней ядер, у которых измерены эти уровни до 30 кэв и выше [1 – 4], приведено на рис.2 (вверху), а такое же распределение для уровней с наибольшей нейтронной шириной (в областях 0 – 50, 50 – 100 кэв и т.д.) приведено внизу рисунка 2. В нижнее распределение включались также ядра V, Mn, Co и Zn с очень большой плотностью уровней, а в положение уровня вводилась небольшая поправка на эффект отдачи ядра. Сравнение распределений рис.1 и 2 позволяет сделать вывод о важности учета одночастичных эффектов при выборе границ усреднения нейтронных сечений и параметров отдельных уровней.

Подобный же анализ можно провести и для области энергий нейтронов до 1 кэв, имея, однако, в виду, что современные теоретические модели для средних и тяжелых ядер не предсказывают каких-либо группирований такого масштаба. Рассмотрим ядра с верхней границей области измеренного спектра нейтронных уровней в 90 – 100 эв и выше.

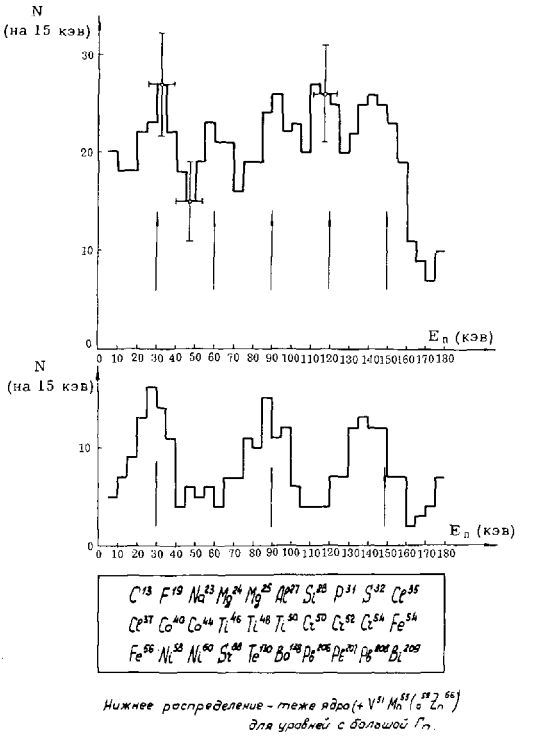

Рис. 2. Распределение положений нейтронных уровней у ядер с границей области исследованных энергий ~ 30 кэв и выше: вверху – все уровни, внизу – уровни с наибольшей нейтронной шириной среди уровней интервала в 50 кэв.

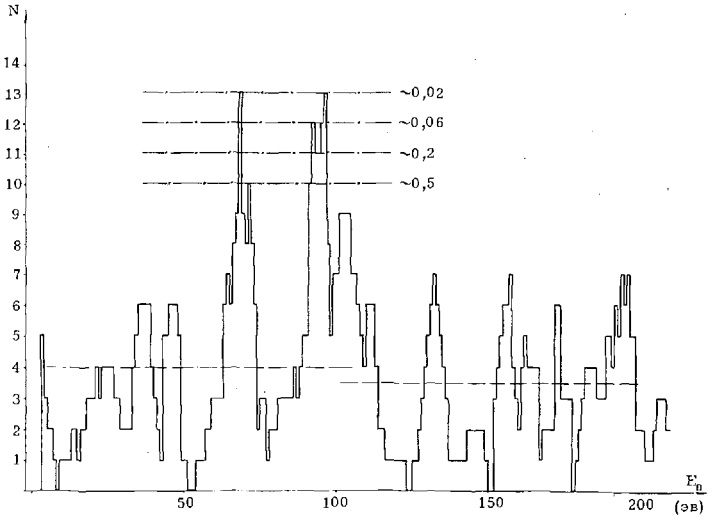

Рис. 3. Оценки вероятности случайного группирования (в интервале ±3 эв) в распределении положений нейтронных уровней с максимальной приведенной нейтронной шириной: – . – . – интегральные оценки случайного появления данного значения N (отнесенные к области 400 эв); ~ – – – среднее значение $\bar{N}$ для интервала 100 эв.

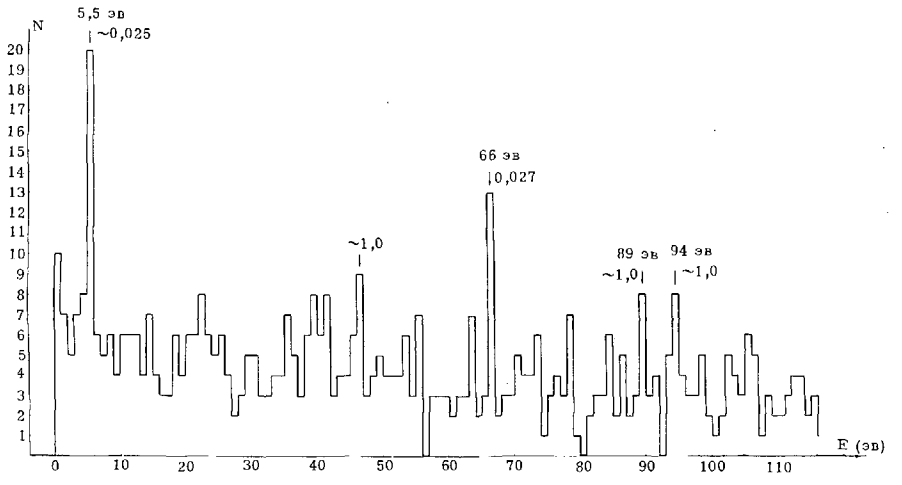

Рис. 4. Распределение положений нейтронных уровней с относительно большими приведенными нейтронными ширинами.

На рис.3 [5] приведено распределение числа "сильных" нейтронных уровней таких ядер (т.е. уровней с небольшими приведенными нейтронными ширинами Γ_n^0 в интервалах 0 – 100 и 100 – 200 эв), попадающих на участок энергетической шкалы в ±3 эв (т.е. 2 $\Delta E = 6$ эв). "Группирование" сильных уровней происходит при энергиях ~ 94 эв и, по-видимому, при 66 – 72 эв, причем вероятность случайного возникновения такого группирования составляет величину в несколько процентов (рис.3). Указанная корреляция сохраняется и при отборе, например, трех сильных уровней на 100 эв в каждом ядре.

Распределение положений уровней с наибольшей Γ_n^0 (среди уровней интервала в 10 эв) показано на рис.4 (2 $\Delta E = 1$ эв). В это распределение входят практически все уровни N-четных ядер-мишеней, и только у четно-четных составных ядер, имеющих высокую плотность состояний, отбираются, таким образом, лишь "сильные" резонансы. Группирования уровней при 5,5 эв и 66 эв могут быть охарактеризованы вероятностями случайного возникновения их в несколько процентов (цифры вверху гистограммы – оценки по распределению Пуассона). Если интервал в 5,5 эв не может существенно повлиять на средние значения силовых функций (так как область измерений обычно превосходит его во много раз), то группирование нейтронных уровней с относительно большими Γ_n^0 в районах 70 и 90 эв может следующим образом отразиться на их величине: когда силовые функции получены усреднением нейтронных ширин резонансов, расположенных ниже 70 – 90 эв, можно ожидать, что они в среднем будут занижены. С ростом числа данных по нейтронным резонансам средних и тяжелых ядер можно надеяться проверить и уточнить отмечавшиеся выше корреляции, представляющие (в случае их реальности) несомненный интерес.

ЛИТЕРАТУРА

[1] ГОРДЕЕВ И.В. и др., "Ядерно-физические константы" (Справочник), Госатомиздат, 1963, стр.52.

[2] БЮЛЛЕТЕНЬ ИНФОРМАЦИОННОГО ЦЕНТРА ПО ЯДЕРНЫМ ДАННЫМ (выпуск первый), Атомиздат, 1964, стр.18.

[3] БЮЛЛЕТЕНЬ ИНФОРМАЦИОННОГО ЦЕНТРА ПО ЯДЕРНЫМ ДАННЫМ (выпуск второй), Атомиздат, 1965, стр.25.

[4] STEHN, J.R. et al., BNL 325, Second Edition, Suppl. 2 (1964).

DISCUSSION

J. JULIEN (Chairman): Did you compare your calculations with experimental data?

S.I. SUKHORUCHKIN: Yes, we used data from the works listed in the references.

ПЛОТНОСТЬ УРОВНЕЙ И СТРУКТУРА АТОМНЫХ ЯДЕР

Ю.Н. ШУБИН, А.В.МАЛЫШЕВ, В.С.СТАВИНСКИЙ
ФИЗИКО-ЭНЕРГЕТИЧЕСКИЙ ИНСТИТУТ, ОБНИНСК
СССР

Abstract — Аннотация

LEVEL DENSITY AND THE STRUCTURE OF ATOMIC NUCLEI. The paper analyses experimental data on neutron resonance density on the basis of a nearly independent-particle model taking into account residual interaction (pairing energy). A detailed correlation is established between a basic theoretical parameter – the single-particle level density near the Fermi surface – and the nuclear shell structure. It is observed that this correlation is connected not only with the type of filling of single-particle levels of real nuclei, but also with their grouping in shells as determined by proton and neutron magic numbers. A formula is derived for calculating this parameter for a nucleus with a given number of protons and neutrons.

The analytical results give reason to hope that the more extensive experimental information on nuclear level density will make it possible to determine more exactly the character of the spectrum of elementary excitations in a degenerate system of strongly interacting fermions.

ПЛОТНОСТЬ УРОВНЕЙ И СТРУКТУРА АТОМНЫХ ЯДЕР. В работе анализируются экспериментальные по плотности нейтронных резонансов на основании модели почти независимых частиц с феноменологическим учетом остаточного взаимодействия (энергия спаривания). Установлена детальная корреляция основного параметра теории – плотности одночастичных уровней вблизи поверхности Ферми – с оболочечной структурой ядер. Обнаружено, что эта корреляция связана не только с деталями в схеме заполнения одночастичных уровней реальных ядер, но и с их группировкой по оболочкам, определяемым магическими числами протонов и нейтронов. Получена формула, позволяющая рассчитывать этот параметр для ядра с данным числом протонов и нейтронов.

Результаты анализа позволяют надеяться, что более обширная экспериментальная информация о плотности ядерных уровней даст возможность уточнить характер спектра элементарных возбуждений в вырожденной системе сильно взаимодействующих фермионов.

NEUTRON STRENGTH FUNCTION MEASUREMENTS IN THE MEDIUM AND HEAVY NUCLEI

C.A. UTTLEY, C.M. NEWSTEAD AND K.M. DIMENT
ATOMIC ENERGY RESEARCH ESTABLISHMENT,
HARWELL, DIDCOT, BERKS,
UNITED KINGDOM

Abstract

NEUTRON STRENGTH FUNCTION MEASUREMENTS IN THE MEDIUM AND HEAVY NUCLEI.
Neutron total cross-section measurements have been made between 100 eV and 1 MeV on nuclei near the mass 100 and mass 240 p-wave size resonances using the Harwell "booster" pulsed neutron source and the 120-m and 300-m spectrometers. The s-wave strength function s_0 and distant level parameter R_0^∞ have usually been separately determined at lower energies and the corresponding p-wave parameters are obtained from a least-squares fit to the higher energy (> 10 keV) total cross-section using the average collision function expression from R-matrix theory. The d-wave strength function is also determined using plausible assumptions on the average parameters of the higher partial waves. The nuclei studied are $^{93}Nb_{41}$, $^{98}Mo_{42}$, $^{100}Mo_{42}$, $^{103}Rh_{45}$ and $^{232}Th_{90}$, $^{233}U_{92}$, $^{235}U_{92}$, $^{238}U_{92}$ and $^{239}Pu_{92}$.

1. INTRODUCTION

Neutron transmission measurements have been made between 100 eV and 10 MeV on several nuclei of interest to both reactor and nuclear physics using the Harwell booster pulsed neutron source and the 120-m and 300-m spectrometers. Nuclei near the mass 100 and mass 240 p-wave size resonances are of special interest for study over the energy region 100 eV to 1 MeV since the analysis of thin and thick sample transmission data enables the p-wave strength function s_1 and the magnitude and sign of the p-wave distant level parameter R_1^∞ to be determined. Both these parameters, but particularly the magnitude and mass variation of the p-wave strength function, are important to nuclear models and the values near mass 240 for the fissile and fertile nuclei enable more accurate calculations to be made of partial cross-sections and the contribution of unresolved resonances to quantities affecting reactor design and safety.

In the case of the common fissile nuclei, the analysis of the average total cross-section is the only method of determining the average s-wave parameters s_0 and R_0^∞ due to the occurrence of strong interference effects in the fission component of resonances in these nuclei with $\Gamma \sim D$ [1] and also, in the case of ^{239}Pu, due to the broad mean fission width associated with resonances of one spin sequence [2]. Thus rarely, if ever, does the total cross-section between resonances fall to the effective potential scattering level and the redistribution of the partial widths which occur with strong interference effects, along with the occurrence of broad fission resonances, results in too low a value of the strength function from individual resonance analysis.

2. EXPERIMENTAL DETAILS

The 300-m flight path has an intermediate detector station at 120 m at which point is inserted a ^{10}B metal powder plug canned in Al of sufficient thickness (0.7 g/cm^2) to prevent overlap neutrons from the previous burst from reaching the 300-m detector. This boron plug is surrounded by four NaI(Tl) crystals and forms a transmission detector at 120 m. The 300-m detector is a mixture of ^{10}B and vaseline in equal volumes canned in aluminium and is 5 in. in diameter by 4 in. thick surrounded by four $4\frac{1}{2} \times 1\frac{1}{2}$ in. NaI(Tl) crystals and 5 in. photomultipliers. The time jitter introduced by the vaseline is much less than the time channel width of $1/8\,\mu$s and simply serves to increase the efficiency of the detector at high energies without affecting the performance at lower energies. Pulses from each detector are fed to the same 8 Mc/s, 16-track tape recorder, two bits being used to code the detector and the position in or out of the beam of the sample mounted on an automatic sample changer.

No significant time-dependent background has been observed at the 300-m detector by the insertion of resonance filters in the neutron beam, and a measurement of the carbon total cross-section over the useful energy range of the 300-m spectrometer from 10 keV to 10 MeV is in very good agreement with other measurements [3]. A time-dependent background is observed at 120 m and its shape is determined from time spectrum measurements using sufficient thicknesses of Al and Mn in the neutron beam to remove spectrum neutrons from all the main resonances in these nuclei below 90 keV. The time-independent background for each detector is monitored continuously by scaling the detector pulses in a 100-μs gate which is open just before the next pulse. Separate scalers are used for the sample in and out positions and the spectrum neutrons over this short time interval will have been removed by the appropriate overlap filters for the two flight path lengths. The pulse repetition frequency of the electron linear accelerator is ~200 pps which results in a useful energy range under good spectrum-to-background conditions for the 120-m detector of from ~ 70 eV to 100 keV, the upper energy limit being set by the uncertainty in the level of the time-dependent background. Thus the two spectrometers have an energy region of overlap from 10 keV to 100 keV, and measurements are made simultaneously over the energy range < 100 eV to 10 MeV. In practice 13 bits are used to record time-of-flight and the magnetic tape is analysed on a 16 000 channel PDP-4 computer.

3. DATA ANALYSIS

3.1. Theoretical considerations

The average total cross-section $\bar{\sigma}_t(l)$ for neutrons of incident orbital angular momentum l is determined by the average collision function $\bar{U}(l)$ over many levels by the expression [4]

$$\overline{\sigma_t(l)} = 2(2l+1)\,\pi\,\lambda\!\!\!^{-2}(1 - \mathrm{Re}\,\bar{U}(l)) \qquad (1)$$

$$\overline{U(l)} = e^{-2i\phi_l}\ \frac{1 - \hat{L}_l^{*} R_l}{1 - \hat{L}_l R_l} \qquad (2)$$

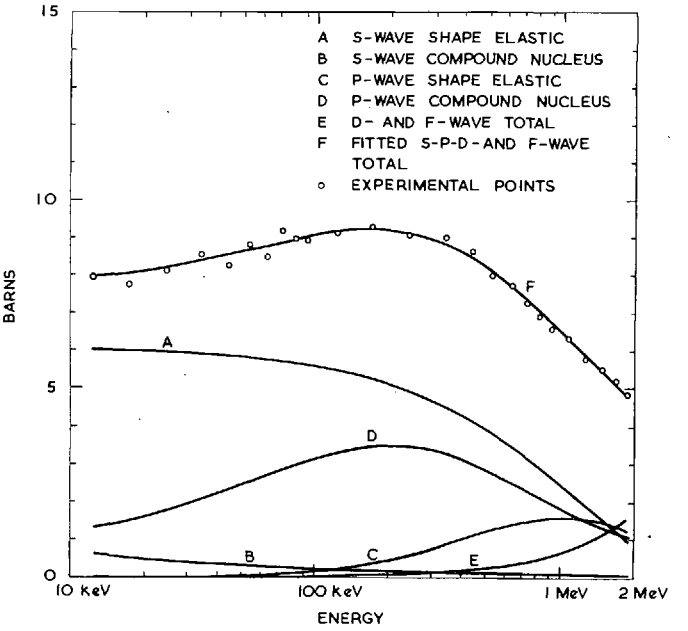

FIG.1. Least-squares fit to niobium-93

In Eq. (2) ϕ_l is the phase shift for l-wave particles scattered from a hard sphere of radius R; $\hat{L}(= L+1)$ where L is the logarithmic derivative of the outgoing wave at radius R and is related to the modified shift factor S_l $(= S_l + 1)$ and the penetration factor P_l according to $L_l = S_l + iP_l$; $R_l = R_l^\infty + i\pi s_l$ is the R-function in which R_l^∞ is the overall effect of very distant levels and s_l is the strength function. It is seen that for each partial wave l only two parameters enter into the total cross-section, the distant level parameter R_l^∞ and the strength function s_l. It is instructive to note that the total cross-section can be split into two other functions of the average collision function [5]

$$\sigma_{se}(l) = (2l+1)\,\pi\lambda^2 \left|1 - \overline{U(l)}\right|^2 \tag{3}$$

$$\sigma_{CN}(l) = (2l+1)\pi\lambda^2 (1 - \left|\overline{U(l)}\right|^2) \tag{4}$$

called the shape elastic and compound nucleus cross-sections respectively which sum to give the total cross-section in Eq. (1). For s- and p-wave neutrons in particular the shape elastic and compound nucleus cross-sections have a completely different energy variation over the energy region of importance in determining their average parameters. This fact is illustrated in Figs. (1) and (2) in which the shape elastic and compound nucleus cross-sections for both s and p-wave neutrons are drawn separately in the fit to the niobium and ^{235}U cross-sections. It is seen that the dominant contribution to the total cross-section up to at least 1 MeV is due to the s-wave shape elastic scattering. Thus it is important to determine s_0, and particularly R_0^∞, in order to obtain

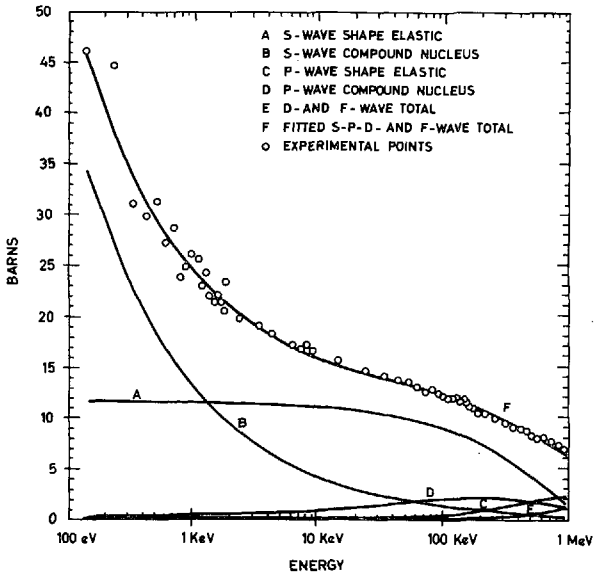

FIG.2. Least-squares fit to uranium-235

reliable values of the p-wave average parameters and possibly the d-wave strength function from the cross-section at higher energies.

For s-wave neutrons $l = 0$, $\hat{S}_0 = 0$, $\phi = kR = \rho$ and $P_0 = \rho$ where k is the incident neutron wave number. Substitution of these quantities into Eqs. (2), (3) and (4) gives

$$\sigma_{se}(0) = 4\pi \lambda^2 \left[\frac{(\sin\rho - R_0^\infty \rho \cos\rho)^2 + (\frac{\pi}{2}\sqrt{E}\, S_0 \cos\rho)^2}{(1+\frac{\pi}{2}\sqrt{E}\, S_0)^2 + (R_0^\infty \rho)^2} \right] \tag{5}$$

$$\sigma_{CN}(0) = 4\pi \lambda^2 \left[\frac{\frac{\pi}{2}\sqrt{E}\, S_0}{(1+\frac{\pi}{2}\sqrt{E}\, S_0) + (R_0^\infty \rho)^2} \right] \tag{6}$$

At low energies and for nuclei outside an s-wave size resonance Eq. (5) reduces to the potential scattering corss-section σ_{pot} (alternatively put $s_0 = 0$ in Eq. (5)) where

$$\sigma_{pot} = 4\pi \lambda^2 \left[\frac{(\sin\rho - R_0^\infty \rho \cos\rho)^2}{1 + (R_0^\infty \rho)^2} \right] = 4\pi\lambda^2 \sin^2(\rho - \arctan \rho R_0^\infty)$$

$$\rightarrow 4\pi R^2 (1 - R_0^\infty)^2 = 4\pi R'^2 \quad (\rho \text{ small}) \tag{7}$$

3.2. Determination of average s-wave parameters

For most nuclei it is not possible to obtain a sufficiently accurate value of the low energy potential scattering cross-section, and thus R_0^∞ ,

from the average total cross-section as a function of energy. Experimentally it is very difficult to measure the true average total cross-section below a few keV due to the necessity of using very thin samples to avoid self-screening. Even though the s-wave strength function of most of the nuclei studied is small ($\leqslant 1\times 10^{-4}$), the large level spacing ($\geqslant 20$ eV) means that the s-wave resonances are strong. Furthermore, the large spacing causes large fluctuations in the low energy average total cross-section due to the small number of resonances involved in averaging. It is fortunate that for the case of the common fissile nuclei the small level spacing, weak resonance structure and relatively broad widths minimize the problems associated with self-screening and wildly fluctuating cross-section because, as mentioned earlier, the analysis of the low energy average cross-section ($E < 20$ keV) is the only method of determining the correct s-wave parameters [2]. For the other nuclei studied the average total cross-section was not measured below 1 keV, and in the case of ^{238}U, ^{232}Th and the molybdenum isotopes not below 10 keV. Two methods are used to determine the lower energy limit above which the true average total cross-section is being measured. The first is to compare the measured total cross-section from transmission measurements on samples of different thicknesses and to observe the energy at which the cross-sections for the two thinnest samples begin to deviate. The second, which is useful when the resolution width is small compared with the total resonance width, is to compare the 'measured' average total cross-section $\bar{\sigma}_m$ obtained from the average transmission over several time channels i according to

$$\overline{T} = \exp(-n\bar{\sigma}_m) = \frac{\Sigma_i T_i \Delta E_i}{\Sigma_i \Delta E_i}$$

with that obtained from averaging the channel total cross-sections $\Sigma_i \sigma_i \Delta E_i / \Sigma_i \Delta E_i$ ($\sigma_i = 1/n \ln 1/T_i$). The procedure adopted to determine the important s-wave distant level parameter R_0^∞ is firstly to measure the reduced neutron widths, and thus the s-wave strength function, from high resolution transmission measurements on samples of different thicknesses. For niobium and rhodium the published resonance parameters of Julien et al. [6] and Ribon et al. [7] have been used. With a knowledge of the reduced neutron widths and thus the strength function s_0 over a significant energy range, two methods of determining R_0^∞ are available.

(a) The effective potential scattering cross-section between resonances at several energies is determined from the high resolution, thick sample transmission measurements. This effective potential scattering radius R_{eff} is corrected for the long range resonance potential interference effects due to the measured resonances at higher and lower energies according to the expression

$$R' = R(1 - R_0^\infty) = R_{eff} - \frac{\lambda\!\!\!^{-}_0}{2} \sum_r g\Gamma^0_{n,r} / E - E_r$$

where R' is the potential scattering radius, $R(=1.35 A^{\frac{1}{3}}$ cm) is taken as the nuclear radius, R_{eff} is the measured effective potential scattering

radius at energy E between any pair of reasonably separated resonances and $\lambda\!\!\!^{-}_0$ is the neutron wavelength at 1 eV.

(b) Lynn [8] has shown that the average transmission as a function of energy of a sample thick enough to involve a high degree of s-wave resonance self-screening can be analysed to determine both R_0^∞ and the p-wave strength function s_1. The average transmission at energy E is given by

$$\langle T(E)\rangle = \langle T_r(E)\rangle \exp\left[-n(\sigma_c(E)+\sigma_p(E))\right]$$

$$\langle T_r(E)\rangle = 1 - \tfrac{1}{2}D\int_0^\infty d\Gamma_n\,(\Gamma_n+\Gamma_\gamma)A_x\frac{\exp(-\Gamma_n/2\bar{\Gamma}_n)}{(2\pi\Gamma_n\bar{\Gamma}_n)^{\frac{1}{2}}} \qquad (8)$$

where $\langle T_r(E)\rangle$ is the mean transmission of neutrons over many s-wave resonances at energy E obtained by weighting average transmission over a single resonance over the Porter-Thomas neutron width distribution. A_x is the Doppler-broadened area function for a resonance of neutron width Γ_n in a sample of thickness n atoms/barn, $\sigma_c(E)$ is the s-wave potential scattering cross-section given by Eq. (7) and $\sigma_p(E)$ is the p-wave compound nucleus cross-section which is the only other partial wave cross-section of importance for E < 50 keV and assumes only that the p-wave resonances are not self-screened. The function $\langle T_r(E)\rangle$ can be calculated from a knowledge of the s-wave strength function and mean level spacing obtained from the low energy high resolution measurements. Alternatively it can be obtained by generating a resonance total cross-section about an energy E from a random selection of neutron widths and spacings from their appropriate distribution functions and then calculating the average transmission over the sample of resonances selected. The experimental average transmission values over the energy range 2 to 50 keV are divided by the computed values of $\langle T_r(E)\rangle$ to leave the exponential term in Eq. (8) from which both R_0^∞ and s_1 are determined from a least-squares fit, using Eqs. (2) and (4) (with l=1) for $\sigma_p(E)$ and Eq. (7) for $\sigma_c(E)$. The energy range selected in this work ($\leqslant$ 50 keV) is too low for terms in Eq. (4) involving R_1^∞ to be important. Lynn has applied this method of analysis to the average transmission of both a thick sample of ^{238}U and ^{232}Th as a function of energy from 2 to 50 keV and more recently to data on three different thick samples of ^{232}Th supplied by the authors. The self-screening of p-wave resonances has been taken into account and his results on ^{232}Th for R_0^∞ and s_1 are compared in Table I with those obtained by method (1) above, and the average total cross-section at higher energies $\leqslant$ 1 MeV.

3.3. Determination of the higher partial wave parameters

In the case of the nuclei near mass 100, the diffraction maximum in the total cross-section due to the nuclear Ramsauer effect occurs at much higher energies (~ 8 MeV) than that for the heavy nuclei (~ 3 MeV). Thus a fit to the average total cross-section up to 1 MeV for the heavy nuclei and up to 2 MeV for the medium nuclei is attempted. The total cross-section is energy averaged over 1-keV intervals up to 10 keV, over two 5-keV steps to 20 keV, over 10-keV intervals to 100 keV, then in 100-keV intervals to 1 MeV or 2 MeV. The average total cross-section is now fitted using a least-squares computer programme with

the s-wave parameter R_0^∞ and sometimes s_0 as fixed parameters. A fit to the data over the whole energy range is carried out for l=1, 2 and 3 using Eqs. (1) and (2) with the appropriate hard sphere phase shift, penetration and level shift factors for each partial wave. The restrictions that $s_3 = s_1$, $R_2^\infty = R_3^\infty = 0$ were fed into the programme. These assumptions are reasonable because firstly one expects from the optical model that p and f-wave size resonances at thermal energies are close together in mass number and secondly, the d and f-wave shape elastic scattering cross-sections are small (~0.1 b) below 1 MeV and either greater or smaller than for $R_2^\infty = R_3^\infty = 0$ depending on the signs of these parameters. Thus the average parameters found are s_1, R_1^∞ and s_2. It is instructive to fit the data first up to 100 keV and then in increasing energy intervals of 100 keV up to 1 or 2 MeV in order to check the sensitivity of the average parameters to increasing neutron energy, since one would expect a significant change in s_1 and R_1^∞ over this energy range, with probably a smaller variation in s_2 and the s-wave parameters. In this investigation it is best to place some restriction on the d-wave strength function below 500 keV, such as $s_2 = s_0$, due to the small d-wave contribution below this energy arising from the small penetrability. Two conclusions can be drawn from this procedure:

(a) No variation in the p-wave strength function s_1 is obtained from fits to the total cross-section with increasing energy. The reason for this is that the p-wave compound nucleus cross-section reaches a maximum near 200 keV and is largely determined by s_1. At this energy it is the dominant contribution to the total cross-section, after the s-wave shape elastic cross-section, and is much larger than the other partial wave components, including p-wave shape elastic scattering. Above 200 keV the p-wave compound nucleus cross-section decreases and p-wave shape elastic scattering becomes increasingly important along with the higher partial wave compound cross-sections at still higher energies. Thus any energy variation in s_1 would be reflected in changes in R_1^∞ and s_2 necessary to fit the higher energy cross-section since the fit obtained below 200 keV must be maintained.

(b) It is found that only small changes in R_1^∞ and s_2 are required to fit the total cross-section as energy increases for most of the medium and heavy nuclei studied. The worst change observed is in niobium where R_1^∞ decreases from +0.34 to +0.22 between 500 keV and 2 MeV while s_2 increases from 0.6×10^{-4} to 0.9×10^{-4}. This change in R_1^∞ is to increase the p-wave contribution slightly indicating, along with the need for an increasing d-wave contribution, that the p-wave parameters change over this energy range.

4. RESULTS AND COMPARISON WITH THEORY

The average resonance parameters obtained from the analyses discussed above are listed in Table I, and examples of the fits to the data for niobium and ^{235}U are shown in Figs. 1 and 2.

The errors on the average parameters s_1, R_1^∞ and s_2 are largely determined by the uncertainty on R_0^∞ and so far have been determined by fitting the total cross-section after changing R_0^∞ by one standard deviation. It is interesting to note that the value of s_1 for ^{93}Nb is in good agreement with that of the Saclay group [6] of $(5 \pm 1)10^{-4}$ obtained

TABLE I. AVERAGE RESONANCE PARAMETERS FOR NUCLEI IN THE 3P AND 4P SIZE RESONANCES

Nucleus	s_0 ($\times 10^4$)	R_0^∞	s_1($\times 10^4$)	R_1^∞	s_2($\times 10^4$)	Comments
^{93}Nb	0.17 ± 0.06 0.35^a	$-0.14^a \pm 0.02$ -0.14^a	5.16 ± 0.24 4.89	$+0.34 \pm 0.02$ +0.35	0.7 ± 0.2 1.6	s_0 from resolved resonances [6]
^{98}Mo	0.42^a	$-0.22^a \pm 0.03$	$6.8^{+0.5}_{-0.5}$	$-0.31^{+0.09}_{-0.01}$	$0.3^{+0.6}_{-0.4}$	
^{100}Mo	0.55^a	$-0.23^a \pm 0.03$	$4.6^{+0.5}_{-0.4}$	$-0.66^{+0.03}_{-0.06}$	$0.5^{+0.1}_{-0.1}$	
^{103}Rh	$0.40^{+0.05}_{-0.08}$	$-0.023^a \pm 0.029$	$5.07^{+0.53}_{-0.29}$	$-0.08^{+0.03}_{-0.03}$	$0.4^{+0.1}_{-0.6}$	
^{232}Th	0.8^a	$-0.178^a \pm 0.015$	1.64 ± 0.24	$+0.019 \pm 0.005$	$0.74^{+0.44}_{-0.17}$	s_0 from Asghar et al.[11]
	0.7^a	$-0.178^a \pm 0.015$	$1.67^{+0.18}_{-0.26}$	$+0.026^{+0.002}_{-0.008}$	$0.76^{+0.16}_{-0.24}$	s_0 from Garg et al.[12]
	0.7^a	-0.189 ± 0.005	1.95 ± 0.20			Lynn [9] analysis of <T> 2 to 50 keV
^{235}U	1.03^a	$-0.158^a \pm 0.015$	$1.76^{+0.24}_{-0.26}$	$+0.02^{+0.03}_{-0.00}$	$0.6^{+0.62}_{-0.10}$	s_0 and R_0^∞ from Uttley [10]
^{238}U	1.0^a	$-0.098^a \pm 0.016$	$2.47^{+0.16}_{-0.28}$	$+0.06^{+0.00}_{-0.04}$	$0.05^{+0.30}_{-0.40}$	s_0 and R_0^∞ from Lynn [8]

[a] Parameters separately determined and fixed in least-squares fit.

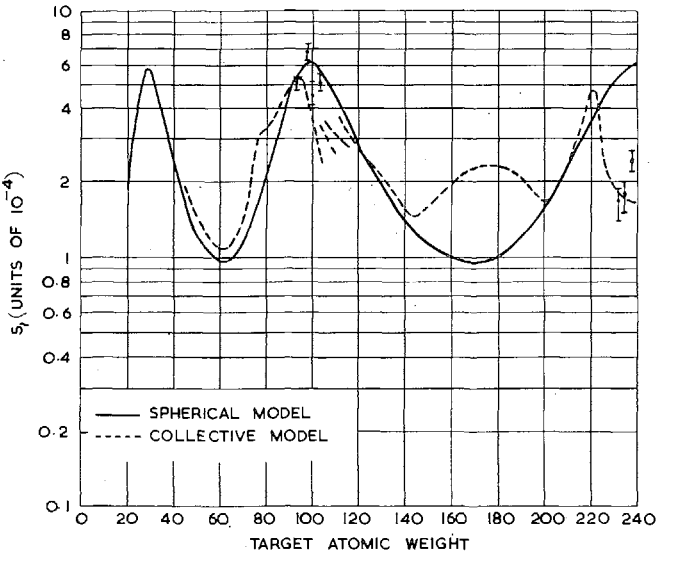

FIG.3. Comparison of theory and experiment for the p-wave strength function

from the identification of p-wave resonances, and with the value of $(5.8 \pm 0.5)10^{-4}$ obtained by Seth et al.[13] from average transmission measurements. The agreement with Seth et al. on ^{93}Nb does not extend to ^{103}Rh or the heavy mass nuclei, the values of s_1 obtained here being significantly higher. The present value of s_1 for ^{238}U of 2.48×10^{-4} is in accord with that obtained by Lynn [8] from the analysis of a thick sample average transmission measurement up to 50 keV.

The p-wave strength function values are compared with theoretical models in Fig. 3. It is seen that, in general, reasonable agreement is observed with the Buck and Perey calculations [14](dashed line)which include the effect of coupling nuclear collective motions to the neutron-nuclear optical potential. The relatively low values of s_1 near mass 240 support the strong rotational splitting of the 4P size resonance obtained by Buck and Perey and are in marked contrast to calculations using just the spherical part of the optical potential. The situation in the region of the 3P size resonance is more confused. The experimental values do not appear to be in good agreement with the vibrational optical model of Buck and Perey as illustrated by the dashed line in Fig. 3. However, the strength function obtained from this model is strongly dependent on the quadrupole deformation parameter β_2 and the energy of the 2+ state excited in quadrupole vibrations such that as the deformation increases and and E_{2+} decreases, the p-wave strength function decreases for a given nuclear species. The calculations of Buck and Perey from A = 94 to A = 104 are for the even-even isotopes of Mo and Ru for which the changes in β_2 and E_{2+} are fairly gradual except for a violent change in β_2 in going from ^{100}Mo to ^{98}Mo. It is likely that a smooth variation in β_2 with mass number has been used by Buck and Perey and that the sudden drop in β_2 for ^{98}Mo explains the high value of s_1 for this nucleus. This assumption is supported by a calculation by Sarius at Bologna [15] who used the Buck and Perey model explicitly to calculate s_1 for ^{98}Mo and ^{100}Mo. The values obtained of 6.2×10^{-4} for ^{98}Mo and 3.9×10^{-4} for ^{100}Mo are in reasonable

agreement with the experimental values in Table I. Calculations for the odd mass nuclei ^{93}Nb and ^{103}Rh have not been made but it is noted that the experimental value of s_1 for ^{93}Nb is in agreement with the predictions of the spherical and collective models which coincide near this mass number.

The signs of R_1^∞ obtained for nuclei in the mass 100 region are also those expected from the optical model. According to this model, for an isolated giant resonance,

$$R_1^\infty = \frac{(E_p - E)\gamma_p^2}{(E_p - E)^2 + W_0^2}$$

where E_p is the energy of the giant resonance, E is the particle energy, γ_p^2 is the reduced single-particle width and W_0 is the imaginary part of the potential. Thus R_1^∞ is positive for nuclei with mass numbers such that $KR < 3\pi$ (where K is the neutron wave number in the real part of the potential) corresponding to $E<E_p$, and is negative for nuclei with radii such that $KR > 3\pi$. It is seen from Table I that ^{93}Nb has a positive R_1^∞ while those for ^{98}Mo, ^{100}Mo and ^{103}Rh are negative. The positive values of R_1^∞ for the heavy mass nuclei indicate that the strength function increases above mass 240 to a second maximum at least as large as the one illustrated in Fig. 3.

REFERENCES

[1] LYNN, J.E., Proc.Int.Conf. on the study of nuclear structure with neutrons, Antwerp 1965, paper 125.
[2] UTTLEY, C.A., Proc.Int.Conf.on the study of nuclear structure with neutrons, Antwerp 1965, paper 98.
[3] UTTLEY, C.A., DIMENT, K.M., Nucl.Phys.Div.Progr. AERE Rep. PR/NP 9 (1966).
[4] LANE, A.M., THOMAS, R.G., Rev.Mod.Phys. 30 (1958) 257.
[5] WEISSKOPF, V.F., Proc.Int.UN Conf. PUAE 2 (1956) 23.
[6] LE POITTEVIN, G., DE BARROS, S., HUYNH, V.D., JULIEN, J., MORGENSTERN, J., NETTER, F., SAMOUR, C., Nucl. Phys. 70 (1965) 497.
[7] RIBON, P., LOTTIN, A., MICHAUDON, A., TROCHON, J., Proc.Int.Conf.on the study of nuclear structure with neutrons, Antwerp 1965, paper 165.
[8] LYNN, J.E., Proc.Phys.Soc. 82 (1963) 903.
[9] LYNN, J.E., Private communication.
[10] UTTLEY, C.A., Harwell Report AERE M1272.
[11] ASGHAR, M., CHAFFEY, C.M., MOXON, M.C., PATTENDEN, N.J., RAE, E.R., UTTLEY, C.A., Nucl.Phys. 76 (1966) 196.
[12] GARG, J.B., RAINWATER, J., PETERSON, J.S., HAVENS, W.W. Jr., Phys.Rev. 134 (1964) B985.
[13] SETH, K.K., TABONY, R.H., BILPUCH, E.G., NEWSON, H.W., Phys.Lett. 13 (1964) 70.
[14] BUCK, B., PEREY, F., Phys.Rev.Lett. 8 (1962) 444.
[15] SARIUS, A.M., Private communication.

DISCUSSION

J. JULIEN (Chairman): Could you give us your opinion regarding the strength function values deduced from average capture cross-section measurements?

C.A. UTTLEY: In my opinion, they are unreliable, since they are subject to the assumption that $<\Gamma_\gamma>/D_0$ for p-wave neutrons is the same as for s-wave neutrons.

ETUDE DE LA DISTRIBUTION DES LARGEURS RADIATIVES PARTIELLES DE ^{195}Pt A L'AIDE D'UN DETECTEUR AU Ge-Li

C. SAMOUR, H.E. JACKSON*, P.L. CHEVILLON, J. JULIEN
ET J. MORGENSTERN
CEA, CENTRE D'ETUDES NUCLEAIRES DE SACLAY,
FRANCE

Abstract — Résumé

LITHIUM-DRIFTED GERMANIUM DETECTOR STUDY OF THE DISTRIBUTION OF PARTIAL RADIATIVE WIDTHS OF ^{195}Pt. In the past, the distributions of partial radiative widths could not be determined correctly because of the poor resolution of detectors. With germanium detectors, the distributions of partial radiative widths in the case of $^{195}Pt + n$ can be studied accurately. The authors present and discuss the results obtained for a large number of resonances in the 0-600 eV energy range.

ETUDE DE LA DISTRIBUTION DES LARGEURS RADIATIVES PARTIELLES DE ^{195}Pt A L'AIDE D'UN DETECTEUR AU Ge-Li. Les distributions des largeurs radiatives partielles n'ont pu dans le passé être obtenues correctement à cause de la mauvaise résolution des détecteurs. L'emploi de détecteurs au germanium a permis une étude précise des distributions des largeurs radiatives partielles dans le cas de $^{195}Pt + n$. Les auteurs présentent et discutent les résultats obtenus pour un grand nombre de résonances dans le domaine d'énergie compris entre 0 et 600 eV.

Dans une étude de capture radiative de neutrons de résonance, il importe, en tout premier lieu, d'essayer de préciser la loi de fluctuation de résonance en résonance de même spin des largeurs radiatives partielles, c'est-à-dire des probabilités de transition par émission de rayonnement gamma entre le niveau de formation du noyau composé et un niveau final donné.

En 1956, Porter et Thomas [1] ont élaboré une théorie statistique rendant compte plus spécialement des fluctuations des largeurs de neutrons. Ils supposent que la distribution d'une largeur quelconque de réaction peut être représentée par une loi en χ^2 à ν degrés de liberté. Ainsi, il est maintenant bien établi que les largeurs réduites de neutrons suivent une loi en χ^2 à 1 degré de liberté et que les largeurs de fission suivent une loi à quelques degrés de liberté.

Le paramètre ν semble donc représentatif du nombre de voies ouvertes de réaction. Ainsi, si le traitement de Porter et Thomas est appliqué aux transitions qui parviennent directement à l'état fondamental du noyau final, ou à un état excité quelconque, une largeur radiative partielle Γ_{γ_i} qui correspond à un rayon gamma d'énergie bien définie, et, par conséquent, à une seule voie de réaction, devrait fluctuer beaucoup de résonance en résonance si cette distribution correspond à un degré de liberté $\nu = 1$.

Cette distribution a été justifiée d'abord par Porter et al. [1, 2] par l'hypothèse statistique selon laquelle les éléments de matrice de l'opérateur hamiltonien, qui définit les états propres du noyau composé,

---

* En congé de l'Argonne National Laboratory, Argonne, Ill., Etats-Unis d'Amérique

suivent une distribution normale. Krieger et Porter [3] ont présenté plus récemment une approche plus générale du problème fondée sur l'indépendance des niveaux du noyau composé et sur l'invariance de la distribution par rapport à une transformation orthogonale des vecteurs propres de ces niveaux.

Le noyau composé ^{195}Pt + n est un cas particulièrement favorable pour étudier la distribution des largeurs radiatives partielles. En effet, il offre un nombre intéressant de résonances isolées de spin J = 1- et, en outre, un certain nombre de raies suffisamment intenses et isolées. Il a fait jusqu'ici l'objet de plusieurs études effectuées par la méthode du temps de vol [4-6] mais, d'une part, l'imperfection, quant à leur résolution, des détecteurs utilisés (cristaux NaI(Tl)) qui rendait les spectres gamma fort complexes, et, d'autre part, le nombre restreint de résonances analysées, limitaient l'efficacité de ces mesures, bien que des dispositifs spéciaux [6] et des techniques d'analyses élaborées [5,6] aient pu être utilisés. Si toutes ces expériences n'ont pu permettre de préciser la valeur de ν, elles ont mis néanmoins très nettement en relief de larges fluctuations de Γ_{γ_i} et ont conduit à penser que ν était vraisemblablement petit, de l'ordre de 2.

Le développement récent des détecteurs au Ge-Li, dont les mérites sont maintenant bien connus [7], nous a conduit à reprendre une telle expérience auprès de l'accélérateur linéaire de Saclay de 45 MeV, à l'aide d'une cible de platine naturel de 5 mm d'épaisseur placée à 45° par rapport à l'axe du faisceau de neutrons. Le détecteur utilisé, fabriqué par H. Mann, au Laboratoire d'Argonne, avait un volume utile de 6 cm^3 et était distant de 10 cm de l'axe du faisceau de neutrons. Ses performances seront discutées en détail dans un autre mémoire [8]. La résolution de l'ensemble de détection était de 6 keV à 1330 keV (^{60}Co) et d'environ 15 keV à 7000 keV. Il est bon de noter que les pics observés avaient une forme triangulaire.

Toute la chaîne électronique était stabilisée digitalement à l'aide d'un générateur de très grande stabilité. La base de temps de vol utilisée avait une longueur de 29 m. La largeur des impulsions de neutrons était de 100 ns. La résolution globale en temps de vol était de 10 ns/m à 700 eV. Afin d'éviter toute surcharge de l'électronique due à la bouffée des rayons γ instantanés, le système était bloqué pendant 20 μs après le début de chaque cycle. Le domaine d'énergie des neutrons étudié allait de 10 à 700 eV. La restitution de l'ensemble était telle que l'étalonnage en énergie des spectres de rayons γ était rigoureusement identique pour toutes les résonances étudiées.

Les données ont été enregistrées à l'aide d'une chaîne d'analyse multidimensionnelle Intertechnique fonctionnant en deux dimensions. Douze digits binaires ont été utilisés pour la définition du temps d'arrivée et 10 pour la définition de l'amplitude d'une impulsion. Cette chaîne comprenait notamment un codeur en temps du type accordéon HC25 (largeur de canaux variable) et un codeur en amplitude CA25 à 1024 canaux.

Nous avons étudié 22 résonances et nous nous sommes limités aux trois transitions 1- → 0+, 1- → 2+ et 1- → 2+ aboutissant à l'état fondamental du noyau ^{196}Pt et aux deux états excités situés à 356 et 689 keV [9]. L'efficacité du détecteur était constante pour ces trois transitions [8].

La résolution en temps de vol était suffisante pour séparer convenablement les doublets et en particulier ceux apparaissant à 66,9-67,5 eV,

à 119-119,6 eV, à 149,9-154,1 eV, à 256,9-261,7 eV, à 558-560 eV et à 590,4-603,3 eV. Cela est une nécessité fondamentale pour le calcul des largeurs partielles, les écrans utilisés étant toujours suffisamment épais pour accroître le taux de comptage. Cependant nous n'avons pu séparer le quadruplet situé à 490 eV; nous n'avons donc pas analysé les trois résonances de spin J = 1 - de ^{195}Pt situées à 485, 490 et 491 eV.

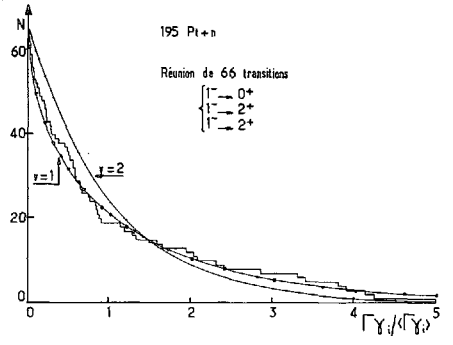

FIG.1. Courbe en temps de vol correspondant au spectre d'amplitude global

La figure 1 montre la courbe en temps de vol correspondant au spectre d'amplitude global. Le tableau I donne les intensités relatives I_i des trois rayonnements γ correspondants, d'énergies respectives 7920, 7564 et 7230 keV. Pour chaque résonance, l'intensité d'une raie donnée est définie comme étant le rapport de l'aire de cette raie à l'aire du spectre global. Le tableau I fait très nettement ressortir de larges fluctuations de résonance en résonance; on voit aussi que chaque résonance présente généralement une seule transition intense, les deux autres étant très faibles. La figure 2 montre l'allure de quelques spectres obtenus. Les données du tableau I montrent que, aux erreurs statistiques près, les intensités $\langle I_i \rangle$ des trois transitions, moyennées sur l'ensemble des résonances, sont sensiblement égales [8]. Cela nous permet de réunir les trois familles partielles pour former une population de 66 éléments et de sommer, pour chaque résonance, les trois intensités.

Un certain nombre de méthodes plus ou moins élaborées ont été développées pour calculer la valeur la plus probable de ν. Nous n'aborderons ici que les points essentiels, nous réservant de détailler les méthodes que nous avons utilisées à Saclay dans une prochaine publication. En appliquant le traitement de Porter et Thomas [1], fondé sur la méthode statistique du maximum de vraisemblance, à la population des 66 largeurs partielles formées à partir de trois familles partielles, en supposant ces dernières indépendantes, ou trouve $\nu = 1,31 \pm 0,20$, valeur compatible avec une loi à 1 degré de liberté. La distribution des largeurs expérimentales réduites $x_i = I_i / \langle I_i \rangle$ a été tracée sur la figure 3, ainsi que les deux distributions en χ^2 à 1 et 2 degrés de liberté. Une simple comparaison confirme le résultat du calcul et montre que les données sont incompatibles avec une loi exponentielle (ν=2). Cet aspect se trouve confirmé si l'on examine la distribution de la somme de ces trois transitions; on trouve en effet

TABLEAU I. PROBABILITES RELATIVES DES TROIS TRANSITIONS ABOUTISSANT A L'ETAT FONDAMENTAL ET AUX DEUX PREMIERS ETATS EXCITES DE ^{196}Pt, POUR LES RESONANCES J = 1-

Energie de résonance (eV)	Transition $1^- \rightarrow 0^+$ (7920 keV)	Transition $1^- \rightarrow 2^+$ (7564 keV)	Transition $1^- \rightarrow 2^+$ (7231 keV)
11,8	3193 ± 66	102 ± 30	24 ± 34
19,4	704 ± 43	194 ± 33	318 ± 46
67,5	1690 ± 87	1317 ± 78	64 ± 49
111,7	710 ± 85	615 ± 91	480 ± 97
119,6	2077 ± 113	4 ± 50	689 ± 87
139,5	552 ± 75	227 ± 74	3537 ± 182
149,9	289 ± 54	59 ± 41	230 ± 60
188,5	756 ± 145	145 ± 107	1724 ± 215
222,2	1069 ± 120	2751 ± 179	62 ± 109
256,9	115 ± 53	42 ± 52	469 ± 106
280	469 ± 115	169 ± 114	1615 ± 234
285,6	2376 ± 178	9 ± 75	423 ± 114
302,3	15 ± 59	2821 ± 170	44 ± 81
382,8	41 ± 49	390 ± 83	187 ± 90
410,1	481 ± 88	181 ± 78	9 ± 86
529,3	717 ± 155	497 ± 154	4165 ± 322
548,8	3266 ± 266	1915 ± 252	633 ± 208
558,7	950 ± 147	1106 ± 161	1366 ± 188
590,4	3440 ± 336	992 ± 217	380 ± 213
632,6	535 ± 438	107 ± 430	535 ± 545
659,8	417 ± 150	246 ± 124	25 ± 123
680	187 ± 108	80 ± 107	27 ± 134

ν=3,71 ± 1,00 soit environ trois fois la valeur précédente, ce qui justifie en outre l'hypothèse d'indépendance.

Contrairement aux largeurs de neutrons, aucun niveau ne peut échapper à la détection dans le cas d'une expérience de capture radiative partielle. Cependant, certains niveaux peuvent avoir des largeurs radiatives faibles et entachées d'erreurs importantes. Afin d'éviter la correction assez délicate suggérée par Porter et Thomas [1] pour rendre compte de ce seuil expérimental, nous avons repris et étendu la méthode préconisée par Garrison [10], c'est-à-dire utilisé une distribution en χ^2 tronquée dans laquelle se trouve inclus le seuil α, en deçà duquel les intensités réduites x_i sont trop imprécises. En prenant α = 0,1, on trouve, pour les 66 probabilités, ν = 1,35 ± 0,42 et, pour la

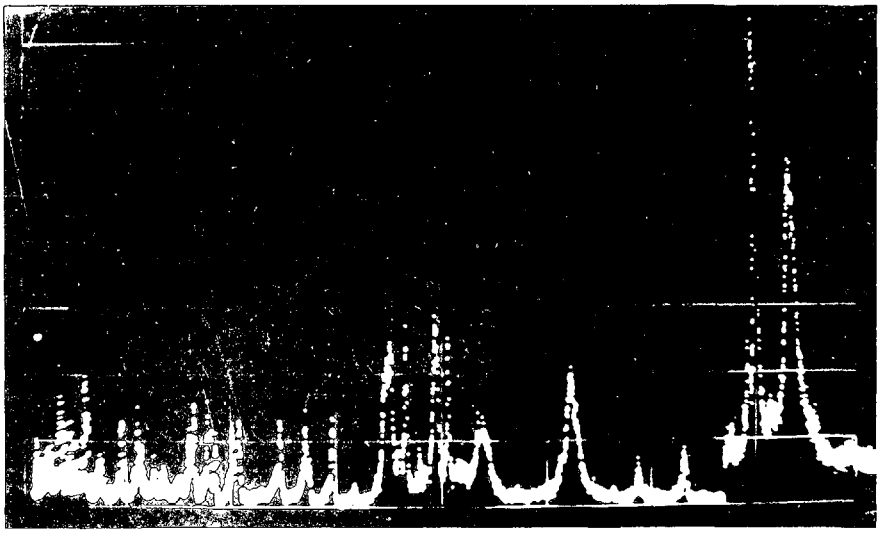

FIG.2. Spectres d'amplitude des résonances situées à 11,8 eV, 19,7 eV, 302 eV et 529 eV

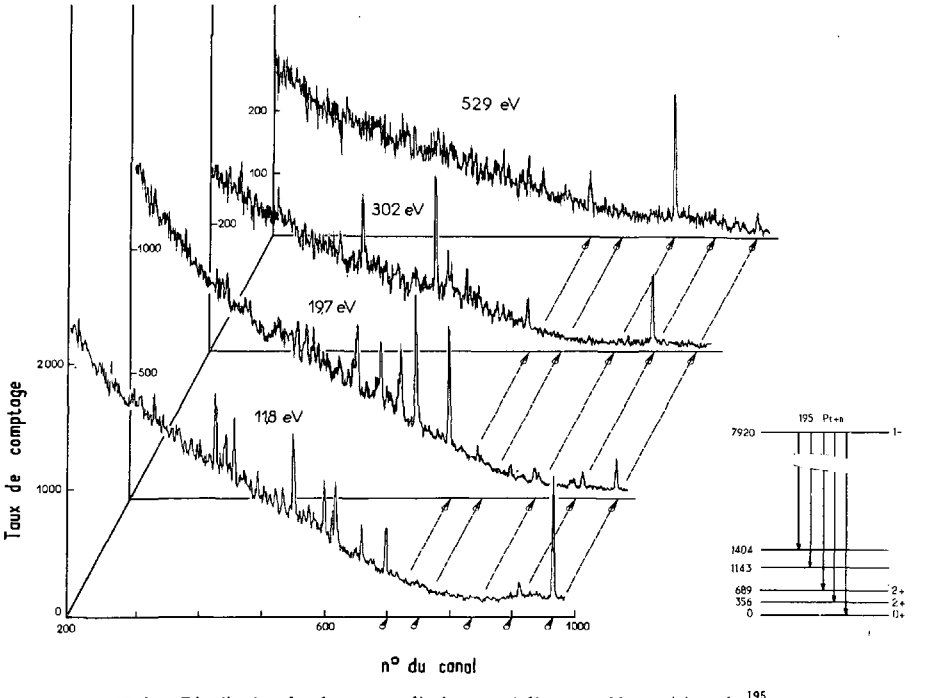

FIG.3. Distribution des largeurs radiatives partielles pour 66 transitions de ^{195}Pt

somme des trois transitions, $\nu = 3,1 \pm 1,2$. Il est intéressant de noter que ces valeurs sont relativement peu sensibles à la valeur du seuil, la taille de l'échantillon étant relativement élevée.

Il est un autre point, à priori plus délicat, dans une telle étude. Certains niveaux ont des intensités relatives élevées, conduisant à des valeurs de x de l'ordre de 0,3 ou 0,6, mais entachées d'une grande erreur. En effet, bien que l'aire des pics des transitions de haute énergie soit faible, l'aire relative du spectre global est également faible. Dans le cas de ^{195}Pt, heureusement, seules deux résonances de ce type interviennent pour chaque transition; on peut voir leur effet sur la distribution en faisant varier leurs intensités dans un large domaine. Les résultats obtenus restent voisins des précédents.

A cause de la faible dimension de leur échantillon, Bollinger, Coté, Carpenter et Marion [5] ont utilisé une procédure plus élaborée, fondée sur la méthode de Monte-Carlo. Rappelons que l'idée générale est de comparer l'échantillon expérimental, qui suit une distribution dont le paramètre ν est inconnu, avec une série d'échantillons mathématiques équivalents formés au hasard par un calcul de Monte-Carlo à partir d'une population régie par une distribution en χ^2 pour laquelle ν prend une valeur donnée ν_0. La méthode consiste à comparer la valeur ν_p de l'échantillon physique, donnée par la méthode du maximum de vraisemblance, à la distribution des valeurs ν_m obtenues par la même méthode pour les échantillons mathématiques. Si la valeur ν_p tombe près du centre de cette distribution des ν_m, les données expérimentales sont compatibles avec la valeur présumée ν_0 de ν. Cependant, pour tenir compte des erreurs expérimentales, les auteurs ont introduit une correction quelque peu arbitraire.

Nous avons développé à Saclay une procédure qui, dans son principe, nous semble serrer de plus près la réalité physique et qui joint les avantages de la méthode de Garrison à ceux du calcul de Monte-Carlo mais qui, cependant, reste très approximative dans ses applications. Elle consiste à ne conserver, dans les échantillons mathématiques, que les valeurs de x_i qui sont supérieures au seuil α déterminé à partir des valeurs expérimentales. En prenant $\alpha = 0,1$ et $\nu_p = 1,35$ on trouve finalement $\nu_0 = 1,30^{+0,42}_{-0,40}$.

Il apparaît donc que les trois méthodes d'analyse conduisent au même résultat et que nos données expérimentales sont compatibles avec une distribution à 1 degré de liberté et ce, pour la première fois, sans ambiguïté aucune. Il est intéressant de noter que, dès que l'échantillon est important, la méthode simple de Porter et Thomas donne un résultat très approché et qu'il n'est pas nécessaire de faire appel à une méthode plus complexe.

Deux autres éléments, ^{238}U et ^{183}W, ont également suscité un vif intérêt durant ces dernières années [6, 11, 12], en particulier en vue de l'étude d'éventuels effets de corrélation entre différentes largeurs radiatives partielles. Nous avons entrepris à Saclay l'étude de ^{238}U à l'aide d'une cible de 4,5 mm d'épaisseur et d'un détecteur de Ge-Li de 12 cm^3, sur une base de temps de vol de 25 m. Nous entreprendrons prochainement celle de ^{183}W sur une base de 50 m.

REFERENCES

[1] PORTER, C.E., THOMAS, R.G., Phys.Rev. 104 (1956) 483.
[2] BLUMBERG, S., PORTER, C.E., Phys.Rev. 110 (1958) 786.

[3] KRIEGER, T.J., PORTER, C.E., J.Math.Phys. 4 (1963) 1272.
[4] CHRIEN, R.E., BOLOTIN, H.H., PALEVSKY, H., Phys.Rev. 127 (1962) 1680.
[5] BOLLINGER, L.M., COTE, R.E., CARPENTER R.T., MARION, J.P., Phys.Rev. 132 (1963) 1640.
[6] HUYNH, V.-D., MEINADIER, J.P., DE BARROS, S., JULIEN, J., LE POITTEVIN, G., MORGENSTERN, J., NETTER, F., SAMOUR, C., Nucl.Instr. Methods 36 (1965) 29.
HUYNH, V.-D., DE BARROS, S., BREZINSKI, C., JULIEN, J., LE POITTEVIN, G., MORGENSTERN, J., NETTER, F., SAMOUR, C., Nucl. Struct.Study with Neutrons, North Holland Publ. Co., Amsterdam (1966) No.79.
[7] EWAN, G.T., TAVENDALE, A.J., Can.J.Phys. 42 (1964) 2286.
[8] JACKSON, H., SAMOUR, C., BLOCH, A., JULIEN, J., LOPATA C., MORGENSTERN, J., « Etude des spectres de rayonnement gamma de capture à l'aide de détecteurs au germanium », ces comptes rendus I, CN-23/66 (résumé seulement).
[9] IKEGAMI, H., SUGIYAMA, K., YAMAZAKI, T., SAKAI, M., Nucl.Phys. 41 (1963) 130.
[10] GARRISON, J.D., Ann.Phys. 30 (1964) 269.
[11] JACKSON, H.E., Phys.Rev. 134B (1964) 921.
[12] SAMOUR, C., DE BARROS, S., CHEVILLON, P.L., HUYNH, V.-D., JULIEN, J., LE POITTEVIN, G., MORGENSTERN, J., Nucl.Struct.Study with Neutrons, North Holland Publ. Co., Amsterdam (1966) No.89.

DISCUSSION

J.E. LYNN: I should like to mention that your result has been confirmed by measurements of Rae, Moyer, Fullwood and Andrews at Rensselaer Polytechnic Institute. They used a 20-cm^3 lithium-drifted germanium detector to examine 29 transitions in four resonances in the cross-section of ^{199}Hg. The distribution of their results (Fig. 1) was

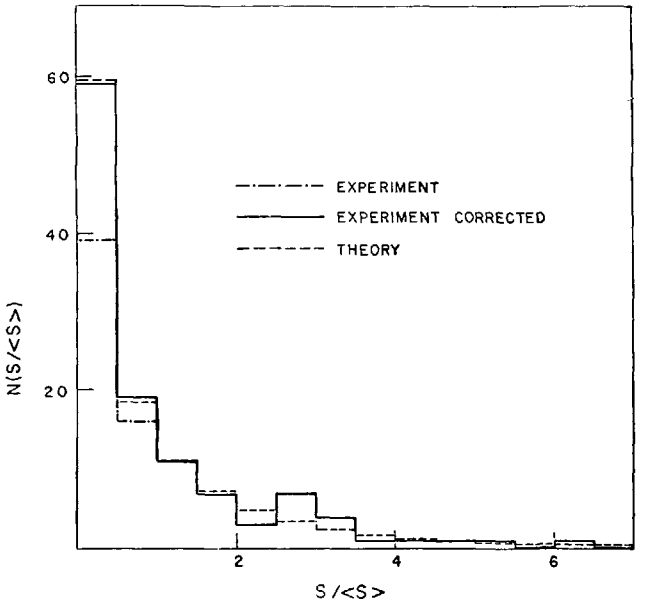

FIG.1. Distribution of 29 transitions in four resonances in the cross-section of ^{199}Hg

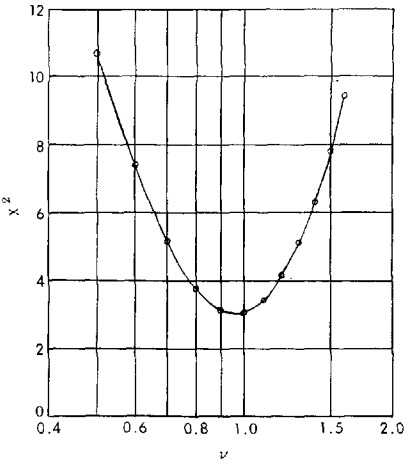

FIG.2. Statistical test against the chi-squared family for results shown in Fig.1.

tested statistically against the chi-squared family and it was found (Fig. 2) that $\nu = 0.96 \begin{smallmatrix}+0.24\\-0.17\end{smallmatrix}$. The results are a vindication of the classical work carried out with the help of sodium iodide crystals by Bollinger and co-workers at Argonne National Laboratory.

VALEUR DE LA FONCTION DENSITE S_0 ET DU RAYON DE DIFFUSION R' EN FONCTION DU NOMBRE DE MASSE ET FLUCTUATION DE S_0 EN FONCTION DE L'ENERGIE DANS LE DOMAINE D'ENERGIE COMPRIS ENTRE 0 ET 300 keV

J. MORGENSTERN, S. DE BARROS*, P. L. CHEVILLON,
M. J. GAUTHIER, H. JACKSON**, J. JULIEN
ET C. SAMOUR
CEA, CENTRE D'ETUDES NUCLEAIRES DE SACLAY, FRANCE

Abstract — Résumé

THE STRENGTH FUNCTION S_0 AS A FUNCTION OF MASS NUMBER AND FLUCTUATION IN S_0 AS A FUNCTION OF ENERGY IN THE 0 to 300-keV ENERGY RANGE. The authors studied the strength function S_0 as a function of mass number A in the range between 50 and 200, especially in the vicinity of the 3S and 4S giant resonances. The maximum of S_0 for A ~ 145 appears to be less wide than had been estimated by the various models. Fluctuations in S_0 as a function of neutron energy (in the case of Co, Pr and others) are indicated and discussed.

VALEUR DE LA FONCTION DENSITE S_0 ET DU RAYON DE DIFFUSION R' EN FONCTION DU NOMBRE DE MASSE ET FLUCTUATIONS DE S_0 EN FONCTION DE L'ENERGIE DANS LE DOMAINE D'ENERGIE COMPRIS ENTRE 0 ET 300 keV. Les auteurs ont étudié la fonction densité S_0 en fonction du nombre de masse A dans l'intervalle $50 < A < 200$, particulièrement au voisinage des résonances géantes 3S et 4S. Le maximum de la fonction densité S_0 pour A ~ 145 paraît moins large que celui qui est prévu par les différents modèles. Les auteurs présentent et discutent des fluctuations de la fonction densité S_0 en fonction de l'énergie des neutrons (Co, Pr, etc.).

1. INTRODUCTION

Les expériences de transmission de neutrons réalisées auprès de l'accélérateur linéaire de Saclay (45 MeV) couvrent un domaine d'énergie compris entre quelques eV et quelques centaines de keV, et des masses nucléaires variant de 30 à 240. Nous nous trouvons dans la région des résonances individuelles de neutrons et nous déterminons les paramètres de ces résonances (énergie, largeur, parité, spin...) ainsi que la valeur de la section efficace de diffusion potentielle.

Nous pouvons à partir de là calculer la valeur de la fonction densité et du rayon de diffusion potentielle R'. Dans cet exposé nous nous limiterons au cas de la fonction densité S_0 correspondant aux résonances induites par des neutrons s. Ces quantités sont reliées à la section efficace totale moyenne $\langle \sigma_t \rangle$ (la moyenne étant prise sur un intervalle d'énergie grand par rapport à l'espacement des résonances mais petit par rapport à la largeur des niveaux de particule indépendante). Nous avons, à basse énergie ($kR' \ll 1$), $\langle \sigma_t \rangle = 4\pi R'^2 + \alpha k S_0$, α étant une constante qui dépend

* Centre brésilien des recherches physiques, Rio de Janeiro, Brésil.

** Laboratoire national d'Argonne, Argonne, Ill., Etats-Unis d'Amérique.

des unités et k le nombre d'onde du neutron. $\langle\sigma_t\rangle$ est identifié à la section efficace totale calculée à partir d'un modèle optique.

Pour que la détermination de la fonction densité ait une précision convenable il faut pouvoir analyser au moins plusieurs dizaines de résonances. Pour 50 résonances par exemple, l'erreur d'échantillonnage est égale à environ 20%; elle est la plus importante. En effet, avec le même nombre de résonances, l'erreur sur S_0, due à l'imprécision expérimentale, est inférieure à 2%.

2. CONDITIONS EXPERIMENTALES

Notre résolution accrue nous a permis d'étudier un domaine d'énergie de plus en plus élevé; l'énergie maximale possible dépend de l'espacement moyen des résonances. Pour les noyaux au-dessous de la masse 60, nous avons fait des mesures jusqu'à une énergie de 500 keV. Nous avons utilisé des bases de temps de vol de 53 m, 103 m et 199 m. Les largeurs d'impulsion de l'accélérateur linéaire variaient de 20 ns à 100 ns suivant les expériences. Nous avons utilisé un codeur de temps de 65 536 canaux à largeur de canaux variable depuis 10 ns. Ce codeur, fabriqué par la société Intertechnique, était connecté à des blocs mémoire à ferrites. Le nombre de canaux utilisé dans une expérience était le plus souvent égal à 8192.

Notre détecteur était une boîte de 45 × 17 cm contenant 2,7 g/cm^2 de ^{10}B, entouré de huit cristaux de NaI(Tl) couplés à des photomultiplicateurs 54 AVP.

Nous détectons le γ de 478 keV qui suit la désexcitation de ^{7}Li produit dans la réaction (n, α) sur ^{10}B. Nous avons deux sorties d'impulsion sur les photomultiplicateurs; une sortie « lente » sur la dernière dynode, qui permet de sélectionner le pic photoélectrique du γ de 478 keV, et une sortie « rapide » sur l'anode, qui fournit une impulsion saturée permettant d'avoir une bonne définition en temps; on fait ensuite une coïncidence entre la voie lente et la voie rapide.

La résolution de notre ensemble électronique, y compris les cristaux et les photomultiplicateurs, a été mesurée et trouvée égale à 12 ns. En tenant compte de tous les facteurs, notre résolution minimale était 0,17 ns/m. Cette résolution a été testée par l'analyse de forme d'une résonance dont l'aire était connue (la mesure de l'aire est indépendante de la résolution) (fig. 1).

3. ANALYSE DES RESONANCES

La figure 2 donne un exemple de spectre expérimental à analyser. Pour analyser les résonances dues aux neutrons s, nous avons utilisé différents formalismes. Nous utilisons dans de nombreux cas la formule proposée par Bethe [1]:

$$\sigma_t = \sigma_d + \sigma_c = \pi\lambda^2 \sum_J g_J \left[\left| \exp(2ikR') - 1 + \sum_\lambda \frac{i\Gamma_{n\lambda}}{E - E_\lambda + \frac{\Gamma_\lambda}{2}} \right|_J^2 + \sum_\lambda \frac{\Gamma_{n\lambda}(\Gamma_\lambda - \Gamma_{n\lambda})}{(E-E_\lambda)^2 + \frac{\Gamma_\lambda^2}{4}} \right] \quad (1)$$

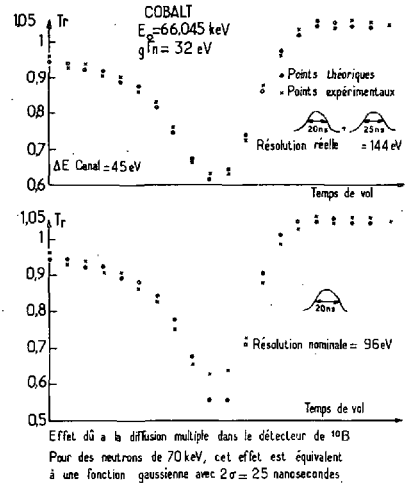

FIG.1. Comparaison de la courbe expérimentale et de la courbe calculée pour une résonance, suivant la valeur de la fonction de résolution

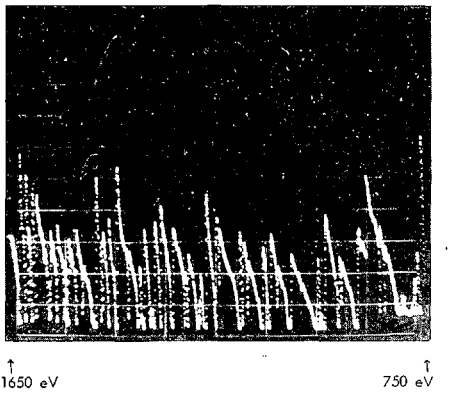

FIG.2. Spectre de transmission analysé par temps de vol d'un échantillon d'or de 2 cm d'épaisseur, dans le domaine d'énergie compris entre 750 eV et 1650 eV - n = 0,113 at/b - résolution: 0,8 ns/m

où σ_t est la section efficace totale, σ_d la section efficace de diffusion, σ_c la section efficace de capture, λ la longueur d'onde réduite du neutron, g_J le facteur statistique des résonances de spin J, R' le rayon de diffusion potentielle, Γ_λ et $\Gamma_{n\lambda}$ la largeur totale et la largeur de diffusion de la résonance d'énergie E_λ.

Cette formule est valable lorsque les largeurs des résonances de même spin sont très inférieures à leur espacement; c'est le cas pour Ga, As, Br, Se, Y, Zr, Nb, Ag, Ba, Pr, Tm, Pt, Au, Hg.

Pour les noyaux où cette condition n'était pas remplie, c'est-à-dire pour Mn, Co, Cu, nous avons utilisé les formalismes rigoureux de Humblet et Rosenfeld [2] et la matrice dérivée [3].

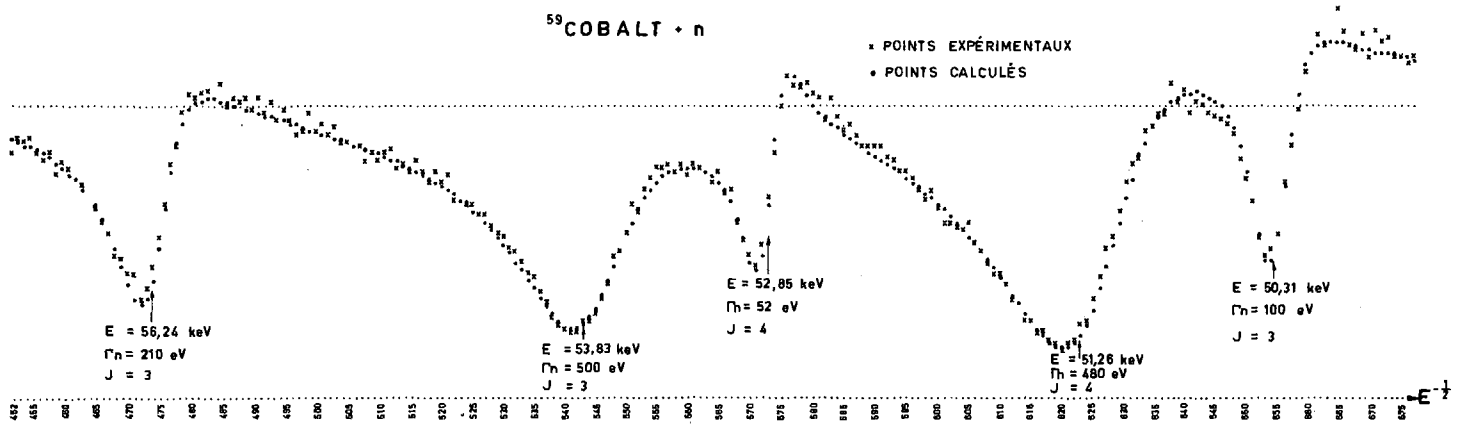

FIG. 3. Adaptation d'une courbe de transmission expérimentale par une courbe calculée à partir d'une formule à plusieurs niveaux

Dans nos expériences, nous étions alors toujours dans le cas où la largeur radiative était négligeable par rapport à la largeur totale: $\Gamma_{n\lambda} = \Gamma_\lambda$. Dans ce cas ces formalismes se simplifient.

- Dans le cas du formalisme de Humblet et Rosenfeld, nous avons

$$\sigma_t = \sigma_d = \pi \sum_J g_J \left| C(E) + \sum_\lambda \frac{2\gamma_\lambda^2}{E - E_\lambda + i\Gamma_{n\lambda}} \right|_J^2 \qquad (2)$$

où C(E) est une fonction qui varie lentement avec l'énergie, et où γ_λ^2 est un coefficient complexe dans le cas général, qui devient égal à $\Gamma_{n\lambda}/2k_\lambda$ lorsque la largeur des résonances est petite par rapport à leur espacement.

- Dans le cas de la matrice dérivée, cette matrice se réduit à une fonction lorsque $\Gamma_{n\lambda} = \Gamma_\lambda$ car il n'y a alors plus qu'une voie. Cette fonction s'écrit

$$\mathscr{R} = \frac{1}{2k_a} \sum_\lambda \frac{\Gamma_{n\lambda}}{E_\lambda - E}$$

où a est le rayon de la voie.

La section efficace est donnée par

$$\sigma_t = \sigma_d = \frac{\pi}{k^2} \left| 1 - e^{-2ikR'} \frac{1 + ik_a\mathscr{R}}{1 - ik_a\mathscr{R}} \right|^2 \qquad (3)$$

L'emploi des formules (2) et (3) conduit sensiblement aux mêmes valeurs des largeurs de résonances même dans le cas de résonances de même spin rapprochées, cela dans la limite de notre précision expérimentale.

Des programmes [4] écrits par Corge et Bianchi tenant compte de l'effet Doppler et de l'effet de résolution permettent de calculer la transmission d'un échantillon d'épaisseur donnée, en utilisant les formules (1), (2) et (3).

Ces programmes permettent de faire le calcul en prenant jusqu'à 50 résonances simultanément. On compare ensuite la courbe calculée à la courbe expérimentale et les paramètres choisis sont ceux qui minimisent la valeur du χ^2.

Les paramètres obtenus sont les valeurs de E_λ, Γ_λ, $\Gamma_{n\lambda}$, $g_J R'$. La figure 3 montre un exemple d'adaptation de la courbe expérimentale par la courbe calculée.

4. VARIATION DE S_0 ET DE R' EN FONCTION DE A

Le tableau I donne les résultats pour les noyaux que nous avons étudiés. Pour chaque noyau nous donnons l'intervalle d'énergie étudié et le nombre de résonances analysées dans cet intervalle.

La valeur de la fonction densité est calculée suivant la relation

$$S_0 = \frac{\Sigma g\, \Gamma_n^0}{\Delta E}$$

TABLEAU I. LISTE DES FONCTIONS DENSITE ET DES RAYONS DE DIFFUSION

Elément	Valeurs de S_0 mesurées (10^{-4} $eV^{-\frac{1}{2}}$)	Rayon de diffusion R' (10^{-13} cm)	Intervalle d'énergie (eV)	Nombre de résonances analysées
^{55}Mn [8]	4,0	3,6 ± 0,4	0 - 75 000	44
^{59}Co [8, 9]	3,9	5,4 ± 0,4	0 - 120 000	86
^{63}Cu [10]	2,2	7 ± 0,8	0 - 14 000	13
^{65}Cu [10]	1,3	7 ± 0,8	0 - 14 000	12
^{69}Ga [11]	1,2	6,3 ± 1	0 - 2 500	7
^{75}As [11]	1,75	7 ± 0,8	0 - 4 000	55
^{77}Sc [12]	1,5		0 - 1 500	9
^{79,81}Br [13]	1,5	7 ± 0,8	0 - 2 000	47
^{89}Y [14]	0,6	6,6 ± 0,7	0 - 16'000	5
^{91}Zr [15]	0,45	7 ± 1	0 - 2 500	11
^{93}Nb [16]	0,35	7,1 ± 0,3	0 - 4 100	37
^{107,109}Ag [17]	0,6		0 - 760	109
^{135}Ba [18]	0,8	5,8 ± 0,8	0 - 1 350	20
^{137}Ba [18]	0,3	5,8 ± 0,8	0 - 1 350	3
^{141}Pr	2,1	4,9 ± 0,6	0 - 6 000	80
^{169}Tm [17]	1,5	7,7 ± 0,8	0 - 760	88
^{194}Pt [17]	1,2	8,7 ± 0,5	0 - 825	4
^{195}Pt [17]	1,7	8,7 ± 0,5	0 - 825	40
^{197}Au [19]	1,8	8,7 ± 0,5	0 - 1 000	64
^{198}Hg	1,5	9,8 ± 0,7	0 - 420	5
^{199}Hg	2,2	9,8 ± 0,7	0 - 700	7
^{201}Hg	1,3	9,8 ± 0,7	0 - 700	7

S_0 est égale à la fonction densité pour chaque état de spin quand ces fonctions sont égales et à une moyenne pondérée par les facteurs statistiques correspondant aux différents spins quand ces fonctions ne sont pas égales; cette façon de calculer la moyenne est commode car, dans le cas où l'on ne peut pas donner le spin de la résonance, on peut tout de même obtenir la valeur du produit $g\Gamma_n^0$ correspondant à cette résonance.

Sur la figure 4 nous avons porté les valeurs expérimentales de S_0 et les valeurs calculées:

1) par Campbell et al. [5] en utilisant un potentiel sphérique de Saxon-Woods avec une absorption de volume;
2) par Chase et al. [6] en utilisant un potentiel trapézoïdal déformé avec absorption de volume;
3) par Buck et Perey [7] en utilisant un potentiel de Saxon-Woods pour la partie réelle avec une absorption de surface, et en tenant compte du couplage avec les états collectifs.

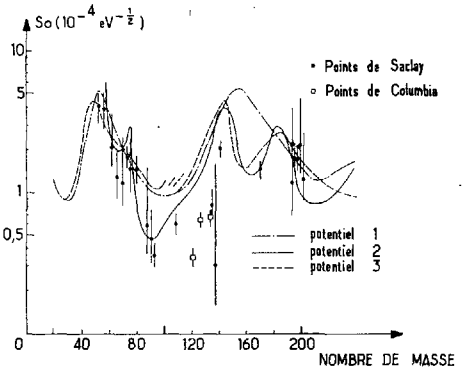

FIG.4. Variation de la fonction densité S_0 en fonction du nombre de masse - points expérimentaux et courbes calculées à partir de potentiels du modèle optique par: 1. Campbell et al.[5], 2. Chase et al. [6] et 3. Buck et Perey [7]

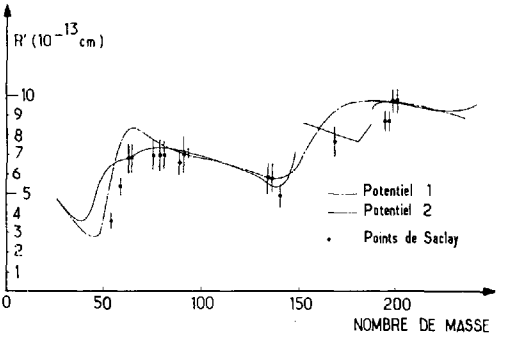

FIG.5. Variation du rayon de diffusion R' en fonction du nombre de masse - points expérimentaux et courbes calculées à partir de potentiels du modèle optique par 1. Campbell et al.[5] et 2. Chase et al. [6]

La meilleure adaptation est obtenue avec le potentiel 2 mais le second pic, dont le maximum est vers A = 150, apparaît beaucoup plus étroit que celui prévu par la théorie.

Sur la figure 5 nous avons porté les valeurs de R' que nous trouvons et les valeurs calculées avec les potentiels 1 et 2.

L'accord est assez bon avec le potentiel 2 sauf entre A = 50 et A = 60, où la valeur calculée est supérieure à la valeur mesurée.

5. VARIATION DE S_0 EN FONCTION DE E

La figure 6 montre la variation de $\sum_0^E g\,\Gamma_n^0$ en fonction de E jusqu'à 120 keV pour les résonances du cobalt. On voit que cette courbe présente trois régions de pentes différentes.

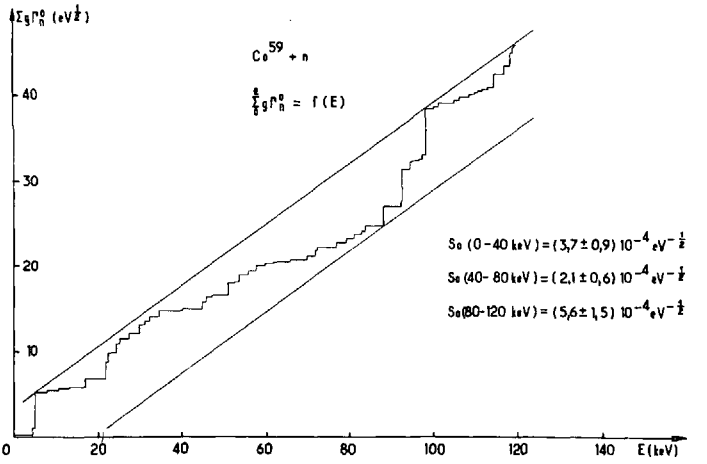

FIG.6. Variation de la quantité $\sum_0^E g\,\Gamma_n^0$ en fonction de l'énergie E pour les résonances du cobalt

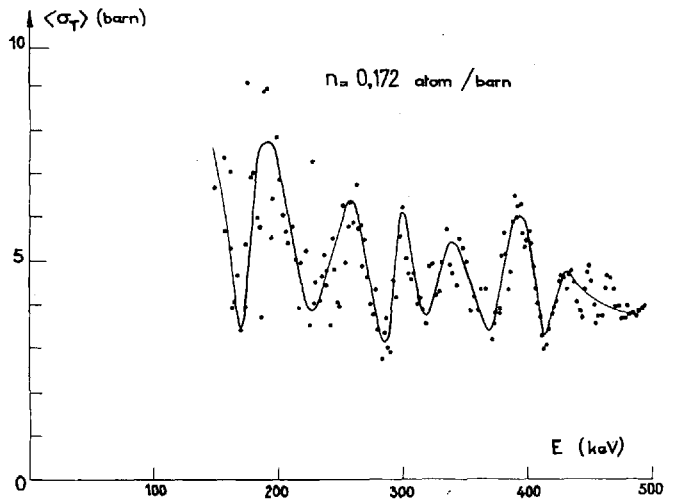

FIG.7. Points représentant la section efficace totale moyenne du cobalt aux neutrons - La courbe représentée ici est une courbe moyenne passant à travers ces points

On trouve: $S_0 = (3,9 \pm 1,0)\,10^{-4}\ eV^{-\frac{1}{2}}$ entre 0 et 40 keV
$S_0 = (2,1 \pm 0,55)\,10^{-4}\ eV^{-\frac{1}{2}}$ entre 40 et 80 keV
$S_0 = (5,6 \pm 1,5)\,10^{-4}\ eV^{-\frac{1}{2}}$ entre 80 et 120 keV.

Cet effet semble confirmé à plus haute énergie comme le montre la figure 7, qui représente la variation de la section efficace moyenne en fonction de l'énergie (la moyenne a été prise sur des intervalles d'énergie de l'ordre de 2 à 4 keV). On voit que cette courbe présente des oscillations dont la largeur est de l'ordre de 30 à 40 keV.

Ces variations de la fonction densité pourraient correspondre à des structures intermédiaires entre, d'une part, les états à une particule qui donnent le comportement moyen de la fonction densité dans des intervalles d'énergie de l'ordre de grandeur des largeurs des niveaux de particules indépendantes, et, d'autre part, les configurations complexes correspondant aux résonances individuelles.

REFERENCES

[1] BETHE, H. A., Rev. mod. Phys. 9 (1937).
[2] HUMBLET, J., ROSENFELD, Nucl. Phys. 26 (1961) 529.
[3] WIGNER, E. P., EISENBUD, L., Phys. Rev. 72 (1947) 29.
[4] CORGE, C., Rapport CEA (à paraître).
[5] CAMPBELL, E. J., FESBACH, H., PORTER, C. E., WEISSKOPF, V. F., MIT Laboratory for Nuclear Science, Technical Report No. 73 (1960).
[6] CHASE, D. M., WILETS, L., EDMONDS, A. R., Phys. Rev. 110 (1958) 1080.
[7] BUCK, B., PEREY, F., Phys. Rev. Lett. 8 (1962) 444.
[8] MORGENSTERN, J. et al., Int. Conf. on the Study of Nuclear Structure with Neutrons, Antwerp (July 1965) No. 86.
[9] MORGENSTERN, J. et al., Nucl. Phys. 62 (1965) 529.
[10] JULIEN, J. et al., Int. Conf. on the Study of Nuclear Structure with Neutrons, Antwerp (July 1965) No. 80.
[11] JULIEN, J. et al., Phys. Lett. 10 (1964) 86.
[12] JULIEN, J. et al., Phys. Lett. 3 (1962).
[13] JULIEN, J. et al., Nucl. Phys. 66 (1965) 433.
[14] BIANCHI, G. et al., J. Phys. 24 (1963) 996.
[15] CORGE, C. et al., J. Phys. Radium 22 (1961) 719.
[16] LE POITTEVIN, G. et al., Nucl. Phys. 70 (1965) 497.
[17] DE BARROS, S., Thèse, Université de Paris (1966).
[18] CHEVILLON, P. L., Thèse, Université de Paris (1966).
[19] JULIEN, J. et al., Nucl. Phys. 76 (1966) 391.

DISCUSSION

J. E. LYNN: It appears to me that, in fitting the two-level cobalt cross-section, you assumed the channel-pole phase factors to be independent parameters. I should therefore like to take this opportunity to point out something that has not been made clear in the literature. The S-matrix formalism of Humblet and Rosenfeld contains more parameters than the R-matrix theory. The reason for this is that unitarity, the condition of conservation of flux in the stationary wave representation of the nuclear reaction, is built into R-matrix theory, but has to be imposed as an extra condition on the Humblet-Rosenfeld theory. The result of

imposing unitarity on the S-matrix is that correlations among the parameters are introduced. In the two-level case, in particular, the channel-pole phase factors become strongly related to the partial width quantities. These relations cannot be ignored if a meaningful fit to the data is required.

J. MORGENSTERN: You are quite right. However, if the adaptation of our experimental curve is correct, the parameter values obtained are those which one would find if one could calculate the correlations among the parameters. We simply wished to show that the resonance width values in the Humblet-Rosenfeld formalism are only slightly different from those in the R-matrix theory, even for resonances having the same spin and lying very close together.

DISTRIBUTIONS DES ESPACEMENTS DES RESONANCES ET VALEURS DES COEFFICIENTS DE CORRELATION ENTRE LES DIFFERENTS PARAMETRES

S. DE BARROS*, P.L. CHEVILLON, H. JACKSON**,
J. JULIEN, J. MORGENSTERN ET C. SAMOUR
CEA, CENTRE D'ETUDES NUCLEAIRES DE SACLAY,
FRANCE

Abstract — Résumé

RESONANCE SPACING DISTRIBUTIONS AND CORRELATION FACTORS BETWEEN THE DIFFERENT PARAMETERS. The distribution of spacings and the values of the correlation coefficients are very sensitive to the number of undetected levels. The paper compares experimental distributions with those predicted by theory for certain nuclei (Tm, Am and others), in which both the number of omitted resonances and the values of the correlation coefficients is very small. The authors discuss the effects of a lack of resolution on the distributions obtained for other nuclei and the desirability of knowing the behaviour of such distributions.

DISTRIBUTIONS DES ESPACEMENTS DES RESONANCES ET VALEURS DES COEFFICIENTS DE CORRELATION ENTRE LES DIFFERENTS PARAMETRES. Les distributions des espacements et les valeurs des coefficients de corrélation sont très sensibles au nombre de niveaux non détectés. Les auteurs comparent des distributions expérimentales avec les prévisions pour quelques noyaux (Tm, Au, etc.) où le nombre de résonances omises est très faible, ainsi que les valeurs des coefficients de corrélation. Ils discutent l'incidence d'un manque de résolution sur les distributions obtenues pour d'autres noyaux et l'intérêt de connaître le comportement de telles distributions.

1. INTRODUCTION

L'étude des distributions des espacements entre résonances et le calcul des coefficients de corrélation entre espacements adjacents ou autres est valable si un échantillon statistique suffisant de niveaux est disponible. Les progrès réalisés tant dans l'amélioration des conditions expérimentales que dans les méthodes d'analyse permettent maintenant la comparaison des résultats expérimentaux et des prédictions théoriques [1 à 16].

Les distributions employées pour adapter les histogrammes expérimentaux sont déduites des relations suivantes (distributions de Wigner):

$$p(x) = \frac{\pi}{2}\, x \exp\left(-\frac{\pi}{4} x^2\right) \qquad (1)$$

pour une famille de spins

* Centre Brasileiro de Pesquisas Fisicas, Rio de Janeiro, Brésil
** En congé de l'Argonne National Laboratory, Argonne, Ill., Etats-Unis d'Amérique

$$p(x) = \frac{\pi}{2}\, x \left\{ \frac{1}{(1+R)^3} \left[1-\mathrm{erf}\left(\sqrt{\frac{\pi}{2}}\,\frac{Rx}{1+R}\right)\right] \exp\left(-\frac{\pi}{2}\,\frac{x^2}{(1+R)^2}\right) \right.$$

$$\left. + \frac{R^3}{(1+R)^3} \left[1-\mathrm{erf}\left(\sqrt{\frac{\pi}{2}}\,\frac{x}{1+R}\right)\right] \exp\left(-\frac{\pi}{4}\,\frac{R^2 x^2}{(1+R)^2}\right) \right\} \qquad (2)$$

$$+ \frac{2R}{1+R^2} \exp\left(-\frac{\pi}{4}\,\frac{1+R^2}{(1+R)^2}\, x^2\right)$$

avec

$$x = \frac{D}{\langle D \rangle} \qquad \text{et} \qquad R = \frac{\langle D \rangle_{I-1/2}}{\langle D \rangle_{I+1/2}}$$

pour deux familles de spins, R étant égal au rapport I/(I+ 1), I spin du noyau cible.

On présente les résultats pour quelques noyaux (Au, Tm, Pt, Ag), considérés soit isolément, soit groupés. La signification des résultats obtenus sera discutée en fonction des méthodes expérimentales.

2. RESULTATS

2.1. Distribution pour un même noyau (I = 1/2) de deux populations

Les figures 1 et 2 représentent respectivement les histogrammes expérimentaux de ^{169}Tm et de ^{197}Au, et leur comparaison avec les distributions théoriques. On peut constater que le nombre des faibles espacements est compatible avec la courbe théorique, à l'opposé des résultats obtenus pour d'autres noyaux [17]. Cela est dû à des con-

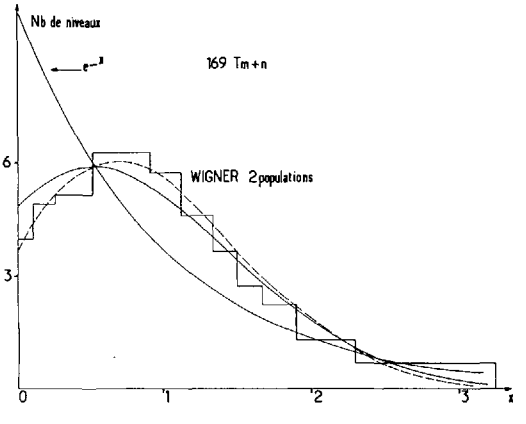

FIG.1. Histogramme expérimental des espacements de ^{169}Tm pour un domaine d'énergie de 0 à 750 eV et comparaison avec la distribution au hasard e^{-x} et les distributions de Wigner à deux populations, α représentant le rapport des espacements moyens I = 1/2, α = 1/3, I = 3/2, α = 5/8

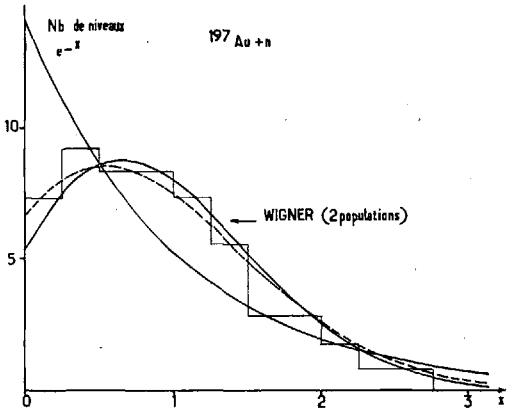

FIG.2. Histogramme expérimental des espacements de ^{197}Au pour un domaine d'énergie de 0 à 900 eV et comparaison avec les mêmes courbes théoriques que pour ^{169}Tm

ditions expérimentales meilleures et en particulier aux méthodes d'analyse. Le nombre des espacements pour l'or est 63 et pour le thulium 94. Le pas le plus faible choisi est $\Delta x = 0,1$; si $\Delta x < 0,1$, les histogrammes changent peu. Pour le thulium, dans ce cas, un plus faible espacement serait nécessaire, mais pour ce noyau nous estimons ne pas détecter entre 5 et 8 niveaux. Cela expliquerait le nombre important de grands espacements de l'histogramme de ce noyau. Pour l'or, le nombre de niveaux non détectés sera égal à 1 ou nul pour le domaine d'énergie considéré. Nous étudierons plus loin l'incidence des niveaux omis dans l'interprétation des résultats expérimentaux.

2.2. Distributions résultant d'un mélange de populations supérieur à deux

Les figures 3 et 4 représentent les histogrammes obtenus en combinant les résonances de ^{169}Tm et de Pt pour deux domaines d'énergie, 0 à 760 eV, 0 à 550 eV. Dans le domaine d'énergie de 0 à 550 eV le nombre

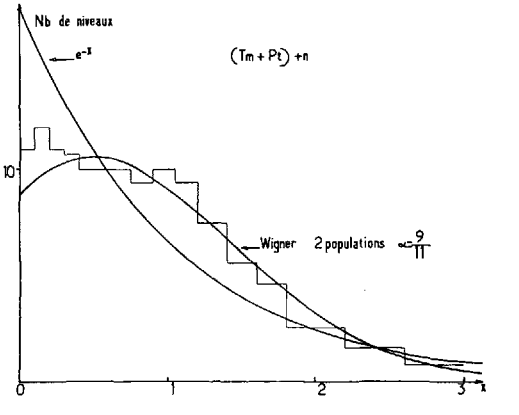

FIG.3. Histogramme expérimental des espacements obtenus en combinant les niveaux de ^{169}Tm et de Pt pour un domaine d'énergie de 0 à 760 eV

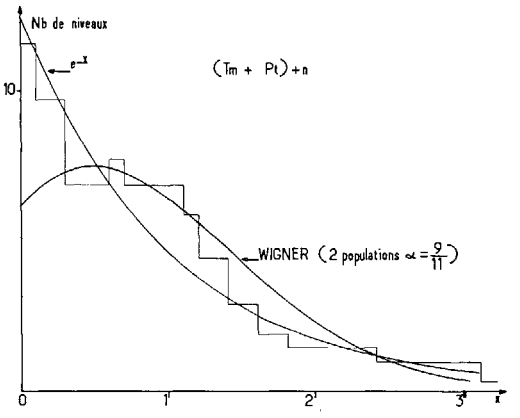

FIG.4. Histogramme expérimental des espacements obtenus en combinant les niveaux de ^{169}Tm et de Pt pour un domaine d'énergie de 0 à 550 eV

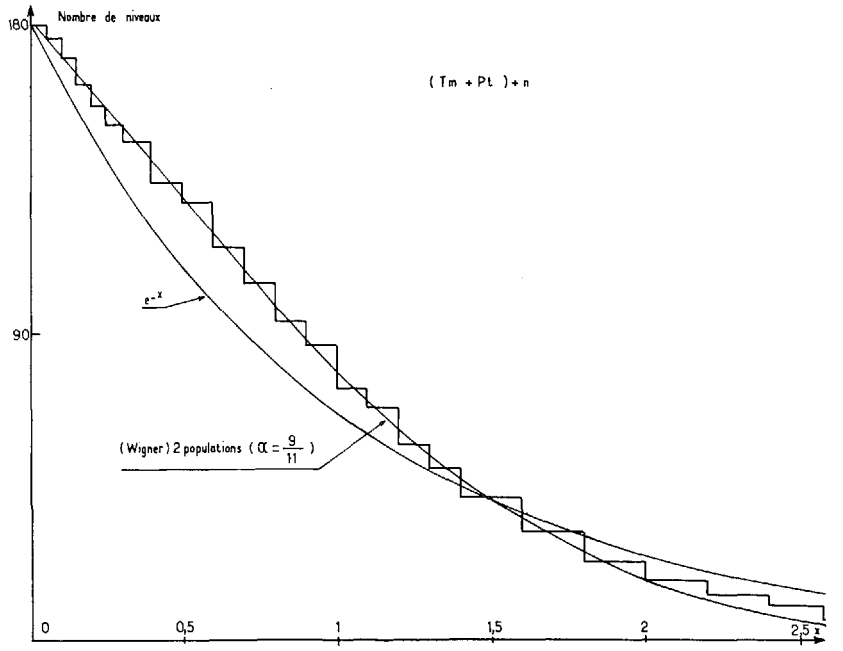

FIG.5. Distribution intégrale des espacements de la figure 3 et comparaison avec la loi au hasard e^{-x} et la distribution intégrale de Wigner à deux populations (α = 9/11)

de niveaux non détectés est faible et le nombre de faibles espacements croît sensiblement. Il est vrai qu'à faible énergie les méthodes d'analyse et la résolution expérimentale permettent de mettre en évidence les doublets plus aisément. La courbe 4 révèle toutefois un nombre important d'espacements pour la valeur x = 1. Il faut combiner beaucoup de populations pour obéir à la distribution au hasard e^{-x}. La figure 5 représente les distributions intégrées de la courbe 3. La figure 6 représente l'histogramme obtenu en combinant les résonances de Pt.

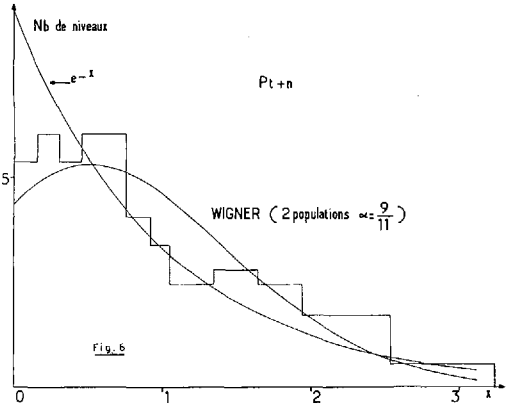

FIG.6. Histogramme des espacements de Pt

La figure 7 représente l'histogramme obtenu en combinant les résonances de Ag, Tm, Pt. Le nombre des faibles espacements $X < 0,1$ est grand mais il y a un manque d'espacements $X \sim 0,20$ et un trop grand nombre d'espacements $X \sim 0,6$. Le nombre total de résonances était égal à 288. Le nombre de niveaux de Ag croissant avec l'énergie ne permet pas de combiner des populations d'espacement moyen respectif à peu près égal.

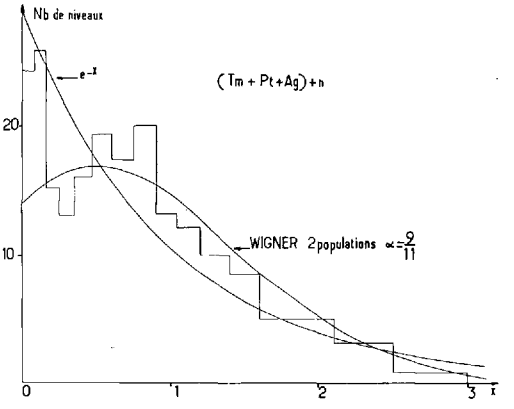

FIG.7. Histogramme exponentiel obtenu en combinant les niveaux de $^{107,\ 109}$Ag, ^{169}Tm, Pt dans un domaine d'énergie de 0 à 760 eV

La figure 8 représente l'histogramme dans un domaine d'énergie de 0 à 550 eV.

2.3. Influence des niveaux omis

L'obtention de résultats significatifs exige des échantillons de 100 niveaux au moins. Un tel chiffre ne peut être atteint sans omettre des niveaux.

D'abord le pas choisi pour tracer l'histogramme peut fournir des résultats bizarres. La figure 9 représente l'histogramme de ^{238}U dans le domaine d'énergie de 0 à 3200 eV, le pas choisi étant voisin de 0,25. La courbe de Wigner à une population adapte bien les résultats

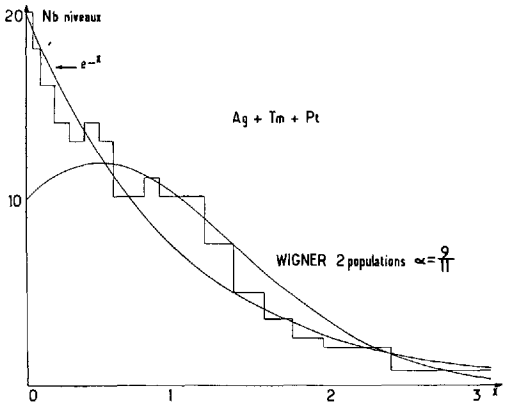

FIG.8. Histogramme exponentiel obtenu en combinant les niveaux de ^{107,109}Ag, ^{169}Tm, Pt dans un domaine d'énergie de 0 à 550 eV

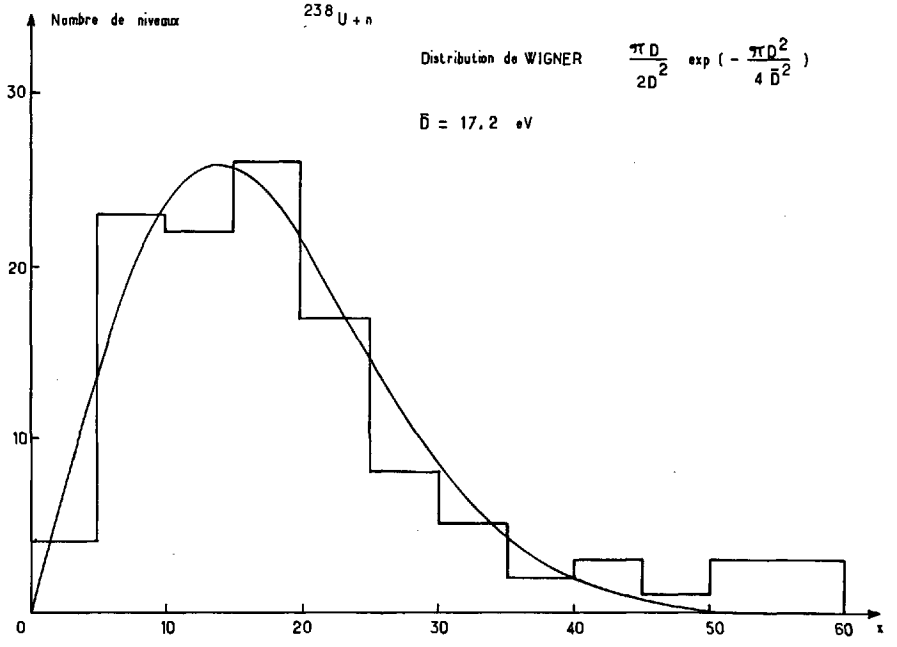

FIG.9. Histogramme des espacements de ^{238}U dans un domaine d'énergie de 0 à 3200 eV

expérimentaux (I = 1/2 pour ^{238}U). Si nous choisissons un pas deux fois plus petit, le nouvel histogramme est entièrement différent: deux pics apparaissent (fig. 10). Nous traçons maintenant le même histogramme pour les domaines d'énergie de 1200 à 2250 eV et de 3200 à 2250 eV (fig. 11). Les deux pics apparaissent séparément, cela pour des valeurs de x sensiblement doubles. La résolution dans le domaine de 2200 à 3200 eV est insuffisante pour détecter tous les niveaux, aussi la valeur $\langle D \rangle$ = 17 eV est très différente du $\langle D \rangle$ expérimental pour cet intervalle d'énergie; le maximum vers x = 1 est donc déplacé vers x ~ 2 et, la réso-

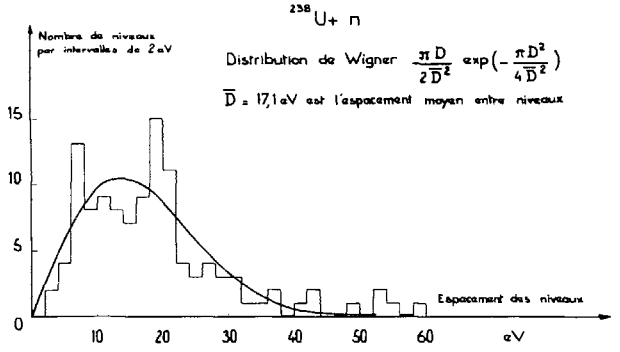

FIG.10. Histogramme des espacements de ^{238}U dans un domaine d'énergie de 0 à 3200 eV, avec un pas deux fois moindre qu'à la figure 9

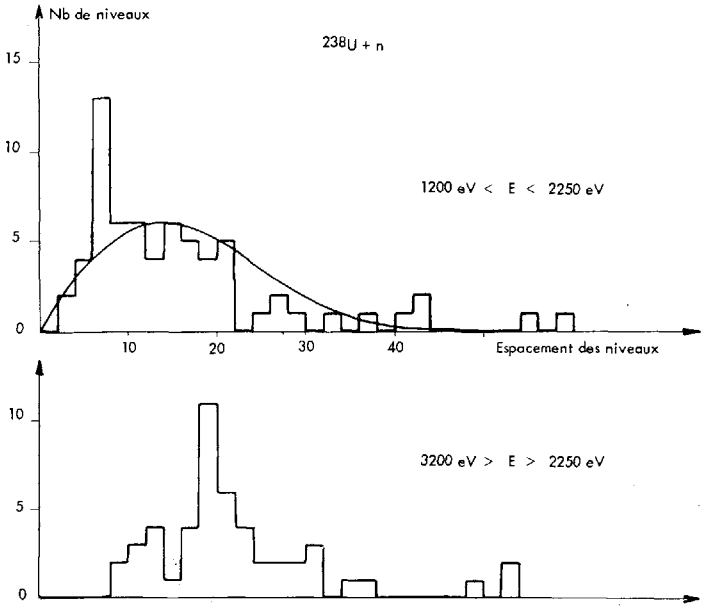

FIG.11. Histogramme des espacements de ^{238}U, avec le même pas qu'à la figure 10 mais pour deux domaines d'énergie

lution étant mauvaise, on ne peut plus distinguer des doublets, d'où un nombre nul des faibles espacements. Dans le domaine d'énergie de 1200 à 2250 eV, la valeur $<D>$ choisie est en fait plus élevée que celle effective pour cet intervalle; le maximum est donc situé à une valeur $x = D_i / <D>$ plus faible que la valeur vraie, ici environ 0,7. Il est donc nécessaire, avant d'interpréter des résultats, d'analyser des données sûres. Les figures 3 et 4 montrent combien les histogrammes peuvent être différents même pour un faible nombre de niveaux omis.

Même en supposant que la résolution expérimentale est suffisante comparée à la largeur totale Γ et l'espacement moyen $<D>$, il faut envisager le cas de non-détection de niveaux très rapprochés. Ainsi pour 100 niveaux détectés et pour un noyau cible de spin $I = 3/2$, le nombre

d'espacements $D_i < 0,05 <D>$ sera de l'ordre de deux. Si $<D> = 15$ eV, on a $D_i = 0,075$ eV. Il est plus probable (distribution de Porter et Thomas) d'avoir deux résonances peu intenses rapprochées. Une faible résonance voisine d'une résonance intense sera très difficile aussi à mettre en évidence. Certains exemples ont déjà été cités [18, 19]. On peut conclure en disant qu'il n'est guère possible actuellement de détecter plus de 100 niveaux avec une perte de un ou deux niveaux. Une manière de connaître la sensibilité de mise en évidence des niveaux rapprochés est d'étudier simultanément des noyaux ayant des résonances très voisines et d'analyser les données pour connaître ce seuil de détection. Les résultats expérimentaux concordent bien avec ceux déduits de courbes simulées à l'aide d'ordinateurs.

2.4. Conclusion

Il est difficile de connaître si les formalismes proposés rendent bien compte des résultats expérimentaux.

Il semble, lorsqu'on dispose de données sûres mais peu nombreuses malheureusement, que les distributions de Wigner à une et deux populations soient vérifiées convenablement.

3. COEFFICIENT DE CORRELATION

La valeur du coefficient de corrélation ρ pour des espacements adjacents est

$$\rho = \frac{\Sigma X_i X_{i+1}}{\Sigma X_i^2}$$

avec

$$X_i = \frac{D_i}{<D>} - 1$$

L'erreur sur p est $\frac{1-p^2}{\sqrt{n}} = \Delta\rho$.

Leff a calculé les valeurs de ρ pour un mélange de deux populations et différentes valeurs du rapport $\alpha = D_{I+1/2}/D_{I-1/2}$:

$\alpha = 1/3$	$\rho = -0,19$
$\alpha = 3/5$	$\rho = -0,26$
$\alpha = 1$	$\rho = -0,29$

3.1. ^{169}Tm

La valeur de ρ a été calculée pour différents domaines d'énergie:

Domaine énergie	ρ	$\Delta\rho$	ΣX_i^2	Nombre de niveaux
0 à 360 eV	-0,11	± 0,14	24	50
0 à 548 eV	-0,175	± 0,11	39,6	70
0 à 760 eV	-0,14	± 0,10	47	95

TABLEAU I. ESSAI D'ATTRIBUTION DE LA VALEUR DU SPIN EN S'IMPOSANT UNE VALEUR DU FACTEUR DE CORRELATION ρ EGALE A -0,25

E (eV)	J	E (eV)	J	E (eV)	J	E (eV)	J
4,91	2	58	1	4,91	2	58	1
46,5		78,43	1	46,5		78,43	1
60,25	2	144,2	1	60,25	2	144,2	1
107	2	162,9	1	107	2	162,9	1
122,2		189,9	1	122,2		189,9	1
151	2	261,9	1	151	2	208,9	
164,9	2	330,3	1	164,9	2	261,9	1
208,9		375,1				330,3	1
240,3	2	* 401,5		240,3	2	375,1	
255,3		440,2	1	255,3		*401,5	
273,6		489,7	1	273,6		440,2	1
293,1	2	548,5	1	293,1	2	489,7	1
329	2	580,8	1	329	2	548,5	1
355,1	2	624,6	1	355,1	2	580,8	1
370,7	2	658,7		370,7	2	624,6	1
381,5	2	695,7	1	381,5	2	658,7	
* 400,3		759,9	1	* 400,3		695,7	1
450,9	2	773,8	1	450,9	2	759,7	1
477,3	2	813,5		477,3	2	773,8	1
493,8	2	930		493,8	2	813,5	1
534	2	961,2	1	534	2	930	
561,4		*1040		561,4		961,2	1
579	2			579	2	*1040	
586,7				586,7			
602,8	2			602,8	2		
617,2	2			617,2	2		
628,2	2			628,2	2		
638,7	2			638,7	2		
685,9				685,9			
699	2			699	2		
715,6	2			715,6	2		
738,4				738,4			
784,3	2			784,3	2		
796	2			796	2		
819,5	2			819,5	2		
825	2			825	2		
864,2				864,2			
879,5				879,5			
932,4	2			932,4	2		
956,1				956,1			
984,2	2			984,2	2		
988,5	2			988,5	2		
995,4	2			995,4	2		
*1050				*1050			
$p^{(0)} = -0,24$		$p^{(0)} = -0,25$		$p^{(0)} = -0,275$		$p^{(0)} = -0,215$	
0-534 eV $p^{(0)} = -0,30$				0-550 eV $p^{(0)} = -0,45$			
534-1050 eV $p^{(0)} = -0,23$				550-1050 eV $p^{(0)} = -0,23$			

Note: Les astérisques signifient que dans la colonne de l'autre valeur du spin il y a une résonance d'énergie voisine et que la permutation est possible.

Si la valeur de ρ réelle est -0,19, la valeur de p sera très sensible au changement d'un produit $X_i\ X_{i+1}$ si la quantité ΣX_i^2 du dénominateur est faible. En effet si la quantité $\Sigma X_i X_{i+1}$ varie par exemple de 0,7 la valeur de ρ passe de -0,11 à 0,06 dans le cas du ^{169}Tm pour le domaine d'énergie de 0 à 360 eV. La tendance de ρ à rester négatif et voisin de -0,15, et cela pour un nombre de niveaux omis très faible,

semble indiquer que la valeur réelle de ρ est de cet ordre de grandeur (la valeur théorique étant $\rho = -0,19$).

3.2. ^{197}Au

Pour ce noyau, la probabilité de manquer un niveau est très faible. On trouve $\rho = -0,22 \pm 0,12$ dans le domaine d'énergie de 0 à 980 eV.

Les valeurs des spins étant connues pour un grand nombre de résonances, on s'est efforcé de trouver la valeur du spin des autres en séparant les niveaux en deux groupes de spin 1 et 2 tout en s'efforçant de trouver $\rho = -0,25$ ou une valeur voisine. Les résultats sont représentés dans le tableau I. En particulier, pour la famille de résonances $J = 1$, il était essentiel qu'une résonance soit située vers l'énergie de 930 eV pour obtenir une valeur ρ convenable. Cette résonance a été détectée récemment en employant un écran d'or de 3 cm d'épaisseur. Sans cette résonance, la valeur ρ pour l'ensemble des résonances était de $-0,10$ seulement. Cela est encore un exemple de la sensibilité de ρ au nombre total de niveaux considérés et au nombre de ceux omis.

3.3. Mélange de plusieurs populations

La valeur de ρ pour l'ensemble des résonances mélangées de Ag, Tm et Pt est égale à $-0,09 \pm 0,06$.

4. CONCLUSION

Le calcul du coefficient de corrélation ρ est très délicat et il semble difficile de tirer des conclusions significatives des résultats expérimentaux. Ces derniers, même s'ils sont corrects, sont encore en nombre insuffisant et cela est vrai aussi pour les distributions des espacements.

REFERENCES

[1] MEHTA, M.L., Nucl. Phys. 18 (1960) 395.
[2] MEHTA, M.L., GAUDIN, M., Nucl. Phys. 18 (1960) 420.
[3] MEHTA, M.L., GAUDIN, M., Nucl. Phys. 22 (1961) 340.
[4] PORTER, C.E., Nucl. Phys. 40 (1963) 167.
[5] PORTER, C.E., J. Math. Phys. (1963).
[6] WIGNER, E.P., ORNL 2309 67 (1956).
[7] WIGNER, E.P., Ann. Math. 67 (1958) 325.
[8] KAHN, P.B., Nucl. Phys. 41 (1959) (1963).
[9] DYSON, F.J., J. Math. Phys. 3 (1962) 140.
[10] DYSON, F.J., J. Math. Phys. 3 (1962) 157.
[11] DYSON, F.J., J. Math. Phys. 3 (1962) 166.
[12] DYSON, F.J., J. Math. Phys. 3 (1962) 1191.
[13] DYSON, F J., J. Math. Phys. 3 (1962) 1193.
[14] LEFF, H.S., Bull. Am. phys. Soc. 8 (1962) 31.
[15] LEFF, H.S., Thèse (non publiée).
[16] GAUDIN, M., Nucl. Phys. 25 (1961) 447.
[17] GARG, J.B., Phys. Rev. 137 (1965) B457.
[18] JULIEN, J. et al., Nucl. Phys. 76 (1966) 391.
[19] JULIEN, J., Proc. Int. Conf. on the Study of Nuclear Structure with Neutrons, Antwerp (July 1965) p.156.

DISCUSSION

R. JOLY (Chairman[1]): You stated that the level spacing distribution for $^{238}U + n$ in, say, the energy range 1200 - 2250 eV was in good agreement with the Wigner distribution for a single population. Did you eliminate the levels corresponding to p waves to obtain this agreement, and, if so, how did you identify them?

J. JULIEN: We did not identify the p resonances; this appears to be very difficult in the case of ^{238}U. Earlier results for ^{238}U were presented to demonstrate the strange nature of the experimental results when one does not have excellent resolution within a given energy range (in this case 2200 - 3000 eV). I feel that experimental results and theoretical predictions should be compared only if very few levels are omitted.

A. MICHAUDON: You have shown several cases where the merging of a large number of populations leads to an exponential distribution (e^{-x}). The most interesting distribution, however, is that of the spacings of a single family, as in the case of an even-even isotope (for example, ^{238}U and ^{232}Th).

In the case of ^{238}U, good agreement is found with the Wigner distribution for a single population, although the distribution is disturbed by the p resonances that have not been eliminated. One might well ask whether this agreement is not a spurious one since, even with excellent resolution, the measurements are disturbed by the natural width of the resonances and the Doppler effect.

For example, we have calculated the total cross-section of ^{238}U and ^{232}Th as broadened by the Doppler effect. Taking into account only resonances observed in the total cross-section, we found a spacing distribution that was in agreement with the Wigner distribution for one population, even though two populations were present. In this case, therefore, the agreement is completely spurious.

Thus, it is difficult to verify the Wigner distribution, since it is above all sensitive to small spacings, which are difficult to detect in the case of resonances induced by neutrons.

J. JULIEN: Our aim was to show that, under excellent experimental conditions, the spacings for the two spin families of a nucleus were in agreement with the Wigner distribution for two populations. Earlier results had revealed an absence of small spacings, due in our opinion to the resolution.

We have also shown that, when the resolution is not excellent, it is, as one might expect, difficult to find an e^{-x} distribution for a large number of populations (8-10).

In your total cross-section calculations for ^{238}U and ^{232}Th, you appear to have taken distributions at random and simulated a total cross-section curve, from the examination of which you have found that the two populations are in agreement with the Wigner distribution for a single population. Like me, you attribute this to the effect of experimental resolution. However, I have one reservation regarding your calculations: you do not allow for the value of the correlation coefficient p (= -0.25), which is zero for your two populations. Actually, one should diagonalize matrices, as Porter and co-workers have done, in order to obtain

[1] During presentation and discussion of this paper R. Joly (France) took the chair.

spacings corresponding exactly to those of a real case. J. B. Garg [Phys. Lett. 12 (1964) 240] has shown that the merged experimental results for ^{238}U and ^{232}Th correspond to the Wigner distribution for two populations. In this example there is probably a merging of the s and p resonances.

We are able to combine two spin families only if they have the same spacing, otherwise the distribution of the family with small spacing will dominate; in fact, we combined the S = 1 resonances of gold and the S = 0 resonances of ^{169}Tm. The sample was poor (40 levels), but we found a considerable number of small spacings, which is typical of a Wigner distribution for two populations. The combination of the S = 2 resonances of gold and the S = 1 resonances of ^{195}Pt (the mean spacing $< D >$ is essentially the same) gives the same result. We conclude that, for energy regions in which virtually all the levels are detected, our experimental results are in agreement with the different Wigner distributions. A simple calculation shows that, if one wished to obtain a population of 100 levels with a minimum number of undetected levels, a standard nucleus would be one having a mean spacing $< D >$ of about 16 eV and an S_0 value of about 2×10^{-4} for a resolution of approximately 0.3 ns/m.

DEPENDANCE DE LA FONCTION DENSITE S_0 SUIVANT LA VALEUR DU SPIN

J. JULIEN, S. de BARROS, P. L. CHEVILLON, V. D. HUYNH,
J. MORGENSTERN, F. NETTER ET C. SAMOUR
CEA, CENTRE D'ETUDES NUCLEAIRES DE SACLAY,
FRANCE

Abstract — Résumé

DEPENDENCE OF THE STRENGTH FUNCTION S_0 ON SPIN. The assignment of the value for spin to a large number of resonances makes it possible to study various quantities as a function of the two spin states, $J = I \pm 1/2$. The authors observed, in particular, the strength function S_0 for target nuclei of spin $I = 1/2$ (Y, Ag, Tm, Pt). S_0 is the same for the spins $J = 0$ and $J = 1$. For target nuclei of spin $I = 3/2$ (Cl, Cu, Ga, As, Br, Ba, Au), S_0 for spin state $J = 2$ is twice as large as for $J = 1$. There is a discussion of the results obtained in the energy range of a few keV.

DEPENDANCE DE LA FONCTION DENSITE S_0 SUIVANT LA VALEUR DU SPIN. L'attribution de la valeur du spin à un grand nombre de résonances permet l'étude de différentes quantités en fonction des deux états de spin $J = I \pm 1/2$. La fonction densité S_0 a été en particulier étudiée pour des noyaux cibles de spin $I = 1/2$ (Y, Ag, Tm, Pt); la valeur S_0 est la même pour les valeurs de spin $J = 0$ et $J = 1$. Pour les noyaux cibles $I = 3/2$ (Cl, Cu, Ga, As, Br, Ba, Au), la valeur S_0 pour l'état de spin $J = 2$ est deux fois plus grande que la valeur S_0 pour $J = 1$. Les résultats obtenus dans le domaine d'énergie de quelques keV sont présentés et discutés.

DISCUSSION

G. ROHR: We have measured the total neutron cross-section for ^{51}V and ^{55}Mn at energies up to 220 keV, and have found no spin dependence of the strength function when the whole energy range was taken into account. When a small part, about 50 keV, of this energy range was considered, however, the ratio of the strength functions of the two possible spin systems assumed different values.

In the case of ^{51}V, for example, the ratio has a value of about five in the energy range 0.50 keV, indicating strong spin dependence, whereas in the range 50-100 keV there is no spin dependence. In the range 100-160 keV the ratio is 0.2, indicating strong reverse spin dependence.

These results show that, for this isotope, an energy range of 50 keV is too small for significant measurements of spin dependence. This effect, which is due to the structure caused by intermediate states, may have influenced your results, since you took energy ranges smaller than 10 keV in most cases.

J. MORGENSTERN: The important point in seeking a spin dependence of the strength function is the number of resonances analysed within each energy range. With vanadium the level density is low and one has to take a fairly large energy range to have sufficient resonances.

Last year, we published results indicating that, in the case of manganese, there was no dependence of strength function on spin at energies up to 80 keV.

With regard to nuclei with spin 3/2, for which we have found spin dependence, and those with spin 1/2, for which we have found no spin dependence, the number of resonances analysed for each nucleus was so high that a statistical accident is most unlikely.

Session IV

(n,p), (n,α), (n, 2n)-REACTIONS, ETC. AND INVERSE REACTIONS

THE (n, 2n) CROSS-SECTIONS OF ^{9}Be AND D IN THE THRESHOLD REGIONS

M. HOLMBERG AND J. HANSEN
FÖRSVARETS FURSKNINGSANSTALT,
STOCKHOLM, SWEDEN

Abstract

THE (n, 2n) CROSS-SECTIONS OF ^{9}Be AND D IN THE THRESHOLD REGIONS. The (n, 2n) cross-sections of ^{9}Be and D have been measured in the energy regions 2. 0 - 6. 5 MeV and 4. 2 - 6. 5 MeV, respectively. The two neutrons in the (n, 2n) reaction were detected by a large liquid scintillator by the use of a special technique which was based on the time correlation between the pulses due to the two neutrons. The efficiency for detecting an (n, 2n) event was about 40%. The determination of the number of (n, 2n) events was made with an accuracy corresponding to a cross-section of the order of 5-10 mb. This made it possible to study the energy region below 2. 7 MeV where earlier measurements of ^{9}Be have given contradictory results and also the energy region 4. 2 - 6. 1 MeV for D where no measurements exist. The (n, 2n) cross-sections at 6. 5 MeV were measured with an accuracy of about 10% and the relative errors were of the order of 5%.

The excitation function measured for ^{9}Be confirms the earlier measurements which show that the cross-section mainly is due to the inelastic scattering to the 2. 43-MeV level of ^{9}Be, which subsequently decays by neutron emission. However, below the threshold at 2. 7 MeV there exists a cross-section which is (25 ± 5) mb at 2. 5 MeV and (10 ± 5) mb at 2. 2 MeV. Below 2. 1 MeV the cross-section is < 5 mb. The excitation function for deuterium indicates that the cross-section below 4. 6 MeV is < 10 mb.

DISCUSSION

R. BATCHELOR: In your (n, 2n) measurements you have used a rather different technique with your liquid scintillator to that previously used. What are the advantages of your method?

M. HOLMBERG: The liquid scintillator measurements carried out by the Livermore group used a post-deflection system, which reduced the ion current of the accelerator by a factor of 50-100. In the present technique the full intensity of the accelerator current was available, so that a collimation system could be used to reduce the background and in addition we could use a thin target.

ETUDE DE LA REACTION $^{9}Be(n,2n)$ A 14 MeV

R. BOUCHEZ, J. C. GONDRAND, P. PERRIN,
C. PERRIN, A. GIORNI, R. DARVES-BLANC ET P. QUIVY
LABORATOIRE DE PHYSIQUE NUCLEAIRE DE L'UNIVERSITE
ET CENTRE D'ETUDES NUCLEAIRES DE GRENOBLE, FRANCE

Abstract

STUDY OF THE $^{9}Be(n,2n)$ REACTION AT 14 MeV. The authors studied the $^{9}Be(n,2n)$ reaction using double time-of-flight spectrometry, and found that it takes place mainly through the formation of $^{9}Be^{*}$ resonance states (6.76 and 7.94 MeV). The contribution of the direct process $^{8}Be + n_1 + n_2$ is small in spite of the weak binding (1.66 MeV) of the peripheral neutron $p_{3/2}$ in the ^{9}Be, compared with the incident energy $E_n = 14.5$ MeV.

Measurements made at $\varphi_1 = -\varphi_2 = 30°$, 60°, 80° and at $\varphi_1 = 30°$, $\varphi_2 = -15°$ show anisotropy of the (n,2n) reaction, predominantly towards the forward angles.

ETUDE DE LA REACTION $^{9}Be(n,2n)$ A 14 MeV. Les auteurs ont étudié la réaction $^{9}Be(n,2n)$ par double spectrométrie à temps de vol. On observe qu'elle se produit principalement par formation d'états résonnants de $^{9}Be^{*}$ (6,76 et 7,94 MeV), la part du processus direct $^{8}Be + n_1 + n_2$ étant faible malgré l'état peu lié (1,66 MeV) du neutron périphérique $p_{3/2}$ dans ^{9}Be, comparé à l'énergie incidente $E_n = 14,5$ MeV.

Les mesures effectuées à $\varphi_1 = -\varphi_2 = 30°$, 60°, 80° et $\varphi_1 = 30°$, $\varphi_2 = -15°$ ont montré une anisotropie de la réaction (n,2n) avec prédominance vers les angles avant.

DISPOSITIF EXPERIMENTAL

La réaction $^{9}Be(n,2n)$ a été étudiée à 14 MeV à l'aide d'un double spectromètre à temps de vol (base de vol 1,50 m, résolution instantanée $1,5 \cdot 10^{-9}$ s [1].

Une réaction à trois corps a neuf degrés de liberté, auxquels il faut ajouter un paramètre supplémentaire si l'état d'excitation de la particule intermédiaire (ici le $^{8}Be^{*}$) n'est pas connu. Une étude complète nécessitera donc la mesure de dix paramètres. Nous avons associé les quatre relations cinématiques (une de conservation d'énergie plus trois de conservation d'impulsion) à la mesure des deux paramètres (angle et énergie) pour trois particules, soit les neutrons incidents n_0 et émis n_1 et n_2.

Le faible taux d'acquisition, 1,8 événement (n,2n)/h, a nécessité l'automatisation de l'expérience, les paramètres relatifs à chaque événement étant enregistrés et traités ensuite avec la machine à calculer Gamma 30 du Centre d'études nucléaires de Grenoble.

Les résultats sont présentés sous forme d'une matrice $|T_1, T_2|$ pour les neutrons émis, les neutrons incidents étant monocinétiques ($E_0 \approx 14,5 \pm 0,1$ MeV).

La résolution en énergie obtenue (0,6 MeV à $E_1 \approx 6$ MeV) a permis une bonne séparation du bruit de fond constitué d'événements fortuits reportés sur tout le plan et d'événements corrélés parasites dus à la diffusion des neutrons d'un détecteur sur l'autre.

Une condition de compatibilité entre le temps de vol du neutron et l'énergie de recul du proton a permis d'éliminer une grande partie des neutrons et γ parasites de faible énergie.

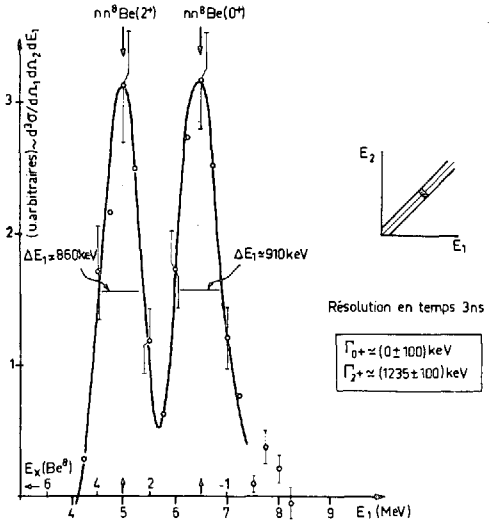

FIG.1. Mise en évidence des réactions $nn^8Be(0^+)$ et $nn^8Be(2^+)$ - Spectre de la réaction suivant $E_1 \approx E_2$ corrigé du bruit de fond et de l'efficacité des détecteurs

CINEMATIQUE

Les différentes voies possibles de désintégration pour le système ^9Be + n sont:

a) Désintégration en quatre particules $\alpha\alpha nn$
Faible importance: limite supérieure 10% dans notre expérience.

b) Résonance à trois corps: par exemple $^8Be^*$ nn
Les événements se situent pratiquement sur une droite du plan T_1, T_2 correspondant à la corrélation $\alpha\alpha$ pour former $^8Be(0+)$ ou $(2+)$.

c) Résonance à deux corps: par exemple $^9Be^*$ n
Les événements se situent sur un segment de la droite précédente $(0+)$ ou $(2+)$, la largeur d'un segment est celle du niveau $^9Be^*$ correspondant.

MESURES

Nous avons fait quatre mesures dans le plan horizontal avec les géométries suivantes:

ϕ_1	30°	60°	80°	30°
ϕ_2	-30°	-60°	-80°	-15°

La figure 1, pour la géométrie (30°, -30°), met en évidence la désintégration en trois corps $^8Be^*$ nn, par conséquent le passage par les niveaux 2+ et 0+ du ^8Be. La figure 2 montre l'évolution angulaire de la réaction $^9Be(n,nn)\alpha\alpha$. Il y a une prédominance marquée vers les angles avant, en accord avec les mesures de Myachkova [2] faites par émulsions nucléaires.

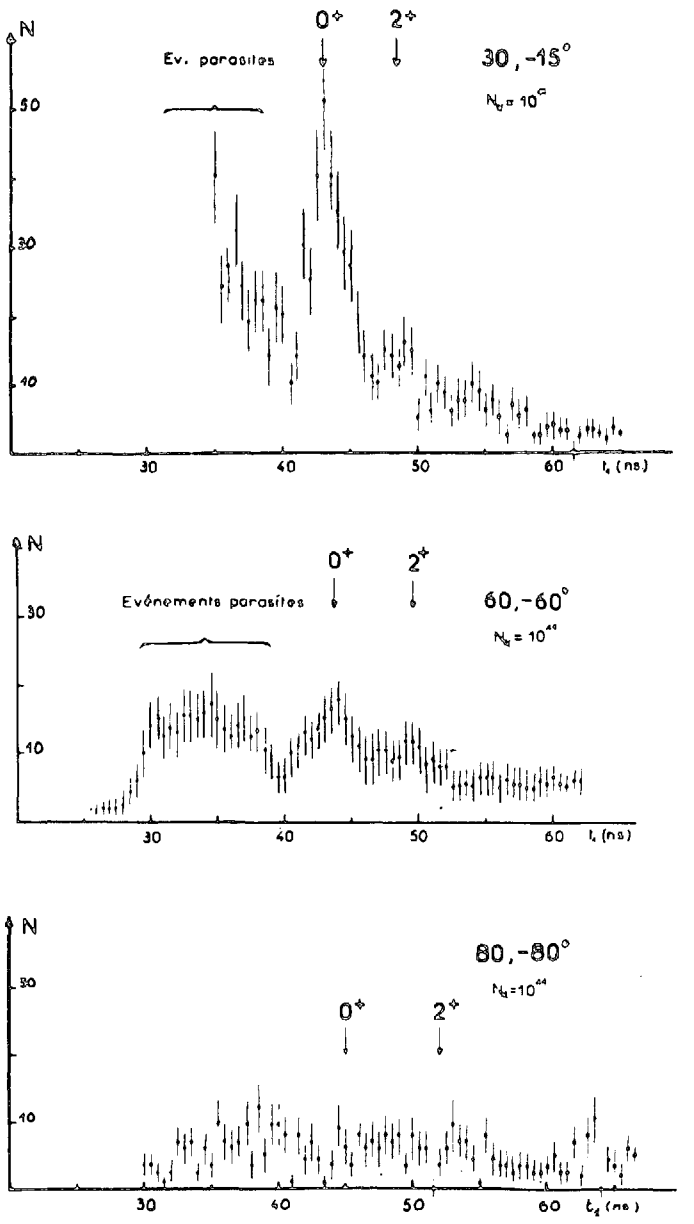

FIG.2. Evolution angulaire de la réaction $^{9}Be(n,nn)\,\alpha\alpha$ - Spectres de la réaction suivant $E_1 \approx E_2$ non corrigés du bruit de fond et de l'efficacité des détecteurs

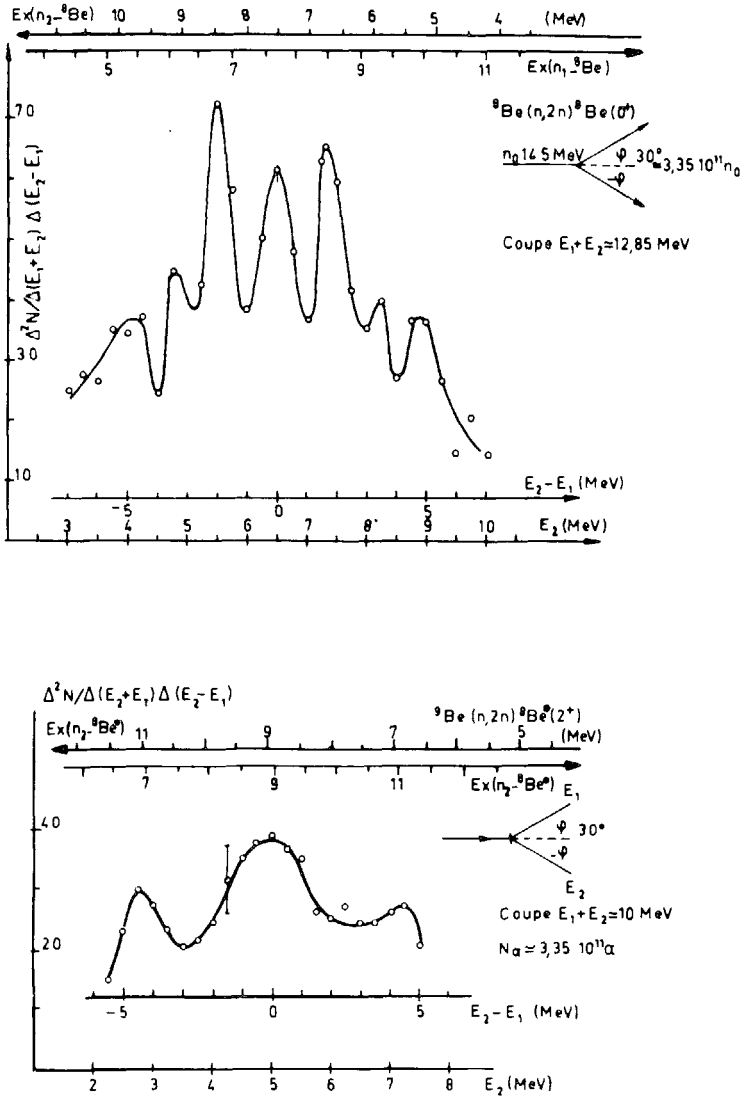

FIG.3. Distribution des événements (n, n) avec formation intermédiaire du ^{8}Be mettant en évidence l'excitation des niveaux du ^{8}Be

L'analyse le long des lignes cinématiques, correspondant au passage par ^{8}Be(0+) ou (2+), montre une forte structure résonnante (fig.3) associée à une suite de désintégrations en deux corps:

$$n + {}^{9}Be \rightarrow n_1 + {}^{9}Be^{*} \begin{cases} \nearrow n_2 + {}^{8}Be^{*}(0+) \\ \searrow n_2' + {}^{8}Be^{*}(2+) \end{cases}$$

TABLEAU I. SECTIONS EFFICACES DIFFERENTIELLES A (30°, -30°)

Réaction	Niveau ^{9}Be (MeV)	$d^2\sigma/d\Omega_1 \cdot d\Omega_2$ (mb/sr^2)
^{8}Be(0+) n, n	6,76	0,6 ± 0,1
	7,94	0,25 ± 0,05
	9,1	très petit
^{8}Be(2+) n, n	6,76	non mesuré
	7,94	très petit
	9,1	0,6 ± 0,1

La présence d'un seuil sur chaque voie de neutrons ($E_n > 1,5$ MeV) et les corrections d'efficacité à leur voisinage ont limité l'étude des niveaux du ^{9}Be dans cette expérience.

Finalement, nous avons observé les sections efficaces différentielles à (30°, -30°); les résultats sont donnés au tableau I.

On observe, en outre, que les niveaux du ^{9}Be* se désintègrent de préférence vers un seul des niveaux (0+) ou (2+) du ^{8}Be; par exemple, le niveau 6,76 MeV du ^{9}Be va vers le ^{8}Be(0+); par contre le niveau 9,1 MeV du ^{9}Be va vers le ^{8}Be(2+), indiquant que la structure des objets ^{9}Be à 6,76 MeV ou 9,1 MeV est formée de préférence avec $|^8\text{Be}(0+)\text{-n}>$ ou $|^8\text{Be}(2+)\text{-n}>$.

La distribution des événements dans le diagramme de Dalitz $|T_1, T_2|$ (fig.4) n'a pas mis en évidence une désintégration en quatre corps $n + {}^9\text{Be} \rightarrow \alpha\alpha nn$. De même, la structure observée le long des lignes cinématiques ^{8}Be(0+) et ^{8}Be(2+) indique que ni une interaction directe concernant le neutron $P_{3/2}$ peu lié (1,66 MeV) du ^{9}Be [3], ni un autre processus à

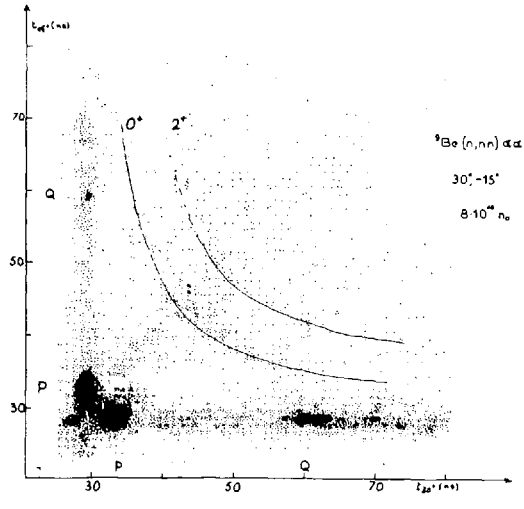

FIG.4. Distribution des événements dans le plan t_1, t_2 pour ($\varphi_1 = 30°$, $\varphi_2 = -15°$)

trois corps n'est prédominant à cette énergie dans la transition vers le ^{8}Be.

Il apparaît ainsi que cette transition est dominée par un processus séquentiel à deux corps: d'abord une interaction directe $^{9}Be(n,n')^{9}Be^{*}$, suivie par une désintégration en $^{8}Be(0+)$ ou $^{8}Be(2+)$.

REFERENCES

[1] BOUCHEZ, R., J. Phys. , Colloque n° 1 (1966) C1-79.
[2] MYACHKOVA, S. A., PERELYGIN, V. P., Soviet Phys. JETP 13 (1961) 876.
[3] BALIAN, R., GILLET, V. P., Nucl. Phys. 17 (1960) 448.

MEASUREMENTS OF 14-MeV NEUTRON-INDUCED REACTION CROSS-SECTIONS ON ENRICHED ISOTOPES OF CALCIUM

P. N. TIWARI AND E. KONDAIAH
TATA INSTITUTE OF FUNDAMENTAL RESEARCH,
BOMBAY, INDIA

Abstract

MEASUREMENTS OF 14-MeV NEUTRON-INDUCED REACTION CROSS-SECTIONS ON ENRICHED ISOTOPES OF CALCIUM. Some (n, t), (n, d), (n, p), (n, α) and (n, 2n) reaction cross-sections have been measured by the activation of enriched ^{40}Ca, ^{42}Ca, ^{43}Ca, ^{44}Ca, ^{48}Ca and specifically pure Al and K. Gamma counting by specially shielded and calibrated NaI(Tl) well-type crystals was employed to determine the absolute activities. The sensitivity of the counting system is such that with a neutron flux of the order of 10^{7} to 10^{8} n/s cm^{2}, cross-sections in the micro-barn region can be measured. The method adopted for measuring (n, d) cross-sections can be used to measure many of these cross-sections that have not yet been measured.

CROSS-SECTIONS FOR SOME (n, p) REACTIONS NEAR THRESHOLD

A. PAULSEN AND H. LISKIEN
CENTRAL BUREAU FOR NUCLEAR MEASUREMENTS,
EURATOM, GEEL, BELGIUM

Abstract

CROSS-SECTIONS FOR SOME (n,p) REACTIONS NEAR THRESHOLD. Cross-sections for the (n,p) reactions on ^{31}P, ^{32}S, ^{58}Ni and ^{64}Zn were measured near threshold in about 60-keV intervals compared with earlier measurements. Monoenergetic neutrons in the energy range 1.0 - 2.2 MeV were obtained by means of the T(p,n)^{3}He reaction and a 3-MeV Van de Graaff accelerator. The T(p,n) angular distribution was remeasured at E_p = 3 MeV with a recoil proton telescope. The results are compared with theoretical cross-sections after the method of Hauser and Feshbach. The application of these reactions as threshold detectors is discussed.

1. INTRODUCTION

Neutron-induced threshold reactions have up to now been widely used in nuclear reactors for fast flux integration and neutron spectra determination. The (n, p) reactions on ^{31}P, ^{32}S, ^{58}Ni and ^{64}Zn are the most important threshold reactions, with thresholds between 1- and 2-MeV neutron energy. An inquiry by EURATOM [1] about the necessary accuracy for the differential cross-sections of these threshold reactions showed a demand for accuracies between 2 and 4% in the energy region near threshold. Certainly such accuracies can hardly be reached today, but discrepancies between existing data have been much larger up to now [2]. The aim of this work is to ameliorate the situation by measuring the above-mentioned (n, p) reactions in the energy region from 1.0 to 2.2 MeV by the same technique with which these reactions will be used, i.e. by the activation technique.

2. EXPERIMENTAL

2.1. Activation procedure

The metallic samples of nickel and zinc and pressed pellets of sulphur and phosphorus mixed with 1% graphite and 20% paraffin, respectively, were disk-shaped, with dimensions of 20-mm diameter and 5-mm thickness. These samples were irradiated with neutrons from the T(p, n)^{3}He reaction at 3-MeV proton energy. An analysed beam of about 12 μA struck an occluded T-Ti target of 2.3-mg/cm^2 thickness which gave rise to a total neutron energy spread of $\pm$ 87.5 keV for 0°. The geometrical size of the neutron source is defined by the beam spot at the target, this being limited by an aperture to a width of 3 mm and a height of 8 mm. The samples were suspended from a graduated circle of 90.6-mm radius with their diameter in the direction of this radius. In

this way it was possible to irradiate simultaneously 26 probes between 0 and 90°, corresponding to 2.2 - 0.92 MeV neutron energy.

At the same time the neutron energy spread due to the finite solid angle for the sample viewed from the target is minimized in this irradiation geometry. On the other hand, it was necessary to apply corrections for neutron flux attenuation in the samples and for elastic in-scattering of neutrons from sample to sample. All these corrections never exceeded 8%. The reason for these corrections are obvious if one realizes that the T(p, n) angular distribution and the (n, p) activation excitation

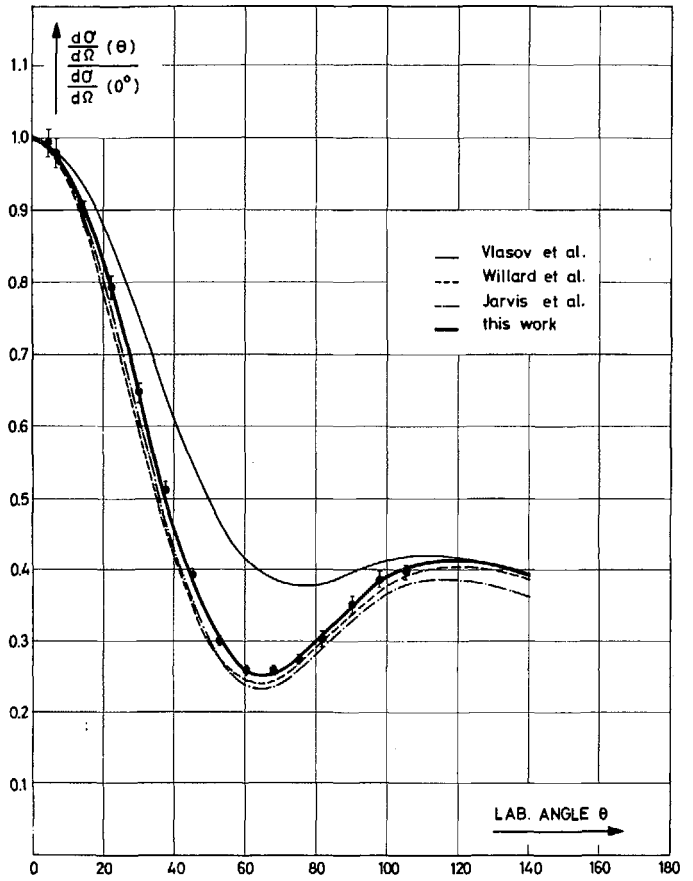

FIG.1. Angular distributions for the reactions $T(p, n)^3He$ at 3.0 MeV. The earlier measurements of Vlasov et al. [4], Willard et al.[5], and Jarvis et al. [6] were carried out with long counters. The present experiment is a telescope measurement.

functions amplify each other with respect to the resulting activities. An in-scattering from a sample of higher neutron energy and intensity to a probe at correspondingly lower values is therefore strongly enhanced in weight.

With a mirror system the graduated circle which carried the samples was adjusted with its centre above the geometrical centre of the proton beam spot.

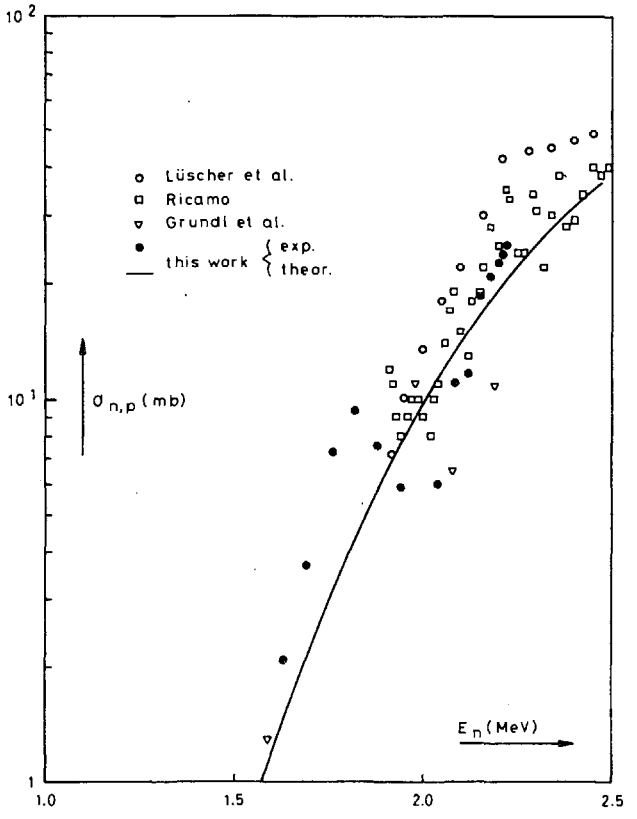

FIG.2. Cross-sections for the reaction $^{31}P(n, p)^{31}Si$. The earlier measurements of Lüscher et al.[12] and Ricamo [13] were normalized to (74 ± 15) mb at 3.0 MeV. The results of Grundl et al.[14] are related to the ^{238}U fission cross-section at the same energies. Our results are normalized to 25 mb at 2.2 MeV.

2.2. Activity determination

The induced ^{31}Si-activities in the phosphorus pellets were determined with simple GM end-window counters, while a GM end-window counter in anticoincidence with a NaI well-crystal was used for the determination of ^{32}P in the sulphur pellets. Relative counter efficiencies were checked by means of highly activated probes.

The reaction products ^{58}Co and ^{64}Cu were identified by their annihilation radiation and their half-lives in NaI coincidence counters. A ^{22}Na-source was used to check the relative efficiencies.

Also a lithium-drifted Ge-detector was used to observe the γ-spectra of the Zn and Ni samples. This detector showed in the case of zinc a considerable γ-line at 440 keV due to ^{69}Zn formed by neutron capture. As this γ-line is normally not resolved from the 511-keV annihilation radiation by scintillation counters and as the half-life of the isomeric state of ^{69}Zn is nearly the same as that of ^{64}Cu, measurements not using coincidence techniques may contain errors that cannot be neglected. This is a disadvantage of this reaction for threshold detector purposes. Probabilities for positron emission were taken from Ref. [3].

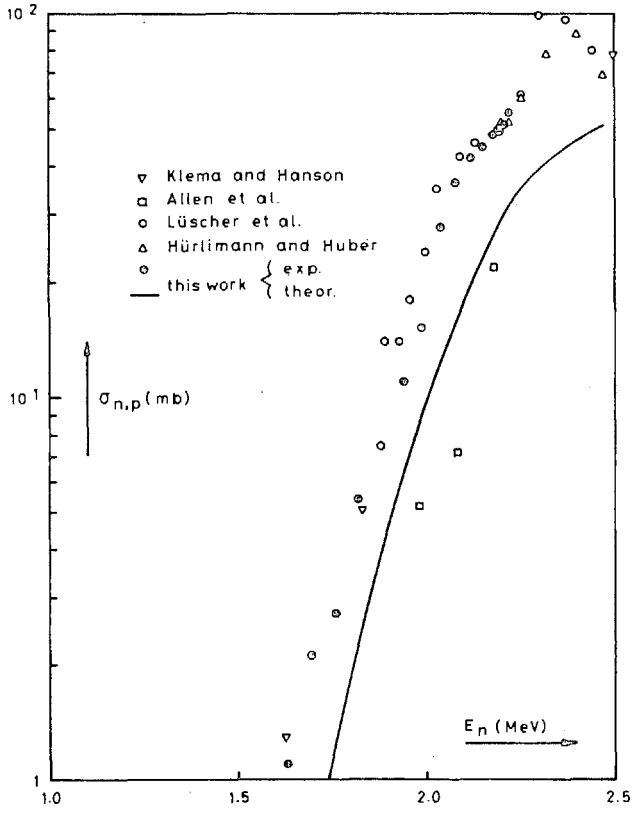

FIG.3. Cross-sections for the reaction $^{32}S(n,p)^{32}P$. The earlier results of Klema and Hanson [15] and Allen et al.[16] are related to the ^{238}U fission cross-sections. The results of Lüscher et al.[12] are normalized to those of Klema and Hanson [15]. Hürlimann and Huber [17] have determined the neutron flux with a Hornyak button of calculated efficiency. The results of the present work were normalized to this last measurement.

2.3. The T(p, n) angular distribution

For the evaluation of the activation cross-sections it was necessary to know the T(p, n) angular distribution. There are three earlier measurements [4-6] available which were all carried out with long counters. One of these [4] shows large discrepancies from the others [5, 6]. This was the reason for remeasuring the angular distribution by means of a telescope counter. This counter has been described already in a previous paper [7]. For use at these relatively low neutron energies the telescope counter was improved by replacing the CsI crystal by a large-area Si-diode. The angle of 105° corresponding to a neutron energy of 0.75 MeV was the lower limit for the telescope. The results of this measurement are shown in Fig. 1 together with the earlier results. Only these new results which agree well with those of Refs. [5, 6] were used for the activation cross-section evaluation. The relative uncertainty of the angular distribution is about ± 3%.

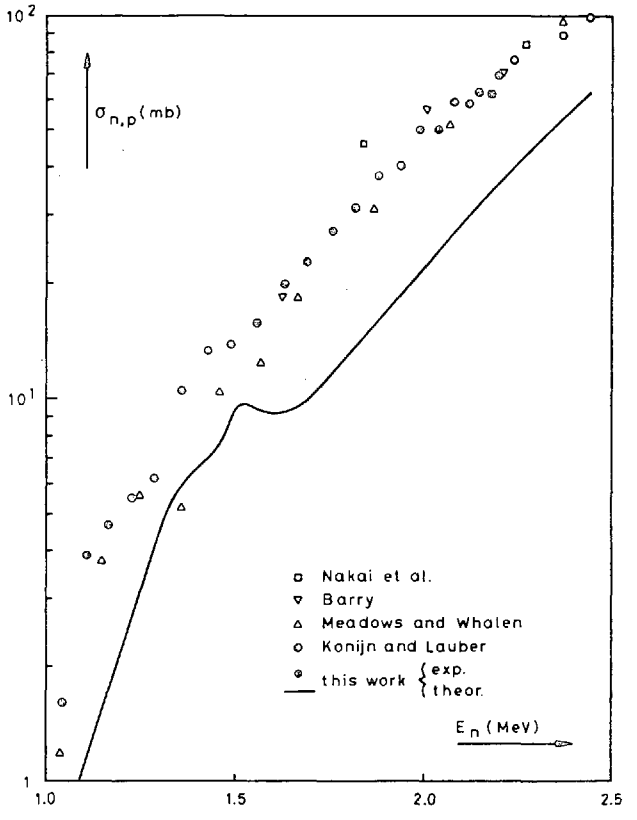

FIG.4. Cross-sections for the reaction $^{58}Ni(n, p)^{58}Co$. Nakai et al.[18] have performed absolute cross-section determinations, while Barry [19] and Meadows and Whalen [20] related their results to the ^{235}U fission cross-sections. Konijn and Lauber [21] have applied direct proton counting with semiconductor detectors. Our results were normalized to 70 mb at 2.2 MeV.

3. RESULTS

Reproducibility checks of the measurements showed good agreement in the relative shape of the excitation functions. Absolute values were obtained by using a proton recoil telescope for absolute flux measurements. The absolute activities were determined in the case of ^{31}Si and ^{32}P by liquid scintillation and bremsstrahlung counting [8] while the ^{58}Co and ^{64}Cu activities were compared with ^{58}Co and ^{22}Na standard sources.

But unfortunately all the absolute cross-section values were reproduced very poorly. The reasons for these discrepancies have not yet been found. Therefore we can present now only these relative excitation functions normalized to some earlier measurements. The results are shown in Figs. 2 to 5. To give a clear survey the diagrams do not contain error indications. The uncertainties of the earlier measurements can be found in Ref. [2]. The relative uncertainty of this work amounts to ± 4%. For the reaction $^{31}P(n, p)^{31}Si$ a peak was found in the excitation curve at 1.8 MeV. Good overall concurrence with the earlier measurements can be stated.

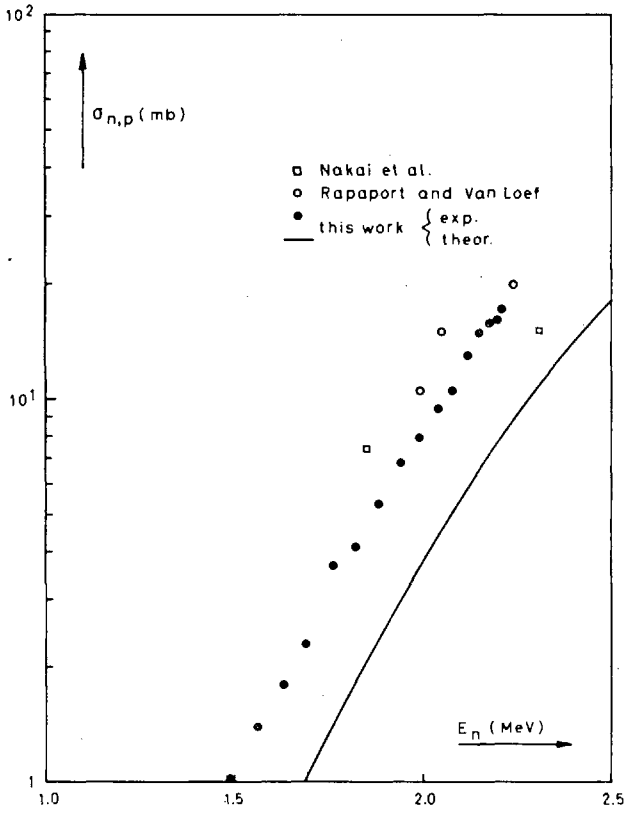

FIG.5. Cross-sections for the reaction $^{64}Zn(n,p)^{64}Cu$. The measurement of Nakai et al.[18] is based on absolute determinations. Rapaport and Van Loef [22] have related their results to the $^{31}P(n,p)^{31}Si$ cross-section at 3.55 MeV. Our results are normalized to 16 mb at 2.2 MeV.

4. HAUSER-FESHBACH CALCULATIONS

Figures 2 to 5 contain also as solid lines the results of statistical model calculations after the method of Hauser and Feshbach [9]. In this so-called partial statistical model the product nuclei are regarded as being excited in the discrete level region only. A computer programme (for IBM 7090) was written which contains the transmission coefficients for the various competing decay channels of the compound nucleus as input data. These transmission coefficients were used in steps of 100 keV from optical model calculations [10, 11]. Since most of the discrete-level spins and parities are unknown the computer programme contains a sub-programme for averaging over all possible spins and parities using the spin distribution function.

$$W(I) = (2I + 1) \exp\left[-(I+\frac{1}{2})^2/2\sigma^2\right]$$

and equal probabilities for both parities. The agreement between theory and experiment is very good for the reaction $^{31}P(n, p)^{31}Si$ as shown in Fig. 2. With increasing mass number the agreement in absolute values becomes worse, while the relative shapes are concurring in all cases.

These are rather encouraging results for a complete theoretical approach. This kind of calculation may be a helpful tool for interpolations and extrapolations of experimental results in this energy region. The reason for the shifts at higher mass numbers may perhaps be found in the fact that the product nuclei have larger level densities in this region. A certain number of rather low-lying levels may be unknown till now (see e. g. for ^{58}Co) because they are not populated with usual nuclear reactions due to spin selection rules.

5. CONCLUSIONS

The relative shapes of the (n, p) excitation functions on ^{31}P, ^{32}S, ^{58}Ni and ^{64}Zn were measured near threshold with ± 4% accuracy in good concurrence with earlier measurements and Hauser-Feshbach calculations. One may hope that better knowledge of nuclear-level schemes will result in a very good reliability of statistical model calculations. The experimental determination of the absolute reaction yields seems to be somewhat difficult for these reactions at the rather low monoenergetic neutron fluxes available by accelerators. One possible source of error was revealed in the case of $^{64}Zn(n, p)^{64}Cu$. Absolute cross-sections are under study.

ACKNOWLEDGEMENTS

The authors wish to thank Messrs. A. Spernol, R. Vaninbroukx and Dr. H. Schmid from the CBNM and Dr. L. Wallin from the ENEA for valuable help.

REFERENCES

[1] DELATTRE, P., Rep. EANDC(E) 51 "L" (1964).
[2] LISKIEN, H., PAULSEN, A., Rep. EUR. 119.e (1962).
[3] Nuclear Data Sheets, National Academy of Sciences, Washington (1959/60).
[4] VLASOV, N. A., KALININ, S. P., OGLOBLIN, A. A., SAMOILOV, L. N., SIDOROV, V. A., CHUEV, V. I., JETPUSSR 28 (1955) 639.
[5] WILLARD, H. B., BAIR, J. K., KINGTON, J. D., Phys. Rev. 90 (1953) 865.
[6] JARVIS, G. A., HEMMENDINGER, A., ARGO, H. V., TASCHEK, R. E., Phys. Rev. 79 (1950) 929.
[7] PAULSEN, A., LISKIEN, H., Nucl. Phys. 56 (1964) 394.
[8] VANINBROUKX, R., "Precise measurement of extended beta sources", Standardization of Radionuclides, IAEA, Vienna (1967) SM-79/38.
[9] HAUSER, W., FESHBACH, H., Phys. Rev. 87 (1952) 366.
[10] AUERBACH, E. H., PEREY, F. G. J., Rep. BNL 765 (1962).
[11] WALLIN, L., ENEA Gif-sur-Yvette, private communication.
[12] LÜSCHER, E., RICAMO, R., SCHERRER, P., ZÜNTI, W., Helv. phys. Acta 23 (1950) 561.
[13] RICAMO, R., Nuovo Cim. VIII (1951) 383.
[14] GRUNDL, J. A., HENKEL, R. L., PERKINGS, B. L., Phys. Rev. 109 (1958) 425.
[15] KLEMA, E. D., HANSON, A. O., Phys. Rev. 73 (1948) 106.
[16] ALLEN, L., Jr., BIGGERS, W. A., PRESTWOOD, R. J., SMITH, R. K., Phys. Rev. 107 (1957) 1363.

[17] HÜRLIMANN, T., HUBER, P., Helv. phys. Acta 28 (1955) 33.
[18] NAKAI, K., GOTOH, H., AMANO, H., J. phys. Soc. Japan 17 (1962) 1215.
[19] BARRY J.F., J. nucl. Energy A/B 16 (1962) 467.
[20] MEADOWS, J.W. WHALEN, J.F., Phys. Rev. 130 (1963) 2022.
[21] KONIJN, J., LAUBER, A., Nucl. Phys. 48 (1963) 191.
[22] RAPAPORT, J., VAN LOEF, J.J., Phys. Rev. 114 (1959) 565.

DISCUSSION

J. SPAEPEN (Chairman): Could you comment on the possible causes of discrepancies in the absolute measurements?

A. PAULSEN: The discrepancies seem to be partly connected with the different counting efficiencies of the lithium-drifted germanium detector and the NaI crystals normally used for determining absolute activity. Our knowledge of the photopeak efficiency curves of these detectors may be inadequate. However, the discrepancies for the formation of the pure β-emitters ^{31}S and ^{32}P must be due to something else, since the results obtained with the two methods of absolute β-counting (using bremsstrahlung and liquid scintillation) are not in agreement. The reasons have not yet been found. The absolute cross-sections are still under study; we hope to reach $\pm 6\%$ in total uncertainty.

CROSS-SECTIONS OF SOME (n, p), (n, t) AND (n, α) REACTIONS IN THE NEUTRON ENERGY REGION 13-19 MeV

M. BORMANN, F. DREYER, H. NEUERT, I. RIEHLE AND U. ZIELINSKI
I. INSTITUT FÜR EXPERIMENTALPHYSIK, UNIVERSITÄT HAMBURG, HAMBURG, FEDERAL REPUBLIC OF GERMANY

Abstract

CROSS-SECTIONS OF SOME (n, p), (n, t), AND (n, α) REACTIONS IN THE NEUTRON ENERGY REGION 13-19 MeV. The activation method was used for measuring the cross-sections of some neutron reactions at several neutron energies in the region 13-19 MeV. Results are presented in tabular form for (n, p) in ^{16}O, ^{25}Mg, ^{34}S, ^{58}Ni, ^{75}As, ^{74}Se and ^{85}Rb, for (n, t) in ^{32}S and ^{40}Ca and for (n, α) in ^{26}Mg, ^{75}As and ^{85}Rb. Monochromatic neutrons were produced by the reaction $^{3}H(d,n)^{4}He$ in titanium-tritium targets using the deuteron beams of a 3-MeV or a 1.5 MeV Van de Graaff generator. Gamma and positron activities were detected by means of a 3 in. × 2 in. NaI well-crystal or a $\gamma\gamma$-coincidence spectrometer consisting of two 3 in. × 3 in. NaI crystals. A pneumatic sample transport system was used in those cases where the activities had short half-lives. The neutron flux was measured by counting the recoil protons in a stilbene crystal.

Most of the (n, p) and (n, α) reactions investigated in the present work reach a maximum cross-section in the energy region considered. From these results and from corresponding data in the literature a simple expression can be deduced for the approximative determination of the neutron energy E_n^{max}, at which the (n, p) and (n, α) reactions reach their maximum cross-section as long as the target nuclei are restricted to the mass region of A = 20 - 100.

To continue earlier investigations [1] the activation method was used for measuring the excitation functions of some neutron-induced reactions with charged particle emission in the neutron energy region 13-19 MeV. In most cases gamma activities were detected by integral bias gamma counting with a 3 in. $\phi \times 2$ in. NaI well-crystal, the well of which had the dimensions 1 in. $\phi \times 1$ in. All pulses of the gamma spectrum above the threshold corresponding to 50-keV gamma energy were registered. For this discrimination setting the counting efficiency of the well-crystal was calculated for each activity produced after the method of Pollehn and Peuckert [2].

In some cases where the product nuclei decayed by positron emission this activity was measured by detecting the annihilation gamma quanta with a coincidence spectrometer consisting of two 3 in. $\phi \times 3$ in NaI crystals. The counting efficiency of this spectrometer was determined by means of the reactions $^{63}Cu(n, 2n)^{62}Cu$ and $^{19}F(n, 2n)^{18}F$ at 14.1-MeV neutron energy. The product nuclei of these reactions are also positron emitters and the cross-sections of the reactions at 14.1 MeV are well known, the values 478 mb ± 8% [3] and 41.2 mb ± 5.3% [1], respectively, were adopted.

Neutrons were produced in water-cooled thin titanium-tritium targets by the reaction $^{3}H(d,n)^{4}He$. For this purpose the 3-MeV and 1-MeV deuteron beams of two available Van de Graaff generators were

TABLE I. EXPERIMENTAL CROSS-SECTIONS

$^{16}O(n,p)^{16}N$		$^{25}Mg(n,p)^{25}Na$		$^{34}S(n,p)^{34}P$		$^{58}Ni(n,p)^{58}Co$	
E_n (MeV)	σ (mb)	E_n (MeV)	σ (mb)	E_n (MeV)	σ (mb)	E_n (MeV)	σ (mb)
13.35 ± 0.14	47.0 ± 4.8	13.00 ± 0.16	52.5 ± 5.3	14.00 ± 0.22	78 ± 7.5	12.95 ± 0.20	532 ± 44
13.58 ± 0.14	43.4 ± 4.4	13.25 ± 0.18	50.0 ± 5.0	14.96 ± 0.23	73 ± 7.0	13.5 ± 0.25	473 ± 39
14.00 ± 0.14	44.0 ± 4.5	13.55 ± 0.14	53.0 ± 5.3	15.92 ± 0.26	62 ± 6.0	14.1 ± 0.25	411 ± 30
14.10 ± 0.22	40.1 ± 4.1	14.00 ± 0.14	49.0 ± 4.9	16.17 ± 0.28	58 ± 5.6	14.9 ± 0.30	373 ± 31
14.25 ± 0.14	37.7 ± 3.8	14.28 ± 0.16	43.0 ± 4.3	16.42 ± 0.30	57 ± 5.5	15.6 $^{+0.30}_{-0.35}$	317 ± 26
14.53 ± 0.14	38.9 ± 4.0	14.74 ± 0.20	40.0 ± 4.0	16.65 ± 0.20	53 ± 5.1		
14.82 ± 0.16	35.8 ± 3.7	15.21 ± 0.28	37.0 ± 3.7			16.3 $^{+0.30}_{-0.35}$	277 ± 23
15.08 ± 0.17	32.2 ± 3.3	15.68 ± 0.29	36.0 ± 3.6				
15.30 ± 0.18	33.2 ± 3.4	15.92 ± 0.23	37.5 ± 3.8			17.25 $^{+0.25}_{-0.40}$	246 ± 20
15.54 ± 0.19	34.0 ± 3.5	16.17 ± 0.28	36.0 ± 3.6				
15.76 ± 0.19	31.8 ± 3.2	16.42 ± 0.30	34.0 ± 3.4			18.0 $^{+0.25}_{-0.35}$	221 ± 18
15.93 ± 0.21	31.3 ± 3.2	16.65 ± 0.20	27.5 ± 2.8				
16.17 ± 0.28	31.0 ± 3.2					18.9 $^{+0.15}_{-0.30}$	209 ± 17
16.50 ± 0.30	29.7 ± 3.0						
16.65 ± 0.26	26.0 ± 2.7					19.6 $^{+0.15}_{-0.25}$	215 ± 18

TABLE I (cont.)

$^{75}As(n,p)^{75}Ge$		$^{74}Se(n,p)^{74}As$		$^{85}Rb(n,p)^{85}Kr^{m}$		$^{32}S(n,t)^{30}P$	
E_n(MeV)	σ (mb)	E_n(MeV)	σ(mb)	E_n(MeV)	σ(mb)	E_n(MeV)	σ(μbam)
12.54 ± 0.17	16.4 ± 1.5	12.95 ± 0.20	174 ± 52	12.94 ± 0.36	3.3 ± 0.5	14.70 ± 0.35	7.5 ± 0.7
13.31 ± 0.23	18.3 ± 1.6	13.5 ± 0.25	107 ± 32	13.51 ± 0.38	3.6 ± 0.5	16.05 ± 0.95	471 ± 61
14.10 ± 0.27	20.3 ± 1.8	14.1 ± 0.25	105 ± 20	14.10 ± 0.47	4.3 ± 0.3	17.05 ± 0.95	737 ± 96
14.88 ± 0.30	18.4 ± 1.7	14.9 ± 0.30	111 ± 33	14.88 ± 0.53	4.7 ± 0.5	$18.00^{+0.70}_{-0.90}$	1000 ± 130
$15.62^{+0.31}_{-0.35}$	17.5 ± 1.6	$15.6^{+0.30}_{-0.35}$	73 ± 22	$15.62^{+0.55}_{-0.51}$	4.6 ± 0.5	$18.70^{+0.50}_{-0.75}$	1260 ± 160
$16.31^{+0.30}_{-0.38}$	16.4 ± 1.5	$16.3^{+0.30}_{-0.35}$	81 ± 24	$16.31^{+0.54}_{-0.61}$	4.6 ± 0.5	$19.60^{+0.20}_{-0.30}$	1380 ± 180
$17.23^{+0.26}_{-0.42}$	15.4 ± 1.4	$17.2^{+0.25}_{-0.40}$	79 ± 24	$17.23^{+0.48}_{-0.67}$	4.2 ± 0.4		
$18.02^{+0.24}_{-0.37}$	15.1 ± 1.4	$18.0^{+0.25}_{-0.35}$	70 ± 21	$18.02^{+0.43}_{-0.60}$	3.8 ± 0.4		
$18.89^{+0.15}_{-0.22}$	14.1 ± 1.3	$18.8^{+0.15}_{-0.30}$	72 ± 22	$18.89^{+0.29}_{-0.50}$	3.0 ± 0.3		
19.58 ± 0.14	13.7 ± 1.2	$19.6^{+0.15}_{-0.25}$	69 ± 21	19.58 ± 0.17	2.4 ± 0.2		

TABLE I (cont.)

$^{40}Ca(n,t)^{38}K^{g}$		$^{26}Mg(n,\alpha)^{23}Ne$		$^{75}As(n,\alpha)^{72}Ga$		$^{85}Rb(n,\alpha)^{82}Br$	
E_n (MeV)	σ (μ barn)	E_n (MeV)	σ (mb)	E_n (MeV)	σ (mb)	E_n (MeV)	σ (mb)
$14.9^{+1.4}_{-1.2}$	31 ± 5	13.00 ± 0.16	90.0 ± 9.0	12.54 ± 0.17	9.9 ± 0.9	12.94 ± 0.36	5.2 ± 0.5
16.1 ± 1.4	93 ± 11	13.25 ± 0.18	81.0 ± 8.1	13.31 ± 0.23	11.2 ± 0.9	13.51 ± 0.38	6.5 ± 0.7
$17.1^{+1.3}_{-1.4}$	135 ± 15	13.55 ± 0.14	88.5 ± 8.9	14.10 ± 0.27	12.5 ± 1.0	14.10 ± 0.47	7.0 ± 0.5
		14.00 ± 0.14	84.0 ± 8.4	14.88 ± 0.30	13.2 ± 1.1	14.88 ± 0.53	8.1 ± 0.8
$17.7^{+1.2}_{-1.4}$	157 ± 17	14.28 ± 0.16	77.0 ± 7.7	$15.62^{+0.31}_{-0.35}$	12.8 ± 1.0	$15.62^{+0.55}_{-0.51}$	8.5 ± 0.8
		14.74 ± 0.20	66.5 ± 6.7				
$18.0^{+1.0}_{-1.3}$	158 ± 17	15.21 ± 0.28	61.0 ± 6.1	$16.31^{+0.30}_{-0.38}$	12.3 ± 1.0	$16.31^{+0.54}_{-0.61}$	9.6 ± 0.9
		15.68 ± 0.29	59.0 ± 5.9				
$18.7^{+0.7}_{-1.2}$	188 ± 20	15.92 ± 0.23	64.0 ± 6.4	$17.23^{+0.26}_{-0.42}$	10.6 ± 0.8	$17.23^{+0.48}_{-0.67}$	10.0 ± 0.9
		16.17 ± 0.28	61.0 ± 6.1				
$19.6^{+0.2}_{-0.3}$	169 ± 18	16.42 ± 0.30	59.0 ± 5.9	$18.02^{+0.24}_{-0.37}$	10.3 ± 0.8	$18.02^{+0.43}_{-0.60}$	10.2 ± 0.9
		16.65 ± 0.20	53.0 ± 5.3				
				$18.89^{+0.15}_{-0.22}$	9.4 ± 0.7	$18.89^{+0.29}_{-0.50}$	9.7 ± 0.8
				19.58 ± 0.14	8.2 ± 0.6	19.58 ± 0.17	9.5 ± 0.7

used. Because of the angular dependence of the neutron energy for the source reaction, monochromatic neutrons in the energy range 12.6-19.6 MeV and 13.0-16.7 MeV, respectively, could be selected by varying the angle of irradiation.

The neutron flux was measured absolutely with a 1 in. $\phi \times 1$ in. stilbene recoil proton spectrometer at that angle which corresponded to 14.1-MeV neutron energy [4]. From this result the neutron intensities at other angles, that means for other neutron energies, were calculated with the help of the differential cross-sections for the reaction $^{3}H(d,n)^{4}He$ as measured by Paulsen and Liskien [5].

The samples consisted of powders of pure elements or of compounds. Only in the case of ^{40}Ca a metallic calcium cylinder was used. Sample quantities of the order of 10 g were irradiated. At the smaller accelerator a pneumatic sample transport system was available which allowed the measurement of activities with half-lives down to about 1 s.

Excitation functions for the following reactions were measured:

(a) With the NaI well-crystal
(n, p) for ^{16}O, ^{25}Mg, ^{34}S, ^{75}As and $^{85}Rb(n,p)^{85}Kr^{m}$,
(n, α) for ^{26}Mg, ^{75}As and ^{85}Rb.

(b) With the coincidence spectrometer
(n, p) for ^{58}Ni and ^{74}Se
$^{32}S(n,t)^{30}P$ and $^{40}Ca(n,t)^{38}K^{g}$

The results are given in Table 1 and also shown in graphical form in Figs. 1-12. The errors quoted for the cross-sections mainly consist of the statistical error of the sample activities, the uncertainty in the neutron flux on the sample (6% due to the error of the flux measurement at 14.1 MeV, the irradiation geometry and the differential cross-sections for the $^{3}H(d,n)^{4}He$ reaction), the error in the counting efficiency (1.5% for the well-crystal, 8% for the coincidence spectrometer), and the uncertainty in the correction for neutron absorption in the sample (1%).

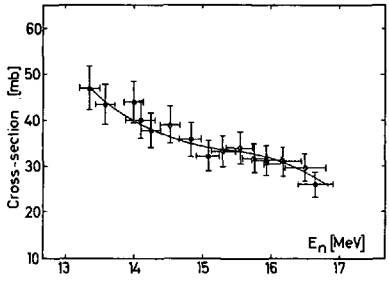

FIG. 1. Cross-sections for $^{16}O(n,p)^{16}N$

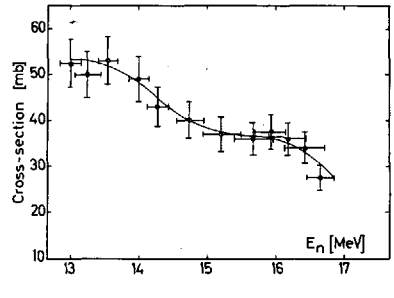

FIG. 2. Cross-sections for $^{25}Mg(n,p)^{25}Na$

The level schemes and transition probabilities for the product nuclei were taken from the Nuclear Data Sheets [6]. No errors of these data have been accounted for. For this reason some cross-sections may have additional systematic errors. The given neutron energy spread is due to the finite solid angle of the samples, the thickness of the tritium

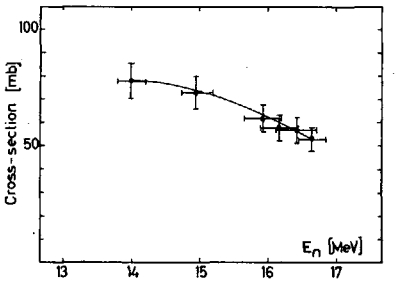

FIG. 3. Cross-sections for $^{34}S(n, p)^{34}P$

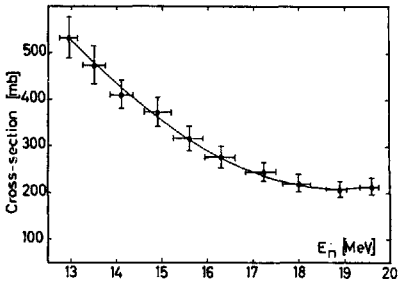

FIG. 4. Cross-sections for $^{58}Ni(n, p)^{58}Co$

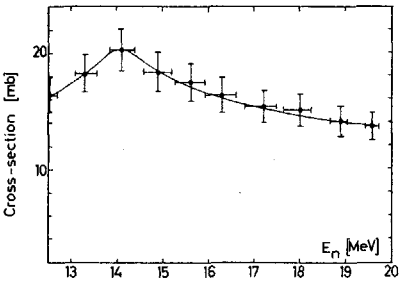

FIG. 5. Cross-sections for $^{75}As(n, p)^{75}Ge$

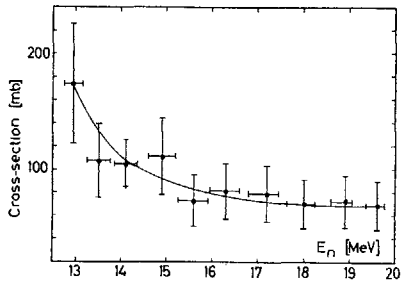

FIG. 6. Cross-sections for $^{74}Se(n, p)^{74}As$

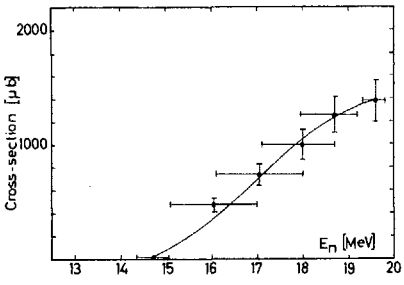

FIG. 7. Cross-sections for $^{32}S(n, t)^{30}P$

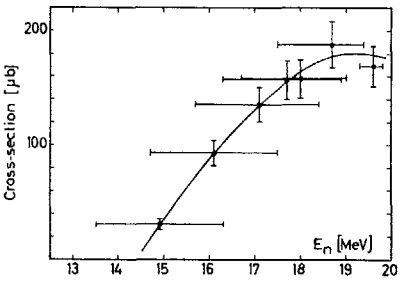

FIG. 8. Cross-sections for $^{40}Ca(n, t)^{38g}K$

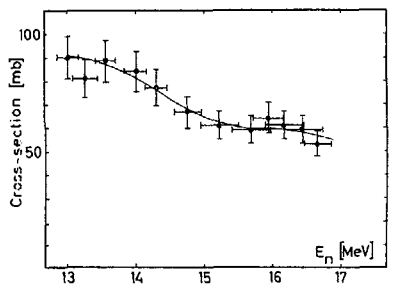

FIG. 9. Cross-sections for $^{26}Mg(n, \alpha)^{23}Ne$

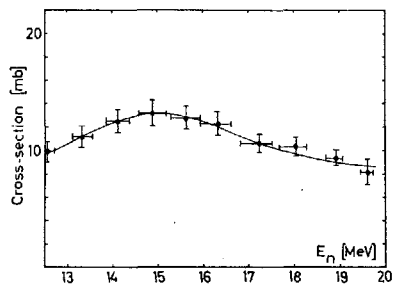

FIG. 10. Cross-sections for $^{75}As(n, \alpha)^{72}Ga$

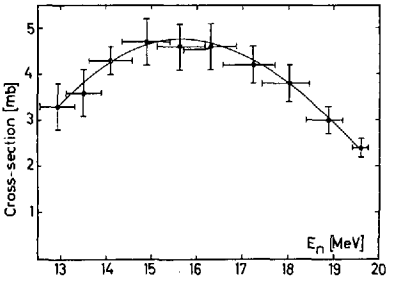

FIG. 11. Cross-sections for $^{85}Rb(n, p)^{85m}Kr$

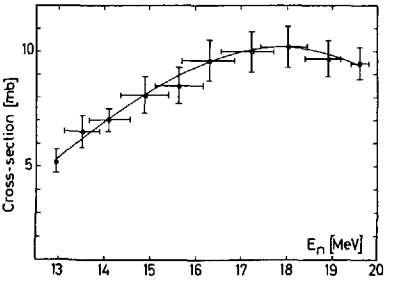

FIG. 12. Cross-sections for $^{85}Rb(n, \alpha)^{82}Br$

target and the error in the deuteron energy. This energy spread is largest for the (n, t) reactions. In this case, due to the small cross-sections, the samples had to be irradiated at small distances from the neutron source, giving large solid angles.

The (n, p) and (n, α) cross-sections measured are of the order of 100 mb for the lighter nuclei and of 10 mb for the heavier ones. The (n, t) cross-sections are much smaller; the excitation functions start at about 14 MeV and reach values of 1 mb at 19 MeV.

Some of the (n, p) and (n, α) excitation functions show a maximum in the energy region considered. The existence of a simple relation for the energy $E_n(\sigma^{max})$ at which these cross-sections reach the maximum values has been investigated. It is well established that the (n, p) and (n, α) reactions for nuclei in the mass region from about A = 20 to 90 and in the energy region considered in the present work can be interpreted as being mainly compound nucleus reactions which follow the predictions of the statistical theory [7-9]. According to this theory the cross-section of a special reaction depends strongly on the probabilities of other competitive reactions. The most competitive processes for the reactions (n, p) and (n, α) are the reactions (n, pn) and (n, αn), respectively. So it is expected that the (n, p) and (n, α) reactions reach their maximum cross-sections at about that neutron energy where the competitive reactions just start to have considerable intensities. Statistical theory calculations show that the excitation function for a reaction (n, xn), where x stands for a proton or an alpha particle, begins to increase rapidly at about that neutron energy E_n^* where the total reaction energy $E_n^* + Q_{n,xn}$ is equal to the height $E_C(x)$ of the coulomb barrier of the product nucleus for the charged particle x. Therefore the reaction (n, x) should have its maximum cross-section at the energy $E_n(\sigma_{n,x}{}^{max}) = E_n^*$ or $E_n(\sigma_{n,x}{}^{max}) \approx E_C(x) - Q_{n,xn}$ where $Q_{n,xn}$ is the negative Q-value for the competing reaction (n, xn). To check this relation for the (n, p) and (n, α) reactions in the mass region A = 20 to 90 all those experimental excitation functions of the present work and of the literature [10] were considered, where a maximum is clearly established. The quantities $[E_n(\sigma_{n,p}{}^{max}) + Q_{n,pn}] / E_C(p)$ and $[E_n(\sigma_{n,\alpha}{}^{max}) + Q_{n,\alpha n}] / E_C(\alpha)$ have been drawn against the mass number A of the target nuclei in Figs. 13 and 14, respectively. If the relation given above holds, these quantities should have values near unity. As can be seen from the figures this actually is the case. So there is a method given for a quick, rough estimate

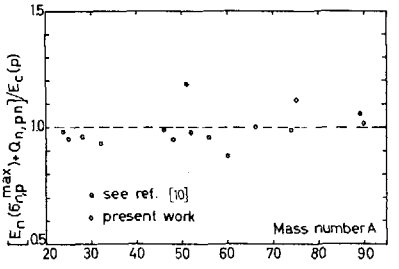

FIG.13. Neutron energy for the maximum (n, p) cross-section as a function of the target mass number A

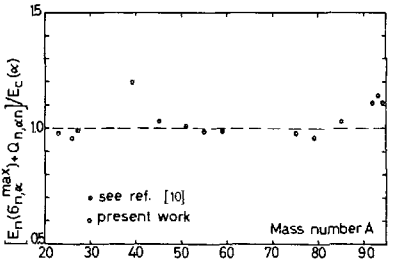

FIG.14. Neutron energy for the maximum (n, α) cross-section as a function of the target mass number A

of the neutron energy at which (n, p) and (n, α) reactions reach their maximum cross-sections as long as the statistical theory reaction mechanism dominates.

REFERENCES

[1] BORMANN, M. et al., Nucl. Phys. 63 (1965) 438.
[2] POLLEHN, H., PEUCKERT, K.H., Univ. Hamburg, unpubl.
[3] BORMANN, M. et al., Z. Physik 166 (1962) 477.
[4] BORMANN, M. et al., 14 MeV neutron flux measurement with a stilbene scintillator, EURATOM Rep. EUR 1815.e (1964) 246.
[5] PAULSEN, A., LISKIEN, H., Nucl. Phys. 56 (1964) 394.
[6] NUCLEAR DATA SHEETS, ed. by The NUCLEAR DATA GROUP of ORNL (1960).
[7] FACCHINI, U. et al., Nucl. Phys. 51 (1964) 460.
[8] SAETTA-MENICHELLA, E. et al., Nucl. Phys. 51 (1964) 449.
[9] ALLAN, D.L., Nucl. Phys. 24 (1961) 274.
[10] JESSEN, P. et al., Nucl. Data 1 (1966) 103.

$^{16}O(n,\alpha)^{13}C$ REACTION CROSS-SECTIONS FROM THE $^{13}C(\alpha,n)^{16}O$ REACTION

A.S. DIVATIA, K.K. SEKHARAN AND M.K. MEHTA
ATOMIC ENERGY ESTABLISHMENT TROMBAY,
BOMBAY, INDIA

Abstract

$^{16}O(n,\alpha)^{13}C$ REACTION CROSS-SECTIONS FROM THE $^{13}C(\alpha,n)^{16}O$ REACTION. Total cross-sections for the $^{16}O(n,\alpha)^{13}C$ reaction have been obtained from the total cross-sections for the $^{13}C(\alpha,n)^{16}O$ reaction, using the principle of reciprocity. The incident neutron energy covered ranges from 3.95 to 6.50 MeV. The $^{13}C(\alpha,n)^{16}O$ reaction was studied by bombarding an enriched ^{13}C target, about 35-keV thick for 3-MeV alphas, with singly charged He ions obtained from the Trombay Van de Graaff accelerator, in the energy range 1.95 to 5.50 MeV, in steps of 5 to 8 keV. The total neutron yield was measured by a calibrated 4π neutron detector, consisting of a BF_3 counter-paraffin assembly, and the absolute cross-sections were measured to an accuracy of ±15%. About twenty resonances were observed, corresponding to energy levels in the compound nucleus ^{17}O, in the excitation energy region 7.9 - 10.5 MeV. For isolated levels, total widths have been deduced. For resonances corresponding to the levels in ^{17}O at 8.40, 8.50, 9.19, 9.50, 9.73 and 9.88 MeV, the $^{16}O(n,\alpha)^{13}C$ reaction cross-sections are 70.8, 132, 43.1, 33.1, 149 and 134 mb, respectively. For these six levels, partial widths for neutron and alpha emission have been obtained, using Breit-Wigner dispersion theory.

1. INTRODUCTION

The measurement of the $^{16}O(n,\alpha)^{13}C$ reaction cross-section is important, both for understanding the level structure of ^{17}O, as well as for fast reactor calculations. Direct measurements of this cross-section have been made by Seitz and Huber [1], Davis et al. [2] and Lister and Sayers [3]. Another approach is to measure the $^{13}C(\alpha,n)^{16}O$ reaction cross-sections and obtain the $^{16}O(n,\alpha)^{13}C$ reaction cross-sections from them by the reciprocity theorem. The differential cross-sections for the $^{13}C(\alpha,n)^{16}O$ reaction have been measured by Becker and Barschall [4] and by Walton et al. [5] for the incident alpha particle energy range 2-3.5 MeV, and by Bonner et al. [6] for the energy range 2-5.1 MeV. Even though the integrated cross-sections have been obtained from these measurements, no direct measurement of the integrated cross-sections for the $^{13}C(\alpha,n)^{16}O$ reaction is available. Such a direct measurement was undertaken with the 5.5-MeV Van de Graaff Accelerator at the Atomic Energy Establishment Trombay and a 4π-geometry neutron counter.

2. EXPERIMENTAL METHOD

An excitation function for the $^{13}C(\alpha,n)^{16}O$ reaction was obtained for incident particle energies ranging from 1.95 to 5.5 MeV, in steps of 5 to 8 keV. The neutrons were detected by a 4π-geometry neutron counter [7] consisting of a BF_3 counter-paraffin assembly shown in Fig. 1. The counter was calibrated using the $^{7}Li(p,n)^{7}Be$ reaction; the cross-section for the $^{7}Li(p,n)^{7}Be$ reaction is known, and the thick-

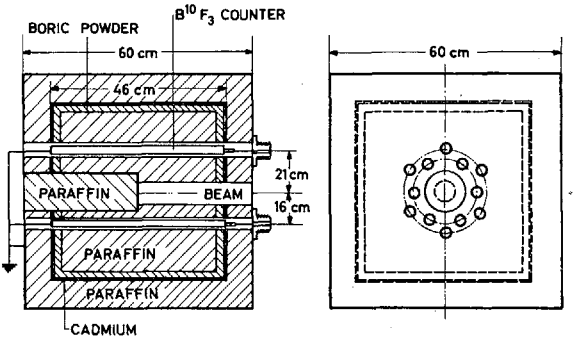

FIG.1. The 4π-neutron counter

ness of ^{7}Li could be determined by the ^{7}Li(p, p)^{7}Li reaction, the lithium being deposited on a thin carbon backing. The efficiency of the counter was determined to an accuracy of ±12%.

An electromagnetically enriched ^{13}C (enrichment ≈30%) target, obtained from the Atomic Energy Research Establishment, Harwell, where the carbon was deposited on a thick tantalum backing, was used. The thickness of carbon was 31 keV for 3.1-MeV alpha particles, as determined from the widths of the resonances in the excitation function. Since the ^{13}C(p, n)^{13}N reaction cross-section has been measured [8], the number of ^{13}C nuclei in the target was determined by measuring the neutron yields from the ^{13}C(p, n)^{13}N reaction.

The current integration was done by a current integrator [9] built at Trombay, based on a design by Smulders and Smith [10]. The integration was accurate to ±2%.

The overall accuracy of the cross-section measurements is ±15%. The factors contributing to the error are, (i) determination of the efficiency of the neutron counter, (ii) determination of the number of ^{13}C nuclei in the target, and (iii) current integration. Of these, the first factor contributes the largest error.

3. RESULTS AND DISCUSSION

According to the reciprocity theorem, the cross-section σ(a, b) for a reaction A(a, b)B can be expressed in terms of the cross-section σ(b, a) for its inverse reaction by means of the relationship,

$$\frac{\sigma(a,b)(2I_A+1)(2I_a+1)}{\lambda\!\!\!^{-2}_a} = \frac{\sigma(b,a)(2I_B+1)(2I_b+1)}{\lambda\!\!\!^{-2}_b} \qquad (1)$$

where I_A, I_B, I_a, I_b = the spins of nuclei A, B, a, b; $\lambda\!\!\!^{-}_a$, $\lambda\!\!\!^{-}_b$ = $1/2\pi \times$ the De Broglie wave length of the particle a, b in the centre-of-mass system. For the ^{16}O(n, α)^{13}C reaction,

$$\frac{\sigma(n,\alpha)}{\lambda\!\!\!^{-2}_n} = \frac{\sigma(\alpha,n)}{\lambda\!\!\!^{-2}_\alpha} \qquad (2)$$

Figure 2 shows the excitation function for the ^{16}O(n, α)^{13}C reaction for

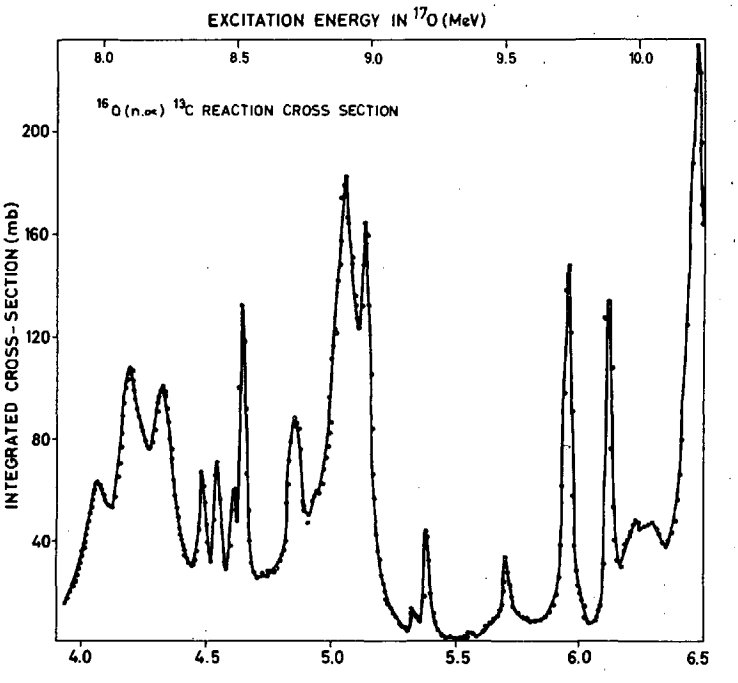

FIG.2. The excitation function for the $^{16}O(n, \alpha)^{13}C$ reaction

the incident neutron energy range E_n = 3.95 to 6.50 MeV obtained by this relationship. About twenty resonances are observed, corresponding to energy levels in the compound nucleus at ^{17}O, in the excitation energy region 7.9-10.5 MeV. The overall agreement with the resonances observed in the differential cross-section measurements mentioned

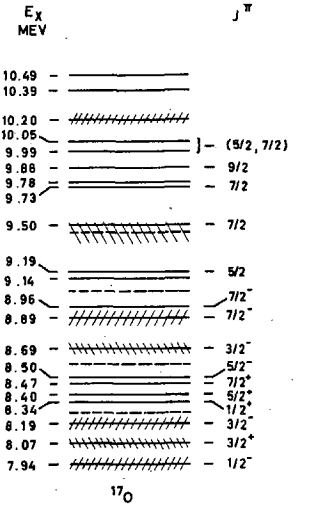

FIG.3. Energy level diagram of ^{17}O in the region 7.9-10.5 MeV. Continuous lines indicate levels observed in the present work (Table II); dashed lines indicate levels observed in other reactions. Level widths $\geq$ 50 keV are indicated by slanting lines.

TABLE I. INTEGRATED PEAK CROSS-SECTIONS FOR THE $^{16}O(n, \alpha)^{13}C$ REACTION

Incident neutron energy, E_n (MeV)	Integrated peak cross-sections (mb) according to:		
	Wisconsin Walton et al. [5] ± 20%	Rice Davis et al. [2] ± 20%	Trombay present work ± 15%
4.05	76	73	63
4.18	140	125	107
4.32	125	105	102
4.47	102	48	67
4.53	92	52	71
4.60	75	--	60
4.64	194	90	132
4.84	68	82	88
5.05	190	182	183
5.13	153	150	164
5.32		10	12
5.38		19	43
5.71		20	33
5.95		80	149
6.11		70	134
6.23		43	47
6.29		--	47

earlier [4-6] is good. Two resonances, corresponding to the levels in ^{17}O at 9.99 and 10.05 MeV, are partially resolved, and indicate two separate levels 60 keV apart. This is in disagreement with the assignment of a single broad level in this region, by Bonner et al.[6]. The cross-sections at the maxima of the resonances are given in Table I, along with the earlier measurements of Walton et al.[5] and Davis et al.[2].

For the isolated levels, total widths deduced from the $^{13}C(\alpha, n)^{16}O$ excitation function are given in Table II. For levels which are narrow compared to the target thickness the total width Γ was determined by the leading edge method of Richards [11], and for levels which are wide, it was obtained directly from the experimental width $\Gamma_{exp.}$ and the target thickness T, since $\Gamma^2_{exp.} = \Gamma^2 + T^2$.

A knowledge of the integrated cross-section at the resonant energy and the spin and the total width of a level enables one to calculate the partial alpha width Γ_α and the partial neutron width Γ_n, since, according to the Breit-Wigner single-level theory, the cross-section $\sigma(\alpha, n)$ at an energy E is given by

$$\sigma(\alpha, n) = \pi \lambda_{\alpha}^{2} \frac{(2J+1)}{(2I+1)(2i+1)} \frac{\Gamma_{\alpha}\,\Gamma_{n}}{(E-E_{r})^{2} + (\Gamma/2)^{2}} \qquad (3)$$

where λ_{α} = $1/2\pi \times$ the De Broglie wavelength of the incident particle in the centre-of-mass system
J = total angular momentum of the compound nucleus state excited
I = spin angular momentum of the target nucleus
i = spin angular momentum of the incident particle
Γ = total width of the compound nucleus level,
$\Gamma_{\alpha}, \Gamma_{n}$ = partial alpha and neutron widths, respectively
E_{r} = resonance energy of the level.

TABLE II. TOTAL WIDTHS FOR LEVELS IN ^{17}O OBTAINED FROM THE $^{13}C(\alpha, n)^{16}O$ REACTION CROSS-SECTIONS

Incident alpha energy E_{α} (lab) (MeV)	Excitation energy E_{x} in ^{17}O (MeV)	Integrated peak cross-section (mb) ±15%	Total width Γ(keV) (centre-of-mass)
2.10	7.94	46.4	79 ± 10[b]
2.27	8.07	75.0	71 ± 8[b]
2.43	8.19	68.7	71 ± 5[b]
2.62	8.34	43.6	9 ± 3[a]
2.70	8.40	45.2	4 ± 3[a]
2.78	8.47	37.9	7 ± 3[a]
2.83	8.50	82.0	5 ± 3[a]
3.08	8.69	52.7	50 ± 3[b]
3.34	8.89	105.2	101 ± 3[b]
3.44	8.96	93.1	21 ± 3[b]
3.67	9.14	6.7	4 ± 3[b]
3.73	9.19	23.5	4 ± 3[a]
4.13	9.50	17.3	8 ± 3[a]
4.44	9.73	75.6	15 ± 3[a]
(4.50)	(9.78)	—	—
4.63	9.88	67.0	5 ± 3[a]
(4.78)	(9.99)	(23.2)	—
(4.86)	(10.05)	(22.9)	—
5.06	10.20	113.1	50 ± 3[b]
5.30	10.39	147.7	—
5.42	10.49	197.4	—

(a) Determined by the leading edge method of Richards [11].
(b) Determined directly as explained in the text.

TABLE III. PARTIAL WIDTHS Γ_α AND Γ_n FOR LEVELS IN ^{17}O

Incident alpha energy E_α(lab) (MeV)	Excitation energy E_x in ^{17}O (MeV)	Spin J^π	Partial alpha width Γ_α (keV)	Partial neutron width Γ_n (keV)	Γ_n/Γ_α
2.70	8.40	$5/2^+$	0.31	3.69	11.9
2.83	8.50	$5/2^-$	0.82	4.18	5.1
3.73	9.19	5/2	0.22	3.78	17.2
4.13	9.50	7/2	0.26	7.74	29.8
4.44	9.73	7/2	2.75	12.27	4.5
4.63	9.88	9/2	0.63	4.37	6.9

The partial widths, evaluated for the levels in ^{17}O at 8.40, 8.50, 9.19, 9.50, 9.73 and 9.88 MeV, are listed in Table III. In this evaluation it is necessary to make the assumption that $\Gamma_n > \Gamma_\alpha$. In view of the coulomb barrier for the alpha particles, this is a reasonable assumption; however, it may not be valid in all cases. The spins assumed for these levels have been listed in the table [12, 13].

An energy level diagram of ^{17}O in the region 7.9-10.5 MeV is shown in Fig. 3; it summarizes the available information [12-14], including that obtained in the present work.

REFERENCES

[1] SEITZ, J., HUBER, P., Helv.phys.Acta 28 (1955) 227.
[2] DAVIS, E.A., et al., Nucl.Phys. 48 (1963) 169.
[3] LISTER, D., SAYERS, A., Phys.Rev. 143 (1966) 745.
[4] BECKER, R.L., BARSCHALL, H.H., Phys.Rev. 102 (1956) 1384.
[5] WALTON, R.B., CLEMENT, J.D., BORELI, F., Phys.Rev. 107 (1957) 1065.
[6] BONNER, T.W., et al., Phys.Rev. 102 (1956) 1348.
[7] MARION, J.B., et al., Nucl.Instr. Methods 8 (1960) 297.
[8] GIBBONS, J., H., MACKLIN, R.L., Phys.Rev. 114 (1959) 571.
[9] DIVATIA, A.S., A.E.E.T. Rep. A.E.E.T./N.P./8 (1964) 12.
[10] SMULDERS, P.J.M., SMITH, P.B., Nucl. Instr.Methods 8 (1960) 40.
[11] RICHARDS, H.T., "Charged particle reaction", Ch.I.D, Nuclear Spectroscopy, Part A (AJZENBERG-SELOVE, F., Ed.), Academic Press, N.Y.(1960).
[12] AJZENBERG-SELOVE, F., LAURITSEN, T., Nucl.Phys. 11 (1959) 1.
[13] BARNES, B.K., BELOTE, T.A., RISSER, J.R., Phys.Rev. 140 (1965) B 616.
[14] FOSSAN, D.B., et al., Phys.Rev. 123 (1961) 209.

Session V

CROSS-SECTIONS AND CONSTANTS USED AS STANDARDS

PRIMARY STANDARD DATA AND STANDARD SAMPLES

J. SPAEPEN
CENTRAL BUREAU FOR NUCLEAR MEASUREMENTS,
EURATOM, GEEL, BELGIUM

Abstract

PRIMARY STANDARD DATA AND STANDARD SAMPLES. The accuracy requirements for primary standard cross-sections, in the interval from thermal energy to 15 MeV, are derived from the needs for precise neutron data, requested for reactor purposes. The accuracy attained at present for possible standard cross-sections is discussed, and the situation is reviewed as far as the properties of corresponding samples and detectors are concerned. The $^{10}B(n,\alpha)^{7}Li,Li^{*}$ (below 100 keV) and $^{1}H(n,n)$ (above 100 keV) cross-sections are proposed as primary standards for flux measurements and recommended values are given, where possible. On the other hand, energy regions where improvement of accuracy is still needed, are indicated.

Suggestions for future work are given in the conclusions. It is pointed out, in particular, that a high precision measurement of the $^{10}B(n,\alpha)$ cross-section near 100 keV would establish a sufficiently accurate primary standard in the 1-100 keV-region if the cross-section behaves still as 1/v at 100 keV.

The suggestions pertain also to secondary working standards of which a brief list is given, without, however, reviewing the present status in detail.

1. INTRODUCTION

Nuclear energy has matured during recent years into the stage of industrial competition. The need to design "conventional" power reactors as economically and safely as possible, and to develop fast reactors for the future, has created a demand for precise data pertaining to interactions of neutrons with fissile, moderating, coolant and structural materials, to in-pile neutron spectra, to isotopic composition of fissile and moderating material, etc.

To ensure uniformity and avoid confusion, the measurement of such data has to be carried out within the framework of a well-defined system of units, making use of carefully chosen secondary working standards, which are in turn based on a few very precisely known primary reference data and carefully assayed reference samples.

It is in this sense that the terms standard data and standard samples (measurement standards) are used in the present article, leaving out any considerations about engineering standards, radiation protection standards, etc. Also, to remain within the scope of this Conference, our considerations will be limited to measurement standards closely linked to reactor needs, without discussing, for example, calibrated radioactive sources for biological, medical or agricultural applications or standards for calibrating radiation protection measuring equipment.

The main difficulty with most absolute measurements of neutron data lies in the determination of the neutron flux. An important part of the discussion is therefore devoted to this problem. For flux measurement, most experiments refer in the last instance to a few absolute cross-sections, such as $\sigma_{n,n}(^{1}H)$ or $\sigma_{n,\alpha}(^{10}B)$. It is a pity, however, that the origin and the accuracy of the reference values used are not always carefully checked; this gives rise to much confusion. Unfortunately also,

reference cross-sections are inaccurate in energy intervals which are very important with respect to the accuracy of many neutron data requested by reactor designers and other users.

The present article is mainly concerned with primary standards. It is an attempt to review the present situation, mostly based on very recent progress, as excellent reviews exist for different sectors of interest (e.g. several chapters in Refs.[1] and [2]). As a basis for discussion, suggestions are advanced concerning a system of primary and secondary standard cross-sections and related quantities. It points out which recommended values could already be adopted and indicates areas in which improvement is needed.

The general use of a recommended value for a standard cross-section is, of course, an important step. However, it must be supplemented by careful preparation and precise assay of the corresponding reference sample. Part of the discussion is therefore devoted to such reference samples.

2. STANDARD METHODS FOR NEUTRON FLUX DETERMINATION

There are several methods to measure the absolute number of neutrons emitted by a source.

2.1. Associated particle counting

The method of counting the associated charged particles from a neutron-producing reaction has been often applied to the $^{3}H(d,n)$ reaction at about 14 MeV and accuracies of 1% are normally attained [3]. At lower energies the associated protons from the $^{2}H(\gamma,n)$ reaction have been counted [4]. Leroy's group [5] reports at this Conference their attempts to apply this method to the $^{3}H(p,n)$-reaction at energies of a few hundred keV. Difficulties lie in the preparation of the very thin tritiated titanium targets, in the high charged particle background and in the coulomb scattering of ^{3}He in the target.

2.2. Bath methods

The total yield of a source can be measured by immersing it in a medium which completely absorbs the neutrons in such a way that every neutron captured gives rise to a radionuclide, which can be conveniently counted. The best technique at present is the manganese sulphate bath. The method does not provide any information about the neutron spectrum of the source. The latter is so essential that it limits the use of (α,n) sources to a very few applications. Recently, important progress has been made, however, in calibrating monoenergetic (γ,n) sources at the National Physical Laboratory, U.K., resulting in an accuracy of $\pm$ 0.6% for a ^{124}Sb-Be source [6]. This accuracy estimate may be too optimistic, as shown by the results of a recent intercomparison organized by the Bureau International des Poids et Mesures [7]: values obtained for the same Ra(α,n)Be source by the manganese bath technique by eight of the world's best standards laboratories are spread over more than 3%, although normalized to the same manganese and hydrogen thermal capture cross-sections.

2.3. Flat response counters

Other 4π-counters are the long counter of Hanson and McKibben [8] and the graphite sphere neutron detector of Macklin [9], which allows the calibration with a known source to be extrapolated to other neutron energies, thanks to a nearly constant and known efficiency versus neutron energy. Especially in the keV region the calculated efficiency curve seems to be better known for the graphite sphere than for the long counter.

2.4. Induced activity method

The number of neutrons produced in a nuclear reaction has been deduced in some cases from the activity of the radioactive product. Pönitz reports the measurement of the ^{7}Be-activity from the ^{7}Li(p, n) reaction [10]. ^{51}V(p, n)^{51}Cr is another example of this technique [11, 12].

2.5. Methods based on standard cross-sections

All more or less direct methods of flux determination mentioned above present particular advantages in special cases but remain of limited application. The most generally applied methods of flux measurement are based on cross-sections for reactions such as ^{3}He(n, p), ^{10}B(n, α), ^{6}Li(n, α), and on the hydrogen scattering cross-section. It is possible to measure those cross-sections to a high precision provided the contribution of competing processes to the total cross-section remains very small, a transmission measurement being independent of the number of neutrons in a given energy interval and of the detector efficiency. In this way the reaction cross-sections for ^{3}He and ^{10}B in the thermal region (the scattering cross-section being relatively small) and the hydrogen scattering cross-section up to 40 MeV (competing reactions being small) have been measured to a very high precision. However, as soon as the difficultly measured scattering cross-section becomes relatively important, an ordinary total cross-section measurement becomes too inaccurate, which is the case, for example, with ^{10}B and ^{6}Li above 100 eV. Another type of transmission experiment has been tried in this region. The so-called spherical shell transmission is in fact related to the absorption cross-section. The unavoidable multiple scattering corrections, however, diminish somewhat the accuracy which can be expected from this technique. At this Conference Bogart [13] reports an improved analysis of sphere transmission experiments and Belanova et al. [14] discuss their experiments at 24 keV.

3. ACCURACY OF STANDARD DATA

Uncertainties (or accuracies) quoted in this article should be regarded as standard deviations for a single measurement[1].

To estimate the accuracy needed for standard data we have to consider the more stringent accuracies requested by reactor designers for

[1] We would have preferred to quote each uncertainty as a sum of statistical and systematic errors, and to distinguish between both sources of error. It is, however, often difficult to derive this distinction from the information given in the original articles.

TABLE I. ACCURACIES REQUESTED FOR REACTOR DESIGN

Energy range	$\sigma_{n,f}$ (%)	$\sigma_{n,\gamma}$ (%)	$\sigma_{n,n}(E;\theta)$ $\sigma_{n,n}(E;E',\theta)$ (%)	$\sigma_{n,p}$, $\sigma_{n,\alpha}$, $\sigma_{n,2n}$, $\sigma_{n,n'}$ (%)	$\bar{\nu}$ (%)
Thermal	0.5	1-5	2-10	-	0.5
< 40 keV	0.5-3	2-5	5-10	-	2
> 40 keV	0.5-2	2-5	3-10	-	0.5
up to 3 MeV above threshold	-	-	-	2-5	-
from 3 to 5 MeV above threshold	-	-	-	3-10	-
from 5 MeV above threshold	-	-	-	10-30	-

TABLE II. FLUX STANDARD ACCURACY REQUIREMENTS

Energy range (keV)	Flux standard accuracy corresponding to	
	requested accuracy (%)	acceptable accuracy (%)
Thermal	0.1-0.3	0.1-0.3
< 40	0.1-0.3	0.6-1.5
> 40	0.1-0.3	0.4-1

microscopic data of many isotopes (Table I). The best accuracies listed are those really needed, but as designers realize that most of them cannot be met with present techniques, they have added less stringent accuracies which, if met, would already be greatly welcomed as substantial intermediary improvements.

The main difficulty in meeting some of the requested accuracies lies in the precise neutron flux measurement. Depending on the precision of the method used for comparison with a flux standard, the value of the latter has to be known 2 to 5 times better than the tolerated errors listed in Table I. Once the fundamental problem of flux measurement is solved, suitable secondary reference data can be measured, especially adapted to the kind of cross-section and the energy region. We will therefore

first discuss standard data for neutron flux, which are in fact primary standards, followed by a brief list of useful secondary reference data.

The most stringent accuracies, listed in Table I, pertain to fission cross-sections: 0.5% is requested over the complete energy range, although even 3% would be welcomed below 40 keV and 2% above this energy. This establishes the goal for flux determinations. Depending on the precision of the applied technique of fission cross-section measurement, the flux standard should have the accuracy given in Table II. Let us now examine the present accuracy of direct methods for flux measurement and of basic cross-sections (Table III).

Condensing information as in Table III is impossible without a lot of simplification, and some comments have to be added.

3.1. Associated particle

Associated particle counting using the $^{3}H(d,n)$ reaction provides a precise method of flux determination in an energy region where the hydrogen scattering becomes anisotropic and its cross-section small. The extension of the technique to lower energies has been pioneered by Fort and Leroy [5], using the $^{3}H(p,n)$ reaction. These efforts should continue, because they will allow interesting cross checks with recoil proton counters.

3.2. Monoenergetic sources

The ^{124}Sb-Be source appears very attractive from Table III. It should be stressed, however, that precision measurements are hampered by the neutron energy spread, mainly resulting from moderation in the beryllium shell, leaving in a typical case only an estimated 72% of the neutrons in the 23-25 keV interval [15]. Also the high γ-activity may give rise to difficulties. No experience in the use of other sources (such as ^{24}Na-Be and ^{228}Ra-^{2}H) at other neutron energies for precision purposes has been reported up to now.

3.3. Induced activity

Counting the activity induced in a neutron-producing target also has some drawbacks. All neutrons produced have to be used in the experiment, otherwise the angular distribution of the neutrons has also to be known, which in turn depends upon a precise knowledge of the efficiency of the detector. The kinematic collimation of the neutrons may require excellent energy stability of the charged particle beam. On the other hand the counting of, for example, Be could be improved, by improving the accuracy of the branching ratio and of the γ-efficiency of the counter, which would allow a flux determination to better than 1%. This applies also to the $^{51}V(p,n)^{51}Cr$ reaction, which, however, suffers from a low yield.

4. STANDARD CROSS-SECTIONS

In the following paragraphs the situation on standard cross-sections will be discussed with reference to Table III.

TABLE III. ACCURACIES ATTAINED AT PRESENT

Method or cross-section	Energy range				
	Thermal	1-100 keV	100-500 keV	500 keV-10 MeV	10-15 MeV
Associated particle					
$^{3}H(d,n)$	-	-	-	-	1% at 14 MeV
$^{3}H(p,n)$	-	-	3% [5]	-	-
$^{2}H(\gamma,n)$	-	-	0.3% [4]	0.3%	-
Monoenergetic source					
^{124}Sb-Be	-	1% at 24 keV [6,7]	-	-	-
Induced activity					
$^{7}Li(p,n)^{7}Be$	-	2.5% at 30 keV [10]	-	-	-
$^{51}V(p,n)^{51}Cr$	-	2% [11,12]	2% [11,12]	-	-
Cross-section					
$^{1}H(n,n)$	-	1%	1%	0.5-1%	1%
$^{3}He(n,p)$	0.2% [24]	10%	>10%	-	-
$^{6}Li(n,\alpha)$	3%	15% up to 30 keV 10% betw. 30-100 keV	-	-	-
$^{10}B(n,\alpha)$	0.15% [68]	5%	-	-	-
$^{10}B(n,\alpha_0)^{10}B(n,\alpha)$	0.1% [63]	5%	-	-	-

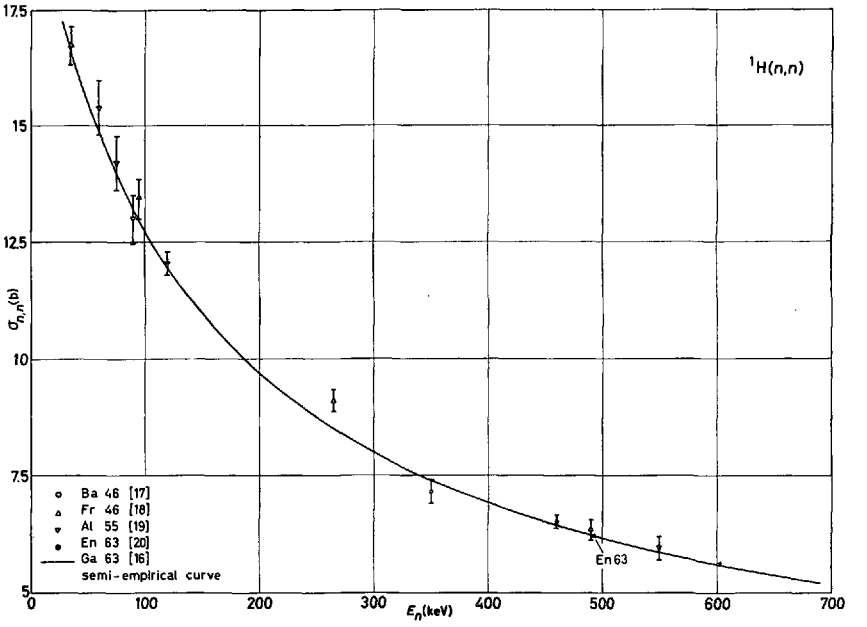

FIG.1. ^{1}H(n, n) cross-section from 10 to 700 keV

TABLE IV. HYDROGEN TOTAL SCATTERING CROSS-SECTIONS

Reference	Energy (MeV)	Measured $\sigma_{n,n}$ (b)	Calculated $\sigma_{n,n}$ Gammel [16] (b)	Discrep. (%)
Engelke [20]	0.4926	6.202 ± 0.18%	6.209	-0.11
Engelke [20]	3.205	2.206 ± 0.31%	2.187	+0.86
Lebowitz [21]	3.204	2.212 ± 0.17%	2.187	+1.13
Lebowitz [21]	5.858	1.465 ± 0.16%	1.446	+1.3

4.1. ^{1}H(n, n)^{1}H

Precise hydrogen recoil proportional counting is impossible below 20 keV, so no attempt was made to list accuracies below 1 keV.

Gammel [16] used an analytical form based on effective range theory to interpolate between values, quoted to about 0.5% up to 4.7 MeV and to about 1% at 14 MeV. He estimates that interpolated values have the same accuracy as the measured points, and states that the region below 1 MeV, however, is more in doubt. As a matter of fact, from a purely experimental point of view, the situation is not so satisfactory. Up to

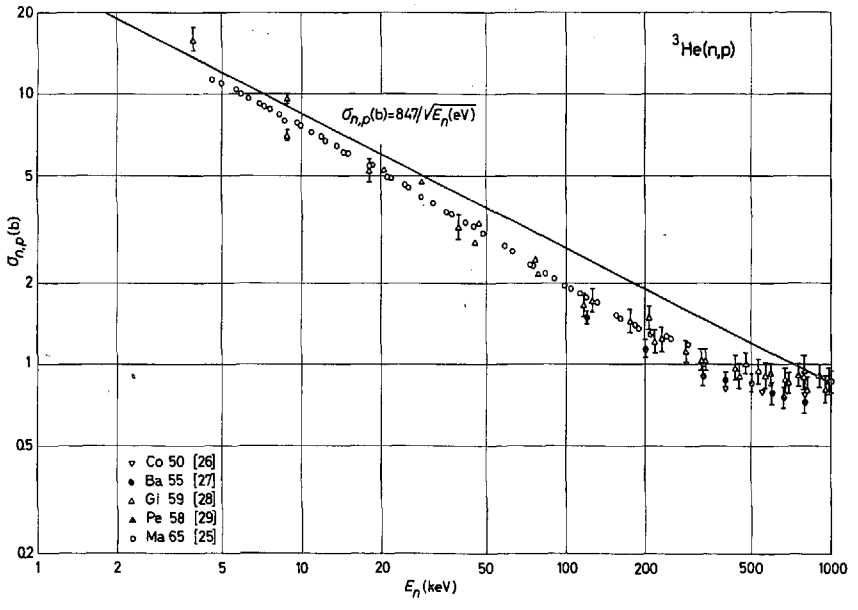

FIG. 2. ^{3}He(n, p) cross-section from 4 to 1000 keV

400 keV, only older measurements are available [17-19] and techniques certainly have been improved considerably since. Between 100 and 400 keV the situation is particularly unsatisfactory (see Fig. 1).

Only one of recently measured high precision values in the energy region of interest to reactors lies precisely on the Gammel curve; the others [20, 21] show discrepancies of about 1%, as can be seen from Table IV. Furthermore, the results of Engelke et al. [20] do not seem fully consistent with recent theoretical considerations [22].

Gammel's interpolation provides total cross-sections probably accurate within 0.5 to 1% between 500 keV and 10 MeV and within 1% above this energy. Below 500 keV the situation is more uncertain. There are, however, precise measurements underway at Harwell, with fast time-of-flight techniques to cover systematically the energy range between 200 keV and 10 MeV instead of just checking a few spots [23]. The extension of such a continuous series of measurements to lower energies could result also in an improvement of the accuracy below 200 keV.

4.2. ^{3}He(n, p)^{3}H

The 2200-m/s value of the ^{3}He(n, p) cross-section is precisely known: (5327 ± 10)b; the 1/v behaviour of this cross-section has been verified up to 11 eV [24].

Recently Macklin and Gibbons [25] have precisely remeasured the total cross-section for the ^{3}H(p, n)^{3}He reaction. They converted their results to ^{3}He(n, p)^{3}H by detailed balance, normalizing to 1980 mb at 100 keV. They conclude that the cross-section departs from 1/v behaviour above 10 keV and perhaps as low as a few keV and that previous discrepancies with direct ^{3}He(n, p) measurements above 100 eV remain (see Fig. 2, where also the older data [26-29] are shown). They point

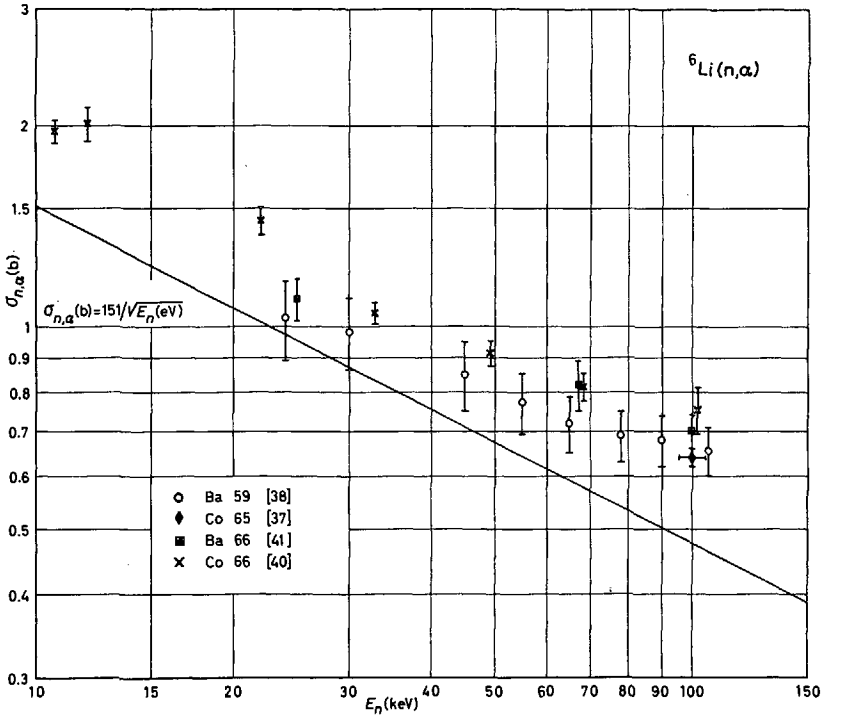

FIG. 3. ^{6}Li(n, α) cross-section from 10 to 100 keV

out that errors in the absolute cross-section normalization could be due to traces of tritium in the target backings. They do not provide information about errors. Judging from the spread of values around 100 keV the normalization point may be 10% in error.

4.3. ^{6}Li(n, α)^{3}H

Most measurements of the thermal cross-section are lifetime or oscillator measurements, relative to boron, performed on natural lithium, without mentioning its isotopic composition. In this respect it should be stressed that geological variations exist up to several percent [30, 31] and variations of the isotopic ratio measurement itself are a well-known phenomenon. For these and other reasons only 1-2% accuracy can be attained in an absolute mass spectrometric determination. No stock of standard lithium exists. Only one transmission measurement [32] has been performed on LiF powder. There is considerable disagreement between the coherent scattering length for ^{6}Li as measured by Peterson and Smith [33], (a_{coh} = + 1.8 fm), and the value (a_{coh} = + 7 fm) as calculated from Shull and Wollan's results [34].

All those reasons force us to put a quite large error on the presently adopted 2200-m/s value of 70.7 b for natural lithium and consequently on the ^{6}Li(n, α) cross-section, as listed in Table III. Because of the interest of Li as a standard (e.g. for measurements with nuclear explosions [35]) the thermal value should be remeasured to a higher precision for different enrichments, by transmission, and also relative to

boron. At CBNM Euratom, work is in progress for accurate chemical and isotopic definition of samples, needed for such measurements.

All recent results above thermal are represented in Fig. 3, with the exception of Schwarz et al. [36]. Schwarz normalized his data to a thermal value of 945 b, assuming a 1/v behaviour below 20 keV. A curve, resulting from a Breit-Wigner single-level fit to the 258-keV resonance has been added to it. Although at 100 keV Schwarz's value is in excellent agreement with the absolute spot point of Condé et al. [37], the data were not included in our graph, because the assumption of a 1/v-behaviour below 20 keV appears too uncertain in the light of other recent absolute measurements. Another reason is that the experiment is based on the assumption that the $^{7}Li(p,n)^{7}Be$ cross-section is isotropic in the centre-of-mass system at proton energies close to the neutron threshold, for which there is no direct proof available up to now.

All new data pertain to the 10-100 keV interval (Fig. 3) and have been obtained in an independent way. Barry [38] measured relatively to White's [39] recent ^{235}U fission cross-sections, which in turn are based on the hydrogen scattering cross-section. Cox [40] applied the absolute method of spherical shell transmission. Condé [37] used a large scintillator tank, calibrated at 100 keV by neutrons scattered from lead (the transmission of the lead samples being measured in the same experiment).

It is striking that all data are well above the 1/v extrapolation from thermal. Even below 35 keV the five results are on average 25% higher. The excellent agreement between Cox's and Barry's values at 100 and 67 keV gives strong support to their data at lower energies, indicating that the cross-section deviates from 1/v even at 10 keV. In this respect, it has to be stressed that in the lower region Cox should have obtained his most reliable data, because the absorption is relatively larger than the scattering and so the important scattering correction is less serious.

Condé's result at 100 keV, although quoted with ± 3% accuracy, is 14% smaller than Cox's value. On the other hand, renormalization of some data of Bame and Cubitt [41] to White's [39] fission cross-sections gives data which are systematically lower, but not inconsistent with the Barry and Cox data.

Summarizing, it can be stated that $^{6}Li(n,\alpha)$ seems to depart from the 1/v behaviour already at 1 keV, and that a fit through recent and renormalized data would be uncertain to at least ± 15% between 1 and 30 keV and to ± 10% between 30 and 100 keV. New measurements are needed.

Above 100 keV, the new results of Fort et al. [5] are plotted in Fig. 4 together with older data [36-38, 40-48]. Fort's method is based on associated particle counting, using the $^{3}H(p,n)$ reaction, the first known application of this absolute method in this energy region. The new data are strikingly higher than older results.

4.4. $^{10}B(n,\alpha)^{7}Li$, $^{7}Li^{*}$

CBNM has just finished a painstaking study of the errors involved in precise isotopic composition measurements of boron. In consequence the Prosdocimi and De Ruytter [49, 50] result has been slightly changed, the actual mean value now being (3836 ± 7)b [51]. Together with the results of Safford et al. [52] and Als-Nielsen et al. [24], this value has now to be considered as the most accurate one, because the main un-

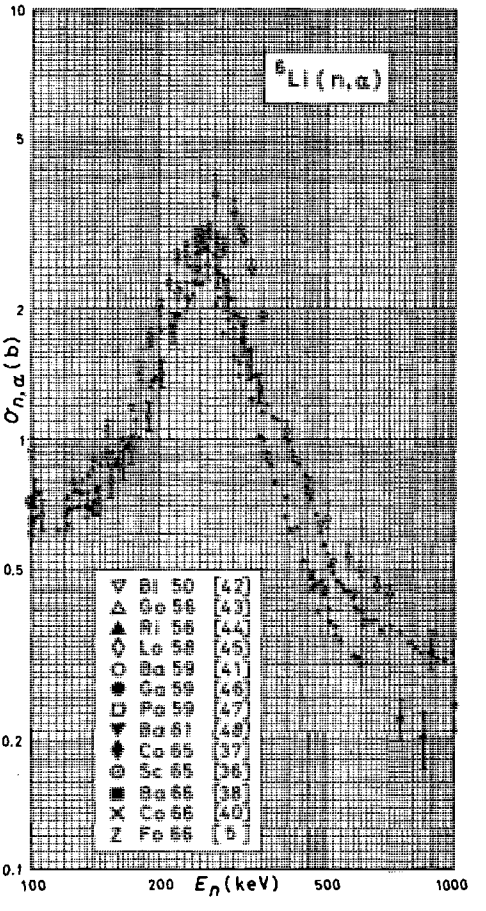

FIG.4. ^{6}Li(n, α) cross-section from 100-1000 keV

certainty in this kind of high precision measurement is due to sample definition. They are in agreement with Meadows and Whalen [53] and Schmitt et al. [54], although the samples used by these authors are less well known. By weighing the results of Ref.[24], [51] and [52], a best value of (3835 ± 10)b is obtained, the error quoted being equal to two standard deviations.

In Fig. 5 five series of measurements above 1 keV are plotted.

Bichsel and Bonner [55] used a long counter for flux measurement and normalized at 20 keV to $\sigma_{n,\alpha}$ extrapolated from a thermal value of 4010 b. Data in the graph are renormalized to $\sigma_{n,\alpha}$ = 3835 b. As with those of Bilpuch et al. [56], they are based on an assumed constant efficiency of a long counter, whilst Davis et al. [57] applied long counter efficiency corrections using the data of Haddad et al. [58].

The very recent results of Cox [40] are of special interest because they are obtained by spherical shell transmission and are the only direct absolute measurements available.

Mooring et al. [59] measured the total and the ratio of scattering to total cross-section and derived the absorption cross-section from them.

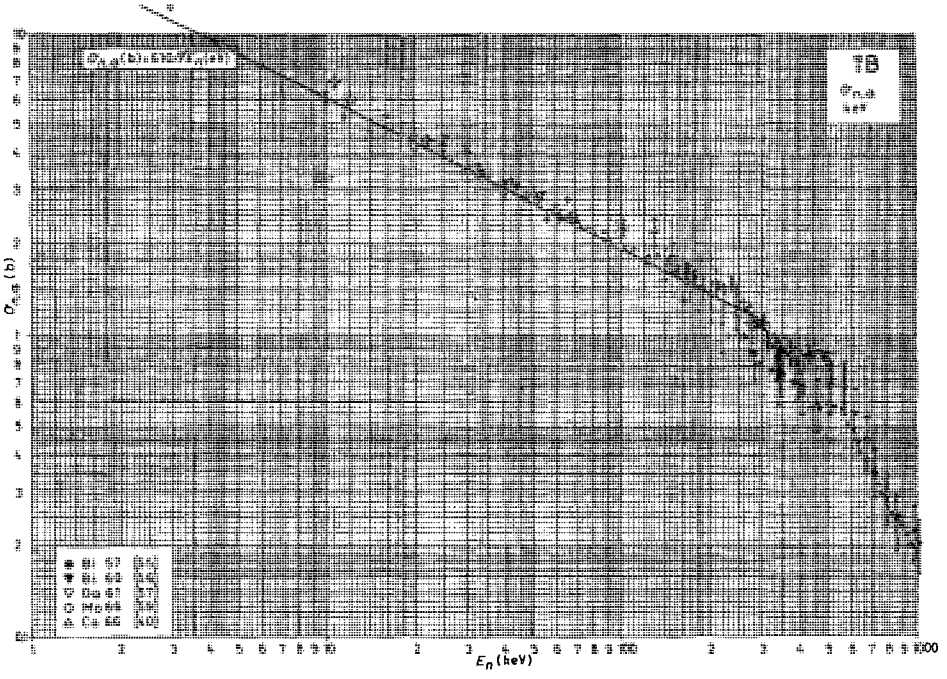

FIG.5. $^{10}B(n, \alpha)$ cross-section from 3 to 1000 keV

They conclude from a discussion of their own measurements and other relevant data that the absorption and (n, α) cross-sections are very nearly equal between 10 and 500 keV. This point is very important. In fact, in addition to the (n, α), the (n, γ), (n, t) and (n, p)-reactions are all energetically possible. The (n, γ) cross-section is presumably negligible above 10 keV [40]. The (n, p) cross-section has been measured to be $\approx$ 3 mb for fission spectrum neutrons [60] and to be smaller than 0.2 b for thermal neutrons. Davis et al. [57] found the (n, t) cross-section to be $\approx$ 5 mb for 1.3-MeV neutrons. Mooring et al. [59] looked for the (n, t) reaction in the 100-keV region but the cross-section was too small for the reaction to be observed. There is therefore evidence that the (n, α) and absorption cross-sections are very nearly equal, certainly below 100 keV.

A 1/v fit through the data from Fig. 4 between 1 and 100 keV gives the result $\sigma_{n,\alpha} = 649/\sqrt{E_n}$ compared to $610/\sqrt{E_n}$, corresponding to the thermal value. The spread of the data is such that a 1/v behaviour within $\pm$ 5% may be assumed. It should be noted, however, that Bogart [61] has recalculated the Bichsel et al. [55] results, based on a long counter efficiency curve derived from $\sigma_{n,\gamma}(Au)$ relative to $\sigma_{n,\alpha}(^{10}B)$ [62]. In this indirect way he finds a significant departure from 1/v variation above $\approx$ 80 keV due to a resonance at 140 keV.

The branching ratio $\sigma_{n,\alpha_0}/\sigma_{n,\alpha}$ has been included in Table III, since in many boron applications detection is via the 478-keV γ-ray which accompanies the (n, α) reaction. The thermal value has been measured very recently at CBNM to a high precision: 0.06308 ± 0.00006 [63]. New data from Sowerby [64], Macklin and Gibbons [65] and Mooring et al. [59] are plotted in Fig. 6 together with previous measurements

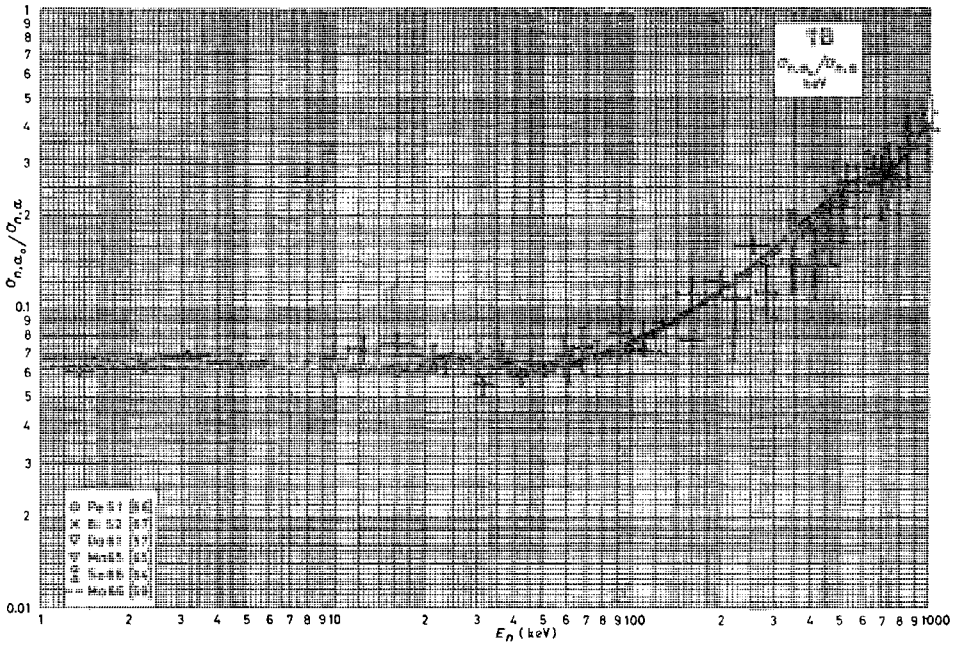

FIG.6. $^{10}B(n,\alpha)$ branching ratio from 1 to 1000 keV

[57, 66, 67]. The ratio remains constant up to about 50 keV where it starts rising. Below 100 keV it is known to 5%.

A detailed analysis by Gubernator of all available data on $^{10}B(n,\alpha)$ and on the branching ratio will appear shortly [68] as an issue of the CBNM-series on compilations of standard cross-sections. Figure 6 contains also the extrapolated thermal value (up to about 50 keV), together with a smooth curve above 50 keV taken from Ref. [68].

5. CHOICE OF PRIMARY FLUX STANDARD DATA

Comparing Tables II and III it becomes clear that the highest accuracy requested is at the moment only met in the thermal region up to 1 keV by a standard based on the $^{10}B(n,\alpha)$ or $^{3}He(n,p)$ cross-sections. After some improvement also the hydrogen scattering cross-section will meet the requirements up to 10 MeV, around which energy the uncertainties created by the error on the anisotropy start to become serious. Luckily the associated particle method allows an independent cross check at those higher energies. The present status of the art for detecting low energy proton recoils makes, however, the application of this cross-section very difficult below 100 keV and impossible below 20 keV.

The main problem lies therefore in the important 1-100 keV region and although it has received a lot of attention in recent years [69] we are still quite far from the needed accuracies.

Monoenergetic neutron sources and induced activity counting offer perhaps opportunities for improvement, but they should only be used to determine the best suited of the reaction cross-sections on ^{3}He, ^{6}Li and

TABLE V. PROPERTIES OF POSSIBLE PRIMARY STANDARDS IN THE 1-100 keV REGION

	$^{3}He(n,p)^{3}H$	$^{6}Li(n,\alpha)^{3}H$	$^{10}B(n,\alpha)^{7}Li, ^{7}Li^{*}$
Cross-section			
Magnitude	≈ equal to $^{10}B(n,\alpha)$	≈ 4 times smaller	≈ equal to $^{3}He(n,p)$
Behaviour	not 1/v	not 1/v	1/v within present error of measurement
Present uncertainty	10%	15% up to 30 keV; 10% between 30-100 keV	5%
Energy of emitted particles	p: ≈ 0.6 MeV; ^{3}H: ≈ 0.2 MeV	α: ≈ 2 MeV; ^{3}H: ≈ 2.8 MeV	α: ≈ 1.8 and ≈ 1.5 MeV
Samples			
Gas	Easy chemical and isotopic analysis. Large uncertainty in flight path. Expensive.	-	-
Foils	-	LiF: Isotopic analysis not yet precise, especially for low concentrations [49]	Very stable and homogeneous ^{10}B-foils. Isotopic, chemical analysis and weighing, allowing 0.3% on 1 mg foil [51, 76-78]. Once a few of such primary foils are assayed, they can be used to calibrate other foils quickly and accurately in a thermal beam (such a service being available at CBNM)

TABLE V (cont.)

Loaded glass scintillators	-	Precise chemical and isotopic analysis extremely difficult.	Precise chemical and isotopic analysis extremely difficult.
Slabs	-	-	Very convenient by detection of γ-ray from $^{10}B(n,\alpha)Li^*$
Fast detectors			
100 g/cm^2 foil + surface barrier detector			
Timing resolution	-	< 5 ns	< 5 ns
Pulse height resolution	-	2% (for solid angle 1/10)	3% (for solid angle 1/10)
Efficiency at 100 keV	-	$\approx 10^{-5}$	$\approx 10^{-4}$
Remarks	-	Very low γ-sensitivity	Very low γ-sensitivity
Loaded glass scintillators (1 cm thick)		5 wt.% ^{6}Li	15 wt.% ^{10}B
Detection time uncertainty	-	3 ns	7 ns

TABLE V (cont.)

	$^{3}He(n,p)^{3}H$	$^{6}Li(n,\alpha)^{3}H$	$^{10}B(n,\alpha)^{7}Li, ^{7}Li^{*}$
Pulse height resolution (at thermal energy)	-	10%	30%
Efficiency at 100 keV	-	$6 \cdot 10^{-3}$	$4 \cdot 10^{-2}$
Remarks	-	Very γ-sensitive (unless thinner than 1.5 mm) but pulse shape discrimination possible. Correction for multiple scattering. Calibration necessary in known thermal flux or by pile oscillator	Very γ-sensitive. Correction for multiple scattering. Calibration necessary in known thermal flux or by pile oscillator.

^{10}B to a higher accuracy, if feasible. These methods are in fact too involved and limited in application; the apparatus is also too cumbersome for general use. Consequently, in this energy region too a cross-section should become the primary standard. Let us, in this respect, first consider the specifications for standards, based on cross-sections.

5.1. Requirements for primary neutron flux standards

A good primary flux standard should respond to the following specifications: The cross-section should be accurately known, smooth and as large as possible, over a broad energy interval. The (n, p) and (n, α) reactions should have a large positive Q-value.

Corresponding standard samples, used for detection, should be relatively easy to prepare and to assay accurately for chemical and isotopic composition, quantity, uniformity and homogeneity. They should remain unaltered under normal conditions of use. Substances used for sample preparation should be easy to obtain in a chemically pure form and suitable for precise mass spectrometric analysis.

A detector of reasonable size should be available, which, if combined with a precise sample, is capable of fast response ($\leq$ 10 ns), has good efficiency and low γ-sensitivity (or good γ-discrimination properties). The fast response is needed in time-of-flight measurements or with Van de Graaffs for eliminating background by time-of-flight selection.

5.2. Recommended primary standard data

Based on the preceding information and requirements, the choice of a primary standard is not difficult above 100 keV and below 1 keV.

Above 100 keV the $^{1}H(n, n)$ cross-section has no equal. Telescope and semiconductor proportional counting can be based on values obtained by Gammel's semi-empirical interpolation, (equation 30 from Ref. [16]), the accuracy of which has been discussed above.

Careful proportional counting of proton recoils allows flux measurements accurate to 2% between 100 keV and 2.5 MeV (White [39, 70]. Semiconductor recoil counting (Dearnaley and Whitehead [71], White [39]) is possible to 3% at 2.2 MeV and to 4% at 5.5 MeV, whilst with the telescope counter flux can be measured to 3% at 4 MeV and to 4% at 14 MeV [3, 72], the uncertainty on the anisotropy of the scattering cross-section of hydrogen becoming dominant above 10 MeV.

The hydrogen content of polythene or similar samples, used as radiators in telescope or semi-conductor counting, is a source of uncertainty. The precision of the chemical analysis should be improved below the present 1% [73].

At the other end of the energy scale the thermal cross-sections of $^{3}He(n, p)$ and $^{10}B(n, \alpha)$ are known to the same high accuracy. Up to 1 keV the $^{10}B(n, \alpha)$ cross-section is strictly $\sim 1/v$, but the same is not yet clearly established for $^{3}He(n, p)$ and $^{6}Li(n, \alpha)$. Boron with its high (n, α) cross-section is therefore an obvious choice as primary standard up to 1 keV. This choice is also supported by the following discussion of the 1-100 keV region. We base it on Table V, which lists advantages and drawbacks of the three possible standards in the 1-100 keV region.

^{3}He cannot be considered as a primary standard because of its low Q-value and the non-availability of a suitable fast detector, allowing

time-of-flight selection. The choice between ^{6}Li and ^{10}B is not so clear cut. ^{6}Li-loaded scintillator glasses offer somewhat better timing, pulse-height resolution [74] and pulse-shape discrimination against γ-rays [75], besides being commercially available. Their efficiency at 100 keV is, however, lower than the efficiency of boron glass scintillators [74] of the same thickness. Moreover, calibration difficulties and multiple scattering corrections remain serious drawbacks of scintillator glasses.

Further, we should not forget that the real need for high accuracy standards in this energy interval stems from fission data requests. Measurements of fission cross-sections have to be performed with foils of fissile isotopes, resulting in a low counting rate and often low signal-to-background ratio. In this respect boron standard foils would behave very similarly, the cross-section being of the same order as the fission cross-sections of the fissile isotopes. However, as can be seen from Table V, boron foils combined with solid state detectors have distinct advantages over LiF foils.

In addition, the boron cross-section is much better known in the energy region of interest and there is a good chance that it will prove to remain 1/v also when measured to a higher accuracy than the present 5%. Moreover, a direct test to check very accurately the 1/v behaviour up to 100 keV is only practicable for $^{10}B(n,\alpha)$. Finally, the γ-ray associated with the $^{10}B(n,\alpha)Li^{*}$ reaction widens considerably the application possibilities of this standard.

To conclude, it is proposed to adopt as primary neutron flux standards $^{10}B(n,\alpha)$ up to 100 keV and $^{1}H(n,n)$ above 100 keV. In consequence, efforts to improve the accuracy of the $^{10}B(n,\alpha)$ cross-section in the 1-100 keV region should be continued. Of course, $^{3}He(n,p)$ may find an interesting application as a secondary flux standard in the thermal region and $^{6}Li(n,\alpha)$ may offer better experimental conditions in some cases (e.g. as a standard for time-of-flight measurements with underground explosions). However, once the 1/v behaviour of $^{10}B(n,\alpha)$ is well established, it will be relatively easy to obtain the $^{6}Li(n,\alpha)$ cross-section by ratio measurements. Advantage could then be taken of the ^{6}Li-loaded scintillator glasses, in cases where their application is better suited.

6. SECONDARY STANDARD CROSS-SECTIONS

As just pointed out, the use of a secondary standard, well established against a primary one, is often more practical for a given kind of measurement. A detailed discussion of such working standards, however, is outside the scope of this article. We shall therefore limit ourselves to particular areas with some indication as to where useful information can be found.

We would like to stress, however, that in our opinion direct measurement of such secondary standard data seems only possible in special cases and within limited energy intervals. Such direct measurements may be very valuable as absolute spot values. However, complete curves over broad energy intervals will be difficult to provide in this way, because these reactions do not show a 1/v behaviour. To complete the secondary standard data, relative measurements, not based on the

recommended primary standard data, will tend to increase the confusion which already reigns in this field, because of the multiplication of "primary reference" data, whose origin and accuracy cannot always be checked with the necessary precision. In this way there exists a real danger of ending up in a vicious circle.

6.1. Flux calibration

Besides the already discussed $^{3}He(n,p)$ and $^{6}Li(n,\alpha)$ cross-sections, the ^{235}U and ^{239}Pu fission cross-sections find wide-spread applications at thermal energies and between 10 keV and 3 MeV. In this respect, attention is drawn to the recent work of Perkin et al. [15], White et al. [39, 79] and Gilboy and Knoll [80]. The thermal activation cross-section of gold and cobalt are also convenient secondary standards.

Although no longer satisfying the requirements for a primary standard above 100 keV (departure from 1/v, unknown contribution of (n,t) reaction, insufficiently known variation of branching ratio) ^{10}B-slabs are used also in this energy region, e.g. for flux measurements with linacs. Study of both $^{10}B(n,\alpha)$ cross-section and branching ratio above 100 keV is therefore recommended.

6.2. Calibration of scattering measurements

The carbon (up to 2 MeV) and lead (up to 10 keV) total cross-sections are practically equal to the scattering cross-sections and are used as standards in scattering measurements.

6.3. Calibration of radiative capture measurements

The $Au(n,\gamma)$ and $In(n,\gamma)$ reactions are often used. Recent contributions are found in Refs. [10, 61, 62, 81-84].

6.4. Calibration of activation measurements on threshold reactions

The (n,p), (n,α), (n,2n) and (n,n') threshold reactions are widely applied for in-pile neutron spectra and integrated flux measurements. The cross-section curve is often measured against a working standard such as $^{32}S(n,p)$ or $^{27}Al(n,\alpha)$. Also used are $^{63}Cu(n,2n)$, $^{65}Cu(n,2n)$ and $^{56}Fe(n,p)$. In other cases flux measurement has been based on $^{238}U(n,f)$.

Best curves for $^{32}S(n,p)$ and $^{27}Al(n,\alpha)$ have been drawn at CBNM by Liskien and Paulsen [3]. They have also made available best curves for $^{24}Mg(n,p)$, $^{31}P(n,p)$, $^{56}Fe(n,p)$, $^{59}Co(n,\alpha)$, $^{58}Ni(n,p)$ and $^{63}Cu(n,2n)$. Detailed discussion of complete data (but no best curves) on 24 threshold reactions has been published by the same authors [85].

6.5. Calibration of $\bar{\nu}$-measurements

$\bar{\nu}$ from spontaneous fission of ^{252}Cf is widely accepted as the standard. At this conference, De Volpi and Porges [86] report a precise measurement of this quantity and Colvin et al. [87] report results obtained by the Harwell Boron Pile. Colvin et al. also discuss the ^{252}Cf $\bar{\nu}$-values obtained by other authors.

7. CONCLUSIONS

(1) The $^{10}B(n,\alpha)^{7}Li$, $^{7}Li^{*}$ (below 100 keV) and $^{1}H(n,n)$ (above 100 keV) cross-sections are proposed as primary standards for flux measurements. Corresponding reference data, as far as they can be recommended at the present stage, are mentioned above, but to satisfy present requests for neutron data, a big effort is needed to enhance the accuracy of the primary standard data in important energy intervals. In the first place, it is necessary to check the 1/v behaviour of $^{10}B(n,\alpha)$ between 1 and 100 keV to a higher accuracy than the present 5%. It is realized that this will be very difficult to achieve, although it would suffice to check one point at about 100 keV. Several independent ways should be tried: Improvement of the associated particle method applied to the $^{3}H(p,n)$ reaction (as e.g. suggested by Fort and Leroy [5]) and extension to lower neutron energies; more accurately known branching ratios of ^{7}Be and better determination of the γ-efficiency of the counter would considerably reduce the uncertainty which affects the induced activity method. As careful proportional recoil proton counting allows flux measurements accurate to 2% around 100 keV (White [39, 70]), this method should be applied to measure the cross-section ratio $^{10}B(n,\alpha)/^{1}H(n,n)$. Generally speaking, repetition of some difficult measurements by other laboratories is advisable, which applies certainly to the sphere transmission measurement on boron at and above 100 keV.

(2) Present techniques allow the improvement of the experimental data for the $^{1}H(n,n)$ total cross-section. The fast time-of-flight measurements, now underway at Harwell, between 200 keV and 10 MeV should be extended below 200 keV. In the MeV range better knowledge of the differential cross-section is needed in the first place. Of course, improvements in proton recoil counting (including assay of hydrogenous sample) should keep pace with increase of cross-section accuracy.

(3) The direct use of the two primary standards may prove less practical for certain applications. Once their cross-section versus energy is well established, they should therefore be compared to secondary standards. In this respect the following ratio measurements are particularly recommended:

$^{6}Li(n,\alpha)/^{10}B(n,\alpha)$ between 1 and 100 keV;
$^{10}B(n,\alpha)/^{1}H(n,n)$ above 100 keV, together with improvements of the $^{10}B(n,\alpha)$-branching ratio;
$^{235}U(n,f)/^{10}B(n,\alpha)$ between 10 and 100 keV;
$^{235}U(n,f)/^{1}H(n,n)$ between 100 keV and 10 MeV.

Moreover, for the purpose of calibration at thermal energies of samples (e.g. ^{6}Li-scintillator glasses) or complete detection devices, the 2200-m/s $^{6}Li(n,\alpha)$ cross-section should be measured to a higher accuracy.

(4) In high precision measurements, sample preparation and assay play an important part. It is felt that the reliability and compatibility of neutron data could be substantially improved if primary and secondary standard samples such as boron foils, boron solutions, fission foils, lithium and boron scintillator glasses were prepared and/or assayed

by standard laboratories, specialized in this field. A first step in this direction would be the exchange on a world-wide scale of standard samples to test the reliability of assaying techniques between interested laboratories. At a later stage complete neutron detection devices, such as long counters and telescope counters could be exchanged.

ACKNOWLEDGEMENTS

The author would like to express his thanks to many colleagues at CBNM for interesting discussions and especially to those who provided results before publication. Special thanks are due to Dr. K. Gubernator for graphs and comments from his compilation on boron and for invaluable help with the preparation of the manuscript. The author would like to thank also Dr. R. Batchelor for many fruitful discussions in the past and Mr. K. Bobin for correcting the English.

REFERENCES

[1] MARION, J.B., FOWLER, J.L. Eds., Fast Neutron Physics, Intersci. Pub., New York (1960).
[2] PHILLIPS, G.C., MARION, J.B., RISSER, J.R. Eds., Progress in Fast Neutron Physics, Chicago (1963).
[3] LISKIEN, H., PAULSEN, A., private communication (1966).
[4] COLVIN, D.W., SOWERBY, M.G., MacDONALD, R.I., paper CN-23/33, these Proceedings I.
[5] FORT, E., LEROY, J.L., paper CN-23/67, these Proceedings I.
[6] AXTON, E.J., CROSS, P., ROBERTSON, J.D., J. nucl. Energy, A/B 19 (1965) 409.
[7] NAGGIAR, V., private communication (1966).
[8] HANSON, A.O., McKIBBEN, J.L., Phys. Rev. 72 (1947) 673.
[9] MACKLIN, R.L., Nucl. Instrum. Meth. 1 (1957) 335.
[10] PÖNITZ, W., paper CN-23/6, these Proceedings I.
[11] HARRIS, K.K., GRENCH, H.A., JOHNSON, R.G., VAUGHN, F.J., Nucl. Instrum. Meth. 33 (1965) 257.
[12] GIBBONS, J.H., MACKLIN, R.L., Nucl. Instrum. Meth. 37 (1965) 330.
[13] BOGART, D., paper CN-23/83, these Proceedings I.
[14] BELANOVA, T.S., VANKOV, A.A., MIKHAILUS, F.F., STAVISSKY, Y.Y., paper CN-23/96, these Proceedings I.
[15] PERKIN, J.L., WHITE, P.H., FIELDHOUSE, P., AXTON, E.J., CROSS, P., ROBERTSON, J.C., J. nucl. Energy, A/B 19 (1965) 423.
[16] GAMMEL, J.L., in Fast Neutron Physics, Intersci. Pub., N.Y. Chapt. V.T. Part II (1960) 2185.
[17] BAILEY, C.L., BENNETT, W.E., BERGSTRAHLH, T., NUCKOLLS, R.G., RICHARDS, H.T., WILLIAMS, J.H., Phys. Rev. 70 (1946) 583.
[18] FRISCH, D.H., Phys. Rev. 70 (1946) 589.
[19] ALLEN, W.D., FERGUSON, A.T.G., Proc. phys. Soc. (Lond.) A68 (1955) 1077.
[20] ENGELKE, C.E., BENONSON, R.E., MELKONIAN, E., LEBOWITZ, J.M., Phys. Rev. 129 (1963) 324.
[21] LEBOWITZ, J., Rep. WASH-1048 (1964) 21.
[22] NOYES, H.P., Nucl. Phys. 74 (1965) 508.
[23] LANGSFORD, A., private communication (1966).
[24] ALS-NIELSEN, J., DIETRICH, O., Phys. Rev. 133 (1964) B 925.
[25] MACKLIN, R.L., GIBBONS, J.H., Proc. Int. Conf. Study of Nuclear Structure with Neutrons, Antwerp, 1965, EANDC-50-S, Vol.I, 13 (1965); ORNL-P-1375 (1965).
[26] COON, J.H., Phys. Rev. 80 (1950) 488.
[27] BATCHELOR, R., AVES, R., SKYRME, T.H.R., Rev. Sci. Instr. 26 (1955) 1037.
[28] GIBBONS, J.H., MACKLIN, R.L., Phys. Rev. 114 (1959) 571.
[29] PERRY, J.E., Jr., HADDAD, E., HENKEL, R.L., JARVIS, G.A., SMITH, R.J., unpublished (1958), reported by J.D. Seagrave, Proc. Conf. Nuclear Forces and the Few Nucleon Problem II, London (1960) 583.

[30] CAMERON, A.E., J. Am. chem. Soc. 77 (1955) 2731.
[31] ORDZHONIKIDZE, K., SHIUTTSE, V., Sov. Phys. JETP. 2 (1956) 396.
[32] HAVENS, W.W., Jr., RAINWATER, J., Phys. Rev. 70 (1946) 154.
[33] PETERSON, S.W., SMITH, H.G., J. phys. Soc. Japan 17 (Suppl. B II) (1962) 335.
[34] SHULL, C.G., WOLLAN, E.O., Phys. Rev. 81 (1951) 527.
[35] DIVEN, B., Conf. Neutron Cross Section Technology, Washington, 1966, Conf. 660303, Book 2 (1966) 1051.
[36] SCHWARZ, S., STRÖMBERG, L.G., BERSTRÖM, A., Nucl. Phys. 63 (1965) 593.
[37] CONDÉ, H., SCHWARZ, S., STARFELT, N., Ark. Fys. 29 (1965) 45.
[38] BARRY, J.F., Conf. Neutron Cross Section Technology, Washington, 1966, Conf. 660303, Book 2 (1966) 763.
[39] WHITE, P.H., J. nucl. Energy, A/B 19 (1965) 325.
[40] COX, S.A., Conf. Neutron Cross Section Technology, Washington, 1966, Conf. 660303, Book 2 (1966) 701; to be published in J. nucl. Energy.
[41] BAME, S.J., CUBITT, R.L., Phys. Rev. 114 (1959) 1580; data are renormalized to recent $\sigma_{n,f}(^{235}U)$ values given in BNL 325, 2nd ed., suppl. no.2 Vol.III (1964).
[42] BLAIR, J.M., HOLLAND, R.E., ANL-4515 (1950); data are re-evaluated by J.J. Devanany, 1955, cited in BNL-325, 2nd ed., suppl. no.2, Vol.I (1964).
[43] GORLOV, G.V., GOKHBERG, B.M., MOROZOV, V.M., OTROSHENKO, G.A., Sov. Phys. Doklady 1 (1956) 705.
[44] RIBE, F.L., Phys. Rev. 103 (1956) 741; data are corrected as suggested by MURRAY, R.B., SCHMITT, H.W., Phys. Rev. 115 (1959) 1707.
[45] LOS ALAMOS GROUP, unpublished, given in BNL 325, 2nd. ed. (1958).
[46] GABBARD, F., DAVIS, R.H., BONNER, T.W., Phys. Rev. 114 (1959) 201.
[47] PARDO, W.B., ROBERTS, J.H., Bull. Am. phys. Soc. 4 (1959) 218.
[48] BABCOCK, R.V., Rep. AFSWC TR 61-57 (1961).
[49] PROSDOCIMI, A., DERUYTTER, A.J., J. nucl. Energy, A/B 17 (1963) 83.
[50] DERUYTTER, A., DEBUS, G., LAUER, K., MORET, H., PROSDOCIMI, A., Rep. EUR 12.e (1962).
[51] DEBUS, G., De BIÈVRE, P., private communication (1966).
[52] SAFFORD, G.J., TAYLOR, T.I., RUSTAD, B.M., HAVENS, W.W.,Jr., Phys. Rev. 119 (1960) 1291.
[53] MEADOWS, J.W., WHALEN, J.F., Nucl. Sci. Engng 9 (1961) 132.
[54] SCHMITT, H.W., BLOCK, R.C., BAILY, R.L., Nucl. Phys. 17 (1960) 109; BLOCK, R., SLAUGHTER, G., PATTENDEN, N., HARVEY, J., Pile Neutron Research, IAEA, Vienna (1962) 535.
[55] BICHSEL, H., BONNER, T.W., Phys. Rev. 108 (1957) 1025.
[56] BILPUCH, E.G., WESTON, L.W., NEWSON, H.W., Ann. Phys. 10 (1960) 455.
[57] DAVIS, E.A., GABBARD, F., BONNER, T.W., BASS, R., Nucl. Phys. 27 (1961) 448.
[58] HADDAD, E., HENKEL, R.L., PERRY, J.E. Jr., SMITH, R.J., private communication (1958), cited by ALLEN, W.D., in Fast Neutron Physics, Interscl. Pub., N.Y. Part I (1960) 374.
[59] MOORING, F.P., MONAHAN, J.E., HUDDLESTON, C.M., Nucl. Phys. 82 (1966) 16.
[60] EGGLER, C., HUGHES, D.J., HUDDLESTON, C., Phys. Rev. 74 (1948) 1239.
[61] BOGART, D., Rep. NASA TR R-240 (1966).
[62] GIBBONS, J.H., MACKLIN, R.L., MILLER, P.D., NEILER, J.H., Phys. Rev. 122 (1961) 182.
[63] DERUYTTER, A., to be published (1966).
[64] SOWERBY, M.G., J. nucl. Energy, A/B 20 (1966) 135.
[65] MACKLIN, R.L., GIBBONS, J.H., Phys. Rev. 140 (1965) B324.
[66] PETREE, B., JOHNSON, C.H., MILLER, D.W., Phys. Rev. 83 (1951) 1148.
[67] BICHSEL, H., HÄLG, W., HUBER, P., STEBLER, A., Helv. Phys. Acta 25 (1952) 119.
[68] GUBERNATOR, K., to be published (1966).
[69] Symposium on the Absolute Determination of Neutron Flux in the Energy Range 1-100 keV, Oxford 1963, EANDC-33-U (1963).
[70] WHITE, P.H., in Symposium on the Absolute Determination of Neutron Flux in the Energy Range 1-100 keV, Oxford, EANDC-33-U (1963) 25.
[71] DEARNALEY, G., WHITEHEAD, A.B., Rep. AERE R-3662 (1961).
[72] BAME, S.J., Jr., HADDAD, E., PERRY, J.E., Jr., SMITH, R.K., Rev. Sci. Instrum. 28 (1957) 997.
[73] LAUER, K.F., private communication (1966).
[74] BOLLINGER, L.M., THOMAS, G.E., GINTHER, R.J., Nucl. Instrum. Meth. 17 (1962) 97.

[75] COCEVA, C., Nucl. Instrum. Meth. 21 (1963) 93.
[76] Van AUDENHOVE, J., ESCHBACH, H., MORET, H., Nucl. Instrum. Meth. 24 (1963) 465.
[77] ESCHBACH, H.L., Proc. Seminar on Preparation and Standardization of Isotopic Targets and Foils, Harwell 1965, Rep. AERE-R 5097 (1965) 37.
[78] MORET, H., LOUWERIX, E., Proc. 5th Inform. Conf. Vacuum Microbalance Techniques, Princeton 1965, in press (1966).
[79] WHITE, P.H., REICHELT, J.M.A., WARNER, G.P., paper CN-23/58, these Proceedings II.
[80] GILBOY, W.B., KNOLL, G.F., paper CN-23/7, these Proceedings I.
[81] BARRY, J.F., J. nucl. Energy, A/B 18 (1964) 491.
[82] HARRIS, K.K., GRENCH, H.A., JOHNSON, R.G., VAUGHN, F.J., FERZINGER, J.H., SHER, R., Nucl. Phys. 69 (1965) 37.
[83] GRENCH, H.A., COOP, K.L., MENLOVE, H.O., VAUGHN, F.J., submitted to Nucl. Phys. (1966).
[84] RYVES, T.B., ROBERTSON, J.C., AXTON, E.J., GOODIER, I., WILLIAMS, A., J. nucl. Energy, A/B 20 (1966) 249.
[85] LISKIEN, H., PAULSEN, A., Rep. EUR 119.e, Vol.1 and 2 (1966).
[86] De VOLPI, A., PORGES, K.G., paper CN-23/40, these Proceedings I.
[87] COLVIN, D.W., SOWERBY, M.G., McDONALD, R.I., paper CN-23/33, these Proceedings I.

DISCUSSION

W. PÖNITZ: You recommend certain reactions as primary standards with the other cross-sections as secondary standards. Now, the ^{10}B (n, α) reaction which you suggest has some very favourable features, but in the keV energy region the experiments which should give the highest accuracy are not suitable for the suggested reactions. I should also like to point out that the recent values of Cox differ by about 20% from other values at 100 and 200 keV. In the keV region capture and fission cross-sections are measured, so it would be good to have both a capture and a fission cross-section as standard.

J. SPAEPEN: I entirely agree that suitable secondary working standards are in many cases better adapted to particular measurements. However, these secondary standards have first to be measured against either a direct method of flux determination, say from the activity induced in a ^{7}Li target by proton bombardment, or a primary standard cross-section such as ^{10}B (n, α).

P. FIELDHOUSE: Table III of your paper gives a figure of 1% for the accuracy of 14-MeV flux determinations with the ^{3}H (α, n)^{4}He reaction. I should like to mention that, using an improved technique which has been developed at the Atomic Weapons Research Establishment, Aldermaston, an accuracy of about 0.6% can be attained. This work is shortly to be published in the Journal of Nuclear Energy.

D. BOGART: I should like to comment that there are very good reasons to believe that the Bichsel and Bonner values and the Davis et al. values for ^{10}B (n, α) cross-sections are low. We have attempted to correct the Bichsel and Bonner values for the efficiency of the unorthodox long counter that was used, and we find the ^{10}B (n, α) to be non-1/v above 80 keV, being $\sim$ 20% above 1/v at 100 keV. These corrected data are in agreement with the recent Cox sphere transmission values. With the Davis data, below 1 MeV, there are difficulties in separating spectra due to (n, α_0) and (n, α_1) groups because of large epithermal background contributions. Accuracy is poor as the incident neutron energy is lowered to several hundred keV.

J. SPAEPEN: If we can show with good accuracy, say by comparison with a proportional proton recoil counter, that the ^{10}B (n, α) is 1/v at 100 keV or slightly above, the problem is solved. It is then unlikely that a resonance exists below 100 keV. If, on the other hand, the shape had to be remeasured with high precision starting at 80 keV this would be a very difficult and tedious task.

R. BATCHELOR (Chairman): I would just like to make a plea for some new measurements on ^{6}Li (n, α) around 10 keV, since I think we have a definite discrepancy there.

M. G. SOWERBY: Paper CN-23/30 on fission cross-sections reports data on spectrum measurements that have been made with detectors based on the ^{6}Li (n, α) and ^{10}B (n, α) reactions. The energy dependence of the ^{6}Li (n, α) cross-section can be obtained from these measurements if it is assumed that the boron cross-section has a 1/v energy dependence. It is found that between 10 eV and 25 keV the energy dependence of the two cross-sections is the same within ± 5%.

S. SCHWARZ: I would like to make a comment on the question of the ^{6}Li(n, T)^{4}He cross-section. During the past year much new information has been received, including the renormalization of Bame and Cubitt to the new ^{235}U fission cross-section, our own corrections due to the discovery of an unexpected effect in the multiple scattering of neutrons in Li-glass, and the absolute measurements of Cox et al. and Leroy et al. Now, the points of Cox indicate a deviation from the 1/v law in the region above 10 keV (which might indicate a large constant term in the expansion), and the points of Leroy give a higher resonance peak than was assumed before. Our own results were only from a relative measurement normalized to a strict 1/v dependence to about 30 keV. As it appears, a renormalization of our points to those of Leroy would bring us into agreement with Cox in the low energy region, which is quite satisfactory. I would like to mention that a review of all this material is being issued as Newsletter No. 3 from the ENEA Neutron Data Compilation Centre.

J. SPAEPEN: After the renormalization, is there still agreement with Condé's absolute spot value at about 100 keV?

S. SCHWARZ: Unfortunately, this is not possible. The Condé point was based on a silicon analysis of the Li-glass and probably this analysis could not be made very accurately as it is a very difficult thing to do.

J. C. HOPKINS: I would like to point out one other area where standards are necessary. This is in the field of cross-section measurements for gamma-ray production in the MeV region. The 4.43-MeV gamma ray from ^{12}C (n, n') $^{12}C^{*}$ has been used, but the cross-section is not properly known.

D. BUTLER: Dr. Spaepen's paper indicated that the accuracy needed for the measurement of fission cross-sections below 40-keV neutron energy could be somewhat less than that required above 40 keV. The accuracy requirement is presumably determined on the basis of fast-reactor considerations. In the future it is very likely that some of the fast reactors built will have major fractions of their neutron spectra below this energy, for example reactors with some moderator like Be or those of very large volume. In either of these cases the fission cross-section below 40 keV is likely to be as important as that above 40 keV, and relaxing the requirement for the fission cross-section will therefore not be appropriate.

K. H. BECKURTS: I have a comment on the $^{6}Li\ (n, \alpha)^{3}H$ cross-section at thermal energy. This quantity was measured a few years ago by Meadows and Whalen at Argonne. They used the pulsed source lifetime method, which yields an absolute value directly without recourse to a standard. They obtained a result to better than 1% accuracy. Since this looked like a very reliable experiment, I would have considered this question as settled.

J. SPAEPEN: Meadows and Whalen did not measure the isotopic composition of the natural lithium used in their experiment. As I explained in my oral presentation, this introduces serious uncertainties.

J. J. SCHMIDT: In regard to what Dr. Butler has just said, I would like to stress the importance of exact fission cross-section knowledge, particularly below 40 keV, for criticality and safety considerations in the design of fast steam-cooled reactors.

MESURE DE LA SECTION EFFICACE DE LA REACTION $^{6}Li(n, \alpha)T$ PAR LA METHODE DE LA PARTICULE ASSOCIEE

E. FORT ET J.L. LEROY
CEA, CENTRE D'ETUDES NUCLEAIRES DE CADARACHE,
FRANCE

Abstract — Résumé

MEASUREMENT OF THE $^{6}Li(n,\alpha)T$ REACTION CROSS-SECTION BY THE ASSOCIATED PARTICLE METHOD. The neutrons are produced by the $T(p,n)^{3}He$ reaction, as obtained in the Van de Graaff accelerator at the Centre d'études nucléaires, Cadarache.

The ^{3}He particles associated with neutrons are detected in a direction making an angle of 10° with the incident proton beam. This detection is made possible by using a tritium-titanium target on a thin backing of copper, and a spectrometer selecting particles according to their charge. Under beam bombardment, the target emits protons of various energies by elastic and inelastic scattering on copper and titanium, together with recoil tritons and ^{3}He particles. These latter are selected by the spectrometer, which is mainly composed of an electrostatic analyser and a silicium solid-state detector. In a second run of measurements, a magnetic separator was added to the device to eliminate completely parasitic protons.

Neutrons associated with detected $^{3}_{2}He$ particles pass through a ^{6}Li-loaded glass scintillator. The ^{6}Li content was determined by a measurement of thermal neutron absorption, using the pile oscillator method.

The detector efficiency is equal to the ratio of the number of coincidences between neutrons and ^{3}He particles to the total number of detected ^{3}He particles.

The coulomb scattering of ^{3}He particles in the target induce a dispersion in energy and direction of associated neutrons. A Monte Carlo calculation has been made to correct for coincidences lost by this effect and for multiple scattering of neutrons in the scintillator.

The resulting cross-section is 3.00 ± 0.1 b at 255-keV neutron energy. Measurements have been carried out in the range between 150 and 280 keV. Further improvements to the method are proposed.

MESURE DE LA SECTION EFFICACE DE LA REACTION $^{6}Li(n,\alpha)T$ PAR LA METHODE DE LA PARTICULE ASSOCIEE. Les neutrons sont produits par le Van de Graaff au moyen de la réaction $T(p,n)^{3}He$.

Les particules ^{3}He associées aux neutrons sont détectées dans une direction formant un angle de 10° avec le faisceau de protons incident. Cette détection est possible grâce à l'utilisation d'une cible de titane-tritium sur support mince de cuivre, et à un spectromètre sélectionnant les particules selon leur charge. La cible émet, lors du bombardement par le faisceau, des protons de toutes énergies, par diffusion élastique ou inélastique sur le cuivre et le titane, des tritons de recul et des particules ^{3}He. Ces dernières sont sélectionnées par le spectromètre qui comprend essentiellement un analyseur électrostatique et un détecteur solide au silicium. Dans une deuxième série de mesures, le dispositif a été complété par un analyseur magnétique. La combinaison des deux champs permet d'éliminer de façon quasi totale les protons parasites.

Les neutrons associés aux $^{3}_{2}He$ détectés traversent un scintillateur de verre chargé au lithium. Le nombre d'atomes de ^{6}Li contenu a été déterminé par une mesure d'absorption réalisée par une oscillation de pile.

L'efficacité du détecteur est égale au rapport du nombre de coïncidences entre neutrons et ^{3}He au nombre total de ^{3}He détectés.

Une partie des coïncidences est perdue à cause de la dispersion angulaire des neutrons provoquée par la diffusion coulombienne des particules chargées dans la cible. Cet effet et celui de la diffusion multiple des neutrons dans le scintillateur ont été calculés par une méthode de Monte-Carlo.

La section efficace trouvée est de 3,00 ± 0,1 b à 255 keV. Les mesures ont été effectuées entre 150 keV et 280 keV. Des perfectionnements à la méthode sont proposés.

1. INTRODUCTION

La réaction $^{6}Li(n,\alpha)T$ est d'un usage commode dans les détecteurs destinés à la mesure absolue des flux de neutrons dont l'énergie est comprise entre quelques keV et quelques centaines de keV, et cet usage a été recommandé au cours du Symposium sur la détermination absolue des flux de neutrons dans le domaine d'énergie de 1 à 100 keV (Oxford, 1963). Des désaccords existent entre les mesures de la section efficace de cette réaction selon différents auteurs [1-4].

L'objet du présent travail est de refaire la mesure de cette grandeur en utilisant une méthode entièrement différente et aussi directe que possible.

2. PRINCIPE DE LA METHODE

Les neutrons sont produits au moyen de la réaction $^{3}_{1}T(p,n)^{3}_{2}He$. Les particules $^{3}_{2}He$ associées aux neutrons sont détectées dans une direction formant un angle de 10° avec le faisceau de protons incident. Cette détection est possible grâce à l'utilisation d'une cible de tritium absorbé dans du titane sur support de cuivre assez mince pour être traversée par le faisceau de protons, et grâce à une combinaison d'analyseurs électrostatique et magnétique qui séparent les particules $^{3}_{2}He$ du flot de protons et de tritons qui les accompagne.

Le compteur à neutrons est un scintillateur de verre chargé au ^{6}Li; il est placé de façon à être traversé par tous les neutrons associés aux particules $^{3}_{2}He$ détectées par l'analyseur. L'efficacité du détecteur à neutrons est égale au rapport du nombre de coïncidences entre les impulsions de neutrons et de $^{3}_{2}He$ au nombre total de particules $^{3}_{2}He$ détectées.

Le calcul de la section efficace de la réaction $^{6}Li(n,\alpha)T$ est fait à partir de l'efficacité mesurée et du nombre d'atomes de ^{6}Li contenus dans le scintillateur, en tenant compte des diffusions de neutrons dans le scintillateur et de divers autres facteurs correctifs.

3. DESCRIPTION DU DISPOSITIF ET DE LA METHODE DE MESURE

Pour pouvoir utiliser cette méthode avec des neutrons d'énergie aussi faible que possible, il faut placer le compteur à neutrons vers l'arrière, et, dans ce cas, les particules $^{3}_{2}He$ doivent être détectées vers l'avant. En outre, elles ont une énergie plus élevée, ce qui facilite la détection.

Par contre, la diffusion coulombienne des protons du faisceau par la cible, à l'angle de 10°, est de plusieurs ordres de grandeur supérieure au taux de la réaction qui nous intéresse. De surcroît, le cuivre et le titane qui supportent le tritium dans la cible donnent lieu à des diffusions inélastiques sur de très nombreux niveaux, ce qui conduit à un spectre pratiquement continu de protons. Enfin, des tritons peuvent être projetés dans la direction de notre compteur. Nous avons pu vérifier que le taux de réaction (p,α) sur le cuivre et le titane n'était pas gênant dans cette expérience.

Il est absolument essentiel, pour la validité de la mesure, que toutes ces particules parasites ne soient pas confondues avec les $^3_2$He. Pour les éliminer, nous avons construit un analyseur comprenant un déflecteur électrostatique, un diaphragme et un détecteur solide au silicium (fig. 1). La géométrie du déflecteur a été choisie de façon à éviter le plus possible

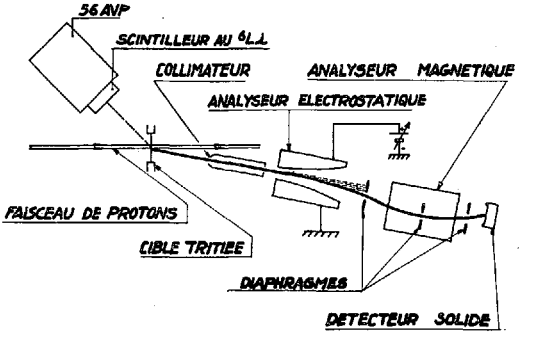

FIG.1. Dispositif expérimental

que les particules provenant de la cible ne puissent être diffusées vers le détecteur par les électrodes. La déviation d'une particule de charge Z et d'énergie E est

$$d = K\frac{Z}{E}V$$

où K est une constante qui dépend uniquement de la géométrie et V est la tension appliquée entre les électrodes du déflecteur.

Avec les dimensions choisies, les particules qui passent le diaphragme ont une énergie définie à 25% près, de sorte que les particules de charge 2 donnent sur le détecteur des impulsions approximativement doubles de celles données par les particules de charge 1. Un discriminateur d'amplitude permet d'éliminer les petites impulsions correspondant aux protons; celles qui dépassent le seuil sont d'une part enregistrées sur une échelle A et d'autre part envoyées dans un convertisseur temps amplitude, dont l'autre voie reçoit les impulsions provenant du compteur à neutrons. Les coïncidences se produisent dans un intervalle de temps égal à 10 ns et sont enregistrées sur un échelle B. Les coïncidences fortuites sont tout à fait négligeables. L'efficacité du détecteur de neutrons est égale au rapport des nombres contenus dans les échelles B et A.

Malgré les précautions prises dans le dimensionnement de l'analyseur électrostatique, la diffusion sur les parois donne, sur le détecteur de particules chargées, des impulsions qu'il n'est pas possible d'éliminer au moyen du seuil, surtout dans les cas où l'énergie des neutrons associés est faible. Pour évaluer cette contribution, on remplace la cible tritiée par une cible comportant les mêmes épaisseurs de cuivre et de titane. La correction ainsi déterminée varie de 10 à 20% du nombre des particules $^3_2$He.

Pour réduire cet effet parasite, on a ajouté un séparateur magnétique après l'analyseur électrostatique, de façon à séparer plus complètement les $^3_2$He et les protons parasites. De cette façon, le taux de comptage obtenu avec la cible non tritiée n'est plus que de 2 à 3% du comptage dû à la cible tritiée. Les mesures effectuées avec les deux dispositifs sont d'ailleurs en accord à mieux que 1% près.

Le compteur à neutrons comporte un verre scintillant, chargé avec 7,5% en poids de ^{6}Li (NE 905). Son diamètre est de 44,4 mm et son épaisseur de 9,5 mm; le taux de comptage des coïncidences est, selon les énergies, de 0,1 à 1 coup/s.

4. CORRECTIONS APPLIQUEES AUX RESULTATS BRUTS ET CALCUL DE LA SECTION EFFICACE DE LA REACTION ^{6}Li(n, α)T

En plus de la correction apportée au nombre de particules ^{3}He, pour tenir compte de la contamination par des particules de charge 1, on a tenu compte de la diffusion des neutrons par les parois de la boîte à cible (1 mm d'aluminium). Cet effet introduit une perte de coïncidences qui varie de 1,5 à 3,5% selon l'énergie des neutrons.

Par ailleurs, la diffusion coulombienne des particules ^{3}He à l'intérieur de la couche tritiée dévie légèrement ces particules, si bien que celles qui sont comptées dans une direction faisant 10° avec la direction du faisceau incident sont émises en réalité dans une direction légèrement différente. Les neutrons associés subissent donc de ce fait une certaine dispersion en direction et en énergie. Il s'ensuit que certains d'entre eux ne traversent pas le détecteur, ce qui correspond à une diminution d'efficacité. L'influence de cet effet a été calculé avec la collaboration de J.L. Huet, par une méthode de Monte-Carlo à partir des hypothèses suivantes:

La probabilité élémentaire de diffusion d'une particule de charge z et d'énergie E par un noyau de charge Z dans un angle solide $2\pi \sin\theta \, d\theta$ est donnée par la formule de Rutherford

$$\phi(\theta)d\theta = \frac{e^4 z^2 Z^2}{16\, E \sin^4(\theta/2)} \, 2\pi \sin\theta \, d\theta$$

A cause de l'effet d'écran des électrons, la déviation éventuelle d'une particule lourde ne peut être, selon Molière [5], inférieure à

$$\theta_{min} = \left(\frac{\lambda\!\!\!^{-}}{0,885a}\right)(1,13 + 3,76\,\alpha^2)^{1/2}$$

avec $\lambda\!\!\!^{-} = \frac{\hbar}{Mv}$ $\qquad \alpha = \frac{z\,Z\,e^2}{\hbar v}$ $\qquad a = \frac{\hbar^2}{e^2 m} Z^{-1/3}$

et M = masse de la particule ^{3}He, m = masse de l'électron, v = vitesse de la particule.

Dans ces conditions, la section efficace de diffusion est donnée par la formule

$$\sigma \simeq \frac{6,5\, z^2\, Z^2}{E^2} \frac{1}{\theta_{min}^2} 10^{-26} \text{ cm}^2 \quad (E \text{ en MeV})$$

La distribution des atomes de tritium dans la couche tritiée, qui doit s'annuler aux extrémités du dépôt de titane, est prise en forme de

demi-sinusoïde (fig. 2). La diffusion des protons avant la réaction est négligée, car la section efficace est beaucoup plus petite que celle relative aux ^{3}He. A partir de ces hypothèses, le calcul de Monte-Carlo se fait en tirant successivement au hasard, selon les lois de probabilité indiquées précédemment, la position de l'atome de tritium donnant lieu

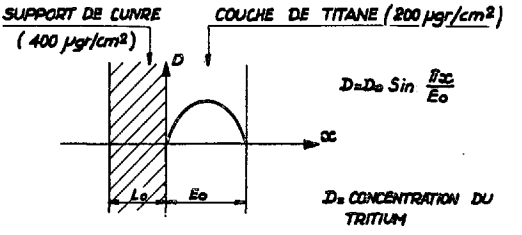

FIG.2. Distribution supposée des atomes de tritium dans la cible

à la réaction, les chocs coulombiens successifs, les angles de déviation correspondants. La combinaison de ces angles donne la déviation de la particule à sa sortie de la cible. En supposant qu'elle part en direction de l'analyseur, on peut calculer l'angle que formait sa direction avec celle du proton incident juste après la réaction qui la produit. L'application des lois de conservation régissant la réaction permet de trouver l'angle d'émission et l'énergie du neutron associé, et finalement de voir si ce neutron traverse le scintillateur à étalonner. On peut, en répétant les opérations pour un nombre suffisamment grand de particules, tracer le spectre d'énergie des neutrons traversant le scintillateur, ainsi que la proportion des neutrons qui ne le traversent pas. Les résultats de

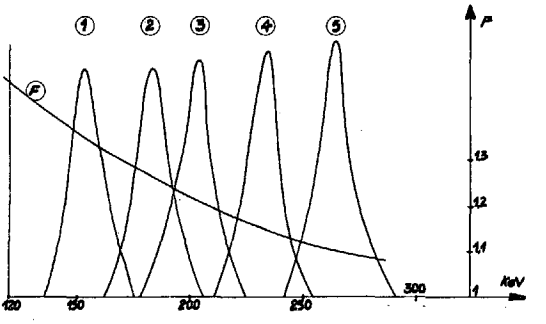

FIG.3. ①②③④⑤ Spectres d'énergie des neutrons détectés; Ⓕ Facteur correctif lié à la diffusion coulombienne

ces calculs sont donnés à la figure 3. Pour vérifier la validité de ce calcul nous avons mesuré la variation de la probabilité de coïncidence en fonction de la position angulaire du compteur à neutrons, en utilisant un scintillateur de plus petit diamètre (25,4 mm) pour lequel l'effet est beaucoup plus fort. La figure 4 représente le résultat de cette expérience ainsi que celui du calcul des mêmes cas fait par la méthode exposée plus haut.

La section efficace de la réaction est donnée par

$$\sigma = \frac{\epsilon S}{Nf}$$

ϵ = efficacité mesurée,
S = surface du scintillateur,
N = nombre total d'atomes de ^{6}Li contenu dans le scintillateur,
f = facteur correctif tenant compte des diffusions multiples dans le scintillateur.

Le facteur f a été calculé par une méthode de Monte-Carlo, par Bluet [6]; il est de l'ordre 1,1.

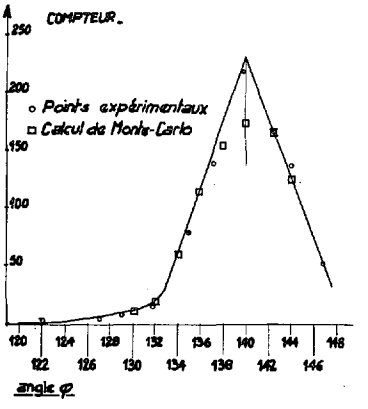

FIG. 4. Variation du taux de coïncidence en fonction de la position angulaire du compteur (θ = 20°)

La détermination du nombre N d'atomes de ^{6}Li a été faite en mesurant l'absorption des neutrons thermiques par un scintillateur au ^{6}Li, par la méthode d'oscillation de pile. Cette mesure a été faite par Carré et Vidal [7] qui ont utilisé la pile ZOE de Fontenay-aux-Roses. La section efficace d'absorption du ^{6}Li a été prise égale à 936 b. Cette valeur est obtenue en divisant la section efficace d'absorption thermique, 70,4 b, trouvée par Meadows and Whalen [8], par la concentration isotopique du ^{6}Li (7,52%). Le scintillateur qui a servi à notre mesure de coïncidence étant trop absorbant pour se prêter à une mesure correcte d'oscillation, on a utilisé dans cette dernière un scintillateur NE 901 de 1 mm d'épaisseur, contenant 2,5% de lithium naturel. Les sensibilités des deux scintillateurs, donc leurs nombres d'atomes de ^{6}Li, ont été comparées dans un flux de neutrons de 250 keV fourni par le Van de Graaff.

5. DISCUSSION DES CAUSES D'ERREURS (tableau I)

La mesure d'efficacité du scintillateur peut être affectée par les causes suivantes:

a) L'erreur statistique est, selon les points, de 1 à 3%;

b) Malgré les précautions prises, une partie des impulsions fournies par le détecteur solide pourrait être due à des particules autres que $^3_2$He; cependant, en procédant comme il a été expliqué précédemment, l'erreur devrait être inférieure à 1%.

c) En ce qui concerne la diffusion coulombienne des particules ^{3}He dans la couche tritiée, l'accord trouvé entre le calcul et la mesure de la dispersion angulaire des neutrons associés aux ^{3}He détectés (fig. 4) permet de penser que l'erreur liée à cet effet ne dépasse pas 2%.

TABLEAU I. RECAPITULATION DES CAUSES D'ERREUR

Erreur statistique	1% à 3%
Erreur sur l'identification des ^3He	1%
Incertitude sur la correction liée à la diffusion coulombienne	2%
Incertitude sur la diffusion multiple	0,5%
Incertitude sur le nombre d'atomes de ^6Li	2,5%
Erreur sur la section efficace	3,5 à 4,5%

En plus des erreurs énumérées ci-dessus, d'autres erreurs s'introduisent dans le calcul de la section efficace à partir de l'efficacité du détecteur; ce sont:

a) L'incertitude sur la correction de diffusion multiple dans le scintillateur, qui peut être évaluée à 0,5%.

b) L'incertitude sur le nombre d'atomes de ^6Li contenus. La détermination de ce nombre fait malheureusement intervenir beaucoup de constantes parmi lesquelles la composition isotopique du lithium utilisé par Meadows et Whalen [8]. L'incertitude sur ce nombre d'atomes est de 2,5%.

6. RESULTATS

Nos résultats sont représentés par la figure 5, sur laquelle on a également reporté les résultats des mesures antérieures de Gabbard et al. [2], de Bame et al. [1] et de Schwarz et al. [4]. Nos mesures sont en assez bon accord avec celles de Bame et Gabbard, mais diffèrent sensiblement de celles de Schwarz.

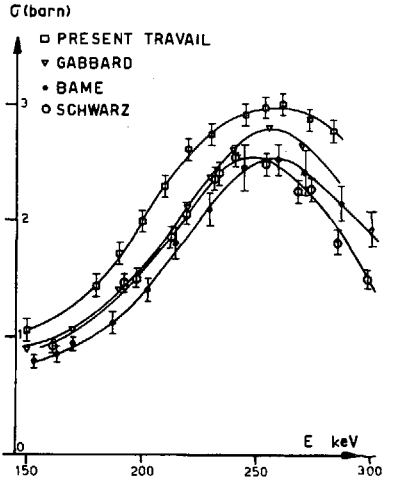

FIG.5. Courbe de la section efficace

Nous n'avons pas effectué de mesures à des énergies inférieures à 150 keV, car la diffusion des particules $^{3}_{2}He$ dans la couche tritiée introduit alors une correction trop forte. D'ailleurs, le taux de comptage des particules ^{3}He diminue rapidement lorsque l'énergie initiale diminue en dessous de 500 keV, car la probabilité de capture d'un électron par les noyaux de ^{3}He devient forte [9]. Le comportement d'un ion $^{3}_{2}He^{+}$ dans l'analyseur est le même que celui d'un triton et il ne peut atteindre le détecteur. Le domaine de mesure a été limité vers les grandes énergies à 280 keV, pour des raisons triviales d'agencement mécanique. Rien ne s'oppose à ce que la méthode soit utilisée jusqu'à 1 MeV environ, et, en détectant les particules $^{3}_{2}He$ à un angle plus élevé, jusqu'à 2 MeV environ.

7. CONCLUSION

Nous considérons ce travail comme la preuve de l'utilité de la méthode de la particule associée dans ce domaine d'énergie où les mesures absolues sont difficiles, et nous comptons poursuivre l'utilisation de cette méthode, en essayant d'étendre son champ d'application.

Pour cela il serait utile de diminuer la diffusion des particules ^{3}He dans la couche tritiée. Un gain appréciable serait certainement obtenu dans ce domaine si le titane qui absorbe le tritium pouvait être remplacé par un élément plus léger, le lithium par exemple.

Par ailleurs, il faudrait perfectionner la méthode de mesure du nombre d'atomes de ^{6}Li dans le scintillateur. Un progrès substantiel serait fait dans cette voie si l'on pouvait disposer, pour la mesure d'oscillation de pile, d'un étalon dont le nombre d'atomes de ^{6}Li soit connu avec précision.

REMERCIEMENTS

Les auteurs sont heureux de remercier M. J.P. Marquette de sa collaboration efficace, et le Bureau central des mesures nucléaires (GEEL) qui a mis au point et fabriqué des cibles tritiées sur support mince, grâce auxquelles cette expérience a pu être menée à bien.

REFERENCES

[1] BAME, S.J., Jr., CUBITT, R.L., Phys. Rev. 114 (1959) 1580-83.
[2] GABBARD, F., DAVIS, R.H., BONNER, T.W., Phys. Rev. 114 (1959) 201-08.
[3] GORLOV, G.V., GOCHBERG, B.M., MOROZOV, V.M., OTROSHCHENKO, C.A., Dokl. Akad. Nauk. SSSR 111 (1956) 791.
[4] SCHWARZ, S., STRÖMBERG, L.G., BERGSTRÖM, A., Nucl. Phys. 63 (1965) 593-609.
[5] MOLIERE, G., Z. Naturforsch. 3a (1948) 78.
[6] BLUET, J.C., Rapport CEA R 2971.
[7] CARRE, J.C., Communication privée (1964).
[8] MEADOWS, J.W., WHALEN, J.F., Nucl. Sci. Engng 9 (1961) 132-36.
[9] SNITZER, E., Phys. Rev. 89 (1953) 1237.

DISCUSSION

P. FIELDHOUSE: Do you take account of multiple proton scattering in the titanium-tritide target?

J. L. LEROY: Since the scattering cross-section is proportional to the square of the particle charge and inversely proportional to the square of the energy, the proton scattering is negligible in relation to that of the ^{3}He particles.

J. SPAEPEN: Regarding determination of the number of ^{6}Li atoms in a sample, I should like to point out that the isotopic analysis of natural lithium cannot yet be satisfactorily carried out, so that an error of 1-2% may exist for the absolute values. This error is much smaller in the case of enriched lithium. A programme is underway at the Bureau central de mesures nucléaires (Central Bureau for Nuclear Measurements), at Geel, to try to improve this situation.

AN ABSOLUTE (n, γ) CROSS-SECTION MEASUREMENT FOR GOLD AT 30 keV AND ITS APPLICATION IN THE NORMALIZATION OF OTHER DATA

W.P. PÖNITZ
KERNFORSCHUNGSZENTRUM KARLSRUHE,
FEDERAL REPUBLIC OF GERMANY

Abstract

AN ABSOLUTE (n,γ) CROSS-SECTION MEASUREMENT FOR GOLD AT 30 keV AND ITS APPLICATION IN THE NORMALIZATION OF OTHER DATA. The absolute (n,γ) cross-section of ^{197}Au at 30 keV was determined by the activation method. Kinematically collimated neutrons near the threshold of the reaction ^{7}Li(p,n)^{7}Be were used as the neutron source. The neutron source strength was measured with the ^{7}Be-activity as intensity reference. This activity was calibrated with the aid of the manganese bath technique. The γ-activities of the nuclei ^{7}Be, ^{56}Mn and ^{198}Au were measured relatively by a 4 in. × 3-in. NaI(Tl) detector. The calibration of this detector for the ^{56}Mn and the ^{198}Au activities was carried out with samples of known absolute disintegration rates which were previously determined by the 4πβ-γ-coincidence method. Several corrections needed for the calculation of the radiative capture cross-section were applied.

An attempt was made to get a "best" value of the (n,γ) cross-section of ^{197}Au at 30 keV from the published results of a number of experiments. This value which confirms our experimental result was used to renormalize experimental data in the energy range 1 - 1000 keV, published by other authors. The (n,γ) cross-sections of several other materials were renormalized with the aid of this curve and $\sigma^{X}_{n,\gamma}/\sigma^{Au}_{n,\gamma}$ ratios calculated from $\sigma_{n,\gamma}$ values given by other authors.

1. INTRODUCTION

Due to the considerable importance of the neutron capture cross-sections in the keV-energy region a large number of experiments were performed in the past by a variety of techniques. All available data of the (n, γ) cross-section of gold, which is of interest as a standard cross-section, are shown in Fig. 1. As one can see, there is a considerable disagreement between the results of the different groups in both the absolute values and the shapes of the cross-sections. In this paper we deal mainly with the (n, γ) cross-section of gold and describe a measurement at 30-keV neutron energy.

In Table I a review of the usable methods for capture cross-section measurements in the keV-energy region are given. In Fig. 1 we have included the abbreviations given in Table I. Three main principles exist for the measurements of (n, γ) cross-sections: firstly, the determination of the transmission of neutrons through the sample which allows us to ascertain the loss of neutrons due to absorption if we take into consideration the scattered neutrons. Secondly, the measurement of the reaction rate in the sample due to the (n, γ) process. Thirdly, the observation of the decay of a neutron field in a "sample" moderator. These main principles are subdivided into a large number of methods differing in the kind of determination of the transmission or the measurement of the reaction rate or the neutron flux.

An important feature of an (n, γ) experiment is whether it is performed absolutely or relatively. The first and last class of experiments mentioned above are on principle always absolute, whereas the second class is only absolute if the reaction rate and the neutron flux are determined absolutely. However, we shall consider such methods as approximately absolutely performed which need only the well-known (n, p) scattering cross-section (recoil proton measurements) or thermal absorption cross-sections (integral methods).

The second method mentioned above should be subdivided into a large number of methods which appear in the experiments. However, we have separated in Table I the different methods for the determination of the reaction rate and those for the neutron flux. Generally all possible combinations of these methods are usable in an experiment.

2. A MEASUREMENT OF $\sigma_{n,\gamma}^{Au}$ AT 30-keV NEUTRON ENERGY

The experiment was carried out in two parts (see Fig. 2):

(1) A gold foil (diameter 18 mm, thickness 0.3 mm) was irradiated using kinematically collimated neutrons at the threshold of the $^{7}Li(p, n)^{7}Be$ reaction. The time dependence of the neutron flux was monitored by a long counter. At the end of the irradiation time the γ-activities of the sample (^{198}Au; 411-keV transition of $^{198}*Hg$) and of the target (^{7}Be; 438-keV transition of $^{7}*Li$) were measured using a 4 in. × 3 in. NaI(Tl) detector. To get the absolute disintegration rate in the Au foil, a thin Au foil was activated with thermal neutrons and its absolute disintegration rate measured by the $4\pi\beta$-γ-coincidence apparatus. This foil was used to calibrate the γ-detector. The different γ-self-absorption in the thick and thin foil was calculated with the assumption of a homogeneous activation in the foil.

(2) A LiF target was placed at an end of a channel in the centre of a glass sphere which was filled with $MnSO_4$ solution. The target was bombarded with a proton beam. The neutrons slow down and are captured partly at thermal energy by the ^{55}Mn nuclei. After the irradiation the solution was stirred and the γ-activity of a well-defined quantity was measured using a NaI(Tl) detector. The arrangement used for this measurement was calibrated with a $MnSO_4$ solution of well-known activity which was previously determined by the $4\pi\beta$-γ-coincidence method. The ^{7}Be activity was measured in the same geometric arrangement as in the first experiment.

The relation between the various counts Z in the photopeaks of the transitions considered and the capture cross-section of gold is given by the following relations:

$$Z_{Au} = \epsilon_{Au} \cdot Q_n \cdot d_{Au} \cdot F_{Au} \cdot \sigma_{n,\gamma} \qquad \text{First part of the experiment} \qquad (1a)$$

$$Z_{Be} = \epsilon_{Be} \cdot Q_n \cdot F_{Be} \qquad (1b)$$

$$Z_{Mn} = \epsilon_{Mn} \cdot C_{Mn} \cdot F_{Mn} \qquad \text{Second part of the experiment} \qquad (2a)$$

$$Z_{Be} = \epsilon_{Be} \cdot Q'_n \cdot F_{Be} \qquad (2b)$$

$$F = \frac{1}{\lambda}(1 - e^{-\lambda T})\ (1 - e^{-\lambda\theta})\ e^{-\lambda t}$$

ϵ being the probabilities to get counts in the photopeaks if decays take place. Q_n is the neutron source strength. N is the number of atoms per cm^3 and d the thickness of the gold foil. λ is the decay constant, T is the irradiation time, θ is the counting time and t is the time between the end of the irradiation and the beginning of the counting. The activation of the manganese nuclei, C_{Mn}, being determined by the neutron source strength Q'_n and given in a previous work [36]. ϵ_{Au} and ϵ_{Mn} are known from $4\pi\beta$-γ-coincidence measurements [25, 36, 47]. Thus we know from the second part of the experiment the factor ϵ_{Be} and use it to determine $\sigma^{Au}_{n,\gamma}$ from the first part.

However, there are a few effects which must be taken into account: The scattering of neutrons in the target backing plate, the activation of the foil due to neutrons which are scattered in the foil, the resonance self protection and the influence of the divergence of the neutrons in the cone. All these problems are discussed in a previous work [36] and will not be repeated here. The result of the experiment is:

$$\sigma^{Au}_{n,\gamma}\ (30\ \text{keV}) = (0.598 \pm 0.012)\ \text{b}$$

The advantage of the procedure used in this experiment in contrast to a previously described experiment [36] is the use of a better geometric arrangement of the target and the manganese bath (this means a smaller loss of neutrons due to leakage at the edge of the manganese bath). Detailed values of the quantities defined in Eqs.(1) and (2) are given in Ref. [48].

3. "BEST" VALUES FOR THE CAPTURE CROSS-SECTION OF GOLD AT 30 keV

To get a normalization point for a capture cross-section curve, we consider the independent measured values for gold around 30 keV, given later than 1960. As "independent" we consider values which are not measured relative to other capture cross-sections. The omission of relative measured values is well-motivated: We would like to avoid taking into account one measurement twice, at first directly and then again indirectly in a relative measurement. Not so very clear is the cut at 1960. Our argument was that most measurements before were activation measurements and shell transmission measurements. For the shell transmission measurements, most authors have published newer results. The activation measurements depend on the absolute determination of the activities. The $4\pi\beta$-γ-coincidence method, suggested by Champion [49], came into use around 1959 and gave rise to the determination of absolute activities on a new level.

Table IIa contains a list of these independent cross-section values at 30 keV. If no measured values are available at 30 keV we have used a smooth curve through the measured values and determined the error by the scattering and the errors of the values in the neighbourhood of 30 keV. We have omitted the values of Isakov et al. [39] because a renormalization

was necessary and done by Konks et al. [27]. The original measured values of Moxon and Rae [21] we have averaged over an energy range of 5 keV.

Cross-section values measured relative to the fission cross-section of ^{235}U [18, 51] are included in our discussion; however, we have modified the original values by using the recent ^{235}U fission cross-section values of White [50], determined relative to the n, p scattering cross-section. The original results of experiments 1 to 14 (Table IIa) are shown in Fig. 3.

First, we have calculated the non-weighted and the weighted average values of all data given in Table IIa. We note these values as "A", because it was not taken into consideration that several measurements depend upon the same method or calibration procedure.

In a second step, we have grouped the experiments according to the method for determination of the neutron flux, and have obtained a non-weighted average for each group (Table IIb). The weighted average of the values Nos. 15-21 was noted as "B".

In a last step, we have selected some values: The research of Bogart and Semler [34] has shown recently that the Bethe method for the calculation of the transmission for a spherical shell is not applicable if the cross-sections (scattering and absorption) are not smooth. Therefore we omit the value of Belanova et al. [31] because in this work smooth cross-sections were assumed. Furthermore, we have omitted the value given by Cox [32]. This value makes use of the $^{10}B(n, \alpha)$ cross-section for high energies which is somewhat questionable. The values Nos. 22-27 are calculated, in contrast to those of Nos. 15-21, by weighting the single values. The value No. 25 was evaluated using the value No. 8 and the non-weighted average of Nos. 11 and 14, since these last two values are not independent. The value No. 2 was corrected for activation by scattered neutrons (60%).

To calculate the weighted average of the last group we have included an additional weight for the three cross-section values based on absolute activation measurements. The average of this group was noted as "C" and used as a normalization value. It is of interest that the several procedures to obtain an average value give almost identical results. We should remark that in the "C" average value the cross-section No. 23 has the highest weight.

4. THE SHAPE OF THE CAPTURE CROSS-SECTION OF GOLD IN THE ENERGY REGION 1 - 1000 keV

We have subdivided the existing measurements of the (n, γ) cross-section shape of ^{197}Au [1-36] in three groups: The first group contains all values measured below 30 keV and the third the values above 150 keV. The second group contains the experimental values between 30 and 150 keV. We have used smooth curves through the measured points and the values from these smooth curves at a number of energy points. All measured shapes within the first and the third groups are in fairly good agreement. Between 10- and 20-keV neutron energy the shape of the cross-section measured by Gibbons et al. [15] and by Kompe [59] are in disagreement with the other measurements; this can be explained by the unfavourable true-to-background count ratios in these experiments in this region.

We have normalized these curves at 30 and 150 keV and calculated the average normalized values at all other energies in the two groups. The absolute value at 30 keV is given in the previous section.

The shape of the cross-section in the second range and the absolute value at 150 keV are closely related. The shapes measured by Cox [32], Miskel et al. [18] and Harris et al. [30] are in good agreement between 30 and 150 keV, but if we normalize them at 30 keV, they give at 150 keV a value which is about 20% lower than that of Barry [28] and the values measured relative to $\sigma_{n,f}$ of ^{235}U [5, 11, 14, 18, 33]. The shape measured by Kompe [59] relative to the cross-section curve for the reaction $^{6}Li(n,\alpha)$ given by Schwarz et al. [60] connects the absolute values at 30 and 150 keV mentioned above; however, the shape is in strong disagreement with all other measured values between 30 and 64 keV.

The situation seems to be unclarified up to now. We have used the following assumptions and procedure for deriving a "best" cross-section curve: We assume that the values of Barry [28] and those measured relative to the ^{235}U fission cross-section are correct. For the cross-section between 30 and 150 keV we have used a middle line between the curve given by Kompe [59] (which depends on the data of Schwarz et al. [60]) and a curve which was constructed using the measured values up to 64 keV with a smooth connection between 64 keV and 150 keV. However, the curve is uncertain to ±10% in this range.

The calculated values of the capture cross-section of ^{197}Au and its errors are given in Table III and shown in Fig. 4. In Fig. 4 we have included also fitted cross-section curves given by Bogard [52], Gibbons [53] and Grench et al. [54].

5. RENORMALIZATION OF CAPTURE CROSS-SECTIONS OF SEVERAL ELEMENTS

We have calculated the ratios $\sigma^{X}_{n,\gamma}/\sigma^{Au}_{n,\gamma}$ at several energy points using smooth curves through the measured values of $\sigma^{X}_{n,\gamma}$ and $\sigma^{Au}_{n,\gamma}$ given in Refs [1-38, 55, 56, 57, 58]. All available ratios are averaged and multiplied by the values of $\sigma^{Au}_{n,\gamma}$ determined in the previous section. The results for smooth curves of the capture cross-sections of Mo, Rh, Ag, In, Sb, I, Ta and W are given in Table III. The errors are estimated by the scattering of the different cross-section ratios and by the errors of the gold cross-section. The results are shown in Fig. 5.

6. DISCUSSION

The problem of finding an absolute cross-section value in the keV-neutron-energy region usable for the normalization of cross-section curves seems to be - at least in the author's opinion - solved. However, there are disagreements in the shape of the (n,γ) cross-section of gold between 30 and 150 keV which cannot be explained up to now. Therefore it is not possible to give a standard cross-section in the energy range 1-1000 keV which is better than 7-12%.

The accuracies of the (n,γ) cross-sections of several other materials considered in this paper are not strongly affected by the uncertainty of

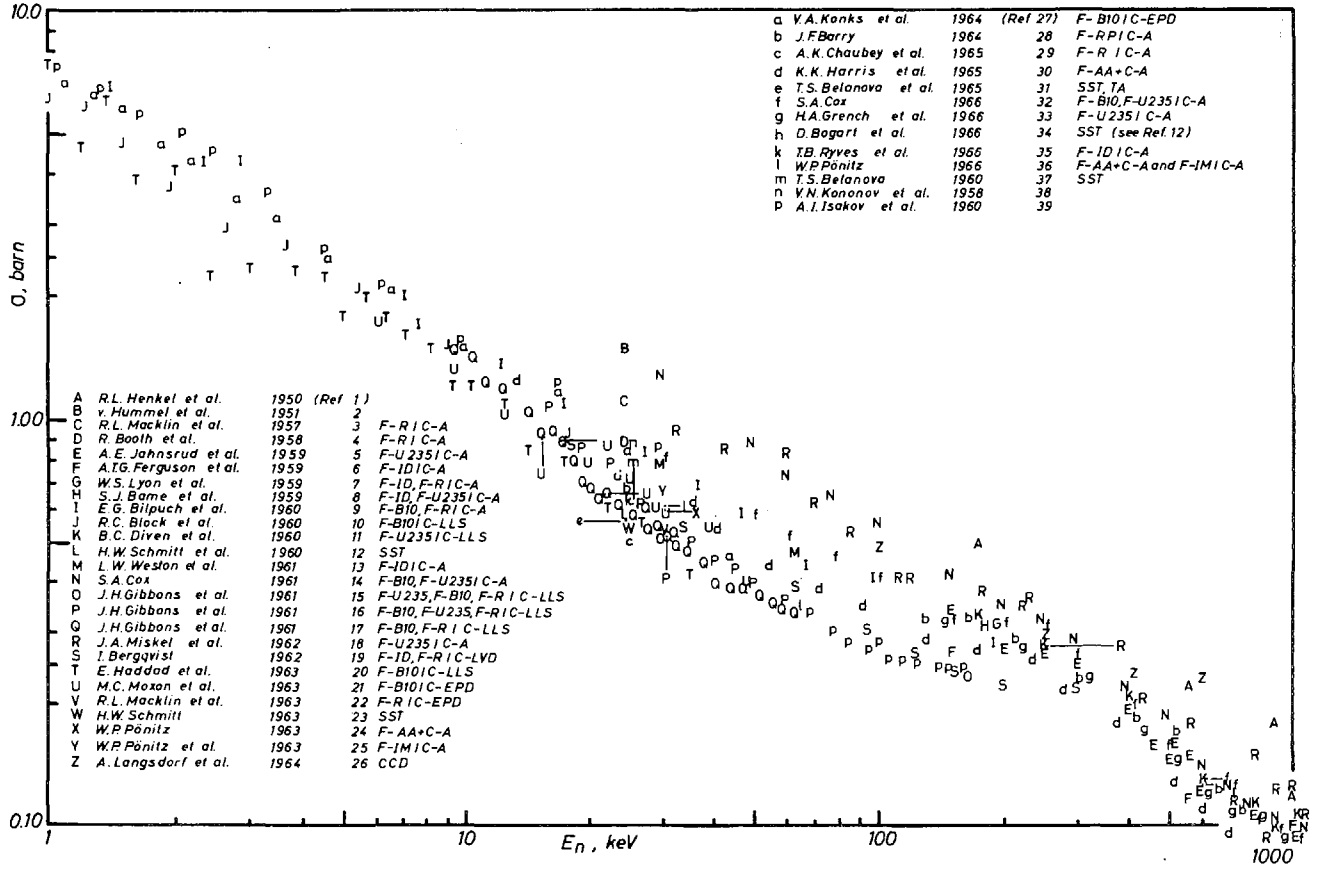

FIG. 1. The neutron-capture cross-section of gold. Comparison of existing data.

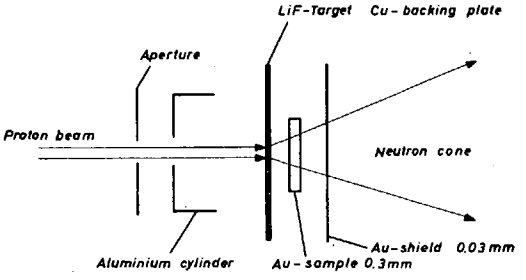

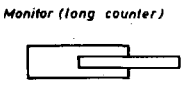

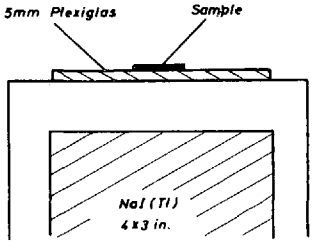

Irradiation arrangement

Detector arrangement

1.st Part of the experiment

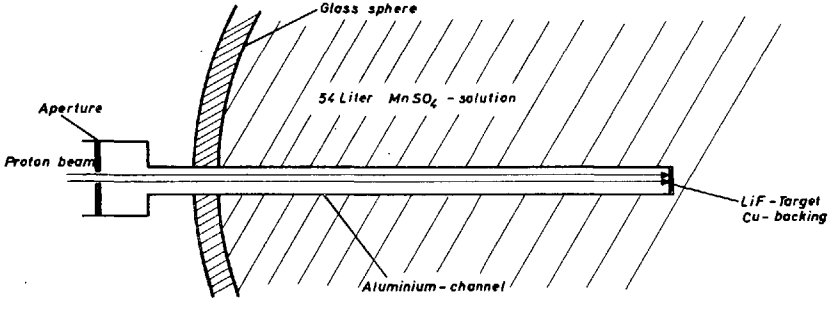

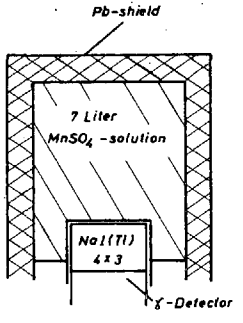

Irradiation arrangement

Detector arrangement

FIG 2. Experimental set-up of second part of the experiment

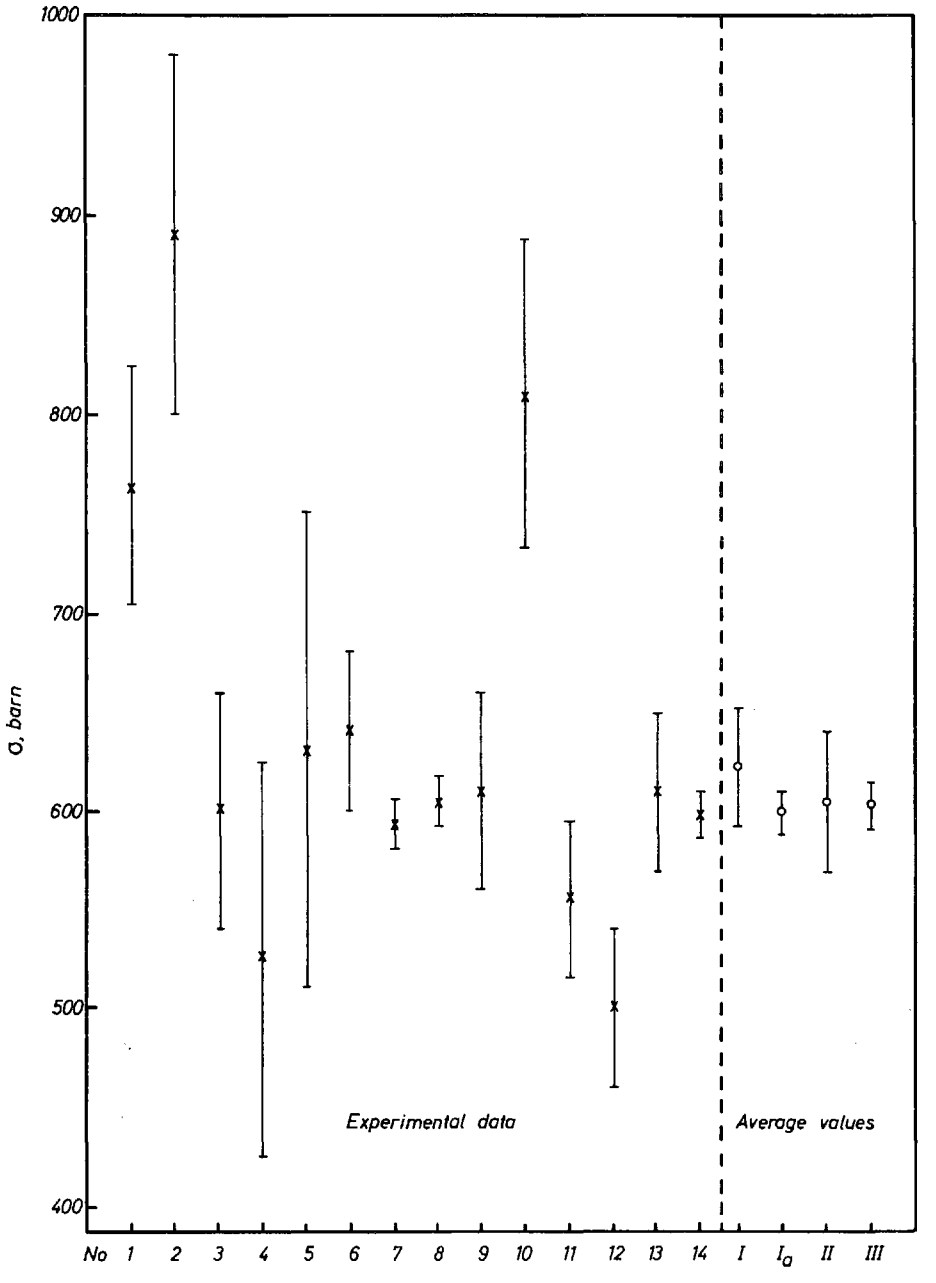

FIG.3. The independent experimental values of $\sigma_{n,\gamma}^{Au}$ at 30-keV neutron energy

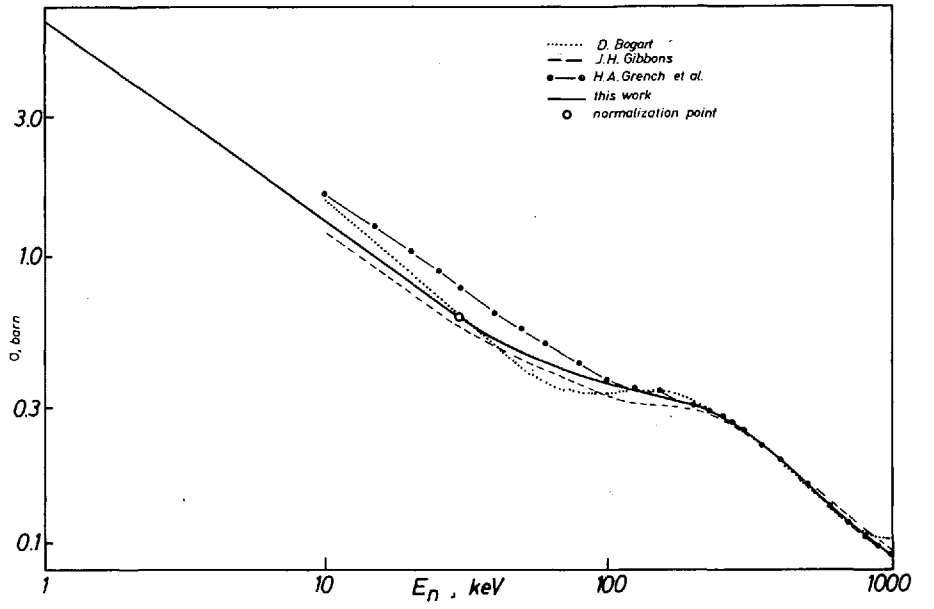

FIG. 4. Comparison of fitted cross-section curves

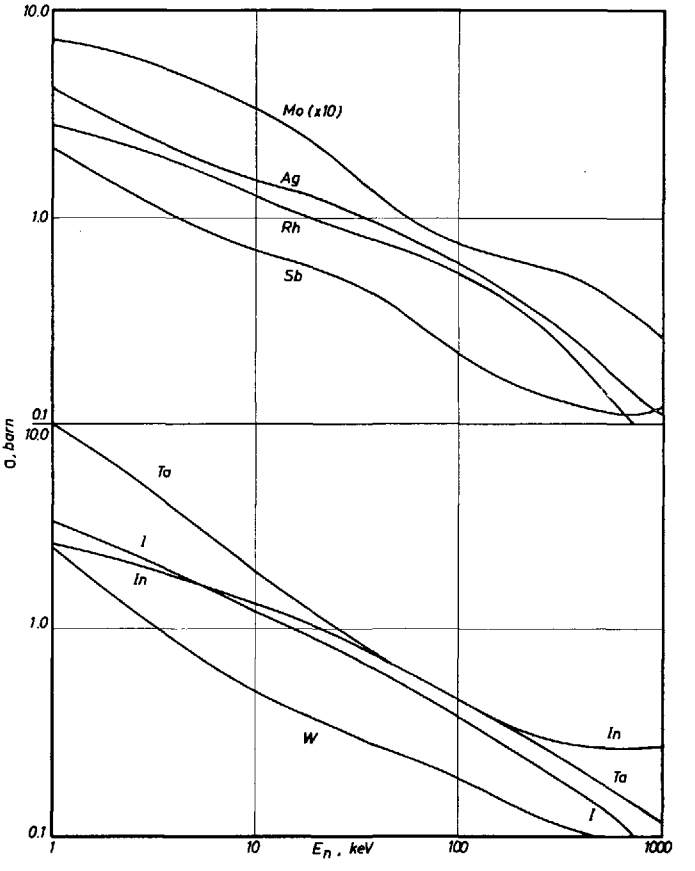

FIG. 5. Capture cross-sections of Mo, Rh, Ag, In, Sb, I, Ta and W in the energy range 1 - 1000 keV

TABLE I. EXPERIMENTAL METHODS FOR CAPTURE CROSS-SECTION MEASUREMENTS

Principle	Abbreviation	Method	Remarks	Ref.
Transmission (Absorption)	SST	Spherical shell transmission	The transmission of a spherical shell is observed. In contrast to a normal transmission experiment, in this geometric arrangement the neutrons which are "scattered out" by that part of the sample which is between the source and the detector are compensated by neutrons which are "scattered in" from the rest of the sample.	[12, 23, 31, 34, 38] and references cited therein
	CCD	Cross-section difference method	The normal transmission due to absorption and scattering in a sample is observed. In addition the scattered neutrons are measured in a 4π-geometry. To eliminate the efficiency of the 4π-detector the same experiment is performed with a "pure" scatterer.	[26]
	TA	Total absorption method	The loss of neutrons due to a sample in a 4π-neutron detector is measured. This method is in principle identical with the method to determine the resonance integral given by Popov.	[31]
Reaction (Capture)	F	Neutron flux measurements		
	F-RP	Recoil proton	The well-known (n,p)-scattering cross-section is used to determine the neutron flux. Because it is difficult to measure the recoil protons for low energies, the lowest neutron energy for which absolute neutron flux measurements have been performed is about 40 keV.	[28]
	F-AA	Associate activity	The associated activity (nucleus B) in the neutron source reaction A(B,n)B being measured and is equal to the neutron source strength. If the (n,γ)-reaction at the sample leads to an activity which is similar to those of the source reaction, the combination F-AA/C-A is an absolute method.	[24, 30, 36]

TABLE I. (cont.)

Principle	Abbreviation	Method	Remarks	Ref.
Reaction (Capture)	F-AP	Associate particle	The associated (charged) particle in the source being detected. This method was not performed for measurements in the keV-energy region, as far as we know, up to now.	[40]
	F-ID	Integral detectors	The neutrons are slowed down in a large moderator and detected at thermal neutron energy in the whole moderator. This means a flat response of the detector as a function of the incident neutron energy, the detector being calibrated in energy regions where good methods for flux measurements exist. (Examples: Long Counter, Macklin sphere, grey neutron detector, large liquid scintillator with a scatterer).	[3,6,9,13,41, 42]
	F-IM	Integral methods (mainly $MnSO_4$-bath technique)	The principle of neutron slowing down is the same as for F-ID. However, the captures at thermal energies lead partly to an activity which can be measured absolutely. This activity together with the ratio of the activation cross-section to the capture cross-section of the moderator determine the neutron flux.	[25,35,36]
	F-R or F-U235	Relative measurements	The neutron flux measurement is avoided by using an (n,γ)-cross-section or the (n,f)-cross-section of ^{235}U as a standard	[4,5,8,9,10,11, 15,18,22,29,32, 33]
	F-B10	Relation to $^{10}B(n,\alpha)$	This procedure is different from F-R inasmuch as the thermal cross-section and an assumption about the energy dependence of the cross-section (1/v-behaviour) is used. Furthermore the measurement of the (n,α) cross-section for ^{10}B using the spherical shell transmission method, in contrast to the (n,γ) measurements, allows the assumption of smooth cross-sections in the keV-energy region.	[9,10,14,20, 21,27,32,39,44]

TABLE I. (cont.)

Principle	Abbreviation	Method	Remarks	Ref.
Reaction (Capture)	F-SD	Slowing-down spectrometer	In principle it should be possible to calculate the neutron flux in a large moderator of heavy nuclei as a function of time (energy) using a pulsed neutron source of constant source energy. A calibration at one energy would determine the flux at all energies. However, this method has not been used in absolute cross-section determination; rather all measurements have been made relative to ^{10}B.	[43]
Reaction (Capture)	C	Capture rate measurements		
	C-LLS	Total absorption of prompt γ-rays (large liquid scintillator)	The prompt γ-rays are detected in an n-geometry using a large liquid scintillator tank. To obtain independence of the efficiency from the changes of the γ-multiplicities in the cascades, it is necessary to use a large scintillator volume.	[10,11,15,20]
	C-EPD	Detection of prompt γ-rays proportional to their energy	The efficiency for the detection of a prompt γ-ray in the cascade is proportional to the energy of this γ-ray. This means that the overall efficiency is independent of the multiplicity in a γ-ray cascade and only proportional to the max. γ-transition energy. (Examples: Proportional counter; Moxon-Rae detector).	[21,27,39,44]
	C-LVD	Detection of prompt γ-rays in large volume scintillation counters	The prompt γ-rays are detected in only a part of the 4π-angle with a large volume scintillation detector. However, most of the detectors are not "black" for the γ-rays and therefore are sensitive to a change in the γ-ray spectra. (Examples: Plastic scintillators, CaF-crystals, NaI-crystals)	[19]
	C-A	Activation	The activity of a sample due to (n,γ)-reactions is determined after the irradiation. Not all stable nuclei yield a radioactive nucleus when undergoing an n,γ reaction; also in many cases it is not possible (because of half-life and/or decay scheme) to determine the induced activity. Therefore the application of this method to the determination of (n,γ) cross-sections is very restricted. However, in a few cases such precise determination of the activity (that is, also of the capture rate) are possible, that this method is very favourable for absolute cross-section measurements.	[1-9,13,14,18, 24,25,28,33, 35,36]

TABLE I. (cont.)

Principle	Abbreviation	Method	Remarks	Ref.
Reaction (Capture)		Relation to capture rates at thermal or eV energy	The elimination of the detector efficiency (in the cases C-LLS, C-EPD, C-LVD and C-A) is possible if one knows either the capture cross-section at thermal neutron energy or the resonance parameters.	[4,20,21,27, 39,44]
Decay time measurement (Absorption)	DTM	Neutron field decay time measurement	The decay time constant $\alpha_0 = v_0 \Sigma_a \cdot D_0 B^2 + CB^4$ is observed to determine the absorption cross-section Σ_a. The moderation effect must be taken into consideration. The result is an effective cross-section averaged over many resonances.	[45,46]

TABLE IIa. EXPERIMENTAL CROSS-SECTION VALUES AT 30 keV

No.	Authors	Ref.	Year	Methods, Remarks	Value (barn) [a]
1	Weston, Lyon	[13]	1961	F-ID/C-A	0.767 ± 0.060
2	Miskel et al.	[18]	1962	F-U235/C-A	0.880 ± 0.090
3	Moxon, Rae	[21]	1963	F-B10/C-EPD Calibration at several resonances	0.600 ± 0.060
4	Haddad et al.	[20]	1964	F-B10/C-LLS Calibration using the 1.46-eV resonance of Au	0.525 ± 0.100
5	Konks et al.	[27]	1964	F-B10/C-EPD Calibration using thermal cross-section and resonance parameter of Au	0.630 ± 0.120
6	Harris et al.	[30]	1965]	F-AA + C-A	0.640 ± 0.040
7	Pönitz	[48, 36]	1966 (Jan.)	F-AA + C-A	0.593 ± 0.012
8	Pönitz	[48, 36]	1966 (Jan.)	F-IM/C-A	0.604 ± 0.011
9	Schmitt, Cook, Bogart, Semler	[12, 34]	1966 (March)	SST (Monte Carlo calculation)	0.608 ± 0.050 [b]
10	Cox	[14, 32]	1966 (March)	F-B10, F-U235/C-A	0.809 ± 0.080
11	Ryves et al.	[35]	1966 (April)	F-IM/C-A	0.555 ± 0.040 [b]
12	Belanova et al.	[31]	1966 (May)	TA, SST (Bethe method)	0.500 ± 0.050 [b]
13	Knoll, Pönitz	[51]	1966 (Aug.)	F-U235/C-A The cross-section ratio given in the referred work and an extrapolated value of $\sigma_{n,\gamma}$ given by White [50] was used	0.608 ± 0.040
14	This work	-	1966	F-IM/C-A	0.598 ± 0.012

[a] The original values are averaged at an energy range of 5 keV

[b] The values are translated from 24.8 keV to 30 keV using the cross-section curve given by Harris et al. [30].

TABLE IIb. REDUCED AND SELECTED CROSS-SECTION VALUES AT 30 keV AND AVERAGE VALUES

No.	No. from Tab. IIa	Method		Value (barn)
15	1	F-ID/C-A		0.767 ± 0.060
16	3, 4, 5	F-B10/C-EPD, C-LLS		0.585 ± 0.095
17	6, 7	F-AA + C-A		0.617 ± 0.026
18	8, 11, 14	F-IM/C-A		0.586 ± 0.021
19	9, 12	SST		0.554 ± 0.050
20	2, 13	F-U235/C-A		0.749 ± 0.065
21	10	F-B10, F-U235/C-A		0.809 ± 0.080
No.	**No. from Tab. IIa**	**Method**	**Add. Weight**	**Value (barn)**
22	1	F-ID/C-A	0.3	0.767 ± 0.060
23	3, 4, 5	F-B10/C-EPD, C-LLS		0.587 ± 0.021
24	6, 7	F-AA + C-A		0.598 ± 0.030
25	8, 11, 14	F-IM/C-A	0.3	0.595 ± 0.030
26	9	SST		0.608 ± 0.05
27	2, 13	F-U235/C-A	0.3	0.644 ± 0.021
No.	**No. from above**	**Notation**		**Average value (barn)**
I	1-14	"A" non-weighted		0.623 ± 0.030
Ia	1-14	"A" weighted		0.600 ± 0.009
II	15-21	"B" weighted		0.615 ± 0.025
III	22-27	"C" weighted		0.603 ± 0.012

the standard cross-section, because the ratios $\sigma^{X}_{n,\gamma} / \sigma^{Au}_{n,\gamma}$ measured by different authors disagree generally about 10-30%.

ACKNOWLEDGEMENT

The author would like to thank H.W. Schmitt for valuable discussions and Professor K.H. Beckurts for his interest in these investigations.

TABLE III. CAPTURE CROSS-SECTION VALUES IN THE ENERGY REGION 1 – 1000 keV

E (keV)	σ (barns)								
	Au	Mo	Rh	Ag	In	Sb	I	Ta	W
1	6.77	0.72	2.82	4.27	2.59	2.13	3.38	10.16	2.49
2	4.08	0.63	2.35	2.91	2.18	1.43	2.50	6.33	1.43
3	3.03	0.56	2.09	2.44	1.98	1.16	2.15	4.61	1.06
5	2.11	0.47	1.73	1.94	1.65	0.91	1.68	3.16	0.75
10	1.31	0.33	1.27	1.52	1.29	0.69	1.17	1.83	0.49
20	0.811	0.234	1.00	1.28	1.02	0.574	0.90	1.18	0.364
30	0.603	0.165	0.85	1.02	0.81	0.480	0.72	0.85	0.292
50	0.460	0.110	0.72	0.85	0.65	0.370	0.570	0.65	0.250
70	0.400	0.090	0.64	0.73	0.56	0.285	0.460	0.545	0.220
100	0.355	0.076	0.54	0.61	0.46	0.216	0.375	0.460	0.192
200	0.304	0.062	0.364	0.406	0.321	0.145	0.246	0.321	0.132
300	0.245	0.056	0.258	0.310	0.287	0.130	0.197	0.256	0.113
500	0.159	0.045	0.150	0.198	0.267	0.114	0.142	0.182	0.095
700	0.118	0.036	0.103	0.150	0.267	0.106	0.102	0.145	0.090
1000	0.093	0.027	0.075	0.112	0.269	0.111	0.073	0.119	0.098
	Δσ/σ (%)								
1-10	7	30	20	10	15	30	20	10	15
10-40	8	20	20	10	10	20	15	10	15
40-200	12	20	20	15	15	15	15	15	15
200-1000	7	20	15	10	15	20	20	20	15

REFERENCES

[1] HENKEL, R.L., BARSCHALL, H.H., Phys. Rev. 80 (1950) 145.
[2] HUMMEL, V., HAMERMESH, B., Phys. Rev. 82 (1951) 67.
[3] MACKLIN, R.L., LAZAR, N.H., LYON, W.S., Phys. Rev. 107 (1957) 504.
[4] BOOTH, R., BALL, W.P., McGREGOR, M.H., Phys. Rev. 112 (1958) 226.
[5] JOHNSRUD, A.E., SILBERT, M.G., BARSCHALL, H.H., Phys. Rev. 116 (1959) 927.
[6] FERGUSON, A.T.G., PAUL, E.B., J. nucl. Energy A10 (1959) 19.
[7] LYON, W.S., MACKLIN, R.L., Phys. Rev. 114 (1959) 1619.
[8] BAME, S.J., CUBITT, R.L., Phys. Rev. 113 (1959) 256.

[9] BILPUCH, E.G., WESTON, L.W., NEWSON, H.W., Ann. of Physics 10 (1960) 455.
[10] BLOCK, R.C., SLAUGHTER, G.G., WESTON, L.W., VONDERLAGE, F.C., Neutron Time-of-Flight Methods (SPAEPEN, J., Ed.) EURATOM, Brussels (1961) 203.
[11] DIVEN, B.C., TERRELL, J., HEMMENDINGER, A., Phys. Rev. 120 (1960) 556.
[12] SCHMITT, H.W., COOK, C.W., Nucl. Phys. 20 (1960) 202.
[13] WESTON, L.W., LYON, W.S., Phys. Rev. 123 (1961) 948.
[14] COX, S.A., Phys. Rev. 122 (1961) 1280.
[15,16,17] GIBBONS, J.H., MACKLIN, R.L., MILLER, P.D., NETLER, J.H., Phys. Rev. 122 (1961) 182.
[18] MISKEL, J.A., MARSH, K.V., LINDNER, M., NAGLE, R.J., Phys. Rev. 128 (1962) 2717.
[19] BERGQUIST, I., Ark. Fys. 23 (1963) 425.
[20] HADDAD, E., WALTON, R.B., FRIESENHAHN, S.J., LOPEZ, W.M., Nucl. Instr. 31 (1964) 125; EANDC-33 "U" (1963).
[21] MOXON, M.C., RAE, E.R., Nucl. Instr. 24 (1963) 445.
[22] MACKLIN, R.L., GIBBONS, J.H., INADA, T., Nucl. Phys. 43 (1963) 353.
[23] SCHMITT, H.W., EANDC-33 "U" (1963) 41.
[24] POENITZ, W.P., EANDC-33 "U" (1963) 164.
[25] POENITZ, W.P., BRUDERMUELLER, G., EANDC-33 "U" (1963) 87.
[26] LANGSDORF, A., LANE, R.O., ELWYN, A.J., Rep. WASH-1046 (1964).
[27] KONKS, V.A., POPOV, Y.P., SHAPIRO, F.L., Soviet Phys. (JETP) 19 (1964) 59.
[28] BARRY, J.F., J. Nucl. Energy A/B 18 (1964) 491.
[29] CHAUBEY, A.K., SEHGAL, M.S., Nucl. Phys. 66 (1965) 267.
[30] HARRIS, K.K., GRENCH, H.A., JOHNSON, R.G., VAUGAN, F.J., FERZIGER, J.H., SHER, R., Nucl. Phys. 69 (1965) 37.
[31] BELANOVA, T.S., VANKOV, A.A., MIKHATLUS, F.F., STAVISSKII, Y.Y., J. Nucl. Energy A/B 20 (1966) 411; Atomnaja Energija 19 (1965) 3.
[32] COX, S.A., Rep. WASH-1068 (1966) 6.
[33] GRENCH, H.A., COOP, K.L., MENLOVE, H.O., VAUGHN, F.J., Rep. WASH-1068 (1966) 75.
[34] BOGART, D., SEMLER, T.T., Rep. NASA TM X-52173 (1966).
[35] RYVES, T.B., ROBERTSON, J.C., AXTON, E.J., GOODLER, I., WILLIAMS, A., J. nucl. Energy A/B 20 (1966) 249.
[36] POENITZ, W.P., EANDC(E)-69 "S"; J. nucl. Energy, to be published (1966).
[37] KONONOV, V.N., STAVISSKII, I.I., TOLSTIKOV, V.A., Soviet J. atom. Energ. 5 (1958) 1483.
[38] BELANOVA, T.S., Soviet J. atom. Energ. 8 (1960) 462.
[39] ISAKOV, A.I., POPOV, Y.P., SHAPIRO, F.L., Sov. Phys. (JETP) 11 (1960) 712.
[40] BETL, H., LE RIGOLEUR, M., LEROY, J.L., EANDC-33 "U" (1963) 150.
[41] POENITZ, W.P., WATTECAMPS, E., EANDC-33 "U" (1963) 102.
[42] GONDE, H., SCHWARZ, S., STARFELT, N., Ark.f. Fysik 39 (1965) 45.
[43] BECKURTS, K.H., Rep. IAK 3/63, Kernforschungszentrum Karlsruhe (1963).
[44] MITZEL, F., PLENDL, H.S., Nukleonik 6 (1964) 371.
[45] BECKURTS, K.H., Rep. IAK 13/64, Kernforschungszentrum Karlsruhe (1964).
[46] MIESSNER, H., ARAI, E., Nukleonik, to be published.
[47] POENITZ, W.P., Rep. KFK-180 (1963).
[48] POENITZ, W.P., Thesis, Karlsruhe (1966).
[49] CHAMPION, P.J., Measurements and Standards of Radioactivity, National Science Series Report 24, Publication No 573.
[50] WHITE, P.H., J. nucl. Energy A/B 19 (1965) 325.
[51] KNOLL, G.F., POENITZ, W.P., to be published.
[52] BOGART, D., Rep. NASA TM X-52 162 (1966).
[53] GIBBONS, J.H., see Ref. [54].
[54] GRENCH, H.A., COOP, K.L., MENLOVE, H.O., VAUGHN, F.J., to be published.
[55] COX, S.A., Phys. Rev. 133 (1964) B378.
[56] HUGHES, D.J., SCHWARTZ, R.B., Rep. BNL-325 (1958).
[57] GORDEEV, I.W., KARDASCHEV, D.A., MALUESCHEV, A.W., Rep. INDSWG-43 (1963).
[58] POPOV, Y.P., Trudy Fiz. Inst. Akad. Nauk XXIV (1964).
[59] KOMPE, D., paper CN-23/10, these proceedings, vol. I.
[60] SCHWARZ, S., STROEMBERG, L.G., BERGSTROEM, A., Nucl. Phys. 63 (1965) 593.

DISCUSSION

D. BOGART: The different shapes of the gold capture cross-section from 30 to 150 keV are completely dependent on whether Li(n, α) or ^{10}B(n, α) is used as flux monitor. The Li(n, α) used here gives rise to a flatter Au(n, γ) curve in this region than the ^{10}B(n, α), which varies as 1/v up to 80 keV. The Au(n, γ) is merely a secondary indicator of erroneous shapes in either the Li(n, α) or the ^{10}B(n, α). The Au(n, γ) curves obtained using these two flux monitors, normalized at 30 keV to an absolute value, differ by as much as 25% between 50 and 100 keV. Precise evaluation of all (n, γ) cross-sections is impossible until either Li(n, α) or ^{10}B (n, α) is chosen as a standard.

W. PÖNITZ: I realize that between 30 and 150 keV there are discrepancies of up to ± 10%. However, I do not think a reaction cross-section should be preferred as a standard for capture cross-section measurement. In choosing a standard the criterion should be the practical applicability. To solve the problem of the shape between 30 and 150 keV we are preparing an experiment at Karlsruhe using a scintillation counter and a grey neutron detector (EANDC-33"U")

M. D. GOLDBERG: In preparing the new edition of BNL-325, we have had to face up to the problem of Au capture. The data are plotted as presented by the author with very few renormalizations. Gibbons suggested that we renormalize the Oak Ridge scintillator tank detector data using a linear correction between 80 and 170 keV, with 0% correction at 80 keV and 15% correction at 170 keV. The curve through the data in BNL-325 was drawn with the assistance of Gibbons and should replace the old Gibbons curve shown in your slide.

W. P. PÖNITZ: The Gibbons data included in Fig. 4 of the paper are taken from a paper by Grench et al. I presume these are the newer Gibbons data.

R. BATCHELOR (Chairman): The fission cross-section in this energy region is an important measurement and it is to be hoped there will be more work on this in the future.

FISSION CROSS-SECTIONS OF SOME PLUTONIUM ISOTOPES IN THE NEUTRON ENERGY RANGE 5-150 keV

W. B. GILBOY AND G. F. KNOLL
KERNFORSCHUNGSZENTRUM KARLSRUHE,
FEDERAL REPUBLIC OF GERMANY

Abstract

FISSION CROSS-SECTIONS OF SOME PLUTONIUM ISOTOPES IN THE NEUTRON ENERGY RANGE 5 - 150 keV. The fission cross-sections of ^{239}Pu and ^{240}Pu have been measured relative to the fission cross-section of ^{235}U over the neutron energy range 5 - 150 keV. A thick lithium target was bombarded with a pulsed and bunched proton beam from the Karlsruhe 3-MeV Van de Graaff to produce a pulsed "white spectrum" of neutrons from the $^{7}Li(p,n)^{7}Be$ reaction. The fissile samples were mounted in xenon gas scintillation counters to detect the induced fissions. Pairs of these fission counters were mounted symmetrically round the pulsed neutron source and the neutron energies were determined from their flight times. The $^{239}Pu/^{235}U$ and $^{240}Pu/^{235}U$ ratios are presented at 10% and 30% lethargy intervals, respectively, and no marked structure is apparent in either case with these energy resolutions.

DIRECT AND ABSOLUTE MEASUREMENTS OF AVERAGE FISSION NEUTRON YIELD FROM URANIUM-235 AND CALIFORNIUM-252*

A. DE VOLPI + AND K.G. PORGES
ARGONNE NATIONAL LABORATORY,
ARGONNE, ILLINOIS, UNITED STATES OF AMERICA

Abstract

DIRECT AND ABSOLUTE MEASUREMENTS OF AVERAGE FISSION NEUTRON YIELD FROM URANIUM-235 AND CALIFORNIUM-252. A recent survey by the IAEA has shown that significant discrepancies exist amongst absolute values of $\bar{\nu}$ and σ_f. For $\bar{\nu}$ (^{235}U) only one measurement, made in 1958 with a quoted precision of 1.5%, is considered independent, and the Westcott group reports that the original value has been lowered so that it is now 2.5% below the recommended least-squares average. There are four accepted values for $\bar{\nu}$ (^{252}Cf), one of which is also about 2.5% lower than the least-squares fit; another is 1.6% lower, while the average of all measurements is 1% below the recommended values derived from the multiparameter fit. A similar situation exists with regard to 2200-m/s fission cross-sections, wherein the discrepancies far exceed the precision quoted for each experiment.

Since these measurements represent the cornerstone of a strongly interrelated structure of nuclear data utilized in reactor physics, it is important that they be independently and accurately evaluated, despite the fact that there exists strong confidence in σ_a, η, and α values which provide an overdetermined set of parameters. The experiment reported in this present paper has been designed to circumvent certain plausible systematic errors which may be responsible for the discrepancies. The total neutron yield has been measured for thermal neutron fission of ^{235}U and also independently for ^{252}Cf with an improved manganese bath apparatus. Evaluation of possible error sources has led to the adoption of a sequence of precision techniques subjected to extensive verification.

The neutron yield of a fission counter was determined with the manganese bath; the accuracy of the bath system was independently corroborated with 0.7% precision against the United States National Bureau of Standards secondary neutron source. Absolute beta-gamma and relative gamma-gamma coincidence techniques are important facets of this calibration.

The fission rate of the fission counter was found in a separate prompt fission-neutron coincidence experiment, borrowing well-established methods from beta-gamma coincidence work. In the course of this calibration it was discovered that angular anisotropy in fission neutron emission is much more a problem than universally realized: it is possible that some of the discrepancies in reported $\bar{\nu}$ and σ_f measurements result from discounting this correction too readily. This conclusion is supported with a series of angular traverses and, in the final analysis, by the contemporary $\bar{\nu}$ results reported in this paper.

1. INTRODUCTION

The purpose of this investigation has been to make a direct and precise measurement of $\bar{\nu}$ for ^{252}Cf and ^{235}U, $\bar{\nu}$ being the average total number of neutrons emitted per fission.

At the present time the best value for $\bar{\nu}(^{235}U)$ is derived indirectly from η — the number of fission neutrons per neutron captured — and relative fission-to-capture cross-sections, as well as by comparison with $\bar{\nu}(^{252}Cf)$ measurements recently reported [1].

Great importance has been attached to having results of this experiment independent of detector efficiencies, neutron leakage, fission energy spectra, cross-section values, background subtractions, and counting statistics.

---

* Work performed under the auspices of the United States Atomic Energy Commission.

+ Submitted in partial fulfillment of requirements for degree of Doctor of Philosophy at Virginia Polytechnic Institute, Blacksburg, Va., USA.

The measurement may be considered to consist of two independent phases: (I) evaluation of the fission rate; and (II) absolute determination of the neutron intensity. A simultaneous measurement of neutron and fission rate is adjusted according to absolute calibrations determined in the two separate phases. The relationship of some essential elements of the experiment are given in the block diagram, Fig. 1.

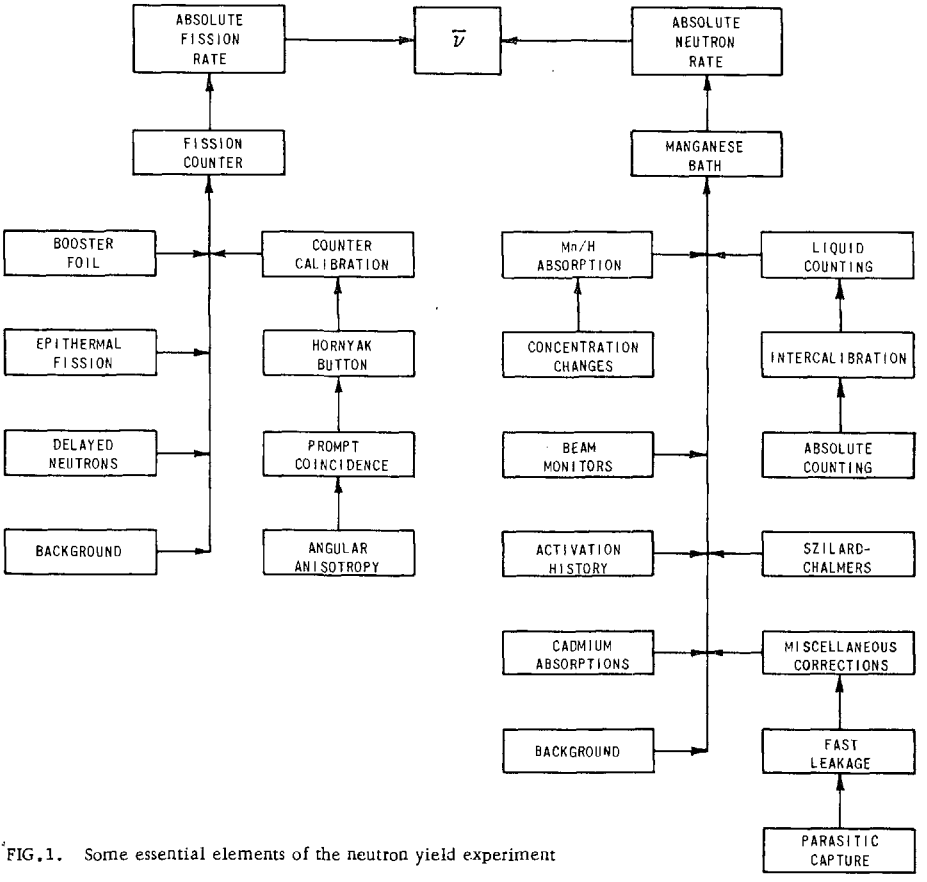

FIG.1. Some essential elements of the neutron yield experiment

The basic equipment for Phase I consists of a fission counter containing material which either fissions spontaneously or can be induced to fission; a fast-acting neutron detector; and electronic circuitry to record the number of single and coincidence counts. The fission counter rate F is in simplified terms proportional to the source rate S, the constant being the fission counter efficiency, ε_f,

$$F = \varepsilon_f S \quad ; \tag{1}$$

the neutron channel rate N contains the desired quantity $\bar{\nu}$ with the neutron detector efficiency ε_n,

$$N = \bar{\nu}\, \varepsilon_n S \quad ; \tag{2}$$

and the coincidence rate C includes all three parameters

$$C = \varepsilon_f \bar{\nu} \varepsilon_n S \quad . \tag{3}$$

Taking the ratio of coincidence and fission counts yields

$$C/F = \varepsilon_n \bar{\nu} \quad . \tag{4}$$

Thus, if the neutron detector efficiency can be evaluated (over the fission neutron energy spectrum), the desired quantity $\bar{\nu}$ is found. Equation (4) represents the method applied to all published precision measurements of the past decade. For work reported in this paper the relation

$$FN/C = S \tag{5}$$

is used to find the fission rate S only.

Phase II consists of a separate measurement of the absolute neutron rate using the manganese bath. The source of ^{235}U fission neutrons is a well-moderated beam emerging from the Argonne CP-5 reactor thermal column. For Phase II the beam is directed (Fig. 2) into the beam channel through the

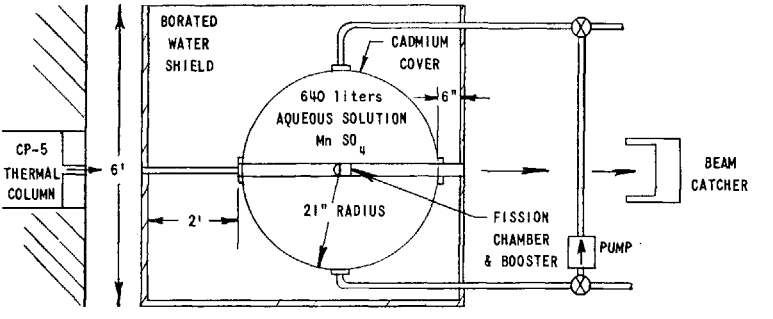

FIG. 2. Manganese bath sphere located at reactor thermal column

shielding tank and into the fission chamber located at the center of the manganese bath sphere used as the basic neutron detector. Transmitted thermal neutrons in the beam pass through the remainder of the collimator and are stopped in an external beam catcher. The beam tube is lined with cadmium to keep scattered thermal neutrons out of the slowing-down sphere. Fission neutrons from the ^{235}U coating of the fission chamber undergo scattering and absorption in both the hydrogen and manganese of the aqueous solution of manganous sulfate.

Adequate source rate is obtained by adding a "booster foil" consisting of additional enriched uranium placed in the umbral region of the chamber coating. The ^{235}U fission counter and booster are concentric hemispheres. For ^{252}Cf no booster is required.

Calibration of the manganese bath counting system requires various supplementary experiments and calculations, as outlined in Fig. 1.

More specific details of the two phases are reported in two papers presented at the Vienna Symposium on Standardization of Radionuclides [2,3].

2. ^{235}U EXPERIMENTS

2.1. Combined Normalized Fission Rate (Phase I)

The quantity obtained from the fission calibration phase of the experiment is the fission counter normalized disintegration rate. The setting for the neutron discrimination level is an important parameter for interpretation. Plots of the data from both ^{235}U fission chambers are given in Figs. 3 and 4.

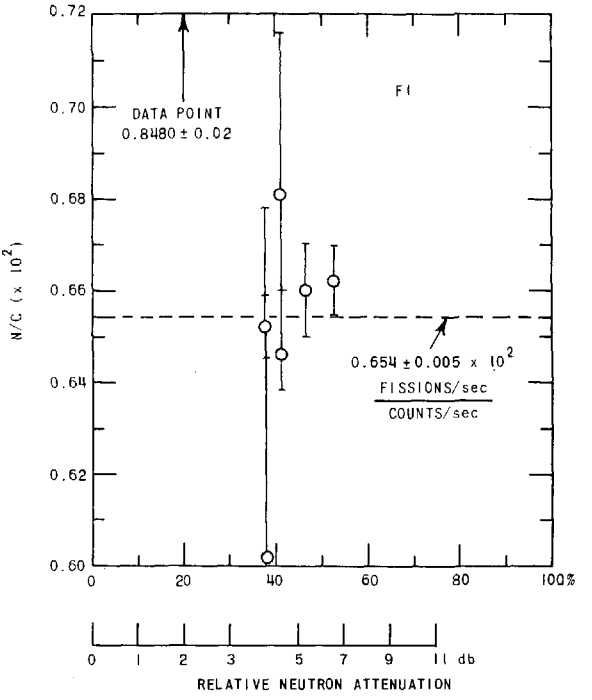

FIG.3. Neutron-coincidence ratio (N/C) as a function of neutron bias level N_U for fission counter F-1. At sufficiently high level, delayed and slower fission neutrons, as well as gamma rays, are biased out.

These represent the basic information derived from this phase of the experiment. The fact that the N/C ratio levels off at sufficiently high bias is taken to mean that gamma background and the slower neutrons have been adequately excluded and that the "plateau" rate represents the "true" N/C ratio. Since there is some latitude in choosing the final slope, this uncertainty has been incorporated in the standard deviation connected with the weighted mean N/C ratios chosen to represent the two fission counters.

2.2. Normalized Absolute Neutron Rate (Phase II)

As stated, the neutron rate is determined with the aid of a calibrated manganese bath system. Samples of activated manganese solution drawn from the bath are counted in a high-stability gamma-gamma coincidence system. The gamma-gamma coincidence facility is frequently intercalibrated with an absolute 4π beta-gamma coincidence counter [4], with data processed by the program COINC [5]. Corrections for relative hydrogen/manganese capture are based on the work of Axton [6]. Independent corroboration of the accuracy of the neutron rate determination has been found by obtaining a value of $(1.185 \pm 0.007) \times 10^6$ neutrons/sec for the secondary source NBS-II, which is given by the U. S. National Bureau of Standards to be $(1.180 \pm 0.013) \times 10^6$ neutrons/sec [7].

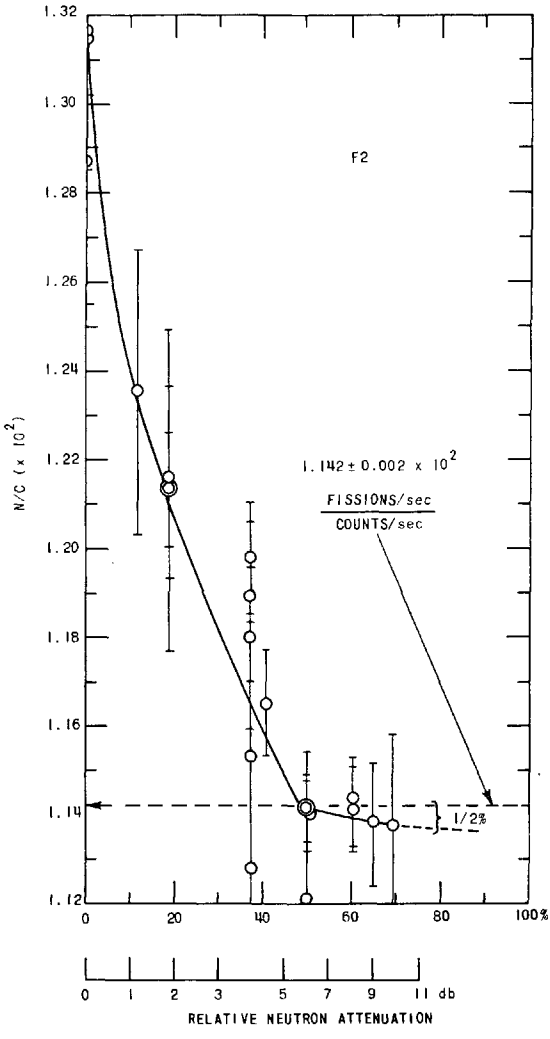

FIG. 4. Neutron-coincidence ratio for fission counter F-2.

In order to correct for reactor-induced background which amounts to 5 or 10% of the signal rate and to adjust for varying reactor power level, a set of monitors as well as the primary fission counter are sources of continuous data for normalization.

2.3. Neutrons/Fission

The final computation for the neutron yield (Table I) is a simple division of the normalized neutron rate of Phase II and the normalized fission rate of Phase I, separately determined for each of the two fission counters. The two values have been equally weighted in averaging together, since the 3.3% spread, which exceeds the standard deviation assigned to each individual counter, is probably dominated by discrepancies associated with orientation of each fission counter, an effect with equal a priori likelihood.

3. DATA AND CALCULATIONS FOR ^{252}Cf

While the measurement of $\bar{\nu}(^{252}Cf)$ is generally very similar to the ^{235}U experiment, there are some important differences. For example, the absence of

TABLE I. $\bar{\nu}$ AVERAGE OBTAINED FROM BOTH FISSION COUNTERS

$$\bar{\nu}_1 = \frac{1.593 \times 10^2 \text{ (n/s)/(c/s)} \pm 1.3\%}{0.654 \times 10^2 \text{ (fis/s)/(c/s)} \pm 0.8\%} = 2.436 \text{ n/fis} \pm 1.5\%$$

$$\bar{\nu}_2 = \frac{2.662 \times 10^2 \text{ (1.011)} \pm 1.0\%}{1.142 \times 10^2 \quad 0.3\%} = 2.357 \text{ n/fis} \pm 1.1\%$$

3.3% spread

$$\bar{\nu} = \frac{\bar{\nu}_1 + \bar{\nu}_2}{2} = 2.40 \pm 0.04 \text{ (1.7\%) n/fis}$$

a reactor-induced neutron background in the manganese bath favors the californium measurements. Furthermore, monitors are not required for normalization, and it is not necessary to make corrections for ^{56}Mn buildup subject to varying reactor power level. The various neutron reference sources (Ra-Be and ^{252}Cf) ensure that the neutron intensity measurements are reproducible over a long span of time.

With regard to the fission rate, the ^{252}Cf result depends on two different fission counters — one with a hemispherical foil and the other with a flat foil. In view of the factors associated with neutron beam and booster alignment and uniformity, the use of the spontaneous fission source represents a significant simplication. Again, the absence of a reactor-induced background in the Hornyak button prompt neutron detector improves the quality of the ^{252}Cf data. In addition, the reproducibility of the ^{252}Cf fission rate makes data assessment much more reliable.

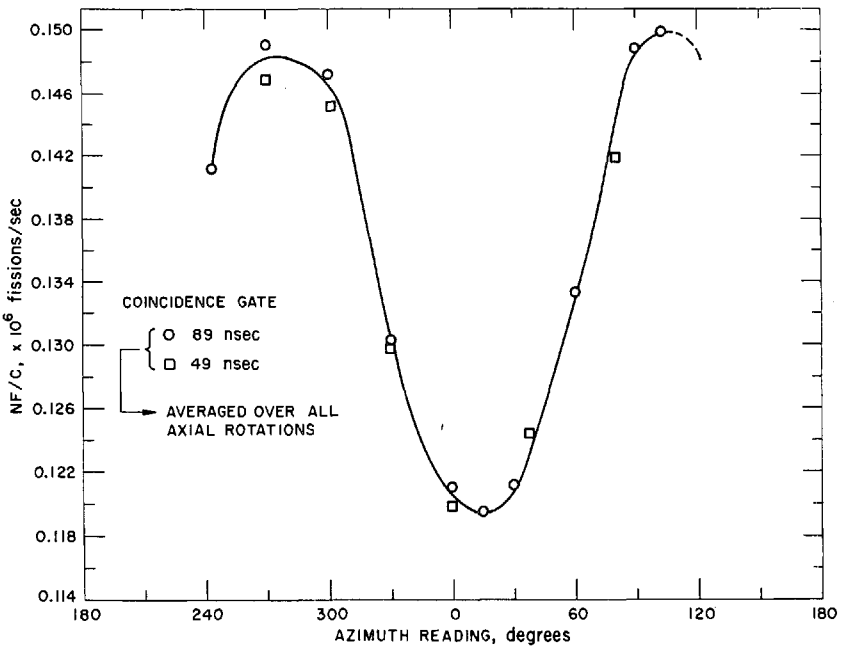

FIG.5. Change in disintegration rate computed from NF/C for a plane foil fission counter moved about an angle between the neutron detector normal and the fission counter normal. Data points are averages over all axial rotations of the fission counter. This variation is essentially a measure of the loss of coincidence counts resulting from correlated fragment-neutron emission for a counter with 60% fragment efficiency.

Roughly half a microgram of ^{252}Of was deposited on a platinum disk used as one electrode of a parallel-plate fission counter. The deposition apparently was not carrier-free, resulting in a net efficiency of the order of 60%. The strong correlation between fragment and neutron emission results in a variation in fission rate determined by the coincidence method according to the angle between the fission foil axis and the neutron detector normal. The results of such an azimuthal scan are shown in Fig. 5. A simple theory, which has been worked out to account for this behavior [3], allows a relatively precise evaluation of the fission rate from these data.

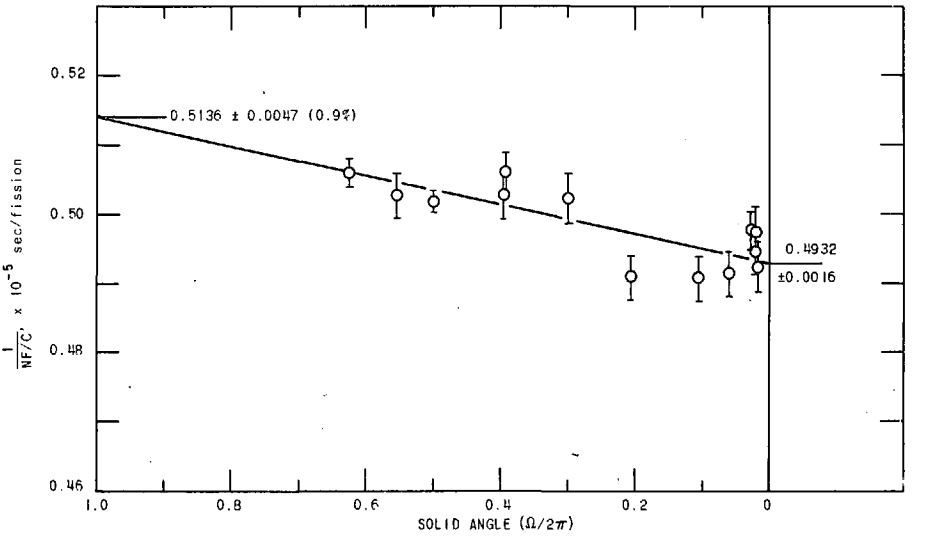

FIG.6. The inverse disintegration rate of the hemispherical counter plotted as a function of solid angle subtended by the neutron detector. Coincidence resolving time is 89 nsec.

The geometry of the hemispherical fission counter does not permit application of a simple theory, but its relatively high efficiency (close to 90%) suggests an extrapolation can be made to a neutron detector with 2π solid angle. Data from such runs obtained by varying the distance between the neutron detector and fission counter along the axis of both detectors is plotted in Fig. 6. In order to ensure that coincidences were not being lost due to the finite flight time of the fission neutrons, the coincidence gate was widened from 49 nsec to 89 nsec.

The neutron yield per fission is calculated from the data separately for the hemispherical counter ($\bar{\nu}_H$) and the flat foil chamber ($\bar{\nu}_F$) in Table II. The two results are weighted with inverse variances.

Agreement between two methods of determining the fission rate of the hemispherical counter tends to support the validity of the underlying procedures. Since, however, the hemispherical shape is not directly suitable for the analysis, it was decided to increase the 0.1% standard error obtained in the angular scan to 0.5%, providing an over-all weighted error in the fission rate of 0.4%. (All errors quoted are one standard deviation.)

4. DISCUSSION

The results listed in Tables I and II, [$\bar{\nu}(^{235}U) = 2.40$ and $\bar{\nu}(^{252}Cf) = 3.750$], give estimated errors of 1.7% for the ^{235}U measurement and 0.75% for ^{252}Cf. The californium results have smaller standard deviations because the conditions for measurement are much better than those encountered for ^{235}U in a reactor environ-

TABLE II. NEUTRON YIELD PER FISSION FOR ^{252}Cf COUNTERS

Hemisphere (Decay Corrected to 10/15/65)	
Neutron Intensity (Weighted Average)	= 7.277 × 10 n/sec ± 0.7%
Reciprocal Fission Rate (Weighted Average)	= 0.5153 × 10^{-5} sec/fis ± 0.4%
$\bar{\nu}_H$	= 3.750 × 0.030 (±0.8%) n/fis
Flat Foil (Decay Corrected to 7/27/65)	
Neutron Intensity (Weighted Average)	= 5.15 × 10^5 n/sec (±1.8%)
Fission Rate (Weighted Average)	= 1.374 × 10^5 fis/sec (±0.5%)
$\bar{\nu}_F$	= 3.748 ± 0.095 (±1.8%) n/fis
$\bar{\nu}(^{252}Cf)$(Weighted Average)	= 3.750 ± 0.028 (±3/4%) n/fis

ment. Aside from additional corrections applied to ^{235}U data, the ^{252}Cf result essentially confirms most but not all of the procedures used in the ^{235}U experiments.

On account of the well-thermalized character of the CP-5 reactor beam, the ^{235}U measurement can be considered to be equivalent to a 2200 m/s value; the increase in neutron emission at increasing energies is quite small over the Maxwellian beam range.

It is pertinent to note at this point that the values quoted for our ^{235}U work are simply unweighted averages of two fission counter results, and the associated error equals the range of divergence of the two values. This conservative course, which is a temporary expedient for ^{235}U until a return to the CP-5 reactor can be scheduled, is consistent with reasonable expectations that the discrepancy between the two ^{235}U counts is not random but systematic (residual anistoropy due to non-uniformities).

A comprehensive review of the 2200 m/s fission parameters for four fissile nuclides has recently been published [1]. The Westcott survey is exhaustive and up-to-date. Table III contains a comparison of their ^{235}U and ^{252}Cf values next to ours. The first column consists of recommended values derived from a least-squares fit to a set of over-determined constants. The second column lists the data averages which were used as input to the least-squares fitting, and the final column gives the values obtained in this work up to the cut-off date.

It is worthwhile to note that the recommended $\bar{\nu}$ values (which include delayed neutrons) differ from the preferred input data by much more than their associated errors. This means that the recommended values of $\bar{\nu}$ are almost entirely determined by the η and α measurements, implying that the $\bar{\nu}$ data averages are far from their likely values. Note that this is also true for the fission cross-section. Reasons for these discrepancies are extensively discussed in the Westcott report, and they coincide with the evidence available to us.

The International Atomic Energy Agency group, led by Westcott, examined all measurements for consistency; all fission cross-sections were tied to the "gold standard" (98.7 ± 0.2 b) where possible, and other experiments were renormalized with regard to other recent standards or corrected for various spectral indices to obtain uniform criteria for evaluation.

The Westcott group states "……results for $\bar{\nu}(^{252}Cf)$ have been obtained whose scatter is considerably larger than would be expected from the claimed errors." Moreover, they note that "There was only one input datum (for ^{235}U) for a ν measured absolutely, apart from the measurements of $\nu(^{252}Cf)$." This

TABLE III. COMPARISON OF EXPERIMENTAL AND RECOMMENDED VALUES OF ^{235}U AND ^{252}Cf PARAMETERS

	Recommended[a]	Preferred Input Data[b]	This Work[c]
		^{235}U (2200 m/s)	
σ_a	679.9 ± 2.3	680.57 ± 0.009	
σ_f	579.5 ± 2.0	583.49 ± 4.3	
σ_γ	100.5 ± 1.4		
α	0.1734 ± 0.0025	0.1733 ± 0.009	
η	2.071 ± 0.007	2.0740 ± 0.0083	
$\bar{\nu}$	2.430 ± 0.008	2.373 ± 0.029	2.40 ± 0.04
		^{252}Cf	
$\bar{\nu}$	3.772 ± 0.015	3.7488 ± 0.0157	3.750 ± 0.028

[a]Recommended by Westcott group [1] (output of 10-parameter least-squares fit).

[b]Used by Westcott group [1] as input to least-squares fit.

[c]Cutoff date 7/13/66.

single retained measurement [$\nu(^{235}U) = 2.373 \pm 0.029$] is by Kenward and Sanders [8], originally reported as 2.420 ± 0.037. Apparently there has been a recalibration of the ^{240}Pu source, resulting in reduction of their reported value, the information being transmitted by private communication in 1965 to Westcott. In any event, the Kenward and Saunders work was done using a parallel plate geometry, prompt-coincidence technique as all other absolute experiments of $\bar{\nu}$.

The Westcott group in regard to $\nu(^{252}Cf)$ states that ".....since the Third Geneva Conference.....new measurements had produced a rather unsatisfactory situation concerning the absolute values of ν. The results.....obtained using the liquid scintillator technique agree quite well, but the Harwell boron-pile value.....with a claimed accuracy of ±0.4% differs from the other two by about 2%."

Since "the underlaying basis of the least-squares procedure used in the present study is that the errors involved in the various measurements are of a random nature and are not correlated or systematic," one can reasonably conclude that the discrepancies shown in Table III indicate the existence of such a systematic error, and the source of this systematic error may be prevailing experimental arrangement of parallel-plate fission counters in a beam-hole geometry with inadequate correction for fission-neutron fission-fragment correlations. The distinctive aspects of the present experiment in contrast to other determinations of $\bar{\nu}$ warrant emphasis. The four measurements of $\bar{\nu}(^{252}Cf)$ and the one for $\bar{\nu}(^{235}U)$ abstracted by Westcott for inclusion in his least-squares fit all have a common feature; they are based on Eq. (4), $C/F = \varepsilon_n\bar{\nu}$, although different types and sizes of detectors have been used for neutron collection. The present work has avoided some of the problems associated with determining ε_n by relying upon the most precise technique presently available for neutron source calibration and has carefully considered the influence of angular correlations upon the coincidence rate; this procedure is limited, of course, to a few key measurements. On the other hand, the large liquid scintillator and boron pile prompt neutron detectors have been successfully applied to a number of experiments involving evaluation of $\bar{\nu}$ at other energies and for other fissionable materials.

ACKNOWLEDGMENTS

The authors wish to take this opportunity to state their appreciation for encouragement and technical support from a large number of Argonne staff members, particularly S. G. Kaufmann, W. C. Redman, L. M. Bollinger, A. B. Smith, and B. I. Spinrad.

REFERENCES

[1] WESTCOTT, C. H., et al., A survey of values of 2200 m/s constants for four fissile nuclides, Atomic Energy Rev. 3 2 (1965) 3.
[2] DE VOLPI, A., PORGES, K. G., ARMANI, A., Absolute calibrations of fission neutron source strength relying upon an improved manganese bath technique and absolute beta-gamma coincidence counting, Standardization of Radionuclides, IAEA, Vienna (1967) SM 79/56.
[3] PORGES, K. G., DE VOLPI, A., Absolute determination of fission fragment emission rates with a prompt neutron-fission coincidence method, Standardization of Radionuclides , IAEA, Vienna (1967) SM-79/55
[4] PORGES, K. G. A., DE VOLPI, A., LARSEN, R. N., Electronic design of an absolute counting system for Mn^{56}, Nucl. Instr. Meth. 29 (1964) 157.
[5] DE VOLPI, A., PORGES, K. G., JENSEN, G., Computer code for Reduction of Coincidence Counting Data, J. appl. Rad. Isotopes 17 (1966) 277.
[6] AXTON, E. J., CROSS, P., ROBERTSON, J. C., Calibration of the NPL standard Ra-Be photoneutron sources by an improved manganese sulphate bath technique, J. Nucl. Energy 19 A/B (1965) 409.
[7] SPIEGEL, V., Jr., National Bureau of Standards, Private Communication (May 7, 1965).
[8] KENWARD, C. J., RICHMOND, R., SANDER, J. E., A measurement of the neutron yield in thermal fission of ^{235}U, AERE R/R-212 (Rev.) (1958).

CONFIRMATORY EXPERIMENTAL DATA ON THE HARWELL BORON PILE $\bar{\nu}$ VALUES

D.W. COLVIN*, M.G. SOWERBY AND R.I. MACDONALD
ATOMIC ENERGY RESEARCH ESTABLISHMENT,
HARWELL, DIDCOT, BERKS.,
UNITED KINGDOM

Abstract

CONFIRMATORY EXPERIMENTAL DATA ON THE HARWELL BORON PILE $\bar{\nu}$ VALUES. The $\bar{\nu}$ values obtained by the Harwell boron pile experiment, which have been reported previously [Physics and Chemistry of Fission II (1965) 24] are approximately 2% lower than the values obtained with large liquid scintillators and those derived from measured values of η and α. The value of pile efficiency used in these measurements was obtained by using the associated particle technique, i.e. the d(γ,n)p reaction. Two standard neutron sources, a Ra-γ-Be source and the Atomic Weapons Research Establishment ^{240}Pu spontaneous fission source, have now been calibrated at the National Physical Laboratory, Teddington, England and in the boron pile. These measurements also enable the boron pile calibrations to be compared with other laboratories, such as the National Bureau of Standards in Washington, USA, and the National Research Council in Ottawa, Canada. The count rates of the standard sources in the boron pile can be used to obtain a second independent value of the pile efficiency and hence give information on the correctness of the boron pile $\bar{\nu}$-values. The results of these measurements are given together with other information, which demonstrates that the correction procedures used in the boron pile experiment are valid.

1. INTRODUCTION

The values of the average number of neutrons emitted per fission ($\bar{\nu}$) measured in the Boron Pile experiment [1] are lower than the values obtained with liquid scintillators by Hopkins and Diven [2] and Asplund-Nilsson et al.[3]. Other values, which are consistent with either the liquid scintillator or the Boron Pile data, have been obtained by Moat et al. [4, 5] and De Volpi and Porges [6]. Moat et al. used a detector consisting of BF_3 counters embedded in paraffin wax and De Volpi and Porges employed a manganese sulphate bath. The results of these measurements for ^{252}Cf are as follows:

Boron Pile	$\bar{\nu}$ = 3.713 ± 0.015
Hopkins and Diven	$\bar{\nu}$ = 3.780 ± 0.030
Asplund-Nilsson et al.	$\bar{\nu}$ = 3.808 ± 0.034
Moat et al.	$\bar{\nu}$ = 3.684 ± 0.040
De Volpi and Porges	$\bar{\nu}$ = 3.750 ± 0.028

To determine $\bar{\nu}$ accurately in the Boron Pile experiment it was necessary to measure the efficiency of Pile for a fission neutron energy spectrum. This was done to an accuracy of ± 0.3% by using the associated particle technique with the D(γ, n)p reaction. These efficiency measurements can be compared with other independent accurate methods of determining neutron output by using standard neutron sources. These

* Now at ENEA Neutron Data Compilation Centre, Gif-sur-Yvette, France

sources have been measured in the Boron Pile and have also been calibrated by one or both of the following methods:

(i) The Manganese Sulphate Bath of the National Physical Laboratory [7] whose efficiency is determined by adding to the inactive bath a known amount of ^{56}Mn activity.

(ii) The Aldermaston Oil Bath [8] standardized by the $T(d,n)^4He$ reaction.

The intercomparisons will be described elsewhere but the measurements on the standard sources can be used to obtain independent values of the Boron Pile efficiency and these results will be discussed in section 3.

Several meetings to discuss the measurement of $\bar{\nu}$ [9] have been held since the low $\bar{\nu}$ values of the Boron Pile were published [1]. During these discussions questions were raised about the Boron Pile measurements which could not be answered immediately. Since these are important in any evaluation of $\bar{\nu}$ data they will be discussed in section 4. Before any new results are presented, however, it is necessary to recall briefly the details of the Boron Pile experiment.

2. THE BORON PILE EXPERIMENT

The Boron Pile, which is shown in Fig. 1, consists of a graphite stack with a cubic core of side 220 cm in which there is an 11×11 lattice of holes. In each of these holes, except the central one, there are two 5-cm diameter $^{10}BF_3$ counters end to end. Surrounding this core there is a 35-cm graphite reflector and a neutron shield consisting of 0.4 mm of cadmium and 61 cm of concrete. The central hole has a key-hole shape with the circular part 10.1 cm in diameter. The whole assembly has a counting efficiency of approximately 64% for a neutron source placed at the centre.

To measure $\bar{\nu}$ a fission chamber was placed in the middle of the central hole of the Pile and, for neutron-induced fission, a collimated beam of neutrons passed through it. The fission fragments detected in the chamber were used to trigger a gating system which measured ($\bar{R}$) the average number of neutrons detected per fission. When $\bar{R}$ is corrected to $\bar{R}'$ to allow for effects such as pulse overlap which are described in detail in Ref. [1], $\bar{R}'$ is proportional to the number of prompt neutrons emitted per fission.

The Pile was calibrated by replacing the fission chamber with either a gridded fast ionization chamber or a proportional counter both containing tetra-deutero-methane. Use was then made of the deuteron photodisintegration reaction (i.e. the $D(\gamma,n)p$ reaction) in which "ν" is one and the energy of the neutron is known from the incident γ-ray energy. The gating circuit was then triggered by the photoproton pulses and $\bar{R}'$, which is the pile efficiency in this case, was measured as a function of neutron energy by using γ-rays of different energies.

The gating system consisted of two gates of the same length, the "prompt" and "background" gates, separated by a delay. The "prompt" gate was opened by either the fission or photoproton pulse and the background gate was usually opened 20 ms later. The difference between the average neutron counts through the two gates gave the average number of neutrons detected per event for the gate length used. The choice of

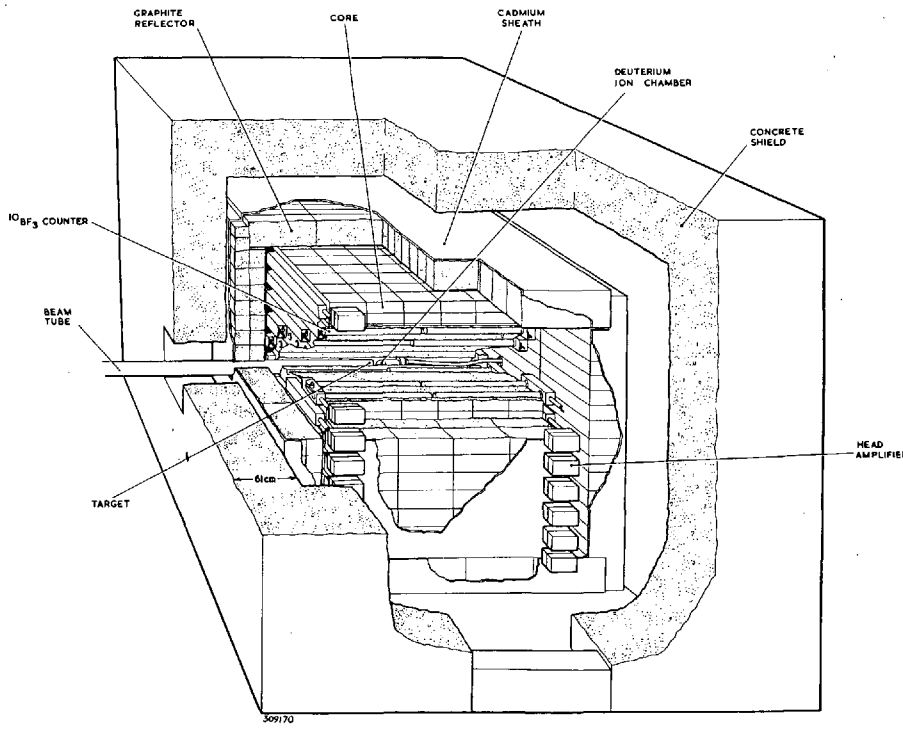

FIG.1. The boron pile

TABLE I. $\bar{R}'$ VALUES

Experiment	Neutron energy	$\bar{R}'$	Error (%)[a]
^{252}Cf Spontaneous fission	Fission	2.3811	0.11
^{235}U Thermal fission	Fission	1.5230	0.40
D(γ, n)p with ThC" γ-rays	190 keV	0.6440	0.60
D(γ, n)p with ^{24}Na γ-rays	265 keV	0.6457	0.21
D(γ, n)p with $^{19}F(p,\alpha,\gamma)$ γ-rays	2.0 MeV	0.6433	0.25
D(γ, n)p with $^{27}Al(p,\gamma)$ γ-rays	4.9 MeV	0.6500	1.24

[a] The errors quoted here do not include all errors in the experiment. For more details see reference [1].

gate length depended upon the experiment being performed; for a typical value of 4 ms approximately 4% of the neutrons were captured after the prompt gate had closed and the cosmic ray neutron background was 0.2 neutrons per gate.

Table I gives the corrected values of the average number of neutrons detected per event ($\bar{R}'$) for various experiments. It is assumed in [1]

that the variation of Pile efficiency as a function of neutron energy is as follows:

(i) Below 2 MeV it follows a straight line through the measurements at 2 MeV and 265 keV.

(ii) Above 2 MeV it follows a curve calculated by the Carlson Sn method which is normalized to the measurements at 2 MeV.

Figure 2 shows the experimental data, the calculated curve and a linear fit to the experimental data, as well as the ^{252}Cf fission neutron energy spectrum. The efficiency for this spectrum was found to be 0.6428 ± 0.0020. The error quoted is only true for a comparison of gated fission and photoneutron measurements and has to be increased when the efficiency is required for an experiment without gating.

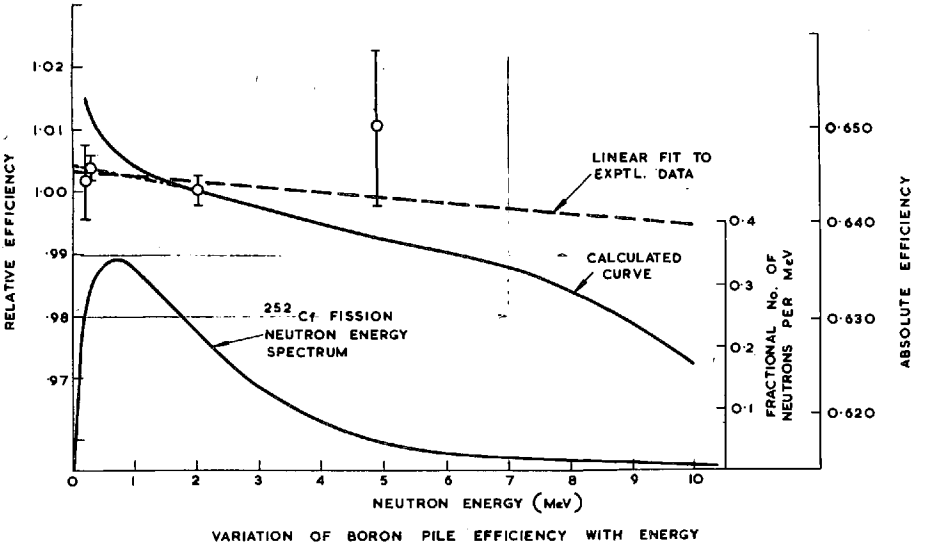

FIG.2. Variation of boron pile efficiency with energy

3. EFFICIENCY MEASUREMENTS USING STANDARD SOURCES

Three standard neutron sources have been counted in the Boron Pile, the Harwell ^{240}Pu spontaneous fission source [10], the Aldermaston ^{240}Pu spontaneous fission source [8] and a Ra-γ-Be source. The Harwell source was measured several times during the calibration of the Pile and the efficiency measurements quoted in the previous section were made when the average count of the Harwell source was 13 099 ± 12 counts per second. The other source counts were all made relative to the Harwell source so that all the measurements could be related to the D(γ, n)p efficiency determinations. It has recently been shown [5] that the spontaneous fission sources are increasing at an annual rate of 0.04% (Harwell source) and 0.1% (Aldermaston source) due to the increase in the (α, n) contribution to the source output. The results given in Table II, which gives the efficiency of the Boron Pile as determined from standard neutron sources, have been corrected for this effect. The values of A given in

the table are the factors by which the neutron output of a source is modified when put in the Pile.

The efficiency of the Pile for the Ra-γ-Be source (0.6475 ± 0.0048) should be the same as for neutrons of approximately 250 keV and so can be compared to the efficiency (0.6457 ± 0.0023) measured by using the D(γ, n)p reaction with ^{24}Na γ-rays (see Table I). The efficiency of the Pile for a ^{240}Pu fission spectrum obtained from sources is the mean of the following values:

(i) The efficiency (0.6433 ± 0.0105) determined using the reassessed Richmond and Gardner calibration [5] of the Harwell ^{240}Pu source. (The other efficiency measurements for this source are not independent of the AWRE ^{240}Pu source).

(ii) The efficiency (0.6459 ± 0.0057) determined using the AWRE ^{240}Pu source.

The result (0.6450 ± 0.0050) is to be compared to the value of 0.6428 ± 0.0028 obtained from D(γ, n)p measurements. (The errors quoted for D(γ, n)p measurements in this section include all the errors and have been increased from those given in Ref. [1] because the "ungated" efficiency is required). The results of the two sets of efficiency measurements are in good agreement and this suggests that (i) the efficiency measurements made by the D(γ, n)p reaction are correct and (ii) the procedures used to correct the raw data [1] are satisfactory. Table III gives the $\bar{\nu}$ values deduced from the efficiency measured by standard neutron sources.

4. CRITICISMS OF THE BORON PILE EXPERIMENT

One of the most important criticisms of the Boron Pile experiment is the possible anisotropy of the Pile efficiency. This could arise in two ways:

(i) The effect of the counter holes

(ii) Capture of neutrons in the dead spaces at the ends of the counters.

These two effects tend to cancel since in the first case the efficiency should be lower for neutrons in the direction of the lattice while in the second case the efficiency should be lower for neutrons emitted perpendicular to the lattice. (There are two counters per lattice hole so the most important dead spaces are midway along the holes).

The anisotropy of the Pile has been investigated by using the anisotropy of the deuterium photodisintegration reaction. Three experiments, which are described in Table IV, were done with ^{24}Na γ-rays. It can be seen that there is no evidence for anisotropy of efficiency for neutrons of 265 keV. No measurements were done at other neutron energies. However, the source counts described in the previous section provide supporting evidence for the view that the effect of any anisotropy is negligible. The very fact that the efficiencies obtained from source counts agree with those based upon the D(γ, n)p reaction suggests that there is no anisotropy. It might be argued that the N. P. L. calibrations are incorrect though this implies that the calibrations at the National Bureau of Standards in Washington, D. C., USA and at the National Research Council in Ottawa, Canada are also wrong. However, if one assumes they are in error, then it is likely that the calibrations of all the sources will be either high or low by the same percentage and the following argument will still be

TABLE II. BORON PILE EFFICIENCY OBTAINED FROM STANDARD NEUTRON SOURCES

Date	Source	Counts/sec	Ratio of efficiency when source counted to efficiency in 1962	Source strength at time of counting	A	Pile efficiency corrected to 1962
Mean of runs in 1962 while pile was being calibrated	AERE ^{240}Pu	13,099	1.000	1.990×10^4 (e) 2.006×10^4 (f)	1.015	0.6485 ± 0.0006 random 0.0046 systematic 0.6433 ± 0.0006 random 0.0104 systematic
8.4.64	AWRE ^{240}Pu	42,867	1.0012	6.560×10^4 (a) 6.499×10^4 (b)	1.011	Mean efficiency 0.6472 ± 0.0006 random 0.0058 systematic (a)
4.3.65	AWRE ^{240}Pu	42,803	0.9954	6.565×10^4 (a) 6.504×10^4 (b)		0.6412 ± 0.0006 random 0.0087 systematic (b)
23.3.65	AWRE ^{240}Pu	42,815	0.9957	6.565×10^4 (a) 6.504×10^4 (b)		0.6459 ± 0.0006 random 0.0056 systematic (d)
9.4.64	Ra-γ-Be Ra(α, n) Photoneutrons by subtraction	36,867 6,998 29,869	1.0012	4.610×10^4 (c)	0.9998	0.6475 ± 0.0010 random 0.0047 systematic

(a) Source calibrated by N.P.L. using $MnSO_4$ bath [8]
(b) Source calibrated by A.W.R.E. using oil bath [8]
(c) Source calibrated by N.P.L. using $MnSO_4$ bath [11]
(d) Mean of calibrations (a) and (b).
(e) Mean result of reassessed calibration [5] if Boron Pile data neglected.
(f) The original calibration of Richmond and Gardner as revised [5]

TABLE III. $\bar{\nu}$-VALUES

	$\bar{\nu}$ with pile efficiency measured by D(γ, n)p reaction	$\bar{\nu}$ with pile efficiency determined from standard sources
^{252}Cf	3.713 ± 0.015	3.700 ± 0.031
^{235}U	2.385 ± 0.015	2.377 ± 0.023
ratio	0.6423	

correct. For the anisotropy to cause an error in $\bar{\nu}$ the anisotropy must be a function of neutron energy. Thus it would be expected that the ratio of the efficiencies for 265-keV neutrons and for a fission neutron energy spectrum would be different for D(γ, n)p measurements and source measurements. (The neutrons in the D(γ, n)p efficiency measurements were predominantly emitted perpendicular to the Pile lattice). The values are 1.0045 and 1.0039 respectively again showing that the effect of any possible anisotropy is negligible. It is therefore concluded that the error of ± 0.2% in $\bar{\nu}$ assigned to this effect in Ref. [1] is reasonable.

The correction applied in the Boron Pile experiment for the neutrons captured after the closing of the "prompt" gate has been questioned. Table V shows for three typical experiments the results obtained, together with their statistical errors, when gate lengths of 2, 4 and 8 ms were used simultaneously. The 8-ms results require little correction; 4-ms gates were used for most of the experiments and 2-ms gates were only used when the signal-to-background in 2-ms was ⩾ 1. It can be seen that the 4- and 8-ms results agree so there is little error in the corrections. Therefore the error of 0.1% in $\bar{\nu}$ given in Ref. [1] for this correction is realistic particularly as any errors in the fission and D(γ, n)p measurements are likely to cancel out.

A possible source of error in this experiment is that fast neutrons produced inside either the fission chambers or the counters used in the photodisintegration experiments may be absorbed in the walls of the counters before they have a chance of entering the Pile. Simple calculations show, however, that a negligible fraction of neutrons are absorbed and so no correction for the effect is needed.

An error can occur in $\bar{\nu}$ measurements if some fissions are not observed because their fragments lose most of their kinetic energy in the layer of fissile material in the fission chamber. If these fissions emit on average a high or low number of neutrons per fission then the measurements of $\bar{\nu}$ will be in error. This effect was investigated experimentally and in Ref. [1] an error of ± 0.3% assigned to the ^{235}U measurements; for ^{252}Cf the error was found to be negligible.

The Boron Pile $\bar{\nu}$ results have been criticized because the values given in a provisional report [12] disagree with the final values [1]; the values for ^{235}U thermal fission being 2.420 ± 0.024 and 2.385 ± 0.015 respectively. The provisional report was issued before all the experimental data had been analysed and the $\bar{\nu}$-values given were based upon hand calculations of a small fraction of the available results. The fact that the $\bar{\nu}$-value was reduced by one and a half provisional standard errors to a value approximately 3 final standard errors lower than the previous

TABLE IV. RESULTS OF MEASUREMENTS MADE TO CHECK ANISOTROPY OF PILE EFFICIENCY

Experiment	Results (errors are those appropriate for making comparisons)	
Efficiency for a ^{24}Na γ-ray source axially in line with cylindrical counter compared with efficiency for the source under the counter	Efficiency (in line) = 0.6449 ± 0.0022	(Neutrons emitted predominantly in plane perpendicular to lattice)
	Efficiency (under) = 0.6456 ± 0.0016	(Neutrons emitted predominantly in a plane containing the lattice direction).
Efficiency measured with counter inside a long annulus of ^{24}Na	Efficiency = 0.6495 ± 0.033	(Neutrons emitted "isotropically")
Collimated ^{24}Na γ-ray source in the "key-hole" under the counter. Efficiency for photoprotons selected from peak in their pulse height distribution compared with photoprotons selected from tail of the distribution. The absolute efficiency is low in this experiment for experimental reasons	"Efficiency" (peak) = 0.6246 ± 0.0022	(Neutrons emitted predominantly in plane containing the lattice direction).
	"Efficiency" (tail) = 0.6227 ± 0.0066	(Neutrons emitted perpendicular to lattice).

TABLE V. THE NUMBER OF NEUTRONS DETECTED PER EVENT DEDUCED FROM GATES OF DIFFERENT LENGTH

Experiment	No. of neutrons detected per event[a]		
	2-ms gate	4-ms gate	8-ms gate
^{240}Pu spontaneous fission	1.3598 ± 0.0036	1.3582 ± 0.0028	1.3570 ± 0.0044
^{240}Pu spontaneous fission	1.3608 ± 0.0040	1.3567 ± 0.0050	1.3578 ± 0.0057
^{24}Na D(γ, n)p	0.6453 ± 0.0008	0.6491 ± 0.0009	0.6476 ± 0.0015
Typical correction required (%)	20.7	4.3	0.1

[a] The errors quoted are the statistical errors.

best value (2.430 ± 0.009)[13] means that the Boron Pile experiment cannot be criticized of the following disturbing practice quoted by Birge[14] (who credits the remark to E.O. Lawrence). "In any highly precise experimental arrangement there are initially many instrumental difficulties that lead to numerical results far from the accepted value of the quantity being measured... Accordingly, the investigator searches for the source or sources of such errors, and continues searching until he gets a result close to the accepted value. Then he stops..... In this way one can account for the close agreement of several different results and also for the possibility that all of them are in error by an unexpectedly large amount". It is not suggested that this practice occurs in accurate nuclear data measurements but evaluators of data should remember that it can occur. As far as the Boron Pile experiment is concerned the data obtained do not agree very well with previous values but no error can be found to explain the differences.

5. DISCUSSION

The results of the measurements of Boron Pile efficiency by using standard neutron sources agree very well with the values obtained by the associated particle technique and the results of the two measurements can be combined to give $\bar{\nu}$-values of 3.711 ± 0.013 (^{252}Cf) and 2.383 ± 0.014 (^{235}U). These values are slightly more accurate than the values (3.713 ± 0.015 and 2.385 ± 0.015) based upon the efficiency measurements using the associated particle technique. However, in the discussion which follows these latter results will be used because they are independent of other experiments (e.g. Moat et al.[4] who use sources for calibration.

The discussion of criticisms of the Boron Pile experiment in section 4 has not brought to light any new effects which make it necessary to modify the result of the experiment or its errors. Therefore the present situation regarding absolute $\bar{\nu}$-values is as follows.

(a) Three accurate values of $\bar{\nu}$ (^{252}Cf) (the accepted standard) have been made using the associated particle technique for calibration. The values are 3.808 ± 0.034 (Asplund-Nilsson et al. [3], 3.780 ± 0.030 (Hopkins and Diven [2]) and the Boron Pile value 3.713 ± 0.015.

(b) Another accurate value of 3.750 ± 0.028 has recently been obtained by De Volpi and Porges [6] by using a manganese sulphate bath.

(c) Moat et al.[4] obtained a value, which has recently been revised [5] to 3.684 ± 0.040, based upon the calibration of the Harwell ^{240}Pu spontaneous fission source.

(d) A value can be obtained from η and α data for ^{235}U combined with the $\bar{\nu}$-ratio for ^{235}U and ^{252}Cf. If the input data for η and α obtained by Westcott et al. [15] (2.0739 ± 0.0083 and 0.17332 ± 0.00086) is combined with their average value for the $\bar{\nu}$-ratio (0.6425 ± 0.0018) a value for $\bar{\nu}$ (^{252}Cf) of 3.787 ± 0.018 is obtained.

The mean value of the direct measurements (i.e. excluding (d)) is 3.736 ± 0.011 (internal error) ± 0.018 (external error). The internal consistency ratio is 1.67 which should be 1 ± 0.35 for this number of observations. Therefore, the spread in $\bar{\nu}$-measurements could still be due to statistical fluctuations. A more important discrepancy is the difference (0.072 ± 0.024) between the Boron Pile datum and that obtained from η and α measurements.

The fact that the absolute values of $\bar{\nu}$ obtained by the Boron Pile are lower than the values obtained with liquid scintillators and from η and α data while $\bar{\nu}$-ratios (see for example Table VII of Westcott et al. [15]) agree suggests that perhaps the Boron Pile efficiency measurements are incorrect. The source measurements described in section 3 do not support this.

6. CONCLUSIONS

The following conclusions can be made as a result of this paper:

(i) All known criticisms of the Boron Pile experiment have been considered but no reason has been found to change the $\bar{\nu}$-values obtained or their errors.

(ii) The efficiency of the Boron Pile has been measured with standard neutron sources and found to give a value close to that obtained with the associated particle technique.

(iii) The spread in direct $\bar{\nu}$-measurements is not significantly greater than that expected as a result of statistical fluctuations. The largest discrepancy is between the $\bar{\nu}$-values obtained by the Boron Pile and η and α measurements.

ACKNOWLEDGEMENTS

The authors wish to express their appreciation to Mr. E. J. Axton, N. P. L. and Messrs. P. Fieldhouse, D. Mather and E. R. Culliford of A. W. R. E. for the calibration of the standard neutron sources and for many helpful discussions. Mr. J. R. Johnson provided admirable

technical backing throughout the Boron Pile experiment and this is gratefully acknowledged.

REFERENCES

[1] COLVIN, D.W., SOWERBY, M.G., Physics and Chemistry of Fission 2 IAEA, Vienna (1965) 25.
[2] HOPKINS, J., DIVEN, B.C., Nucl.Phys. 48 (1963) 433.
[3] ASPLUND-NILSSON, I., CONDE, H., STARFELT, N., Nucl.Sci.Engng 16 (1963) 124.
[4] MOAT, A., MATHER, D.S., McTAGGART, M.H., Reactor Sci.Technol. 15 (1961) 102.
[5] FIELDHOUSE, P., CULLIFORD, E.R., MATHER, D.S., COLVIN, D.W., MACDONALD, R.I., SOWERBY, M.G., J.nucl.En. (Parts A/B) 20 (1966) 549.
[6] DE VOLPI, A., PORGES, K.G., private communication.
[7] AXTON, E.J., CROSS, P., ROBERTSON, J.C., J.nucl.En. (Parts A/B) 19 (1965) 409.
[8] FIELDHOUSE, P., CULLIFORD, E.R., MATHER, D.S., (1966) private communication of results to be published.
[9] STARFELT, N., private communication.
[10] RICHMOND, R., GARDNER, B.J., UKAEA Rep. AERE R/R 2097 (1957).
[11] AXTON, E.J., private communication.
[12] COLVIN, D.W., SOWERBY, M.G., unpublished (1963).
[13] SHER, R., FELBERBAUM, J., USAEC Rep. BNL-722 (1962).
[14] BIRGE, R.T., Nuovo Cimento, Suppl. 6 (1957) 39.
[15] WESTCOTT, C.H., EKBERG, K., HANNA, G.C., PATTENDEN, N.J., SANATANI, S., ATTREE, P.M., Atomic En.Rèv. 3 2 (1965) 3.

DISCUSSION

(on papers CN-23/40 and CN-23/33)

P. FIELDHOUSE: In connection with Dr. De Volpi's paper I should like to refer to the precise determination of $\bar{\nu}$ for ^{252}Cf recently performed by White at the Atomic Weapons Research Establishment (A. W. R. E.), Aldermaston, and by Axton at the National Physics Laboratory (N. P. L.), Teddington. Fissions from a thin ^{252}Cf foil were counted absolutely at A. W. R. E. to an accuracy of about 0. 8% and the neutron output of the same foil was determined to an accuracy of 0. 4% in an $MnSO_4$ bath at the N. P. L. The neutron yield per fission $\bar{\nu}$ given by the ratio of the respective neutron and fission counts can be seen to have an error of about 0. 9%. The provisional value obtained for total $\bar{\nu}$ is 3.798 ± 0.033.

Perhaps I should add that although this measurement is very similar to that reported here by Dr. De Volpi it is rather more direct in that the fissions were counted absolutely in contrast to Dr. De Volpi's work, in which, owing to about 40% loss of fissions, it was necessary to employ a fission-neutron coincidence technique.

A. DE VOLPI: To put this question of the "directness" of the extrapolation technique and the "necessity" of recourse to the coincidence method in perspective, it should be noted that the question, as it is discussed in our paper, is analogous to that of the extrapolation technique in 4π β-counting versus 4π β-γ-coincidence counting.

For our measurements with ^{235}U the extrapolation technique is not available because of the booster. For ^{252}Cf we used two chambers, one with 60% and another with 90% efficiency.

Our experience has made us circumspect with regard to extrapolation, although if a coating with over 99% apparent efficiency is available it is reasonable to expect the extrapolation to zero fragment thickness to be accurate.

One might suspect that the ultimate procedure for evaluation of $\bar{\nu}$ would consist of the fission count rate obtained from a large liquid scintillator or boron pile coincidence experiment, followed by an assessment of the neutron rate in a manganese bath.

P. H. WHITE: I would like to query the low efficiency for the counting of fission fragments quoted by Dr. De Volpi. It has been our experience at Aldermaston that fission fragments from thin foils can be counted with an efficiency of better than 99.5%. From an experimental point of view the efficiencies of 60% and 90% quoted by Dr. De Volpi would seem excessively low. From a theoretical point of view such a high bias may be biassing off part of the fragment energy spectrum since the value of ν is correlated with the fragment mass. Does this bias affect the value of $\bar{\nu}$ that is derived?

A. DE VOLPI: Our calculations indicate that this effect should have a magnitude not exceeding about 0.1% for a fission counter of 90% efficiency; this also coincides with the conclusions of Condé and Diven who have made experimental evaluations of $\bar{\nu}$ as a function of fission counter bias.

P. FIELDHOUSE: I have two small comments relating to values of $\bar{\nu}$ for ^{252}Cf and ^{235}U mentioned by De Volpi and Colvin. A figure of 2.373 ± 0.029 by Kenward and Sanders for thermal $\bar{\nu}_T$ ^{235}U was referred to by Dr. De Volpi in paper CN-23/40. This was taken from Westcott's recent 2200-m/s compilation and is a revision of the original Kenward value. In fact, further work subsequent to the above survey (see J. nucl. Energy 20 (1966) 549) shows that the finally revised value should be $\bar{\nu}_T = 2.370 \pm 0.014$.

The $\bar{\nu}$ value of 3.675 for ^{252}Cf by Moat et al. given by Dr. Colvin in the introduction to paper CN-23/33 is in fact the prompt emission. Since all the other figures given for comparison are for total $\bar{\nu}$ the Moat value should read 3.684 ± 0.040.

N. STARFELT: Dr. De Volpi mentioned the fragment-to-neutron correlation as a possible cause of error in the $\bar{\nu}$-measurements employing parallel plate fission chambers. In the case of ^{252}Cf this effect should be very small. Could he give an estimate of the magnitude of the expected error in $\bar{\nu}$?

A. DE VOLPI: The correlation between fragments and secondary neutrons has been reported to be upwards of 90% for ^{252}Cf. For a fission detector of 90% efficiency and a large liquid scintillator or boron pile with an effective neutron escape angle of 10-20°, this correlation is likely to cause the measured $\bar{\nu}$ to be increased by no more than 1/4 - 1/2%.

N. STARFELT: The work described by Dr. Colvin is, I think, to a large extent a result of the discussions which have taken place between the different groups of $\bar{\nu}$-measurers during the last few years. I would like to thank Colvin and Sowerby for the large amount of work they have done to clear up questions brought up at these discussions.

A. DE VOLPI: I want to say that I tend to agree with Dr. Colvin and his colleagues that present discrepancies in $\bar{\nu}$ may be due to statistical imprecision. Their examination of possible systematic errors is impressive. Nevertheless, there are two factors especially pertinent to coincidence measurements which require explicit comment, particularly since they both operate in such a way as to increase the reported $\bar{\nu}$ value.

The first concerns the angular correlation between fission fragments and secondary neutrons, and in this connection I want to ask what was the efficiency of the fission fragment detector used by Dr. Colvin and to what extent would the effective beam hole of the boron pile contribute to a reduced coincidence rate?

Second, aside from the measurements as a function of gate wid[illegible], what is the magnitude of the correction for the non-detection of m[illegible] neutrons from a single fission event? This factor is a function [illegible] neutron multiplicity distribution and applies only when a fracti[illegible] neutrons of a single fission event are lost.

D. W. COLVIN: The correction for correlation is extre[illegible] The solid angle for the fission counter inside the boron pile is [illegible] The holes are 4 in. in diameter and the pile is about 10 ft lon[illegible] have also filled up the hole with graphite, which the rest of th[illegible] consists of, and we find no effect.

MEASUREMENT OF AVERAGE CROSS-SECTION RATIOS IN FUNDAMENTAL FAST-NEUTRON SPECTRA

J. A. GRUNDL AND G. E. HANSEN
UNIVERSITY OF CALIFORNIA,
LOS ALAMOS SCIENTIFIC LABORATORY,
LOS ALAMOS, NEW MEXICO,
UNITED STATES OF AMERICA

Abstract

MEASUREMENT OF AVERAGE CROSS-SECTION RATIOS IN FUNDAMENTAL FAST-NEUTRON SPECTRA. Average cross-section ratios in basic critical systems persist as vital check-points for fast-reactor computations. Calculational methods for simple one-dimensional systems are hardly open to question today and the properties of elemental fast-neutron criticals are important guides to the use of microscopic data and provide crucial checks of their validity. Measurements reported here seek to improve the worth of spectral indices by comparing the responses of selected detectors in critical spheres of ^{235}U, ^{233}U, and ^{239}Pu to corresponding responses in fission-neutron spectra and in monoenergetic beams. Major emphasis is placed on identifying and evaluating sources of error in order to facilitate tests of microscopic data.

The critical spheres are the long-studied family of Los Alamos fast-critical assemblies that include both bare and natural-uranium-reflected versions. The detector reactions, a conventional but restricted set, possess some of the more reliable excitation functions and test the main features of the fast-neutron distributions involved. They may be grouped as follows:

Low energy	- $In(n,\nu)$, $^{235}U(n,f)$
Intermediate energy	- $Np(n,f)$, $^{238}U(n,f)$
High energy	- $P(n,p)$, $Al(n,p)$, $^{56}Fe(n,p)$, $Al(n,\alpha)$, $^{63}Cu(n,2n)$.

Recommended excitation functions and uncertainties for each reaction are presented in coarse group-structures appropriate for computational checks. They are based on existing cross-section information supplemented by monoenergetic measurements performed at the Los Alamos Van de Graaff accelerator.

Fission detector responses are obtained from fission ionization chambers and activation techniques, both of which give average fission cross-section ratios based on monoenergetic calibration. The comparison of the ^{235}U, ^{233}U, and ^{239}Pu fast-criticals with corresponding thermal-fission-neutron spectra reveals the two inelastic scattering cross-sections for each fissile material which describe the energy-transfer of neutrons to below the response range of the $Np(n,f)$ and $^{238}U(n,f)$ detectors. The same comparisons with the high-energy detectors show a well-preserved fission-neutron spectrum above 2 MeV.

1. INTRODUCTION

Microscopic cross-sections used to describe direction- and energy-transfer in fast-neutron transport computations are far from complete, of varying precision, and often in conflict, even for the primary fissile materials. Basic fast-critical assemblies therefore provide a necessary bridge between disparate information and design requirements for functional chain-reacting systems. The Pajarito Critical-Assemblies Laboratory at Los Alamos has maintained a continuing effort to achieve precise experimental and computational understanding of an important set of elementary critical systems: bare and natural-uranium reflected ^{235}U, ^{233}U, and ^{239}Pu critical spheres [1]. Calculational methods for such one-dimensional systems are well-established so that measured

properties test directly the detailed information provided by microscopic measurements. This report presents spectral indices, as known today, for the neutron spectra at the centre of these critical spheres.

Spectral indices – energy-sensitive average cross-section ratios – are simple to measure in principle, but to be of value must be determined to an overall accuracy of a few percent. Error evaluation, therefore, must be of major concern. Since interpretation of spectral indices for any system inevitably involves comparisons with the same indices for still simpler spectra, it is appropriate to orient the error evaluation by looking upon these measurements as spectral comparisons. By means of energy-sensitive nuclear reactions, the six fast-critical assembly spectra are compared, (1) among themselves, (2) to corresponding fission-neutron spectra, and (3) to neutrons of a single energy. Experimental errors then depend upon reproducibility of detecting systems, spectral distortions due to the presence of detecting systems, and purity of the monoenergetic and fission neutrons. To establish comparisons with computed spectral indices there remains only the uncertainty in detector excitations. Recommended excitation functions and estimated uncertainties for each reaction will be presented in coarse group-structures appropriate for computational checks. They are based on existing cross-section information supplemented by monoenergetic measurements performed at the Los Alamos Van de Graaff accelerator. The observed spectral indices and detector excitations together with their uncertainties provide a set of values that must be met by the microscopic cross-sections for ^{235}U, ^{233}U, and ^{239}Pu via transport computation.

2. FISSION DETECTORS

Responses of the three common fission detectors, $^{235}U(n, f)$, $Np(n, f)$ and $^{238}U(n, f)$, have been obtained at the centres of all six fast-criticals. Additional fission detectors have been employed, but useful information from them cannot be expected until more accurate excitation functions become available. Two techniques have been applied systematically: fission comparisons by means of quadruple ionization counters, and an activation method that employs gross beta-gamma counting of irradiated disks. Both methods compare the fast-critical spectra to mono-energetic "spectra", while the activation method alone was used for the comparison with corresponding fission-neutron spectra.

2.1. Fission ionization chambers

The quadruple fission-comparison chambers were designed and measurements performed by G. A. Jarvis and D. M. Barton (see Ref. [2]). Four fission counters in a $\frac{1}{2}$ in. $\times \frac{1}{2}$ in. cylindrical enclosure present well-resolved pulse-height distributions with 2-3% of the fission pulses below the α-pulse cut-off. Consistent extrapolations to zero pulse height were such that the error from this source should not exceed a few tenths of one percent. Isotopic composition of the fissionable deposits were as follows: for ^{235}U, 99.1 ±0.02% ^{235}U, 0.346 ±0.01% ^{234}U, and 0.552 ±0.01% ^{238}U; for ^{238}U, normal and depleted uranium (140 000 : 1); for ^{237}Np, negligible fissionable impurities. Corrections for isotopic composition, generally less than 1% but as high as 5% for normal uranium, contribute a few tenths of one percent to the uncertainty of interassembly comparisons.

TABLE I. CORRECTIONS FOR DISTORTION OF CENTRAL SPECTRAL INDICES BY FISSION CHAMBER AND CAVITY

Detector ratios	^{235}U sphere bare	^{235}U sphere refl.	^{233}U sphere bare	^{233}U sphere refl.	^{239}Pu sphere bare	^{239}Pu sphere refl.
$\frac{^{235}U(n,f)}{^{238}U(n,f)}$	-1.7%	-3.0%	-1.8%	-4.3%	-2.0%	-4.5%
$\frac{Np(n,f)}{^{238}U(n,f)}$	-0.8%	-1.3%	-0.9%	-1.6%	-0.9%	-1.7%

Cylindrical cavity, $\frac{1}{2}$ in. diam × $\frac{1}{2}$ in. long; chamber material equivalent, 3 g/cm^3 iron.

Reproducibility of measurements in the fast-criticals was routinely better than ± $\frac{1}{2}$% – the average deviation from the mean of fifty counter response ratios at the centre of the six assemblies was ± $\frac{1}{4}$%. Somewhat larger errors are introduced by the spectral distortions due to the chamber cavity containing structural elements of the counter. Perturbation calculations [3] furnished the correction factors for this distortion and are shown in Table I. Errors associated with spectral distortions (estimated standard deviation) are ± $\frac{1}{2}$%.

The fission chambers were calibrated with 2.43 ± 0.18 MeV neutrons from the Los Alamos Van de Graaff accelerator[1] to provide the present basis for fast-critical spectral indices derived from fission counters. This calibration effort was less exhaustive than the fast-critical work and larger errors arise:

	maximum error
Correction for distortion of the neutron beam by chamber materials	± 1$\frac{1}{2}$%
Correction for fissionable impurities	± $\frac{1}{2}$%
Correction for neutron backgrounds (estimated by check of inverse-square, also Ref. [4])	± 1$\frac{1}{2}$%
Reproducibility, pulse-height extrapolation, and energy uncertainty	± 1 %

Total experimental uncertainties have been set at 2$\frac{1}{2}$%.
Values chosen for the cross-section ratios at 2.43 MeV are based on the results of Stein et al. and Smith and Balagna [4] and of Jarvis [5]:

$$\frac{\sigma(^{235}U)}{\sigma(^{238}U)} = \frac{2.5\ \text{MeV}}{2.37 \pm 1\frac{1}{2}\%} \qquad \frac{2.0\ \text{MeV}/2.5\ \text{MeV}}{1.04_2 \pm 1\%}$$

$$\frac{\sigma(^{237}Np)}{\sigma(^{238}U)} = 3.14 \pm 2\% \qquad 1.02_6 \pm 1\%$$

[1] Also carried out at this time were calibrations of ^{235}U, Np and ^{238}U spiral fission chambers which were employed in earlier fast-critical measurements [1]. Though spiral measurements are incomplete for the fast-criticals, and of somewhat poorer precision overall, they agree with the quadruple fission chamber results to within the error structure of Table II, Part A.

TABLE II. VALUES OF CENTRAL SPECTRAL INDICES FOR ELEMENTAL FAST-CRITICAL ASSEMBLIES FISSION DETECTORS

Detector ratios	Method	^{235}U Flattop-25	^{235}U Godiva	^{233}U Flattop-23	^{233}U Jezebel-23	^{239}Pu Flattop-49	^{239}Pu Jezebel-49	Uncertainties (%) Inter-comparison	Monoenergetic calibration exp	Monoenergetic calibration σ
Part A: Spectral indices based on monoenergetic calibration[a]										
$\frac{^{235}U(n,f)}{^{238}U(n,f)}$	Fission chamber	6.86	6.18	5.35	4.80	5.69	4.77	0.6	2½	1½
	Activation	6.78	6.24	5.32	4.71	5.61	4.71	0.9	3	2
$\frac{Np(n,f)}{^{238}U(n,f)}$	Fission chamber	5.31	5.25	4.82	4.78	4.82	4.69	0.7	2½	2
	Activation	5.17	5.14	4.72	4.59	4.72	4.49	0.9	3	2
Part B: Spectral indices relative to corresponding fission-neutron spectra								Fission spectra[c]		
$\frac{^{235}U(n,f)}{^{238}U(n,f)}$	Activation	1.76 ± 0.10	1.62 ± 0.09	(1.38 ± 0.08)[b]	(1.22 ± 0.07)[b]	1.48 ± 0.08	$1.24_5 \pm 0.07$	$\frac{^{235}U}{1.000}$ $(3.85 \pm 6\%)$	$\frac{^{233}U}{-}$	$\frac{^{239}Pu}{0.98_5}$
$\frac{Np(n,f)}{^{238}U(n,f)}$	Activation	$1.23_2 \pm 0.02_5$	$1.22_5 \pm 0.02_5$	$1.13_2 \pm 0.02$	$1.10_0 \pm 0.02$	$1.15_9 \pm 0.02$	$1.10_2 \pm 0.017$	1.000 $(4.20 \pm 3\frac{1}{2}\%)$	0.994	0.971

Designation of fast-criticals: "Flattop" series are 8-in. normal uranium-reflected critical spheres; Godiva and Jezebels are the unreflected versions [1]. Nominal composition of the critical spheres: ^{235}U(94% ^{235}U), ^{233}U(98.1% ^{233}U), ^{239}Pu(95-98% ^{239}Pu).

a Ionization chambers are calibrated at 2.43 MeV [$\sigma_f(^{235}U)/\sigma_f(^{238}U) = 2.37$; $\sigma_f(Np)/\sigma_f(^{238}U) = 3.14$]. Activation detectors are based on monoenergetic excitation measurements normalized at 2.75 MeV [$\sigma_f(^{235}U)/\sigma_f(^{238}U) = 2.34$; $\sigma_f(Np)/\sigma_f(^{238}U) = 3.15$]. See Refs. [4, 5]. Errors apply respectively to fast-critical intercomparison, to calibration experiments, and to cross-section ratios at the calibration energy.

b Measurements in the ^{233}U fission spectrum do not exist; values for the ^{235}U fission spectrum are substituted.

c Ratios of spectral indices among fission spectra, spectral indices for ^{235}U fission neutrons in parentheses. [8]

Fission chamber results for the six fast-criticals are presented in Part A of Table II. Three sets of errors are listed separately and apply, in order, to intercomparisons among the fast-criticals, to calibration experiments with monoenergetic neutron beams, and to cross-section ratio values at the calibration energy. An rms sum of the first two yields the uncertainty applicable to computational checks based on detector excitations given in section 5.1; a further rms sum with the remaining calibration error (σ) yields the total error for the spectral indices as average cross-section ratios.

2.2. Gross counting of induced activity

The activation method is the second main technique for measuring spectral indices. The method has been described in detail elsewhere [6, 7], and its application to fast-criticals, as reported below, presents few additional problems. Detector disks are 0.4-in. diameter aluminium or nickel cans a few mils thick containing about 0.1 g of the fissionable material. After irradiation, gross beta-gamma counting of fission-fragment activity is carried out with thin-window, methane-flow counters operated in the region of limited proportionality. With strict attention to procedural details, a fixed counting scheme, and computer data processing, reproducibility for fission detector responses is better than ±1%. Corrections for isotopic composition important only for the ^{235}U material (5.3% ^{238}U, 1.2% ^{234}U, 93.5% ^{235}U) are in the vicinity of 2% for the fast-critical spectra; precision is $\pm\frac{1}{2}$%. Cavity perturbations for detector-response ratios are similar in magnitude to those for the fission chambers, but are complicated by a wide variation in cavity size ($\frac{1}{2}$-in. diam. × 0.1 - 0.4 in. long), by disk materials, and by disk stacking order. A three energy-group perturbation calculation provided the basis for correction. With uncertainties set at 20% of each applied correction, the errors for interassembly comparison are generally less than $\pm\frac{1}{2}$%. Additional considerations for the assignment of errors to individual detector responses are as follows:

activity of aluminium and nickel cans	< 0.2%
capture activities	
- ^{238}U detector	< 0.3%
- Np detector	< 0.4%
approximation of fission-product decay by a power law	± 0.3%
uncertainty due to natural background activity in Np	± 0.5% (max.)
uncertainty in counter dead-time loss	± 0.3%
uncertainty in detector disk positioning in counter	± 0.5% (max.)
counting statistics	± 0.1 - 0.3%

Monoenergetic measurements by the activation method are described in Refs. [6, 7]. Fission-detector responses were normalized at 2.75 ± 0.18 MeV to cross-section ratios that are consistent with Refs. [4, 5]. Experimental uncertainties for these measurements are ±3%, and arise principally from flux gradients over the detector disks. Errors in cross-section ratios at 2.75 MeV are judged to be 2% for both $\sigma_f(^{235}U/\sigma_f(^{238}U)$ and $\sigma_f(^{237}Np)/\sigma_f(^{238}U)$.

TABLE III. CENTRAL SPECTRAL INDICES FOR ELEMENTAL FAST-CRITICAL ASSEMBLIES RELATIVE TO CORRESPONDING FISSION-NEUTRON SPECTRA – HIGH-ENERGY DETECTORS

Detector ratios	^{235}U		^{233}U		^{239}Pu		Fission spectra[a]		
	Flattop-25	Godiva	Flattop-23	Jezebel-23	Flattop-49	Jezebel-49	^{235}U	^{233}U	^{239}Pu
$\frac{^{238}U(n, f)}{P(n, p)}$	$1.02_2 \pm 0.02_1$	$1.01_8 \pm 0.02_5$	$1.03_8 \pm 0.03_2$	$1.02_6 \pm 0.02$	$1.01_5 \pm 0.02$	$1.01_5 \pm 0.01_6$	1.000	0.976 ± 0.009	0.979 ± 0.009
$\frac{P(n, p)}{Al(n, p)}$	$0.986 \pm 0.01_5$	0.980 ± 0.02	$0.983 \pm 0.02_5$	$0.987 \pm 0.01_7$	$0.984 \pm 0.01_7$	0.984 ± 0.02	1.000	0.966 ± 0.009	0.933 ± 0.009
$\frac{P(n, p)}{^{56}Fe(n, p)}$	0.991 ± 0.02	$0.978 \pm 0.02_5$	0.977 ± 0.03	0.979 ± 0.02	0.968 ± 0.02	$0.968 \pm 0.01_5$	1.000	0.956 ± 0.010	0.898 ± 0.010
$\frac{P(n, p)}{Al(n, \alpha)}$	$0.976 \pm 0.02_5$	0.971 ± 0.03	0.970 ± 0.03	$0.972 \pm 0.02_5$	$0.959 \pm 0.02_2$	$0.959 \pm 0.02_2$	1.000	0.947 ± 0.010	0.868 ± 0.010
$\frac{P(n, p)}{^{63}Cu(n, 2n)}$	0.974 ± 0.03	0.974 ± 0.04	0.990 ± 0.03	0.989 ± 0.03	0.963 ± 0.03	0.952 ± 0.03	1.000	0.931 ± 0.014	0.762 ± 0.016

Designation of fast-criticals: "Flattop" series are 8-in. normal uranium-reflected critical spheres; Godiva and Jezebels are the unreflected versions [1].

[a] Ratios of spectral indices among fission spectra [6, 8].

Activation detector results based on the exposure to monoenergetic neutrons are presented in Table II, Part A. A triplet of errors is assigned and bears the same significance as with the fission chamber results.

The important data supplied by the activation detectors are from the comparison of neutron spectra at the centre of the fast-critical spheres with corresponding fission-neutron spectra. Measurements in the thermal-neutron-induced, fission-neutron spectra of ^{235}U, ^{233}U, and ^{239}Pu have been described [6, 8], and we mention here only the two conspicuous problems which influence the comparison with the fast-criticals. First, uncertain flux gradients across the detector disks during exposure to fission neutrons yield errors larger than those assigned to cavity perturbations above, and second, low-energy neutron backgrounds introduce a 4 to 5% uncertainty in the fission-neutron response of the $^{235}U(n, f)$ detector.

Ratios of spectral indices, fast-critical to corresponding fission-neutrons spectra, are presented in Table II, Part B. Also included are intercomparisons of fission spectra, and spectral indices for ^{235}U fission neutrons from Ref. [8].

3. HIGH-ENERGY DETECTORS

Measurements in fast-criticals and in fission-neutron spectra also made use of five high-energy activation detectors: P(n, p), Al(n, p), $^{56}Fe(n, p)$, Al(n, α), and ^{63}Cu (n, 2n). The general application of these detectors and responses to monoenergetic neutrons have been reported [6, 7, 9]. Problems of background and isotopic composition are not significant, with the exception of $^{63}Cu(n, 2n)$, but cavity perturbations in the fast-criticals and flux gradients in the fission-neutron source-detector arrangement remain important. Reproducibility with the high-energy detectors is in the range 1-3%. Other influences on the primary activities are listed below along with estimated errors:

P(n, p):	capture activity		± 0.2%
	aluminium case activity	1	± 0.1%
Al (n, p):	capture activity	0.6	± 0.3% (max)
	Al(n, α) activity	15	± 0.3% (max)
	saturation effects due to irradiation time-profile uncertainty	<	± 0.5%
^{56}Fe (n, p):	capture activity of copper impurity	1.5	± 0.2% (max)
Al (n, α):	counting statistics		± 0.5%
^{63}Cu (n, 2n):	^{63}Cu capture activity	8-50	± 0.3 - 0.6%
	^{65}Cu capture activity	1-20	± 0.3 - 0.6%

Ratios of spectral indices, fast-critical to corresponding thermal-neutron induced fission-neutron spectra, appear in Table III. Fission spectra comparisons from Ref. [6] are included and make it possible to form intercomparison ratios among the fast-criticals without reference to the corresponding fission source spectra. The error for such a double ratio is roughly one-half of the highest of the two relevant errors listed in Table III.

TABLE IV. CENTRAL SPECTRAL INDICES FOR REFLECTED FAST-CRITICAL SPHERES – IODINE DETECTOR

Detector ratio	Flattop-25	Flattop-23	Flattop-49	Uncertainties (%) Inter-comparison	Uncertainties (%) Monoenergetic calibration (exp)
$\frac{I(n,\gamma)}{^{235}U(n,f)}$	0.0976	0.082_3	0.090_0	2	$3\frac{1}{2}$

4. IODINE CAPTURE DETECTOR

About half of the neutron flux in the fast-criticals lies below 0.8 MeV. This portion of the spectrum is poorly known and to gain some experimental knowledge over the single datum given by the $^{235}U(n,f)$ detector, we introduce in this paper an additional low-energy detector, the capture reaction in iodine. This particular low-energy detector is chosen almost entirely because of an abundance of cross-section information in the literature which gives promise of an excitation function that is reliable and relevant.

The experimental application of iodine is uncomplicated: detector disks containing 106 mg of lead iodide powder yield the 25-min capture activity with interference only from the activities in the aluminium can. These activities are monitored directly by means of the aluminium detector and contribute less than 1% to the iodine response uncertainty. Monoenergetic calibration of iodine against $^{235}U(n,f)$ was carried out at 1.40 ± 0.17 MeV with an experimental uncertainty of $\pm 3\frac{1}{2}$%. Additional activation measurements at seven energies above 1 MeV agree generally with the shape reported by Johnsrud et al. [10] and give a new high-energy value of 5 ± 1 mb at 7.50 ± 0.15 MeV. A fission spectrum response for iodine does not exist. As with the $^{235}U(n,f)$ detector, the preparation of a sufficiently pure fission spectrum for such a low-energy detector presents serious difficulties.

At present, iodine detector responses are available only for the reflected critical spheres. Spectral indices with respect to the $^{235}U(n,f)$ detector are given in Table IV followed by two uncertainties, the first applicable to fast-critical intercomparison and the rms sum of both applicable to computational checks.

5. INTERPRETATION

5.1. Specification of detector excitations

Successful interpretation of observed spectral indices requires accurate but not necessarily high resolution detector excitation functions. Activation measurements tailored to this requirement have been made at the Los Alamos Van de Graaff accelerator where irradiations of the detector set at 18 different energies between 1.7 and 10 MeV sampled

TABLE V. MEAN DETECTOR RESPONSE ENERGY AND RESPONSE RANGE FOR THE ^{235}U FISSION SPECTRUM

Detector	Mean response energy[a] (MeV)	Response range[b] (MeV)
Np(n, f)	1.9	0.80 - 4.3
^{238}U(n, f)	2.7	1.6 - 5.5
P(n, p)	3.7	2.4 - 6.0
Al(n, p)	5.8	3.7 - 8.5
^{56}Fe(n, p)	7.4	5.8 - 10.2
Al(n, α)	8.5	6.9 - 11.2
^{63}Cu(n, 2n)	13.7	12.3 - 16.4

[a] Equal detector response occurs above and below the mean response energy.

[b] Energy range which encompasses 80% of the response with equal exclusion above and below the end-points.

the detector excitations relative to ^{238}U(n, f) [7]. Beam-energy spreads were in the range 200 to 500 keV, and calculations of their shape allow the activation data to be used as constraints in the evaluation of existing cross-section information.

The specifications of detector excitations, except that of iodine, are given in Ref. [7] accompanied by a brief outline of the evaluation leading to them. Two simple characterizations are presented here. The first, in Table V, is a mean response energy for ^{235}U fission neutrons,

$$\overline{E} = \frac{\int E\sigma(E)\chi_{25}(E)dE}{\int \sigma(E)\,\chi_{25}(E)\,dE}$$

and an energy interval that encompasses 80% of the fission-spectrum response. The second, in Table VI, is a seven-group display proper to the structure of the excitations and suitable for simple and flexible methods of spectrum extraction: specifically, for each detector and a Maxwellian description of the ^{235}U fission spectrum, Table VI lists (1) fission-spectrum weighted excitation function values within each energy group (σ_i), (2) estimated uncertainties, and (3) the fraction of the response in each group (r_i). Underlined group-values designate the interval within which the excitation was normalized to a cross-section scale and the detector calibrated. Uncertainty for an underlined or normalization group-value arises from the excitation shape within the group and in no way assesses

TABLE VI. DETECTOR EXCITATION FUNCTIONS IN A SEVEN-GROUP STRUCTURE

Energy groups				^{235}U(n, f)		^{237}Np(n, f)		^{238}U(n, f)		P(n, p)		Al(n, p)		^{56}Fe(n, p)		Al(n, α)		^{63}Cu(n, 2n)	
No.	Range	$\bar{E}_i$[a]	Group flux[b]	σ_i(mb)[c]	r_i[d]	σ_i(mb)	r_i	σ_i(mb)	r_i	σ_i(mb)	r_i	σ_i(mb)	r_i	σ_i(mb)	r_i	σ_i(mb)	r_i	σ_i(mb)	r_i
1	0 - 0.60	0.34	0.1818	1426 ± 7%	0.20	207 ± 20%	0.03	(0.18)		0		0		0		0		0	
2	0.60 - 1.4	0.99	0.2803	1233 ± 6%	0.26	1346 ± 5%	0.28	25 ± 30%	0.03	0		0		0		0		0	
3	1.4 - 2.2	1.78	0.2053	1270 ± 5%	0.21	1690 ± 3%	0.27	410 ± 4%	0.31	7.7 ± 50%	0.07	0		0		0		0	
4	2.2 - 3.0	2.57	0.1333	1205 ± 3%	0.14	1620 ± 2%	0.17	510 ± 2%	0.25	56.9 ± 6%	0.24	0.21 ± 50%	0.01	0		0		0	
5	3.0 - 6.0	4.0	0.1737	1140 ± 6%	0.16	1510 ± 5%	0.21	525 ± 3%	0.33	106.8 ± 12%	0.58	11.6 ± 10%	0.54	0.82 ± 8%	0.13	0.045 ± 30%	0.01	0	
6	6.0 - 11.0	7.3	0.0249	1470 ± 6%	0.03	1920 ± 10%	0.04	855 ± 4%	0.08	134 ± 10%	0.11	63.3 ± 8%	0.43	35.2 ± 6%	0.81	25.2 ± 6%	0.88	0	
7	11.0 - ∞	11.8	0.00070	1700		2140		960		119		84.5 ± 20%	0.02	100 ± 15%	0.06	112.5 ± 10%	0.11	175 ± 8%	1.00

[a] Mean group energy $\bar{E}_i = \int_{\Delta E} E\chi(E)dE / \int_{\Delta E} \chi(E)dE$.

[b] Maxwellian approximation to the ^{235}U fission spectrum: $\chi_{25}(E) = 0.771\sqrt{E}\exp(-0.775\,E)$.

[c] Group cross-section in mb weighted according to $\chi_{25}(E)$.

[d] Fraction of fission spectrum response in each group.

the choice of cross-section scale; other uncertainties are relative to the normalization group-value.

The excitation function for the iodine capture detector was obtained in the following manner. Four I(n, γ) cross-section measurements in the energy range above 200 keV [10-13], all of them relative to $^{235}U(n,f)$, were normalized to 80 mb at 1 MeV. Three additional measurements at lower energies [14-16] were joined to the normalized values [11-13] around 200 keV. These experimental results establish an excitation function between 0.017 and 10 MeV and uncertainties from the spread of the data. A cursory extension to below 17 keV was made on the basis of data from Ref. [17]. Table VII presents the iodine excitation in an eleven-group summary weighted within each group according to the spectral function,

$$N(E) = \left[1 + \frac{q}{2}\right]^{-2} \left[\chi(E) + q\alpha^2 E e^{-\alpha E} + 20\, q^2 E e^{-9E}\right] \qquad (1)$$

$$\alpha = 3.6\, q^{0.21};\ q = 0.63,$$

where $\chi(E)$ is the Maxwellian approximation to the ^{235}U fission spectrum: $0.771\, E^{\frac{1}{2}} \exp(-0.775\, E)$. Equation (1) provides a description of the central Flattop-25 spectrum that matches six-group DSN computations to within 10% [18]. More generally, for energies above 100 keV, this one-parameter expression is consistent with detailed transport computations for equilibrium spectra in enriched uranium ($0.5 < q < 4$ for enrichments between 100% and 6%). Interpretation of Table VII is entirely similar to that of Table VI, and, for comparison, includes the $^{235}U(n,f)$ detector excitation also weighted according to Eq. (1).

5.2. Some implications of measured spectral indices

A thoroughgoing correlation between computational bases and measurement – spectral indices, critical masses, prompt-neutron lifetimes, and reactivity coefficients – is not within the outline of this report. Some implications for our basic fast-criticals, however, may be obtained directly from the spectral indices.

5.2.1. Fission spectrum component

The high-energy detector results in Table III show that for all of the fast-criticals the fission-neutron source spectra are well-preserved above about $2\frac{1}{2}$ MeV. The mild but consistent hardening of the fission spectrum components relative to their thermal-neutron-induced counterparts is in the direction suggested by Terrell's theory of fission-neutron emission [19], but of smaller magnitude. The spectral index $P(n,p)/^{63}Cu(n,2n)$ in Table III, for example, shows less than half of the departure from unity expected for the fast-neutron-induced fission spectra appropriate for the fast-criticals.

5.2.2. Inelastic transfer cross-sections

Spectra in the unreflected fast-critical spheres are nearly independent of spatial position and but little affected by the mild energy dependence of

TABLE VII. EXCITATION FUNCTIONS FOR LOW-ENERGY DETECTORS

Energy division	Approximate Flattop-25 spectrum[a]	I(n, γ) detector σ_i(mb)[b]	I(n, γ) detector r_i[c]	^{235}U(n, f) detector σ_i(mb)	^{235}U(n, f) detector r_i
0.0					
	0.0018	(1843)	0.025	(3398)	0.005
0.017					
	0.0063	1035 ± 15%	0.049	2468 ± 15%	0.012
0.04					
	0.0296	560 ± 10%	0.124	1976 ± 10%	0.044
0.10					
	0.0683	324 ± 8%	0.166	1615 ± 10%	0.083
0.20					
	0.1437	197 ± 7%	0.211	1396 ± 8%	0.150
0.40					
	0.1238	135 ± 6%	0.125	1248 ± 7%	0.115
0.60					
	0.1420	103.4 ± 5%	0.110	1198 ± 6%	0.127
0.90					
	0.1527	76.9 ± 3%	0.088	1256 ± 5%	0.143
1.4					
	0.2164	55.3 ± 5%	0.090	1261 ± 4%	0.214
3.0					
	0.1007	16.3 ± 5%	0.012	1140 ± 6%	0.090
6.0					
	0.0146	3.9 ± 15%	(0.000_4)	1476 ± 6%	0.017
∞					

[a] Group-flux according to Eq. (1)

[b] Group cross-sections weighted according to Eq. (1)

[c] Fraction of the detector response in each group for the approximate Flattop-25 spectrum.

transport and absorption cross-sections. Departures from virgin fission neutron spectra are due primarily to inelastic scattering, and it is useful to define two parameters which describe the net inelastic transfer of neutrons out of the detector response ranges of ^{238}U(n, f) and Np(n, f) [1].

Spectral index ratios S[x, $^{235}U(n,f)/^{238}U(n,f)$] and S[x, $^{235}U(n,f)/Np(n,f)$] for an unreflected fast-critical of isotope x, relative to its fission spectrum source (Table II, Part B), imply inelastic transfer cross-sections σ_{in}[x, $^{238}U(n,f)$] and σ_{in}[x, Np(n, f)] according to the relation,

$$S[x, {}^{235}U(n,f)/\beta] = 1 + \mu_1(x,\beta) + \mu_2(x,\beta)\frac{\sigma_{in}(x,\beta)}{(\overline{\nu\sigma_f})_x}$$

where $\nu\sigma_f$ is averaged over the spectrum of the fast-critical, μ_1 is a calculated correction for energy-dependent absorption and transport [μ_1 ($^{235}U, \beta$) $\simeq$ 0.007 to 0.02; μ_1 ($^{233}U, \beta$) $\simeq$ 0.008; μ_1 ($^{239}Pu, \beta$) $\simeq$ 0.04 to 0.07], and μ_2 is a calculated quantity which exceeds unity due to the enhanced response of the ^{235}U fission detector for inelastically scattered neutrons [$\mu_2(x, {}^{238}U(n,f)) \simeq 1.09$; $\mu_2(x, Np(n,f)) \simeq 1.20$].

Derived values of the inelastic transfer cross-sections in barns are listed below, accompanied by uncertainties due to the experimental errors of Table II, Part B:

$\frac{\beta}{^{238}U(n,f)}$: x:	$\frac{^{235}U}{1.7 \pm 0.2_5}$	$\frac{^{233}U}{1.0 \pm 0.3}$	$\frac{^{239}Pu}{0.8_5 \pm 0.3_5}$
Np(n, f):	$0.8_0 \pm 0.2$	$0.4_5 \pm 0.2_5$	$0.4_0 \pm 0.2_5$

Uncertainties in the computational adjuncts, $\nu\sigma_f$, μ_1 and μ_2, do not contribute significantly to the uncertainties. Smaller errors for these transfer cross-sections must await a better measurement of the $^{235}U(n,f)$ detector response to fission neutrons. Even so, the results materially supplement existing information on inelastic scattering for the fissile isotopes.

5.2.3. Low-energy spectral component

In the spectra of the reflected fast-criticals one-half of the iodine detector response is below about one-third MeV, and the average cross-section is some 50% greater than its computed value for the ^{235}U fission spectrum. By contrast, the mid-response energy for the ^{235}U (n, f) detector is nearly 1 MeV and the average cross-sections in fission spectra and fast-criticals are nearly the same. Thus, the spectral index $I(n,\gamma)/^{235}U(n,f)$ is an excellent computational check of the inelastic transfer into the lowest region of the spectrum, and, for the reflected systems, of the neutron return from the normal-uranium.

Transport computations based on the cross-section sets of Hansen and Roach [20] yield six-group spectra which, when combined with the excitations of Table VII, give the following computed spectral indices at the centres of the reflected fast-critical spheres:

$I(n,\gamma)/^{235}U(n,f)$:	^{235}U	^{233}U	^{239}Pu
	$0.101 \pm 4\frac{1}{2}\%$	$0.091 \pm 4\%$	$0.093 \pm 4\%$

The uncertainties are derived from the I(n, γ) excitation errors given in Table VII and incorporate allowances for systematic departures of the chosen excitation from its true shape; $^{235}U(n,f)$ excitation errors below 1 MeV are excluded since I(n, γ) measurements over the bulk of the

spectrum energy range were made relative to $^{235}U(n,f)$. Agreement with measured values in Table IV for the ^{235}U and ^{239}Pu systems is good and accentuates the high value computed for the ^{233}U system.

REFERENCES

[1] Hansen, G. E., "Status of Computational and Experimental Correlations for Los Alamos Fast-Neutron Critical Assemblies" in Physics of Fast and Intermediate Reactors, IAEA (1962).

[2] Chezem, C. G., Nucl. Sc. and Eng. 8 (1960) 652-669.

[3] Hansen, G. E., Maier, C., Perturbation Computations Applied to the Interpretation of Reactivity Coefficients, Nucl. Sc. and Eng. 8 (1960) 532-542.

[4] Stein, W. E., Smith, R. K., Grundl, J. A., "Relative Fission Cross-Sections of U238, Np237, and U235," Conference on Neutron Cross-Section Technology, Washington, D. C. (March 22-24, 1966). Nucl. Sc. Abstr. 20 13 (1966) 2975.

Smith, H. L., Balagna, J. P., "A Method of Assay of U235, U238, and Np237 Fission Foils," Conference on Neutron Cross-Section Technology, Washington, D. C. (March 22-24, 1966). Nucl. Sc. Abstr. 20 13 (1966) 2794.

[5] Jarvis, G. A., Fission Comparison of U238 and U235 for 2.5 MeV Neutrons, Los Alamos Scientific Laboratory Report LA-1571 (1953).

[6] Grundl, J. A., Los Alamos Scientific Laboratory Report LAMS-2883 (1963). All experimental results have been reworked and are superseded by Refs. [7,8], and this paper.

[7] Grundl, J. A., A Study of Fission-Neutron Spectra with High-Energy Activation Detectors -- Part I, Detector Development. Submitted for publication in Nucl. Sc. and Eng.

[8] Grundl, J. A., A Study of Fission-Neutron Spectra with High-Energy Activation Detectors -- Part II, Fission Spectra. In preparation for publication in Nucl. Sc. and Eng.

[9] Grundl, J. A., Usner, A. A., Nucl. Sc. and Eng. 8 (1960) 598-607.

[10] Johnsrud, A. E., Silbert, M. G., Barschall, H. H., Phys. Rev. 116 (1959) 927.

[11] Cox, S. A., Phys. Rev 133 (1964) B378.

[12] Bame, S. J., Cubitt, R. L., Phys. Rev. 113 (1959) 256.

[13] Stavisskii, Y. Y., Tolstikov, V. A., Kononov, V. W., Reactor Sci. Technol. 16 (1962) 326.

[14] Gabbard, F., Davis, R. H., Bonner, T. W., Phys. Rev. 114 (1959) 201.

[15] Gibbons, J. H., Macklin, R. L., Miller, P. D., Neiler, J. H., Phys. Rev. 122 (1961) 182.

[16] Weston, L. W., Seth, K. K., Bilpuch, E. G., Newson, H. W., Ann. Phys. (N. Y.) 10 (1960) 455-489.

[17] Popov, Yu. P., Shapiro, F. L., J. Exptl. Th. Phys. (USSR) 42 (1962) 988 [Translation: Sov. Phys. JETP 15 (1962) 683].

[18] Engle, L. B., Hansen, G. E., Paxton, H. C., Nucl. Sc. and Eng. 8 (1960) 567.

[19] Terrell, J., Phys. Rev. 113 (1959) 527.

[20] Hansen, G. E., Roach, W. H., Six and Sixteen Group Cross Sections for Fast and Intermediate Critical Assemblies, Los Alamos Scientific Laboratory Report LAMS-2543 (1961). See also Nucl. Sc. and Eng. 8 (1960) 621-651.

DISCUSSION

D. T. GOLDMAN: I completely agree with your general conclusion that integral measurements on simple reactor systems form a very good indication of the accuracy of the basic input data to reactor physics programmes. However, it is my feeling that the calculation of bare critical assemblies cannot be performed to such accuracy that one can assign all discrepancies in integral measurements and calculations to inaccuracy of the nuclear data.

J. A. GRUNDL: Computational bias due to neutron-transport models and arithmetical approximations have been discussed in detail in an earlier paper[1]. For an undiluted and unreflected critical sphere of ^{235}U the computational errors in reproduction number and neutron lifetime are less than 1%. Fission spectrum weighting rather than flux weighting of cross-section data to produce multi-group parameters introduces at most a 1.4% error into the computed spectral index $\bar{\sigma}_f(^{235}U) / \bar{\sigma}_f(^{238}U)$.

We believe that for these elemental chain-reacting systems microscopic data can be transformed into integral properties with arbitrary accuracy.

R. D. SMITH: I would first like to comment that simultaneous discrepancies in both calculated neutron lifetimes and threshold reaction rates are not unexpected. It often happens that fast reactor calculations indicate both too few high-energy neutrons (>1 MeV) and too few low-energy neutrons (< 20 keV).

I would also like to ask what data set was used and what was the age of the microscopic nuclear data included in it.

J. A. GRUNDL: In the fast-critical spheres of nearly pure fissile elements more than 95% of neutron spectrum is above 100 keV and some 40% above 1.4 MeV. It would no doubt be possible to construct a spectrum such that relative to high energy detectors there is agreement between the ^{235}U (n, f) detector (nearly flat response above 100 keV) and neutron lifetime (qualitatively a 1/v detector). Such a spectrum however would contradict what we presume to know about the emission spectra of neutrons from fission and inelastic scattering.

---

[1] HANSEN, G. E., "Status of computational and experimental correlations for Los Alamos fast neutron critical assemblies", Physics of Fast and Intermediate Reactors 1 IAEA, Vienna (1962) 445-455.

In answer to your question, the cross-section sets used to describe these fast-critical spheres of fissile elements are those of Hansen and Roach revised in 1960[2]. The inelastic transfer cross-sections are based largely on sphere transmission measurements of the last decade with some ad hoc adjustment to spectral index values as known in 1960. We would hope that before the end of this decade the experimental obstacles will be overcome and good differential data for inelastic scattering in fissile elements will become available.

J. CHERNICK: I think Dr. Grundl's remarks were pertinent and that clean fast-critical assemblies are useful check-points for measured cross-sections. This is also true of thermal criticals, where measurements of eta combined with alpha measurements may be used to obtain $\bar{\nu}$ values for fissionable isotopes such as ^{235}U. In view of the difficulty of obtaining absolute measurements for $\bar{\nu}$, this approach should receive serious consideration. Unfortunately, there is not enough californium available to obtain criticality data for it as well.

---

[2] HANSEN, G. E. and ROACH, W. H., Six and sixteen group cross-sections for fast and intermediate critical assemblies, Rep. LAMS-2543(1961).

Session VI

NEUTRON CROSS-SECTIONS ABOVE THE RESONANCE ENERGY REGION

THE CALCULATION OF NUCLEAR CROSS-SECTIONS BY THE OPTICAL MODEL

D.T. GOLDMAN
NATIONAL BUREAU OF STANDARDS,
WASHINGTON, D.C.,
UNITED STATES OF AMERICA

Abstract

THE CALCULATION OF NUCLEAR CROSS-SECTIONS BY THE OPTICAL MODEL. It is well recognized that there will always be limitations to the amount and certainty of microscopic nuclear cross-section data which are available for direct input into reactor design calculations. Therefore, scattering models for the interaction between incident nucleons and the target nucleus have been proposed and used to obtain appropriate values of necessary cross-sections, both where experimental data are lacking and to differentiate between conflicting data. The generic term for such computations is conveniently "optical model calculations" wherein the two-body internucleon potential is replaced by an effective nuclear potential.

This paper presents a systematic derivation of nuclear cross-sections beginning with the interaction between an incident particle and the target nucleons. The replacement of the exact potential by an effective potential results, to first order, in the ordinary time-independent Schrödinger equation. This equation, including a complex and spin-orbit potential is solved for the resultant wave function. By writing the wave function in its scattering solution form, it is possible to compute the shape elastic cross-section and the polarization directly in Legendre moment expansions. The compound nucleus cross-section, as given originally by the statistical model of Hauser and Feshbach, arises naturally by examining the total wave function. By using the entire solution, including the complete interaction potential, it is possible to generalize these calculations to include the effect of non-spherical potentials and to derive the distorted wave Born approximation. The equations derived in this manner have been used in writing ABACUS-1 and OPTIC, two widely utilized optical model programmes developed by colleagues and the author at Knolls Atomic Power Laboratory. The results obtained from calculations with suitably adjusted potential parameters, have provided confidence for further use of these optical model techniques in providing cross-section information.

I. INTRODUCTION

With the increasing sophistication of nuclear reactor design and the need for understanding the specifics of neutron interactions in a broad energy band from thermal to resonance and high energy regions, there is added importance in having available both detailed reactor physics design and analysis programs and, the subject of this conference, the nuclear cross-sections which form the basic input data to these programs. The improvement and development of experimental sources of large currents of neutrons has resulted in a much greater amount of experimental data for the interaction of neutrons with target materials than was the case just a few years ago. There are certain areas of measurement such as detailed structure of neutron cross-sections in the resonance region for which it is unlikely that any calculation from first principles is likely to predict these values. Nevertheless, the vast amount of input cross-section information required to properly analyze complex reactor systems has required the use of interaction models to provide the necessary density of points. The major purpose of the nuclear models is for use in extrapolating from and interpolating between experimentally determined values of the cross-section. In addition, calculated results may be used to check the validity and consistency of experimental data and to serve as a guide in selecting regions where experiments should be performed.

A detailed model of the interaction of incident nucleons with a nucleus recognizes the fact that there is an interaction between the incident particle

of each of the nucleons in the target. It is possible, however, to replace these detailed interactions with an effective interaction between the incident particle and the nucleus as a whole. This gives rise to the optical model of nuclear reactions which was first presented in detail by Feshbach, Porter, and Weisskopf.(1) The principal points of this model are discussed in Section II of this paper in sufficient detail so that the physical interpretation of the calculated quantities and the mathematical techniques used in their solution are manifest. In Section III the theory of the formation of a compound nucleus and its decay is treated. In addition, a review of the technique for including the effect of resonances in cross-section calculations is presented as well as a demonstration of the relationship between this statistical model of compound nuclear cross-sections and the resonance cross-sections. Section IV which for more pedagogical reasons might actually be presented first, consists of a development of the optical model equations beginning with the initial two-body interaction, and demonstrates the use of the distorted wave Born approximation. Section V summarizes some modifications made to the basic optical model to account for other known or expected effects due to properties of the target nucleus. Section VI summarizes briefly the work presented.

II. THE OPTICAL MODEL

A. The Basic Equations

This section presents a systematic derivation of nuclear cross-sections beginning with the effective interaction between an incident particle and a target nucleus. The form of the interaction is a central optical model potential well with both imaginary and spin-orbit parts. The time-independent Schroedinger equation is solved for an exact expression for the wave function. The direct part of the cross-section then follows by writing the exact wave function as the sum of an incident plane wave and an outgoing spherical wave. The shape elastic cross-section and polarization are then computed directly in Legendre moment expansion. In the next section the compound nucleus cross-section as given originally by Wolfenstein (2) and Hauser and Feshbach (3) arises naturally by examining the total wave function, thus eliminating the need for the introduction of channel spin notation.

As first observed by Bethe (4) and later by Feshbach, Porter, and Weisskopf if the narrow resonances in neutron scattering data are averaged out, the resulting gross structure can be analyzed on a potential well model. In this model all nuclear coordinates are suppressed (see Section IV) and only the relative coordinate of the incident particle with respect to the center-of-mass of the target remains. The equation describing this system is:

$$-\frac{\hbar^2}{2m}\nabla^2\psi(\vec{r},\vec{\sigma}) + V(\vec{r},\vec{\sigma})\psi(\vec{r},\vec{\sigma}) = E\psi(\vec{r},\vec{\sigma}) \qquad (2.1)$$

where m is the reduced mass of the colliding particles, E is the incident energy in the center-of-mass system and

$$V(\vec{r},\vec{\sigma}) = V_c(\vec{r}) + iW(\vec{r}) + V_s(\vec{r})\,\vec{L}\cdot\vec{S}$$

where $V_c(\vec{r})$ is the real part of the potential
$W(\vec{r})$ is the imaginary part of the potential
$V_s(\vec{r})$ is the spin-orbit part of the potential (for simplicity possessing only a real part) and $\vec{L}$ and $\vec{S}$ are the orbital and spin angular momentum operators, respectively, (measured in units of $\hbar$, so as to be dimensionless quantities).

Analogous to the procedure in the non-spin case (5) of expanding the wave function in spherical harmonics, the total wave function $\psi(\vec{r},\vec{\sigma})$ is expanded as a sum of products of radial functions and functions of the angular and spin coordinates:

$$\psi(\vec{r},\vec{\sigma}) = \sum_{\ell j \mu} K_{\ell j \mu}\,\frac{u^{\mu}_{\ell j}(r)}{r}\,\mathcal{Y}_{\ell j \mu}(\hat{r},\vec{\sigma}) \qquad (2.2)$$

where the $K_{\ell j\mu}$ are a set of constant coefficients to be evaluated later, and $\mathcal{Y}_{\ell j\mu}(\hat{r}, \vec{\sigma})$ is an eigenfunction of the square of the total angular momentum $\vec{J}$:

$$J^2 \mathcal{Y}_{\ell j\mu}(\hat{r}, \vec{\sigma}) = j(j+1)\, \mathcal{Y}_{\ell j\mu}(\hat{r}, \vec{\sigma}) \tag{2.3}$$

The $\mathcal{Y}_{\ell j\mu}$ are defined by vector coupling the orbital and spin angular momentum eigenfunctions:

$$\mathcal{Y}_{\ell j\mu}(\hat{r}, \vec{\sigma}) = \sum_{m_\ell m_s} C^{\ell\ \frac{1}{2}\ j}_{m_\ell\ m_s\ \mu}\, Y^{m_\ell}_{\ell}(\hat{r})\ \chi^{m_s}_{\frac{1}{2}}(\vec{\sigma}) \tag{2.4}$$

The functions $Y^{m_\ell}_{\ell}(\hat{r})$ are normalized spherical harmonics, while $\chi^{m_s}_{\frac{1}{2}}(\vec{\sigma})$ is the spin eigenfunction for a particle of intrinsic spin 1/2. The unit vector $\hat{r}$ stands for the angles (θ, φ) and $\vec{\sigma}$ is the spin coordinate. Because of its definition, (2.4), $\mathcal{Y}_{\ell j\mu}$ is also an eigenfunction of $\vec{L}\cdot\vec{S}$, L^2, S^2, and J_z

$$L^2 \mathcal{Y}_{\ell j\mu} = \ell(\ell+1)\mathcal{Y}_{\ell j\mu} \tag{2.5a}$$

$$S^2 \mathcal{Y}_{\ell j\mu} = 3/4\ \mathcal{Y}_{\ell j\mu} \tag{2.5b}$$

$$\vec{L}\cdot\vec{S}\,\mathcal{Y}_{\ell j\mu} = 1/2\,(J^2 - L^2 - S^2)\mathcal{Y}_{\ell j\mu} = 1/2\,[j(j+1) - \ell(\ell+1) - 3/4]\mathcal{Y}_{\ell j\mu} \tag{2.5c}$$

$$J_z \mathcal{Y}_{\ell j\mu} = \mu \mathcal{Y}_{\ell j\mu} \tag{2.5d}$$

but not of L_z and S_z separately. The Clebsch-Gordan coefficients are denoted by $C^{j_1 j_2 j_3}_{m_1 m_2 m_3}$. (6)

If we now substitute (2.2) into (2.1) make use of (2.5), multiply the resultant equation by $\mathcal{Y}_{\ell j\mu}(\hat{r}, \vec{\sigma})$ from the left and integrate over the coordinates $\hat{r}$ and $\vec{\sigma}$, the resultant equation for the radial wave function can be put in the form

$$\frac{d^2 u_{\ell j}(x)}{dx^2} + \left[1 - \frac{\ell(\ell+1)}{x^2} - \frac{V_c(x) + iW(x)}{E} - \frac{\gamma^j_\ell V_s(x)}{E}\right] u_{\ell j}(x) = 0 \tag{2.6}$$

where $x = kr = \sqrt{\frac{2mE}{\hbar^2}}\, r$

$$\gamma^j_\ell = \frac{\ell}{2} \qquad \text{for} \quad j = \ell + 1/2$$

$$\gamma^j_\ell = \frac{-(\ell+1)}{2} \qquad \text{for} \quad j = \ell - 1/2$$

and the absence of any dependence of $u_{\ell j}$ on μ is made manifest by dropping that subscript.

We are looking for scattered solutions to the Schrodinger Equation. We, therefore, impose on the total wave function the condition that at large distances it have the form of an incident plane wave with its appropriate initial spin wave function plus a spherical outgoing wave

$$\Psi(\vec{r}, \vec{\sigma}) \underset{r\to\infty}{\sim} e^{i\vec{k}\cdot\vec{r}}\, \chi^{m_s}_{\frac{1}{2}}(\vec{\sigma}) + f^{m_s}(\theta, \vec{\sigma})\, \frac{e^{ikr}}{r} \tag{2.7}$$

Using the Legendre expansion of the plane wave,

$$e^{i\vec{k}\cdot\vec{r}} = \sum_{\ell} (2\ell+1) i^\ell j_\ell(kr) P_\ell(\hat{k}\cdot\hat{r})$$

and the addition theorem for spherical harmonics, we can write

$$e^{i\vec{k}\cdot\vec{r}}\chi^{m_s}_{\frac{1}{2}}(\vec{\sigma}) = 4\pi \sum_{\substack{\ell m_\ell \\ j\mu}} i^\ell j_\ell(kr)\, Y^{m_\ell}_\ell(\hat{k})^*\, C^{\ell\ \frac{1}{2}\ j}_{m_\ell\ m_s\ \mu}\, \mathcal{Y}^{j\mu}_\ell(\hat{r}, \vec{\sigma}) \tag{2.8}$$

Asymptotically,

$$j_\ell(kr) \underset{r\to\infty}{\sim} \frac{1}{kr}\sin(kr - \tfrac{\ell\pi}{2})$$

and

$$e^{i\vec{k}\cdot\vec{r}}\chi^{m_s}_{\frac{1}{2}}(\vec{\sigma}) \underset{r\to\infty}{\sim} \frac{2\pi}{ikr}\sum_{\substack{\ell m_\ell \\ j\mu}} i^\ell\, C^{\ell\ \frac{1}{2}\ j}_{m_\ell\ m_s\ \mu}\, Y^{m_\ell}_\ell(\hat{k})^*\, \mathcal{Y}^{j\mu}_\ell(\hat{r}, \vec{\sigma}) \left[e^{i(kr - \frac{\ell\pi}{2})} - e^{-i(kr - \frac{\ell\pi}{2})}\right] \tag{2.9}$$

We now seek the asymptotic solution of Eq (2.6), which is regular at the origin. For potentials falling off faster than 1/r (i.e., for non-Coulomb type interactions), the regular solution to Eq. (2.6) has the form

$$u^j_\ell(r) \underset{r\to\infty}{\sim} \sin(kr - \tfrac{\ell\pi}{2} + \delta^j_\ell) \tag{2.10}$$

where δ^j_ℓ is the nuclear phase shift. (The inclusion of a Coulomb potential makes the analysis somewhat more complicated and is discussed in Appendix C). Splitting (2.10) into complex exponentials and equating coefficients of e^{-ikr} in Eq. (2.7) one can evaluate the coefficient $K_{\ell j\mu}$. Substituting the result into Eq. (2.2) we obtain the following expression for the wave function

$$\Psi(\vec{r}, \vec{\sigma}) = \frac{4\pi}{kr}\sum_{\substack{\ell m_\ell \\ j\mu}} i^\ell\, C^{\ell\ \frac{1}{2}\ j}_{m_\ell\ m_s\ \mu}\, Y^{m_\ell}_\ell(\hat{k})^*\, \mathcal{Y}^{j\mu}_\ell(\hat{r}, \vec{\sigma})\, e^{i\delta^j_\ell}\, u^j_\ell(r) \tag{2.11}$$

Equating the coefficient of e^{ikr} in (2.7), making use of (2.9) and the result for $K_{\ell j\mu}$, we can solve for the scattering amplitude $f^{m_s}(\theta, \vec{\sigma})$ as

$$f^{m_s}(\theta, \vec{\sigma}) = \frac{2\pi}{ik}\sum_{\substack{\ell m_\ell \\ j\mu}} C^{\ell\ \frac{1}{2}\ j}_{m_\ell\ m_s\ \mu}\, Y^{m_\ell}_\ell(\hat{k})^*\, \mathcal{Y}^{j\mu}_\ell(\hat{r}, \vec{\sigma})\, (\eta^j_\ell - 1) \tag{2.12}$$

where $\eta^j_\ell = e^{2i\delta^j_\ell}$ (2.13)

B. The Shape Elastic Cross-Section

The scattering cross-section is obtained by dividing the outgoing current through a sphere enclosing the target by the incident current. (17) Making use of the definition of the quantum mechanical current

$$\vec{j} = \frac{\hbar}{2im}(\Psi^*\nabla\Psi - \Psi\nabla\Psi^*) \tag{2.14}$$

and Eq. (2.7), the cross-section for different final and initial azimuthal spin quantum numbers m_s' and m_s if (f is a function of m_s' through $\mathcal{Y}$)

$$\sigma^{m_s' m_s}(\theta) = \frac{\frac{\hbar k}{m} f^{m_s *} f^{m_s}}{\frac{\hbar k}{m}} = f^{m_s}(\theta)^* f^{m_s}(\theta) \tag{2.15}$$

If we now average over initial spin states and sum over final spin states, the familiar shape elastic differential cross-section results. The difference between the two possible final spin states, spin up and spin down, divided by the shape elastic cross-section, results in an expression for the polarization of the incident beam. If the initial beam is itself polarized, we omit the sum over initial azimuthal quantum numbers. This last result will not be presented in this paper, but can be derived by the method outlined herein.

In order to calculate the shape elastic and polarization cross-sections in unison, we define a generalized scattering function

$$\Phi(\theta) = \tfrac{1}{2} \sum_{m_s' m_s} C_{m_s'} \, f^{m_s *} \, f^{m_s} \tag{2.16}$$

where when $C_{m_s'} = 1$, $\Phi(\theta) = \sigma(\theta)$, the differential cross-section, and when $C_{m_s'} = (-)^{\frac{1}{2}-m_s'}$, $\Phi(\theta) = \sigma(\theta)\, P(\theta)$, where $P(\theta)$ is the polarization of the outgoing particle. From Eq. (2.16), using Eq. (2.13) and the definition of $\mathcal{Y}_{jm}$, we find

$$\Phi(\theta) = \frac{2\pi^2}{k^2} \sum C_{m_s'} (1 - \eta_\ell^j)\,(1 - \eta_{\tilde{\ell}}^{\tilde{j}})^* \, Y_\ell^{m_\ell *}(\hat{k}) \, Y_{\tilde{\ell}}^{\tilde{m}_\ell}(\hat{k}) \, Y_\ell^{m_\ell'}(\hat{r}) \, Y_{\tilde{\ell}}^{\tilde{m}_\ell'}(\hat{r})^* \, C^{\tilde{\ell}\ \frac{1}{2}\ \tilde{j}}_{\tilde{m}_\ell' m_s' \tilde{\mu}} \, C^{\ell\ \frac{1}{2}\ j}_{m_\ell' m_s \mu} \, C^{\tilde{\ell}\ \frac{1}{2}\ \tilde{j}}_{\tilde{m}_\ell m_s \tilde{\mu}} \, C^{\ell\ \frac{1}{2}\ j}_{m_\ell' m_s \mu} \tag{2.17}$$

After a great deal of manipulation as described in Appendix A, the differential cross-section, and its product with the polarization are, respectively

$$\sigma(\theta) = \frac{1}{8k^2} \sum_{\ell j \tilde{\ell} \tilde{j} L} (1 - \eta_\ell^j)\,(1 - \eta_{\tilde{\ell}}^{\tilde{j}})^* \, Z(\ell j \tilde{\ell} \tilde{j};\ \tfrac{1}{2} L)\, P_L(\hat{k}\cdot\hat{r}) \tag{2.18}$$

$$\sigma(\theta)\, P(\theta) = \frac{1}{8k^2 i} \sum_{\ell j \tilde{\ell} \tilde{j} L} \frac{dP_L(\cos\theta)}{d\cos\theta} (-)^{\tilde{\ell}+\frac{1}{2}-\tilde{j}} \, C^{\ell \tilde{\ell} L}_{oo} \, (1 - \eta_\ell^j)\,(1 - \eta_{\tilde{\ell}}^{\tilde{j}})^* \sqrt{(2\ell+1)\,(2\tilde{\ell}+1)\,(2j+1)\,(2\tilde{j}+1)} \sqrt{\frac{3(2L+1)}{L(L+1)}} \, Z(\ell j \tilde{\ell} \tilde{j};\ \tfrac{1}{2} L)\ X(\tilde{j} \ell \tfrac{1}{2};\ j \tilde{\ell} \tfrac{1}{2};\ L L 1) \tag{2.19}$$

where θ is the angle between $\vec{k}$ and $\vec{r}$, and the polarization direction in the last equation is the vector perpendicular to the $(\vec{k} \times \vec{r})$ plane. The remaining quantities are coupling coefficients defined in Appendix A.

The potential scattering cross-section, defined as the angle integration of the shape elastic differential cross-section, can be calculated from Eq. (2.18) by noting that

$$Z(\ell j \tilde{\ell} \tilde{j};\ \tfrac{1}{2} 0) = (-)^{j-\frac{1}{2}} \sqrt{2j+1}\ \delta_{\ell \tilde{\ell}}\ \delta_{j \tilde{j}}$$

Thus $\sigma_{pot} = 2\pi \int_{-1}^{1} \sigma(\theta)\, d(\cos\theta)$

$$= \frac{\pi}{2k^2} \sum_{\ell j} |(1 - \eta_\ell^j)|^2 (2j+1) \tag{2.20}$$

C. Computational Solutions

We note that in the above expressions for the nuclear cross-sections, the exact radial wave functions do not appear explicitly; the phase shifts δ_ℓ^j do. In fact this is the implicit reason for writing the exact wave functions in terms of the phase shifts. However to evaluate the cross-sections the exact equation (2.6) must actually be solved and is described in this section. The procedure follows that presented in Blatt and Weisskopf (7) and is utilized in two computational programs with which the author is most familiar [ABACUS-1 (8) + OPTIC (9)].

Due to the generality of the nuclear potential, it is necessary to use numerical techniques to solve the radial equation (2.6). This is done by choosing some cut-off radius R_c beyond which the potentials can be set equal to zero. In this outside region an analytical solution is possible as described below. Inside R_c, the radial equation is solved numerically, and the real imaginary parts of the solution and their derivatives are matched at the boundary $r = R_c$.

For $r > R_c$, in the absence of a Coulomb potential the radial equation is the spherical Bessel equation. The solution written in asymptotic form above (2.10) can be written exactly as

$$u_\ell^j(x) = \text{constant}\,[e^{2i\delta_\ell^j} u_\ell^+(x) - u_\ell^-(x)] \tag{2.21}$$

$$\text{where } u_\ell^{\pm}(x) = G_\ell(x) \pm iF_\ell(x), \tag{2.22}$$

the free $\begin{Bmatrix}\text{outgoing}\\ \text{incoming}\end{Bmatrix}$ waves

$$\text{where } G_\ell(x) = -xn_\ell(x) \underset{x\to\infty}{\sim} \cos\left(x - \frac{\ell\pi}{2}\right) \tag{2.23a}$$

$$F_\ell(x) = xj_\ell(x) \underset{x\to\infty}{\sim} \sin\left(x - \frac{\ell\pi}{2}\right) \tag{2.23b}$$

the irregular and regular solutions of the potential-free wave equation and $n_\ell(x)$ and $j_\ell(x)$ are the spherical Neumann and Bessel Functions, respectively. (Note the absence of a spin-orbit potential means a dependence on the orbital quantum number only.)

If we now denote the interior solution by $L_\ell^j(x)$, and its logarithmic derivative at the cutoff

$$f_\ell^j \equiv X_c \left.\frac{dL_\ell^j(x)/dx}{L_\ell^j(x)}\right|_{x = kR_c = X_c} \tag{2.24}$$

and the outgoing (incoming) wave logarithmic derivative as

$$X_c \left.\frac{du_\ell^{\pm}/dx}{u_\ell^{\pm}}\right|_{x = X_c} \equiv \Delta_\ell \pm iS_\ell \tag{2.25}$$

the boundary condition involves just the matching of the logarithmic derivatives, defined by (2.24) and (2.25) at the boundary R_c or X_c. Equating the logarithmic derivative yields the following equation for the reflection coefficient, η_ℓ^j

$$\eta_\ell^j = \frac{f_\ell^j - \Delta_\ell + iS_\ell}{f_\ell^j - \Delta_\ell - iS_\ell} \cdot \left.\frac{G_\ell - iF_\ell}{G_\ell + iF_\ell}\right|_{x = X_c} \tag{2.26}$$

Explicit forms for Δ_ℓ and S_ℓ can be derived using (2.22) and (2.25).

$$\Delta_\ell = X_c \left.\frac{G_\ell \frac{dG_\ell}{dx} + F_\ell \frac{dF_\ell}{dx}}{G_\ell^2 + F_\ell^2}\right|_{x = X_c} \tag{2.27}$$

$$S_\ell = X_c \left. \frac{G_\ell \frac{dF_\ell}{dx} - F_\ell \frac{dG_\ell}{dx}}{G_\ell^2 + F_\ell^2} \right|_{x = X_c} = \frac{X_c}{G_\ell^2(X_c) + F_\ell^2(X_c)} \qquad (2.28)$$

The numerical technique used is to solve the differential equation (2.6), (or at least its equivalent difference equation), point by point integrating outward from the origin and evaluating f_ℓ^j for each value of ℓ and j. The remaining terms in (2.26) are combinations of Bessel and Neumann functions and recursion formulas are used in their evaluation. These are used in the calculation of η_ℓ^j, and from this the phase shift.

Before we pass on to uses of phase shifts in other forms of nuclear reactions, let us consider the case where the interaction potential is real. For this case the logarithmic derivative f_ℓ^j is real and the magnitude of η_ℓ^j obtained from (2.26) is unity. Thus the phase shifts themselves are real, a result that will give rise to a null reaction cross-section, as seen in the next section. Alternatively, the size of the imaginary part of the reaction cross-section is a measure of the reaction cross-section affecting it directly, whereas the potential cross-section, written as

$$\sigma_{pot} = \frac{\pi}{k^2} \sum_{\ell j} (2j + 1)\,(1 + e^{-4\delta_I} - 2\cos 2\delta_R e^{-2\delta_I}) \qquad (2.29)$$

where δ_R and δ_I are the real and imaginary parts of the phase shift, respectively, is less directly affected by W(r). This immediately suggests an iterative procedure for fitting phase shifts or, alternatively, the parameters defining the potentials, to experimental values of the cross-section.

III. COMPOUND NUCLEUS CROSS-SECTION

A. The Statistical Model

In this section we utilize the key suggestion of Hauser and Feshbach(3) that the wave function describing the compound state of the incident and target particle be formed statistically, that is, that all intermediate states which conserve energy and angular momentum be permitted in the wave function. The rationale behind this statement is the fact that typically exothermic particle capture processes result in the particle being captured into a high energy state of the compound nucleus where the energy levels are sufficiently dense to validate this approximation.

The final state of this system also consists of two particles formed in the statistical decay of the compound nucleus. The customary application of this is in the calculation of the inelastic scattering of neutrons by a target nucleus whose final state is some excited state of the nucleus. However, if other exit channels are available, such as proton, alpha particle, or gamma ray emission energetically possible, these cross-sections can be calculated by this process and the probability for them must be included in normalizing the cross-sections calculated below.

The total wave function for the system thus includes the angular momentum coupling of the total spin states of the incident and target particles. In analogy to Eq. (2.2), we define the total wave function as a sum of products of radial wave functions and functions of the total (compound nucleus) spin

$$\Psi(\vec{r},\vec{\sigma},\xi) = \sum_{\ell j \mathcal{J} m} \gamma^{m}_{\ell j \mathcal{J}} \frac{u^j_\ell(r)}{r} \mathcal{Y}^{m}_{\ell j \mathcal{J}}(\hat{r},\vec{\sigma},\xi) \qquad (3.1)$$

where $$\mathcal{Y}^{m}_{\ell j \mathcal{J}}(\hat{r},\vec{\sigma},\xi) = \sum_{\mu M_i} C^{j\ J_i\ \mathcal{J}}_{\mu\ M_i\ m}\, y_{j\mu}(\hat{r},\vec{\sigma})\, \Phi^{M_i}_{J_i}(\xi)$$

the generalization of the y-functions, and $\mathcal{J}, m$, and J_i, M_i, are the total

and azimuthal quantum numbers of the compound nucleus and target nucleus, respectively. The initial state of the scattering system can be expressed as

$$e^{i\vec{k}\cdot\vec{r}}\chi_{\frac{1}{2}}^{m_s}(\vec{\sigma})\Phi_{J_i}^{M_i}(\xi) = 4\pi\sum_{\substack{\ell m_\ell \\ j m}} j^\mu i^\ell j_\ell(kr)\, Y_\ell^{m_\ell *}(\hat{k})\, C_{m_\ell m_s \mu}^{\ell\ \frac{1}{2}\ j}\, C_{\mu\ M_i m}^{j\ J_i j}\, \gamma_{\ell j j}^{m}(\hat{r},\vec{\sigma},\xi) \tag{3.2}$$

Substituting into a scattering equation for the asymptotic solutions analogous to Eq. (2.7), and equating coefficients of the incoming exponentials we can evaluate the coefficient $\gamma_{\ell j j}^{m}$. The resultant total wave function is

$$\Psi(\vec{r},\vec{\sigma},\xi) = \frac{4\pi}{k}\sum_{\substack{\ell m_\ell j \mu \\ M_i \mu m_\ell m_s \\ j m}} i\, e^{i\delta^j}\, \frac{u_\ell^j(r)}{r}\, Y_\ell^{m_\ell}(\hat{k})\, \chi_y^{m_s}(\sigma)\, \Phi_{J_i}^{M_i}(\xi)\, Y^{m}(\hat{r})\, C_{m_\ell m_s \mu}^{\ell\ \frac{1}{2}\ j}\, C_{\mu M_i m}^{jJ_i j}\, C_{\mu M_i m}^{jJ_i j}\, C_{m_\ell m_s \mu}^{\ell\ \frac{1}{2}\ j} \tag{3.3}$$

The reaction cross-section is equal to the net flux into target computed from the complete wave function. (7)

$$\sigma = \frac{\frac{-\hbar}{2im}(\Psi^*\nabla\Psi - \Psi\nabla\Psi^*)}{\hbar k/m} \tag{3.4}$$

where the negative sign makes the net flux positive. The radial and angular parts separate conveniently. The cross-section for the formation of compound nucleus of spin j derived explicitly in Appendix B, is

$$\sigma_j = \frac{4\pi^2}{k^2}\sum_{\ell jLM}(-)^{J_i - j - \frac{1}{2}}\sqrt{\frac{2j+1}{4\pi}}\,\frac{(1-|\eta_\ell^j|)^2}{2(2J_i+1)}\,Y_L^M(\hat{k})$$
$$Z(\ell j\ \ell\ j;\ \tfrac{1}{2}L)W(jjjj;\ J_i L)C_{m-M\,m}^{j\ L\ j} \tag{3.5}$$

We now consider the relative probability for the decay of the compound state (j,m). This is obtained by using Eq. (3.5) and the reciprocity theorem. Thus the cross-section for decay is equal to

$$\sigma_j(\text{decay}) = \sum_{\ell_f j_f L_f M_f}(-)^{J_f - j - \frac{1}{2}}\sqrt{\frac{2j+1}{4\pi}}\,\frac{(1-|\eta_{\ell_f}^{j_f}(E')|)^2}{\sum_{\ell_p j_p} T_{\ell_p}^{j_p}(E_p)}\,Y_{L_f}^{M_f}(\hat{k}')$$
$$Z(\ell_f j_f \ell_f j_f;\ \tfrac{1}{2}L_f)\,W(jj_f jj_f;\ J_f L_f)\,C_{m-M_f m}^{j\ L_f\ j} \tag{3.6}$$

where $T_{\ell_p}^{j_p}(E_p') \equiv 1 - |\eta_{\ell_p}^{j_p}(E_p')|^2$ the penetrability, E' is the final energy of the (3.7)

projectile and the summation in the denominator is formed over all energy and spin conserving final states.

The product of Eq. (3.5) and (3.6) is the cross-section for the scattering of an incident spin 1/2 particle by a target of spin (J_i,M_i) through an angle θ by means of a statistically formed compound nucleus. The result is

$$\sigma_{CN}(\theta) = \frac{1}{4k^2} \sum_{\ell_i j_i \ell_f j_f} \frac{T^{j_i}_{\ell_i}(E)}{2(2J_i + 1)} \sum_{\mathcal{J}} \frac{T^{j_f}_{\ell_f}(E')\,(2\mathcal{J} + 1)^2}{\sum_p T^{j_p}_{\ell_p}(E'_p)}$$

$$\sum_{L \text{ even}} (-)^{J_i - J_f} P_L(\cos\theta)\, Z(\ell_f j_f \ell_f \mathcal{J}_f;\ \tfrac{1}{2}L) \qquad (3.8)$$

$$Z(\ell_i j_i \ell_i j_i;\ \tfrac{1}{2}L)\, W(\mathcal{J} j_f \mathcal{J} j_f; J_f L)\, W(\mathcal{J} j_i \mathcal{J} j_i;\ J_i L)$$

where $\cos\theta = \hat{k}\cdot\hat{k}'$

The details are described in Appendix B. This result can be compared with an expression given by Feshbach which is similar but which did utilize the concept of channel spin.(10) By means of a relationship introduced by Ford and Levinson, (11)

$$Z(abcd;\ \tfrac{1}{2}f) = (-)^{b - \frac{1}{2}} \sqrt{(2f + 1)\,(2b + 1)}\ C^{b\ f\ d}_{\frac{1}{2}\ o\ \frac{1}{2}}$$

$$\text{for } a + c + f \text{ even} \qquad (3.9)$$

$$= 0 \text{ for } a + c + f \text{ odd}$$

there appears an alternative expression for the differential cross-section

$$\sigma_{CN}(\theta) = \frac{1}{4k^2} \sum_{\ell_i j_i \ell_f j_f} \frac{T^{j_i}_{\ell_i}(E)}{2(2J_i+1)} \sum_{\mathcal{J}} \frac{T^{j_f}_{\ell_f}(E')\,(2\mathcal{J} + 1)^2}{\sum_p T^{j_p}_{\ell_p}(E'_p)}$$

$$(2j_i + 1)(2j_f + 1) \sum_{L \text{ even}} (-)^{J_i - J_f} P_L(\cos\theta)\, C^{j_f j_f\ L}_{\frac{1}{2}-\frac{1}{2}\ 0}\, C^{j_i j_i\ L}_{\frac{1}{2}-\frac{1}{2}\ 0} \qquad (3.10)$$

$$W(\mathcal{J} j_f \mathcal{J} j_f;\ J_f L)\, W(\mathcal{J} j_i \mathcal{J} j_i;\ J_i L)$$

The total compound nucleus cross-section is the integral of Eq. (3.8) or (3.10) over the surface. The integral yields $4\pi\delta_{LO}$, so that the total cross-section becomes

$$\sigma_{CN} = \frac{\pi}{2k^2(2J_i + 1)} \sum_{\ell_i j_i \ell_f j_f} T^{j_i}_{\ell_i}(E) \sum_{\mathcal{J}} \frac{(2\mathcal{J} + 1)\, T^{j_f}_{\ell_f}(E')}{\sum_p T^{j_p}_{\ell_p}(E'_p)} \qquad (3.11)$$

The reaction cross-section is the sum of the compound nucleus cross-section over all possible final states

$$\sigma_r = \frac{\pi}{2k^2(2J_i + 1)} \sum_{\ell_i j_i} T^{j_i}_{\ell_i}(E) \sum_{\mathcal{J}} (2\mathcal{J} + 1)$$

$$= \frac{\pi}{2k^2} \sum_{\ell_i j_i} T^{j_i}_{\ell_i}(E)\,(2j_i + 1) \qquad (3.12)$$

where we have made use of the fact that the multiplicity of states of the compound system, $\sum(2\mathcal{J} + 1)$ is equal to the multiplicity of states of the initial system, $\mathcal{J}(2j_i + 1)(2J_i + 1)$.

The total cross-section for scattering is the sum of Eqs. (2.19) and (3.12). Thus

$$\sigma_T = \frac{\pi}{2k^2} \sum_{\ell j} (2j+1)\left(|1 - \eta_\ell^j|^2 + 1 - |\eta_\ell^j|^2\right) = \frac{\pi}{k^2} \sum_{\ell j} (2j+1)\,\mathrm{Re}\,(1 - \eta_\ell^j) \tag{3.13}$$

B. Exact Treatment of Resonance Scattering in Single-Channel R-Matrix Appropriation

In this section we shall replace the statistical model for nuclear reactions by a model which includes explicitly the formation of a relatively long-lived compound intermediate state. For ease in calculations, it will be assumed that only a single decay channel is available, viz., the same channel as the incident one. For reactor materials with low atomic masses, such as carbon and oxygen, with a resonance in Mev region, it is important to include the resonance explicitly in optical model calculations, as has been demonstrated by Slaggie. (12) For energies of the compound state which open more than one possible exit channel a multi-channel description is required which is not described here. The reader is referred to a review such as the one given by Preston for the complete version of this theory. (13)

We consider initially the radial equation (1.6) and the two asymptotic solutions (2.23), $G_\ell(x)$ and $F_\ell(x)$ and the exact solution combining them, (2.21). We now choose some radius, a, at which the potential vanishes (but not necessarily R_c) and define $\mathcal{R}_\ell^j$ ("the R-Matrix") which connects the value of the interior solution L_ℓ^j with its derivative.

$$L_\ell^j(ka) = ka\,\mathcal{R}_\ell^j \left(\frac{dL_\ell^j}{dx}\right)_{x = ka} \tag{3.14}$$

Equating the logarithmetic derivatives of the interior and exterior solutions, we can solve for the reflectivity as

$$e^{2i\delta_\ell^j} = \frac{1 - (\bar{\Delta}_\ell - i\bar{S}_\ell)\mathcal{R}_\ell^j}{1 - (\bar{\Delta}_\ell + i\bar{S}_\ell)\mathcal{R}_\ell^j} \cdot \left.\frac{G_\ell - iF_\ell}{G_\ell + iF_\ell}\right|_{x = ka} \tag{3.15}$$

where $\bar{\Delta}_\ell$ and $\bar{S}_\ell$ are defined as before, equations (2.27) and (2.28) but evaluated at $x = ka$ instead of at $x = X_c$. If we now replace the second ratio in (3.15) which is in reality u_ℓ^-/u_ℓ^+, by its value in the absence of an intermediate state, viz. $\exp[2i\delta_\ell^j(\text{optical})]$ where δ_ℓ^j (optical) is the ordinary optical model phase shift (10) then by suitable trigonometric manipulation we can rewrite (3.15) in a particularly convenient form

$$\delta_\ell^j = \tan^{-1}\frac{\mathcal{R}_\ell^j \bar{S}_\ell}{1 - \mathcal{R}_\ell^j \bar{\Delta}_\ell} + \delta_\ell^j(\text{optical}) \tag{3.16}$$

Thus far we have not made use of the model of intermediate states of the compound nucleus. We now do so in evaluating $\mathcal{R}_\ell^j$ in terms of the interior solution $L_\ell^j(x)$. We consider only those solutions $L_\ell^j(x)^{(\lambda)}$ which have a zero derivative at $r = a$ and corresponding eigenvalues E_λ. We thus expand the exact solution

$$u_\ell^j(r) = \sum_\lambda A_\lambda^{(\ell,j)} L_\ell^{j(\lambda)}(r) \tag{3.17}$$

at least for $r < a$. To evaluate $A_\lambda^{(\ell,j)}$ we multiply (2.6) by $L_\ell^{j(\lambda)}$, and the eigenequation for $L_\ell^{j(\lambda)}(r)$ corresponding to (2.6) but with $E = E_\lambda$ by $u_\ell^j(r)$, subtract the resulting equations and obtain

$$L_\ell^{j(\lambda)}(r)\frac{d^2u_\ell^j(r)}{dr^2} - u_\ell^j(r)\frac{d^2L_\ell^{j(\lambda)}(r)}{dr^2} + \frac{2m}{\hbar^2}(E - E_\lambda)\,u_\ell^j(r)L_\ell^{j(\lambda)}(r) = 0 \qquad (3.18)$$

where we have reverted to the coordinate r as the dependent variable. We now integrate (3.18) over r from 0 to a. Integrating the first two terms by parts, we are left with

$$\left[L_\ell^{j(\lambda)}(r)\frac{du_\ell^j}{dr} - u_\ell^j\frac{dL_\ell^{j(\lambda)}}{dr}\right]_0^a = L_\ell^{j(\lambda)}(a)\left.\frac{du_\ell^j}{dr}\right|_{r=a} \qquad (3.19)$$

since $L_\ell^{j(\lambda)}(0) = u_\ell^j(0) = 0$

and $\left.\dfrac{dL_\ell^{j(\lambda)}}{dr}\right|_{r=a} = 0.$*

For the remaining term we substitute equation (3.17) and make use of the orthonormality of the L's:

$$\int_0^a L_\ell^{j(\lambda)}(r)L_\ell^{j(\lambda')}(r)\,dr = \delta_{\lambda\lambda'} \qquad (3.20)$$

to obtain

$$\frac{2m}{\hbar^2}\int_0^a (E - E_\lambda)u_\ell^j(r)L_\ell^{j(\lambda)}(r)dr = \frac{2m}{\hbar^2}(E - E_\lambda)A_\lambda^{(\ell,j)} \qquad (3.21)$$

Using (3.19) and (3.21) we find the coupling coefficient $A_\lambda^{(\ell,j)}$ to be

$$A_\lambda^{(\ell,j)} = \frac{\hbar^2}{2m}\,\frac{1}{E_\lambda - E}\,L_\ell^{j(\lambda)}(a)\left.\frac{du_\ell^j}{dr}\right|_{r=a} \qquad (3.22a)$$

and

$$u_\ell^j(r) = \frac{\hbar^2}{2m}\sum_\lambda \frac{L_\ell^{j(\lambda)}(a)\,L_\ell^{j(\lambda)}(r)}{E - E_\lambda}\left(\frac{du_\ell^j}{dr}\right)_{r=a} \qquad (3.22b)$$

Comparing (3.22) at r = a and (3.14), we find

$$R_\ell^j = \frac{\hbar^2}{2ma}\sum_\lambda \frac{(L_\ell^{j(\lambda)}(a))^2}{E_\lambda - E} = \sum_\lambda \frac{\gamma_\lambda^{2(\ell,j)}}{E_\lambda - E} \qquad (3.23)$$

where $\gamma_\lambda^{(\ell,j)} = \left(\frac{\hbar^2}{2ma}\right)^{\frac{1}{2}} L_\ell^{j(\lambda)}(a)$, the reduced width. Substituting in (3.16), we can write the generalized phase shift as

$$\delta_\ell^j = \tan^{-1}\frac{\frac{1}{2}\Gamma_\lambda^{(\ell,j)}}{E_\lambda - E + D_\lambda^{(\ell,j)}} + \delta_\ell^j(\text{optical}) \qquad (3.24)$$

where

$$\tfrac{1}{2}\Gamma_\lambda^{(\ell,j)} = \gamma_\lambda^{2(\ell,j)}\,\bar{S}_\ell \qquad (3.25)$$

$$D_\lambda^{(\ell,j)} = -\gamma_\lambda^{2(\ell,j)}\,\bar{\Delta}_\ell \qquad (3.26)$$

---

* This restriction is in reality too strict and any arbitrary constant b_ℓ^j would satisfy R-Matrix Theory. The definitions (3.15) would be modified by including b_ℓ^j in the definition of $\bar{\Delta}_\ell$ but the final results (3.23) would be unchanged and (3.24) would be altered to include a further energy shift in the denominator.

Substitution of (3.24) in either (2.20) or (3.13) (they are equal when the phase shift is real) yields the complete Breit-Wigner single level formula, with interference between potential and resonance scattering. The incorporation of this extended phase shift in optical model calculation has enabled Slaggie to calculate the scattering of neutrons by oxygen and carbon in the Mev-resonance region.(14) We note that the presence of this "Breit-Wigner" term means that the phase shift goes through $\pi/2$ rather sharply when $E = E_\lambda + D_\lambda^{(\ell,j)}$, thus giving rise to sharp peaks or resonances, in the total cross-section.

It is possible to generalize the results of this section to the case where more than one decay mode is available to the compound state denoted by λ. The resulting equation for this process is (13)

$$\sigma_{nn} = \sigma_{pot} + \frac{\pi}{k^2} g^{\mathcal{J}} \sum_{\ell j} \frac{\Gamma_{\lambda n}^{(\ell,j)} 2(E - E_\lambda + D_\lambda^{(\ell,j)} \sin 2\delta_\ell^j(\text{optical}) - \Gamma_\lambda^{(\ell,j)}(1-\cos 2\delta_\ell^j)}{(E_\lambda + D_\lambda^{(\ell,j)} - E)^2 - \Gamma_\lambda^2/4} + \Gamma_{\lambda n}\Gamma_{\lambda n}/\left[(E_\lambda + D_\lambda - E)^2 + \Gamma_\lambda^2/4\right] \tag{3.27}$$

where $\Gamma_\lambda = \Sigma\Gamma_{\lambda c}$, σ_{pot} is the optical model potential scattering cross-section, $\delta_\ell^j(\text{optical})$ is the optical model phase shift, and $g^{\mathcal{J}}$ is the statistical factor, $(2\mathcal{J} + 1)/2(2J_i + 1)$.(15)

As the final exercise in this section we shall demonstrate the relationship between the non-elastic cross-section and the statistical model. To do this we consider the average of the last term of (3.27) with the two $\Gamma_{\lambda n}$'s corresponding to different initial and final channels over an energy region large enough to contain one and only one resonance. If we replace the energy-dependent partial and total widths by their values at the energy corresponding to the energy at which the nominator is a minimum: $E_o = E_\lambda + D_\lambda$, then the necessary integral can be carried out.

$$\langle \sigma_{\substack{cc' \\ c\neq c'}} \rangle = \frac{\pi}{k_o^2} \frac{(2\mathcal{J} + 1)}{2(2J_i + 1)} \left\langle \frac{\Gamma_{\lambda c}\Gamma_{\lambda c'}}{\Gamma_\lambda} \right\rangle \frac{2\pi}{\langle D(\mathcal{J}) \rangle} \tag{3.28}$$

where $D(\mathcal{J})$ is the mean spacing between resonances of spin $\mathcal{J}$. Making use of the relationship between the partial width and the penetrability (16)

$$T_\ell^j(E) \cong 2\pi \frac{\langle \Gamma_n \rangle}{\langle D \rangle}$$

and summing over all possible compound nucleus states $\mathcal{J}$, we obtain

$$\langle \sigma_{\substack{cc' \\ c\neq c'}} \rangle = \frac{\pi}{k_o^2 2(2J_i + 1)} T_\ell^j(E) \frac{\sum (2\mathcal{J} + 1)\, 2\pi \langle \Gamma_{c'} \rangle / \langle D \rangle}{\sum_p T_{\ell_p}^{j_p}(E_p') + \frac{2\pi \langle \Gamma_{c'} \rangle}{\langle D \rangle}} \quad \tilde{f}$$

where $\tilde{f} = \left\langle \frac{\Gamma_c \Gamma_{c'}}{\Gamma} \right\rangle \frac{\langle \Gamma \rangle}{\langle \Gamma_c \rangle \langle \Gamma_{c'} \rangle}$

a measure of the fluctuation of the reaction widths over the energy range. Comparing (3.29) and (3.11) we see that in the absence of fluctuations, the statistical model is the energy average over the single-level resonance formula. (17, 18)

IV. NUCLEAR REACTION THEORY AND THE OPTICAL MODEL

In this section we shall consider the exact wave function governing a nuclear system including an incident projectile. After removing the motion of the center-of-mass of the system from the analysis, we write the exact

two-body potential in terms of an average potential between the target and the incident particle which will be defined as the optical model potential, and a residual potential which is not a function just of the coordinate joining the centers of the target and projectile. If we then look for particular scattering solutions to the Schrodinger equation we can see that the formalism derived in great detail in the previous sections can be regarded as a special case of the generalized nuclear reaction theory and indeed suggests obvious modifications to ordinary Optical Model calculations to account for known physical properties of the system. Furthermore, the scattering amplitude in the distorted wave Born Approximation will be derived in a systematic manner.

The time-independent Schrodinger equation satisfied by the system is:

$$H\Psi = \left(\sum_{i=1}^{A} T_i + \sum_{i<j=1}^{A+1} V(\vec{r}_i - \vec{r}_j)\right) \Psi(\vec{r}_1,\cdots\vec{r}_A,\vec{r}_{A+1}) = E_{Lab}\Psi(\vec{r}_1,\cdots\vec{r}_{A+1}) \quad (4.1)$$

where T_i is the kinetic energy for the i^{th} particle and $V_{ij} \equiv V(\vec{r}_i - \vec{r}_j)$ is the interaction potential between the i^{th} and j^{th} particles. There are A nucleons in the target; the incident nucleon is the $A + 1^{st}$.

Since $-\hbar^2/2m_i \nabla^2_{\vec{r}_i}$ is the kinetic energy operator for a particle with position r_i and mass m_i, one can write

$$\frac{\nabla^2_{\vec{r}_1}}{m_1} + \frac{\nabla^2_{\vec{r}_2}}{m_2} = \frac{\nabla^2_{\vec{r}_{12}}}{m_{12}} + \frac{\nabla^2_{\vec{R}_{12}}}{M_{12}} \quad (4.2)$$

where $\nabla^2_{\vec{r}_{12}}$ is the Laplacian operator in the relative coordinate $\vec{r}_{12} = \vec{r}_1 - \vec{r}_2$, m_{12} is the reduced mass $\frac{m_1 m_2}{m_1 + m_2}$, $\nabla^2_{\vec{R}_{12}}$ is the center-of-mass Laplacian operator for particles 1 and 2, $\vec{R}_{12} = \frac{1}{M_{12}}(m_1\vec{r}_1 + m_2\vec{r}_2)$ and $M_{12} = m_1 + m_2$.

Successive applications of (4.2) to the kinetic energy term of (4.1) enables us to split this term into an internal contribution which involves only the coordinates of the A nuclear particles, $\vec{r}_1,\cdots,\vec{r}_A$, a relative term involving, $\vec{r}$, the distance of the incident $A + 1^{st}$ nucleon from the center-of-mass of the A nucleons, and a term involving the coordinates of the center-of-mass of the entire system

$$\vec{R} = \sum_{i=1}^{A+1} m_i\vec{r}_i \Big/ \left[(M = \Sigma m_i) + m_{A+1}\right]$$

For this separation to prove useful, we transfer the coordinates of the interaction term in the same manner. This is possible by grouping the interaction terms into those which involve only the target nucleons, and those which involve the incident neutron as one member of the pair:

$$\sum_{i<j=1}^{A+1} V_{ij} = \sum_{i<j=1}^{A} V_{ij} + \sum_{i=1}^{A} V_{i,A+1} \quad (4.3)$$

$$= V_{int} + V(A+1) \quad (4.4)$$

In (4.4) V_{int} is the internal potential energy and V(A+1) is the true interaction between the neutron and the target nucleus. Because it is extremely difficult to solve the Schrodinger equation with the interaction V(A+1), this term is conveniently split into an average term, $V_{rel}(\vec{r})$ and a remainder

$$V(A+1) = V_{rel}(\vec{r}) + V(r,\xi) \quad (4.5)$$

$V_{rel}(\vec{r})$ is a function only of the relative coordinate between the neutron and the center-of-mass of the target nucleus and, hence, represents the average effect of all the nucleons; it is indeed the optical model potential. $V(r,\xi)$ is, from (4.5), just the difference between the exact potential between the incident particle and the target nucleons, and the model potential $V_{rel}(\vec{r})$. It is a function of both the relative coordinate $\vec{r}$ and all the internal coordinates $r_i(i=1,\cdots,A)$ here denoted by ξ, for convenience.

We can now rewrite (4.1) as

$$\left[H_o(\xi) + H(\vec{r}) - \frac{\hbar^2}{2(M + m_{A+1})}\nabla_R^2 + V(\vec{r},\xi)\right]\Psi(\vec{R},\vec{r},\xi) = E_{Lab}\Psi(\vec{R},\vec{r},\xi) \tag{4.6}$$

where $$H_o(\xi) = T_{int} + V_{int} \tag{4.7a}$$

$$H(\vec{r}) = -\frac{\hbar^2}{2m}\nabla_{\vec{r}}^2 + V_{rel}(\vec{r}) \tag{4.7b}$$

and $$\frac{1}{m} = \frac{1}{M} + \frac{1}{m_{A+1}} \tag{4.7c}$$

It is particularly simple to separate the center-of-mass motion from (4.6) by writing $\Psi(\vec{R},\vec{r},\xi) = e^{i\vec{K}_o\cdot\vec{R}}\,\Psi(\vec{r},\xi)$ and substituting back into (4.6). This is possible since the motion of the center of the mass is unaffected by any interaction. We obtain

$$\left[H_o(\xi) + H(\vec{r}) + V(\vec{r},\xi)\right]\Psi(\vec{r},\xi) = E\Psi(\vec{r},\xi) \tag{4.8}$$

where $E = E_{Lab} - \frac{\hbar^2 K_c^2}{2(M+m_{A+1})}$, the total energy of the interacting system.

Equation (4.8) will be regarded as the basic equation of the total system, analogous to (2.1). It is fairly trivial to show that in the absence of the interaction potential $V(\vec{r},\xi)$, $\Psi(\vec{r},\xi)$ can be written as a product of two wave functions of internal and relative coordinates and the wave equation resulting from this is precisely (2.1), but with the energy E redefined as the total energy less the initial energy of the target system.

In the absence of a potential between the relative coordinate $\vec{r}$, and the internal nuclear coordinates ξ, i.e. when $V(\vec{r},\xi) = 0$, the solution to (4.8) can be written precisely in the form previously chosen, (3.1). We shall therefore consider $V(\vec{r},\xi)$, as a perturbation to the ordinary, separable, Hamiltonian of the system. Multiplying (4.8) on the left by $\Phi_{J'}^{M'}(\xi)^\dagger$ and integrating over the internal coordinates of the target, we obtain

$$\left[H(\vec{r}) - E'(J')\right]\Upsilon_{(\vec{r},\vec{\sigma})}^{(J'M')} = -\int\Phi_{J'}^{M'}(\xi)^\dagger V(\vec{r},\xi)\Psi(\vec{r},\vec{\sigma},\xi)d\xi \tag{4.9}$$

where $$\Upsilon_{(\vec{r},\vec{\sigma})}^{(J'M')} = \int\Phi_{J'}^{M'}(\xi)^\dagger\Psi(\vec{r},\vec{\sigma},\xi)d\xi\,,\quad E'(J') = E - E_{J'} \tag{4.10}$$

and we made use of the eigenequation of the target system

$$H_o\Phi_J^M(\xi) = E_J\Phi_J^M(\xi) \tag{4.11}$$

The new equation is a function of $\vec{r}$ (and $\vec{\sigma}$) only. To solve it we make use of the technique of the Green's function and rewrite (4.9) in the form

$$\Upsilon_{(\vec{r},\vec{\sigma})}^{(J'M')} = \Psi_{(\vec{r},\vec{\sigma})}^{(J')} + \int K_{(\vec{r},\vec{\sigma},\vec{r}',\vec{\sigma}')}^{(J')} F_{(\vec{r}',\vec{\sigma}')}^{(J'M')}d\vec{r}'d\vec{\sigma}' \tag{4.12}$$

where $$F_{(\vec{r}',\vec{\sigma}')}^{(J'M')} = -\int\Phi_{J'}^{M'}(\xi)^\dagger V(\vec{r}',\xi)\Psi(\vec{r}',\vec{\sigma}',\xi)d\xi \tag{4.13}$$

$$\left[H(\vec{r}) - E'(J')\right]K_{(\vec{r},\vec{\sigma},\vec{r}',\vec{\sigma}')}^{(J')} = \delta(\vec{r} - \vec{r}')\delta(\vec{\sigma} - \vec{\sigma}') \tag{4.14}$$

and $\Psi_{(\vec{r},\vec{\sigma})}^{(J')}$ is the "unperturbed" solution to (4.9) defined by

$$\left[H(\vec{r}) - E'(J')\right]\Psi_{(\vec{r},\vec{\sigma})}^{(J')} = 0 \tag{4.15}$$

Equation (4.15) is identical to (2.1), with the energy appropriately redefined, and its solution has been derived in some detail in Section 2.

To determine the solutions to the remaining equations and from these the total wave function requires that we introduce appropriate boundary conditions.

We are interested in the scattering solutions to the complete wave equation (4.1) which we can evaluate by making use of (4.10) and the closure property

$$\sum_{JM} \Phi^M_J(\xi')^\dagger \Phi^M_J(\xi) = \delta(\xi-\xi')$$

The total wave function thus is

$$\Psi(\vec{r},\vec{\sigma},\xi) = \sum_{J'M'} \Phi^{M'}_{J'}(\xi) \mathcal{Y}^{(J'M')}_{(\vec{r},\vec{\sigma})} \tag{4.16}$$

which asymptotically must be the sum of an initial wave function and an outgoing spherical wave. With the use of (4.16) and (4.12), and the previously derived characteristics of $\Psi^{(J)}(\vec{r},\vec{\sigma})$, (cf. (2.7)), these boundary conditions are reflected in the requirement that $K(\vec{r},\vec{r}') \underset{r\to\infty}{\sim} e^{ik'r}$. Furthermore the analyticity of the total wave function at the origin puts another condition on $K^{(J')}(\vec{r},\vec{r}')$. The solution to (4.14) makes use of these two boundary conditions and the fact that except for the δ-function, equations (4.14) and (4.15) are identical in form. Therefore $K^{(J')}(\vec{r},r')$ can be written in terms of the solutions to (4.15). This results in two different solutions, depending upon whether r is greater or less than r'. Specifically, following Mott and Massey (19) we write the Green's function in the partial wave expansion form as

$$K^{(J')}(\vec{r},\vec{\sigma},\vec{r}',\vec{\sigma}') = \frac{-2m}{\hbar^2 k'} \sum_{\ell j\mu} \frac{L^j_\ell(r)}{r} \frac{h^j_\ell(r')}{r'} \mathcal{Y}_{\ell j\mu}(\hat{r},\vec{\sigma}) \mathcal{Y}^\dagger_{\ell j\mu}(\hat{r}',\vec{\sigma}') \qquad r<r' \tag{4.17a}$$

$$= \frac{-2m}{\hbar^2 k'} \sum_{\ell j\mu} \frac{L^j_\ell(r')}{r'} \frac{h^j_\ell(r)}{r} \mathcal{Y}_{\ell j\mu}(\hat{r},\vec{\sigma}) \mathcal{Y}^\dagger_{\ell j\mu}(\hat{r}',\vec{\sigma}') \qquad r>r' \tag{4.17b}$$

where $L^j_\ell(r)$, previously defined, and $h^j_\ell(r)$ are solutions of the radial equation (2.6), differing only in their boundary conditions. $L^j_\ell(r)$ is regular at r = 0 while $h^j_\ell(r)$ is irregular and

$$h^j_\ell(r) \underset{r\to\infty}{\sim} e^{i(k'r - \ell\pi/2 + \delta^j_\ell)} \tag{4.18}$$

and $$k' = \sqrt{\frac{2m}{\hbar^2} E'(J')}$$

Substitution of Equations (4.18), (4.17b), and (4.13) into the asymptotic value of the Green's function term on the right hand side of (4.12) yields

$$\int K^{(J')}(\vec{r},\vec{\sigma};\vec{r}',\vec{\sigma}') F^{(J',M')}(\vec{r}')d\vec{r}'$$

$$\underset{r\to\infty}{\sim} \frac{2m}{\hbar^2} \frac{e^{ik'r}}{r} \int dr' d\sigma' d\xi \sum_{\ell j\mu} \frac{L^j_\ell(r')}{r'} e^{i(\delta^j_\ell - \frac{\ell\pi}{2})} \mathcal{Y}_{\ell j\mu}(\hat{r},\vec{\sigma}) \mathcal{Y}^\dagger_{\ell j\mu}(\hat{r}',\vec{\sigma}') \tag{4.19}$$

$$\Phi^{M'}_{J'}(\xi)^\dagger V(\vec{r},\xi) \Psi(\vec{r}',\vec{\sigma}',\xi)$$

Making use of the definition of the vector spherical harmonic (2.4) we can write equation (4.19) as

$$\int K^{(J')}(\vec{r},\vec{r}') F^{(J',M')}(\vec{r}') d\vec{r}' \underset{r\to\infty}{\sim} \frac{m}{2\pi\hbar^2} \frac{e^{ik'r}}{r} \sum_{m_s} \chi^{m_s}_{\frac{1}{2}}(\vec{\sigma})$$

$$\int d\vec{\sigma}' d\vec{r}' d\xi \; \Psi^\dagger_f(J')(\vec{r}',\vec{\sigma}') \Phi^{M'}_{J'}(\xi)^\dagger V(\vec{r}',\xi) \Psi(\vec{r}',\vec{\sigma}',\xi) \tag{4.20}$$

where cf. (2.11),

$$\Psi^\dagger_{f(r',\vec{\sigma}')}(J') = \frac{4\pi}{k'r'} \sum_{\ell m_\ell j\mu} (-i)^\ell C^{\ell\ \frac{1}{2}\ j}_{m_\ell\ m_s\mu} Y^{m_\ell}_\ell(\hat{k}) \mathcal{Y}^\dagger_{\ell j\mu}(\vec{r}',\vec{\sigma}') e^{-i\delta^j_\ell} L^j_\ell(r') \tag{4.21}$$

$\Psi_f^{(J')\dagger}(\vec{r},\vec{\sigma})$ is the solution to the scattering problem, Eq. (2.1), involving the complex conjugate of the potential well, with an in-going boundary condition.

Substituting (4.20) and (2.7), the asymptotic solution of (4.15), into (4.12), we can write the complete scattering solution (4.16) as

$$\Psi(\vec{r},\vec{\sigma},\xi) = e^{i\vec{k}\cdot\vec{r}}\,\chi_{\frac{1}{2}}^{m_s}(\vec{\sigma})\Phi_{J_i}^{M_i}(\xi) + \frac{e^{ikr}}{r} f^{m_s}(\theta,\vec{\sigma})\Phi_{Ji}^{Mi}(\xi) \tag{4.22}$$

$$+ \frac{m}{2\pi\hbar^2}\frac{e^{ik'r}}{r}\sum_{\substack{J'M'\\ m_s'}}\Phi_{J'}^{M'}(\xi)\chi_{\frac{1}{2}}^{m_s'}(\vec{\sigma})\int d\vec{r}'\,d\vec{\sigma}'\,d\xi'\,\Psi_f^{(J')\dagger}(\vec{r}',\vec{\sigma}')\Phi_{J'}^{M'}(\xi)^{\dagger}V(\vec{r}',\xi)\Psi(\vec{r}',\vec{\sigma}',\xi')$$

Comparing (4.22) with (2.7) we see that an additional scattering amplitude term results. The contribution of this term to the differential cross-section, using (2.14), for a process which leaves the nucleus in the state E_f and the neutron in state m_s' is

$$\sigma(\theta)\Big|_{\substack{E_i\to E_f\\ m_s\to m_s'}} = \frac{k'}{k}\left|\frac{m}{2\pi\hbar^2}\left(\Psi(\vec{r},\vec{\sigma})\Phi_{J_f}^{M_f}(\xi),\ V(\vec{r},\xi)\Psi(\vec{r},\vec{\sigma},\xi)\right)\right|^2 \tag{4.23}$$

where the scalar product notation is used and the integration is over all the coordinates indicated.

The Born Approximation results from the replacement of the total wave function in (4.22) or (4.23) by an iterative solution. If we set $\Psi(\vec{r},\vec{\sigma},\xi)$ equal to the initial wave function $\Psi(\vec{r},\vec{\sigma},\xi) = \Psi_i(\vec{r},\vec{\sigma})\Phi_{J_i}^{M_i}(\xi)$ where Ψ_i is given by (2.11), then the resultant expression for the differential cross-section is the First Order Born Approximation

$$\sigma_{fi}(\theta) = \frac{k'}{k}\left|\left(\Psi_f(\vec{r},\vec{\sigma})\Phi_{J_f}^{M_f}(\xi),\ U(\vec{r},\xi)\Phi_{J_i}^{M_i}(\xi)\Psi_i(\vec{r},\vec{\sigma})\right)\right|^2 \tag{4.24}$$

where $$U(\vec{r},\xi) = \frac{m}{2\pi\hbar^2}V(\vec{r},\xi)$$

Since Ψ_i and Ψ_f appearing in (4.24) are the exact solutions of the wave equation including the effect of the nuclear potential, this particular form of the cross-section is called the Distorted Wave Born Approximation (DWBA). If, on the other hand, the effect of the nuclear potential is neglected in calculating the wave functions appearing in (4.24), the Plane Wave Born Approximation results. Since no appeal to the formation of the compound nucleus was made in deriving the cross-section (4.23), this particular model is called the direct interaction cross-section. Note that when $V(r,\xi)$ is independent of ξ, the integral over ξ' in (4.22) requires that $J' = J_i$, $M' = M_i$, and the third term on the right hand side of (4.22) reduces to a constant multiplied by the outgoing spherical wave

$$\frac{e^{ikr}}{r}\Phi_{J_i}^{M_i}(\xi)\chi_{\frac{1}{2}}^{m_s'}(\vec{\sigma}).$$

This is precisely the same as just modifying the initial optical model to produce a different value for the scattering amplitude, $f(\theta,\sigma)$.

As an aside, it is interesting to note that the scattering of low energy neutrons by atoms of a solid (or liquid or gas) can be treated in this same formalism. In this case, there is no "effective potential" ($V(r) = 0$) and rigorously $\Psi_f \to e^{i\vec{R}\cdot\vec{r}}\chi_{\frac{1}{2}}^{m_s}(\vec{\sigma})$ and $\Psi_i \to e^{i\vec{k}\cdot\vec{r}}\chi_{\frac{1}{2}}^{m_s}(\vec{\sigma})$. If we now utilize the Fermi Pseudopotential Approximation, where the short-range neutron-nucleus potential is replaced by a delta function with an appropriate strength to give the correct total cross-section (20)

$$U(r,\xi) = \sum_{i=1}^{N} a_i\delta(\vec{r} - \vec{r}_i)$$

where a_i is the scattering length for the scattering by a target particle at the i^{th} position, and N is the total number of particles in the scattering system, the resulting differential cross-section is

$$\sigma^{m_s m_s'} = \frac{k'}{k} \left| \sum_{i=1}^{N} \left(\chi_{\frac{1}{2}}^{m_s'}(\vec{\sigma}),\ a_i \chi_{\frac{1}{2}}^{m_s}(\vec{\sigma}) \right) \int \Phi_f^{\dagger}(\vec{r}_i, \cdots, \vec{r}_N) e^{i\vec{K}\cdot\vec{r}_i} \Phi_i(\vec{r}_i, \cdots \vec{r}_N) \prod_{i=1}^{N} d\vec{r}_i \right|^2 \qquad (4.25)$$

where $\vec{K} = \vec{k} - \vec{k}'$, a familiar result and the basic equation for the scattering of long wave length neutrons from target states representing the quantum mechanical motion of the target system. (21)

In the remaining portion of this section we consider examples of the interaction potential $V(\vec{r},\xi)$ and its use in the calculation of nuclear cross-sections. For example, we consider the evaluation of the cross-section for the (n,p) reaction.* One assumes that the initial state is a distorted wave neutron scattering function Eq. (2.11) and a single bound proton and the final state is similar with the roles of the neutron and proton reversed. This has the effect of writing the target wave function in (4.24) in terms of an inert core and a single interacting particle. The result using (4.24) and a Legendre expansion of the two-body neutron-proton potential can be expressed as a sum over geometrical factors multiplied by the product of integrals over the radial coordinate. A similar result can be obtained for photonuclear reactions by means of a multipole expansion of the incident photon wave and calculating the differential cross-section by an equation equivalent to (4.24). The formulas for these types of direct interactions are rather complicated and we refer the reader to other papers for their explicit form, calculations using them and comparisons with experiments. (23,24)

In all of the above a spherically symmetric nuclear potential has been implied in the calculations. As is well known, the presence of collective nucleonic motion in nuclei gives rise to properties of nuclei such as axially symmetric deformations and vibrational bands of energy levels which are consistent with observed experimental results. Tamura has recently written a review paper summarizing a technique for including the effect of a collective nuclear potential in nuclear scattering theory.(25) He chose an explicit form (Saxon-Woods) for the interaction potential (26) V(A+1) (see (4.5)) and writes, for the central part

$$V(A+1) = V(\vec{r},\vec{\Omega}) = -(V + iW) \frac{1}{1 + e^{\frac{r - R(\Omega)}{a}}} \qquad (4.26)$$

where $$R = R_c\left(1 + \sum_{\lambda\mu} \alpha_{\lambda\mu} Y_\lambda^\mu(\Omega)\right) \qquad (4.27a)$$

for "vibrational" nuclei

and $$R = R_o\left(1 + \sum_{\lambda} \beta_\lambda Y_\lambda^o(\Omega)\right) \qquad (4.27b)$$

for "rotational" nuclei, where $\vec{r}'$ is in the body-fixed coordinates for "rotational" nuclei and $\alpha_{\lambda\mu}$ and β_λ are the customary parameters for collective motion. (27) Similar potential terms are used for the spin-orbit and Coulomb parts. Tamura then expands $R(\Omega)$ appearing in (4.26) by means of either form of (4.27) as appropriate and for the first term of the expansion finds the familiar optical model potential. The remaining terms, V(coupling), constitute the interaction between the incident particle and the non-static part of the nuclear motion and an equation analogous to (4.9) results. It can be solved to varying degrees of approximation. The most exact way, called the "coupled channel" method, involves writing the total wave function as

---

* Deuteron stripping, i.e. (d,p) or (d,n) reactions, whose characteristics could not be explained by the formation of a compound nucleus, were the early examples of the use of direct interaction theory. However, before the use of DWBA, the magnitudes of the cross-sections could not be predicted with much confidence. (22)

$$\Psi(r,\sigma,\xi) = \sum_{\substack{n\ell_n j_n \\ m}} \frac{R^{n}_{\ell_n j_n}(r)}{r} \Psi^{m}_{\ell_n j_n}(\hat{r},\vec{\sigma},\xi) \tag{4.28}$$

See (3.1) for the definitions. The index n denotes the "interaction channel" determined by the state of the nucleus

$$H_o(\xi)\Phi^{M_n}_{J_n}(\xi) = E_n\Phi^{M}_{J_n}(\xi) \tag{4.29}$$

Substitution of (4.28) into (4.9), with multiplication on the left by $\Psi^{m}_{\ell_n j_n}(\hat{r},\vec{\sigma},\xi)^{\dagger}$ and integration over all the coordinates but r results in an equation for the radial function $R^{n}_{\ell_n j_n}(r)$

$$\left(\frac{d^2}{dx_n^2} + 1 - \frac{\ell_n(\ell_n+1)}{x_n} - \frac{V(r)}{(E-E_n)}\right) R^{n}_{\ell_n j_n}(r)$$

$$= \frac{1}{(E-E_n)} \sum_{n'\ell'_n j'_n} \left\{ \int d\hat{r}d\vec{\sigma}d\xi \; \Psi^{m}_{\ell_n j_n}(\hat{r},\vec{\sigma},\xi)^{\dagger} V(\vec{r},\xi)_{\text{coup.}} \Psi_{J\; n' j'_n}(\hat{r},\vec{\sigma},\xi) \right\} R^{n'}_{\ell'_n j'_n}(r) \tag{4.30}$$

When $V_{\text{coupling}} = 0$, (4.30) is identical to (2.6). With the term on the right hand side of (4.30) not equal to zero, the solution for the radial function requires a knowledge of the function for all other possible channels, or, alternatively, diagonalization of the matrix equation resulting from (4.30). This procedure is quite lengthy and time consuming and it is reasonable to limit the coupling of only two or a few channels in the calculation. Two-channel programs utilizing these approximations have been written by Dunford (28) and Buck (29) and have proven useful in the calculation of nuclear cross-sections.

A simpler alternative method to the nuclear cross-section calculation is to add to the scattering amplitude $f(\theta,\vec{\sigma})$ appearing in (4.22), the DWBA given by (4.24). Intermediate between these two methods is the adiabatic approximation, wherein it is assumed that the initial state of the target system $\Phi^{M_i}_{J_i}(\xi)$ changes very much more slowly than the projectile wave function $\Psi(\vec{r},\vec{\sigma})$, and $\Psi(\vec{r},\vec{\sigma},\xi)$ in (4.23) is replaced by $\Psi(\vec{r},\vec{\sigma},\xi) \rightarrow \Psi^{i}_{J}(\xi)\Psi(\vec{r},\vec{\sigma})$ where $\Psi(\vec{r},\vec{\sigma})$ is now the solution of the Schrodinger Equation including $V(\vec{r},\xi)$, (or, rather, its matrix element between $\Phi^{M_i}_{J_i}(\xi)$) instead of with $V(r,\xi) = 0$, as in the DWBA.

FURTHER MODIFICATIONS

In the previous sections we went into some detail in deriving the appropriate equations used in optical model calculations and in extending the optical model to include certain properties of the ground state of the system. In this section we shall touch briefly on further modifications that have been made to the simple optical model and include references, where appropriate, for the reader to receive more information on these modifications and results of calculations using the simple and extended optical model.*

As a projectile transverses a nucleus a series of interactions takes place between the projectile and nucleons in the target. The possibility of multiple scattering excitation can be examined through a series of terms in a perturbation expansion. This succession of excitations and de-

* A large variety of nuclear cross-section calculations is being presented here at this conference and it is suggested that the reader look at these papers for detailed results.

excitations produced by the two-body interaction potential can be replaced by an effective imaginary potential as described, e.g. by Brown.(30) This effective imaginary potential is manifestly a non-local operator. Perey and Buck have performed calculations for the scattering of particles from a non-local potential by replacing $V(\vec{r})\Psi(\vec{r})$ in the Schrodinger equation by the integral $\int V(\vec{r},\vec{r}')\Psi(\vec{r}')d\vec{r}'$ and have obtained quite satisfactory comparisons to experimental cross-section results with a single set of non-local potential parameters. In addition, Perey and Buck have evaluated an equivalent local optical model with energy-dependent parameters, to produce good fits to experimental data for a variety of target nuclei.(31) Another approach has been to re-examine the compound nucleus cross-section in terms of the actual probability for the formation of the compound intermediate state, especially in the absence of a sufficiently dense continuum of compound states for the statistical model described earlier in Section 3 to be valid. This can be seen most simply from equation (3.5) with the collision matrix U_{cc}, replacing the phase shift factor $e^{2i\delta}$. The penetrability as given by (3.7) is re-defined as $1 - |U|^2$ which to the first order in the strength function, Γ/D, is given by (3.29). The magnitude of the collision matrix has been written by Krieger as, at least in the absence of channel-channel correlations, (32)

$$|U_{cc}| = \frac{1 - \frac{\pi}{2}\Gamma_{c/D}}{1 + \frac{\pi}{2}\Gamma_{c/D}}$$

which leads to

$$T \equiv 1 - |U_{cc}|^2 = 2\pi\frac{\Gamma c}{D} - 2\pi^2\frac{\Gamma c^2}{D^2} + \ldots$$

A similar type of analysis has been carried out by Moldauer (33), and the machine program NEARREX (34), which accepts phase shifts from ABACUS-2 (35) and modifies the transmission coefficients accordingly, has been used to calculate nuclear cross-sections. Comparison with experiments, especially for incident energies just above the threshold for the excitation of a particular excited level where the statistical model is expected to be the most inaccurate, indicates the necessity for the use of an approach of this sort for predicting experimental results. On the other hand, when the density of compound states is high, the elementary form of compound nucleus theory seems to produce reasonable results and indeed to provide some sort of choice of spins of levels of the outgoing nucleus. (36, 37)

Use of this model in one of its original or corrected forms does require detailed information on all possible final states of the system. Information is frequently lacking at least for more than the first few excited states. For this region the Fermi gas model is used where the incident particle's energy is assumed to raise the nuclear temperature yielding on a purely statistical basis a probability for one of the particles in the nucleus to be ejected. This particular theory is obviously somewhat more difficult to justify on an a priori basis but has been used at least to correlate data in this higher energy range. (38)

VI. SUMMARY

The advent of fast computers has prompted parallel improvements in optical model calculations. From Bjorklund and Fernbach's spin-orbit calculations (39) to the most recent complete coupled calculations of Tamura, there has been an improvement of several orders of magnitude in the speed of digital computer calculations, so that the elapsed time for these two calculations of widely different complexity has probably not changed very much. This brief summary in fact has omitted any mention of earlier, analytic square well potential calculations with no spin-orbit coupling. Thus it has become possible, and indeed customary, to vary the optical model parameters to fit appropriate measured cross-sections and then to calculate with these fitted parameters

a large number of nuclear cross-sections which are needed for reactor physics calculations. A succession of steps has been presented by which the customary formulas for nuclear cross-sections can be derived, as well as suggestions for their modifications based on the work of numerous investigators in this field.

The remaining portion of this section contains a summary of the author's impressions as to the confidence one can place in nuclear cross-section calculations based on these models. (During a recent conference held in Washington this question was discussed.) (40) In the resonance region (that is, for incident neutrons below about 100 Kev in energy for most target nuclei) single or multi-level formulas are used to reproduce point-by-point cross-sections. A method has been presented here in some detail which shows promise in extending optical model calculations to light-weight nuclei where the resonance region includes the Mev region. The great success of the optical model in predicting nuclear cross-sections comes in the Mev region where the averaging process inherent in the model is most appropriate. That is to say, except for possible fluctuations due to the presence of certain open channels, the narrow compound nucleus resonances are inherently broadened into the smooth background by either "Doppler broadening" by the recoil of the target or by the limitations on the experimental energy resolution. This is especially true when the experimental cross-section is not very sensitive to the particular nature of the target nucleus; that is, for quantities such as total cross-sections and angular distributions.(41) There are, however, a variety of cross-sections needed for reactor physics calculations which can be given only very approximately by model calculations described herein, and whether the nuclear designer will accept these computed values depends a great deal on the detail and importance he attaches to a precise knowledge of these numbers. In this latter category are quantities such as (n,γ), $(n,n'\gamma)$, (n,p) and, of course, fission cross-sections.

The optical model has proved useful in reproducing a large variety of nuclear cross-section data, and especially in interpolation between measured values. It also suggests values and provides systematics for unmeasured cross-sections It has proved of lesser value for certain other quantities for which measurements are still required.

Acknowledgements

The author would like to acknowledge the contributions of Dr. N. C. Francis and C. R. Lubitz, who with the author published a version of a portion of this paper. (23) Numerous discussions with members of the Reactor Radiations Division and the Neutron Physics Section of the National Bureau of Standards are also gratefully acknowledged.

APPENDIX A

DEVIATION OF DIFFERENTIAL CROSS-SECTION AND POLARIZATION EQS. (3.5) & (3.6)

Using the definitions of the Racah coefficients as given for example by Rose, (6) the sums over azimuthal quantum numbers appearing in Eq. (2.17) can be carried out. This will result in expressions which are much simpler in appearance as well as concept. Furthermore the introduction of the auxiliary coefficient C_{m_1} enables the differential cross-section and polarization to be derived simultaneously until the very last step.

We make use of the following relationships

$$Y_{\ell}^{m}(\hat{k})^{*}\,Y_{\tilde{\ell}}^{\tilde{m}}(\hat{k}) = \sum_{LM}(-)^{m_\ell}\sqrt{\frac{(2\ell+1)(2\tilde{\ell}+1)}{4\pi\,(2L+1)}}\;C^{\ell\tilde{\ell}L}_{-m_\ell\,\tilde{m}_\ell\,M}\;C^{\ell\tilde{\ell}L}_{oo}\;Y_L^M(\hat{k})$$

$$Y_{\ell}^{m'_\ell}(\hat{r})\,Y_{\tilde{\ell}}^{\tilde{m}'_\ell}(\hat{r})^{*} = \sum_{\mathcal{LM}}(-)^{\tilde{m}'_\ell}\sqrt{\frac{(2\ell+1)(2\tilde{\ell}+1)}{4\pi\,(2\mathcal{L}+1)}}\;C^{\ell\tilde{\ell}\mathcal{L}}_{m'_\ell\,-\tilde{m}'_\ell\,m}\;C^{\ell\tilde{\ell}\mathcal{L}}_{oo}\;Y^{m}_{\mathcal{L}}(\hat{r})$$

$$\sum_{m_\ell\,\tilde{m}_\ell\,m_s}(-)^{m_\ell}\;C^{\ell\,\frac{1}{2}\,j}_{m_\ell\,m_s\,\mu}\;C^{\tilde{\ell}\,\frac{1}{2}\,j}_{\tilde{m}_\ell\,m_s\,\mu}\;C^{\ell\tilde{\ell}L}_{-m_\ell\,\tilde{m}_\ell\,M}$$

$$= (-)^{L+\frac{1}{2}-\tilde{j}}\sqrt{(2j+1)(2L+1)}\;W(j\ell\tilde{j}\tilde{\ell};\tfrac{1}{2}L)\;C^{jL\tilde{j}}_{\mu M\tilde{\mu}}$$

$$\sum_{\mu} C^{\ell\,\frac{1}{2}\,j}_{m'_\ell m'_s\mu}\;C^{jL\tilde{j}}_{\mu M\tilde{\mu}}\sum_{f\varphi}\sqrt{(2j+1)(2f+1)}\;W(\ell\tfrac{1}{2}\tilde{j}L;\,jf)\;C^{\ell f\tilde{j}}_{\tilde{m}_\ell\,\varphi\tilde{\mu}}\;C^{\frac{1}{2}Lf}_{m'_s M\varphi}$$

$$\sum_{m'_\ell\,\tilde{m}'_\ell\,\tilde{\mu}}(-)^{\tilde{m}'_\ell}\;C^{\ell f\tilde{j}}_{m'_\ell\varphi\tilde{\mu}}\;C^{\tilde{\ell}\,\frac{1}{2}\,j}_{\tilde{m}'_\ell m'_s\tilde{\mu}}\;C^{\ell\mathcal{L}\mathcal{L}}_{m'-\tilde{m}\,m}$$

$$= (-)^{\ell+f-\frac{1}{2}}(2j+1)\sqrt{\frac{2L+1}{2}}\;W(\mathcal{L}\ell\tfrac{1}{2}\tilde{j};\tilde{\ell}\,f)\;C^{\mathcal{L}f\frac{1}{2}}_{m\varphi m'_s}$$

$$\sum_{\varphi} C^{\frac{1}{2}Lf}_{m'_s m\varphi}\;C^{\mathcal{L}f\frac{1}{2}}_{m\varphi m'_s} = (-)^{\mathcal{L}+f-\frac{1}{2}}\sum_{g}\sqrt{(2f+1)(2g+1)}\;\delta_{M,-m}$$

$$W(\tfrac{1}{2}L\tfrac{1}{2}\mathcal{L};\,fg)\;C^{\frac{1}{2}g\frac{1}{2}}_{m'_s o m'_s}\;C^{L\mathcal{L}g}_{M-Mo}$$

$$\sum_{f}(2f+1)\,W(\tfrac{1}{2}\tilde{j}L;\,jf)\,W(\;\tfrac{1}{2}\tilde{j};\,\tilde{f})\;\;W(\tfrac{1}{2}L\tfrac{1}{2}\mathcal{L};\,fg) = X(j\tilde{j}\tfrac{1}{2};\,j\ell\tfrac{1}{2};\,L\mathcal{L}g)$$

where X is the X-coefficient, given by Rose.(6)

Substituting all of the above expressions into Eq. (2.17), we obtain

$$\Phi(\theta) = \frac{\pi}{2k^2}\sum_{\substack{\ell j\tilde{\ell}\tilde{j}m'_s\\ LM\mathcal{L}g}} C_{m'_s}\;Y_L^M(\hat{k})\;Y_L^{-M}(\hat{r})(-)^{\ell+\frac{1}{2}-\tilde{j}}(1-\eta_\ell^j)(1-\eta_{\tilde{\ell}}^{\tilde{j}})^{*}(2j+1)$$

$$(2\ell+1)(2\tilde{\ell}+1)(2\tilde{j}+1)\sqrt{\frac{2g+1}{2}}\;C^{\ell\tilde{\ell}L}_{oo}\;C^{\ell\tilde{\ell}\mathcal{L}}_{oo}$$

$$W(j\ell\tilde{j}\;\tilde{\ell};\,\tfrac{1}{2}L)\;X(j\ell\tfrac{1}{2};j\ell\tfrac{1}{2};\,L\mathcal{L}g)$$

$$C^{\frac{1}{2}\,g\,\frac{1}{2}}_{m'_s o m'_s}\;C^{L\mathcal{L}g}_{M-Mo}$$

Examining $C^{\frac{1}{2}\,g\,\frac{1}{2}}_{m'_s o m'_s}$, we see that there are two possible values for g, viz. 0, and 1. For g = 0, $\mathcal{L} = L$. For g = 1, $C^{\mathcal{L}\,L\,1}_{M-M\,o}$ requires that $\mathcal{L} = L$, or $\mathcal{L} = L \pm 1$. From $C^{\ell\tilde{\ell}L}_{oo}$ and $C^{\ell\tilde{\ell}\mathcal{L}}_{oo}$ we see that $\ell+\tilde{\ell}+L$ and $\ell+\tilde{\ell}+\mathcal{L}$ must both be even. This requires that L and $\mathcal{L}$ must be equal, or else differ by an even number. Thus we see that $\mathcal{L} = L$, for both values of g. We consider each case separately.

1) $g = 0$

$$\sum_{m_s m_s'} C_{m_s}\, C^{\frac{1}{2}\ o\ \frac{1}{2}}_{m_s\ o\ m_s'} = 2 \text{ for } C_{m_s'} = 1$$

$$= 0 \text{ for } C_{m_s'} = (-)^{\frac{1}{2} - m_s'}$$

Thus $g = 0$ projects out $\sigma(\theta)$ from (A.1). Furthermore

$$C^{L\ L\ o}_{M-M\ o} = (-)^{L+M} \frac{1}{\sqrt{2L+1}}$$

$$X(\widetilde{j\ell}\tfrac{1}{2};\ j\ell\tfrac{1}{2};\ LLo) = \frac{(-)^{\ell + \frac{1}{2} - \widetilde{j}}}{\sqrt{2(2L+1)}}\ W(\widetilde{j\ell}j\ell;\ \tfrac{1}{2}L)$$

Making use of

$$P_L(\hat{k}\cdot\hat{r}) = \frac{2L+1}{4\pi} \sum_M (-)^M Y_L^M(\hat{k}) Y_L^{-M}(\hat{r})$$

and previous expressions, we find that the differential cross-section is

$$\sigma(\theta) = \frac{1}{8k^2} \sum_{\substack{\ell j \widetilde{\ell} \widetilde{j} \\ L}} P_L(\hat{k}\cdot\hat{r})\ (1 - \eta_\ell^j)\ (1 - \eta_{\widetilde{\ell}}^{\widetilde{j}})^*\ (C^{\ell \widetilde{\ell} L}_{oo})^2$$

$$(2\ell+1)(2j+1)(2\widetilde{\ell}+1)(2\widetilde{j}+1)\ W^2(j\ell\widetilde{j}\widetilde{\ell};\ \tfrac{1}{2}L) \qquad \text{(A.2)}$$

The formula presented in the text Eq. (2.18) results from using the modified Z-coefficient introduced by Blatt and Biedenharn. (42)

$$Z(abcd;\ ef) = \sqrt{(2a+1)\ (2b+1)\ (2c+1)\ (2d+1)}\ C^{a\ c\ f}_{0\ 0}\ W(abcd;\ ef)$$

2) $g = 1$

$$\sum_{m_s m_s'} C_{m_s}\, C^{\frac{1}{2}\ 1\ \frac{1}{2}}_{m_s\ m_s'} = 0 \text{ for } C_{m_s'} = 1$$

$$= \sqrt{\frac{2}{3}} \text{ for } C_{m_s'} = (-)^{\frac{1}{2} - m_s'}$$

and $g = 1$ projects out $\sigma(\theta)P(\theta)$ from (A.1).

Using

$$C^{L\ L\ 1}_{M-M} = (-)^{L-M} \sqrt{\frac{3}{2L+1}}\ \frac{M}{\sqrt{L(L+1)}}$$

$$\sum_M (-)^M M Y_L^M(\hat{k}) Y_L^{-M}(\hat{r}) = \frac{2L+1}{4\pi i} P_L'(\hat{k}\cdot\hat{r})\ (\hat{k} \times \hat{r})_{\text{Z-component}}$$

we find the result quoted in the text. Eq. (2.19).

APPENDIX B

CROSS-SECTION FOR FORMATION OF THE COMPOUND NUCLEUS

Using Eq. (3.3) in Eq. (3.4), the compound nucleus cross-section can be written as

$$\sigma_{\mathcal{J}} = \frac{4\pi^2}{k^2 r^2} \sum_{\substack{\ell m_\ell \tilde{\ell} \tilde{m}_\ell \\ J_i \mu_i \tilde{J}_i \tilde{\mu}_i \\ M_i \mu_i \tilde{M}_i \tilde{\mu}_i \\ m'_\ell m_s \tilde{m}'_\ell \tilde{m}'_s \\ \mathcal{J} m_{\mathcal{J}} s M_i}} \frac{(1 - \eta_{\mathcal{J}}^{j} \eta_{\tilde{\mathcal{J}}}^{\tilde{j}*})}{2(2J_i + 1)} Y_{\ell}^{m_\ell *}(\hat{k}) Y_{\tilde{\ell}}^{\tilde{m}_\ell}(\hat{k}) Y_{\ell}^{m'_\ell}(\hat{r}) Y_{\tilde{\ell}}^{\tilde{m}'_\ell}(\hat{r})^* \chi_{\frac{1}{2}}^{m'_s}(\vec{\sigma}) \chi_{\frac{1}{2}}^{\tilde{m}'_s}(\vec{\sigma})^{\dagger} \Phi_{J_i}^{M'_i}(\xi) \Phi_{J_i}^{\tilde{M}'_i}(\xi)^{\dagger} \quad \text{(B.1)}$$

$$C^{\ell \frac{1}{2} j}_{m_\ell m_s \mu} C^{j J_i \mathcal{J}}_{\mu M_i m_{\mathcal{J}}} C^{j' J_i \mathcal{J}}_{\mu' M'_i m_{\mathcal{J}}} C^{\tilde{\ell} \frac{1}{2} \tilde{j}}_{\tilde{m}_\ell \tilde{m}_s \tilde{\mu}} C^{\tilde{j} J_i \tilde{\mathcal{J}}}_{\tilde{\mu} \tilde{M}_i \tilde{m}_{\tilde{\mathcal{J}}}} C^{\tilde{j}' J_i \tilde{\mathcal{J}}}_{\tilde{\mu}' \tilde{M}'_i \tilde{m}_{\tilde{\mathcal{J}}}} C^{\tilde{\ell} \frac{1}{2} \tilde{j}'}_{\tilde{m}_\ell \tilde{m}_s \tilde{\mu}'},$$

To calculate the total current, we integrate Eq. (B.1) over nuclear coordinates, spins, and the solid angle $\hat{r}$. The result of this operation yields

$$r^2 \delta_{M_i \tilde{M}_i} \delta_{m_s \tilde{m}_s} \delta_{\ell \tilde{\ell}} \delta_{m_\ell \tilde{m}_\ell}.$$

We next use the following vector coupling relation slips,

$$Y_{\ell}^{m_\ell}(\hat{k})^* Y_{\tilde{\ell}}^{\tilde{m}_\ell}(\hat{k}) = \sum_{LM} (-)^{m_\ell} \frac{(2\ell + 1)}{\sqrt{4\pi(2L + 1)}} C^{\ell \tilde{\ell} L}_{0\ 0} C^{\ell \tilde{\ell} L}_{-m_\ell \tilde{m}_\ell M} Y_L^M(\hat{k})$$

$$\sum_{m_\ell \tilde{m}_\ell m_s} C^{\ell \frac{1}{2} j}_{m_\ell m_s \mu} C^{\tilde{\ell} \frac{1}{2} \tilde{j}}_{\tilde{m}_\ell m_s \tilde{\mu}} C^{\ell \tilde{\ell} L}_{-m_\ell \tilde{m}_\ell M} = (-)^{\frac{1}{2} - \tilde{j}} \sqrt{(2j + 1)(2L + 1)}\ W(j \ell \tilde{j} \tilde{\ell}; \tfrac{1}{2} L) C^{j L \tilde{j}}_{\mu M \tilde{\mu}}$$

$$\sum_{m'_\ell m'_s} C^{\ell \frac{1}{2} \tilde{j}}_{m'_\ell m'_s \mu'} C^{\ell \frac{1}{2} j}_{m'_\ell m'_s \mu} = \delta_{j \tilde{j}} \delta_{\mu \tilde{\mu}'}$$

$$\sum_{\tilde{\mathcal{J}} m} C^{j J_i \tilde{\mathcal{J}}}_{\mu M_i m} C^{j' J_i \tilde{\mathcal{J}}}_{\mu' M'_i m} = \delta_{\tilde{\mu} \tilde{\mu}'} \delta_{M_i M'_i}$$

$$\sum_{\mu \mu' M_i} C^{j J_i \mathcal{J}}_{\mu M_i m} C^{j J_i \mathcal{J}}_{\mu' M'_i m} C^{j L j'}_{\mu M \mu'}$$

$$= (-)^{J_i - \mathcal{J} - \frac{1}{2}} \sqrt{(2j+1)(2\mathcal{J}+1)}\ W(\mathcal{J} j \mathcal{J} j; J_i L) C^{\mathcal{J} L \mathcal{J}}_{-m M m}$$

Substitution of these equations into (B.1) yields Eq. (3.5), the cross-section for the formation of a compound nucleus.

The cross-section for the scattering of an incident spin ½ particle through the formation of a compound nucleus, as defined in the text, is given by:

$$\sigma_{C\text{-}N}(\theta) = \frac{4\pi^2}{k^2} \sum_{\substack{\ell_i j_i \ell_f j_f \\ L_i M_i L_f M_f}} (-)^{J_i + J_f - 2\mathcal{J} - i} \frac{(2\mathcal{J} + 1)}{8\pi(2J_i + 1)} \frac{T_{\ell_i}^{j_i}(E)\, T_{\ell_f}^{j_f}(E')}{\sum_P T_{\ell_p}^{j_p}(E'_p)} Y_{L_i}^{M_i}(\hat{k}_i) Y_{L_f}^{M_f}(\hat{k}_f)^* C^{\mathcal{J} L_i \mathcal{J}}_{m M_i - m} C^{\mathcal{J} L_f \mathcal{J}}_{m M_f - m}$$

$$Z(\ell_i j_i \ell_i j_i; \tfrac{1}{2} L_i)\ Z(\ell_f j_f \ell_f j_f; \tfrac{1}{2} L_f)$$

$$W(\mathcal{J} j_i \mathcal{J} j_i; J_i L_i)\ W(\mathcal{J} j_f \mathcal{J} j_f; J_f L_f)$$

Now

$$\sum_{m} C^{\mathcal{L}\, L_i\, \mathcal{L}}_{m\, M_i - m}\; C^{\mathcal{L}\, L_f\, \mathcal{L}}_{m\, M_f - m} = (2\mathcal{L}+1)\,\delta_{L_i L_f}\,\delta_{M_i M_f}$$

$$\sum_{M} Y^{M}_{L}(\hat{k}_i)\, Y^{M}_{L}(\hat{k}_f)^{*} = \frac{2L+1}{4\pi}\, P_L(\hat{k}_i\cdot\hat{k}_f)$$

Substituting into (B.2) we obtain Eq. (3.10) of the text.

APPENDIX C

COULOMB SCATTERING

The total wave function in the presence of a Coulomb potential can be written as (2.2) of the text where $u^{j}_{\ell}(r)$ satisfies the following confluent hypergeometric radial equation (5)

$$\frac{d^2 u^{j}_{\ell}}{dx^2} + \left(1 - \frac{2\eta}{x} - \frac{\ell(\ell+1)}{x^2} - \frac{V_i(x) + iW(x)}{E} - \frac{\gamma^{j}_{\ell}\, V_s(x)}{E}\right) u^{j}_{\ell} = 0 \qquad (C.1)$$

where $x = kr$, $\eta = Z_1 Z_2 e^2 / \frac{2E}{m}\hbar^2$

The regular and irregular solutions of (C.1) are asymptotically (cf. (2.10))

$$F_{\ell} \underset{r\to\infty}{\sim} \sin\left(kr - \eta \ln 2kr - \frac{\ell\pi}{2} + \sigma_{\ell} + \delta^{j}_{\ell}\right) \qquad (C.2a)$$

$$G_{\ell} \underset{r\to\infty}{\sim} \cos\left(kr - \eta \ln 2kr - \frac{\ell\pi}{2} + \sigma_{\ell} + \delta^{j}_{\ell}\right) \qquad (C.2b)$$

where δ^{j}_{ℓ} is the nuclear phase shift

and $\sigma_{\ell} = \arg\Gamma(\ell + 1 + i\eta) = \sigma_0 + \sum_{s=1}^{\ell} \tan^{-1}\frac{\eta}{s}$

The incoming plane wave appearing in (2.7) is replaced by

$$e^{i\vec{k}\cdot\vec{r}} \to e^{i(\vec{k}\cdot\vec{r} + \eta\, \ln kr[1 - \hat{k}\cdot\hat{r}])} = \Psi_c$$

which satisfies the nuclear potential free Schrodinger equation (to order $1/r^2$)

$$(\nabla^2 + k^2 - \frac{2\eta k}{r})\Psi_c = 0$$

Asymptotically $\Psi_c \underset{r\to\infty}{\sim} \sum_{\ell} i^{\ell}(2\ell+1)\,\dfrac{\sin\left(kr - \frac{\ell\pi}{2} - \eta\ln 2kr\right)}{kr}\, P_{\ell}(\hat{k}\cdot\hat{r})$

Proceeding analogously to (2.8) -- (2.13)

$$f^{m_s}(\theta,\vec{\sigma}) = \frac{2\pi}{ik} \sum_{\ell m_\ell j\mu} C^{\ell\, \frac{1}{2}\, j}_{m_\ell\, m_s\, \mu}\; Y^{m}(\hat{k})^{*}\, Y_{\ell j\mu}(\hat{r},\vec{\sigma})\left(e^{2i(\delta^{j}_{\ell} + \sigma_{\ell})} - 1\right) \qquad (C.3)$$

For pure Coulomb scattering, $\delta^{j}_{\ell} = 0$, there is no spin dependence and (5)

$$f_c(\theta) = \frac{\eta}{2k}\csc^2\frac{\theta}{2}\; e^{-2i\eta \ln \sin\frac{\theta}{2} + i\pi + 2i\sigma_0} \qquad (C.4)$$

Thus the scattering amplitude (C.3) can be written as

$$f^{m_s}(\theta,\vec{\sigma}) = f_c(\theta) + f^{m_s}_{N}(\theta,\vec{\sigma})$$

where

$$f_N^{m_s}(\theta,\vec{\sigma}) = \frac{2\pi}{ik} \sum_{\substack{\ell m_\ell \\ j\mu}} C^{\ell\ \frac{1}{2}\ j}_{m_\ell\ m_s\ \mu} Y_\ell^{m_\ell}(\hat{k})^* \mathcal{Y}_{\ell ju}(\hat{r},\vec{\sigma}) e^{2i\sigma_\ell}(e^{2i\delta_\ell^j} - 1) \qquad (C.5)$$

or the scattering cross-section is

$$|f^{m_s}(\theta,\vec{\sigma})|^2 = |f_c(\theta)|^2 + |f_N^{m_s}(\theta,\sigma)|^2 \qquad (C.6)$$

$$+ \text{ interference terms.}$$

The first two terms of (C.6) are easily interpretable. $|f_c(\theta)|^2$ is the ordinary Coulomb scattering cross-section, from (C.4)

$$\sigma_c(\theta) = |f_c(\theta)|^2 = \frac{\eta^2}{4k^2} \csc^4\frac{\theta}{2} = \left(\frac{Z_1 Z_2 e^2}{4E}\right)^2 \csc^4\frac{\theta}{2} \qquad (C.7)$$

$|f_N|^2$ is the nuclear part of the cross-section modified by the appearance of the Coulomb phase factor (note that its magnitude is unity and therefore does not contribute to the reaction cross-section. The interference terms between Coulomb and nuclear part is calculated directly from the product of (C.4) and (C.5).

As is well-known, integration of the Coulomb cross-section over the solid angle gives an infinite result, another manifestation of the non-point source nature of charged particles. Therefore, total cross-sections for charged particles are not meaningful and instead such cross-sections are reported as angular distribution ratios to the pure Coulomb cross-section, (C.7). (13)

The procedures outlined in the text for determining the phase shifts from matching logarithmic derivatives at nuclear cutoff distance R_c are used for Coulomb scattering also. However, the asymptotic spherical Bessel functions (2.23) must be replaced by the asymptotic form of the Coulomb wave function. (44)

References

1. Feshbach, H., Porter, C. E., and Weisskopf, V. F., Phys. Rev. 96, 448 (1954).
2. Wolfenstein, L., Phys. Rev. 82, 690 (1951).
3. Hauser, W., and Feshbach, H., Phys. Rev. 87, 366 (1952).
4. Bethe, H. A., Phys. Rev. 57, 1125 (1940).
5. Schiff, L. I., "Quantum Mechanics," McGraw-Hill, New York (1949) Chap. V.
6. The notation used is that of Rose, M. E., "Elementary Theory of Angular Momentum," Wiley, New York, (1957).
7. Blatt, J. M. and Weisskopf, V. F., "Theoretical Nuclear Physics," Wiley, New York (1952), Chap. VIII.
8. Auerbach, E. H., Francis, N. F., Goldman, D. T., and Lubitz, C. R., "ABACUS-1, A Program for the Calculation of Nuclear Cross Sections Using the Cloudy Crystal Ball Model," KAPL-3020 (1964).
9. Goldman, D. T., Lubitz, C. R., Shanholt, G. A., and Slaggie, E. L., "OPTIC: A Program for the Calculation of Nuclear Cross Sections and Legendre Moments Using the Optical Model," KAPL-3085 (1965).
10. Feshbach, H., "The Complex Potential Model," Ch. VI. D, "Nuclear Spectroscopy," Part B, (Ajzenberg-Selove, Ed.) Academic Press, New York (1960).
11. Ford, K. and Levinson, C., Phys. Rev. 100, 1 (1955).
12. Slaggie, E. L., private communication.

13. Preston, M. A., "Physics of the Nucleus," Addison-Wesley, Reading (1962) Chap. 16.

14. Slaggie, E. L., and Reynolds, J. T., KAPL-3099 (1965).

15. For slow neutron s-wave scattering $\delta_{\ell}^{j} \to \delta_{0}^{\frac{1}{2}} \to ka \ll 1$ and the familiar form of the single level cross section with interference results (see, e.g., Dresner, L., "Resonance Absorption in Nuclear Reactors," Pergamon, New York (1960) Chap. 3.)

16. Reference 10 and Section V below.

17. Rae, E. R., Margolis, B., and Troubetskoy, E. S., Phys. Rev. 112, (1958).

18. Nemirovsky, P. E., Yelagin, Y. P., Nucl. Phys. 45, 156 (1963).

19. Mott, N. F., and Massey, H. S. W., "The Theory of Atomic Collisions," 2nd. Ed., Clarendon Press, Oxford (1949) p. 112.

20. Fermi, E., Ric. Sci. 7, II 13 (1936).

21. See, e.g., Goldman, D. T., and Muehlhause, C. O., "Neutron Physics," Part 9, Chap. 7, Handbook of Physics (Condon, E. U. and Odishaw, H., eds.) 2nd. Ed. McGraw-Hill, New York, in press.

22. Bassel, R. H., Satchler, G. R., Drisco, R. M., and Rost, E., Phys. Rev. 110, 1080 and other papers by these authors which followed.

23. Francis, N. C., Goldman, D. T., and Lubitz, C. R., "Calculation of Nuclear Cross Sections," Sec. 2.2, Naval Reactors Handbook, Vol. I, (Radkowsky, A., Ed.), TID-7030, Supt. of Documents, Washington, (1964).

24. Austern, N., "Direct Reactions," from "Selected Topics in Nuclear Theory," IAEA, Vienna (1963).

25. Tamura, T., Rev. Mod. Phys. 37, 679 (1965).

26. Woods, R. D., and Saxon, D. S., Phys. Rev. 95, 577 (1954).

27. Bohr, A. and Mottelson, B. R., Kgl. Danske Videnskab. Selskab, Mat. Fys. Medd. 27, No. 16 (1953).

28. Dunford, C. L., "2-Plus, A Non-Spherical Optical Model for Fast Neutron Cross Sections," NAA-SR-11706 (1966).

29. Buck, B., Phys. Rev. 130, 712 (1963).

30. Brown, G., Unified Theory of Nuclear Models, North-Holland, Amsterdam (1964) Chap. IX.

31. Perey, F., and Buck, B., Nucl. Phys. 32, 353 (1962).

32. Krieger, T. J., Annals of Physics 31, 88 (1965).

33. Moldauer, P. A., Phys. Rev. 135, B642 (1964).

34. Moldauer, P. A., Engelbrecht, C. A., and Duffy, G. J., "NEARREX, A Computer Code for Nuclear Reaction Calculations," ANL-6978 (1964).

35. Auerbach, E. H., private communication.

36. Goldman, D. T., and Lubitz, C. R., "Calculation of Inelastic Neutron Scattering," KAPL-2163 (1961).

37. Auerbach, E. H., and Moore, S. O., Phys. Rev. 135, B895 (1964).

38. Pearlstein, S., Nucl. Sci. & Eng. 23, 238 (1965).

39. Bjorklund, F. E., and Fernbach, S., Phys. Rev. 109, 1295 (1958).

40. Hemmig, P. B., Ed. "Neutron Cross Section Technology," CONF-660303 (1966). See especially, Perey, F. G., "Filling Gaps with Cross Sections Calculated from Theory," p. 235.

41. Cindro, N., Rev. Mod. Phys. 38, 391 (1966) presents survey of recent results on fast-neutron reactions.

42. Blatt, J. M., and Biedenharn, L. C., Rev. Mod. Phys. 24, 258 (1952).

43. Nodvik, J. S., Duke, C. B., and Melkanoff, M. A., Phys. Rev. 125, 975 (1962).

44. Abramowitz, M., "Coulomb Wave Functions," Ch. 14 of Handbook of Mathematical Functions (Abramowitz, M. and Stegun, I. A., Eds.) National Bureau of Standards, Washington, (1964).

DISCUSSION

K. H. BECKURTS (Chairman): The spin dependence of the neutron strength function now seems to be well-established. Direct cross-section measurements have also been made using polarized neutrons and nuclei. Do you know whether anybody has tried to derive a spin-dependent part of the optical model potential in the sense of a spin-spin coupling?

D. T. GOLDMAN: I do not know of any such attempt. I have the feeling that such a spin-spin potential would not change the results of optical model calculations, which average over all appropriate spins, at least above the resonance energy region.

GAMMA RAYS FROM NEUTRON INELASTIC SCATTERING IN GERMANIUM

J. F. BARRY
ATOMIC WEAPONS RESEARCH ESTABLISHMENT,
ALDERMASTON, UNITED KINGDOM

Abstract

GAMMA RAYS FROM NEUTRON INELASTIC SCATTERING IN GERMANIUM. Measurements have been made of the yield of γ-rays after inelastic neutron scattering in germanium. A lithium-drifted germanium crystal was bombarded with neutrons at various energies in the range 0.5 to 2.3 MeV. The crystal itself acted as detector for the γ-rays produced and the photopeaks observed were identified with the de-excitation of known levels in the various germanium isotopes present. The neutron flux through the crystal was measured at each energy with a fission counter containing neptunium-237, using the known cross-section for fission of this isotope. The resultant γ-ray yield curves were made absolute by normalizing to the inelastic scattering cross-sections where these are known. Inelastic scattering cross-sections can be inferred from the measurements down to energies within a few kilovolts of threshold, and energy region unattainable by neutron detection methods.

INELASTIC SCATTERING OF FAST NEUTRONS FROM ^{58}Ni AND ^{60}Ni

J.H. TOWLE, R. BATCHELOR AND W.B. GILBOY
ATOMIC WEAPONS RESEARCH ESTABLISHMENT,
ALDERMASTON, BERKS,, UNITED KINGDOM

Abstract

INELASTIC SCATTERING OF FAST NEUTRONS FROM ^{58}Ni AND ^{60}Ni. The Aldermaston time-of-flight spectrometer has been used to study neutron scattering from ^{58}Ni and ^{60}Ni with monoenergetic T(p,n) neutrons in the energy range 1.3 to 4.0 MeV. To obtain detailed information on the energy levels of these nuclei, 30-g samples of the separated isotopes (> 99% pure) were used. The natural isotopic abundances of ^{58}Ni and ^{60}Ni are 67.8 and 26.2%, respectively. The data on ^{60}Ni were obtained with a beam pulsed by deflection in the high voltage terminal of the 6-MV Van de Graaff machine giving a mean target current of 0.7 μA. The ^{58}Ni measurements were made after klystron bunching had been installed in the high voltage terminal and the increased target current (~2.5 μA was used) greatly enhanced the rate of data acquisition and offset the disadvantage of a small scattering sample.

Angular distributions were measured between 20° and 135° at incident energies of 2, 3 and 4 MeV. The cross-sections are relative to the well-known H(n,n) cross-sections and have been corrected for multiple scattering and flux attenuation using the Monte Carlo programme MAGGIE. The centre-of-mass angular distributions of the inelastic groups are practically symmetric about 90° in agreement with the statistical model of the compound nucleus. Relative excitation curves were also measured at 0.2-MeV intervals at 125° and normalized to the cross-sections obtained at 2 and 3 MeV. The curves for the strongly excited 2+ levels of ^{58}Ni and ^{60}Ni at 1.45 and 1.33 MeV, respectively, were continued at 0.1-MeV intervals down to threshold by observing the γ-ray peak in the time-of-flight spectrum. There are some large disagreements between the present results for these levels and previous data of Broder et al. and Nishimura et al. who used NaI spectrometers. The excitation curve of the 1.45-MeV ^{58}Ni level has a broad resonance at about 2.6 MeV.

Inelastic scattering cross-sections have been calculated using a Hauser-Feshbach computer programme with width fluctuation correction and are compared with the experimental results.

1. Introduction

These measurements were made in order to investigate the mechanism of neutron interaction with the Ni isotopes and to provide cross-section data for fast reactor calculations. Since the inelastic neutron spectrum from natural Ni is rather complex, highly enriched samples of ^{58}Ni and ^{60}Ni were used which facilitated the resolution of individual energy levels and the acquisition of accurate cross-sections.

The only previous inelastic scattering data for Ni in this energy region is the differential cross-section for the unresolved 1.33-MeV and 1.45-MeV levels measured at 2.45 MeV [1,2]. In this paper we present the excitation curves for the main inelastic groups for ^{58}Ni and ^{60}Ni together with predictions based on a statistical model [3].

2. Experimental

The measurements were made using the Aldermaston time-of-flight spectrometer [4]. The basic methods of the experiment are also

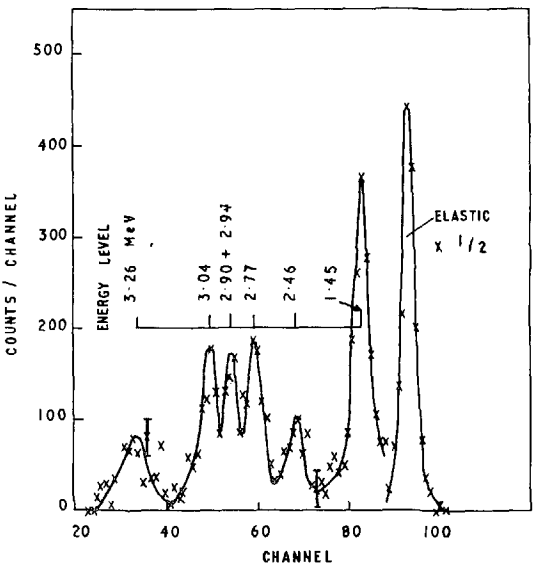

FIG.1. Time-of-flight spectrum for ^{58}Ni measured at 100° with 4.0 MeV incident neutrons. The flight path was 1.7 m.

as described in ref. [4]. Neutrons were obtained from the T(p,n) neutron at 0^{o} using a 2.5 cm long target cell filled to 1 atmosphere with T_2. The ^{60}Ni data were obtained with the proton beam pulsed in the high voltage terminal [5] of the 6-MV Van de Graaff giving a mean target current of 0.7 μA. The ^{58}Ni measurements were made following installation of klystron bunching in the terminal [6] which provided much larger currents ($\sim 2.5\mu$ A) which largely offset the disadvantage of a small scattering sample.

The scattering samples* (isotopic purity > 99%) were about 1 cm diameter, 5 cm long and weighed about 30 g. The cross-sections were established relative to the well known H(n,n) cross-section by observing the scattering from thin polythene samples [4]. The measurments have been corrected for multiple scattering and flux attenuation using the Monte Carlo computer programme MAGGIE [7].

Differential cross-sections for elastic and inelastic scattering were measured at 2.0, 3.0 and 4.0 MeV for ^{60}Ni and 2.2, 3.0 and 4.0 MeV for ^{58}Ni. Relative excitation curves of the inelastic neutron groups were also measured at 0.2-MeV intervals and were normalised to the integrated cross-sections at 2 and 3 MeV. At energies below 2.1 MeV in ^{60}Ni and 2.4 MeV in ^{58}Ni only the first levels (1.33 and 1.45 MeV respectively) are excited so that the γ-ray peak in the T.O.F. spectrum is due solely (after background subtraction) to the corresponding de-excitation γ-ray. Runs

*On loan from the Oak Ridge National Laboratory.

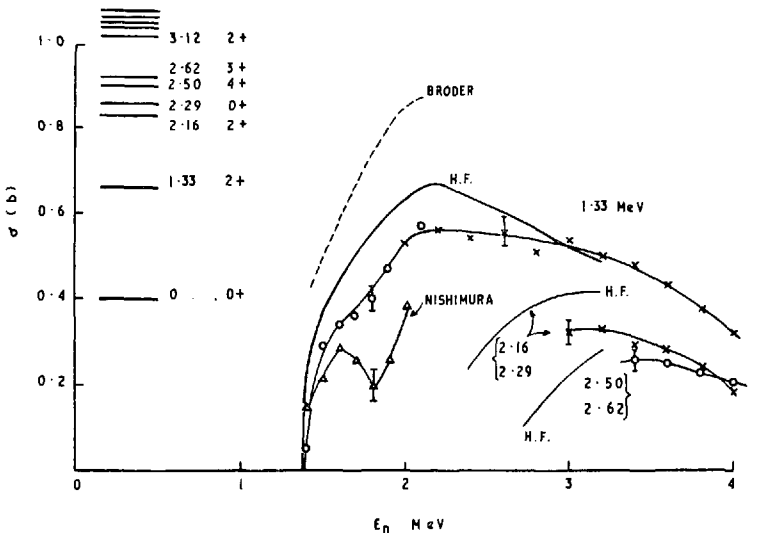

FIG.2. Inelastic scattering cross-sections for ^{60}Ni. The curves denoted H.F. are calculated from Hauser-Feshbach theory (with width fluctuation correction) based on the level spins indicated.

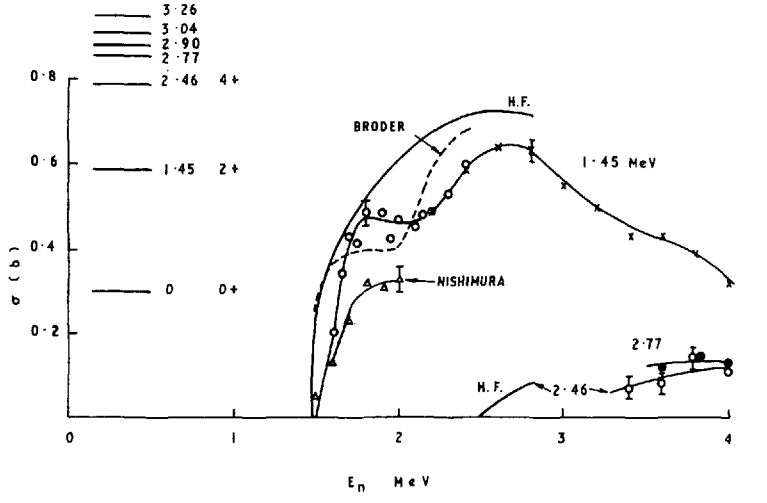

FIG.3. Inelastic scattering cross-sections for ^{58}Ni. See Fig.2 caption.

with a carbon scatterer demonstrated that any contribution from source γ-rays Compton scattered by the sample was negligible. Thus, by observing the γ-ray peak it was possible to measure the excitation curves of the 1.33-and 1.45-MeV levels at 0.1-MeV intervals right down to threshold. For this measurement the circuit normally used to reject γ-ray events was rendered inoperative. The γ-ray excitation curves were normalised to the integrated neutron cross-sections at 2 MeV. All the excitation curve measurements were made at 125^{o} at which angle the differential cross-section is just $1/4\pi$ times the integrated cross-section for a simple

symmetric angular distribution of the form $1 + aP_2(\cos\theta)$ [4] which is a fair approximation for the present case.

3. Results and Discussion

Scattering has been observed to energy levels in ^{58}Ni at 1.45, 2.46, 2.77, (2.90 + 2.94), 3.04, 3.26 and 3.42 MeV, and in ^{60}Ni at 1.33, 2.16, 2.29, (2.50 + 2.62), (3.12 + 3.19) and (3.32 + 3.39) MeV where the brackets denote unresolved groups. The angular distributions at 2, 3 and 4 MeV of these groups are practically all symmetric about 90° in agreement with the statistical theory of Hauser and Feshbach. A time-of-flight spectrum for ^{58}Ni at 4.0 MeV is shown in Fig. 1.

Excitation curves for the main groups are shown in Figs. 2 and 3. The 2+ first excited states at 1.33 MeV (^{60}Ni) and 1.45 MeV (^{58}Ni) are both strongly excited with similar cross-sections, but the detailed shapes of their excitation curves are rather different. In particular the curve for the 1.45-MeV ^{58}Ni level has a sharper rise and a broad resonance at about 2.6 MeV. This resonance is not consistent with a statistical model and is probably due to insufficient averaging over compound nuclear levels. On the basis of the statistical model the shapes of the excitation curves for these two levels should be similar below 2.2 MeV. Above this energy the level structures of ^{58}Ni and ^{60}Ni are different, and the ^{58}Ni(n,p) reaction [8] begins to compete strongly with ^{58}Ni(n,n′).

There are some large discrepancies between the present cross-sections for these 2+ levels and previous measurements [9,10] in which the de-excitation γ-rays were observed using NaI spectrometers and ring scatterers (see Figs. 2 and 3). The cross-sections of Nishimura et al. [9] are smaller than the present ones and there is a pronounced minimum at 1.8 MeV in the curve for the 1.33-MeV level. Nishimura et al. used a natural Ni sample and one suspects that it is a difficult matter using NaI to resolve the 1.33-MeV γ-ray reliably from the 1.45-MeV line which is much stronger since ^{58}Ni is 2.6 times more abundant than ^{60}Ni. The results of Broder et al. [10] for these two γ-rays are represented in Figs. 2 and 3 by broken lines. Their curves which were measured using enriched isotopic samples have similar shapes to the present results but there is a difference in energy scale and the cross-section of the 1.33-MeV ^{60}Ni γ-ray is some 70% larger than our value. A check on the ratio $\sigma(1.45)/\sigma(1.33)$ for 2-MeV neutrons has been provided by a measurement at this laboratory [11] of the γ-ray spectrum from a natural Ni ring sample using a Li-drifted Ge counter. The ratio $\sigma_\gamma(1.45)/\sigma_\gamma(1.33)$ obtained from the total absorption peaks which were well resolved is in excellent agreement with the present results and strongly discordant with the result of Broder et al.

Statistical model calculations of inelastic cross-sections have been made for comparison with experiment (in Figs. 2 and 3) using a Hauser-Feshbach computer program [12] including the correction for level width fluctuation. The transmission coefficients were calculated from an optical model with a Saxon-Woods real potential and a surface absorption potential of differential Saxon-Woods form. The (energy-independent) potential

depths used which were based on those obtained by fitting the differential elastic cross-sections were U = 45.5 MeV, W = 14 MeV for ^{58}Ni and U = 49.0 MeV, W = 12 MeV for ^{60}Ni. The other parameters were $R_u = 1.29A^{1/3}$, $a_u = 0.66$, $R_w = 1.25A^{1/3}$ and $a_w = 0.48$ (all in fm).

The level structure of ^{60}Ni is known up to 3.2 MeV [13] so the excitation curves could be calculated up to that energy, but in ^{58}Ni the spins and parities of the levels at 2.77 MeV and above are not known [14]. With ^{58}Ni there is the added complication of the ^{58}Ni(n,p)^{58}Co reaction (Q = 0.39 MeV), the cross-section of which rises rapidly from an effective threshold at about 1.5 MeV through 0.4 b at 4 MeV [8]. Only the ground and 0.025-MeV states of ^{58}Co have known spin and parity which are 2+ and 5+ respectively [14]. Two other levels in ^{58}Co recently discovered at 1.055 MeV and 1.395 MeV [15] were also included with assumed assignments of 3+ and 4+ respectively according to theoretical expectations [16]. The optical model potentials for the (^{58}Co + p) channels were assumed the same as for (^{58}Ni + n) with the addition of a coulomb potential due to a uniformly charged sphere with the same radius as the real potential.

In Fig. 2 we see that the predicted curve for the 1.33-MeV level of ^{60}Ni is about 20% higher than the experimental results in the region below 2.5 MeV, but is in better agreement near 3 MeV. This difference in shape may reflect the need for some energy dependence in the potentials but this possibility has not yet been investigated. The predicted cross-section for the (2.16 + 2.29) MeV doublet is 25% higher than observed at 3 MeV, but the result for the (2.50 + 2.62) MeV doublet is in better agreement with observation. Calculations at 2 MeV and 3 MeV using potentials equivalent to the Perey-Buck non-local potential [17] gave practically the same cross-sections as the above calculations.

In the case of ^{58}Ni (Fig. 3) one again notes that the predicted cross-section of the 2+ level is about 20% high and as already noted, the shape of the observed curve is not too consistent with the statistical model. Changing W from 14 to 12 MeV slightly worsened the agreement. The curve calculated near threshold for the 2.46-MeV 4+ level is probably not inconsistent with the points measured between 3.4 and 4 MeV when one considers that competition from the 2.77, 2.90, 3.04 and 3.26 MeV levels will cause the curve to turn down at higher energies.

The agreement between the experimental and calculated inelastic cross-sections for both isotopes is fairly reasonable, the calculated results being slightly higher. The agreement for the strongly excited groups would be considerably worsened if the calculation did not include the width fluctuation correction. For example, the cross-sections for the 1.33-MeV and 1.45-MeV 2+ levels would have been about 1050 mb instead of 620 mb at 2.0 MeV. In the present cases therefore the correction appears to be well justified.

The excitation function calculated up to 2.8 MeV for the ^{58}Ni(n,p)^{58}Co reaction has the same shape as the experimental curve [8] but is too low

by about a factor of two. Some 95% of the calculated (n,p) reaction led to the ground and 0.025 MeV levels. Reasons for this discrepancy might be (a) the possible existence of further ^{58}Co levels not included in the calculation, and (b) possible unsuitability of the potential used for calculating the transmission coefficients for (^{58}Co + p).

REFERENCES

[1] CRANBERG, L., LEVIN, J.S., Phys. Rev. 103 (1956) 343.

[2] GOLDBERG M.D., et al., BNL 400, 2nd Ed. Vol. II (1962).

[3] HAUSER, W., FESHBACH, H., Phys. Rev. 87 (1952) 366.

[4] TOWLE, J.H., GILBOY, W.B., Nuclear Physics 32 (1962) 610.

[5] TOWLE, J.H., GILBOY W.B., Nuclear Physics 44 (1963) 256.

[6] ANDERSON, J.H., et al., Nucl. Instr. Meth. 41 (1966) 30.

[7] PARKER, J.B., et al., Nucl. Instr. Meth. 30 (1964) 77.

[8] BARRY, J.F., Reactor Science and Technology 16 (1962) 467.

[9] NISHIMURA, K., et al., Nuclear Physics 70 (1965) 421.

[10] BRODER, D.D., et al., Atomnaya Energiya 16 (1964) No. 2 103.

[11] COLES, R.E., POPE, R.A., Private communication.

[12] WILMORE, D., AERE Report R 5053.

[13] MOHINDRA, R.K., VAN PATTER, D.M., Phys. Rev. 139 (1965) B274.

[14] WAY, K., et al., Landolt-Bornstein New Series 1/1 Springer-Verlag, Berlin (1961).

[15] CROISSIAUX, M., et al., J. Phys. (Paris) 25 (1964) 906.

[16] DE SHALIT, A., Phys. Rev. 91 (1953) 1479.

[17] PEREY, F., BUCK, B., Nuclear Physics 32 (1962) 353. See also WILMORE, D., AERE Report R 4649.

NEUTRON INELASTIC SCATTERING FROM ^{56}Fe

E. BARNARD, J.A.M. DE VILLIERS AND D. REITMANN
ATOMIC ENERGY BOARD, PELINDABA,
SOUTH AFRICA

Abstract

NEUTRON INELASTIC SCATTERING FROM ^{56}Fe. Previous measurements of the cross-section for excitation of the 845-keV level in ^{56}Fe close to threshold were made by detecting the gamma rays after inelastic neutron scattering. These results indicated severe structure over the first 250 keV above threshold. To determine whether the same effects would also show up in measurements on the inelastically scattered neutrons, a ^{10}B + NaI detector was constructed. With this detector and time-of-flight techniques to resolve the inelastically scattered neutrons, measurements were made down to an incident neutron energy of 893 keV. Excellent agreement was found between the two types of measurement over the entire region of overlap.

Since the structure in the excitation curve appeared to persist toward higher energies, measurements were extended as far as 1500-keV incident energy. At the higher energies, a conventional plastic scintillator was employed. Where both neutron detectors were used at the same energies, very good agreement was found.

All measurements were done with a 3-MeV pulsed Van de Graaff and the $^{7}Li(p,n)$ reaction as neutron source. Targets were between 5 and 15 keV thick and pulse lengths of either 3 or 10 ns were used, depending on the resolution required. Flight paths varied between 1 and 3 m. Absolute cross-sections were obtained by using elastic scattering from carbon as a standard. Flux attenuation and multiple scattering corrections were calculated at several representative energies by means of a Monte Carlo method. These corrections were found to be small.

The excitation curve was measured from 893 to 1500 keV at intervals of approximately 10 keV for a scattering angle of 90°. A number of strong resonances were observed, many of which had not been previously recorded. Angular distributions were measured at several of the more prominent peaks and valleys. No systematic variation was, however, obtained. The angular distributions would thus seem unable to shed any more light on the origin of the sharp resonances.

1. INTRODUCTION

The $^{56}Fe\ (n,n')\ ^{56}Fe$ reaction has been studied very carefully by various authors. Two methods of measuring the inelastic scattering cross-section were employed i.e. observation of the de-excitation gamma rays from the 845 keV level to the ground state [1-9] or by separating the inelastically scattered neutrons from those elastically scattered and then registering the former.

Neutrons of different energies were separated either by using the property that for neutrons of different energies different pulse heights are registered by the detector like the ^{3}He spectrometer used by Glazkov [10], who made measurements at 1.0 MeV and 1.2 MeV neutron energy, or by employing the time-of-flight method [11-15]. Because of the nature of the detectors used previously only neutrons of relatively high energies were observed by means of the latter method. Gilboy and Towle [11] measured over the range 1.40 - 3.01 MeV incident neutron energy, Wilenzick et al. [12] for 6.04 MeV neutrons and Hopkins and Silbert [13] over the range 2 - 5 MeV. Cranberg and Levin [15] did time-of-flight measurements on Fe for an incident neutron energy of 2.45 MeV.

On the other hand, for a study of the inelastic scattering cross-section by observing the de-excitation gamma rays the reaction threshold can be approached from the high energy side relatively closely without having an effect on its detection efficiency. For this reason the energy region just above threshold has been covered only by observing gamma

rays and it was the purpose of this experiment to cover this region by observing the inelastically scattered neutrons and compare the results with those of the gamma ray measurements.

2. EXPERIMENTAL METHOD

Measurements were done on the 3-MeV pulsed Van de Graaff which is extremely suitable for time-of-flight spectroscopy. The pulse lengths were either 3 or 10 nanoseconds, depending on the resolution required, with corresponding repetition rates of either 5 Mc/s or 1 Mc/s.

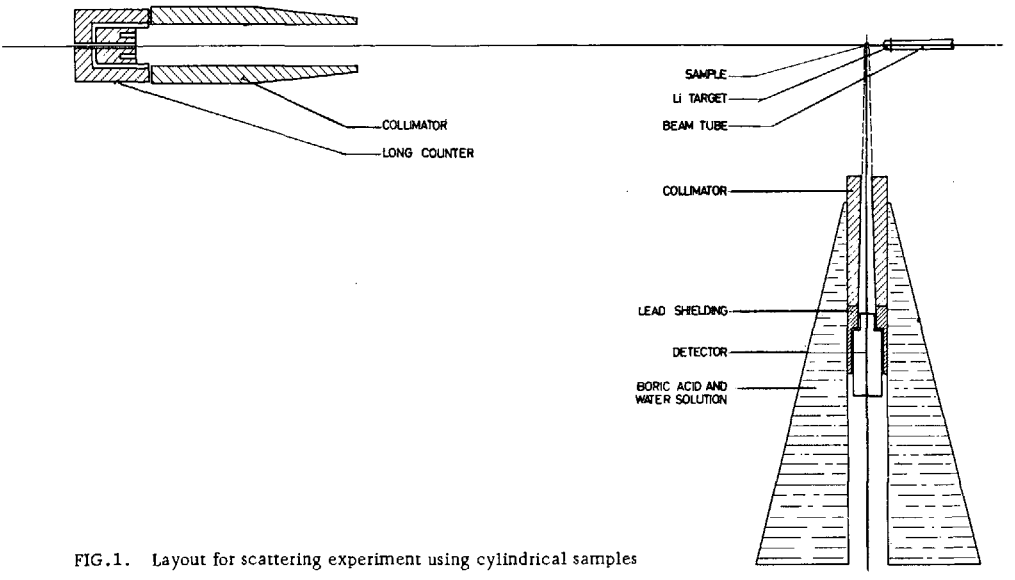

FIG.1. Layout for scattering experiment using cylindrical samples

Neutrons were produced by the ^{7}Li (p,n) reaction and pure Li metal targets were prepared by vacuum evaporation of Li onto a tantalum backing. Target thickness (as measured at threshold) varied between 5 and 15 keV, depending on which energy region was being studied. These were used in conjunction with flight paths ranging from 1 to 3 metres.

Basically the detector system was a 58 AVP photomultiplier coupled to a scintillator. A fast pulse from the anode was used to start the time-to-pulse-height converter. A signal from an electrostatic beam pick-up cylinder in the beam tube acted as stop pulse for the time-to-pulse-height converter, the output of which was fed directly to a 512-channel Nuclear Data pulse height analyser.

A slow signal from a suitable dynode of the photomultiplier was fed via an amplifier, differential discriminator and delay circuit to the coincidence input of the pulse height analyser.

For observing neutrons close to the threshold, a ^{10}B + NaI detector was constructed. Experiments were done with different thicknesses of ^{10}B, i.e. 0.5, 1.0 and 2 cm ^{10}B, and were further combined with two thicknesses of NaI, namely 2.5 cm and 7.6 cm. The ^{10}B slabs as well as the NaI crystals were 10 cm in diameter. For the actual measurements, 1 cm ^{10}B on the 7.6 cm NaI was coupled to a 58 AVP photomultiplier.

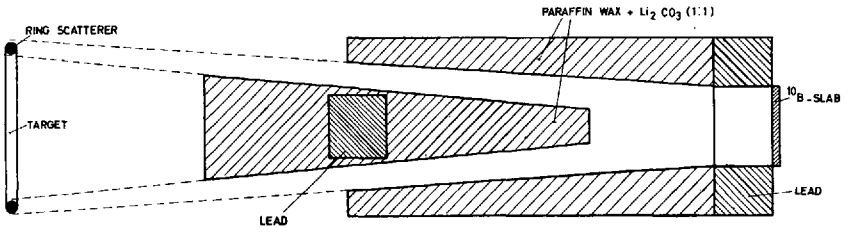

FIG.2. Geometry for ring scattering

In order to improve on the timing resolution of the system the fast trigger from the anode was set extremely low in the noise region. To protect the time-to-amplitude converter from a too high count rate, a second fast pulse was taken, this time from the last dynode, and the trigger was set appreciably higher than the former but still low enough so as not to interfere with the slow discriminator bias. In order to trigger the time-to-amplitude converter a coincidence was required between the two fast pulses mentioned.

On the slow side the differential discriminator window was set so as to include only the photopeak due to the 480-keV gamma ray from the first excited state of ^{7}Li. Unfortunately it was not possible to separate the 480-keV gamma ray from the 511-keV annihilation peak. The efficiency of this detector was carefully measured by comparing its response to that of a long counter. Both were placed at 90^{o} to the proton beam in such a way that they subtended the same solid angle at the target and the required neutron energy region was covered by adjusting the proton beam energy accordingly. Further, during scattering runs, an elastic scattering measurement from C was done after each iron measurement. The energy for the carbon run was chosen in such a way that the energy of the neutrons reaching the detector from the carbon was the same as that of the inelastically scattered neutrons from the Fe. In this way an absolute cross-section could be derived because the carbon cross-section is well known [16].

For the higher energies starting at 1025 keV a 2.54 cm thick 10 cm diameter plastic scintillator (NE 102 A) coupled to a 58 AVP photomultiplier was used as detector. The time resolution of this detector was better than the shortest pulses from the machine and at higher energies the efficiency was appreciably higher than that of the ^{10}B + NaI system. Carbon was again used to obtain absolute cross-sections and at the same time served as a check on the efficiency curve over the energy region where scattering measurements were done.

Two types of geometry were used, as shown in Figs. 1 and 2. In Fig. 1 the samples were 2.54 cm by 2.54 cm diameter hollow cylinders with 0.3 cm wall thickness for the iron sample and 0.48 cm for carbon. These samples (Fe and C) were suspended at 0^{o} at distances between 7 cm and 12 cm from the target, depending mostly on what angle was measured and resolution required.

The detector was housed in a large tank filled with a saturated solution of boric acid. A 10 cm lead ring was placed immediately around the detector and, between the detector and samples, tapered collimators, made out of a 1:1 mixture of lithium carbonate and paraffin wax, were inserted, as shown in Fig. 1. The tank was placed on a trolley which could rotate round a pivot point below the sample and had further provision for changing the distance between the detector and sample. A shadow bar consisting of the same mixture of $Li_2 CO_3$ + paraffin wax shielded the collimator end from direct neutrons from the target and when required 13 cm of lead was added for attenuating gamma rays from the target.

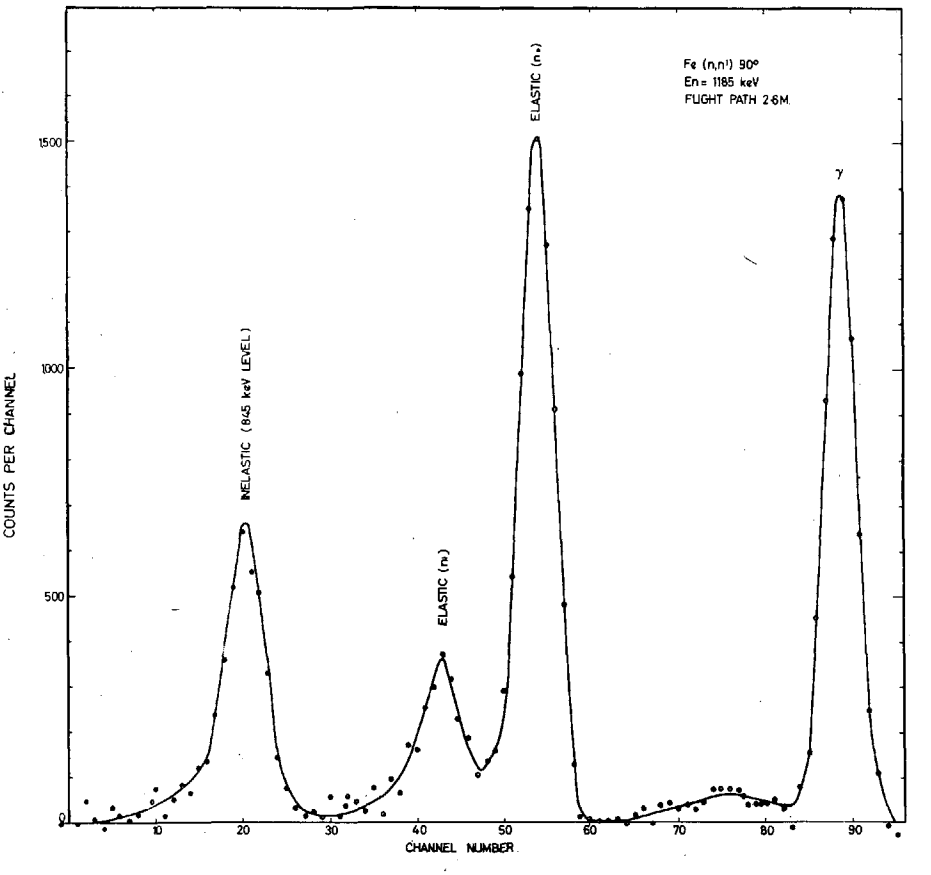

FIG.3. Time-of-flight spectrum for En = 1185 keV

One long counter at 0^{o}, another at 90^{o} and a third at various positions between 0^{o} and 90^{o} were used as flux monitors; for measuring the amount of charge delivered to the target a current integrator was used. The 0^{o} long counter "sample out" readings were used to relate runs of different energies to one another.

The presence of two neutron groups from the ^{7}Li (p,n) reaction for neutron energies smaller than 120 keV in the 0^{o} direction complicated calibration runs with carbon, which could be used down to only 102 keV inelastic neutron energy for a 90^{o} scattering measurement. For this and for intensity reasons the lower part of the measurements was done using ring geometry, as shown in Fig. 2.

Both the iron and carbon samples were 20.1 cm mean diameter and 1.26 cm in cross-section. These were placed at 90^{o} to the proton beam 1 meter from the detector. A shadow bar (Li_2CO_3 and paraffin wax 1:1 and 7.6 cm lead) at 0^{o} placed between the target and detector ensured that the detector could only see the ring and not the direct neutrons or gamma rays from the target.

3. RESULTS

A typical time-of-flight spectrum for an incident neutron energy of 1185 keV and $\theta_{LAB} = 90^{o}$ is given in Fig. 3. The background has been subtracted. For this run the

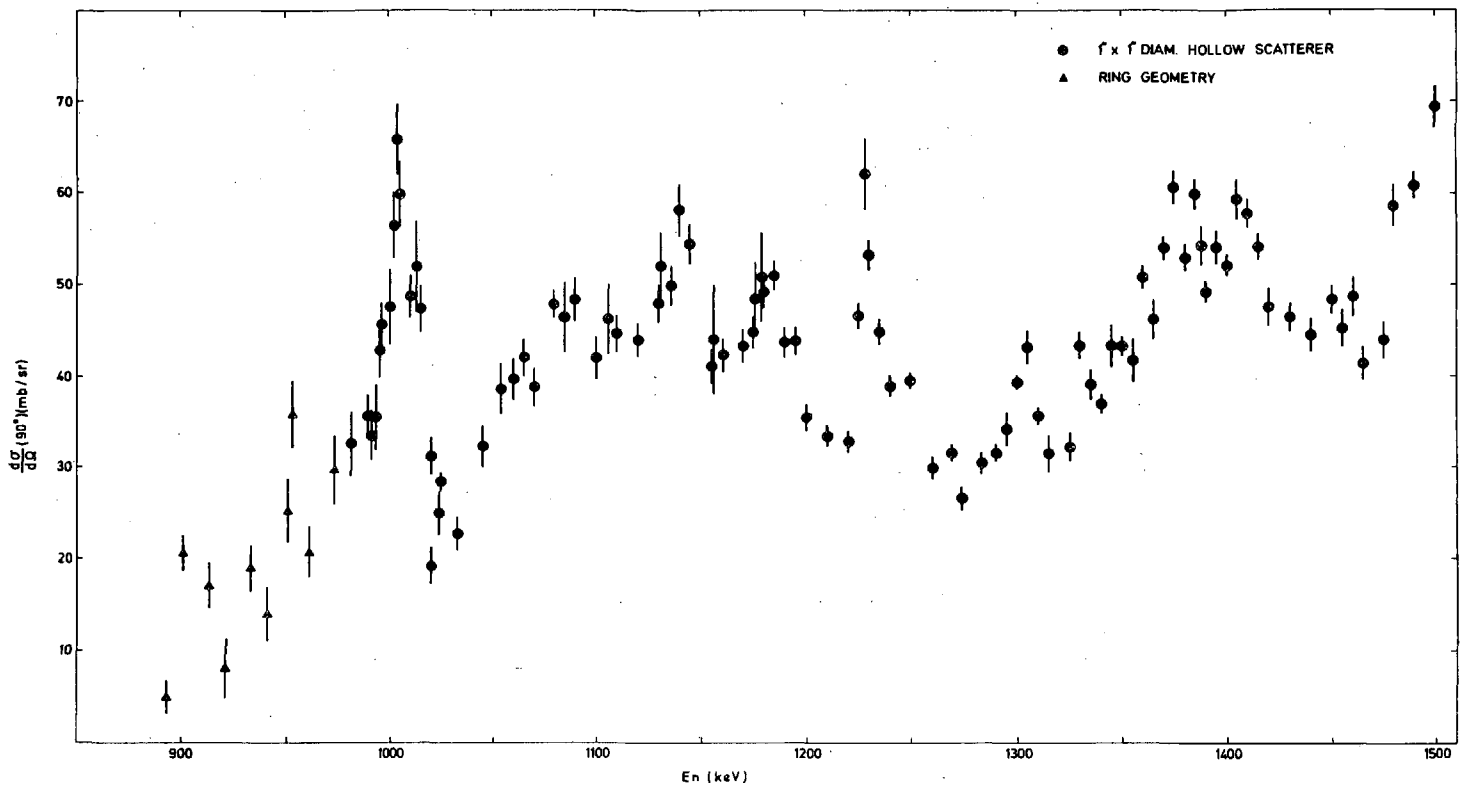

FIG.4. Differential inelastic scattering cross-section for the 845-keV level at 90°

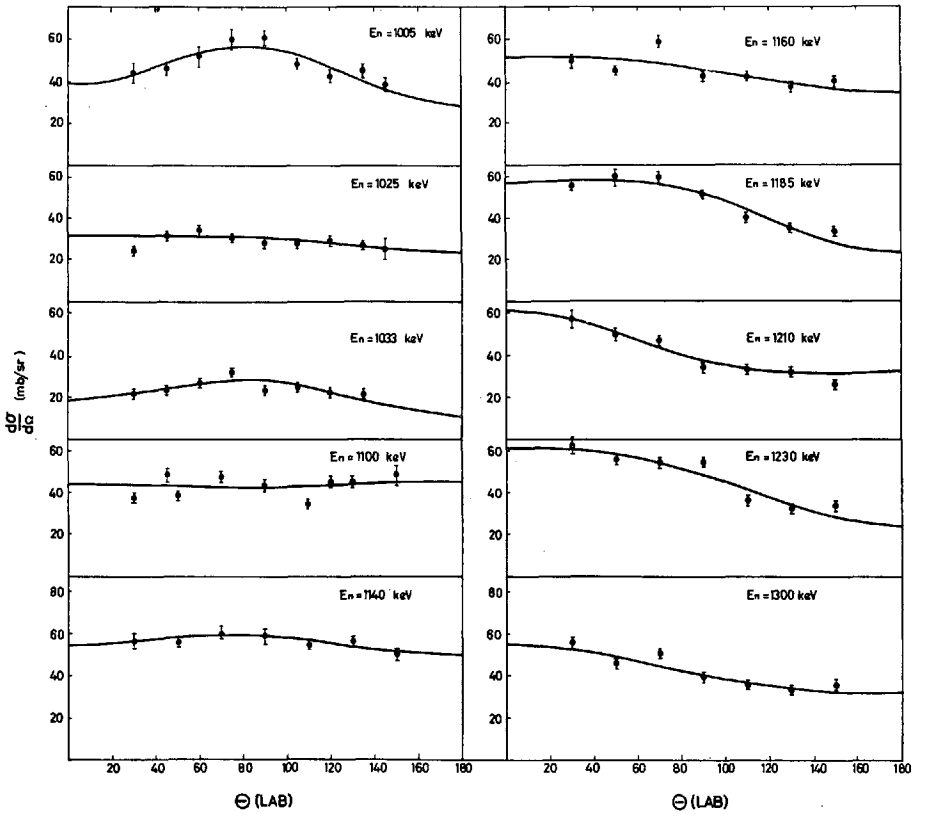

FIG. 5. Angular distributions for the 845-keV level in ^{56}Fe for several incident neutron energies

accelerator pulse was of the order of 10 ns, but with a flight path of 2.6 metres the inelastic peak is well resolved. The plastic detector was used during the above run.

Fig. 4 shows the differential inelastic scattering cross-section for incident neutron energies ranging from 893 keV to 1500 keV. The cross-section is given for the ^{56}Fe isotope and for the energy in the laboratory system. Ring scatterers were used for measuring between 893 keV and 973 keV; for the region En = 981 - 1500 keV the scatterers were the 2.54 x 2.54 cm diameter hollow cylinders.

The results have been corrected for flux attenuation using the method suggested by Cranberg [17], but not for multiple scattering.

Using a Monte Carlo Method, multiple scattering corrections were calculated for several combinations of extreme values of σ_{el}, σ_{in} and the coefficients of the polynomial fits to the elastic angular distributions, as encountered in the measurements, and the corrections were found to be smaller than 7%. In general it means that the values in Fig. 4 have to be reduced by about 5%.

The errors given in Fig. 4 are purely statistical. Because the measurements were done relative to carbon there is an additional error of 5% due to uncertainty of the latter.

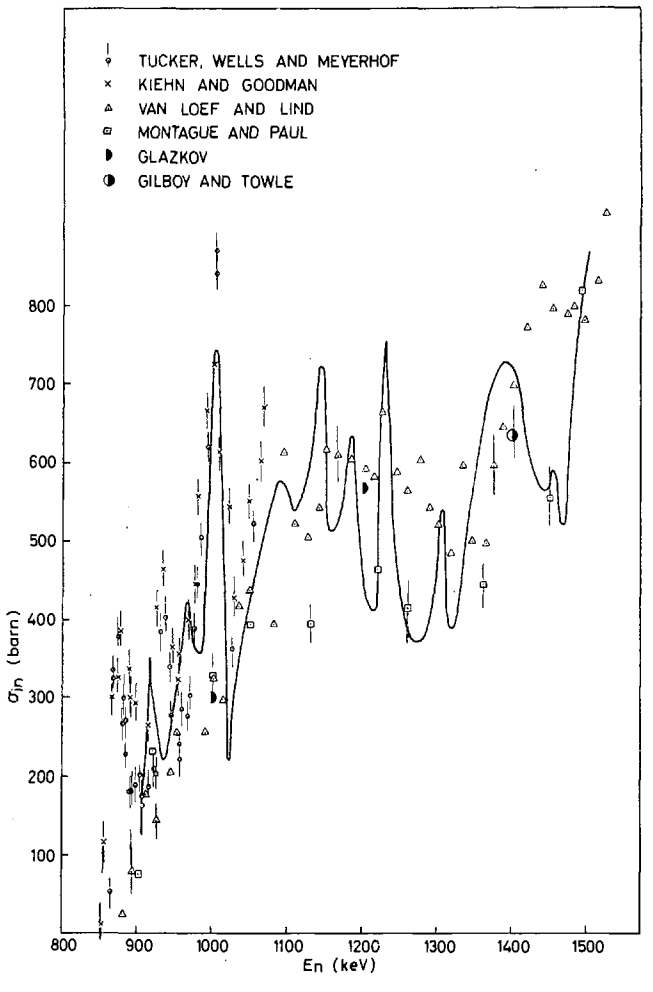

FIG.6. Total inelastic scattering cross-section for the 845-keV level

Because Fig. 4 shows such severe structure the neutron energies at which angular distributions were done were chosen to correspond to the most prominent peaks and valleys in order to see whether these would supply any special explanation for this structure. Measurements were, therefore, done at the following incident neutron energies: 1005, 1025, 1033, 1100, 1140, 1160, 1185, 1210, 1230 and 1300 keV, as shown in Fig. 5.

The solid lines are polynomial fits by means of the method of least squares of a Legendre series of the form

$$\frac{d\sigma}{d\Omega} = \frac{\sigma_{in}}{4\pi}\left[1 + \sum_{i=1}^{n} \omega_i P_i\right] \qquad (1)$$

where σ_{in} is the total inelastic scattering cross-section, P_i Legendre polynomials and ω_i coefficients determined from the experimental points. Although higher order fits were applied, a P_2 fit was found adequate.

In order to have some kind of comparison between the results from this experiment and those from other laboratories the following procedure was followed. Because for a scattering angle of 90^{o}, $P_1 = 0$ and, therefore, if ω_2 is known, σ_{in} can be calculated for this angle by using equation (1).

$$\sigma_{in} = 4\pi \frac{d\sigma}{d\Omega} (90^{o})/(1 - {}^{1}/_{2}\,\omega_2) \qquad (2)$$

Assuming $\omega_2 = 0$ at threshold and drawing a smooth curve through the ω_2 values obtained from the fits to the angular distributions, the ω_2 values for energies where no angular distributions were available were read off. From these σ_{in} was calculated and a smooth curve drawn through the points, as shown in Fig. 6. Also shown are the experimental points by Tucker et al. [3] (ΔEn = 15 keV) and Kiehn & Goodman [9] (ΔEn = 20 keV) which were done with about the same spread in neutron energy as this experiment (ΔEn = 14 keV).

The data from Montague and Paul [4] (ΔEn = 50 keV) and Van Loef and Lind [8] (ΔEn = 80 keV) were obtained with considerably larger energy spread and this must be borne in mind when comparisons are made. Data from Glazkov [10] and Gilboy and Towle [11] are also shown. Where necessary, results from other authors have been converted to the laboratory system and cross-sections to that of the ^{56}Fe isotope.

Although this may not be a very exact way of comparing results, it is nevertheless obvious that the same resonance structure (apart from immediately above threshold) is shown in this experiment, as was found by Tucker et al. and by Kiehn & Goodman.

The resonances observed in the inelastic scattering cross-section are surprisingly sharp and well separated. The fact that no strong forward-backward asymmetry appears to be associated with resonances would seem to indicate that they are not due to strong direct interaction. Furthermore, the fact that these angular distributions at the resonances are not very different from those obtained in between resonances would indicate that there are also no strong interference effects present and, therefore, it seems that the structure is just the ordinary variation of cross-section with energy.

REFERENCES

[1] BENJAMIN, R.W., BUCHANAN, P.S., MORGAN, I.L., Nucl. Phys. 79 (1966) 241.
[2] NISHIMURA, K., OKANO, K., KIKUCHI, S., Nucl. Phys. 70 (1965) 421.
[3] TUCKER, A.B., WELLS, J.T., MEYERHOF, W.E., Phys. Rev. 137 (1965) 1181.
[4] MONTAGUE, J.H. PAUL, E.B., Nucl. Phys. 30 (1962) 93.
[5] BORING, J.W., McELLISTREM, M.T., Phys. Rev. 124 (1961) 1531.
[6] DAY, R.B., WALT, M., Phys. Rev. 11 (1960) 1330.
[7] MORGAN, I.L., Phys. Rev. 103 (1956) 1031.
[8] VAN LOEF, J.J., LIND, D.A., Phys. Rev. 101 (1956) 103.
[9] KIEHN, R.M., GOODMAN C., Phys. Rev. 95 (1954) 989.
[10] GLAZKOV, N.P., Atomnaya Energiya 15 (1963) 416.
[11] GILBOY, W.B. TOWLE J.H., Nucl. Phys. 64 (1965) 130.
[12] WILENZICK, R.M., SETH, K.K., BEVINGTON, P.R., LEWIS, H.W., Nucl. Phys. 62 (1965) 511.
[13] HOPKINS, J.C., SILBERT, M.G., Nucl. Sci. Engng. 19 (1964) 431.
[14] LANDON, H.H., ELWYN, A.J., GLASOE, G.N., OLESKA, S., Phys. Rev. 112 (1958) 1192.
[15] CRANBERG, L., LEVIN, J.S., Phys. Rev. 103 (1956) 103.
[16] LANGSDORF, A. Jr., LANE, R.O., MONAHAN, J.E., Neutron scattering angular distribution. ANL-5567 (Rev.) (1961).
[17] CRANBERG, L., Los Alamos Scientific Laboratory Report No. LA-2177 (1959) (Neutron scattering by ^{235}U, ^{239}Pu and ^{238}U. - Appendix II. LEVIN, J.S.).

DISCUSSION

(on papers CN-23/35 and CN-23/86)

A. T. G. FERGUSON: I should like to ask Dr. Towle what was the energy spread of his incident neutrons. Would he also comment on the differences in structure seen in the excitation functions shown by Barnard for Fe(n, n') and by him for Ni(n, n')?

J. H. TOWLE: The energy spread of the incident neutrons in the nickel experiments varied from about 100 keV at 1.5 MeV to 60 keV at 4 MeV. I think the main reason for the greater structure on the iron curve in Barnard's paper is that people have looked at iron with finer resolution. In the case of nickel, the data of Broder and Nishimura were obtained with energy spreads similar to our own. I am not aware of any work on nickel with thin targets, which might well produce similar results to those seen for iron. In the results I showed, the averaging in the compound nucleus was not as good for ^{58}Ni as for ^{60}Ni.

H. GOLDSTEIN: I should like to make a few comments on Dr. Barnard's paper. Since the term "resonance" has often been applied to the structure observed in the inelastic excitation functions, it is perhaps worthwhile to repeat the view that these "resonances" are unlikely to be identified with individual nuclear levels. The structure observed in the total iron cross-section strongly suggests that the fluctuations in the excitation function represent rather incomplete overlapping and averaging of the nuclear levels. If this is true, one should not regard the asymmetry of the angular distribution as sure evidence of direct interaction. The theoretical prediction of symmetry for compound nuclear processes requires complete statistical averaging over the compound nucleus levels, which may very well not have been the case here.

R. BATCHELOR: Could any requester present say whether it is essential, from the practical point of view, to strive for the very fine resolution used to give results like those presented by Dr. Barnard?

R. D. SMITH: The fast-reactor physicist does not yet know exactly how great the interest is in the fine structure of inelastic scattering for fast-reactor calculations. It is clear, however, that the main interest at present lies in the calculation of "transfer" cross-sections for multi-group calculations. For these, the overall effective cross-section for inelastic scattering of neutrons from say 900 keV to 1 MeV into a similar energy band near 200 keV is of more interest than detailed fluctuations of the cross-sections only a few keV wide.

INELASTIC SCATTERING OF FAST NEUTRONS BY ^{235}U

B. H. ARMITAGE, A. T. G. FERGUSON, J. H. MONTAGUE AND N. STARFELT*
ATOMIC ENERGY RESEARCH ESTABLISHMENT,
HARWELL, DIDCOT, BERKS.,
UNITED KINGDOM

Abstract

INELASTIC SCATTERING OF FAST NEUTRONS BY ^{235}U. Measurements of the spectra of neutrons scattered by ^{235}U have been made by time-of-flight techniques using the Harwell 3-MeV pulsed accelerator at incident neutron energies of 0.12, 0.2, 0.4, 0.55, 0.75, 1.0, 1.5 and 1.8 MeV. All the data were obtained at an observation angle of 90° with a flight path of 1.5 m. The cross-sections for inelastic neutron scattering have been calculated after subtraction of contributions from fission and radioactivity. Even with a resolution of about 10 keV, only the low-lying levels were sufficiently well resolved to give structure in the scattered neutron spectrum.

Introduction

In typical modern fast reactors, U^{235} may form at least 20% of the atoms of the core and in many zero energy assemblies, a higher proportion of this element is used. Inelastic scattering in this material is therefore important in determining the equilibrium spectrum in the core. For this reason a measurement has been requested of $\sigma_{n,n'}$ for U^{235} to an accuracy of 20% over the incident energy range up to 4.0 MeV. Very little experimental information existed prior to this work, the main source being the work of Cranberg who has also reviewed earlier work.[1] More recently, Smith[2] has measured angular distributions of elastically scattered neutrons.

The difficulty of measurement arises from a number of causes. Firstly, there is the very high level density of this odd neutron nucleus. Knowledge of the level scheme of this nucleus comes from the study of the α-decay of Pu^{239} by Baranov et al.[3] and from the reactions $U^{234}(d,p)$ and $U^{236}(d,t)$ studied by Braid et al. of which a preliminary report is given in ref. [4]. These two processes are both subject to strong selection rules but have shown at least 25 levels below 500 keV. Thus, the cross-section for inelastic scattering is divided among many channels giving a nearly continuous energy distribution of secondary neutrons and, as a result, the cross-section to any one level is low. Further, due to the low-lying levels, it is hard to separate the elastic and inelastic groups. Secondly, the substantial fission cross-section gives rise to an unavoidable background. In the earlier measurements of Cranberg, the radioactivity of the sample provided a significant background, but the much higher instantaneous intensities available from modern machines make this source of background relatively small.

The work described in this paper used the time-of-flight technique to observe the spectrum of secondary neutrons arising from the bombardment of a sample of U^{235} with monoenergetic neutrons. Measurements will be reported here at incident neutron energies of 130, 400, 550, 710, 1000, and

* On leave from the A. B. Atomenergi, Studsvik, Sweden.

1500 keV. All measurements were made at a scattering angle of 90°. It should be emphasised that this is a preliminary report and results and especially errors may be subject to revision.

Experimental Method

The arrangement of the neutron time-of-flight apparatus is shown in Fig. 1. This is almost identical with that used by Barnard et al. in the study of inelastic scattering in U^{238} [5]. Pulses of protons of ~ 1 ns

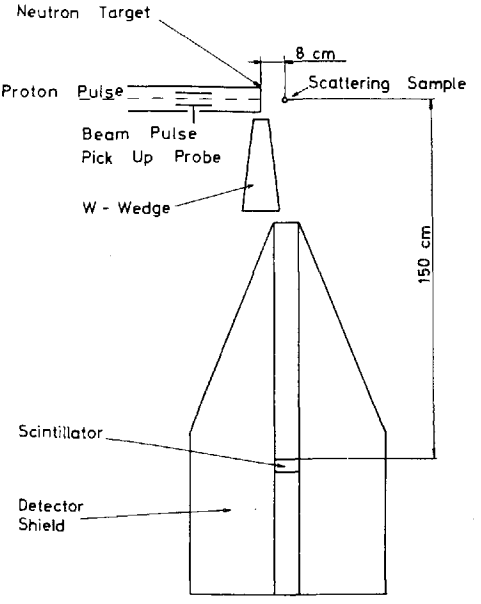

FIG.1. Typical geometrical layout of scattering experiment

duration from the IBIS 3-MeV Van de Graaff accelerator at Harwell[6] were directed onto targets either of Li metal or tritium gas to produce mono-energetic neutrons by the Li(p,n) and T(p,n) reactions. These were scattered from a sample of U^{235} metal (97% U^{235}) placed typically at 8 cm from the target. Two U^{235} samples were used, one 0.5 in. diameter and 1.0 in. long the other 0.6 in. diameter and 1.2 in. long, of weight 70 and 100 gr respectively. The scattered neutrons were detected in a plastic scintillator 10 cm diameter and 2.5 cm thick viewed by two photomultipliers. A detailed description of the detector is given in ref. [7]. This detector could have the bias set to give a threshold lower than 50-keV neutron energy. The threshold used in a given measurement was chosen to optimise signal-to-background ratio without cutting off an excessive fraction of the secondary neutron spectrum.

At a given energy, time-of-flight spectra were obtained with and without the U^{235} scatterer in position, the "sample in" and "sample out" runs being interleaved. The difference between these runs gave the complete secondary neutron spectrum from the U^{235}. This spectrum contains a random time contribution due to the activity of the sample. The magnitude of this could be estimated beyond the γ-ray peak and at a position such that the bias of the counter completely eliminated all neutrons (Fig. 2).

Before and after each scattering run from U^{235}, a run with a lead scatterer, dimensionally identical to the uranium was made. The use of this

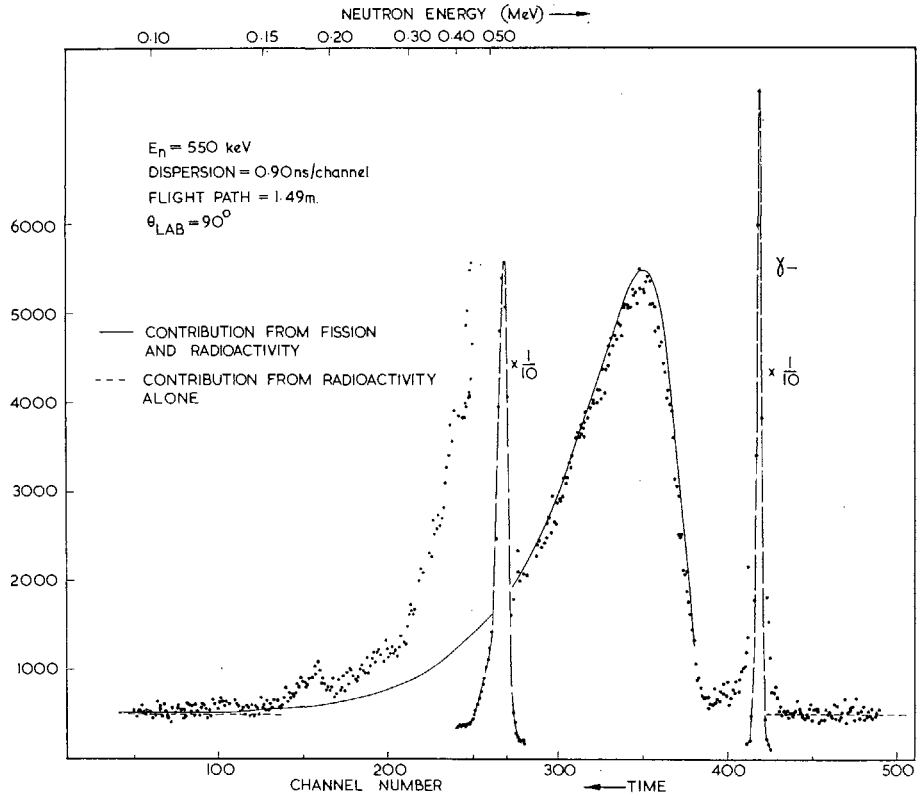

FIG.2. Time-of-flight spectrum of secondary neutrons from ^{235}U with 550-keV neutrons incident. Only the sample-out background has been subtracted.

in the analysis is described below. Runs with a carbon scatterer were also made so that all other cross-sections could be normalised to the well-known elastic scattering cross-section for carbon[10]. A typical spectrum is shown in Fig. 2. This illustrates the major features of the raw spectrum, viz - elastic peak, fission neutron spectrum and radioactive background. The shape of the fission component was determined in an auxiliary experiment in which fission was induced by low energy neutrons, other conditions being kept constant. This procedure is justified by the slow change in the fission spectrum with neutron energy as predicted for example by Terrell[8] and confirmed experimentally in a number of cases by Barnard et al[9]. The shape determined in this way is normalised to the part of the fission spectrum with an energy greater than that of the elastic peak. Due to the existence of low lying levels, the "elastic" peak contains components due to inelastic scattering. To separate these, the spectrum of neutrons scattered from a natural lead sample was measured. This shape was normalised to the high energy edge of the observed "elastic" peak and the area of the normalised "lead shape" was used in determining the true U^{235} elastic cross-section. By subtraction of the normalised "lead shape" a measure of the inelastic scattering cross-section to the low-lying levels could, in principle, be obtained although at the higher energies, very large errors are associated with this process.

The variation of the efficiency of the detector with neutron energy was determined by comparison with a calibrated long counter as described in ref. [7].

All the observed cross-sections have been corrected for sample attenuation and multiple scattering using a Monte Carlo computer programme devised by Parker[11].

Results

Elastic scattering

Since extensive measurements of elastic angular distributions had been made by Smith[2] no attempt was made to repeat this work and only differential cross-sections at 90° are reported here. The errors are mainly of a systematic nature, statistical errors being negligible. These arise mainly

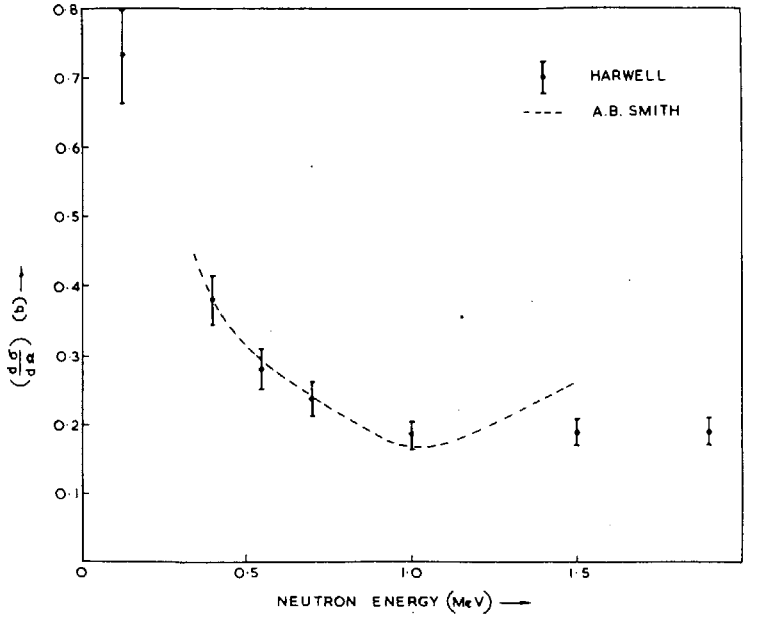

FIG.3. Differential cross-section for elastic scattering of neutrons from ^{235}U. Scattering angle 90°.

in fitting the lead shape but also include uncertainties in the C^{12} cross-sections. Runs in which the lead shape changed during the course of the U^{235} run have been rejected. The estimated overall error was ± 10%. The results are shown in Fig. 3 where they are compared with a smooth line fitted to the measurements of Smith. The agreement appears satisfactory although the tendency to rise near 1.5 MeV is not confirmed by our work.

Inelastic Scattering

Measurements of the spectrum of neutrons inelastically scattered through 90° were made at 130, 400, 550, 710, 1000 and 1500 keV incident neutron energy. At 550 keV, which is experimentally favourable, a run was made with resolution of 25 keV. This run (see Fig. 4) showed peaks which correspond to known levels or level groups in U^{235}. For the other energies the resolution was in general worse than this (see Figs. 5 and 6) and little structure appeared. It was decided therefore to present the data in the form of a histogram of basic step width 50 keV, combining these to 100 keV and 200-keV bands where statistics were inadequate. The results obtained are shown in Table I. The cross-sections shown here are the differential

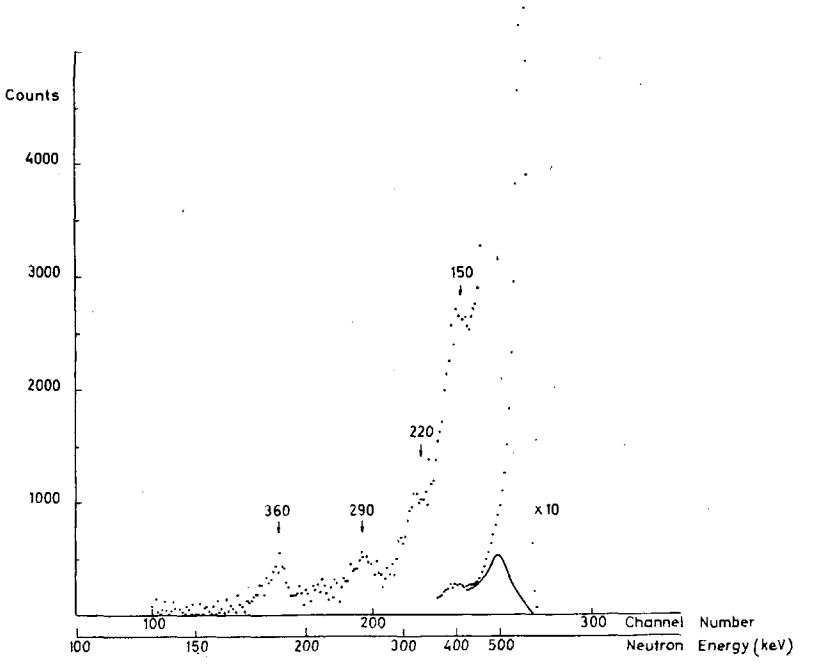

FIG.4. Spectrum of inelastically scattered neutrons from ^{235}U. Incident neutrons energy 550 keV. The fission neutrons have been subtracted, and the effect of removing the "elastic" group is shown.

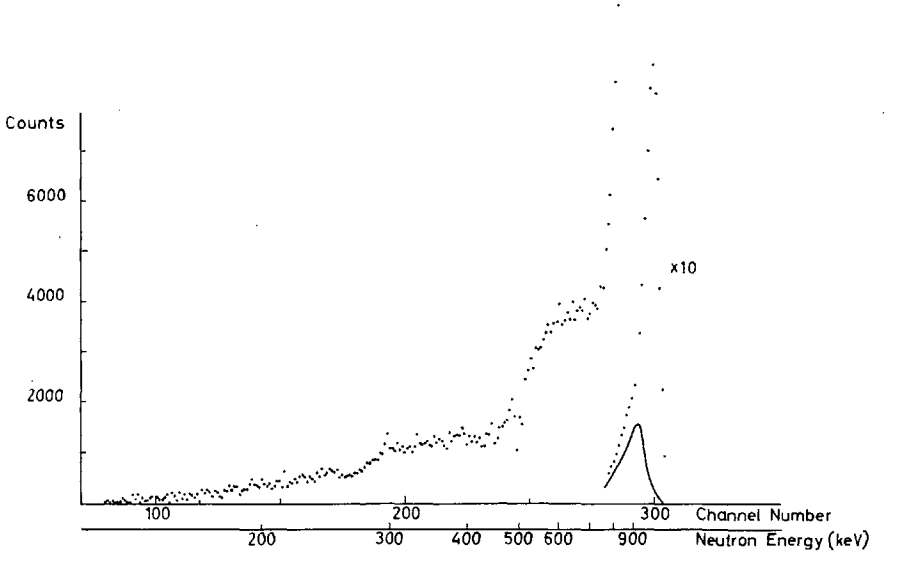

FIG.5. Spectrum of inelastically scattered neutrons from ^{235}U. Incident neutron energy 1000 keV. The fission neutrons have been subtracted, and the effect of removing the "elastic" group is shown.

cross-section at 90° multiplied by 4π. Determining the inelastic cross-section for low-lying levels by subtraction of the elastic peak gives rise to very large uncertainties. For this reason, at each incident neutron energy E_n, the first interval for which cross-sections are quoted in

Table I

Summary of inelastic cross-sections (mb)

Incident Energy (keV)	Cross-section for Excitation Energy Intervals (keV) in U^{235}																Total Inelastic (mb)	Low Neutron Entry Cut off (keV)
	0-25	25-50	50-100	100-150	150-200	200-300	300-400	400-500	500-600	600-700	700-800	800-900	900-1000	1000-1100	1100-1200	1200-1300	1300-1400	
130	344	238																582	70
400	37	306	616	327	184	350*												1820	170
550		92	314	224	236	203	229	66*										1364	110
710		45	211	221	191	245	285	359	206*									1763	130
1000			182	178	130	166	187	177	126	172	157	89*						1564	130
1500			90	159	102	94	68	47	48	69	94	121	159	195	166	110	54*	1576	140

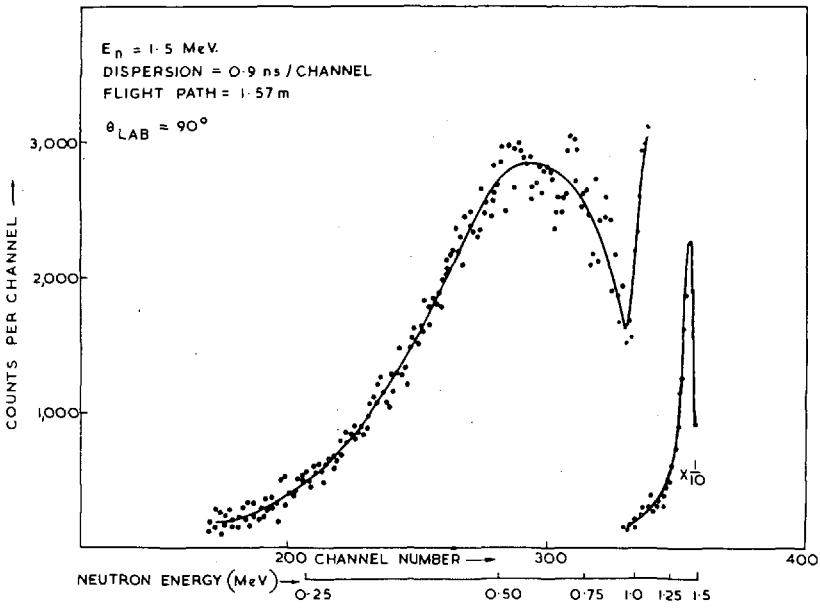

FIG.6. Spectrum of inelastically scattered neutrons from ^{235}U. Incident neutron energy 1500 keV. The fission neutrons have been subtracted, and the effect of removing the "elastic" group is shown.

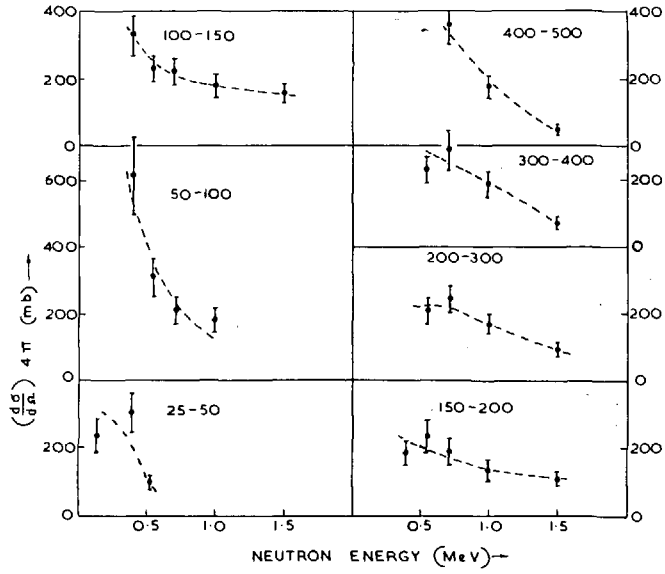

FIG.7. Cross-sections $\left(\frac{d\sigma}{d\Omega}(90°) \times 4\pi\right)$ for excitation of bands of levels in ^{235}U. The boundaries of the bands (keV) are shown on each section of the figure.

Table I has lower boundary at approximately .05 E_n. For each energy, the table shows the "low energy limit", the minimum energy of neutrons reliably observed. This limit forms the upper boundary of the highest step in the histogram. Where this differs from the nominal boundary, the corresponding

cross-sections are starred in Table I. The same data is presented as a function of energy in Fig. 7. The overall estimated error including statistics and systematic errors is thought to be about ± 20%. This value is preliminary and subject to re-examination.

From the above results, a "total inelastic cross-section" has been computed, defined as the cross-section for inelastic scattering with energy loss between 0.05 E_n and (E_n - L) where L is the "low energy limit" shown in Table I. The estimated error in the "total inelastic" cross-section is about ± 10%. The values obtained are shown in Fig. 8. For comparison, the values quoted in the compilation of Parker[12] are also shown. Our results lie systematically higher, by, however, an amount not greatly in excess of the error quoted.

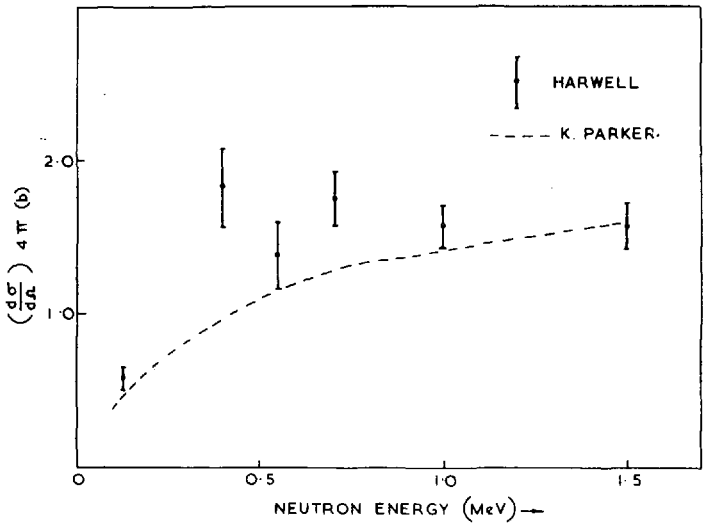

FIG.8. The total inelastic cross-section (see text for definitions) of ^{235}U as a function of neutron energy. For comparison the estimate of this quantity by Parker [12] is shown as a full line.

Discussion

Comparison with earlier experimental work is very difficult due to differences in resolution etc. The total inelastic cross-section is compared in Table II with the results of Allen[13] and Beyster[14]. These authors used biassed threshold detectors to determine the total inelastic cross-section directly. The agreement with our results is excellent. Our cross-sections are rather higher, which is consistent with the inclusion in our total of scattering to lower lying levels which would not appear in the work of Allen or Beyster.

A further comparison, with the work of Cranberg[1] is made in Table III. Here, at both incident energies of 550 keV and 1 MeV there appears to be disagreement in the cross-sections for the energy band closest to the elastic group. This discrepancy should be examined further. The higher groups are in good agreement at both energies.

It is intended to compare these results with theoretical predictions of the corrected Hauser-Feshbach model of compound nuclear reactions and attempt to obtain information about level density in this nucleus.

Table II

Total Inelastic Cross-Section (barns)

Incident Neutron Energy (MeV)	E'_{max} MeV	σ_{in} (barns)	Ref.
0.5	0.46	1.28 ± 0.4	Allen [14]
0.5	0.425	0.95 ± 0.35	Allen [14]
0.55	0.525	1.36 ± 0.14	This work
1.0	0.85	1.28 ± 0.35	Allen [14]
1.0	0.80	1.26 ± 0.3	Beyster [15]
1.0	0.95	1.56 ± 0.15	This work

Table III

Comparison with measurements of Cranberg

Incident Neutron Energy (MeV)	Cross-Section (mb) for inelastic scattering with $-Q_2 < -Q < -Q_1$ MeV				Reference
	$-Q_1$ 0.09 $-Q_2$ 0.20	0.20 0.30	0.15 0.50	0.50 0.75	
0.55	250 ± 50	200 ± 50			Cranberg [1]
0.55	460 ± 60	203 ± 30			This work
0.98			360 ± 60	310 ± 60	Cranberg [1]
1.00			680 ± 100	378 ± 40	This work

References

[1] Cranberg, L., Los Alamos Report LA2177 (1959).

[2] Smith, A.B., Nuc. Sci. Eng. 18 (1964) 126.

[3] Baranov, S.A., Koulakov, V.M., Belenki, S.N. Zhur. Eksp. Teor. Fiz. 43 (1962) 1135; Nuc. Phys. 41 (1963) 95.

[4] Braid, T.H., Chasman, R.R., Erskine, J.R. and Friedman, A.M., Phys. Lett. 18 (1965) 149.

[5] Barnard, E., Ferguson, A.T.G., McMurray, W.R. and Van Heerden, I.J. Nuc. Phys. 80 (1966) 46.

[6] Ferguson, A.T.G. Contemp. Phys. 5 (1964) 269.

[7] Adams, J.M., Barnard, E., Ferguson, A.T.G., McMurray, W.R. and Van Heerden, I.J. Nucl. Inst. 34 (1965) 21.

[8] Terrell, J. Phys. Rev. 113 (1959) 527.

[9] Barnard, E. et al. Nucl. Phys. 71 (1965) 228.

[10] Langsdorf, A. Ann. of Phys. 12 (1961) 135.

[11] Parker, J.B., et al. Nucl. Instr. 30 (1964) 77.

[12] Parker, K. U.K.A.E.A. report AWRE - 0-82/63 (1963).

[13] Allen, R.C., Nuc. Sci. Eng. 2 (1957) 737.

[14] Beyster, J.R. et al. Phys. Rev. 104 (1956) 1319.

DISCUSSION

A. B. SMITH: One of the slides showed some of our data, and the reason for the discrepancy mentioned by Dr. Ferguson is that there is a characteristic optical dip for these heavy nuclei between 1 MeV and 1.5 MeV across the 90° angle. Measurements at 90° and 95° can easily give 20 or 30% difference in the measured cross-section. We measured at around 85° and 92° or 93°, while Dr. Ferguson measured at 90°. The angle is very important in these measurements.

ETUDE DE LA DIFFUSION ELASTIQUE ET INELASTIQUE DES NEUTRONS DE 14 MeV PAR LES NOYAUX ^{6}Li, ^{7}Li ET ^{9}Be

F. MERCHEZ, V. REGIS, NGUYEN VAN SEN, R. DARVES-BLANC, PHAM DINH LIEN ET R. BOUCHEZ
LABORATOIRE DE PHYSIQUE NUCLEAIRE DE L'UNIVERSITE, ET CENTRE D'ETUDES NUCLEAIRES DE GRENOBLE, FRANCE

Abstract — Résumé

STUDY OF ELASTIC AND INELASTIC SCATTERING OF 14-MeV NEUTRONS BY ^{6}Li, ^{7}Li AND ^{9}Be NUCLEI. The authors studied the scattering of 14-MeV neutrons on ^{6}Li, ^{7}Li and ^{9}Be, using a simple time-of-flight method (total resolution ≈ 1 ns). The results were corrected for multiple scattering by a Monte Carlo method:

^{6}Li(n,n'): In addition to the fundamental level and the first 2.18-MeV level, excitation is shown of the levels 0^+ (3.56 MeV), 2^+ (4.52 MeV) and 5.3 MeV. The differential cross-sections for Q = 0 and Q = - 2.18 MeV were measured between 15° and 150° (L).

^{7}Li(n,n'): In addition to the doublet $P_{3/2}$ - $P_{1/2}$ and the excitation of the 4.63-MeV level, for which the angular distributions were measured between 15° and 130°, a study was also made of the group of levels between 6 and 7 MeV: the existence of the disputed 5.7-MeV level is indicated and the 3/2+ level at 6.3 MeV is suggested.

^{9}Be(n,n'): Measurements were made of the differential cross-sections of elastic scattering from 10° to 140° and inelastic scattering (Q = - 2.43 MeV) from 20° to 140°.

ETUDE DE LA DIFFUSION ELASTIQUE ET INELASTIQUE DES NEUTRONS DE 14 MeV PAR LES NOYAUX ^{6}Li, ^{7}Li ET ^{9}Be. La diffusion des neutrons rapides de 14 MeV sur ^{6}Li, ^{7}Li et ^{9}Be a été étudiée par une méthode de simple temps de vol (résolution totale ≈ 1 ns). Les résultats ont été corrigés de la diffusion multiple par une méthode de Monte-Carlo:

^{6}Li(n,n'): On a mis en évidence, outre le niveau fondamental et le premier niveau de 2,18 MeV, l'excitation des niveaux 0+ (3,56 MeV), 2+ (4,52 MeV) et 5,3 MeV. Les sections efficaces différentielles pour Q = 0 et Q = - 2,18 MeV ont été mesurées de 15° à 150° (Lab).

^{7}Li(n,n'): Outre le doublet $P_{3/2}$ - $P_{1/2}$ et l'excitation du niveau de 4,63 MeV, pour lesquels les distributions angulaires ont été mesurées de 15° à 130°, on a étudié le groupe des niveaux entre 6 et 7 MeV, indiquant l'existence du niveau contesté à 5,7 MeV et suggérant le niveau 3/2+ à 6,3 MeV.

^{9}Be(n,n'): On a mesuré la section efficace différentielle de diffusion élastique de 10° à 140° et inélastique (Q = - 2,43 MeV) de 20° à 140°.

Les spectres de neutrons de la diffusion de neutrons de 14 MeV sur les noyaux ^{6}Li, ^{7}Li, ^{9}Be ont été mesurés par une spectrométrie par temps de vol pour des angles de 12° à 155°.

Le faisceau de neutrons était produit par la réaction d+T → n+α et la particule α associée a été utilisée pour définir le temps zéro. Les neutrons étaient détectés dans un scintillateur plastique après une

base de vol de 1,5 m à 4 m, la résolution obtenue étant environ de $1 \cdot 10^{-9}$ s.

Les sections efficaces différentielles ont été mesurées d'après la surface des pics dans les spectres, les corrections pour la diffusion multiple, l'absorption secondaire et la résolution angulaire étant faites par une méthode de Monte-Carlo.

Lorsque cela a été possible, les sections efficaces totales ont été mesurées par intégration des distributions angulaires.. La normalisation absolue des résultats a été donnée par le nombre de particules associées

Lithium-6

Les mesures ont été faites pour des angles de 15° à 150°(Lab). Les pics correspondant à l'excitation de l'état fondamental et des niveaux de 2,18, 3,56, 4,52, 5,35 et 5,5 MeV ont été séparés. Les sections efficaces totales et différentielles pour les transitions vers l'état fondamental et le niveau de 2,18 MeV ont été mesurées. Les distributions angulaires sont données dans la figure 1; les valeurs des sections efficaces totales pour ^{6}Li(n, n) et ^{6}Li(n, n') à $E_n \approx 14$ MeV, comparées avec celles des résultats des travaux précédents, sont les suivantes:

	Livermore [1] (mb)	Los Alamos [2] (mb)	Grenoble (mb)
σ_{el}	824[1]	883 ± 95	850 ± 90
$\sigma_{inel\ (2.18\ MeV)}$	45[1]	35 ± 10	100 ± 25

Lithium-7

Il n'a pas été possible de séparer le premier état excité (0,478 MeV)) de l'état fondamental du ^{7}Li. La section efficace élastique mesurée contient donc une certaine contribution de cette transition inélastique.

Les sections efficaces différentielles ont été obtenues pour la diffusion élastique et inélastique pour le niveau de 4,63 MeV, pour des angles de 15° à 155°(Lab), et sont données dans la figure 2; les sections efficaces totales pour ^{7}Li(n, n) et ^{7}Li (n, n') à $E_n \approx 14$ MeV sont les suivantes:

$\sigma_{el} + \sigma_{inel\ (0,478\ MeV)}$	975 ± 90 mb
$\sigma_{inel\ (4.63\ MeV)}$	135 ± 20 mb

Les sections efficaces différentielles pour les autres transitions ont été mesurées à $\theta = 12°$. L'excitation du niveau de 5,7 MeV a été mise en évidence, niveau pour lequel il existait déjà des études théoriques [3, 4] et expérimentales [5-7]. En outre, ont été vus le niveau de 7,47 MeV et une transition qui pourrait correspondre au niveau 6,3 MeV (3/2+) déjà introduit par Marion [8] et par Beaumevieille [7].

Les valeurs mesurées pour ^{7}Li(n, n') sont les suivantes ($\theta_{Lab} = 12°$):

Energie d'excitation (MeV)	$\sigma_{12°}$ (mb/sr)
5,7	1,9 ± 0,5
6,3	≈ 2,8 ± 0,7[2]
7,47	1,5 ± 0,5

[1] Valeurs intégrées par Armstrong [2]

[2] L'incertitude sur cette valeur est due à la présence possible d'un niveau non résolu à 6,8 MeV.

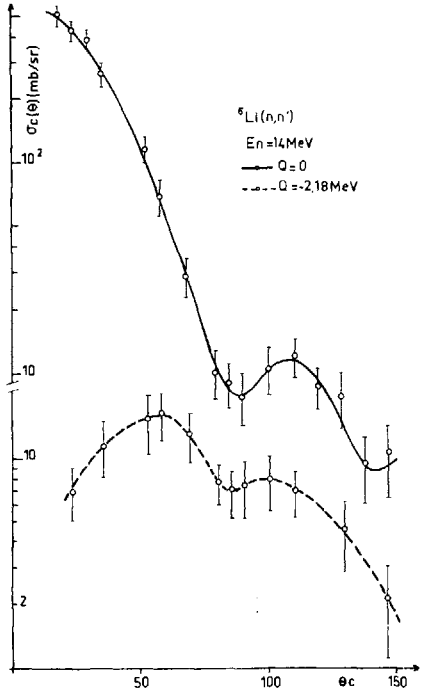

FIG.1. Distributions angulaires de la diffusion élastique (Q = 0 MeV) et inélastique (Q = -2, 18 MeV) des neutrons de 14 MeV sur le ^{6}Li

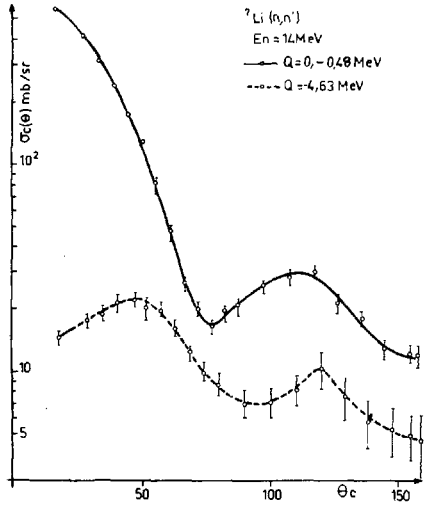

FIG.2. Distributions angulaires de la diffusion élastique (Q = 0 MeV) et inélastique (Q = -4,63 MeV) des neutrons de 14 MeV sur le ^{6}Li

Béryllium-9

Les sections efficaces différentielles ont été mesurées pour la diffusion élastique et inélastique (2,43 MeV), pour des angles entre

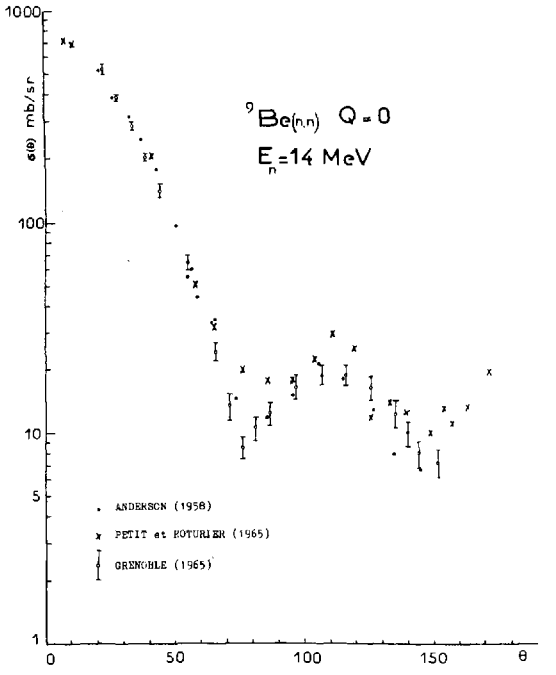

FIG.3. Distribution angulaire de la diffusion élastique (Q = 0 MeV) des neutrons de 14 MeV sur le ^{9}Be

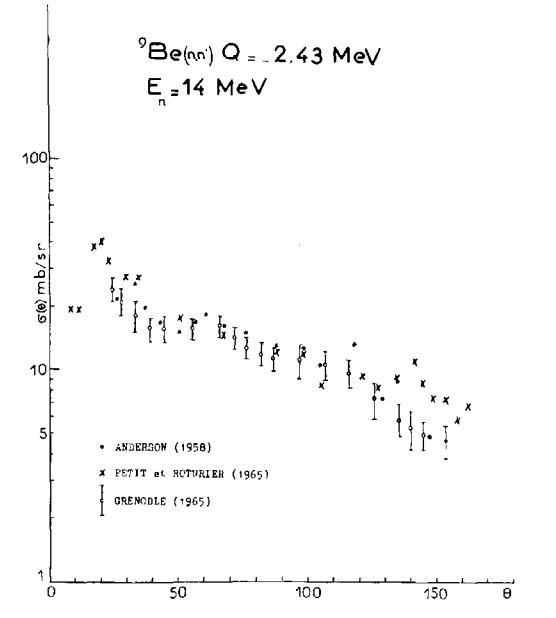

FIG.4. Distribution angulaire de la diffusion inélastique (Q = -2,43 MeV) des neutrons de 14 MeV sur le ^{9}Be

20° et 150°(Lab). Les figures 3 et 4 montrent les présents résultats ainsi que ceux d'autres groupes [9, 10]. Les sections efficaces totales pour $^{9}Be(n,n)$ et $^{9}Be(n,n')$ à $E_n \approx 14$ MeV sont les suivantes:

	Anderson [9] (mb)	Roturier [10] (mb)	Grenoble (mb)
σ_{el}	940 ± 50	-	950 ± 70
$\sigma_{inel\ (2.43\ MeV)}$	170 ± 30	174 ± 20	150 ± 20

REFERENCES

[1] WONG, C., ANDERSON, J.D., NAKADA, M.P., Nucl.Phys. 33 (1962) 680.
[2] ARMSTRONG, A.H., GAMMEL, J., ROSEN, L., FRYE, G.M., Jr., Nucl.Phys. 52 (1964) 505.
[3] SOPER, J.M., Phil.Mag. 2 (1957) 1219.
[4] CHESTERFIELD, C.M., SPICER, B.M., Nucl.Phys. 41 (1963) 675.
[5] LEVINSON, C.A., BANERJEE, M.K., Annls Phys. 2 (1957) 471.
[6] BISHOP, G.P., BERNHEIM, H., Phys.Lett. 8 (1964) 48.
[7] BEAUMEVIEILLE, H., LONGEQUEUE, J.P., LONGEQUEUE, N., BOUCHEZ, R., J.Phys. 25 (1964) 933.
[8] MARION, J.B., WEBER, G., MOZER, F.S., Phys.Rev. 104 (1956) 1402.
[9] ANDERSON, J.D. et al., Phys.Rev. 111 (1958) 572.
[10] PETIT, G.Y., ROTURIER, J., IRIGARAY, J.L., C.r.hebd.Séanc.Acad.Sci., Paris 260 (1965) 4491.

DISCUSSION

K. H. BECKURTS (Chairman): May I ask how you derived absolute cross-sections from your data; in other words, how did you normalize your data?

F. MERCHEZ: We normalized our results by scattering on hydrogen.

R. BATCHELOR: Could you please refresh my memory by saying whether this is the first time the levels at about 3.6 MeV and above have been seen in the reaction, or did the United States groups see them?

F. MERCHEZ: I don't think the first experiments showed the existence of these levels. For the Q = 3.56-MeV level the cross-sections we obtained are considerably higher than those from previous experiments. The situation is just the same when one compares our results with pp' scattering and n, p and p, n reactions for ^{6}Li: these three reactions also give an isobaric triplet A = 6 [$J = 0^+$, T = 1].

MICROSCOPIC NEUTRON SCATTERING CROSS-SECTIONS FOR REACTOR DESIGN*

A. B. SMITH AND D. LISTER
ARGONNE NATIONAL LABORATORY, ARGONNE,
ILLINOIS, UNITED STATES OF AMERICA

Abstract

MICROSCOPIC NEUTRON SCATTERING CROSS-SECTIONS FOR REACTOR DESIGN. Results obtained from a comprehensive experimental study of elastic and inelastic neutron scattering are reported. The incident neutron energy interval is 0.3 to 1.5 MeV and scattering from 50 elements extending from Be to U is investigated. Fast neutron time-of-flight techniques including a multi-angle detector system and fully automated computer control are utilized to achieve a good scattered neutron resolution. Differential elastic and inelastic scattering cross-sections are determined at eight or more angles at incident neutron energy intervals of 50 keV or less. The elastic angular distributions are expressed as Legendre expansions of up to six terms. The observed differential inelastic cross-sections are integrated to obtain the respective inelastic excitation cross-sections. The experimental results are compared with optical model Hauser-Feshbach calculations and it is shown that interpolations of experimental values, based on the model, are valid. Experimental evidence for intermediate resonance structure, width fluctuation effects and nuclear deformation is presented. The influence of each on calculation is illustrated.

1. Introduction

The objective of this study was the acquisition of a systematic experimental knowledge and a physical understanding of neutron scattering at incident energies of $\lesssim$ 1.5 MeV. Emphasis was given to scattering from reactor materials in the mass interval A = 8-239 but generality was maintained in order to provide the basic understanding of neutron scattering requisite to sound interpolation and extrapolation of measured values. Elastic and inelastic processes were examined in detail as is necessary if contributions from various compound-nucleus reaction channels are to be assayed.

Subsequent portions of this paper will: a) outline a highly automated fast neutron time-of-flight system employed in the work, b) describe experimental elastic and inelastic scattering results extending over a sufficent mass-energy interval to provide a general understanding of the scattering process, c) compare experimental results with calculations based upon a general optical potential and compound-nucleus theory, and d) explore details of the scattering process including effects due to deformation, resonance width fluctuations, shell closures, and possible intermediate resonance structure. Throughout, the discussion will be oriented toward the needs of the reactor analyst.

2. Experimental Technique and Method

The experimental measurements required good scattered neutron resolution and sensitivity, as complex and weakly excited scattered neutron groups were of interest, and techniques capable of the acquisition and processing of large amounts of experimental information. These requirements were

* This work was supported by the United States Atomic Energy Commission

largely satisfied by the automated pulsed beam fast neutron time-of-flight system shown in Fig. 1-A.[1] A pulsed Van de Graaff and a magnetic ion bunching system were used to produce short ($\sim$ 1 nsec), intense, and essentially monoenergetic neutron bursts. Neutron production was usually achieved by means of the $Li^7(p,n)Be^7$ source reaction. Some of the source neutrons struck the samples and were scattered into detectors placed several (2-3) meters distant at as many as 10 angles between 20 and 155 deg. The time interval between the source burst and the detection of the scattered neutron was determined and recorded in a digital computer center. Ten scattered neutron velocity spectra were obtained concurrently. The computer center selects meaningful events, partially processes the incoming information and exercises on-line control of the entire system including the accelerator. A representative time spectrum obtained by scattering 650-keV neutrons from W^{186} is shown in Fig. 1-A. The elastically scattered and the inelastically scattered (Q = -0.1 MeV) neutrons were clearly resolved at all observational angles. The sensitivity of the system is a few milli-barns per steradian and the optimum scattered neutron resolution $\sim$ 15 keV.

The system output was compatible with the input of a large central computer. After completion of a set of measurements the information was transferred to this central facility. Special purpose computational programs reduced the measurements to cross-sections and applied necessary corrections such as those for multiple scattering. The corrected cross-section values were rapidly available in both graphical and numerical form. The operation of the entire system was under programmed control thereby achieving a high degree of operational efficiency from the initial measurement to the final cross-section.

III. Results, Interpretation, and Discussion

Differential elastic and inelastic neutron scattering cross-sections were measured at $\lesssim$ 25-keV incident energy intervals from 0.3 to 1.5 MeV. The experimental resolution was sufficient to uniquely determine the inelastic excitation cross-sections corresponding to most energetically available excited nuclear states. The totality of the experimental results provided the comprehensive knowledge of both elastic and inelastic processes over a wide mass-energy region necessary for: a logical interpretation of the nuclear reaction mechanisms, a meaningful extrapolation and interpolation of measured values, and an insight into nuclear structure not otherwise obtainable. The representative measured differential elastic scattering cross-sections are illustrated by those of Sn shown in Fig. 1-B. The elastic cross-sections and the coefficients of the elastic angular distributions expressed in the form of the indicated Legendre expansion are given in the figure.

At the relatively low incident neutron energies of these experiments ($\lesssim$ 1.5 MeV) compound-nucleus processes contributed to both elastic and inelastic scattering. Each type of scattering must be considered if a reasonable understanding of the physical measurements is to be obtained. The chosen method of interpretation is the optical model and the Hauser-Feshbach compound nucleus theory.[2,3] These concepts are statistical in nature and can be most meaningfully compared with experiment in the context of a large body of experimental information as is available from this work.

Calculations were carried out with the intent of obtaining the best possible agreement with experiment over a wide mass-energy region using a single nuclear potential. This objective was pursued using the optical

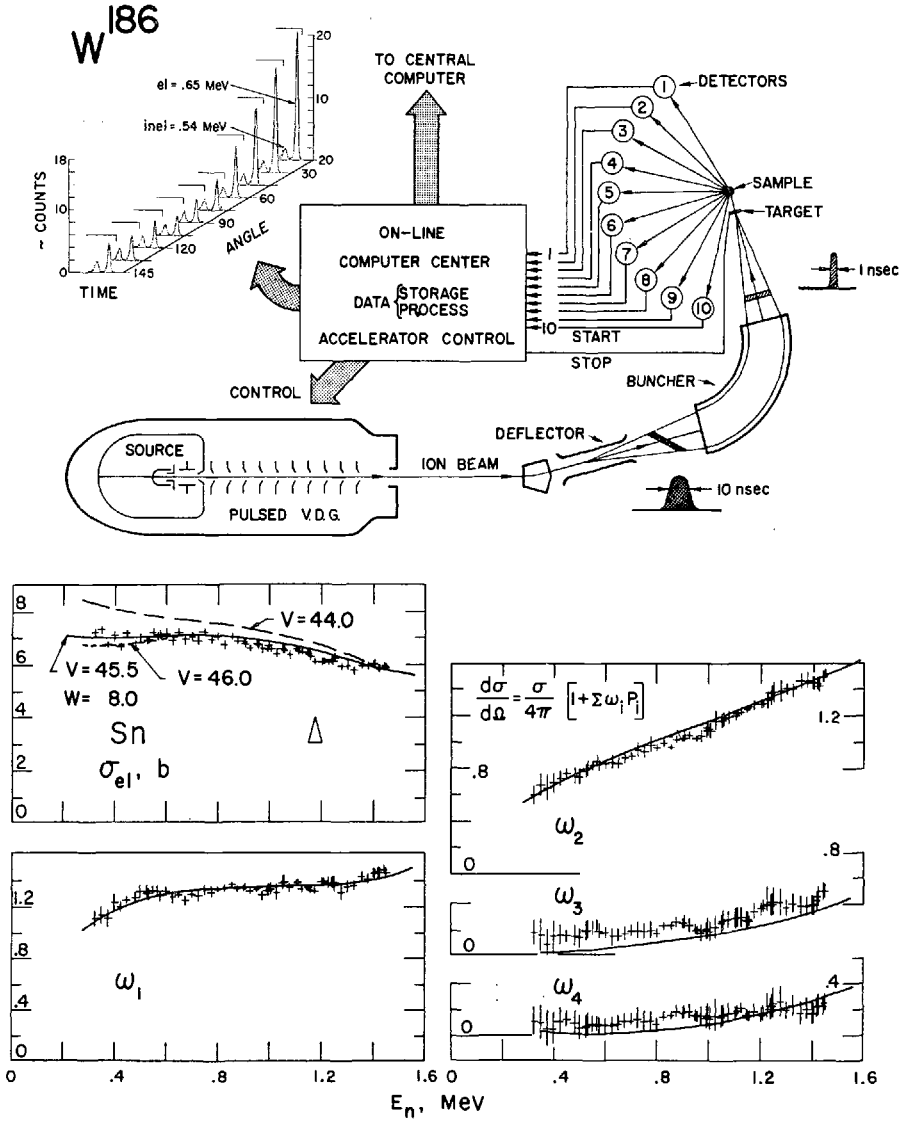

FIG.1. Above: Schematic diagram of the experimental system. Below: Differential elastic scattering cross-sections of Sn. Curves represent results of calculation (see text).

potential suggested by Moldauer[4] which is spherical consisting of: a Saxon real term V, a gaussian imaginary term W centered slightly outside the mean nuclear radius, and a spin-orbit term. Initially, calculations were made using spin and parity assignments reported in the literature or derived from systematics. Subsequently adjustments of real, V, and imaginary, W, potential parameters and level assignments were made to obtain the best overall agreement with the measured elastic and inelastic scattering cross-sections. It was required that a single set of potential parameters be used throughout the mass interval A = 23-239 and energy region 0.3 to 1.5 MeV.

An example of the agreement between the calculated and measured differential elastic scattering cross-sections of Sn is given in Fig. 1-B. The curves represent cross-sections calculated with various indicated values of the real potential V while maintaining the imaginary potential W = 14 MeV. Evidentally, under these conditions the experiment defines V to within $\sim$ 1% ($\sim$ 0.5 MeV). Actually, V = 46 MeV proved to yield the best overall agreement between calculation and experiment although in this particular example of scattering from Sn, V = 45.5 MeV appears slightly more desirable. Similar adjustments of the imaginary potential W were carried out with W = 14 MeV giving the best general agreement with experiment. The measurements were not sensitive to choices of the spin-orbit potential nor did the introduction of energy-dependent potentials lead to appreciably better agreement with experiment. The latter result is reasonable as the known energy dependence of parameters is slight and the incident energy range of these experimental measurements was relatively small.

The observed inelastic neutron scattering was often exceedingly complex and analysis established the characteristics of a number of previously unknown excited nuclear states. This information led to a better knowledge of nuclear structure not easily available by other methods. This observed complexity makes it difficult to convey the experimental results in total and recourse is made to the examples of measured inelastic excitation cross-sections shown in Fig. 2-A. In this figure measured inelastic excitation cross-sections (data points) are indicated for selected states in nuclei distributed throughout the periodic table. The particular nuclear structure involved in the respective inelastic processes is indicated by the schematic structure diagram in each portion of the figure. The solid curves on the figure represent the results of Hauser-Feshbach calculations using the optical potential established in the analysis of the experimental elastic scattering results. The observed angular distributions of inelastically scattered neutrons seldom differed significantly from isotropy or symmetry about 90 deg. An exception was the deformed nuclei where there was often observed a slight preference for scattering toward forward angles. The results shown in Fig. 2-A are the angle-integrals of the observed differential inelastic scattering cross-sections.

The inelastic scattering cross-sections of light nuclei, Na for example, are strongly influenced by isolated resonances. Thus the measured values should be averaged over several hundred keV intervals before comparison with calculations. When this is done the agreement is reasonably good. Near inelastic scattering thresholds where a limited number of exit channels are available, the effect of resonance width fluctuations should be most pronounced. The calculated inelastic excitation cross-sections were corrected for this fluctuation effect following the concepts of Moldauer.[5] The resulting corrected cross-sections are indicated by the dashed curves of Fig. 2-A. In those instances where the fluctuation correction should be largest, Zr and Nb for example, the results of calculations including these corrections are in better agreement with experiment than are those obtained using the Hauser-Feshbach formula alone (solid curve). Some of the excitation cross-sections shown in Fig. 2-A pertain to inelastic scattering from appreciably deformed nuclei; the excitation of the 2^+ (44 keV) state in U^{238} for example. Such inelastic scattering from deformed nuclei should not, in principle, be well described by calculations based upon a spherical potential such as was used to obtain the illustrated curves. Despite this fundamental invalidity the cross-sections calculated from the general spherical potential are in qualitative agreement with the measured inelastic cross-sections of these deformed nuclei.

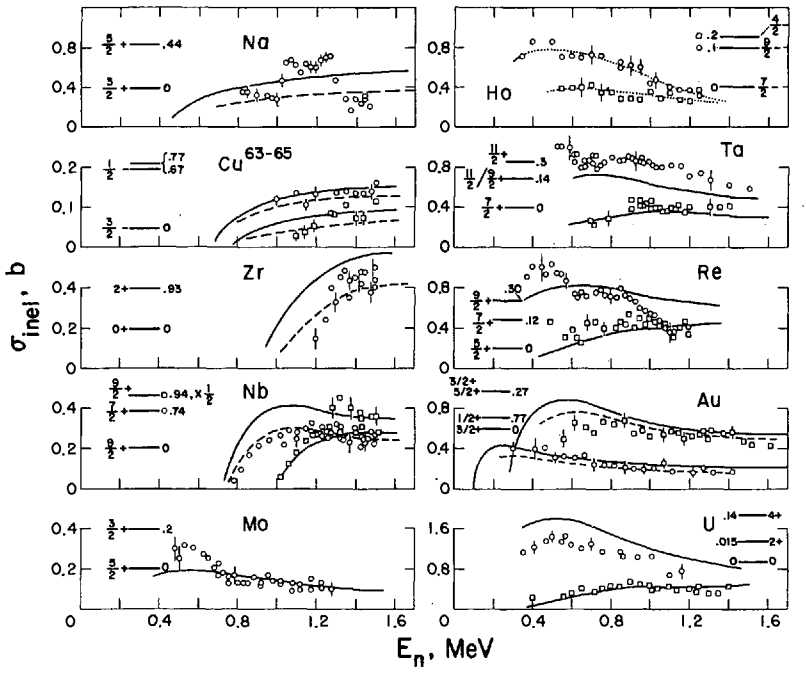

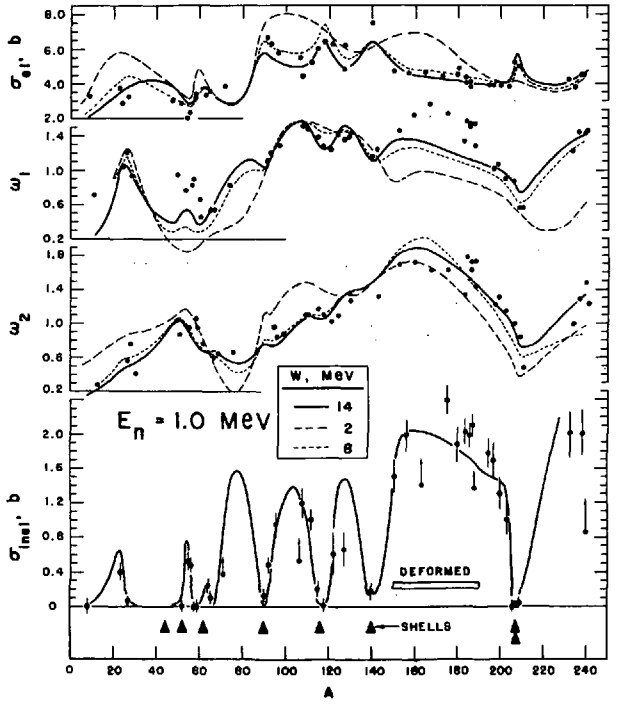

FIG.2. Above: Representative inelastic excitation cross-sections. Curves represent calculations, data points the measuremental values. Below: Comparison of measured and calculated elastic and inelastic scattering cross-sections at 1.0 MeV (see text for description).

At very low incident neutron energies the experimental and calculated neutron scattering is strongly influenced by a few excited states and is unique to the individual nuclei. Thus it is difficult to observe any general trends in the scattering cross-sections. However, as the incident energy increases a systematic behavior of both elastic and inelastic cross-sections emerges and persists to $\sim$ 1.5 MeV where both calculation and experiment become increasingly unreliable due to uncertainties in the excited nuclear structure and the respective cross-sections. At an incident neutron energy of 1.0 MeV a number of nuclear states are energetically available for inelastic excitation and there is a reasonably definitive knowledge of nuclear structure and measured cross-sections. Thus comparisons of calculation and experiment at 1.0 MeV are particularly revealing as shown in Fig. 2-B. Here are plotted the elastic scattering cross-sections, the first two coefficients of Legendre expansion of the elastic angular distributions and the total inelastic cross-sections, all as a function of mass number, A. The solid data points indicate the experimental values. The three types of curves represent the results of calculations using the potential described above with the real parameter V = 46 MeV and the imaginary parameter W varying from 2 to 14 MeV as indicated. Cross-sections were calculated for each measured element and for enough unmeasured elements to reasonably define the curves. Certain quantitative features are immediately evident. The measured and calculated cross-sections are strongly influenced by the shell dependence of nuclear level densities. This is due, of course, to variations in the partition of the reaction cross-section into elastic and inelastic components as the nuclear shells are traversed. The spherical potential employed is not strictly applicable to deformed nuclei such as Yb and the calculated cross-sections are not in quantitative agreement with experiment in these cases. The application of the model to light elements, Na and Al for example, is not commensurate with the underlying physical assumptions, thus good agreement between calculation and experiment is not obtained. Detailed adjustment of parameters, particularly the introduction of volume absorption, can improve the agreement but probably is not physically justified. With the exception of the light and the deformed nuclei the general optical potential employed with a W = 14 MeV together with compound-nucleus theory gives a quantitative description of elastic scattering, elastic angular distributions and inelastic scattering over a large part of the periodic table. The agreement between calculation and experiment shown in Fig. 2-B is more striking when one notes that the potential parameters and the illustrated calculated curves were obtained prior to measuring some 40% of the data shown in the figure. Thus measurements made after the calculations were found to be similar to the predicted values. This experience encourages the use of this or similar general nuclear potentials for the calculation of neutron scattering properties needed for reactor design.

Detailed study of Fig. 2-B and specific examination of relevant measurements reveal that the optical potential is dependent on nuclear shell structure. The effect on the observed cross-sections is in addition to that attributed to variations in level densities noted above. The dependence is most evident near the doubly closed shell at A = 208.[6] As this "doubly magic" mass is approached, the calculated differential elastic cross-sections require a decreasing imaginary potential in order to maintain a good agreement with experiment; the value of W decreasing from a general 14 MeV to 2-5 MeV at A = 208. Similar but less pronounced effects are noted near neutron number N = 50 (Zr and Nb) and proton number Z = 50 (Ag, Cd, In, Sn, and Te).

The detailed resonance structure of intermediate weight nuclei (A $\sim$ 50) near energies of $\sim$ 1.0 MeV presents an enigma to both the reactor and nuclear

structure physicist. A microscopic resonance analysis of the complex resonance structure is a formidable if not insoluble problem. Other physical interpretations leading to structure information and providing descriptions useful in applied calculations are urgently needed. A promising physical concept is that of the intermediate or quasi-particle resonance in the sense of Block and Feshbach.[7] In this concept the compound-nucleus fine-structure resonances are entered through an intermediate two particle-one hole or more complex "doorway" configuration. These intermediate configurations have a definable but relatively short lifetime and thus are observed as an intermediate resonance structure with a relatively wide width and spacing ($\sim$ 100 keV). They should be evident experimentally as a modulation of the average compound nucleus resonance structure. An apparent example of such intermediate structure in Fe is shown in Fig. 3-A. The observed high resolution total cross-section of iron consists of a multitude of narrow resonances mostly due to S and P waves. In practice it is exceedingly difficult to analyze such a complex curve. Furthermore, it is evident that the experimental values of the cross-section will depend violently on the exact experimental energy and resolution employed. The upper portion of Fig. 3-A shows a corresponding energy interval of the elastic scattering cross-section and the first Legendre coefficient of the angular distributions. The measured values have been averaged over 50-keV resolution increments. A gross structure is evident in these scattering cross-sections corresponding to an envelope of the average fine or compound-nucleus resonance structure. The gross structure persists over a wide range of experimental resolution functions and is characterized by a width and spacing of $\sim$ 100-250 keV. Similar gross structure has been observed in a number of other nuclei in the same mass region. The gross structure does have the qualitative characteristics predicted by the theoretical intermediate state concept. The observed gross structure can be analyzed using standard resonance formalism, the R-matrix formula for example, and the respective resonance parameters obtained. Such an analysis describes a highly transitory nuclear phenomena but it does provide a rational physical description of the average behavior of a very complex resonance cross-section. Such an interpretation should provide the reactor physicist with the nuclear cross-sections he needs without the ambiguities and even experimental deceptions too often inherent in the use of the high resolution fine resonance data.

Many of the nuclei studied here, and those most important to reactor design are deformed. Their excited structure consists of well defined collective rotational and vibrational states which may be directly excited in the neutron scattering process. As pointed out above, the general spherical optical potential and compound-nucleus calculations must be considered as qualitative interpretations of scattering from such deformed nuclei as U^{238}. More exact coupled-channel calculations using deformed potentials, though tedious, can give an improved agreement with experiment. This is illustrated in Fig. 3-B where the inelastic excitation cross-sections of W^{186} calculated by Dunford (solid curves) are compared with the measured values. These results were obtained from coupled-channel calculations using a deformed potential and including width fluctuation corrections. The same calculations gave a good agreement with the measured elastic scattering angular distributions and predicted the slight tendency toward forward inelastic scattering that was observed experimentally. At incident energies of $\sim$ 1.5 MeV the direct excitation of the 2^+ state in W^{186} was calculated to be $\sim$ 20% of the respective cross-section. For comparison Fig. 3-B indicates, with a dashed line, the results of calculations using the spherical potential described above. The latter are not in agreement with either experiment or the results of the deformed calculations.

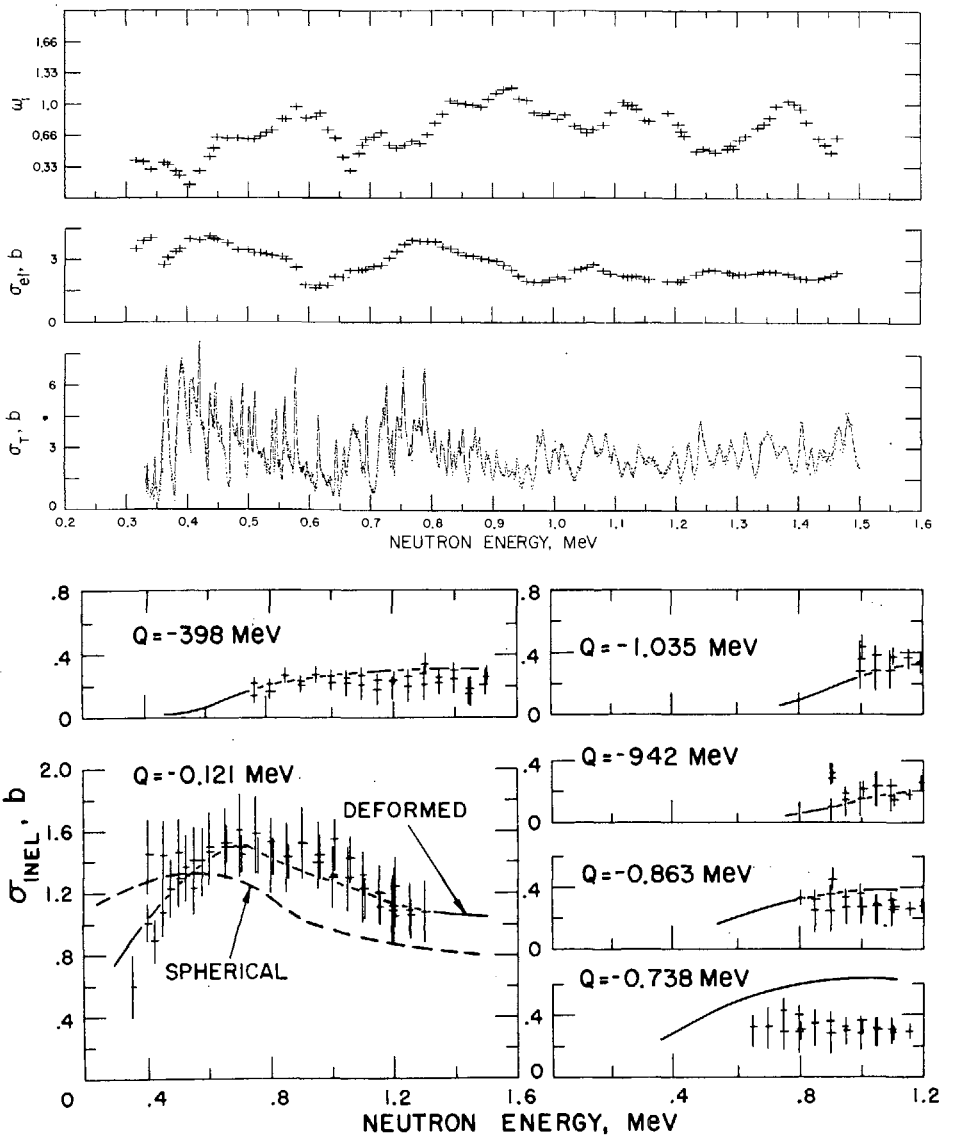

FIG.3. Above: High resolution total cross-section of Fe and 50-keV average of measured elastic scattering cross-section of Fe. Intermediate structure is evident. Below: Inelastic scattering cross-sections of ^{186}W. Both deformed (solid curves) and spherical (dashed curves) calculations are compared with experiment.

IV. Conclusion

These experiments have provided at energies of $\lesssim$ 1.5 MeV a phenomenological basis for the understanding, the interpolation and the extrapolation of neutron scattering data. This foundation has been used to examine the validity of a general optical potential which, together with compound nucleus

theory, provided a good qualitative description of the measured results over a wide mass-energy region. This or similar broadly based models can serve as a point of departure for more quantitative calculations including such detailed effects as deformation, resonance width fluctuations, shell dependence and intermediate resonance structure. Such refined calculations have the potential of satisfying a large part of the low energy scattering needs of the reactor physicist. At higher energies the scattering process is far less known. The appreciable ignorance of the respective excited nuclear structure limits quantitative calculation and the experiments become more difficult and less definitive as the incident neutron energy increases. Some reactor requirements are very precise: a few percent in cross-section uncertainty. Such precise determinations of scattering cross-sections are beyond the present capabilities of the theory and the requisite experimental measurements are exceedingly difficult with usually relatively small effects such as multiple scattering becoming important. However, both the higher energy region and the precision determinations of scattering cross-sections are amenable to successful experimental attack. This is particularly true if the most advanced techniques are employed as is not now the case.

References

[1] Smith, A. B. et al., "Multi-angle fast neutron time-of-flight system," (to be published).

[2] For review see, "The optical model of elastic scattering," P. Hodgson, Oxford Press, New York, 1963.

[3] Hauser, W., Feshbach, H., Phys. Rev. 87 (1952) 366.

[4] Moldauer, P. A., Nucl. Phys. 47 (1963) 65.

[5] Moldauer, P. A., Rev. of Mod. Phys. 36 (1964) 1079.

[6] Vonach, W. G. et al., Phys. Letters 11 (1964) 331.

[7] Feshbach, H., Ann. of Phys. 5 (1958) 353. See also Feshbach, H., "Proc. Intern'l Conf. on the Study of Nuclear Structure with Neutrons," North-Holland Press (1966) 257.

[8] Dunford, C., (private communication).

DISCUSSION

J. H. TOWLE: In some of the papers just presented, we have seen several cases of excitation curves agreeing nicely with Hauser-Feshbach theory after correction for width fluctuations. I wonder whether Dr. Smith has any significant amount of data agreeing better with the uncorrected Hauser-Feshbach theory?

A. B. SMITH: There are such apparent cases, but the level density is then relatively high and the correction term is small, usually within the experimental uncertainty.

N. STARFELT: Moldauer has discussed inelastic neutron scattering through the reaction $(n, \gamma n')$. Do you have any evidence for this reaction in your measurements?

A. B. SMITH: No. We have calculated the effect for appropriate nuclei, including cadmium. The resulting calculated cross-section, integrated over all angles at 1.5 MeV, is about 9 mb. Moreover, it is a continuum, not a discrete level. This is well below the experimental sensitivity.

R. BATCHELOR: Why isn't ^{238}U a good nucleus to study for the $(n, \gamma n')$ reaction? According to Moldauer it has a reasonably high cross-section.

A. B. SMITH: As I recall it, the calculated $n, \gamma n'$ cross-section for ^{238}U at $\sim$ 1.2 MeV is $\sim$ 100 mb over a wide energy region. Such a contribution would be very difficult to observe at these energies as any effect would be heavily masked by the more conventional inelastic neutron scattering.

K. H. BECKURTS (Chairman): In the curve representing the elastic scattering cross-section of iron as a function of energy, you seem to have an intermediate structure with levels about 300 keV apart. Have you tried to interpret this assuming particle-hole states?

A. B. SMITH: Yes. Unfortunately a computer calculation we were doing just before I left the United States did not converge. If it had, we would have had results.

AN OPTICAL MODEL STUDY OF NEUTRONS ELASTICALLY SCATTERED BY IRON, NICKEL, COBALT AND COPPER IN THE ENERGY REGION 1.5 TO 4.6 MeV

B. HOLMQVIST AND T. WIEDLING
AB ATOMENERGI, STUDSVIK, NYKÖPING, SWEDEN

Abstract

AN OPTICAL MODEL STUDY OF NEUTRONS ELASTICALLY SCATTERED BY IRON, NICKEL, COBALT, AND COPPER IN THE ENERGY REGION 1.5 TO 4.6 MeV. Angular distributions of neutrons elastically scattered by cobalt and copper have been measured at seven energies between 1.5 and 4.6 MeV, by natural nickel at four energies between 3.0 and 4.6 MeV, and by natural iron at one energy 4.6 MeV by using time-of-flight technique. The observed angular distributions were corrected for neutron flux attenuation, multiple elastic scattering, and the finite geometry of the source-sample detector system by using a Monte Carlo programme.

Theoretical angular distributions have been fitted to the experimental angular distributions by using an optical model potential of the form

$$V(r) = Uf(r) + iWg(r) + U_{so}\left(\frac{\hbar}{\mu_\pi c}\right)^2 \frac{1}{r}\frac{d}{dr}|f(r)|\vec{\sigma}\cdot\vec{\ell}$$

where U, W, and U_{so} are the real, imaginary, and spin-orbit potential depths. The form factors f(r) and g(r) are given by the expressions $f(r) = [1+\exp(r-R_U)/a]^{-1}$ and $g(r) = 4[1+\exp(r-R_W)/b]^{-2}\exp(r-R_W)/b$ where a and b are the diffuseness parameters and $R_U = r_{oU}A^{1/3}$ and $R_W = r_{oW}A^{1/3}$ are the radii. The automatic search routine of the Abacus II computer programme was used to find the values of U, W, a, r_{oU}, and r_{oW} which give the best fittings to the experimental distributions when U_{so} and b were kept constant. Good fittings were obtained with the values; b = 0.36 fm and U_{so} = 8 MeV for iron and nickel, and b = 0.48 fm and U_{so} = 8 MeV for cobalt and copper. The compound elastic contribution was taken into account in each case. The parameters U, W, a, r_{oU}, and r_{oW} are essentially independent functions of the neutron energy.

The present investigations were performed to obtain neutron elastic cross-sections for comparison with calculated cross-sections from the optical model as well as supplying nuclear data for reactor design. The purpose of the optical model study was also to make a systematic study of the parameters involved in the optical model potential describing the interaction between neutrons and nuclei.

Angular distributions of neutrons elastically scattered by cobalt and natural copper have been measured at seven energies between 1.5 and 4.6 MeV, by natural nickel at four energies between 3.0 and 4.6 MeV, and by natural iron at 4.6 MeV. The velocity spectrum of scattered neutrons was determined by measuring the time between the source burst and the detection of the scattered neutrons. The differential scattering cross-sections were determined relative to the well-known neutron scattering cross-sections of hydrogen except at the neutron energy 1.5 MeV where the carbon cross-section was used. The experimental angular distributions have been corrected for the anisotropy of the neutron flux from the source, attenuation of the neutron flux in the scatterer, multiple elastic neutron scattering, and the finite source-

TABLE I. EXPERIMENTAL DIFFERENTIAL ELASTIC NEUTRON CROSS-SECTIONS OF IRON AND NICKEL

The cross-sections are given in mb/sr in the centre-of-mass system. The errors are ±5%.

Element	Fe	Ni			
E_n (MeV)	4.56	3.00	3.49	4.00	4.56
$\cos \theta_{cm}$	$d\sigma/d\Omega$ mb/sr				
0.969	1532				1367
0.938	1200	953	964	1110	1257
0.862	750	663	711	726	752
0.813	602				
0.759	401	368	396	373	352
0.698	254				
0.633	147	174	184	148	138
0.562	94				
0.487	55	83	62	50	45
0.408	23				25
0.327	20	45	35	20	21
0.243					23
0.157	30	45	36	31	27
-0.018	51	65	65	54	46
-0.190	60	85	73	67	49
-0.359	64	89	82	73	45
-0.513	57	90	74	59	42
-0.653	33	78	62	41	27
-0.773	28	75	48	31	21
-0.825					21
-0.870	28	81	4F	32	25
-0.909					32
-0.942	32	104	62	44	38

TABLE II. EXPERIMENTAL DIFFERENTIAL ELASTIC NEUTRON CROSS-SECTIONS OF COBALT
The cross-sections are given in mb/sr in the centre-of-mass system. The errors are ± 5%.

E_n (MeV)	1.46	2.00	2.47	3.00	3.49	4.00	4.56
$\cos\theta_{cm}$	$d\sigma/d\Omega$ mb/sr						
0.938	746	867	867	946	1019	1115	1283
0.903							1050
0.862	559	619	623	707	706	647	720
0.759	419	385	393	345	408	416	382
0.633	296	266	183	233	177	157	138
0.487	203	137	107	77	62	55	36
0.327	146	75	52	37	28	27	18
0.157	122	81	55	44	35	42	38
-0.018	132	97	75	62	61	62	55
-0.190		112	93	88	78	76	69
-0.359	151	129	115	94	75	75	51
-0.513		134	107	91	71	59	40
-0.653	172	133	96	72	48	41	28
-0.773		124	79	55	33	25	13
-0.870	196	97	78	46	25	23	15
-0.909							18
-0.942					33	31	27

sample and sample-detector geometries using a Monte Carlo computer programme [1]. The corrected differential elastic cross-sections are given in the centre-of-mass system as a function of the neutron energy in Tables I-III. The relative errors of the differential cross-sections are ± 5%. The uncertainties of the neutron energies are ± 0.05 MeV.

The experimental angular distributions have been compared with theoretical angular distributions using an optical potential of the form

$$V(r) = Uf(r) + i\,Wg(r) + U_{so}\left(\frac{\hbar}{\mu_\pi c}\right)^2 \frac{1}{r}\frac{d}{dr}\left|f(r)\right|\vec{\sigma}\cdot\vec{\ell}$$

TABLE III. EXPERIMENTAL DIFFERENTIAL ELASTIC NEUTRON CROSS-SECTIONS OF COPPER

The cross-sections are given in mb/sr in the centre-of-mass system. The relative errors are ± 5%.

E_n (MeV)	1.46	2.00	2.47	3.00	3.49	4.00	4.56
$\cos \theta_{cm}$	$d\sigma/d\Omega$ mb/sr						
0.965							1439
0.938	574	740	763	890	1048	1155	1205
0.862	460	562	552	575	589	595	684
0.814							450
0.760	354	352	351	282	290	237	286
0.633	256	207		141	114	114	90
0.488	147	123	74	52	31	25	22
0.410							24
0.328	118	80	47	26	23	22	26
0.158	114	85	59	49	43	40	47
-0.016	109	105	92	84	81	60	
-0.033							60
-0.189		116	114	101	90	69	
-0.237							53
-0.356	133	129	114	104	89	58	55
-0.512		131	105	84	54	48	34
-0.652	132	121	83	57	40	29	
-0.663							18
-0.774		115	72	43	25	18	15
-0.824							16
-0.870	134	87	67	36	27	21	
-0.886							25
-0.909							25
-0.942					44	33	39

TABLE IV. OPTIMUM VALUES OF THE OPTICAL POTENTIAL PARAMETERS OF IRON AND NICKEL OF THE FIVE-PARAMETER ANALYSIS
The calculated total elastic cross-sections σ_{el} and the experimental total elastic cross-sections are also included as well as the corresponding total cross-sections σ_T.

Element	Fe			Ni			
E_n (MeV)	3.01	3.99	4.56	3.00	3.49	4.00	4.56
U (MeV)	51.19	46.97	47.43	51.35	50.54	49.63	48.79
W (MeV)	14.40	11.23	12.25	12.02	11.52	12.10	14.17
r_{oU} (fm)	1.23	1.26	1.25	1.18	1.18	1.21	1.19
r_{oW} (fm)	1.35	1.29	1.25	1.19	1.18	1.22	1.22
a (fm)	0.60	0.67	0.63	0.72	0.72	0.71	0.78
σ_{el}(b)	2.07	2.21	2.13	2.12	2.14	2.03	2.01
σ_{el}exp(b)	2.00±0.06	2.17±0.09	2.10±0.09	2.15±0.10	2.06±0.09	2.00±0.08	2.00±0.09
σ_T(b)	3.17	3.57	3.46	3.39	3.49	3.44	3.57
$\sigma_T$exp(b)	3.48±0.08	3.70±0.06	3.72±0.07	3.35±0.12	3.52±0.11	3.50±0.09	3.64±0.09
	Ref.[6]	Ref.[6]	Ref.[6]	Ref.[6]	Ref.[6]	Ref.[6]	Ref.[6]

The functions f(r) and g(r) are of the Saxon-Woods and derivative Saxon-Woods forms

$$f(r) = [1 + \exp(r-R_U)/a]^{-1}$$

$$g(r) = 4\,[1 + \exp(r-R_W)/b]^{-2}\ \exp(r-R_W)/b$$

where $R_U = r_{oU}\ A^{1/3}$ and $R_W = r_{oW}\ A^{1/3}$ are the radii, and a and b are the diffuseness parameters. The third term of the potential describes the spin-orbit interaction.

In the low neutron energy region it is necessary to take into account the presence of the compound elastic scattering. The compound elastic differential cross-sections of copper and cobalt were calculated at 1.5 and 2.0 MeV by using the formalism of Hauser and Feshbach corrected for width fluctuations according to Moldauer's theory [2]. The properties of the copper and the cobalt levels excited at the higher neutron energies are, however, not very well known and for this reason no calculations of the compound elastic cross-sections were possible. By assuming isotropic distributions the compound elastic cross-sections were estimated in these cases by the formula $\sigma_{ce} = \sigma_A - \sigma_{ne}$, where σ_A

TABLE V. OPTIMUM VALUES OF THE OPTICAL POTENTIAL PARAMETERS OF COBALT AND COPPER OF THE FIVE-PARAMETER ANALYSIS
The calculated total elastic cross-sections σ_{el} and the experimental total elastic cross-sections are also included as well as the corresponding total cross-sections σ_T.

Element	Co						
E_n (MeV)	1.46	2.00	2.47	3.00	3.49	4.00	4.56
U (MeV)	45.34	45.48	48.79	48.71	48.89	50.34	48.31
W (MeV)	8.69	9.35	11.78	9.97	11.68	10.83	11.17
r_{oU} (fm)	1.34	1.32	1.24	1.23	1.22	1.20	1.23
r_{oW} (fm)	1.34	1.36	1.22	1.24	1.20	1.11	1.20
a (fm)	0.57	0.59	0.65	0.65	0.65	0.65	0.65
σ_{el}(b)	2.78	2.42	2.15	2.09	2.02	2.06	2.03
σ_{el}exp(b)	2.88±0.19	2.46±0.11	2.16±0.10	2.11±0.10	2.03±0.08	2.07±0.08	2.03±0.09
σ_T(b)	3.54	3.49	3.42	3.45	3.45	3.48	3.54
$\sigma_T$exp(b)	3.5	3.3	3.37±0.15	3.59±0.10	3.65±0.09	3.65±0.08	3.74±0.08
	Ref.[7]	Ref.[7]	Ref.[6]	Ref.[6]	Ref.[6]	Ref.[6]	Ref.[6]

Element	Cu						
E_n (MeV)	1.46	2.00	2.47	3.00	3.49	4.00	4.56
U (MeV)	47.90	47.14	49.09	48.55	47.89	47.40	47.97
W (MeV)	8.15	10.19	9.42	9.73	9.98	10.19	9.90
r_{oU}((fm)	1.27	1.28	1.23	1.24	1.25	1.24	1.23
r_{oW} (fm)	1.26	1.24	1.18	1.20	1.19	1.20	1.20
a (fm)	0.67	0.61	0.69	0.67	0.68	0.69	0.71
σ_{el}(b)	2.43	2.25	2.07	1.93	1.91	1.97	2.04
σ_{el}exp(b)	2.35±0.16	2.26±0.09	2.01±0.08	1.85±0.09	1.82±0.09	1.75±0.10	1.85±0.08
σ_T(b)	3.53	3.36	3.39	3.40	3.55	3.70	3.78
$\sigma_T$exp(b)	3.0±0.2	3.42±0.25	3.25±0.13	3.24±0.06	3.45±0.06	3.54±0.05	3.71±0.05
	Ref.[8]	Ref.[6]	Ref.[6]	Ref.[6]	Ref.[6]	Ref.[6]	Ref.[6]

is the absorption cross-section calculated from the optical model and σ_{ne} is the experimental non-elastic cross-section. The compound elastic cross-sections of iron and nickel were calculated from the Hauser and Feshbach theory by using existing level schemes for these nuclei [3, 4]. The higher excited levels of the target nuclei with unknown spins and parities were treated in the Hauser and Feshbach calculations

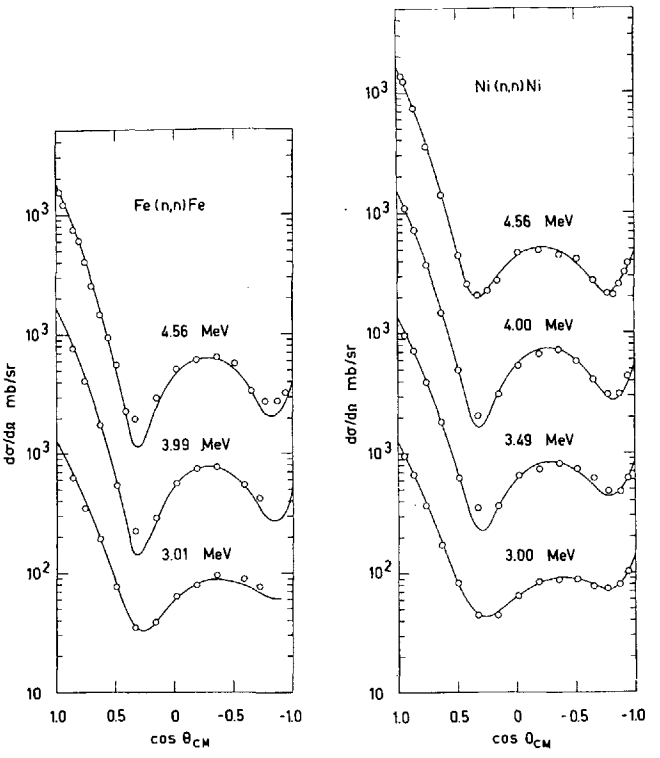

FIG.1. The experimental and the calculated angular distributions of neutrons elastically scattered by Fe and Ni. The circles represent the corrected experimental data and the solid lines are the best fittings obtained from the optical model calculations.

by using different sets of spins and parities for these levels. It was observed by using different values of the spins and parities that the properties of the higher excited levels of the target nucleus have no large influence on the compound elastic differential cross-sections.

The elastic angular distributions have been analysed with the previously given nuclear potential with five adjustable parameters. The optimum values of these parameters, i.e. U, W, r_{oU}, r_{oW}, and a, were calculated by using the automatic parameter search routine of the Abacus II computer programme. The diffuseness parameter b and the spin-orbit potential depth U_{so} were kept constant in the calculations. Good fittings were obtained with the following values: b = 0.36 fm and U_{so} = 8 MeV for iron and nickel, and b = 0.48 fm and U_{so} = 8 MeV for cobalt and copper. A variation of U_{so} has only a slight effect on the calculated angular distributions. The optimum values of the parameters of iron and nickel are shown in Table IV and of cobalt and copper in Table V. The parameter values of iron at the neutron energies 3.01 and 3.99 MeV are also included in Table IV. These values have been calculated outgoing from the experimental data of Gilboy and Towle [5].

The experimental (open circles) and calculated (solid lines) angular distributions of iron and nickel are shown in Fig. 1 and of cobalt and copper in Fig. 2. The agreement is good between the experimental and

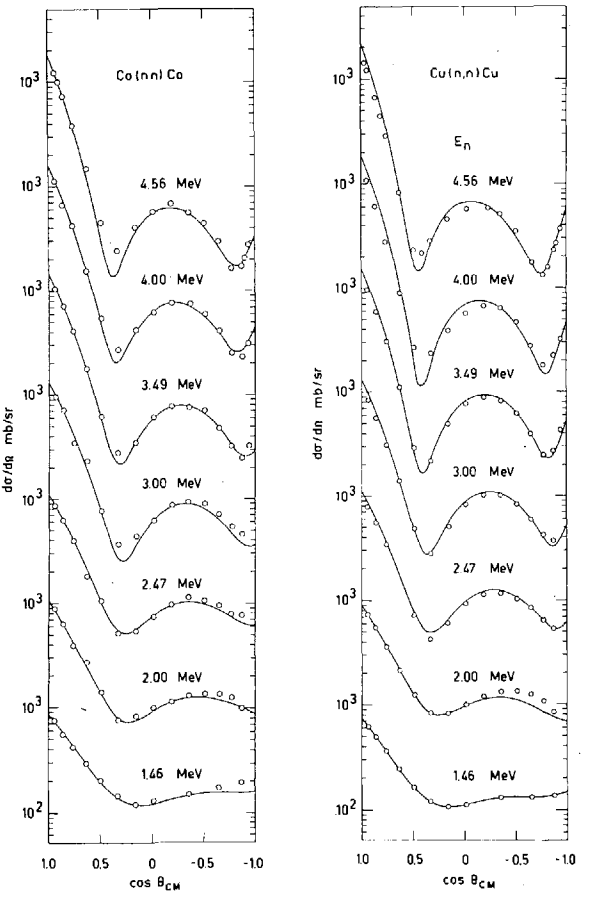

FIG. 2. The experimental and the calculated angular distributions of neutrons elastically scattered by Co and Cu. The circles represent the corrected experimental data and the solid lines are the best fittings obtained from the optical model calculations.

theoretical angular distributions. A comparison between the experimental and computed total elastic cross-sections as well as the experimental and computed total cross-sections show good agreement except at the copper measurement at 1.46-MeV energy.

The optimum values of the adjustable parameters of the investigated elements are plotted as a function of the neutron energy in Fig. 3. The parameters are largely independent of the neutron energy. However, in the case of cobalt and copper all five parameters seem to indicate anomalies at the lowest two energies probably caused by compound nucleus effects. The real potential depth of nickel is a slowly decreasing function of the neutron energy as may be the case also for iron.

It is quite clear that the experimental elastic angular distributions reported here are adequately described by the local optical model potential and that satisfactory agreement is also obtained between experimental and computed total cross-sections. It is believed that

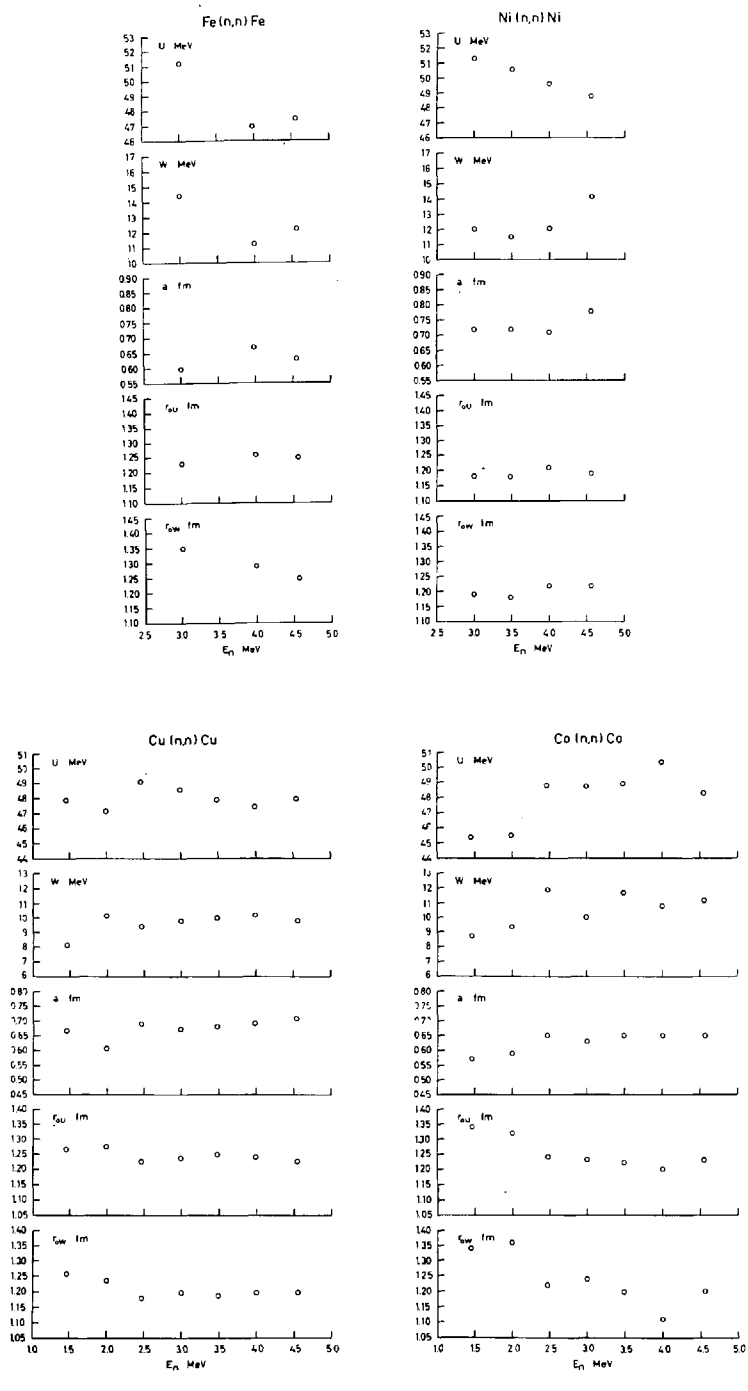

FIG.3. The optical potential parameter values U, W, a, r_{oU}, and r_{oW} from the five parameter analyses of Fe, Ni, Co, and Cu plotted as functions of the neutron energy.

the experimental differential cross-sections and the optical model parameters obtained in the present work can be used for interpolation purposes to obtain cross-sections at intermediate energies as well as the the corresponding data of intermediate nuclei in the mass number region covered.

REFERENCES

[1] GUSTAVSSON, B., HOLMQVIST, B., WIEDLING, T., A Monte Carlo programe for calculation of neutron attenuation and multiple scattering corrections, (To be published).
[2] MOLDAUER, P.A., Average compound nucleus cross sections, Rev.mod.Phys. 36 (1964) 1079.
[3] Nuclear Data Sheets, National Academy of Sciences, National Research Council U.S. Government Printing Office, Washington, D.C.
[4] MacDONALD, J.R., private communication.
[5] GILBOY, W.B., TOWLE, J.H., A neutron scattering study of Fe^{56}, Nucl.Phys. 64 (1965) 130.
[6] FOSTER, D.G., Jr., private communication.
[7] WALT, M., BECKER, R.L., OKAZAKI, A., FIELDS, R.E., Total fast neutron cross sections of Co, Ga, Se, Cd, Te, Pt, Au, Hg, and Th, Phys.Rev. 89 (1953) 1271.
[8] MILLER D.W., ADAIR, R.K., BOCKELMAN, C.K., DARDEN, S.E., Total cross sections of heavy nuclei for fast neutrons, Phys.Rev. 88 (1952) 83.

PULSED FAST NEUTRON RESEARCH AT THE LOS ALAMOS VAN DE GRAAFF ACCELERATOR*

THE NEUTRON TIME-OF-FLIGHT GROUP+
LOS ALAMOS SCIENTIFIC LABORATORY,
LOS ALAMOS, NEW MEXICO,
UNITED STATES OF AMERICA

Abstract

PULSED FAST NEUTRON RESEARCH AT THE LOS ALAMOS VAN DE GRAAFF ACCELERATOR. Pulsed-neutron research and development with the Los Alamos Van de Graaff accelerator are discussed. The salient features of this facility include a Van de Graaff accelerator providing a pulsed beam of protons or deuterons, Mobley-type beam-pulse compression apparatus, and fast electronic systems. The average target current is several microamperes, the pulse length is 1 ns, and the frequency is 2 MHz. Monoenergetic neutrons with energies from 30 keV to 7.5 MeV can be produced as can energies in the 14- to 24-MeV region. Future plans call for the installation of a klystron buncher on the Los Alamos tandem accelerator. This will provide access to the neutron energy interval between 7.5 and 14 MeV.

Four experimental programmes of particular interest to fast reactor designers are being actively pursued: (1) investigation of the gamma rays after neutron inelastic scattering; (2) investigation of elastically and inelastically scattered neutrons; (3) the measurement of the elastic and (n,2n) cross-sections of deuterium, and the elastic, (n,2n) and (n,3n) cross-sections of tritium by time-of-flight techniques; and (4) precision fission cross-section measurements. The first employs a NaI(Tl) detector surrounded by a large NaI(Tl) anticoincidence shield. The nuclides of immediate interest include Al, Si, Fe, Nb, W, ^{235}U, and ^{239}Pu. The differential cross-sections for gamma-ray production are measured for gamma rays with energies greater than 0.5 MeV. Solid-state gamma-ray detectors are being developed to replace the NaI detectors. Neutron elastic and inelastic scattering experiments are performed by directly measuring the flight times of the scattered neutrons over known distances up to 6 m. Nuclides of particular interest include ^{6}Li, ^{7}Li, ^{10}B, Si, Nb, and ^{209}Bi. The deuterium and tritium cross-section measurements use similar techniques. The scattering samples are liquid hydrogen isotopes. Precision fission cross-section ratios have been measured with ^{235}U as the standard. Solid-state counters have been used to study ^{237}Np and ^{238}U from 1 to 5 MeV.

1. INTRODUCTION

The facilities, activities, and plans of the Los Alamos time-of-flight group will be discussed. The various projects will be described, with examples chosen from several of the experiments. The technical details will be minimized except where unique facilities are involved. Similarly, the rather interesting physics resulting from some of the experiments will be neglected in favor of presenting a brief catalog of what can be done, what is being done, and what may be done in the future.

The salient features of this facility include a Van de Graaff accelerator capable of producing a chopped beam of protons or deuterons in the energy range of 1.5 to 8.0 MeV. The pulse length, from the accelerator, is variable from 2 to 10 ns with a repetition rate of 2 MHz and an average current from 2 to 10 μA. A Mobley magnet system is employed to compress

* Work performed under the auspices of the United States Atomic Energy Commission.

+ The group for this paper consists of: H. Condé (guest scientist from the Research Institute of National Defence, Sweden), D.M. Drake, J.C. Hopkins, P.W. Keaton, J.D. Seagrave, R.K. Smith, W.E. Stein and A.R. Sattler (Sandia Laboratory, Albuquerque, New Mexico)

the pulse length to 1 ns. The neutron sources are the $T(p,n)^3He$ reaction for neutrons with energies up to 5 MeV, the $D(d,n)^3He$ reaction for neutron energies between 5 and 9 MeV, and the $T(d,n)^4He$ reaction for neutron energies between 17 and 22 MeV.

There are two specifications which are roughly common to most of the experiments. They are the incident neutron energy resolution and the detector angular resolution. These numbers are 30 to 80 keV and 1 to 3 degrees respectively. The numbers depend upon many factors at the disposal of the experimenter, e.g. the energy, counting rate, sample size, etc.

This comprises the basic facility. The samples, detectors, and shields are distinct for the separate experimental programs.

2. EXPERIMENTAL PROJECTS

2.1. Gamma-ray production cross-sections

The purpose of these investigations is to measure the gamma-ray production cross-sections for various elements of interest in the calculation of radiation shields and in other problems concerning the use of nuclear energy. Special attention is paid to the incident neutron energy region between 5 and 7.5 MeV which has not been very well covered by earlier measurements.

The experimental setup is shown in Figure 1. The prominent characteristics are the NaI(Tl) gamma-ray detector surrounded by the large

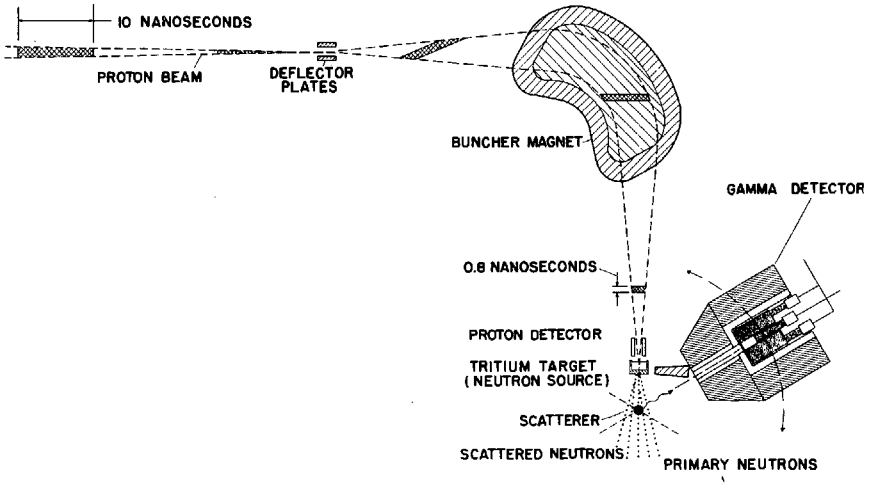

FIG.1. Experimental arrangement of the time-of-flight facility with the gamma-ray detector in position.

NaI anti-coincidence shield. Gamma rays between 300 keV and 7 MeV are detected. The resolution of the ^{137}Cs line at 0.662 MeV is 10%. Time-of-flight techniques are used to sort the gamma rays from the neutron background. Figure 2 shows the time spectrum of gamma rays detected by the central detector. The time resolution is 3.2 ns FWHM, which is very good. This feature permits a short flight path and consequently a small physical size for the scattering samples. The advantage of this is that the corrections for neutron and gamma-ray attenuation are small. Details of these

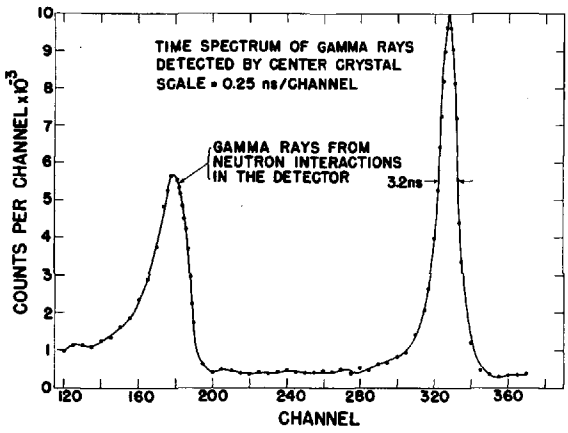

FIG.2. Time spectrum taken with the NaI(Tl) gamma-ray detector.

corrections, of spectrometer efficiency measurements, of background subtraction, and of data handling will not be discussed.

Differential cross-section data have been collected for ^{239}Pu, ^{235}U, W, Nb, Fe, Al, and Si, with 4.0, 6.0, and 7.5 MeV neutrons, for ^{12}C with 6.0 and 7.5 MeV neutrons, and for oxygen with 7.0 MeV neutrons. A proton recoil telescope was employed at each energy to measure the neutron flux.

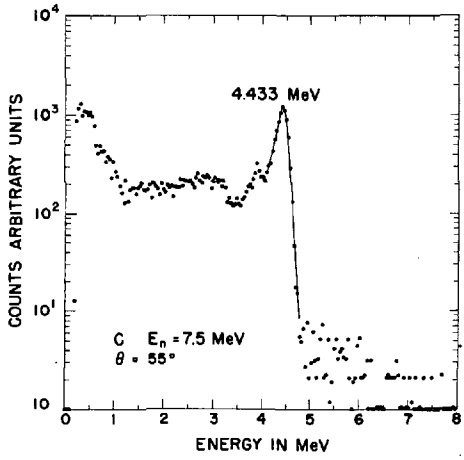

FIG.3. Gamma-ray spectrum from the reaction $^{12}C(n,n'\gamma)^{12}C$

Figures 3 and 4 show examples of gamma-ray energy spectra from ^{12}C and Si respectively for 7.5 MeV neutrons. Figures 5 and 6 show the angular distributions of two of those gamma rays for three incident neutron energies. These are preliminary results and have not yet been corrected for multiple scattering and other smaller effects.

The principal lesson is that 90^{o} is the worst angle to choose to investigate gamma-ray production if only one angle is measured and the resulting differential cross-section is multiplied by 4π to obtain the

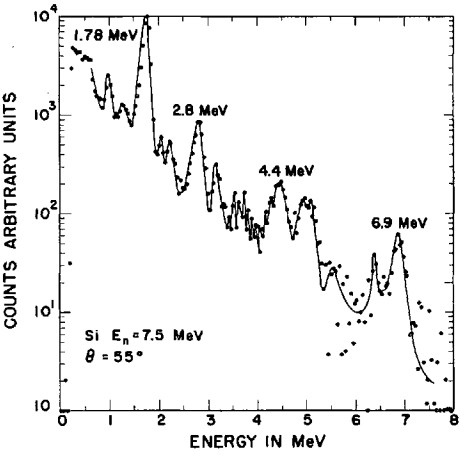

FIG.4. Gamma-ray spectrum from the reaction $^{28}Si(n, n' \gamma)^{28}Si$

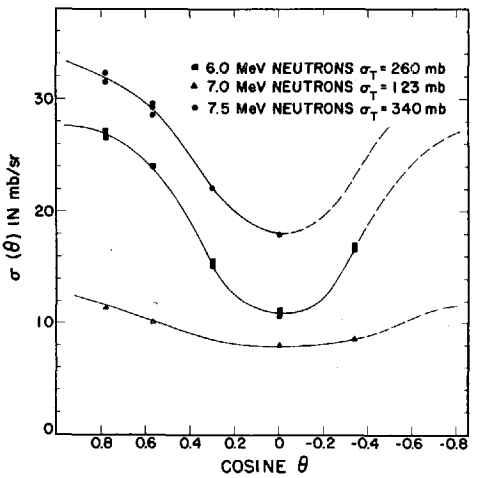

FIG.5. Angular distributions of the 4.43-MeV line from $^{12}C(n, n' \gamma)^{12}C$ at 6.0, 7.0, and 7.5 MeV of incident neutron energy.

integrated cross-section. This discovery is not new, but it does bear repeating.[1]

The raw data are now being reduced to absolute differential cross-sections. These will be compared with whatever cross-sections already exist and, in some cases, with theoretical predictions.

2.2. Neutron Elastic and Inelastic Scattering Cross-Sections

The purpose of these investigations is to measure the elastic and inelastic neutron scattering cross-sections of various elements of interest to reactor designers and engineers. These experiments complement the gamma-ray production cross-section measurements discussed in the previous section. Together they can be used to describe, with varying degrees of success, how a nucleus is excited and how it decays.

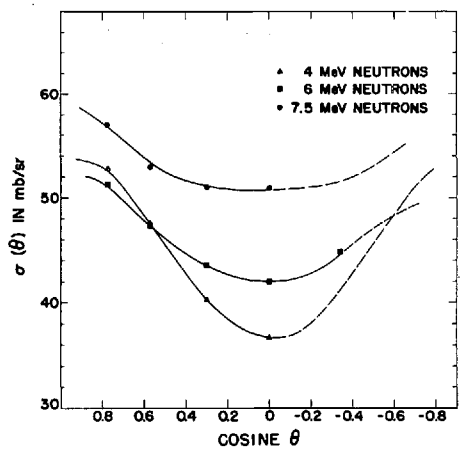

FIG.6. Angular distributions of the 1.78-MeV line from $^{28}Si(n, n' \gamma)^{28}Si$ at 4.0, 6.0, and 7.5 MeV of incident neutron energy.

Figure 1 would show the experimental setup if the gamma-ray detector were exchanged for a neutron detector. Data acquisition and handling are very much the same. In both cases an on-line computer is used as a two-dimensional pulse height analyzer, storing time and energy information. The various electronic settings are, of course, adjusted to emphasize different features.

Differential cross-section data have been collected for ^{6}Li, ^{7}Li, natural Si, and ^{93}Nb. Various energies have been used between 3.35 and 7.5 MeV; however, most of the emphasis is now being placed upon the region above 5 MeV where little data exist.

Figure 7 shows a time spectrum of neutrons elastically and inelastically scattered from Si at 7.5 MeV and 135°. The time resolution

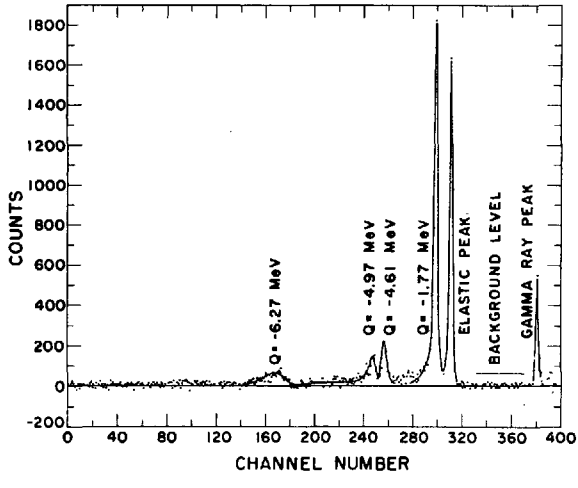

FIG.7. Time spectrum of neutrons elastically and inelastically scattered from Si at 7.5 MeV and a laboratory angle of 135°; 0.81 ns/channel

is about 2 ns. The energy resolution is about 5% at 7.5 MeV and slowly deteriorates as the scattered neutron energy decreases.

The cross-sections are measured relative to the well known neutron scattering cross-section of hydrogen. Figure 8 shows the differential elastic scattering cross-sections for Si at 7.5 MeV. The experimental data

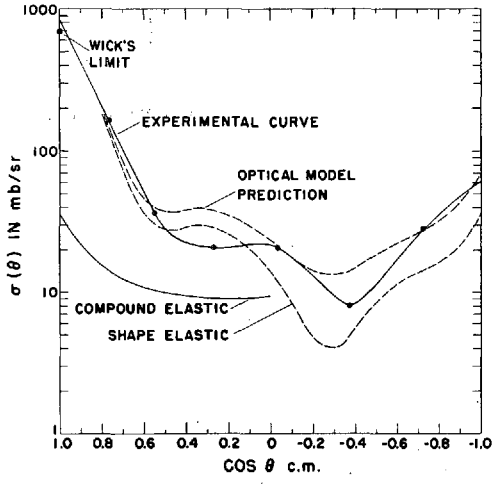

FIG.8. Elastic angular distribution for Si at 7.5 MeV. A theoretical prediction with no fitting or normalization is shown. Wick's limit, derived from the optical theorem, is the minimum value that the zero degree cross-section can assume.

have been corrected for multiple scattering and attenuation. The standard deviations are roughly five percent. The solid line through the experimental points is a visual fit based upon a shape suggested by an optical model prediction. The optical model prediction is shown in Figure 8 as a dot-dashed line. The potential well parameters are those developed by L. Rosen and his collaborators from polarization and elastic scattering data.[2] Transmission coefficients are determined by the optical model code and employed in a Hauser-Feshbach calculation to obtain the compound elastic cross-section. The compound and shape elastic cross-sections are shown separately. No fitting or normalization has been done.

Figure 9 shows the differential inelastic scattering cross-sections for Si at 7.5 MeV. No theoretical prediction is shown. A Hauser-Feshbach calculation would give symmetry about 90°. The main point is that fairly small cross-sections, in the few mb region, can be measured with absolute accuracy of 10 to 20 percent. Data are now being reduced to cross-sections and are being compared with theoretical predictions.

2.3. Neutron scattering from deuterium and tritium

This project will be described separately. The apparatus and the analysis are distinct from the neutron scattering experiments described in Section 2. The purpose of these experiments is to measure the differential cross-sections for neutron scattering from deuterium and tritium by observation of the outgoing neutron. These cross-sections are of interest for basic physics reasons as well as for our practical developmental programs. The incident neutron energies are 6 to 9 MeV and 15 to 24 MeV. At the lower energies the predominant process is elastic scattering whereas at higher energies the n,2n or n,3n reactions may have substantial cross-sections.

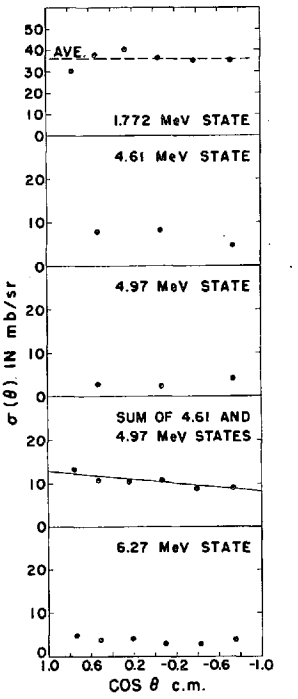

FIG.9. Differential inelastic cross-sections for ^{28}Si at 7.3 MeV of incident neutron energy. These data are isotropic within 10 to 18% relative uncertainty.

The experimental setup is unique. The scattering samples are one-mole volumes of liquid hydrogen, deuterium, or tritium. As in the scattering experiments described in Section 2.2, the cross-sections are measured relative to the n-p scattering cross-section. The samples are contained in a liquid hydrogen cryostat specifically designed for these experiments. The technical problems associated with handling 60 000 Ci of tritium are formidable. The experimental details will be completely described in a future report.

The neutron detector and shield for these experiments are different from those used for the other neutron scattering experiments. The higher neutron energies have required substantially more shielding and have required the incorporation of neutron-gamma discrimination circuits.

Data have been collected for neutron scattering from deuterium at 5.6, 7.0, 8.0, and 9.0 MeV. An example of neutron elastic scattering at 8 MeV is shown in Figure 10 along with the elastic p-d data of Brolley, et al.[3] These n-d data are preliminary and should be considered only as examples. The solid line represents the experimental data after shape correction for multiple scattering. The precision of the relative values is approximately 7%. The absolute cross-section may change as the attenuation analysis progresses. There is no explanation for the disagreement with the p-d data. This problem, of course, will be pursued.

Some data have been collected at 20 MeV. These have not been analyzed. More data will be taken on the n-d scattering at low and high energies. The neutron production cross-section should be determined in the 15 to 24 MeV region. Data have not been taken with tritium. These measurements will follow the experiments with deuterium.

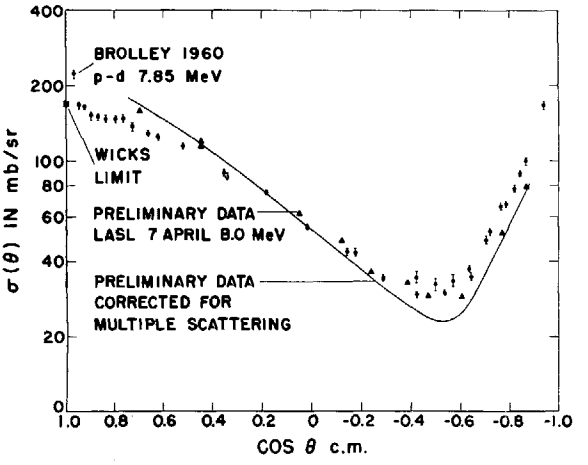

FIG.10. An example of neutron elastic differential cross-section data from deuterium at 8 MeV. These data are preliminary and do not contain the final attenuation or relative efficiency corrections. Also shown are the elastic p-d data of Ref.[3].

2.4. Relative fission cross-sections

The purpose of the present measurements is to provide more accurate values of various fission cross-section ratios in the neutron energy range of 1.0 to 5.0 MeV. The nuclides of interest are ^{235}U, ^{236}U, ^{238}U, and ^{237}Np. Emphasis has been placed on the use of pulsed, monoenergetic neutrons and fast electronic systems to discriminate against fissions induced by scattered neutrons. In addition, careful attention has been given to the evaluation of the necessary corrections to be applied to the data.

The experimental method involves counting fission fragments emitted by each of two known masses of fissile material exposed to the same neutron flux. Both solid-state and xenon gas scintillators have been used as fission fragment detectors. Fragments are recorded during and a few nanoseconds after the arrival time of each neutron burst. Time-of-flight techniques are used to sort out fissions induced by scattered neutrons.

A list of the various experimental problems would include: foil assay, both chemical and isotopic, foil preparation, detector efficiency determination, inscattering corrections, and extrapolation of the fission spectrum under the α peak. Many of these problems are inherent in any precision fission cross-section measurement and presently limit the accuracy to about 2% in a cross-section ratio. The largest single uncertainty, by a factor of 4, is in the assay of the foils.

Figure 11 shows the cross-section ratio $\sigma(^{237}Np)/\sigma(^{235}U)$ and $\sigma(^{238}U)/\sigma(^{235}U)$ versus incident neutron energy. The vertical error bars represent relative standard errors based on statistics and the uncertainties associated with the various corrections applied to the data. The overall standard deviation is ±2.5%. For comparison purposes the ratios obtained from the data of Smith, Henkel, and Nobles[4] and from Henkel[5] are included in Fig. 11. It has been suggested that the steps in the ratios result from the onset of quasi-particle excitations in the saddle-point nucleus. Further work with ^{236}U is in progress to evaluate this hypothesis.

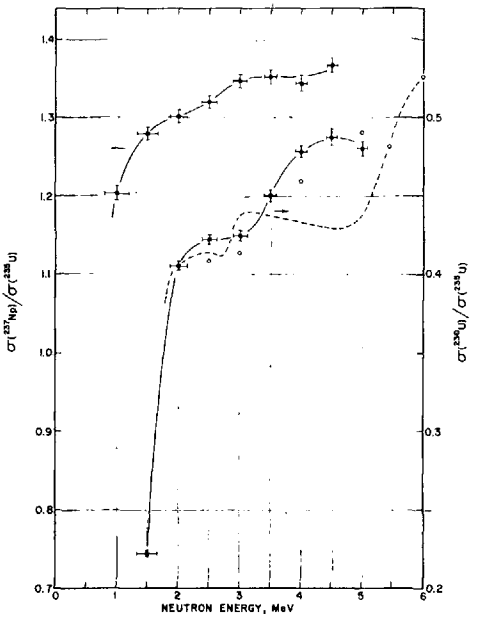

FIG.11. Relative fission cross-sections. Solid circles represent results of this work. Horizontal error bars give estimates of neutron energy spread. Vertical error bars give relative or point-to-point standard errors. Open circles are data of Reference 4. Dashed line represents data from Reference 5.

3. FUTURE PLANS

Briefly, the future plans call for a continuation of the programs outlined. A gradual decrease in the programmatic responsibilities accompanied by an increase in the proportion of the basic physics is expected. Technological improvements are being incorporated as time permits. An example of such is the shift to Li-drifted Ge gamma-ray detectors.

A time-of-flight facility is planned for the Los Alamos tandem accelerator. This will provide access to the 8 to 14 MeV region. It is expected that cross-section work of an applied nature will be undertaken with that facility from time to time to meet the needs of the various laboratory programs.

REFERENCES

[1] MORGAN, I. L., MATHUR, S. C., and NELLIS, D. O., Gamma-ray production cross sections in (n,n'γ) reactions by Satchler theory calculations, Paper D-4, Conference on Neutron Cross Section Technology, March 22-24, 1966, Washington, D.C. (to be published).

[2] ROSEN, L., BEERY, J. G., GOLDHABER, A. S., and AUERBACH, E., Elastic scattering of 10.5 and 14.5 MeV polarized protons from nuclei and the optical model potential at intermediate energies, Annals of Phys. 34 1 (1965) 96.

[3] BROLLEY, J. E., Jr., PUTNAM, T. M., ROSEN, L., and STEWART, L., Hydrogen-helium isotope elastic scattering processes at intermediate energies, Phys. Rev. 117 5 (1960) 1307.

[4] SMITH, R. K., HENKEL, R. L., and NOBLES, R. A., Neutron-induced fission cross sections for ^{233}U, ^{235}U, and ^{239}Pu from 2 to 10 MeV, Bull. Am. Phys. Soc. 2 4 (1957) 196.

[5] HENKEL, R. L., Fast neutron cross sections, U.S.A.E.C. Report LA-2122, Los Alamos Scientific Laboratory, June 1957.

DISCUSSION

M. GOLDBERG: You mentioned an upper limit above 20 MeV for your facility. Are you making measurements in the energy region from 15 to over 20 MeV?

J. C. HOPKINS: Yes. We are measuring the elastic and inelastic scattering cross-sections for deuterium and tritium between 18 and 23 MeV.

K. H. BECKURTS (Chairman): Did you use a germanium detector for the inelastic scattering γ-ray work which you describe? If so, what time resolution could you get? I think it is most important to have an extremely good time resolution if lithium-drifted germanium detectors are to be used in fast-neutron time-of-flight experiments.

J. C. HOPKINS: No, we did not use germanium detectors. The energy resolution is not necessary in these measurements. The time resolution and efficiency of germanium detectors are inferior to those of NaI(Tl), though I believe one could obtain time resolutions better than 10 ns with large germanium detectors.

J. H. TOWLE: I would like to mention that Gilboy at Aldermaston has a 20-cm^3 lithium-drifted germanium detector with which he gets between 7 and 10 ns time-resolution. He is starting some inelastic scattering work with this counter, and we hope to buy a large sodium iodide annulus, like the one mentioned in this paper, to put round it.

EVALUATION OF HEAVY EVEN-EVEN NUCLIDE ELASTIC AND INELASTIC CROSS-SECTIONS BY MEANS OF A NON-SPHERICAL OPTICAL MODEL*

C. L. DUNFORD
ATOMICS INTERNATIONAL DIVISION,
NORTH AMERICAN AVIATION, INC.,
CANOGA PARK, CALIFORNIA,
UNITED STATES OF AMERICA

Abstract

EVALUATION OF HEAVY EVEN-EVEN NUCLIDE ELASTIC AND INELASTIC CROSS-SECTIONS BY MEANS OF A NON-SPHERICAL OPTICAL MODEL. The neutron cross-section data for heavy even-even nuclides are important to both fast breeder reactors and large-scale isotopic heat sources. Only for the isotopes ^{238}U and ^{232}Th have many experimental measurements of fast neutron cross-sections been made. Even for these isotopes, there is insufficient information about elastic scattering cross-sections, angular distributions and inelastic excitation functions to generate an adequate library of fast microscopic cross-sections. In the light of these deficiencies, the evaluator must fill in the gaps in experimental knowledge, decide between conflicting data, and choose a best curve through data which has large associated errors.

While one might want to know a particular cross-section in fine detail from an esthetic point of view, in practice only accurate averages are necessary. Most nuclear models that are used to calculate fast neutron cross-sections yield only energy-averaged cross-sections with little energy detail. Hence, it is conceivable that nuclear theory could be used as an important evaluation tool when sufficient confidence is gained. The important feature of a theoretical analysis would be the applicability of any particular model to a group of isotopes of interest.

The heavy even-even isotopes have been investigated with a combined non-spherical potential optical model and compound nucleus theory. Compound nucleus theory provides a method for treating all the reaction cross-sections (fission, capture, (n,n), (n,2n)). An analysis of ^{238}U and ^{232}Th for which considerable data is available has justified the usefulness of this approach to evaluation. The non-spherical optical model permits the evaluator to separate the elastic and inelastic components of a measured angular distribution for these isotopes.

Combined with an appropriate nucleus model, it is possible to differentiate between conflicting sets of ^{238}U capture data between 10 and 100 keV.

With a knowledge of the systematics of this combined model for fast cross-sections of heavy even-even nuclei, it is possible to generate with some confidence nuclear data for such isotopes as ^{238}Pu, ^{242}Pu and ^{244}Cm. One of these isotopes ^{242}Pu is important in fast breeder reactors, and the others are being considered for large radioisotope heat sources.

The evaluation and production of neutron cross-sections according to an appropriate theoretical model is an important tool in the cross-section evaluator's repertoire.

1. Introduction

In order to remove some of the subjectivity of cross-section evaluation, more extensive use should be made of theory as an evaluation guide. This concept is not a new one and has been used with good results by Slaggie and Reynolds in a recent oxygen evaluation. [1] Difficulties arise in the practical application of nuclear models to evaluation either through lack of appropriate theory or lack of confidence in the extrapolative and interpolative powers of the various nuclear models.

* Work supported by the United States Atomic Energy Commission.

At the present time, there are no theories appropriate to all nuclides and all energies. It is therefore necessary to develop a comprehensive model for a given class of nuclei and energy region. In addition, because of the many-body nature of the problem, there is no nuclear theory which can predict the detailed structure of the energy dependence of neutron cross-sections. However, average characteristics can be calculated from theory. Such average behavior is in fact all that is required for many applications.

The heavy even-even nuclide neutron cross-sections can be evaluated with the aid of an appropriate comprehensive nuclear scheme. Such a scheme has been investigated and applied to ^{238}U, for which extensive experimental data are available. Nuclear theory is used to analyze experimental data; for example, separating an experimental angular distribution into its component parts. A best curve drawn through a set of experimental data with the aid of nuclear theory is illustrated by an evaluation of the ^{238}U capture cross-section.

2. Interaction Models

The number and types of possible reactions between neutrons and nuclei increase with increasing neutron energy. Different reaction models are required to describe different subsets of these reaction types. These different models have been unified into a coherent scheme to analyze the experimentally measured neutron cross-sections, and to produce an evaluated library of microscopic cross-sections for an isotope.

In order to describe the neutron-nucleus interaction, an effective interaction potential is introduced and the quantum scattering problem is solved for this potential. Solutions to the Schrodinger equation give information about the total cross-section, the compound nucleus formation cross-section, and the potential scattering cross-sections. Models for the interaction potential have increased in sophistication in direct proportion to the availability of high speed, large storage digital computers. Recognition of the diffuse nature of the nuclear surface and the possibility of formation of a compound nucleus has led to the Woods-Saxon type potential and the complex potential, respectively. A spin-orbit interaction is required to account for neutron polarization. This introduces a different interaction potential for each total angular momentum state of the neutron.

Heavy nuclei are known to be highly deformed, and their level structure is well described by a collective model.[2] In particular, heavy even-even nuclei, e.g. ^{238}U and ^{232}Th, have a well-defined rotational band with a 0^+ ground state and a 2^+ first-excited level. Therefore, these nuclei should be described by a deformed interaction potential.

Several authors[3-6] have investigated the deformed potential for neutrons, protons, and alpha particles. The deformed potential may be written

$$V\left[r - R(\vec{\Omega})\right] = V(r - R) - \sum_m T_2^m(r - R, A) Y_2^m(\vec{\Omega}), \qquad (1)$$

and

$$T_2^m(r - R, A) \sim \beta \frac{dV(r - R)}{dr}, \qquad (2)$$

where β is the nuclear deformation parameter. The spherical part of the nuclear potential, V(r - R), may have many forms, but the present work is restricted to the following commonly used potential.

$$V(r-R) = \underbrace{-\frac{V_R}{1+\exp\left(\frac{r-R}{a}\right)}}_{\text{(Woods-Saxon)}} \underbrace{- i\frac{4W_I \exp\left(\frac{r-R'}{b}\right)}{\left[1+\exp\left(\frac{r-R'}{b}\right)\right]^2}}_{\text{(Imaginary Saxon derivative)}}$$

$$\underbrace{-\left(\frac{\hbar}{m_\pi c}\right)^2 \left|\frac{1}{r}\frac{d}{dr}\left[\frac{1}{1+\exp\left(\frac{r-R}{a}\right)}\right]\right| \vec{\ell}\cdot\vec{\sigma}}_{\text{(Spin-orbit)}}, \qquad (3)$$

The quadrupole term of the deformed potential is proportional to the derivative of the spherical part of the potential and is therefore complex, also. However, if the assumed coupling is real, then the numerical solution to the scattering equation is simplified. In certain ranges of incident neutron energy, this simplifying assumption is valid, but in other regions the full complex quadrupole potential should be used.

The several reaction cross-sections are calculated using a statistical theory for the decay of the compound nucleus. A cross-section for formation of the compound nucleus is given by the deformed nucleus-scattering calculation. This cross-section is separated into its constituent decay channels by the statistical model calculation. Since charged particle emission is strongly inhibited in the energy range of interest by the large charge on the heavy nuclei, these decay modes are neglected. The channels to be considered include (n,n), (n,n′), (n,f), (n,nf), (n,2n), and (n,γ).

The statistical theory for the decay of the compound nucleus,[7,8] with modifications to account for correlations of the incoming and outgoing channels,[9,10] is used. The basic expression is

$$\sigma_{n,x} = \frac{\pi}{2k_0^2}\sum_{\alpha\beta}(2J+1)\left\{\frac{\langle\Theta_{\alpha\mu}\rangle\langle\Theta_{\beta\mu}\rangle}{\langle\Theta_\mu\rangle}S_{\alpha\beta} - \frac{Q}{4}\langle\Theta_{\alpha\mu}\rangle^2\delta_{\alpha\beta}\right\} \qquad (4)$$

where

$$\Theta_{\alpha\mu} \sim 2\pi\left\langle\frac{\Gamma_{\alpha\mu}}{D}\right\rangle$$

$$\Theta_\mu = \sum_\alpha\langle\Theta_{\alpha\mu}\rangle, \quad \alpha = \text{all open channels}$$

$$S_{\alpha\beta} = \frac{\langle\Theta_{\alpha\mu}\Theta_{\beta\mu}/\Theta_\mu\rangle}{\langle\Theta_{\alpha\mu}\rangle\langle\Theta_{\beta\mu}\rangle/\langle\Theta_\mu\rangle}$$

Q = parameter dependent on the nucleus, $0 \le Q \le 2$

Neutron capture is described by a model for emission of dipole radiation by the compound nucleus, and may be written as

$$\langle\Theta_{\gamma\mu}\rangle = 2\pi\left\langle\frac{\Gamma_\gamma}{D}\right\rangle_0 f(A,J,E). \qquad (5)$$

In this equation, $\langle \Gamma_\gamma / D \rangle_0$ is generally taken as the value given by measured low energy s-wave resonances. The correction factor, f(A,J,E), gives the mass, energy, and spin dependence of the dipole emission probability and is calculated from the Weisskopf radiation formula.[11] At energies around 1 Mev and above, a correction has been applied to the capture cross-section to account for the (n,γn') reaction.[11]

The fission channels, (n,f) and (n,nf), are given by the Hill-Wheeler[12] fission model. This model is described by a channel parameter $\langle \Theta_{f\mu} \rangle$ given by

$$\langle \Theta_{f\mu} \rangle = \frac{N}{1 + \exp - \left(\frac{E - E_o}{\hbar\omega} \right)} \tag{6}$$

where N is the number of open fission channels, E_o is the fission barrier energy, and $\hbar\omega$ is a characteristic energy. This expression is assumed to be independent of the spin of the compound nucleus.

For the heavy even-even nuclei, the level structure of the target nucleus is usually well known up to 1.25 Mev above the ground state. The values for $\langle \Theta_{n'\mu} \rangle$ may be related to the penetrabilities calculated in the interaction potential approximation.[11]

$$\langle \Theta_{n'\mu} \rangle = T_{n'} + \frac{1}{Q} \left[1 - \sqrt{1 - 2QT_{n'}} \right]^2 . \tag{7}$$

Neutron penetrabilities for the ground state and the first excited level (2^+) were obtained from the solution to the deformed nucleus scattering problem. All penetrabilities for higher excited states were calculated with a spherical potential model. Angular distributions for the compound elastic and first inelastic (2^+) level neutrons were calculated without considering the competing (n,γ), (n,f) or continuum (n,n') channels, or the correlation corrections. The distributions were then renormalized to the corrected channel cross-section as calculated for the complete model.

At energies above 1.25 Mev, many levels have not been observed experimentally and those levels which have been observed often do not have spin and parity assignments. Decay of the compound nucleus to these levels was represented by a continuum neutron emission model in which the parameter $\langle \Theta_{n'(\text{cont.})\mu} \rangle$ is specified as piecewise linear and independent of compound nucleus spin,

$$\langle \Theta_{n'(\text{cont.})\mu} \rangle = 2\pi \left[\left\langle \frac{\Gamma_{n'}}{D} \right\rangle_0 + \left\langle \frac{\Gamma_{n'}}{D} \right\rangle_1 E \right] . \tag{8}$$

The continuum model and the discrete-level inelastic model were used from 1.15 to 3.00 Mev in the present evaluations. The systematic analysis of (n,2n) reactions by Pearlstein[13] was used to separate the inelastic continuum neutron emission cross-section into (n,2nγ) and (n,n'γ) components after the competing (n,nf) reaction cross-section was subtracted.

3. Evaluation of ^{238}U

Nuclear theory has been applied to the evaluation of ^{238}U neutron cross-sections over the energy range from 10 Kev to 15 Mev. Many ^{238}U cross-sections have been measured in sufficient detail to give an adequate test of the computational scheme and the nuclear models to be used.

The total neutron cross-section does not depend on the combination of several models, but depends only on the optical model chosen and its well parameters. The well parameters used for all heavy even-even nuclei are those given in Table I. The deformation parameter, β, is 0.244 which is in good agreement with that obtained from electromagnetic transition measurements [14] and scattering experiments.[15] The results are illustrated in Figure 1. The calculations are in general agreement with experimental data. Most of the data lying below the calculated values at energies below 1 Mev are recent measurements of Seth.[17] In the energy region between 2.0 and 7.0 Mev, the calculations lie below all measured experimental points. A larger discrepancy between theory and experiment exists in this region when a spherical optical model is used. It appears that better agreement should result when the 4^+ level is included in the deformed nucleus calculation.

TABLE I

OPTICAL MODEL PARAMETERS

V_R	$46.53 - 0.42\ E$
R	$r_o A^{1/3}$ f
a	0.65 f
W_I	$4.27 + 1.03\sqrt{E}$
R'	$r_o A^{1/3}$ f
b	0.47 f
r_o	1.25 f

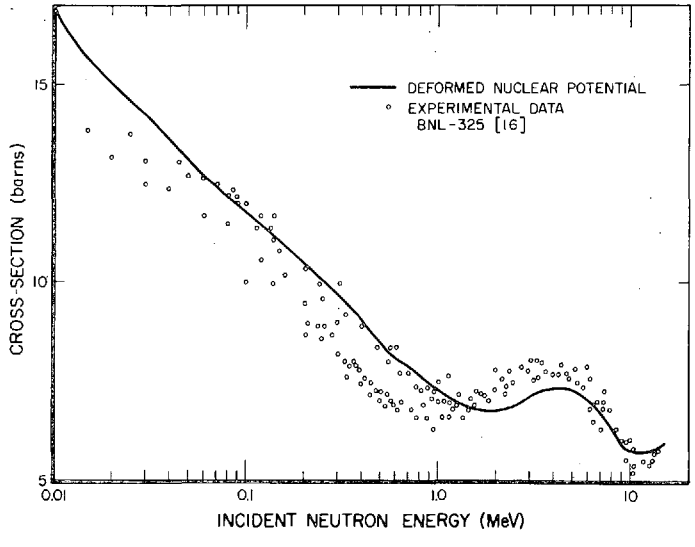

FIG.1. Total cross-section of ^{238}U. Solid line is derived from a deformed nucleus calculation. Open circles represent data from various sources reported in BNL-325 [16].

All other reactions considered rely in part both on an optical model calculation and compound nucleus theory. Figure 2 shows the level structure chosen for the resolved resonances, and is taken from a recent analysis by Barnard.[18] The other unresolved levels in ^{238}U were treated in

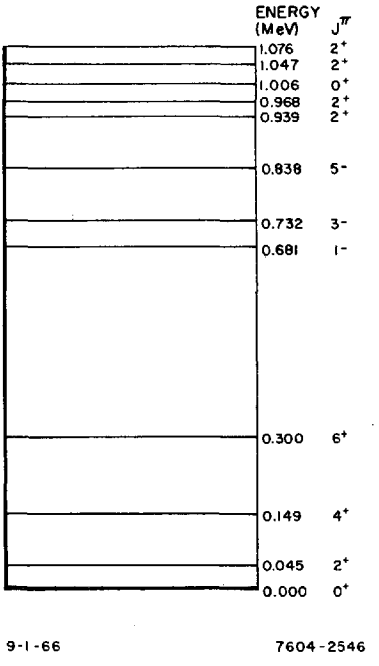

FIG.2. Level structure of ^{238}U from work of Barnard et al.[18]

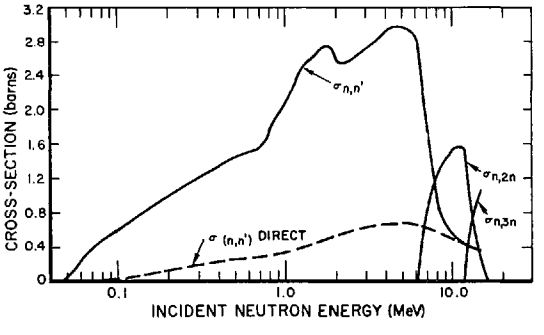

FIG.3. Calculated neutron emission cross-sections for ^{238}U.

a lumped continuum approximation. Up to 1.5 Mev, only discrete level data were calculated; to 3.0 Mev, level data and continuum inelastic scattering were included; above 3.0 Mev, only continuum and direct inelastic scattering were considered. The continuum inelastic scattering was considered as the sources of the (n,2n) and (n,3n) reactions.

Figure 3 shows a composite of all the neutron emission cross sections. The importance of the direct excitation of the 45 Kev level (2+) is clear. In fact, above 10 Mev, this cross section constitutes nearly all of the inelastic cross section.

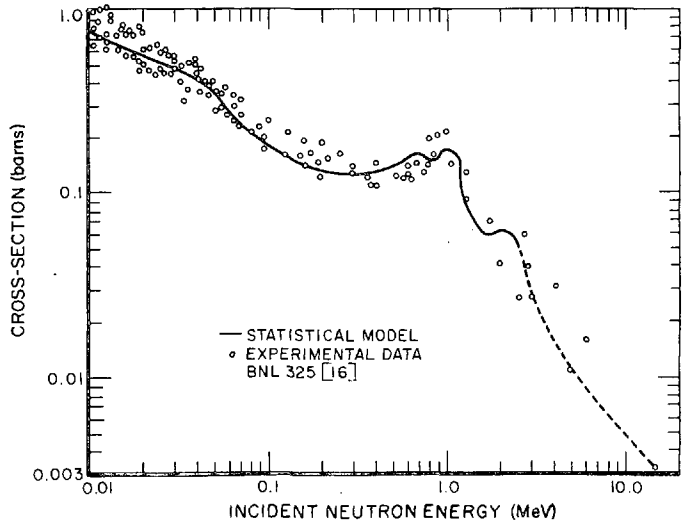

FIG.4. Capture cross-section of ^{238}U. Broken line indicates region in which dipole model is incorrect, and therefore only an estimate was made.

Capture cross-sections were treated with the Weisskopf level density formula and the dipole radiation emission approximation. Additional parameters of the model are the average value of $\langle\Gamma_\gamma/D\rangle_0$, for the measured low energy s-wave resonances and the separation energy of the last neutron of the (A + 1) - nucleon system. Figure 4 compares the model predictions with the data presented in BNL-325. The data lying well above the curve near 10 Kev are the recent data of Macklin and Gibbon.[19] In order to get agreement with those data, either the compound nucleus cross-section or $\langle\Gamma_\gamma/D\rangle_0$ would have to be 50 percent larger.

TABLE II

FISSION MODEL PARAMETERS

Reaction	N	E_o	$\hbar\omega$
n,f	8	1.67	0.105
n,nf	14	6.8	0.50
n,2nf	20	14.3	1.00

The fission cross-section for ^{238}U were treated with the Hill-Wheeler model.[12] The parameters used are shown in Table II. Each fission mode [i.e. (n,f), (n,nf), etc.] could be represented by one fission barrier and associated parameters. The experimental and theoretical fission cross-sections are shown in Fig. 5. The various components are also shown. The values of $\langle\Gamma_n\rangle/\langle\Gamma_\gamma\rangle$ required are smaller than those reported by Vandenbosch and Huisenga.[20] However, this is understandable, since their analysis included the direct inelastic scattering as a part of the compound nucleus cross-section.

Figure 6 illustrates the energy dependence of the average elastic scattering cosine (μ). The experimental points were taken from an analysis of

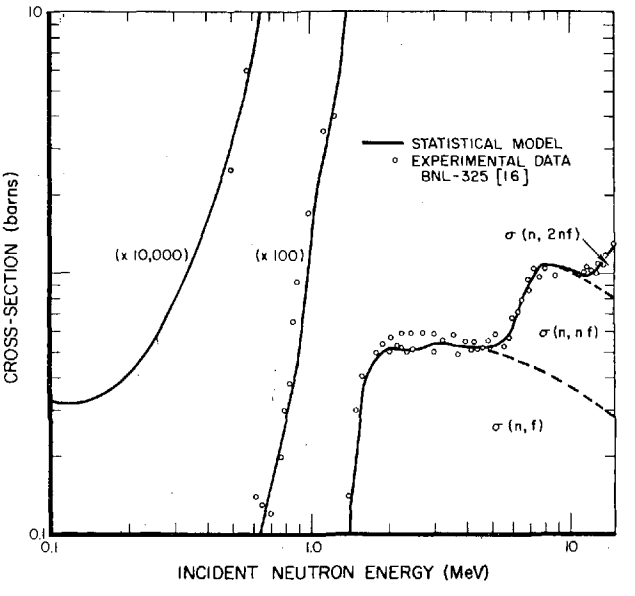

FIG. 5. Fission cross section of ^{238}U.

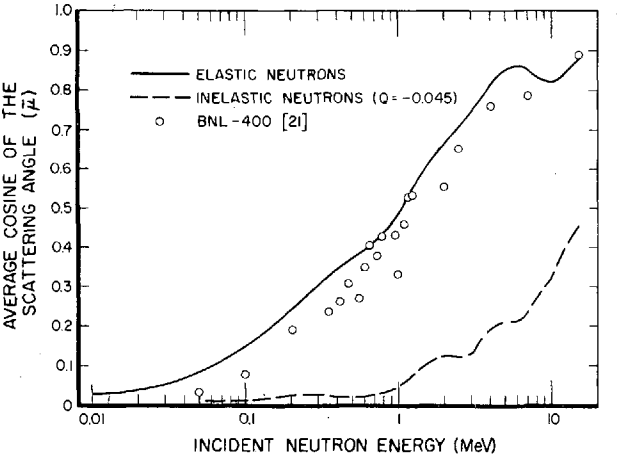

FIG 6. Average cosine of neutrons scattered by ^{238}U.

angular data in BNL-400.[21] In most cases, the values of μ derived from experimental data are smaller than from calculated angular distributions. At energies above 5 Mev, this difference is caused by inelastic neutrons. The discrepancy at lower energies is probably caused by the least-squares fitting techniques used to generate Legendre coefficients from data measured between 30° and 150°.

The average cosine of secondary neutrons from excitation of the 45 Kev level in ^{238}U is nonzero because of the direct interaction contribution to the inelastic scattering.

4. Comparison of Reaction Models

A comparison of the results of calculations using different models and approximations brings out many important problems which should be considered when analyzing experimental data for the heavy nuclei.

An analysis of 15-Mev neutrons scattered by uranium is shown in Fig. 7. Only a deformed nuclear potential will predict a potential inelastic cross-section; a spherical optical model predicts only potential elastic scattering. However, it is clear from Fig. 7 that direct inelastic scattering makes an important contribution to experimentally measured angular distributions. This contribution is most important in the minima of the angular distribution diffraction pattern, where inelastic neutrons are often more numerous than elastic neutrons. The consequence in measured neutron angular distributions for heavy nuclei is the absence of very sharp minima that would be predicted by a spherical optical model.

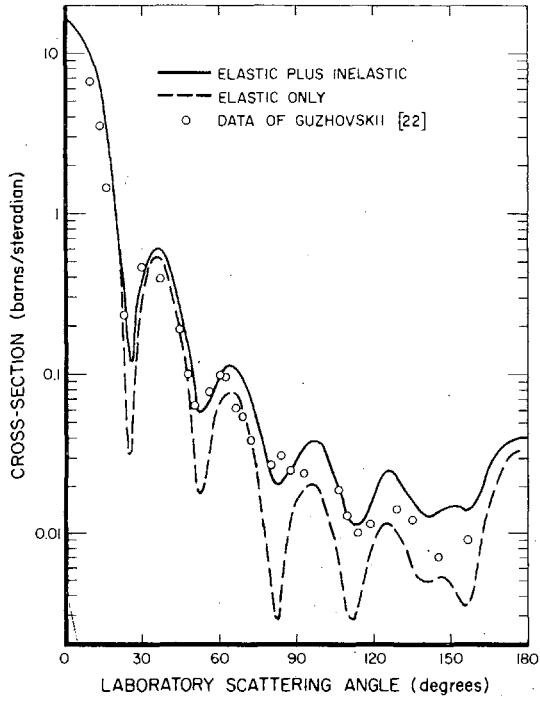

FIG. 7. Angular distribution of 15-Mev neutrons scattered by uranium. Experimental data are those of Gushovskii [22]. The broken line represents contribution of elastic neutrons only, and solid line represents a sum of elastic plus inelastic neutrons scattered after direct excitation of the 45-Kev level of ^{238}U.

The differences between results predicted by a complex and a real quadrupole potential are significant. The complex potential predicts more forward and more backward scattering in the elastic angular distribution. Inelastic angular distributions exhibit similar differences. The complex potential predicts a cross-section about 20 percent larger than the real potential, most of the difference being produced by increased backward scattering. In contrast, a spherical potential predicts no excitation of the 45 Kev level; and any compound nucleus mechanism is negligible at

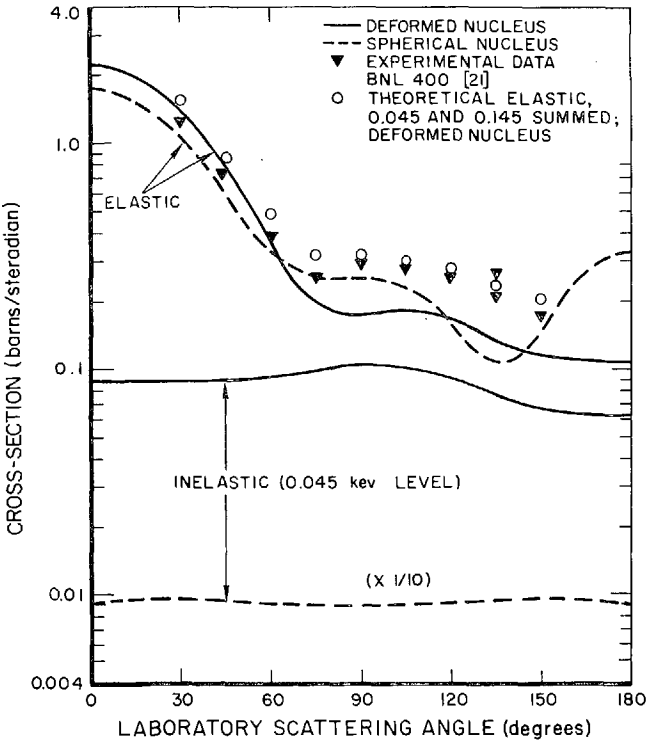

FIG. 8. Scattering of 1-Mev neutrons by uranium. Solid lines represent a deformed nucleus calculation with the compound nucleus contributions added. Broken lines are spherical model calculations. The triangles represent experimental data reported in BNL-400 [21] for scattering of 1-Mev neutrons by uranium. Open circles represent angular distribution predicted by the deformed nucleus model when the elastic and inelastic neutrons have been summed.

higher energies. Therefore, an important and highly anisotropic inelastic cross-section is neglected in a spherical model calculation, and is mistakenly included as a part of the compound nucleus cross-section.

At somewhat lower energies, compound nucleus reactions contribute significantly to both elastic and inelastic cross-sections. Results of two calculations for 1-Mev neutrons are shown in Fig. 8. In both cases, the level width fluctuation corrections have been applied and competition from other neutron, capture, and fission channels included. Neither model gives good agreement with experiment when only elastic neutrons are considered. However, reported experimental angular distributions contain inelastic neutrons from the excitation of at least the first two levels in ^{238}U. The improved agreement between theory and experiment, when this correction was made, is indicative of the significant contribution of inelastic neutrons to measured angular distributions in this energy region.

Similar improvement of the agreement with experimental data for the spherical model is noted when the same corrections are made. However, the spherical model predicts too little forward elastic scattering and too much backward scattering. This difficulty is usually surmounted by "appropriate adjustment" of the spherical model parameters.

The cross-section for excitation of the first level in ^{238}U is dominated by the compound nucleus contribution. The direct excitation cross-section does introduce small but noticeable odd Legendre components to the angular distribution. Such differences are difficult to detect experimentally, but have been noted by Barnard, et al.[18]

Corrections to Hauser-Feshbach (H-F) theory are essential to obtain the correct energy dependence of inelastic excitation functions. The results shown in Fig. 9a and b illustrate the difference between an uncorrected H-F calculation and a calculation in which the level width fluctuation correction has been applied. The elastic scattering cross-section is increased throughout the energy region where compound nucleus reactions are important.

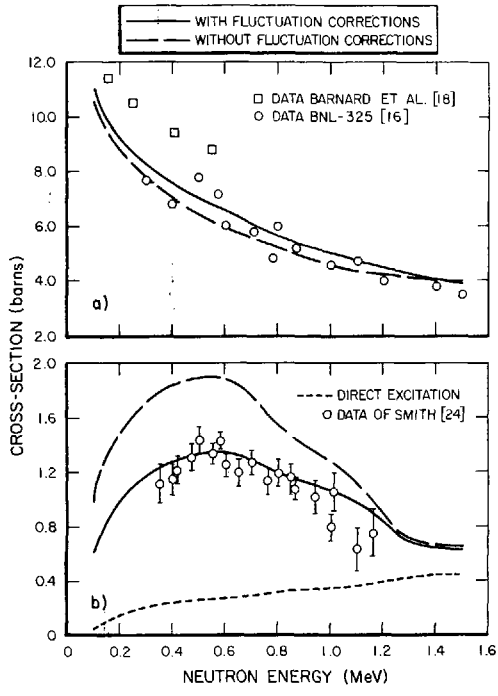

FIG.9. Effects of level width fluctuations on ^{238}U elastic (a) cross-section and inelastic (b) excitation of the 45-Kev level. Solid line includes fluctuation corrections, broken line does not.

The improved agreement between theory and experiment for excitation of the first level (45 Kev) in ^{238}U as a result of application of the corrections is striking. Figure 9b also shows the direct component of the inelastic excitation function. This component ranges from about 20 percent at 0.5 Mev to 50 percent at 1.2 Mev, and to 100 percent at 3 Mev where compound inelastic scattering to the 45-Kev level is negligible.

Similar improvement is noted when the spherical model H-F calculations are corrected for level width fluctuations. Up to energies of 1.2 Mev, there is little difference between spherical and deformed nucleus predictions of the excitation function of the 45 Kev level of ^{238}U. This is true in spite of the fact that the direct inelastic contribution may be as

much as 50 percent of the excitation function. The much larger calculated reaction cross-section for the spherical model (30 to 40 percent) produces this apparent agreement. In general, odd parity penetrabilities are lower and even parity penetrabilities are increased.

In Fig. 10, a comparison of the predicted and measured excitation function for the second excited level (4^+) of ^{238}U is shown. This level is a member of the ground state rotational band. In contrast to the first excited level, the deformed nucleus calculation gives a rather good description of the shape but a poor description of the absolute magnitude of the cross-section.

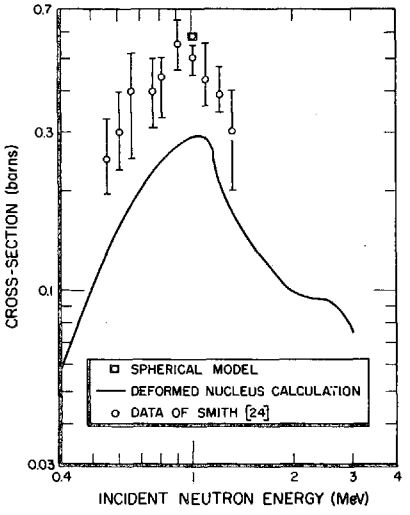

FIG. 10. Inelastic neutron excitation of the 149-Kev level in ^{238}U.

One calculated spherical model point shows rather good agreement with the measured value. Such a discrepancy also exists for the analysis of the 6^+ member of the ground state band. This discrepancy occurs because the penetrabilities for these higher levels are calculated with a spherical model whereas the penetrabilities for the incoming channels are calculated with a deformed potential. It is the $(7/2)^-$ incoming channel which contributes most to the excitation of this 4^+ level. The deformed potential reduces the probability of formation of a compound nucleus with odd parity, and hence the reduction of the 4^+ level excitation function. The reduction of the compound nucleus cross-section for excitation of the first excited level in the ground-state rotational band, which occurs when the deformed nucleus calculation is made, is compensated by the direct excitation of the 2^+ level. By analogy, one would expect that the direct scattering from the 4^+ level should be about 0.26b at 1 Mev, or nearly 50 percent of the total excitation function at that energy.

Calculations at 10 Kev have been made to determine strength functions for ^{238}U. The two s-wave calculations bracket the measured value of approximately 1.0×10^{-4}. However, the deformed nucleus calculation for the p-wave strength function is in better agreement with the experimental value of 1.7×10^{-4}.

5. Conclusion

The analysis of ^{238}U described in this paper and similar analyses of ^{238}Pu, ^{242}Pu, and ^{244}Cm have demonstrated the utility of using a comprehensive scheme of nuclear theory to assist in evaluating neutron cross-sections and preparing data libraries. It has been shown that the most sophisticated models must be used in such an analysis.

Most previous analyses of neutron inelastic scattering have neglected the important low energy level width fluctuation corrections. The optical model parameters obtained from such analyses are strongly dependent on energy as well as target nucleus, thereby restricting the model's utility as an interpolative or extrapolative tool. In the present case, both restrictions have been effectively removed by using a more detailed model, instead of relying on parameter adjustment in a simpler model.

The importance of including the deformed characteristic of the heavy even-even nuclei has been demonstrated. Observed anisotropy of the secondary inelastic neutrons scattered from the 45 Kev level [18] has been predicted, and a method for correcting measured angular distributions for inelastic neutrons has been shown. Strong coupling of the remaining members of the ground state rotational band is evidenced by the discrepancy between experimental data and values of the excitation function for the 0.145 Kev 4^+ level obtained in this analysis.

Finally, the theoretical calculations serve as a guide to an evaluator when several sets of conflicting experimental data exist. Present calculations tend to agree with the lower measured values of the ^{238}U capture cross-section around 10 Kev, and support higher values of the total cross-section below 1 Mev. Nuclear theory thus provides another useful tool to aid in cross-section evaluation.

REFERENCES

[1] SLAGGIE, E. L., REYNOLDS, J. T., USAEC Rep. KAPL-M-6452 (1965).

[2] PRESTON, M. A., Collective nuclear motion, Ch. 10, Physics of the Nucleus, Addison-Wesley, Reading (1962).

[3] CHASE, D. M. WILLITS, L., EDMONDS, A. R., Rotational-optical model for scattering of neutrons, Phys. Rev. 110 (1958) 1080.

[4] BUCK, B., Calculation of elastic and inelastic proton scattering with a generalized optical model, Phys. Rev. 130 (1963) 712.

[5] BALDONI, B., SARUIS, A. M., A rotational-optical model analysis of fast-neutron scattering by ^{238}U nucleus, Nuovo Cim. 33 (1964) 1145.

[6] DUNFORD, C. L., Neutron scattering from non-spherical nuclei, thesis, Massachusetts Institute of Technology, 1964 (unpublished).

[7] HAUSER, W., FESHBACH, H., The inelastic scattering of neutrons, Phys. Rev. 87 (1952) 366.

[8] WOLFENSTEIN, L., Conservation of angular momentum in the statistical theory of nuclear reactions, Phys. Rev. 82 (1951) 690.

[9] LANE, A. M., LYNN, J. E., Fast neutron capture below 1 Mev: the cross sections for ^{238}U and ^{232}Th, Proc. Phys. Soc. A70 (1957) 557.

[10] MOLDAUER, P. A., Average compound-nucleus cross sections, Rev. Mod. Phys. 36 4 (1964) 1079.

[11] MOLDAUER, P. A., ENGLEBRECHT, C. A., DUFFY, C. J., USAEC Rep. ANL-6978 (1964).

[12] HILL, D. L., WHEELER, J. A., Nuclear constitution and interpretation of fission phenomena, Phys. Rev. 89 (1953) 1102.

[13] PEARLSTEIN, S., USAEC Rep. BNL 897 (1964).
[14] STELSON, P. H., GRODZINS, L., Nuclear transition probability, B(E2) for 0^+_{gs} 2^+_{first} transitions and deformation parameter, β_2, Nuclear Data 1 1 (1965) 21.
[15] TAMURA, T., Analysis of the scattering of particles by collective nuclei in terms of the coupled-channel calculation, Rev. Mod. Phys 37 4 (1964) 679.
[16] STEHN, J. R. et al., USAEC Rep. BNL-325, Vol. III (1965).
[17] SETH, K. K., private communication (1964).
[18] BARNARD, E., FERGUSON, A. T. G., McMURRAY, W. R., VAN HEERDEN, I. J., Scattering of fast neutrons by ^{238}U, Nucl. Phys. 80 (1966) 46.
[19] MACKLIN, R. L., GIBBONS, J. H., private communication (1964).
[20] VANDENBOSCH, R., HUISENGA, J. R., Proc. 2nd UN Int. Conf. PUAE 15 (1958) 284.
[21] GOLDBERG, M. D., MAY, W. M., STEHN, J. R., USAEC Rep. BNL-400, Vol. II, (1962).
[22] GUZHOVSKII, B. YA., The elastic scattering of neutrons with an energy of 15 Mev by nuclei of copper, lead, and ^{238}U, Atomnaya Energiya 11 (1961) 395.
[23] WALT, M., BEYSTER, J. R., USAEC Rep. LA-2061 (1956).
[24] SMITH, A. B., Scattering of fast neutrons from natural uranium, Nucl. Phys. 47 (1963) 633.

DISCUSSION

D. WILMORE: I would like to make a comment on the competition between fission and inelastic neutron scattering. I have investigated this for the case of ^{240}Pu. At about 1 MeV, I find that wide variations in the distribution of fission cross-section amongst the different compound spins have only a slight effect on the inelastic neutron cross-section for states of low spin. However, the cross-section for the state of spin 4 is changed by about 40%.

C. L. DUNFORD: My calculation was performed on the assumption that the fission width is independent of compound nucleus spin. What you say may account for the discrepancy between my calculations and experimental data for the 145-keV level.

A. T. G. FERGUSON: I am glad that Dr. Dunford has drawn our attention to the substantial cross-section calculated for direct excitation of the rotational levels in rotational nuclei. Unfortunately, present techniques have insufficient resolution to show these effects experimentally. The cross-section he calculates considering only the 2^+ level would be shared with the 4^+ level.

J. J. SCHMIDT: I am rather surprised that above 1.2 MeV you get such a large direct contribution to the excitation cross-section of the 45-keV level. Did you take into account the coupling of this state with the higher levels of the ground-state rotational band? If so, I would expect a smaller direct contribution than that you mention.

C. L. DUNFORD: The calculations did not include coupling with the higher levels of the ground-state rotational band.

F. H. BÜHLER: We have made coupled channel calculations and find that the inelastic cross-section to the first excited level is lowered about 20% if we include the 4^+ rotational level.

A. T. G. FERGUSON: In reply to Dr. Bühler's comment I should like to say that one would expect this, since direct excitation of the 4^+ level will be predominantly a two-step process, i.e. it goes $0^+ \rightarrow 2^+ \rightarrow 4^+$. Thus the $2^+ \rightarrow 4^+$ process depopulates the 2^+ level. Direct $0^+ \rightarrow 4^+$ is probably negligible.

ELASTIC AND INELASTIC NEUTRON CROSS-SECTIONS

D. WILMORE
ATOMIC ENERGY RESEARCH ESTABLISHMENT,
HARWELL, DIDCOT, BERKS,
UNITED KINGDOM

Abstract

ELASTIC AND INELASTIC NEUTRON CROSS-SECTIONS. Computer programmes have been developed for the calculation of elastic and inelastic scattering of particles from nuclei. These programmes are written in the S2 dialect of FORTRAN, and run on an IBM-7030 computer.

One programme calculates the shape elastic cross-section, the total cross-section and the absorption cross-section according to the optical model. The time taken in performing an optical calculation depends mainly upon the efficiency of the method used to perform the integration of the radial Schrödinger equation. A method is used which takes advantage of the absence of the first derivative term, and this gives a great improvement over more general methods. A least-squares fitting procedure is used which enables any number of parameters to be varied. The number of optical model calculations which are needed for a least-squares fit is less than with usual methods.

Another programme will calculate compound nucleus reactions according to the Hauser-Feshbach theory, with or without the fluctuation correction. This programme will accept target and projectiles of any spin and parity, so that deuteron and alpha channels, as well as nucleon channels, may be taken into account.

A third programme enables least-squares fits of elastic scattering to be done by taking into account the compound elastic contribution as calculated by the Hauser-Feshbach theory.

The use of these programmes is illustrated by the analysis of the inelastic scattering of neutrons from ^{238}U. The elastic scattering cross-sections were used to obtain optical potentials by a least-squares fitting method. These potentials were subsequently used to predict the inelastic cross-sections to a large number of excited states. The results using the fluctuation correction are in good agreement with experiment.

A further example of their use is shown in the analysis of neutron and proton scattering from light nuclei. Proton cross-sections were analysed to obtain potentials which were then used to calculate neutron cross-sections. The results are in reasonable agreement with experiment when it is considered that this is a region of the periodic table where the optical model is not particularly good.

A NOVEL METHOD FOR VERY HIGH RESOLUTION CROSS-SECTION MEASUREMENTS

S. CIERJACKS, P. FORTI, D. KOPSCH, L. KROPP AND H. UNSELD
INSTITUT FÜR ANGEWANDTE KERNPHYSIK,
KERNFORSCHUNGSZENTRUM KARLSRUHE,
FEDERAL REPUBLIC OF GERMANY

Abstract

A NOVEL METHOD FOR VERY HIGH RESOLUTION CROSS-SECTION MEASUREMENTS. A neutron time-of-flight spectrometer has been put into operation with the Karlsruhe isochronous-cyclotron as a very intense pulsed neutron source. The very high recurrence frequency of the micro-structure bunches from the cyclotron was reduced using a novel "bunching-deflection" system to avoid frame overlap problems while largely preserving the high average neutron intensity available from the internal beam. The performance data of the spectrometer are as follows: flight path 57 m, neutron pulse length 1 ± 0.3 ns full width at half maximum, integrated time-averaged neutron flux ($0.2 \leq E_n \leq 50$ MeV) $\phi = (5 \pm 2) \times 10^4$ n/cm^2 s at 57 m, while using a thick natural uranium target and deuterons of (45 ± 5) MeV.

With the present flight path a maximum resolution of 0.02 ns/m has been determined for the spectrometer. The time-of-flight apparatus and the first total cross-section measurements for some light- and medium-weight nuclei in the energy region between 0.5 and 10 MeV are presented.

A NEW METHOD FOR THE MEASUREMENT OF NEUTRON CROSS-SECTIONS

M.J. OHANIAN, R.B. PEREZ AND R.E. UHRIG
UNIVERSITY OF FLORIDA,
GAINESVILLE, FLORIDA,
UNITED STATES OF AMERICA

Abstract

A NEW METHOD FOR THE MEASUREMENT OF NEUTRON CROSS-SECTIONS. A new technique for the measurement of elastic and inelastic differential neutron cross-sections, based on pseudo-random pulsing techniques and statistical correlation methods, is described. The method allows an increase in energy resolution without a reduction in the signal-to-noise ratio because of the inherent 50% duty cycle of the input signal and the ability to reduce the effects of detector and other extraneous noise signals by cross-correlation. The improvement in signal-to-noise ratio and energy resolution that may be achieved over conventional time-of-flight methods is also shown.

INTRODUCTION

In this paper a new method for the measurement of elastic and inelastic differential neutron cross-sections is described. The proposed method is based on pseudo-random pulsing and statistical correlation techniques and should be of particular interest for cross-section measurements in the 0.5-10 MeV region where there is significant need for such data [1]. The method is akin to the noise analysis techniques [2] used in the determination of nuclear reactor system characteristics in both the critical and subcritical states. It falls in the category of experiments in which an external random disturbance is applied to the system under study.

The advantage of this method over conventional time-of-flight techniques is that it allows an increase in energy resolution without a decrease in signal-to-noise ratio for a given instrumentation and accelerator configuration. This advantage is inherent in the pseudo-random pulsing technique on the one hand and the correlation methods on the other: the neutron beam is modulated at a 50% duty cycle thus considerably increasing the beam intensity in comparison to conventional pulsing methods and the correlation procedure eliminates the effects of detector noise or other extraneous noise signals.

PRINCIPLE OF THE METHOD

To describe the principle of the method it is assumed that the sample whose differential scattering cross-section is to be measured may be

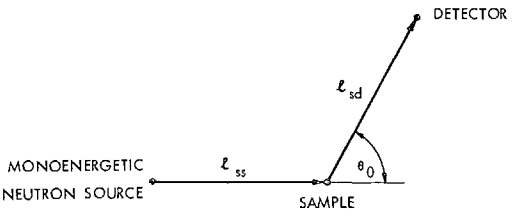

FIG.1. Point geometry representation of the experiment.
ℓ_{ss} = source-to-sample flight path
ℓ_{sd} = sample-to-detector flight path

approximated as a point sample. A similar assumption is made for the detector. The geometry of the experiment is shown in Fig.1. Let

i(t) = monoenergetic neutron current emitted by the source at time t. The time dependence of these neutrons will be given by a stationary "white noise" type signal.

$\sigma(E_0, E, \mu_0)$ = differential scattering cross-section of sample ($\mu_0 = \cos\theta_0$)

With regard to Fig.1, the number of neutrons with energies dE about E absorbed per unit volume of the detector at time t may be written as

$$0_d(E_0, E, \mu_0, t)dE = \epsilon_d(E)\sigma(E_0, E, \mu_0)i(t-\lambda_{ss}-\lambda_{sd})dE \tag{1}$$

where $\epsilon_d(E)$ is the detector efficiency and λ_{ss} and λ_{sd} are the flight times (i.e. $\lambda = \ell/\sqrt{2E/m}$). Since the detector will be sensitive to neutrons of different energies over a certain characteristic range the total response will be given by

$$0_d(E_0, \mu_0, t) = \int_0^\infty \epsilon_d(E)\sigma(E_0, E, \mu_0)i(t-\lambda_{ss}-\lambda_{sd})dE \tag{2}$$

Now a cross-correlation is performed between the "white noise" input signal and the detector response, Eq.(2)

$$\phi_{i0}(E_0, \mu_0, \tau) = \lim_{T\to\infty} \frac{1}{2T}\int_{-T}^{T} i(t)0_d(E_0, \mu_0, t+\tau)dt \tag{3}$$

The result, after reversing the order of integration, is

$$\phi_{i0}(E_0, \mu_0, \tau) = \int_0^\infty \epsilon_d(E)\sigma(E_0, E, \mu_0)\phi_{ii}(\tau-\lambda_{ss}(E_0)-\lambda_{sd}(E))dE \tag{4}$$

where ϕ_{ii} is the autocorrelation function of the input signal. It is convenient to change from the E to the λ_{sd} variable

$$\phi_{io}(E_0, \mu_0, \tau) = \int_0^\infty \epsilon_d(\lambda_{sd})\sigma(E_0, \lambda_{sd}, \mu_0)\phi_{ii}(\tau - \lambda_{ss}(E_0) - \lambda_{sd})d\lambda_{sd} \tag{5}$$

Since the input signal was assumed to have the characteristics of "white noise" its autocorrelation function

$$\phi_{ii}(\tau - \lambda_{ss} - \lambda_{sd}) = \delta(\tau - \lambda_{ss} - \lambda_{sd}) \tag{6}$$

and therefore

$$\phi_{io}(E_0, \mu_0, \tau) = \epsilon_d(\tau - \lambda_{ss})\sigma(E_0, (\tau - \lambda_{ss}), \mu_0) \tag{7}$$

or

$$\sigma(E_0, \tau, \mu_0) = \frac{\phi_{io}(E_0, \mu_0, \tau)}{\epsilon_d(\tau)} \quad \tau \geqslant \lambda_{ss} \tag{8}$$

since for a given initial energy λ_{ss} is constant.

Thus the differential scattering cross-section may be obtained by taking the cross-correlation of the input signal i(t) with the detector response, dividing by the corresponding detector efficiency and introducing the appropriate Jacobian for the transformation to the energy variable $\left(\text{viz. } \left|\frac{d\tau}{dE}\right| = \tau^3/m\ell_{sd}^2\right)$.

In practice it is not possible to obtain a "white noise" type signal, since this implies infinite power. Instead a class of signals known as discrete, binary pseudo-random signals [3] are used. This type of signal closely approximates the characteristics of "white noise" in that its autocorrelation function approximates a delta function. These signals are periodic but are random within a period. The corresponding autocorrelation function has the same periodicity as the input signal. In general the length of the period P is given by

$$(2^N - 1)\Delta t \tag{9}$$

if the signal is generated by a maximum length binary shift register sequence. N is the number of stages of the shift register and Δt corresponds to the reciprocal of the frequency at which the shift register is being driven. A 4-stage shift register sequence and its autocorrelation function are shown in Fig. 2. It should be noted that due to the nature of this type of signal the input autocorrelation function has constant sidebands of magnitude $-1/(2^N - 1)$ when the function is normalized to unity at its peak value. For the sequences used in practice (i.e. $N \geqslant 7$) these sidebands are of small amplitude and corrections may be applied in a straightforward manner.

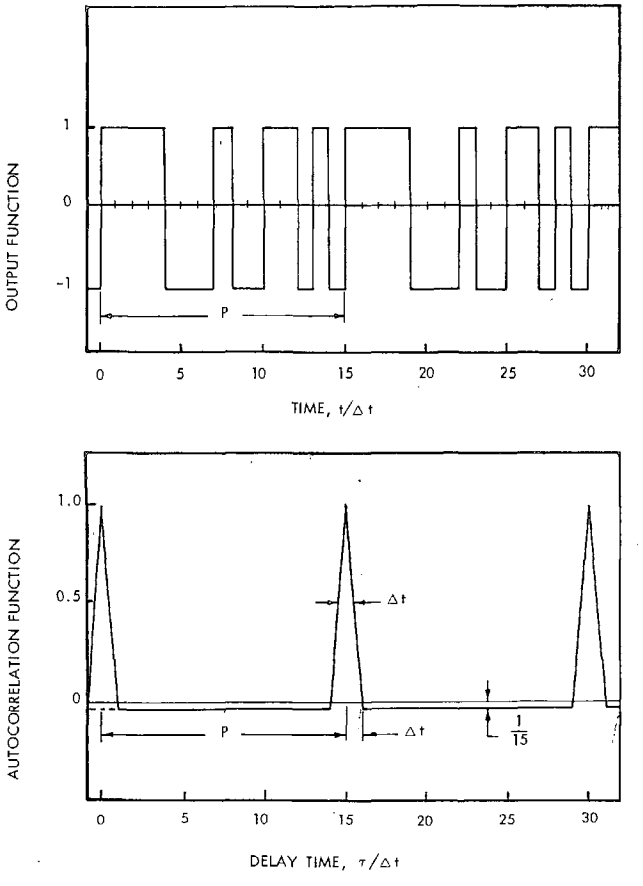

FIG.2. A typical maximum length pseudo-random sequence (N=4) and its autocorrelation function.

When the neutron source is modulated with this signal Eq.(8) is not exact, and the time (and therefore energy) resolution of an experiment is dictated by the width of the autocorrelation function of the input. The latter point is easily seen by considering the measurement of the elastic scattering cross-section. Since in this case

$$\sigma(E_0, \lambda_{sd}, \mu_0) = \sigma(E_0, \mu_0)\delta(\mu_0 - f(E_0, \lambda_{sd})) \tag{10}$$

Eq. (5) becomes

$$\phi_{i0}(E_0, \mu_0, \tau) = \epsilon_d(\lambda_{sd})\sigma(E_0, \mu_0)\phi_{ii}(\tau - \lambda_{ss}(E_0) - \lambda_{sd}(E_0, \mu_0)) \tag{11}$$

Thus, the sharper the input autocorrelation function, the better will the cross-correlation function represent the elastic scattering cross-section.

The fact that the best time resolution attainable by this method is Δt imposes a severe technological problem if one has to build a very fast

pseudo-random signal generator to drive a high voltage supply capable of switching an ion beam at the accelerator terminal. The best that can be achieved yields Δt = 50 ns with 0.6-mA beam current [4]. It is, however, feasible to obtain Δt's of the order of a few nanoseconds by the following scheme:

The accelerator is operated in the steady state and the ion beam is swept, in a circular fashion, over a mask which has, around its perimeter, a set of slits with apertures and spacings located in the desired pseudo-random pattern. The neutron target is placed close to the mask so that the resulting neutron beam is generated with a pseudo-random time dependence. The circular motion of the ion beam can be obtained by means of two sets of deflection plates driven by a high voltage power supply with high frequency sinusoidal modulation. The design parameters obtained for a pseudo-random sequence with N = 7 are given in Table I [5]. It should be noted that this method of generating the pseudo-random modulation of the neutron beam allows for repetitive pulsing in a very simple way.

TABLE I. DESIGN PARAMETERS FOR PSEUDO-RANDOM SIGNAL GENERATOR (N = 7)

Plate separation = 1.5 in	Operating voltage = 21 kV
Plate length = 12 in	Sweep frequency =
Drift length = 90 in	1.58 MHz (Δt = 5 ns)
Deflection radius = 2 in	7.88 MHz (Δt = 1 ns)
	Slit width/Δt at deflection radius = 0.1 in

Since the input signal being used is periodic, it is necessary to ensure that the period P be longer than the flight time of the neutrons of interest. For example, a 1-MeV neutron will traverse a 1-m flight path in 72.3 ns. If a pseudo-random input signal with N = 7 is used, P = 127 Δt; i.e. for Δt = 2 ns, P = 254 ns, which is sufficiently longer than the flight time. In general the requirement on the period may be expressed by

$$\Delta t \ll \ell/\sqrt{2E/m} < P \tag{12}$$

COMPARISON WITH CONVENTIONAL TIME-OF-FLIGHT METHODS

The index of comparison for the two methods will be taken as the signal-to-noise ratio (S). In each case the parameters are distinguished by the subscripts pr (pseudo-random) and tf (time-of-flight). If it is assumed that the signal-to-noise ratio for the raw data from the pseudo-random method is the same as that from the conventional time-of-flight method one has

$$S_{pr}/S_{tf} = \eta(\ell_{tf}/\ell_{pr})^2 (I_{pr}/I_{tf})(d_{pr}/d_{tf}) \tag{13}$$

where η = improvement in signal-to-noise ratio due to cross-correlation process
ℓ = flight path
I = peak current
d = duty cycle

For neutrons of a given energy

$$\ell_{tf}/\ell_{pr} = (\Delta E_{pr}/\Delta E_{tf})(\Delta t_{tf}/\Delta t_{pr}) \tag{14}$$

so that Eq.(13) may also be written as

$$S_{pr}/S_{tf} = \eta(\Delta E_{pr}/\Delta E_{tf})^2 (\Delta t_{tf}/\Delta t_{pr})^2 (I_{pr}/I_{tf})(d_{pr}/d_{tf}) \tag{15}$$

For purposes of illustration and comparison the following rather optimum operating characteristics of a Van de Graaff accelerator with a nanosecond pulsing capability are chosen

I_{tf} = 5 mA
d_{tf} = 1.0% (2 ns pulse width and 5 MHz repetition rate)

These parameters are those expected for the 4-MeV University of Florida machine with klystron bunching. The corresponding parameters in the pseudo-random pulsing mode are

$$I_{pr} = 0.4 \text{ mA}$$
$$d_{pr} = 50\%$$

The beam current is the maximum at steady state and the 50% duty cycle is intrinsic to the method. With these parameters Eq.(15) becomes

$$S_{pr}/S_{tf} = 4\eta(\Delta E_{pr}/\Delta E_{tf})^2 (\Delta t_{tf}/\Delta t_{pr})^2 \tag{16}$$

A value of $\eta = 10$ is reasonable [6]. In Table II the signal-to-noise ratios, as well as the energy resolution and length of flight paths are compared for three representative values of Δt_{pr}. The value of Δt_{tf} was fixed at 2 ns. It should be noted that in making these comparisons the time uncertainties due to the instrumentation were not considered since these would be the same in both cases.

CONCLUDING REMARKS

This initial study of the application of pseudo-random pulsing and cross-correlation techniques to the measurement of differential neutron scattering cross-sections shows it to be a promising method. It seems well suited for use with a Van de Graaff accelerator and eliminates the need for a terminal pulsing system. There are, however, two main problems in the experimental implementation of the method. The first is related to the generation of the pseudo-random modulation and the second to

TABLE II. COMPARISON OF METHODS

Δt_{pr} (ns)	S_{pr}/S_{tf}	$\Delta E_{pr}/\Delta E_{tf}$	ℓ_{pr}/ℓ_{tf}
4	10	1	2
4	2.5	0.5	4
2	40	1	1
2	10	0.5	2
2	2.5	0.25	4
1	160	1	0.5
1	40	0.5	1
1	10	0.25	2

the instrumentation and in particular the availability of a fast time analysis system. The feasibility study of the first problem shows that the pseudo-random modulation with $\Delta t \approx 1$-5 ns is relatively easy to accomplish. The difficulties with the instrumentation are more significant; however the present availability of time-of-flight units with 1-10 ns channel width is encouraging [7].

REFERENCES

[1] Reactor Physics Efforts Required in Support of the Fast Breeder Development Program, USAEC Rep. WASH-1066 (1966).

[2] Symposium on Neutron Noise, Waves and Pulse Propagation, University of Florida, in press as USAEC - TID document (1966).

[3] PETERSON, W.W., Error Correcting Codes, John Wiley & Sons, New York (1961).

[4] SCHLOFKE, D., Private communication, Oak Ridge Technical Enterprises, Corp. (1966).

[5] SWANDER, J.E., Private communication, University of Florida (1966).

[6] BALCOMB, J.D., "Crosscorrelation method of measuring system dynamic response" Noise Analysis in Nuclear Systems (Uhrig, R.E., Ed.) TID-7679 (1964) 183.

[7] TOBACK, P., Private communication, Packard Instruments Corp. (1966).

DISCUSSION

K. H. BECKURTS (Chairman): I think it is gratifying to see that reactor physicists are now teaching new techniques to nuclear physicists after a long period during which nuclear physicists were teaching reactor physicists. I have only one immediate comment. One normally uses these cross-correlation techniques to study phenomena which are very smoothly time-dependent, i.e. relaxation effects in reactors, etc. In the cross-section case, however, you will have very strongly fluctuating effects, especially if you apply the technique to the resonance region.

Are you not afraid that you might have great difficulties in unscrambling the time spectra in these cases?

M. J. OHANIAN: Initially, we plan to apply the method in the region above resonances. However, even when strong fluctuations exist, it should be possible to unscramble the time spectra since the time resolution obtainable is at least as good as for the conventional time-of-flight method. Of course, we will need experimental confirmation of this.

R. E. UHRIG: In connection with the remarks made by Dr. Beckurts I should like to say that resolving resonances calls for the use of very small time increments (shift times) for the shift register, which generates the pseudo-random sequence. We have solved the electronic problems in generating the pseudo-random sequence. However, we must now get the neutron generating target to produce a pseudo-random variation of neutron intensity. The principal problem is to develop such a target.

L. N. USACHEV: I should like to comment that a similar proposal for using a pseudo-random function in neutron spectrometry was made by A. I. Mogilner, O. A. Salnikov and L. A. Timokhin. Details were published in Prib. Teh. Eksp. 2 (1966) 22-27.

CHAIRMAN'S SUMMARY

K. H. BECKURTS: In summarizing Session VI, I believe I can say that great progress has been reported in regard to fast-neutron scattering. For the first time, inelastic scattering data on fissile nuclei have been presented at an international conference. For non-fissile nuclei, data now exist over a very wide range of energies and mass numbers. The optical model and the Hauser-Feshbach theory enable us to calculate and interpret these data with surprising accuracy. However, these theories become very sophisticated and such subtle effects as, for instance, width fluctuations must be taken into account. A new aspect is the study of intermediate structure effects in inelastic excitation functions, and although these may not be important for reactor design purposes, they are certainly of great interest from the point of view of our understanding of nuclear reactions.

Session VII

NEUTRON RADIATIVE CAPTURE

ИЗМЕРЕНИЕ СЕЧЕНИЙ ПОГЛОЩЕНИЯ НЕЙТРОНОВ С ЭНЕРГИЕЙ 24 КЭВ В СФЕРИЧЕСКОЙ ГЕОМЕТРИИ

Т.С.БЕЛАНОВА, А.А.ВАНЬКОВ, Ф.Ф.МИХАЙЛУС, Ю.Я.СТАВИССКИЙ
(Доклад представил А.И.Абрамов)
ФИЗИКО-ЭНЕРГЕТИЧЕСКИЙ ИНСТИТУТ, ОБНИНСК СССР

Abstract — Аннотация

MEASUREMENT OF ABSORPTION CROSS-SECTIONS FOR NEUTRONS WITH A MEAN ENERGY OF 24 keV BY TRANSMISSION IN A SPHERICAL GEOMETRY. The paper describes the measurement of fast-neutron absorption cross-sections σ_a, by the method of transmission in a spherical geometry. The authors report the results of experiments for neutrons from a Sb-Be source with a mean energy of 24 keV for the following elements: Cr, Ni, Cu, Zn, Sr, Zr, Nb, Mo, Ag, Cd, In, Sn, Sb, W, Au, Hg, Pb, Bi, Th, ^{238}U, ^{235}U, ^{239}Pu. In the case of fissionable isotopes the sum of the fission and radiative capture cross-sections $\sigma_f + \sigma_r$ was measured. As neutron detectors the authors used a counter of independent length and a system comprising a water tank and fission chambers for recording thermal neutrons. To investigate the effect of the resonance blocking of fast neutrons they used samples of absorbent material diluted with a lead-bismuth alloy as scatterer; the thickness of the samples was also varied.

The experimental data were processed on the basis of a calculation of transmissions which was carried out by the Monte Carlo method on a computer. Partial results of the calculation are presented in tables of various coefficients, in a form suitable for interpolation. The possibilities and limitations of the spherical transmission method are discussed from the point of view of obtaining absolute values for absorption cross-sections.

ИЗМЕРЕНИЕ СЕЧЕНИЙ ПОГЛОЩЕНИЯ НЕЙТРОНОВ С ЭНЕРГИЕЙ 24 кэв В СФЕРИЧЕСКОЙ ГЕОМЕТРИИ. Работа посвящена измерению сечений поглощения σ_a быстрых нейтронов методом пропускания в сферической геометрии. Приведены результаты эксперимента для нейтронов Sb – Be источника со средней энергией 24 кэв для следующих элементов: Cr, Ni, Cu, Zn, Sr, Zr, Nb, Mo, Ag, Cd, In, Sn, Sb, W, Au, Hg, Pb, Bi, Th, U^{238}, U^{235}, Pu^{239}. В случае делящихся изотопов измерялась сумма сечений деления и радиационного эахвата $\sigma_f + \sigma_\gamma$. В качестве детекторов нейтронов служили независимо длинный счетчик и система водяного бака с камерами деления, регистрирующими тепловые нейтроны. С целью исследования влияния резонансной блокировки быстрых нейтронов использовались образцы поглотителей, разбавленных свинцово-висмутовым сплавом в качестве рассеивателя, а также варьировались толщины образцов.

Обработка экспериментальных данных проводилась на основе расчета пропусканий, выполненного методом Монте-Карло на электронно-вычислительной машине. Частичные результаты расчета представлены в таблицах некоторых коэффициентов в виде, пригодном для интерполирования. Обсуждаются возможности и ограничения метода сферического пропускания с точки зрения получения абсолютных сечений поглощения.

Систематическое расхождение сечений поглощения, измеренных различными методами (например, методами активации и регистрации γ-лучей захвата), сказывается на точности существующей системы ядерно-физических констант. Весьма вероятно, что это расхождение обусловлено различием в способах абсолютной калибровки сечений. С этой точки зрения измерения сечений поглощения в сферической геометрии [1 – 3] представляют большой интерес, так как получаемые результаты являются абсолютными.

МЕТОДИКА ЭКСПЕРИМЕНТА

Измерения проводились в прямой сферической геометрии с Sb – Be нейтронным источником $\bar{E}_n = 24$ кэв диаметром 30 мм, толщиной бериллиевой оболочки 2 – 4 мм и интенсивностью примерно 10^8 нейтр/сек. В качестве нейтронных детекторов использовались независимо система "длинных" счетчиков и система водяного бака с набором миниатюрных камер деления, содержащих слои урана-235. В баке имелась сферическая полость диаметром 1 м, в центре которой помещался источник, окружавшийся образцом в виде сферического слоя. Относительное изменение скорости счета из-за поглощения нейтронов в образце измерялось как отношение интегралов от распределения тепловых нейтронов в воде по сферическим слоям. Преимущество системы водяного бака по сравнению с длинным счетчиком заключается в отсутствии таких эффектов, как энергетическая зависимость эффективности в области 10 – 30 кэв; и чувствительность к угловому распределению падающего потока нейтронов. Однако в измерениях с водяным баком необходимо учитывать эффект поглощения тепловых нейтронов в образце. Этот эффект рассчитывался на основании результатов дополнительных экспериментов. Благодаря большому размеру полости в баке соответствующая поправка была небольшой. В случае длинных счетчиков контрольные измерения с рассеивающими сферами из графита и висмута позволили определить оптимальные условия эксперимента, при которых поправка на угловую и энергетическую чувствительность детектора сравнима с ошибками измерений.

Особое внимание в эксперименте было уделено исследованию эффекта резонансной блокировки быстрых нейтронов в образце. Метод заключался в варьировании толщины образцов и разбавлении исследуемого материала рассеивателем, сечение которого характеризуется слабо выраженной резонансной структурой в пределах действующего спектра нейтронов. В качестве разбавителя использовался свинцово-висмутовый сплав с объемной концентрацией в образце ~70%. Таким образом, сечения поглощения для большинства элементов были получены в результате измерения двумя независимыми регистрирующими установками пропусканий нейтронов через образцы различных толщин и различных концентраций исследуемого элемента. Пример измерений с различными образцами приведен в табл.1. Эксперимент показал, что величина эффекта резонансной блокировки не превышает ошибок измерений.

ОБРАБОТКА РЕЗУЛЬТАТОВ

При обработке экспериментальных результатов были учтены в виде поправок следующие эффекты:

1. Немоноэнергетичность источника (наличие 5% группы нейтронов с энергией ~380 кэв; смягчение спектра за счет рассеяния в бериллиевой оболочке источника, в образцах).
2. Неточечность источника и поглощение в нем.
3. Депрессия теплового потока в баке.
4. Поглощение в свинцово-висмутовом сплаве.
5. Деление примеси урана-235 в природном уране-238.

Результирующая величина поправок по отношению к эффекту поглощения была различной для различных образцов и колебалась в пределах

ТАБЛИЦА 1. ИЗМЕРЕНИЯ С РАЗЛИЧНЫМИ ОБРАЗЦАМИ

Элемент	Толщина образца*	Разбавление	Сечение поглощения	$\Delta\sigma_a$ (σ_{tr}), мбн
	0,089	Нет	1180 ± 110	30
Ag	0,222	Нет	1065 ± 60	35
	0,445	Нет	1005 ± 65	45
σ_{tr} = 7,6 ± 0,3	1,335	Нет	1105 ± 55	50
	0,772	Нет	398 ± 28	25
Cd	1,580	Pb–Bi	424 ± 18	10
	2,12	Pb–Bi	436 ± 18	14
σ_{tr} = 6,4 ± 0,4	2,71	Pb–Bi	419 ± 20	18
	0,639	Нет	375 ± 18	10
	1,28	Нет	377 ± 15	12
$U^{235}_{ест}$	1,92	Нет	377 ± 15	13
	3,21	Нет	376 ± 16	14
σ_{tr} = 13,5 ± 0,3	2,24	Pb– Bi	400 ± 24	9
	2,98	Pb – Bi	408 ± 16	12
	3,70	Pb – Bi	410 ± 18	15

* В единицах длины свободного пробега.

ТАБЛИЦА 2. ОКОНЧАТЕЛЬНЫЕ РЕЗУЛЬТАТЫ ИЗМЕРЕНИЙ

Элемент	σ_a, мбн	элемент	σ_a, мбн	элемент	σ_a, мбн
Cr	10 ± 4	Mo	192 ± 30	Au	570 ± 30
Ni	23 ± 6	Ag	980 ± 60	Hg	233 ± 30
Cu	58 ± 8	Cd	384 ± 20	Pb	43 ± 7
Zn	64 ± 7	In	776 ± 66	Bi	3 ± 3
Sr	108 ± 15	Sn	128 ± 9	Th	615 ± 25
Zr	19 ± 5	Sb	580 ± 73	U^{238}	412 ± 18
Nb	270 ± 15	W	300 ± 25	$U^{238}_{ест}$	376 ± 15
				U^{235}	2910 ± 170
				Pu^{239}	2690 ± 170

5 ÷ 25%. Поэтому поправки не явились серьезным источником дополнительных погрешностей по сравнению с ошибками измерений и ошибками за счет неопределенности полного транспортного сечения, являющегося параметром, при расчете пропускания.

В табл.1 последний столбец иллюстрирует последний вид ошибок.

Расчет пропускания как функции поглощения проводился в односкоростном транспортном приближении для точечного источника нейтронов методом статистических испытаний (Монте-Карло). При этом была

достигнута статистическая точность расчета 0,1 ÷ 0,5% по отношению к поглощенной доле нейтронов $\delta[\Sigma_a; R_1/R_2;\ \Sigma_t(R_i - R_1)]$, зависящей от отношения внутреннего и наружного радиусов образца R_1/R_2 и его оптической толщины $\Sigma_t(R_2 - R_1)$.

В табл.2 приведены окончательные результаты (средние сечения и погрешности), полученные путем обработки данных различных вариантов измерения с помощью длинного счетчика и водяного бака. Для изотопов урана-235 и плутония-239 приведены значения $\sigma_\gamma + \sigma_f$, полученные в измерениях с баком [2].

Сравнение результатов эксперимента с данными работы [3], в среднем указывает на удовлетворительное согласие. Некоторое различие возникает из-за введения в работе [3] заметной расчетной поправки на эффект резонансной блокировки.

ЛИТЕРАТУРА

[1] БЕЛАНОВА Т.С. и др. "Атомная энергия", 19, 3 (1965).
[2] ВАНЬКОВ А.А., СТАВИССКИЙ Ю.Я. "Атомная энергия", 19, 41 (1965).
[3] SCHMITT, H., COOK C., Nucl. Phys. 20, (1960) 202.

РАДИАЦИОННЫЙ ЗАХВАТ БЫСТРЫХ НЕЙТРОНОВ

А.И.АБРАМОВ, А.А.ВАНЬКОВ, В.Н.КОНОНОВ, А.В.МАЛЫШЕВ, Ю.Я.СТАВИССКИЙ, В.А.ТОЛСТИКОВ, А.В.ШАПАРЬ
ФИЗИКО-ЭНЕРГЕТИЧЕСКИЙ ИНСТИТУТ, ОБНИНСК СССР

Abstract — Аннотация

RADIATIVE CAPTURE OF FAST NEUTRONS. The paper discusses the present state of the data on the radiative capture cross-sections of the nuclei of various elements for fast neutrons (with energies above 1 keV). The principal methods of measuring these cross-sections are briefly analysed with a view to evaluating the reliability and accuracy of the information obtained, and also with a view to elucidating possible causes of observed discrepancies. The available experimental data are compared with calculated results, to determine the reliability of such calculations in the case of nuclei for which there are no experimental data, e.g. unstable fission fragments. The authors present their conclusions regarding the most appropriate directions for future work on radiative capture.

РАДИАЦИОННЫЙ ЗАХВАТ БЫСТРЫХ НЕЙТРОНОВ. Рассматривается состояние сведений по сечениям радиационного захвата быстрых нейтронов (с энергиями выше 1 кэв) на ядрах различных элементов. Кратко анализируются основные методы измерения этих сечений с целью оценки достоверности и точности получаемой информации, а также для выяснения возможных причин наблюдаемых разногласий. Имеющиеся экспериментальные данные сравниваются с результатами расчетов сечений с целью определения степени уверенности в правильности таких расчетов для ядер, по которым экспериментальные данные отсутствуют (например, для нестабильных осколков деления). В заключение делаются выводы о наиболее целесообразных направлениях дальнейших исследований радиационного захвата.

Радиационный захват является одним из основных процессов взаимодействия нейтронов с ядрами в области низких и средних энергий возбуждения. Интерес к изучению радиационного захвата нейтронов в диапазоне энергий от нескольких килоэлектронвольт до нескольких мегаэлектронвольт в значительной степени определяется потребностью в константах для прикладных областей ядерной физики.

Одним из первых "потребителей" данных по сечениям захвата в этой области энергий явилась теория происхождения и распространенности элементов, до сих пор базирующая свои основные выводы на механизме последовательного захвата нейтронов.

В реакторостроении данные по сечениям захвата нейтронов в диапазоне энергий до нескольких мегаэлектронвольт широко используются при расчетах ядерных реакторов различных типов, и особенно реакторов на быстрых нейтронах. Несомненна также большая роль исследований радиационного захвата нейтронов для развития физики ядра, ибо сравнение с теорией измеренных сечений захвата и их зависимости от энергии нейтронов и от атомного номера ядра-мишени позволяет судить о справедливости используемых представлений о структуре ядра и механизме ядерных реакций.

Если несколько лет назад представляли интерес любые сведения по сечениям захвата, то сейчас на первый план выдвигается проблема на-

дежности и полноты накопленной информации. Поэтому анализ общего состояния наших сведений о сечениях радиационного захвата и особенно достигнутой к настоящему времени точности измерений, был бы весьма важен. Однако задача объективной оценки точности результатов отдельных исследований очень трудна, и сделанные в настоящем докладе попытки оценить достоверность опубликованных данных можно рассматривать лишь как первый этап подобной работы.

ЭКСПЕРИМЕНТАЛЬНЫЕ МЕТОДЫ ИССЛЕДОВАНИЯ СЕЧЕНИЙ РАДИАЦИОННОГО ЗАХВАТА НЕЙТРОНОВ

Для большинства ядер среднего и тяжелого веса в интересующей нас области энергий сечения захвата усреднены по многим уровням и являются плавной функцией энергии нейтронов. Это позволяет разбить процесс измерения сечений на два практически независимых этапа: 1) определение зависимости сечений от энергии путем сравнения с процессами, имеющими хорошо известный ход (например, B^{10} (n, α), U^{235} (n, f) и т.п.) и 2) абсолютные измерения сечений при одной-двух энергиях с последующей привязкой к ним полученных первым методом кривых.

Определение зависимости сечений от энергии нейтронов производится либо путем регистрации мгновенного гамма-излучения (см. например, [1]), либо путем измерения наведенной активности (см. например, [2]). Наиболее простым и надежным методом абсолютных измерений является метод сферической геометрии [3].

Метод сферической геометрии

Опыты в сферической геометрии заключаются, как известно, в определении пропускания нейтронов сферическим образцом. Величина пропускания T, являющаяся отношением скоростей счета детектора нейтронов при установленном образце и без него, зависит от геометрических размеров образца, плотности ядер, транспортного сечения и сечения захвата нейтронов σ_c. Если достаточно точно рассчитать зависимость пропускания T от величины σ_c, считая при этом, что транспортное сечение известно, то, сравнивая результаты расчета с экспериментально измеренной величиной пропускания, можно определить величину σ_c. При этом следует особо отметить, что абсолютная величина сечения находится этим методом из относительных измерений, при которых не требуется знать ни величины потока нейтронов, ни эффективности детекторов. Это делает получаемые результаты весьма надежными.

При измерениях в сферической геометрии обычно пользуются фотонейтронными источниками. При этом возможность проведения измерений лишь при некоторых дискретных значениях энергии нейтронов вполне окупается природной стабильностью спектральной линии и сферической изотропностью излучения. Детекторами нейтронов служат обычно такие всеволновые системы, как длинный счетчик, водяной бак и т.п.

Точность измерений в сферической геометрии определяется, в основном, точностью расчета зависимости T (σ_c), ошибками в величине транспортного сечения и корректностью введения различных поправок.

Для описания зависимости T (σ_c) в ряде работ использовались экспоненциальные формулы [4] или формула Бете, Бейстера и Картера [5],

но все они по тем или иным причинам (например, из-за большой толщины образцов) не позволяли получить точность выше нескольких процентов. В 1964 году А.А.Ваньков и Ф.Ф.Михайлус для обработки результатов экспериментов в сферической геометрии использовали метод Монте-Карло [6]. Составленные ими таблицы позволяют обрабатывать результаты экспериментов с образцами практически любых размеров.

При проведении опытов в сферической геометрии приходится сталкиваться с целым рядом эффектов, которые могут исказить величину измеряемого пропускания образца (смягчение спектра нейтронов при неидеальной всеволновости детектора, конечное расстояние между источником и детектором и т.п.). Особо следует отметить эффект резонансной блокировки нейтронов в образце. В работе [5] на этот эффект путем расчета вводились значительные поправки, однако в нашей работе [3] было экспериментально показано, что поправка на эффект резонанс-

ТАБЛИЦА 1. РЕЗУЛЬТАТЫ ИЗМЕРЕНИЙ СЕЧЕНИЙ ЗАХВАТА НЕЙТРОНОВ В СФЕРИЧЕСКОЙ ГЕОМЕТРИИ ДЛЯ Au и U ПРИ ЭНЕРГИИ НЕЙТРОНОВ 24 кэв

	Радиусы образцов, см		Использованное значение σ_{tr}, барны	σ_c, мбарны	Источники ошибок, миллибарны	
	Внутренний	Внешний			Эксперим. расчет, поправки	Неопредел. в σ_{tr}
Au	2,05	3,55	13,5 ±0,3	570+30	15	25
U^{238}	3,5	6,5	13,5 ±0,3	412 ±16	9	13

ной блокировки для большой группы веществ лежит в пределах ошибок. Что касается других причин возможных искажений, то при соответствующем выборе условий эксперимента роль большинства из них может быть сведена к нулю, а для остальных можно достаточно корректно ввести поправки, так что общая погрешность оказывается относительно небольшой.

В качестве примера, иллюстрирующего точность измерений в сферической геометрии, можно привести результаты недавно проведенных измерений σ_c для Au и U^{238}. Как видно из табл.1, существенным ограничением точности результатов является неопределенность полных (транспортных) сечений. Тем не менее, точность измерений оказывается порядка 4 – 6%, что пока достаточно для практических целей. Однако для элементов, имеющих очень малые сечения захвата, точность измерений, естественно, хуже.

Регистрация гамма-лучей захвата

Интенсивность возникающего при захвате нейтронов гамма-излучения пропорциональна потоку нейтронов, числу ядер в образце и сечению захвата, поэтому по числу отсчетов детектора гамма-лучей можно, в принципе, определить величину σ_c. Такой метод является наиболее прямым, позволяет детально измерять зависимость σ_c от энергии нейтро-

нов для широкого круга ядер. Однако, трудности определения абсолютных значений потока нейтронов и эффективности детектора дают возможность надежно измерять, как правило, лишь ход кривой $\sigma_c(E_n)$. При таких измерениях необходим монитор нейтронного потока (любой детектор с известным энергетическим ходом или какой-либо процесс, сечение которого можно считать хорошо известным). Следует особо отметить, что вероятность регистрации гамма-квантов, вообще говоря, меняется с изменением энергии нейтронов, ибо возможно изменение спектра гамма-лучей захвата с изменением энергии ядра.

В работах рассматриваемого типа используются как детекторы с малой эффективностью, регистрирующие гамма-кванты в узком телесном угле (кристаллы NaJ и CaF_2 и др.), так и системы, регистрирующие гамма-лучи в телесном угле, близком к 4π и с эффективностью, близкой к 100% (большие сцинтилляционные баки). Первые гораздо проще [7], [8], зато вторые значительно менее чувствительны к изменениям спектра гамма-лучей захвата [9], [10]. Значительный интерес представляют результаты, получаемые с помощью спектрометра по времени замедления в свинце [11] и детектора Моксон-Рея [12]. Высокое временное разрешение больших детекторов гамма-лучей захвата позволяет использовать метод времени пролета как для уменьшения фона, так и для одновременного измерения сечений при различных энергиях нейтронов.

Эффективность регистрации гамма-лучей сцинтилляционным баком определяется его размерами и энергетическим порогом. Наличие низко-энергетического фона вынуждает использовать довольно высокие пороги (≥ 1 Мэв), поэтому эффективность регистрации оказывается меньше 100%, и для определения полного числа отсчетов детектора приходится прибегать к экстраполяциям, что естественно, приводит к ошибкам при измерениях σ_c. Если для детекторов большего объема (~ 4000 л) с хорошим энергетическим разрешением соответствующая погрешность $\sim 2\%$, то для баков меньшего размера она может вырасти до 5 – 7%. Правда, при измерениях усредненных сечений требования к высокой эффективности снижаются, ибо при одновременном возбуждении многих уровней трудно ожидать существенных изменений спектров гамма-лучей при изменении энергии нейтронов. Поэтому оказывается возможным применение баков относительно небольших размеров (100 л), у которых фон посторонних импульсов во много раз меньше [1].

Помимо неопределенности в экстраполяции, общая точность рассматриваемого метода лимитируется следующими факторами: ошибкой в опорных сечениях ($\sim 5 - 6\%$), экспериментальной ошибкой ($\sim 5\%$), неопределенностью в поправках на резонансную блокировку и среднюю длину пути нейтронов в образце (2 – 3%) и погрешностью в определении отношения эффективностей регистрации гамма-квантов от исследуемого образца и эталона (5 – 7%). Таким образом, общая точность определения сечений методом сцинтилляционного бака оказывается порядка 10 – 15%.

Активационные измерения

Активность, наведенная в образце при облучении его нейтронами, пропорциональна сечению захвата, поэтому измерение этой активности позволяет определить величину σ_c. У данного метода есть много об-

щего с предыдущим: наблюдаемый эффект аналогично зависит от величины потока нейтронов и от эффективности аппаратуры, и поэтому метод активации обычно тоже используется для относительных измерений. Основные преимущества метода – возможность измерения сечений для отдельных изотопов с образцами из естественной смеси (путем разделения эффектов по периодам распада). Однако активацию нельзя использовать для измерений сечений неактивируемых изотопов, таких, как железо-56, железо-57 и др. В отличие от методов регистрации гамма-лучей, абсолютную привязку снятых кривых производят или путем измерения абсолютной бета-активности, или нормировкой на сечения для тепловых нейтронов. Использование результатов опытов в сферической геометрии здесь не всегда удается, ибо набор одноизотопных элементов ограничен, а с разделенными изотопами измерения в сферической геометрии пока не проводились.

Основные погрешности при активационных измерениях связаны: 1) с побочными активностями, создаваемыми фоном рассеянных нейтронов и параллельно идущими реакциями; 2) с погрешностями при абсолютном бета-счете (которые обычно не удается опустить ниже 2% [13]); 3) с ошибками в опорных сечениях эталона и монитора. Зависимость эффективности регистрации наведенной активности от энергии нейтронов обычно не наблюдается, если только не возбуждаются метастабильные уровни. В последнем случае из-за зависимости изомерных отношений от энергии нейтронов может изменяться состав и спектр излучения при радиоактивном распаде образца.

Экспериментальная оценка роли всех отмеченных выше факторов позволяет надеяться получить с помощью активационных измерений весьма высокую точность. Так, например, в работе [14] для сечений золота указана ошибка в относительном ходе $\sim 4{,}7\%$. Однако приходится отметить, что разброс данных, полученных различными авторами, оказывается гораздо больше.

РАСЧЕТ СЕЧЕНИЙ

При теоретической интерпретации радиационного захвата нейтронов с энергиями от сотен электронвольт до 14 Мэв обычно используются представления о двух предельных механизмах, соответствующих сильному и относительно слабому взаимодействию частицы с нуклонами ядра-мишени. В первом случае образуются относительно долгоживущие промежуточные конфигурации (промежуточное ядро), во втором – реакция захвата протекает через прямые [15] или "коллективные" механизмы [16], [17]. В области до 5 – 6 Мэв для ядер среднего и тяжелого веса механизм составного ядра является основным. Как показывают проведенные расчеты, применение статистической теории дает возможность получения достаточно надежных количественных оценок сечений, если проницаемости поверхности ядра в нейтронных каналах вычисляются по оптической модели с потенциалом Вуда-Саксона, а плотность ядерных уровней – в модели "почти независимых частиц" с феноменологическим учетом остаточных взаимодействий (энергия спаривания в ядрах с четным Z и N) и оболочечных эффектов.

Для удобства весь интервал кинетических энергий нейтронов можно разбить на три части, каждая из которых удобна для исследования определенной группы вопросов.

а) Несколько кэв $\leq E_n \leq 100$ кэв

В этой области:

1. Основной вклад в сечение вносят нейтроны с $\ell = 0$.
2. Конструкция (n, n') отсутствует или пренебрежимо мала.
3. $\overline{\Gamma}_\gamma / \overline{D}_J$ можно считать постоянными.

Анализ данных по $\sigma_c(E)$ дает возможность получения информации о $\overline{\Gamma}_\gamma / \overline{D}_J$ [18] и о S_1 – силовой функции p-нейтронов, главным образом вблизи ее максимума ($A \sim 100$ [19]), а также о плотности одночастичных состояний вблизи поверхности Ферми (параметр a в выражении для ρ (u, j) [20]. Особый интерес в этой связи представляют сечения, измеренные с фотонейтронными источниками ($E_n = 24$ кэв) для разделенных изотопов.

б) 100 кэв $\leq E_n \leq$ Мэв

1. Становится существенным вклад более высоких орбитальных моментов.
2. Конкуренция неупругого рассеяния с возбуждением отдельных уровней существенно влияет на ход $\sigma_c(E)$.
3. Необходимо учитывать зависимость от энергии $\overline{\Gamma}_\gamma$ и $\overline{D}_J$. При специфической структуре уровней остаточного ядра может происходить увеличение сечения в отдельных интервалах энергии за счет роста плотности уровней составного ядра. Непосредственно за порогом неупругого рассеяния сечение захвата может резко уменьшиться [21]. Анализ этих сбросов в сечениях четно-четных ядер, обусловленных возбуждением уровня 2^+, может дать информацию о силовой функции нейтронов с $\ell = 2$ [22].

в) Несколько Мэв $\leq E_n \leq 14$ Мэв

1. Оценка сечений по статистической теории дает правильный результат лишь для легких ядер. Для ядер среднего и тяжелого веса основной вклад в сечение дают другие механизмы реакции.
2. Становится необходимым статистический учет конкуренции неупругого рассеяния.
3. Оказывается не пренебрежимо малым вклад многофотонных радиационных ширин, хотя вылет нейтронов на промежуточных каскадах значительно более вероятен, чем испускание следующего гамма-кванта.

Анализ зависимости $\sigma_c(E)$ по статистической теории дает возможность проверки функции плотности уровней не только в составном ядре, но и в остаточном ядре (после n, n') при относительно низких энергиях возбуждения. Рассчитанное сечение для йода-127 в интервале энергий от 0,001 Мэв до 14 Мэв с единственным параметром a, полученным из резонансных данных, количественно согласуются с экспериментом до 6 Мэв [23]. В тех случаях, когда о свойствах ядер практически ничего неизвестно, (например, для нестабильных осколков деления), расчет позволяет оценить величину сечения при энергиях до 1 – 2 Мэв с точностью до двух-пяти раз, что иногда оказывается достаточным для практических целей. При $E_n \sim 14$ Мэв расчет приводит к сечениям примерно в 10^3 раз меньшим экспериментальных значений. В этой области энергий согласие с экспериментом может быть получено при использовании механизма "коллективного" захвата [17], [18].

ТАБЛИЦА 2. СРАВНЕНИЕ РЕЗУЛЬТАТОВ РАБОТ [3] И [5] ПО ИЗМЕРЕНИЯМ СЕЧЕНИЙ ЗАХВАТА НЕЙТРОНОВ В СФЕРИЧЕСКОЙ ГЕОМЕТРИИ ПРИ ЭНЕРГИИ 24 кэв

	$\sigma' \pm \Delta\sigma'$ [3]	$\sigma'' \pm \Delta\sigma''$ [5]	$\bar{\sigma}$	$\Delta\bar{\sigma}$	$\delta\sigma$
Cu	58 ± 8	42 ± 15	50	11	8
Zn	64 ± 7	64 ± 20	64	13	0
Ag	980 ± 60	1185 ± 20	1083	40	53
Cd	384 ± 20	515 ± 70	449	45	65
In	776 ± 66	823 ± 60	800	63	24
Sb	580 ± 73	565 ± 45	572	59	8
Au	570 ± 30	585 ± 60	578	45	8
Hg	233 ± 30	380 ± 100	307	65	73
Pb	43 ± 7	3 ± 9	23	8	20

В этой таблице $\bar{\sigma} = \frac{\sigma' + \sigma''}{2}$, $\Delta\bar{\sigma} = \frac{\Delta\sigma' + \Delta\sigma''}{2}$, $\delta\sigma = \left|\frac{\sigma' - \sigma''}{2}\right|$. Как видно, средние ошибки $\Delta\bar{\sigma}$ оказываются, как правило, больше отклонений отдельных результатов от средних значений $\delta\sigma$.

РЕЗУЛЬТАТЫ ИЗМЕРЕНИЙ СЕЧЕНИЙ РАДИАЦИОННОГО ЗАХВАТА БЫСТРЫХ НЕЙТРОНОВ

Наибольшее число абсолютных измерений сечений в сферической геометрии проводилось при энергии нейтронов 24 кэв [3 – 5]. Имеются также сообщения об измерениях при более высоких энергиях нейтронов 220 и 830 кэв [4], однако, трудно учитываемая роль неупругого рассеяния нейтронов делает результаты этих измерений менее надежными. В табл.2 приведены данные из [5] и [3] по элементам, которые исследовались в обеих работах. Из рассмотрения этой таблицы видно, что результаты, полученные в различных лабораториях при различных способах обработки, как правило, согласуются между собой в пределах ошибок опыта, что еще раз подтверждает надежность метода сферической геометрии.

Что касается сведений о зависимости сечений от энергии нейтронов, то положение представляется значительно менее благоприятным. Это заключение можно подтвердить на примере золота – элемента, по которому имеется, пожалуй, наибольшее число экспериментальных данных. На рисунке представлены результаты лишь некоторых последних работ. Здесь же пунктиром показана расчетная кривая сечения, вычисленная по статистической теории при следующих значениях параметров: энергия связи нейтрона в промежуточном ядре $B_0 = 6{,}5$ Мэв, средняя радиационная ширина $\bar{\Gamma}_\gamma = 0{,}17$ эв, среднее расстояние между уровнями $\bar{D} = 0{,}49$ эв, параметр плотности уровней $a = 17$ Мэв$^{-1}$. Как видно, в отдельных точках данные разных авторов расходятся более, чем в два раза, и, по крайней мере, в области ниже 1 Мэв расхождение оказывается нигде не ниже ±20%. Особенно неприятно то, что расходятся не только абсолютные значения, но и формы кривых $\sigma_c(E_n)$. Вполне понятно, что такое положение дел не может считаться удовлетворительным, поскольку

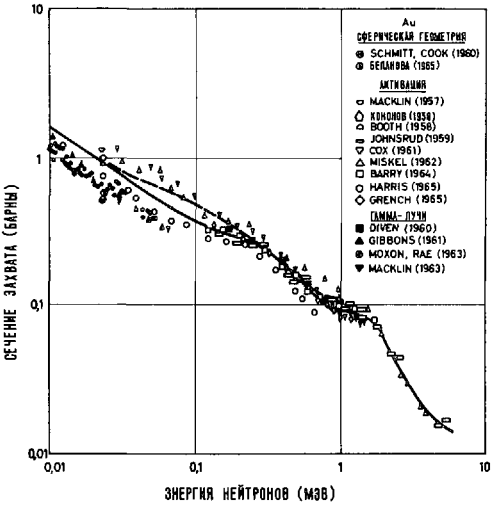

Рис. Кривые сечения для золота по данным различных авторов

возможности экспериментальных методов измерений сечений позволяют как будто бы получить значительно более высокую точность. Делались попытки уменьшить разброс точек путем пересчета старых данных с учетом новых значений опорных сечений [24]. По ряду специально отобранных работ авторы сообщения [24] получили "наилучшую" кривую ("best fit curve"), которая на рисунке показана сплошной линией. Однако необходимо отметить, что при получении этой кривой полностью отбрасывались результаты ряда измерений, и в том числе – измерений в сферической геометрии, которые являются, по-видимому, одними из наиболее надежных. Кроме того, в области энергий ниже 100 кэв явно видна тенденция к объединению точек в две четко выраженные группы. Это, возможно, указывает на наличие каких-то неучтенных систематических ошибок. Поэтому вопрос о точности, с которой известно сейчас сечение захвата нейтронов золотом, по-прежнему остается открытым.

Аналогичная картина наблюдается и для других элементов с той только разницей, что экспериментальных данных по ним гораздо меньше, а для некоторых элементов, и в частности – для отдельных изотопов – экспериментальные данные и вовсе отсутствуют. Особенно неблагоприятна ситуация в области энергий выше 2 – 3 Мэв, в которой применим пока практически только один метод проведения экспериментов – активационный со всеми присущими ему ограничениями. В то же время эта область особенно интересна с точки зрения представлений о вкладе различных механизмов захвата.

ЗАКЛЮЧЕНИЕ

Из рассмотрения всей совокупности данных по радиационному захвату быстрых нейтронов можно сделать вывод о том, что ни их количество, ни достигнутая точность не являются удовлетворительными. В

самом деле, как было отмечено выше, реальная точность абсолютных величин сечений захвата в самых лучших случаях оказывается не выше 10 – 15%. В то же время, для расчета коэффициента воспроизводства ядерного горючего в больших реакторах с ошибкой не более 2 – 5% необходимо знать σ_c (уран-238) в области до 1,5 Мэв с точностью 1 – 2%, σ_c (Fe) в области около 50 кэв с точностью ~ 7% и т.д. [25]. Анализ возможностей экспериментальных методик показывает, что уже сейчас измерения сечений захвата могут проводиться с более высокой точностью, чем ±10%. Поэтому проведение новых измерений и учет всех возможных причин наблюдаемых расхождений является одной из основных задач исследования радиационного захвата нейтронов для практических целей. С этой точки зрения наиболее интересны измерения σ_c для урана-238 и тория-232, для которых требуется наиболее высокая точность.

Для потребностей экспериментальных методик необходимо иметь надежные кривые $\sigma_c(E_n)$ для элементов, часто используемых в качестве эталонов: In, J, Au. Для того, чтобы эти элементы действительно могли служить хорошими эталонами, необходимо знать их сечения с точностью не хуже 1 – 2%.

До некоторой степени недостаток знаний сечений захвата может быть восполнен теоретическими расчетами. Однако на данной стадии в теоретических расчетах всегда присутствует элемент неопределенности, поэтому полностью заменить эксперимент расчеты не в состоянии.

Для теории радиационного захвата особенно желательны измерения сечений для нейтронодефицитных и нейтроноизбыточных ядер, так как из таких измерений может быть получена дополнительная информация о плотности ядерных уровней. С этой же точки зрения желательны более тщательные измерения в области энергий выше 2 Мэв. При еще более высоких энергиях, порядка 6 – 20 Мэв интересны исследования роли различных механизмов захвата. Для проверки спиновой зависимости плотности ядерных уровней целесообразно детальное изучение энергетической зависимости изомерных отношений.

Дальнейшие исследования усредненных значений радиационного захвата несомненно дадут весьма полезную информацию, как для ядерных констант, используемых при расчете реакторов, так и для теории атомного ядра.

ЛИТЕРАТУРА

[1] КОНОНОВ В.Н., СТАВИССКИЙ Ю.Я., ЧИСТОЗВОНОВ С.Р., ШОРИН В.С., Доклад на Парижской конференции 1966 г. См. в данном издании CN-23/99.
[2] КОРОЛЕВА В.П., ТОЛСТИКОВ В.А., КОЛЕСОВ В.Е., ДОВБЕНКО А.Г., Доклад на Парижскую конференцию 1966 г. См. в данном издании CN-23/103.
[3] ВАНЬКОВ А.А., МИХАЙЛУС Ф.Ф., СТАВИССКИЙ Ю.Я., Доклад на Парижскую конференцию 1966 г. См. в данном издании CN-23/96.
[4] БЕЛАНОВА Т.С., ЖЭТФ 34, 574 (1958); "Атомная энергия", 8, 549 (1960).
[5] COOK, C.V., SCHMITT, H.W., Nuclear Physics 20 (1960) 202.
[6] БЕЛАНОВА Т.С., ВАНЬКОВ А.А., МИХАЙЛУС Ф.Ф., СТАВИССКИЙ Ю.Я., "Атомная энергия", 19, 3(1965).
[7] СТАВИССКИЙ Ю.Я., ШАПАРЬ А.В., "Атомная энергия" 15, 323 (1963).
[8] СТАВИССКИЙ Ю.Я., ШАПАРЬ А.В., КРАСНОКУТСКИЙ Р.Н., "Атомная энергия" 19, 42 (1965).
[9] DIVEN, B.C., TERREL, J., HEMMENDINGER, A., Phys. Rev. 120 (1960) 556.
[10] GIBBONS, J.H., Phys. Rev. 122 (1961) 182.
[11] ШАПИРО Ф.Л., Труды Физического института АН СССР XXIV, 3 (1964).
[12] MOXON, M.C., RAE, E.R., Nucl. Instr. & Meth. 24 (1963) 445.

[13] BARRY, J.F., J. Nucl. Energy 18 (1964) 491 .
[14] HARRIS, K.K., GRENCH, H.A. et al., Nucl. Phys. 69 (1965) 37.
[15] ДОВБЕНКО А.Г., ЗАХАРОВА С.М., КОЛЕСОВ В.Е., МАЛЫШЕВ А.В., "Атомная энергия" 18, 114 (1965).
[16] BROWN, G.E., Nuclear Physics 57 (1964) 339.
[17] LANE, A.M., International Conference on the Study of Nuclear Structure with Neutrons. Antwerpen, 1965.
[18] КОНКС В.А., ФЕНИН Ю.И., Доклад на Антверпенской конференции 1965 г.
[19] БЕРГМАН А.А., КАПЧИГАШЕВ С.П., ПОПОВ Ю.П., РОМАНОВ С.А., Доклад на Антверпенской конференции 1965 г.
[20] ДОВБЕНКО А.Г., ЗАХАРОВА С.М., КОЛЕСОВ В.Е., МАЛЫШЕВ А.В., "Атомная энергия" 18, 114 (1965).
[21] КОНОНОВ В.Н., СТАВИССКИЙ Ю.Я., КОЛЕСОВ В.Е., ДОВБЕНКО А.Г., НЕСТЕРЕНКО В.С., МОРОКА В.И., "Ядерная физика", 4, 282 (1966).
[22] КОНОНОВ В.Н., Журнал "Ядерная физика" (в печати).
[23] ЗАХАРОВА С.М., МАЛЫШЕВ А.В., Доклад на Антверпенской конференции, 1965.
[24] GRENCH, H.A., COOP, K.L., MENLOVE, H.O., VAUGHN, F.J., WASH-1068, 75 (1966).
[25] MOORHEAD, T.P., Доклад SM-18/15 на семинаре по физике быстрых и промежуточных реакторов, Вена, 1961 г.

СЕЧЕНИЯ РАДИАЦИОННОГО ЗАХВАТА БЫСТРЫХ НЕЙТРОНОВ ДЛЯ ИЗОТОПОВ Ag, Dy, W, Ta и Re.

В.Н.КОНОНОВ, Ю.Я.СТАВИССКИЙ,
С.Р.ЧИСТОЗВОНОВ, В.С.ШОРИН
(доклад представил А.И.Абрамов)
ФИЗИКО-ЭНЕРГЕТИЧЕСКИЙ ИНСТИТУТ, ОБНИНСК
СССР

Abstract — Аннотация

RADIATIVE CAPTURE CROSS-SECTIONS FOR FAST NEUTRONS FOR Ag, Dy, Ta, W AND Re. The authors have measured the capture cross-sections for 30 to 170-keV neutrons for the isotopes ^{107}Ag, ^{109}Ag, ^{161}Dy, ^{162}Dy, ^{164}Dy, ^{182}W, ^{184}W and ^{186}W and a natural mixture of Ta, W and Re isotopes.

The neutron capture events were recorded by a liquid scintillation detector measuring the prompt capture gamma rays. The measurements were carried out on a Cockcroft-Walton pulsed accelerator, by the nanosecond time-of-flight technique for discriminating the background and measuring the neutron energy.

СЕЧЕНИЯ РАДИАЦИОННОГО ЗАХВАТА БЫСТРЫХ НЕЙТРОНОВ ДЛЯ ИЗОТОПОВ Ag, Dy, W, Ta и Re. Измерены сечения захвата нейтронов с энергией 30 – 170 кэв для изотопов серебро-107, серебро-109, диспрозий-161, диспрозий-162, диспрозий-164, вольфрам-182, вольфрам-184, вольфрам-186 и для естественной смеси изотопов тантал, вольфрам и рений.

События захвата нейтронов регистрировались жидкостным сцинтилляционным детектором по мгновенным гамма-лучам захвата. Измерения проводились на импульсном ускорителе Кокрофта-Уолтона с использованием наносекундной техники времени пролета для дискриминации фона и измерения энергии нейтронов.

Изучение сечений радиационного захвата нейтронов в киловольтной области энергий для разделенных изотопов представляет несомненный интерес, особенно для теории ядерных реакций и совершенствования методов расчета ядерно-физических констант для быстрых реакторов, а также теории звездного нуклеосинтеза. Однако такие исследования стали возможными только в последнее время, когда были созданы спектрометр по времени замедления нейтронов в свинце и детектор Моксон-Рэя.

В публикуемой работе приводятся результаты сечений радиационного захвата нейтронов в диапазоне энергий 30 – 170 кэв для ряда изотопов, выполненных с помощью сцинтилляционного детектора сравнительно небольшого объема (125 л) и наносекундной техники времени пролета, которая используется для измерения энергии падающих нейтронов и дискриминации фона. Применение сцинтилляционного бака малого объема, обладающего значительно меньшим уровнем фона, по сравнению с большими детекторами, позволило резко повысить чувствительность метода при сравнительно небольшой потере эффективности регистрации актов захвата. Эффективность этого детектора более сильно зависит от формы спектра регистрируемых γ-квантов. Однако, для широкого класса ядер тяжелых элементов нет заметного различия в спектрах

возникающего γ-излучения и, следовательно, значительной неопределенности в эффективности детектора при исследовании разных ядер.

Измерения проводились на сплошном спектре нейтронов из реакции $T(p, n)He^3$ на мишени пульсирующего ускорителя Кокрофта-Уолтона. Пролетная база составляла 1,5 м при временном разрешении 20 – 30 нсек. Детальное описание эксперимента дано в работе [1]. В качестве монитора нейтронного потока был выбран образец индия, ход сечения которого детально измерялся относительно сечения $B^{10}(n, \alpha)Li^{7*}$ реакции и сечения поглощения урана-235, а позднее относительно хода сечения деления урана-235 в Ок-Риджской лаборатории [2]. Для абсолютной привязки использовались сечения, полученные абсолютным методом пропускания в сферической геометрии [3]. Результаты данной работы представлены на рис.1 и 2. Неопределенность величины сечения обусловлена, в основном, среднеквадратичной экспериментальной ошибкой, ошибкой в измерении относительной эффективности детектора и ошибкой в абсолютной привязке и лежит в пределах 10 – 15% при энергетическом разрешении около 10%.

Приведенные сечения хорошо совпадают с результатами измерений на спектрометре по времени замедления нейтронов в свинце (за исключением Re) [4, 5], полученные с другим методом калибровки, и данными

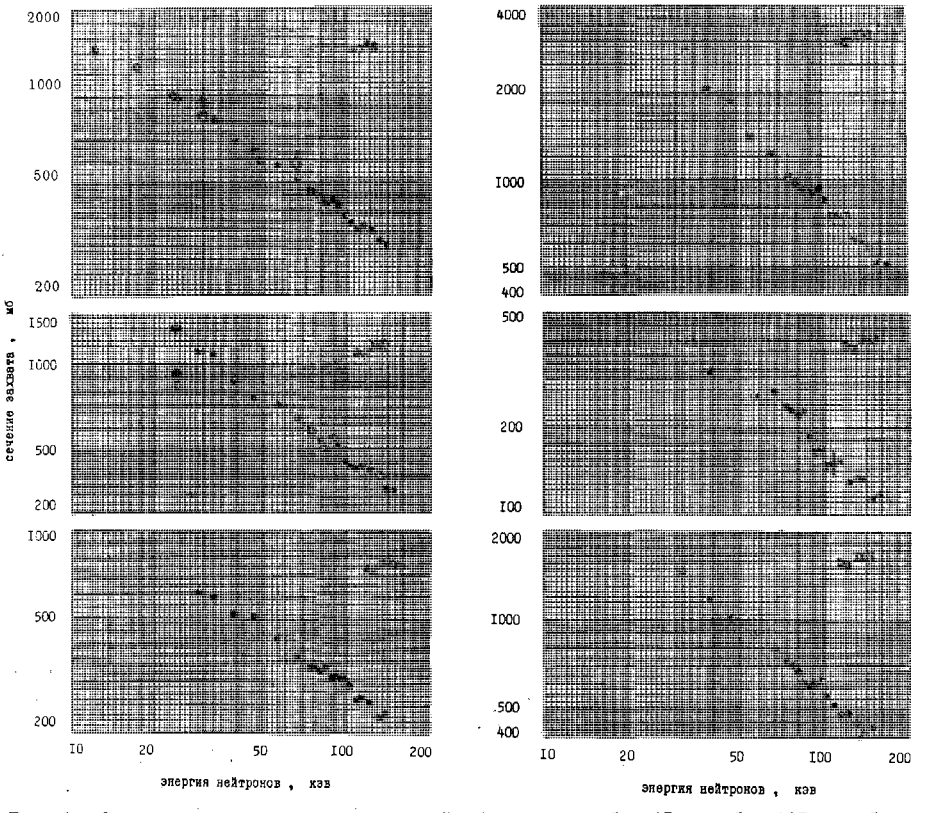

Рис. 1. Сечения радиационного захвата нейтронов для серебра-47, серебра-107, серебра-109; диспрозия-161, диспрозия-162, диспрозия-163: ● – данная работа; ○ – Попов [4]; □ – Macklin et al. [2]; ◇ – Беланова и др. [3]; ◊ – Chaubeg et al. [6]; △ – Macklin et al. [11]; ▽ – Кононов и др. [7].

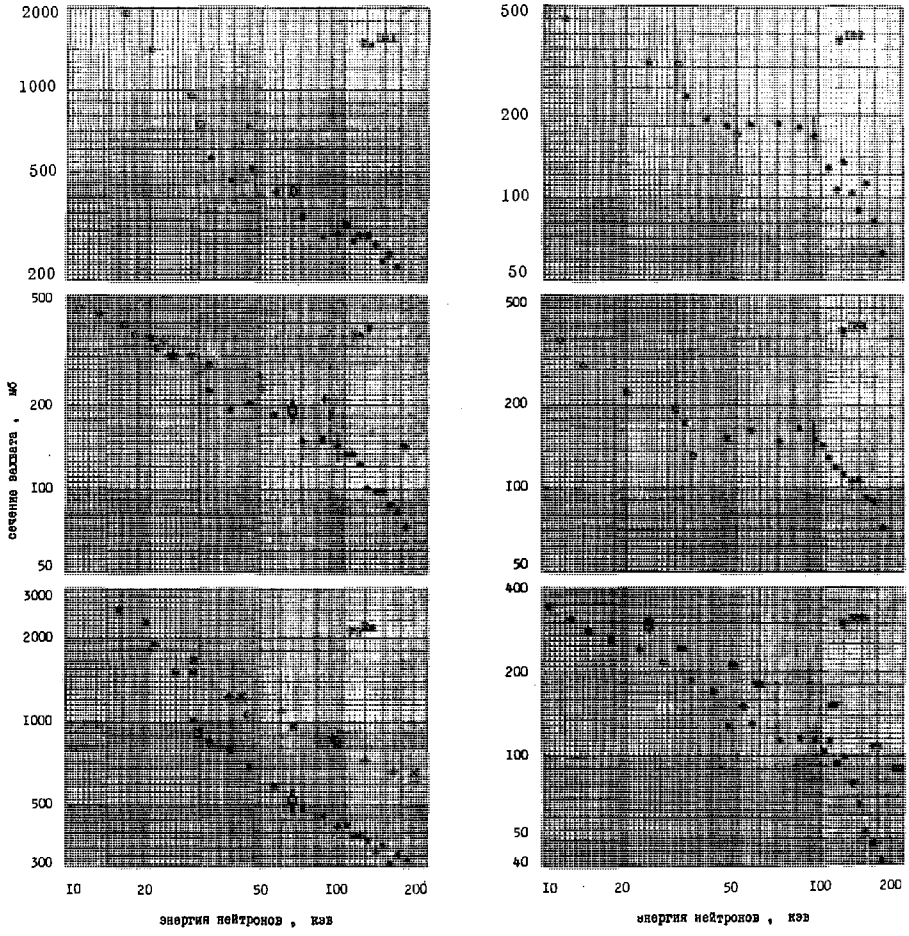

Рис. 2. Сечения радиационного захвата нейтронов для тантала-181, вольфрама-74 вольфрама-182, вольфрама-184, вольфрама-186, рения-75: ● – данная работа; ○ – Попов [4]; □ – Macklin et al. [2]; + – Стависский и др. [9]; × – Stupegia et al. [10]; ◇ – Беланова и др. [3]; ▭ – Стависский и др. [8]; △ – Macklin et al. [11]; ▽ – Кононов и др. [7].

Ок-Риджской лаборатории [2], где использовался аналогичный метод измерения и процедура калибровки. Надежность процедуры нормировки для детекторов сравнительно небольшого объема подтверждается согласием сечения захвата серебра, вычисленного по измеренным в данной работе изотопным сечениям серебра-107 и серебра-109, с результатами Гиббонса [2] и Ванькова [3]. Расхождение наших результатов с активационными данными [7, 8, 10, 11] и результатами Дивена [12], привязанными по сечению поглощения урана-235, является систематическим. Однако следует отметить, что в настоящее время многие авторы производят перенормировку полученных активационных сечений, используя новые данные по сечению деления урана-235. Такая перенормировка приводит к уменьшению расхождения. Причиной расхождения с данными Дивена является, по-видимому, сильное расхождение спектров γ-лучей деления и радиационного захвата. Нормировка по абсолютным сечениям

поглощения в сферической геометрии представляется нам более надежной и подтверждается результатами измерений сечений захвата золота в диапазоне энергии нейтронов 0,01 эв – 50 кэв [13]. Привязка по тепловому сечению захвата золота, известному с точностью 1%, привела к хорошему согласию с сечением, полученным в работе [3] при 24 кэв, что является довольно веским аргументом в пользу выбранной нормировки.

ЛИТЕРАТУРА

[1] КОНОНОВ В.Н., СТАВИССКИЙ Ю.Я., КОЛЕСОВ В.Е., ДОВБЕНКО А.Г., НЕСТЕРЕНКО В.С., МОРОКА В.И., "Ядерная физика", 4, №2 (1966).

[2] GIBBONS, J.H., MACKLIN, R.L., MILLER, P.D., NEILER, J.H., Phys. Rev. 122 (1961) 182.
MACKLIN, R.L., GIBBONS, J.H., INADA, I., Phys. Rev. 129 (1963) 2695.
MACKLIN, R.L., GIBBONS, J.H., Bull. Am. Phys. Soc. Ser II, 11 (1966) 167.

[3] БЕЛАНОВА Т.С., ВАНЬКОВ А.А., МИХАЙЛУС Ф.Ф., СТАВИССКИЙ Ю.Я., "Атомная энергия", 19, 3 (1965).

[4] ПОПОВ Ю.П., Труды ФИАН 24, III (1964).

[5] Бюллетень Информационного центра по ядерным данным, выпуск I. Атомиздат, 1964.

[6] CHAUBEG, A.K., SCHGAL, M.L., Nucl. Phys. 66 (1965) 267.

[7] КОНОНОВ В.Н., СТАВИССКИЙ Ю.Я., ТОЛСТИКОВ В.А., "Атомная энергия", 5, 564 (1958).

[8] СТАВИССКИЙ Ю.Я., ТОЛСТИКОВ В.А., Ядерные реакции при малых и средних энергиях, АН СССР Москва, 1962 стр. 562.

[9] СТАВИССКИЙ Ю.Я., ШАПАРЬ А.В., "Нейтронная физика", Атомиздат, М., 1961, стр.310.
СТАВИССКИЙ Ю.Я., ШАПАРЬ А.В., КРАСНОКУТСКИЙ Р.Н. "Атомная энергия", 19, 42 (1965).

[10] STUPEGIA, P.S., SCHMIDT, M., MADSON, A.A., J. Nucl. Energy (Part A/B Reactor Sci. Technol) 19 (1965) 767.

[11] MACKLIN, R.L., LASAR, N.H., LYON, W.S., Phys. Rev. 107 (1957) 504.

[12] DIVEN, B.S., TERREL, J., HEMMENDINGER, A., Phys. Rev. 120 (1960) 556.

[13] HADDAD, E., WALTON, R.B., FRIESENHAHN, S.J., LOPEZ, W.M., Nucl. Instr. & Methods. 31 (1964) 125.

РАДИАЦИОННЫЙ ЗАХВАТ БЫСТРЫХ НЕЙТРОНОВ ЯДРАМИ ИТТРИЯ-89 И ИРИДИЯ-193

В.П.КОРОЛЕВА, В.А.ТОЛСТИКОВ, В.Е.КОЛЕСОВ, А.Г.ДОВБЕНКО
(Доклад представил А.И.Абрамов)
ФИЗИКО-ЭНЕРГЕТИЧЕСКИЙ ИНСТИТУТ, ОБНИНСК СССР

Abstract — Аннотация

RADIATIVE CAPTURE OF FAST NEUTRONS BY THE NUCLEI ^{89}Y AND ^{193}Ir. The radiative capture cross-sections of the six nuclei were measured by the activation method in the 0.15-7 MeV energy range. As neutron source the authors used T(p,n) and D(d,n) reactions obtained on a Van de Graaff accelerator. The neutron flux was monitored by fission chambers with layers of ^{235}U and the induced β-activity was measured by end-window β-counters. As reference cross-sections the authors took the fast and thermal fission cross-sections of ^{235}U and the radiative capture cross-sections of the nuclei of these isotopes for thermal neutrons. The results obtained are compared with the results of other authors and with calculations made according to the statistical theory of nuclear reactions. In calculating the penetration factors for the nuclear surface use was made of the optical model of the nucleus with a diffuse edge, and account was taken of spin-orbit coupling.

РАДИАЦИОННЫЙ ЗАХВАТ БЫСТРЫХ НЕЙТРОНОВ ЯДРАМИ ИТТРИЯ-89 И ИРИДИЯ-193. Методом активации были измерены сечения радиационного захвата шести ядер в области энергий 0,15 – 7 Мэв. Источником нейтронов служили T(p, n) и D(d, n) реакции, осуществляемые на ускорителе Ван-де-Граафа. Монитором нейтронного потока служили камеры деления со слоями урана-235. Наведенная β-активность измерялась торцевыми β-счетчиками. В качестве опорных сечений использовались сечения деления урана-235 быстрыми и тепловыми нейтронами и сечения радиационного захвата тепловых нейтронов ядрами изучаемых изотопов. Полученные результаты сравниваются с результатами других авторов и расчетами по статистической теории ядерных реакций. При расчете коэффициентов проницаемости ядерной поверхности использовалась оптическая модель с размытым краем и учитывалась спин-орбитальная связь.

Методом активации были измерены сечения радиационного захвата нейтронов с энергией 0,17 – 3,7 Мэв ядрами иттрия-89 и иридия-193. Источником моноэнергетических нейтронов служила реакция T(p, n)He^3, осуществляемая на ускорителе Ван-де-Граафа.

Измерение сечений радиационного захвата проводилось относительно сечения деления урана-237, который в виде слоя находился в ионизационной камере деления. Метод измерений ранее был подробно описан [1].

Для определения из экспериментальных данных сечений радиационного захвата были использованы следующие опорные сечения: сечение захвата тепловых нейтронов в иттрии-89 с образованием активности с $T_{1/2}$ = 64,4 часа – 1,26 ± 0,08 барна [2]; сечение с $T_{1/2}$ = 19,7 часа – 130 ± 30 барна [2]; сечение деления урана-235 тепловыми нейтронами 577,1 ± 0,9 барна [3]. Сечения деления урана-235 быстрыми нейтронами брали по рекомендованной кривой из работы Паркера [4]. Результаты измерений в сравнении с работами других авторов приведены на рисунках 1 и 2. Ошибки измерений, указанные на рис.1 для иттрия-89 полные,

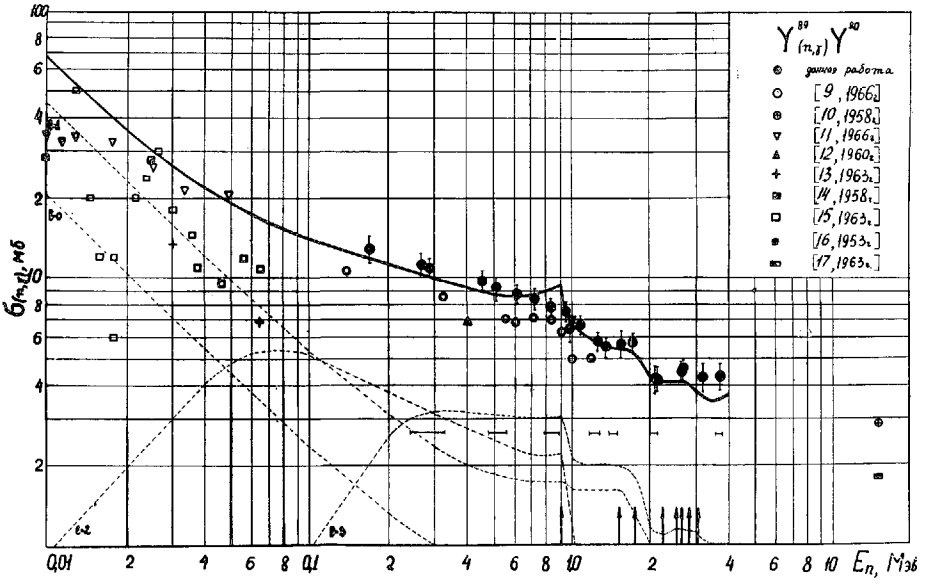

Рис. 1. Результаты измерений сечений радиационного захвата нейтронов иттрия-89 в сравнении с результатами других работ и теорий.

т.е. включают в себя погрешности эксперимента и ошибки в опорных сечениях. Ошибки, указанные на рис.2 для иридия-193 – ошибки в энергетической зависимости сечения радиационного захвата, т.е. не включают в себя ошибки тепловых сечений. На рисунках приведены также результаты расчетов сечений радиационного захвата иттрия-89 и иридия-193 по статической теории ядерных реакций. Метод расчета излагался нами в [5, 6]. Коэффициенты проницаемости ядерной поверхности вычислялись по оптической модели ядра для потенциала, в котором было учтено спин-орбитальное взаимодействие. Были приняты следующие параметры ядерного потенциала [6]:

$V_0 = 45$ Мэв; $d = 0{,}5 \cdot 10^{-13}$ см; $\xi = 0{,}1$; $\kappa = 0{,}35 \cdot 10^{-26}$ см^2;

$R = 6{,}05 \cdot 10^{-13}$ см для иттрия-89 и $7{,}9 \cdot 10^{-13}$ см для иридия-193.

Параметры составных ядер, использованные в расчете, имели следующие значения: B_n для иттрия-89 равна 6,84 Мэв [2], $a = 8{,}8$ Мэв$^{-1}$, B_n для иридия-193 равна 6,13 Мэв [2], $a = 20{,}8$ Мэв$^{-1}$.

Параметр a взят из результатов анализа средних расстояний между нейтронными резонансами вблизи энергии связи нейтронами.

Необходимые для расчета значения энергий, спинов и четностей возбужденных уровней ядра-мишени иттрия-89 были взяты из [7], а для иридия-193 из [8].

Сплошные линии на рисунках – полные сечения захвата, пунктирные – сечения захвата нейтронов с различными угловыми моментами l. Вертикальные стрелки указывают положения возбужденных уровней ядер-мишеней.

Наилучшее согласие теории с экспериментом для иттрия-89 было получено при $\overline{\Gamma}_\gamma = 0{,}3$ эв и $\overline{D} = 6000$ эв, которые находятся в согласии с приведенными в [2] экспериментальными значениями, а значение $\overline{D}$ согласуется со значением a, использованным в расчете. Хорошее со-

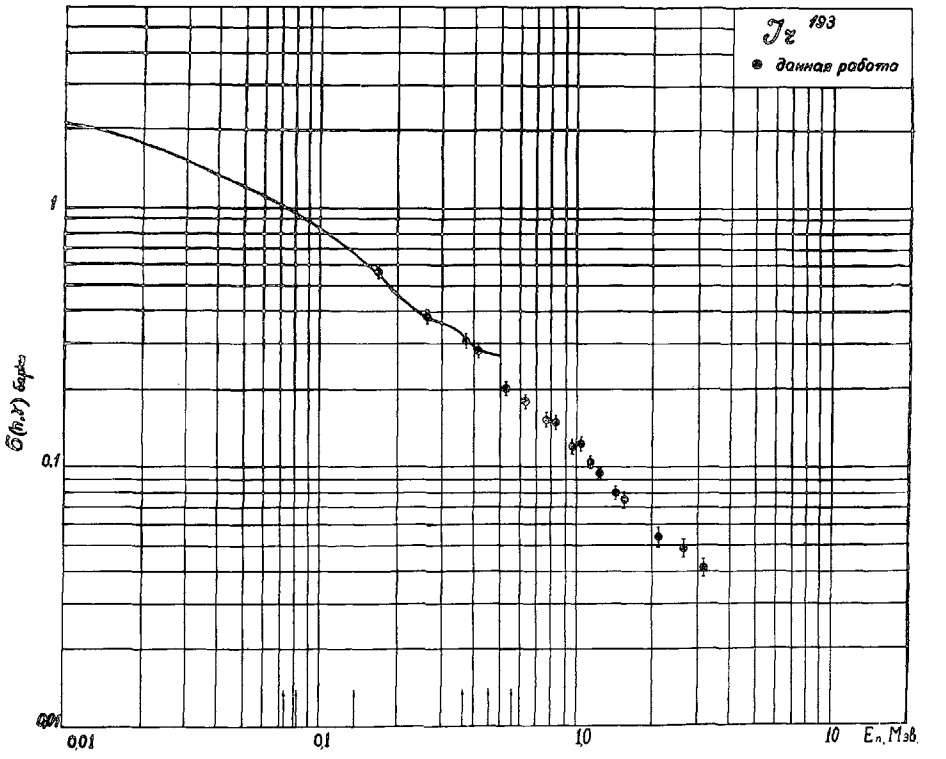

Рис. 2. Результаты измерений сечений радиационного захвата нейтронов иридия-193 в сравнении с теорией. ⊕ – данные публикуемой работы.

гласие теории с экспериментом для иридия-193 было получено при $\overline{\Gamma}_\gamma = 85$ эв и $\overline{D} = 10{,}5$ эв. Для нейтронов с энергией свыше 0,4 Мэв, к сожалению, расчет для иридия-193 провести нельзя из-за отсутствия данных о характеристиках возбужденных уровней.

Авторы благодарят А.Абрамова, А.Малышева и Ю.Стависского за постоянный интерес к данной работе.

ЛИТЕРАТУРА

[1] СТАВИССКИЙ Ю.Я., ТОЛСТИКОВ В.А. Ядерные реакции при малых и средних энергиях. Тр. Второй Всесоюзной конф. Июль, 1960 г. Изд. АН СССР, М., 1962, стр.562.

[2] ГОРДЕЕВ И.В., КАРДАШЕВ Д.А., МАЛЫШЕВ А.В. Ядерно-физические константы. Госатомиздат, М., 1963.

[3] Neutron Cross Sections, BNL-325, second Edition, Supplement No.2, vol.III, Z = 88 to 98, February, 1965.

[4] PARKER, K., AWREO - 82/63, December 1963.

[5] ТОЛСТИКОВ В.А., КОЛЕСОВ В.Е., ДОВБЕНКО А.Г., СТАВИССКИЙ Ю.Я., "Атомная энергия", 17, 6 (1964) 505.

[6] ТОЛСТИКОВ В.А., КОРОЛЕВА В.П., КОЛЕСОВ В.Е., ДОВБЕНКО А.Г., Радиационный захват быстрых нейтронов изотопом Cu^{63}. "Атомная энергия", июль 1966.

[7] SHAFROTH, S.M., TREHON, P.N., VAN PATTER, D.M., Phys. Rev., vol. 129 (1963) 704.

[8] ДЖЕЛЕПОВ Б.С., ПЕКЕР Л.К., СЕРГЕЕВ В.О. Схемы распада радиоактивных ядер, A ≥ 100. Изд. АН СССР, М. – Л., 1964.
[9] GRENCH, H.A. et al., WASH-1064 (1966) 67.
[10] PERKIN, J.L. et al., Proc. Phys. Soc. 72, Pt.4, No.466 (1958) 505.
[11] КАПЧИГАШЕВ С.П. Частное сообщение.
[12] DIVEN, B.C., TERRELL, J., HEMMENDINGER, A., Phys. Rev. 120, N2 (1960) 556.
[13] MACKLIN, R.L. et al., Phys. Rev. 112 (1958) 226.
[14] BOOTH, R. et al., Phys. Rev. 112 (1958) 226.
[15] MACKLIN, R.L. et al., Nucl. Phys. 43 (1963) 353.
[16] HUGHES, D. et al., Phys. Rev. 91 (1953) 1423.
[17] BRAMLITT, E.T. et al., Phys. Rev. 131 (1963) 2649.

DISCUSSION

(on papers CN-23/96, CN-23/98, CN-23/99 and CN-23/103)

W. PÖNITZ: In part of their work the authors of paper CN-23/96 have used a geometric arrangement (involving a water bath) which conflicts with their theoretical assumptions of a point source, a spherical shell and a point detector located at a considerable distance from the shell. Would you care to comment on this?

A.I. ABRAMOV: Perhaps I should first make it clear that the experiments involving a spherical geometry and long counters were carried out by Belanova, while those involving a water bath were performed by Vankov. The results obtained by these two methods were compared and averaged. Of course, conditions differed somewhat as between the work carried out with long counters and that done with a water bath, so that the corrections that had to be made differed somewhat in character. Allowance was made for the fact that the source used was not a point source and that the geometry was not ideal, as well as for a number of other factors, but the corrections were nevertheless small. In this connection, I should like to mention that, when the internal radius of the tank is much greater than the radius of the spherical sample, the observed effect is the same as when a point detector is used.

W. PÖNITZ: I should like to raise a further point, concerning the liquid scintillator bath measurements. The data presented are in agreement with the data of other workers at low energies, but there is a strong disagreement at higher energies. This may be due to the use of a bath that is too small. At higher energies one has mainly capture contributions from neutrons with higher spin orbit values, and the gamma-ray spectrum therefore changes.

A.I. ABRAMOV: Of course, the efficiency of a small tank depends to a larger extent on the gamma-ray spectrum. However, present data do not lead one to expect any substantial spectrum changes in the energy region considered. The discrepancies noted by you are therefore probably due to other causes.

W. PÖNITZ: With regard to the cross-section for gold, many investigators (such as Cox) have renormalized their values, which are now in better agreement; in the case of values measured independently since 1960, the disagreement is only about 20%. The four curves suggested by Grench and co-workers, Bogart, Gibbons and myself also agree within these limits. I should be interested to hear your comments on this point.

A.I. ABRAMOV: I quite agree that renormalization of data can result in better agreement. It should be remembered, however, that the fission cross-section values used in this procedure have changed several times in recent years, and there is no guarantee that they will not change in the future. We therefore feel that the true accuracy of the data for gold is given by the scatter of the points - that is to say, about 20%, which is much greater than the error given in your paper (CN-23/6) for an energy of 30 keV.

D. BOGART: With regard to the fact that no self-protection effects were observed in the sphere transmission experiments with Sb-Be sources (experiments which covered a range of sphere thicknesses and various degrees of atom dilution by lead), I should like to point out that, in my

opinion, dilution by lead does not get to the heart of the self-protection problem.

Semler and I have shown that all mean capture cross-section values that satisfy a given sphere transmission value and allow for the resonance nature of the cross-sections are larger than those obtained by analysis using energy-independent cross-sections. We have analysed (paper CN-23/83) Belanova's water bath and long counter data for gold and silver, and find that our mean capture cross-section values are consistently larger than her results - by about 10% for silver and approximately 15% for gold. We believe this to be the magnitude of the "correction" to a mono-energetic sphere analysis.

It is possible that all the reported experiments lack this correction, in that the sensitivity of analysis and experiment is insufficient.

A.I. ABRAMOV: It is possible that the self-protection effect calculated by you, but for some reason not found in experiments with a Pb-Bi sphere, really does exist; but it is also possible that your calculations fail to allow for certain additional factors that nullify the effect. At all events, experiments with "diluted" specimens yield some additional information which should help us to gain a deeper understanding of the self-protection effect. Perhaps we should also try to devise another means of investigating this effect experimentally.

R. BATCHELOR: In the case of heavy elements, the capture cross-section at 24 keV is small relative to the elastic scattering. This means that the multiple scattering corrections are large, and one would expect experimenters to know the $\sigma_{nn}(\theta)$ cross-sections accurately to make reliable corrections. Why is it that experimenters do not appear to ask for this information?

A.I. ABRAMOV: As stated in the paper, analysis of the experimental data was performed by the Monte Carlo method, with which it is easy to take into account the dependence of the differential cross-section on the scattering angle. Under the actual experimental conditions, however, it is reasonable to expect that the transport approximation would give sufficiently good results.

MESURES DES SECTIONS EFFICACES ET DES INTEGRALES DE RESONANCE PAR LA METHODE D'OSCILLATION

J.C. CARRE ET R. VIDAL
CEA, CENTRE D'ETUDES NUCLEAIRES DE FONTENAY-AUX-ROSES, FRANCE

Abstract — Résumé

MEASUREMENT OF CROSS-SECTIONS AND RESONANCE ABSORPTION INTEGRALS BY THE OSCILLATION METHOD. The authors used the oscillation method to measure reaction rates and to derive the cross-sections from them. To obtain maximum efficiency from the method they developed original applications designed to produce, depending on the nature of the material and cross-section to be investigated, measurement conditions which would permit the attainment of maximum accuracy and at the same time facilitate interpretation of the results in work with a fully known neutron spectrum.

The phase oscillation method was used at ZOE to measure the thermal absorption cross-sections of materials with little capacity for capture but marked capacity for scattering, since it permits attenuation of the diffusion effect by a considerable factor with a measuring point located in the reflector, i.e. in a well-thermalized medium. The results obtained by this method for absorption cross-sections at 2200 m/s are given.

The conventional amplitude oscillation method was used at the MINERVE reactor to measure the reaction rates produced by small samples. The measurements were made at the centre of the core, without a cadmium filter, in a spectrum with a great abundance of epithermal neutrons. By deducting the thermal part, the authors derived the resonance integral from the measured cross-section by calibration with reference to gold. The samples used were in the form of solutions or plates. To derive the values at infinite dilution or at zero thickness, they extrapolated the results obtained for different concentrations or thicknesses, adopting the self-shielding factors calculated according to the ZUT programme and checking to see that they confirmed the experimental results. The resonance integrals measured, not including the 1/V part, are given.

For materials whose resonance parameters are known with sufficient accuracy, the measured values are compared with those calculated or measured by different authors.

MESURES DES SECTIONS EFFICACES ET DES INTEGRALES DE RESONANCE PAR LA METHODE D'OSCILLATION. La méthode d'oscillation a été utilisée pour mesurer les taux de réaction et en déduire les sections efficaces effectives. Pour tirer le maximum de cette méthode, on en a développé des applications originales afin d'obtenir, suivant la nature du matériau et la section efficace à mesurer, des conditions de mesure permettant d'atteindre la précision maximale tout en rendant plus aisée l'interprétation des résultats en travaillant dans un spectre de neutrons parfaitement connu.

La méthode d'oscillation de phase a été utilisée à ZOE pour mesurer les sections efficaces d'absorption thermiques de corps peu capturants mais très diffusants, car elle permet d'atténuer l'effet de la diffusion d'un facteur important avec un point de mesure situé dans le réflecteur, donc dans un milieu bien thermalisé. On donne les résultats obtenus à l'aide de cette méthode.

La méthode classique d'oscillation d'amplitude a été utilisée à MINERVE pour mesurer les taux de réaction produits par de petits échantillons. Les mesures sont effectuées au centre du cœur, sans filtre de cadmium, dans un spectre très riche en neutrons épithermiques. De la section efficace effective mesurée on déduit, en retranchant la partie thermique, la valeur de l'intégrale de résonance en étalonnant par rapport à l'or. Les échantillons utilisés sont en solutions ou en plaques. Pour déduire les valeurs à la dilution infinie ou à l'épaisseur nulle, on extrapole les résultats obtenus pour différentes concentrations ou épaisseurs, en adoptant les facteurs d'autoprotection calculés à l'aide du programme ZUT, et en vérifiant qu'ils confirment les résultats expérimentaux. Les valeurs des intégrales de résonance mesurées, non compris la partie en 1/V, sont données.

Pour les corps dont les paramètres de résonance sont connus avec une précision suffisante, les valeurs mesurées sont comparées à celles qui ont été calculées ou mesurées par différents auteurs.

INTRODUCTION

La méthode d'oscillation permet de mesurer les taux de réaction et d'en déduire des sections efficaces effectives. Pour tirer le maximum d'efficacité de cette méthode, on en a développé des applications originales afin d'obtenir, suivant la nature du matériau et la section efficace à mesurer des conditions de mesure permettant d'atteindre la précision maximale.

La méthode d'oscillation de phase a été utilisée auprès du réacteur ZOE pour mesurer les sections efficaces d'absorption thermique de corps peu capturants mais très diffusants. Elle permet d'effectuer des mesures précises dans un spectre bien thermalisé et atténue de façon très importante et d'un facteur connu l'effet de la diffusion.

La méthode classique d'oscillation d'amplitude a été utilisée à MINERVE pour déterminer les intégrales de résonance de capture à partir des sections efficaces effectives. Les mesures sont effectuées au centre du cœur, sans filtre de cadmium, dans un spectre très riche en neutrons épithermiques. De la section efficace effective mesurée, on déduit la valeur de l'intégrale de résonance en retranchant la partie thermique.

A. MESURE DES SECTIONS EFFICACES THERMIQUES D'ABSORPTION PAR LA METHODE D'OSCILLATION DE PHASE

La méthode d'oscillation de phase a été mise au point sur ZOE il y a plusieurs années par Breton [1]. Un échantillon oscillant dans un réacteur produit simultanément une modulation de flux s'étendant à tout le réacteur et une perturbation qui n'est sensible que localement. Pour une chambre d'ionisation placée judicieusement, on montre que le déphasage entre les signaux obtenus avec deux échantillons d'absorption différente est proportionnel à leur différence de capture. Cette méthode possède la propriété d'affaiblir l'influence de la diffusion d'un facteur important qui peut être mesuré avec précision.

1. Principe de la méthode

Pour des conditions d'oscillation bien définies, amplitude du mouvement mécanique, position moyenne d'oscillation, dimensions d'échantillon, position de la chambre de détection, le déphasage α entre le signal résultant recueilli sur une chambre d'ionisation placée au voisinage de la trajectoire de l'échantillon et le mouvement mécanique est fonction des surfaces de capture S_c et de diffusion S_d de l'échantillon et de son support. On obtient la relation fondamentale

$$\alpha = f\left(\frac{S_c}{S_d}\right) \qquad (1)$$

Sur un support de graphite ayant des surfaces de capture S_c et de diffusion S_d, on place l'échantillon à mesurer. S'il produit des variations faibles de capture ΔS_c et de diffusion ΔS_d par rapport à celles du support, la différence de phase des signaux résultants produits par le support seul

α_0 et par le support chargé de l'échantillon à mesurer α peut s'écrire

$$\Delta\alpha = \alpha - \alpha_0 = f\left(\frac{S_c + \Delta S_c}{S_d + \Delta S_d}\right) - f\left(\frac{S_c}{S_d}\right) \cong f'\left(\frac{S_c}{S_d}\right) \cdot \Delta\left(\frac{S_c}{S_d}\right) \quad (2)$$

$$= a\left[\Delta S_c - \frac{S_c}{S_d}\Delta S_d\right] \quad (3)$$

Le deuxième terme du second membre de la relation (3) représente la correction de diffusion. Avec un support de graphite, le rapport S_c/S_d est voisin de 10^{-3}, ce qui rend cette correction très faible. On a vérifié expérimentalement cette relation avec un échantillon de béryllium sur lequel on a ajouté des cales de graphite.

On détermine le coefficient a qui relie la variation de phase à la capture apparente de l'échantillon étudié à l'aide d'un étalon de bore de diffusion négligeable.

En introduisant dans la relation (3) le nombre de noyaux N de l'échantillon et sa section efficace de diffusion σ_d, on en déduit sa capture apparente

$$\sigma_{ap} = \frac{\Delta\alpha}{aN} = \sigma_c - \frac{S_c}{S_d}\sigma_d \quad (4)$$

d'où

$$\sigma_c = \frac{\Delta\alpha}{aN} + \frac{S_c}{S_d}\sigma_d \quad (5)$$

2. Réalisation expérimentale

Le support est une brique de graphite qui possède une cavité dans laquelle on dispose, soit l'échantillon à mesurer, soit l'étalon, et qui est animée d'un mouvement sinusoïdal dans un canal tangentiel du réacteur ZOE. Le signal est recueilli sur une chambre d'ionisation placée au voisinage de la trajectoire de l'échantillon et envoyé sur un ensemble analyseur analogique donnant son amplitude et sa phase par rapport au mouvement mécanique.

L'étalonnage en capture est effectué à l'aide d'une solution d'acide borique dans l'eau lourde, spécialement fabriquée et dosée par le Bureau central de mesures nucléaires de l'EURATOM. Le bore provient du standard européen servant de référence, dont la teneur isotopique est

$$e = 19,81 \pm 0,02\% \ [2]$$

Pour des neutrons ayant une vitesse de 2200 m/s, en adoptant pour la section efficace microscopique de capture du bore-10

$$\sigma_{B\text{-}10} = 3838 \pm 10 \text{ b } [3]$$

on obtient pour le bore naturel

$$\sigma_0 = 760 \pm 2 \text{ b}$$

3. Mesure des sections efficaces de capture

Pour obtenir la section de capture à 2200 m/s à partir de la section efficace apparente déterminée par la relation (4), il faut effectuer un certain nombre de corrections.

a) Correction de diffusion

D'après la relation (5) elle est égale à $(S_c/S_d)\sigma_d$. Le rapport S_c/S_d, pour le support de graphite utilisé, est égal à $0,83 \cdot 10^{-3}$, ce qui rend cette correction très faible.

b) Correction des captures résonnantes

Le spectre régnant dans la brique support, au point de mesure, a été déterminé expérimentalement par une série de rapports cadmium d'alliage plomb-indium, qui ont donné avec les notations de Wescott [4]

$$r = 0,008 \pm 0,001$$

Les corrections dues aux captures résonnantes sont donc très petites pour la plupart des matériaux courants qui possèdent une intégrale de résonance faible.

c) Correction d'auto-absorption thermique

Le facteur d'auto-absorption F peut se décomposer en deux termes:

$$F = G_0 H \tag{6}$$

Le coefficient G_0 a été calculé en appliquant la théorie d'Amouyal-Benoist-Horowitz [5] qui tient compte de la diffusion.

$$G_0 = (1 - P_c)\left[1 + P_c\left(1 - \frac{\Sigma_0}{\Sigma_t}\right)\right] \tag{7}$$

Σ_t, Σ_c : Sections efficaces macroscopiques totale et de capture de l'échantillon.

P_c : Probabilité de collision donnée par les tables de Case, Hoffmann et Placzek [6] pour des plaques, des cylindres ou des sphères. Cette formule a été vérifiée expérimentalement dans le cas des oscillations sur ZOE avec des échantillons de fer, de cuivre et de cobalt de différentes géométries.

Les mesures étant effectuées dans du graphite, on peut négliger les effets de la dépression de flux et adopter $H = 1$.

d) Précision des mesures

Les principales sources d'erreurs sont les suivantes:

- L'erreur statistique de mesure, qui est déterminée à partir de plusieurs séries de mesure sur le même échantillon et comprend l'erreur due au coefficient d'étalonnage. Elle est en général inférieure à $\pm 0,2$ mm^2.

TABLEAU I. SECTIONS EFFICACES DE CAPTURE σ_0

Matériau	Valeurs mesurées σ_0 (b)	BNL (1960) [7] σ_0 (b)	BNL (1958) [7] σ_0 (b)	Rose (1958) [8,9] σ_0 (b)
Aluminium	$(229 \pm 3) \cdot 10^{-3}$	$(241 \pm 3) \cdot 10^{-3}$	$(230 \pm 5) \cdot 10^{-3}$	$(246 \pm 3) \cdot 10^{-3}$
Magnésium	$(64,2 \pm 1,5) \cdot 10^{-3}$	$(63 \pm 3) \cdot 10^{-3}$	$(69 \pm 2) \cdot 10^{-3}$	$(73 \pm 2) \cdot 10^{-3}$
Fer	$2,53 \pm 0,03$	$2,62 \pm 0,06$	$2,53 \pm 0,06$	$2,75 \pm 0,07$
Cuivre	$3,74 \pm 0,04$	$3,85 \pm 0,03$	$3,77 \pm 0,03$	$4,00 \pm 0,1$
Cobalt	$38,0 \pm 0,3$	$38,0 \pm 0,7$	$37,0 \pm 1,5$	$38,2 \pm 0,7$
Molybdène	$2,60 \pm 0,05$	$2,60 \pm 0,05$	$2,70 \pm 0,04$	$2,70 \pm 0,04$
Zirconium	$(182 \pm 2) \cdot 10^{-3}$	$(180 \pm 4) \cdot 10^{-3}$	$(185 \pm 4) \cdot 10^{-3}$	$(190 \pm 4) \cdot 10^{-3}$

- L'erreur sur l'étalon de capture, qui provient en particulier de l'imprécision sur la teneur en bore de la solution étalon. Elle est égale à $\pm 0,1\%$.
- L'erreur sur la correction de diffusion, qui provient presque uniquement de la section efficace de diffusion utilisée.
- L'erreur sur la correction d'auto-absorption, qui n'est due qu'à l'incertitude de la méthode de calcul de G_0. Cette dernière ayant été vérifiée expérimentalement, la contribution de cette erreur sur le résultat final est faible.

4. Résultats

Les échantillons des différents métaux mesurés se présentent en général sous forme de plaques d'environ 15 cm de longueur et 4 cm de largeur, dont l'épaisseur est variable suivant la capture du matériau de façon à réduire au minimum la correction d'auto-absorption. La plupart des échantillons sont usinés à partir de matériaux très purs et soigneusement analysés. Pour le zirconium, on a utilisé plusieurs échantillons de même géométrie mais à teneur en hafnium croissante. En effet, ce matériau ne peut pas être obtenu parfaitement pur et contient toujours des traces de hafnium et de terres rares. Ces impuretés étant difficilement dosables avec précision, on a préféré extrapoler les résultats expérimentaux à la teneur nulle en hafnium.

Les valeurs obtenues sont présentées dans le tableau I et comparées à d'autres valeurs publiées. Il faut remarquer que, pour certains matériaux très diffusants (Mg et Zr), une partie importante de l'erreur provient de l'incertitude sur les sections efficaces de diffusion. Une meilleure connaissance de ces valeurs entraînerait une amélioration sensible de la précision sur les sections d'absorption.

B. MESURE DES INTEGRALES DE RESONANCE D'ABSORPTION PAR LA METHODE D'OSCILLATION

Les mesures d'intégrales de résonance ont fait l'objet, il y a plusieurs années, de nombreuses publications [9-11], car c'était le seul moyen de les connaître avec une précision suffisante. Depuis, grâce aux progrès des mesures des sections efficaces différentielles et des méthodes de calcul, il est apparu que l'on pouvait obtenir une meilleure précision en utilisant les paramètres de résonance. Cependant, ils conduisent dans certains cas à des incertitudes qui peuvent atteindre 20% sur l'intégrale de résonance calculée, principalement à cause de la mauvaise résolution aux hautes énergies, de l'incertitude sur la valeur du facteur statistique g, des résonances non résolues et aussi des effets d'ombre de résonances voisines. Le but de cette étude est donc de comparer les valeurs des intégrales de résonance pour la dilution infinie, mesurées dans un spectre en 1/E, à celles calculées pour le même spectre à partir des paramètres, et ainsi de contrôler la validité des sections efficaces différentielles publiées.

Plusieurs méthodes ont déjà été utilisées pour mesurer les intégrales de résonance d'absorption et d'activation:

- Mesure de la variation de réactivité produite par l'oscillation des échantillons à l'intérieur d'un tube de cadmium placé au centre d'un réacteur.
- Mesure du taux d'activation des échantillons nus et sous cadmium.
- Mesure de la variation de réactivité produite par l'oscillation des échantillons dans des spectres de neutrons ayant des proportions différentes de neutrons épithermiques.

Les difficultés inhérentes aux deux premières méthodes sont nombreuses; il faut en particulier tenir compte de la distorsion du spectre produite par le cadmium à l'endroit de la mesure et définir la valeur de l'énergie correspondant à la coupure effective du cadmium. Les méthodes par activation ne peuvent être utilisées que pour les matériaux qui, par irradiation aux neutrons, donnent des isotopes radioactifs ayant une période de décroissance convenable et ne permettent que la mesure des intégrales de résonance d'activation.

La dernière méthode, qui permet d'éviter l'utilisation du filtre de cadmium, est particulièrement adaptée au cas où l'intégrale de résonance est faible vis-à-vis de la capture thermique car, pour ces matériaux, l'incertitude sur la valeur de la coupure effective du cadmium entraîne des erreurs importantes qui sont très souvent à l'origine du désaccord entre les valeurs mesurées par différents auteurs.

Pour certains matériaux, la correction de diffusion nécessite un soin particulier, car elle intervient directement sur la valeur du signal mesuré.

1. Définition des sections efficaces effectives et des intégrales de résonance

Nous exprimons le spectre en adoptant le formalisme d'Horowitz-Tretiakoff pour le cas du milieu homogène [12, 13] dans lequel la densité

de neutrons est donnée par

$$N(x) = M(x) + 2\, r_H\, E(x) \tag{8}$$

x : Vitesse réduite égale à V/V_{T_0} où $V_{T_0} = \sqrt{2KT_0}$ est la vitesse la plus probable d'un neutron en équilibre thermique avec le milieu.

M(x): Maxwellienne correspondant à la température ambiante T normalisée à l'unité: $\int_0^\infty M(x)\,dx \equiv 1$.

E(x): Fonction d'intégrale nulle se comportant à l'infini comme $1/x^2$: $\int_0^\infty E(x)\,dx \equiv 0$.

r_H : indice qui caractérise l'importance relative du spectre épithermique.

La section efficace effective est définie par la relation

$$\hat{\sigma} = \frac{\int_0^\infty \sigma(x)\, N(x)\, x\, dx}{x_0 \int_0^\infty N(x)\, dx} \tag{9}$$

qui peut s'écrire

$$\hat{\sigma} = \int_0^\infty \sigma_0 N(x)\,dx + \int_0^{x_c} \left[\frac{\sigma(x)}{x_0} - \frac{\sigma_0}{x}\right] N(x)\,x\,dx + \sqrt{\frac{T}{T_0}} \int_{x_c}^\infty \left[\sigma(x) - \sigma_0 \frac{x_0}{x}\right] N(x)\,x\,dx \tag{10}$$

x_c: vitesse réduite correspondant à l'énergie limite E_c.

$\sigma_0 = \sigma(E_0)$ avec $E_0 = 0,025$ eV.

La première intégrale est égale à σ_0 et la deuxième représente l'écart de la section efficace par rapport à une loi en $1/v$ dans la partie du spectre inférieure à E_c qui est constituée par la Maxwellienne. On associe ces deux intégrales en un seul terme égal à $g\sigma_0$.

Pour les énergies supérieures à quelques eV, N(x) est très voisin de $2r_H/x^2$, ce qui nous permet d'écrire la dernière intégrale de l'expression (10)

$$\sqrt{\frac{T}{T_0}} \int_{E_c}^\infty \left[\sigma(x) - \sigma_0 \frac{x_0}{x}\right] 2r_H \frac{dx}{x} = r_H \sqrt{\frac{T}{T_0}} \int_{E_c}^\infty \left[\sigma(E) - \sigma_0 \sqrt{\frac{E_0}{E}}\right] \frac{dE}{E} = \alpha I \tag{11}$$

avec

$$\alpha = r_H \sqrt{\frac{T}{T_0}} \tag{12}$$

Pour tous les corps que nous avons étudiés, les résonances sont situées au-delà de quelques eV et nous pouvons écrire leur section efficace effective sous la forme

$$\hat{\sigma} = g\sigma_0 + \alpha I \tag{13}$$

avec

$$I = \int_{0,55\,eV}^\infty \left[\sigma(E) - \sigma_0 \sqrt{\frac{E_0}{E}}\right] \frac{dE}{E} \tag{14}$$

I est l'intégrale de résonance au-dessus de la partie en 1/v; nous désignerons par I_R l'intégrale de résonance totale

$$I_R = \int_{0,55\ eV}^{\infty} \sigma(E) \frac{dE}{E} \qquad (15)$$

Ces deux définitions (14) et (15) se rapportent à la dilution infinie.

Remarque: On fixe la limite inférieure à 0,55 eV suivant les recommandations de l'EANDC, ce qui conduit à ne considérer que les résonances dont l'aile est éteinte à cette énergie, donc pratiquement à ne prendre en compte que celles qui sont supérieures à 1 eV. Dans ce cas la correction, pour tenir compte de la déviation du spectre suivant la loi en 1/E dans la zone de thermalisation, est faible, puisqu'elle ne porte que sur l'aile de la résonance.

2. Principe de la méthode

L'oscillation dans le réacteur en un point où la densité est N(x) d'un échantillon contenant N noyaux produit une variation de réactivité Δk proportionnelle au taux de réaction

$$R = N \int_0^{\infty} \sigma(x)\, N(x)\, x\, dx = N x_0 \hat{\sigma} \qquad (16)$$

Dans une première approximation, en ne tenant compte que de l'effet de capture des neutrons et en admettant que l'importance moyenne sur la réactivité des neutrons absorbés est indépendante de l'énergie, on peut écrire que la variation Δk est de la forme

$$\Delta k = QN\hat{\sigma} = QN(G_0 g \sigma_0 + G_r \alpha I) \qquad (17)$$

G_0 et G_r : Coefficients d'auto-absorption thermique et d'autoprotection résonnante.

Q : Constante déterminée par étalonnage avec un corps de référence, le bore, dont la section efficace suit une loi en 1/V.

L'extrapolation de la courbe $\Delta k/QN$ en fonction de l'épaisseur ou de la concentration pour une dilution infinie permet d'obtenir la section efficace effective pour laquelle $G_0 = G_r = 1$.

La valeur de l'intégrale de résonance s'écrit alors

$$I = \frac{\hat{\sigma} - g\sigma_0}{\alpha} \qquad (18)$$

Les sections efficaces thermiques σ_0 sont choisies parmi les meilleures valeurs publiées et la constante α qui caractérise la dureté du spectre est déterminée expérimentalement par étalonnage avec des échantillons d'or.

3. Réalisation expérimentale

Les mesures ont été effectuées au centre du réacteur MINERVE, pile piscine, dont le cœur, constitué d'éléments combustibles d'uranium en-

richi à 90%, est réfléchi sur ses faces latérales par des blocs de graphite. Deux séries de mesures ont été effectuées, l'une avec des échantillons en solution dans l'eau légère, l'autre avec des échantillons sous forme de plaques se déplaçant dans un canal d'air au centre du cœur.

Les configurations utilisées sont choisies pour obtenir des conditions de mesure optimales, en particulier une grande sensibilité et un spectre riche en neutrons épithermiques.

Un tube porte-échantillon se déplace dans le canal central (mouvement carré avec une période de 10 s et une course totale de 600 mm). Les solutions et les dépôts utilisés ont été fabriqués et dosés par le Bureau central de mesures nucléaires de l'EURATOM.

L'oscillation de l'échantillon produit une variation de réactivité qui se traduit par une modulation du niveau de puissance de la pile. Le signal modulé recueilli sur une chambre d'ionisation placée dans le réflecteur est envoyé sur un analyseur analogique d'harmoniques qui donne l'amplitude et la phase du fondamental du signal.

4. Mesure des intégrales de résonance

a) Etalonnage avec le bore

L'étalonnage est effectué avec des étalons de bore se présentant sous la forme de solutions d'acide borique dans l'eau légère ou de dépôts sur aluminium. La variation de réactivité produite par un échantillon contenant N noyaux de bore est égale à

$$\Delta k = QNG_0\sigma_0 \tag{19}$$

G_0: facteur d'auto-absorption fonction de la concentration ou de l'épaisseur de l'échantillon.

σ_0 : 760 b pour le bore standard EURATOM.

Le coefficient Q est déterminé en extrapolant les résultats expérimentaux à une dilution infinie suivant une exponentielle. La figure 1 représente $QG_0 = \Delta k/N\sigma_0$ en fonction de la capture par unité de surface pour les dépôts de bore sur aluminium.

b) Facteur d'auto-absorption

On détermine le facteur G_0 à partir des résultats expérimentaux obtenus avec les échantillons de bore. Pratiquement on obtient

$$G_0 = 1 - \gamma\epsilon\sigma_0 \tag{20}$$

Les valeurs expérimentales sont en accord avec la formule d'Amouyal-Benoist-Horowitz.

c) Caractéristique du spectre

En adoptant l'or comme étalon, on peut déterminer α à partir de la relation (18) par

$$\alpha = \frac{\sigma_{or} - g\sigma_{0_{or}}}{I_{or}} \tag{21}$$

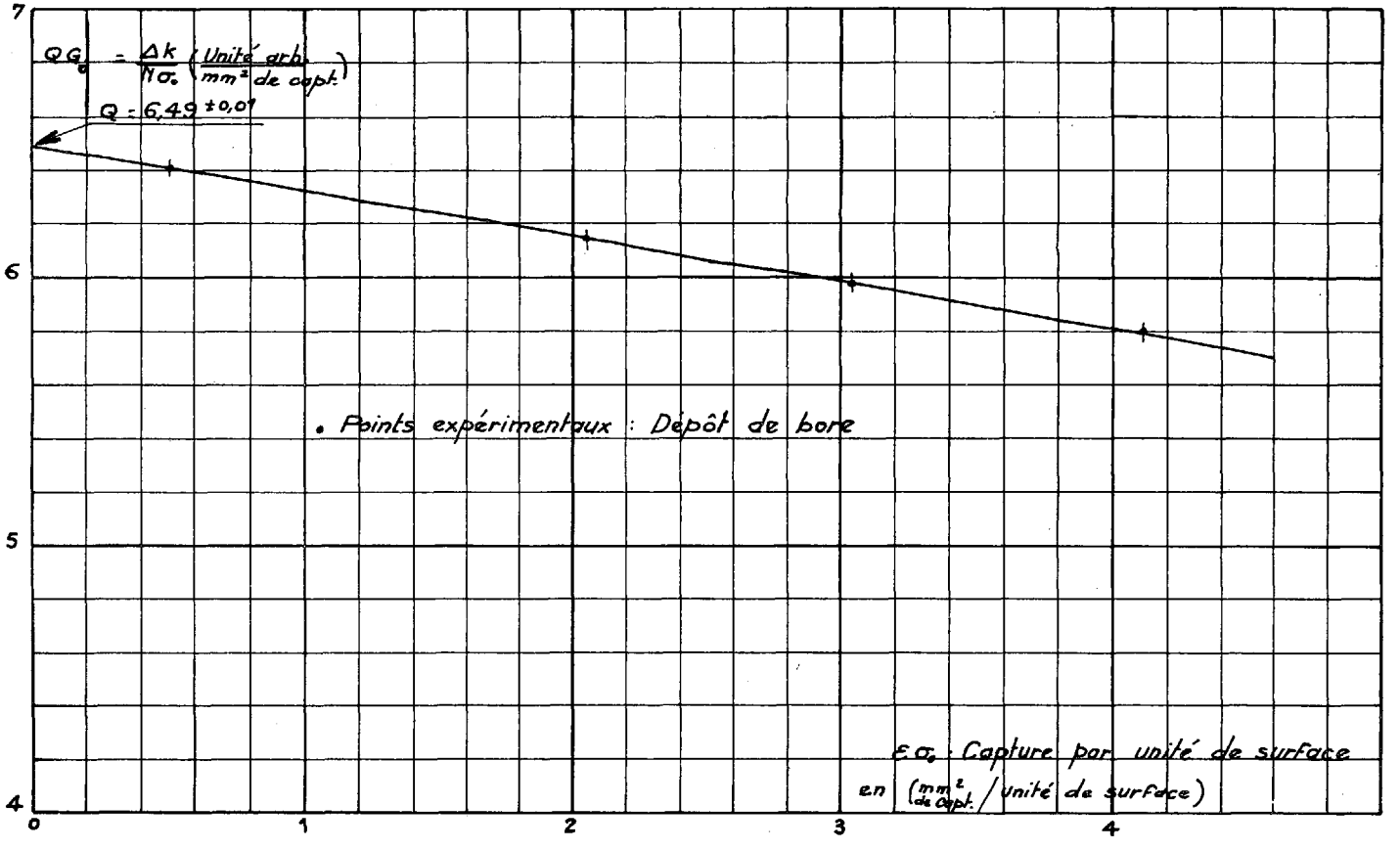

FIG.1. Etalonnage avec le bore

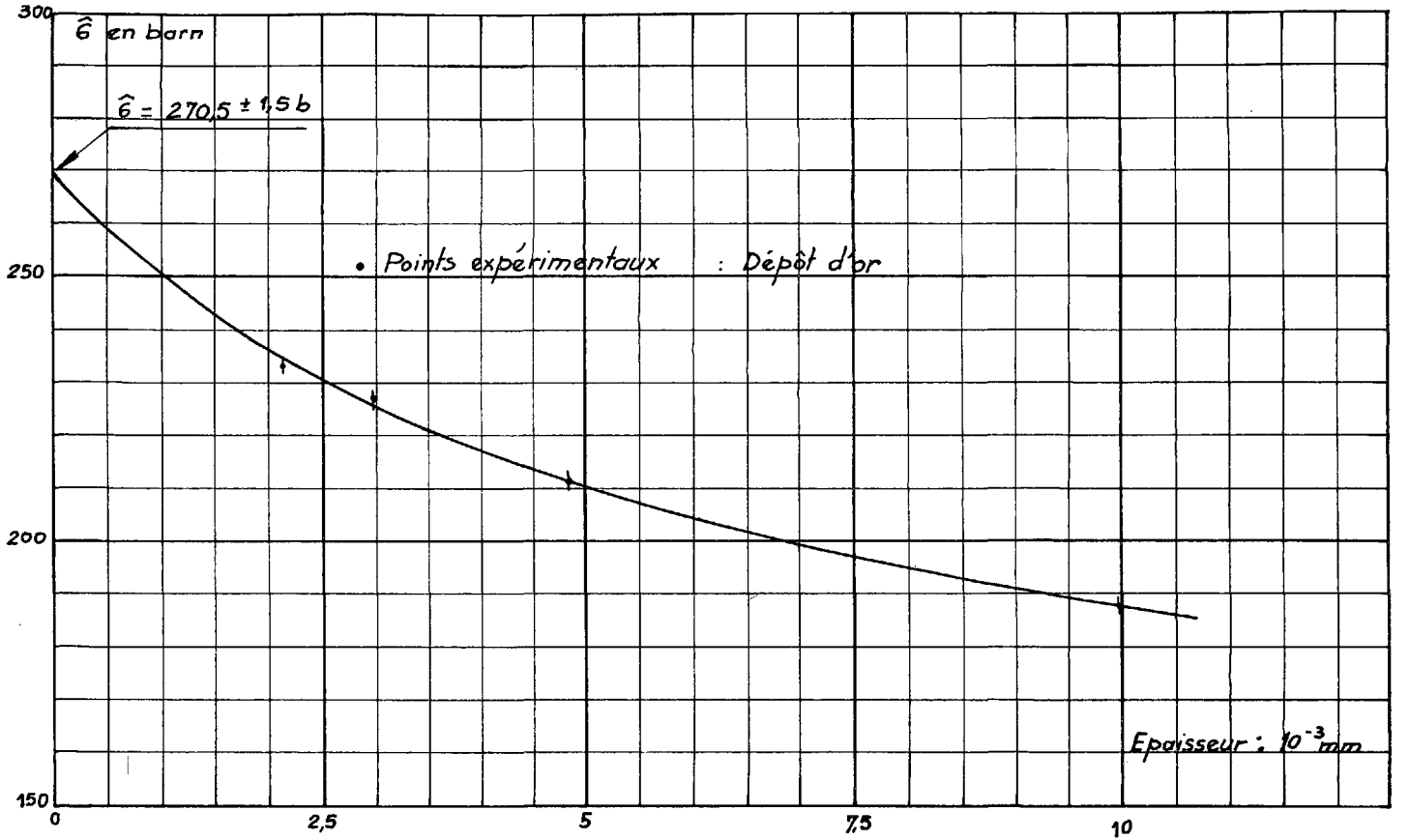

FIG. 2. Section efficace effective de l'or

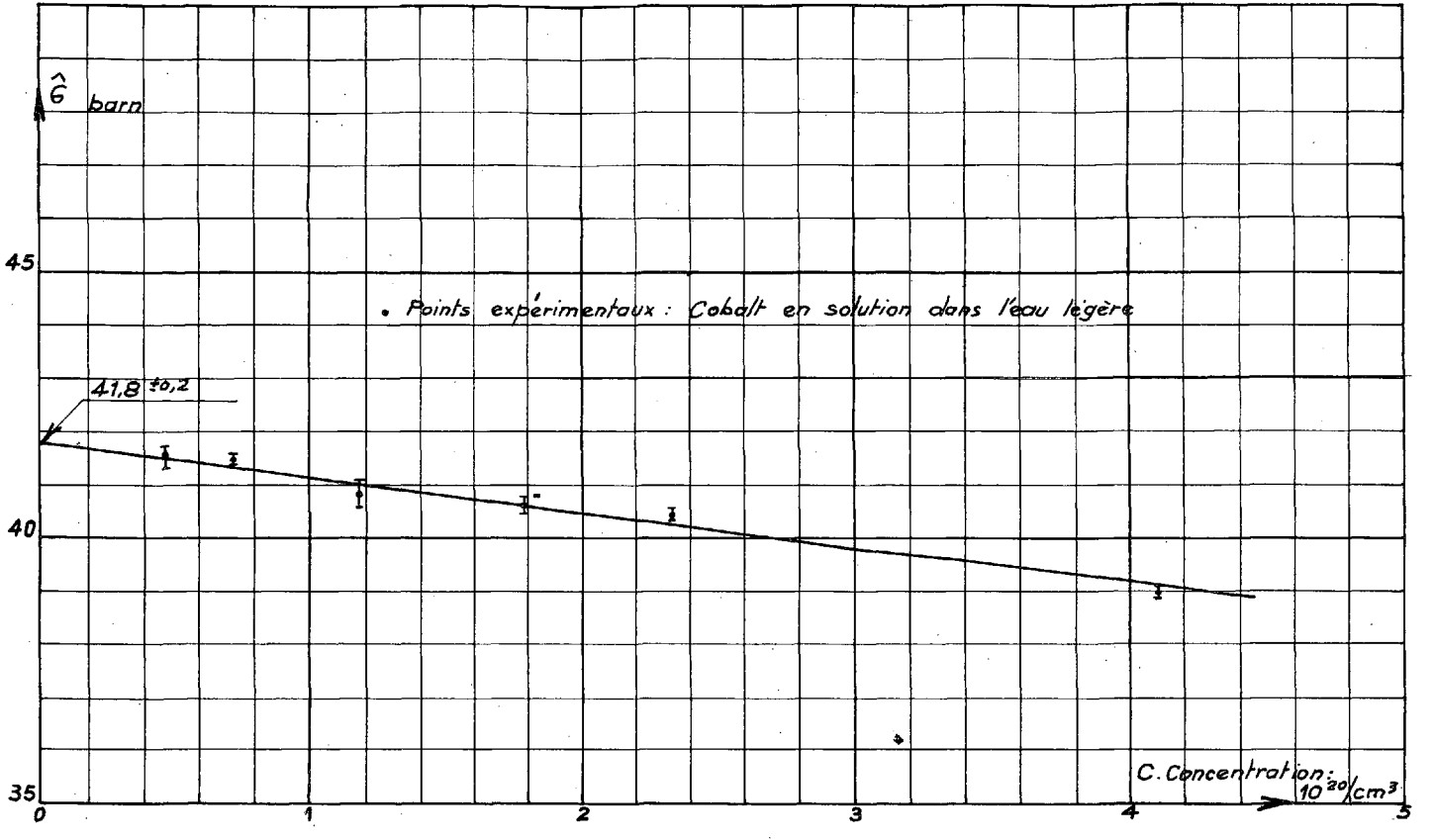

FIG.3. Section efficace effective du cobalt

On utilise des échantillons d'or, en solution ou en dépôt, pour lesquels on adopte $\sigma_0 = 98,9$ b [14] et $I = 1540$ b, calculés à partir des paramètres de résonance [15].

On a obtenu respectivement $\alpha_s = (82,7 \pm 0,6)10^{-3}$ et $\alpha_p = (111 \pm 1)10^{-3}$ pour les configurations dans lesquelles on a mesuré les échantillons sous forme de solutions et de plaques.

d) Extrapolation à la dilution infinie

On utilise plusieurs échantillons d'un même matériau d'épaisseurs ou de concentrations différentes, pour lesquels on mesure la section efficace effective $\hat{\sigma}$ et on extrapole ces valeurs pour en déduire celle correspondant à la dilution infinie en adoptant une loi exponentielle qu'on ajuste par une méthode de moindres carrés. On vérifie que cette loi est identique à celle que l'on obtient en calculant les facteurs d'autoprotection.

L'intégrale de résonance effective est calculée pour chaque épaisseur à partir des paramètres en utilisant le code ZUT écrit suivant la méthode de calcul proposée par Nordheim et al. [16].

Sur la figure 2 on a porté la section efficace effective de l'or sous forme de dépôt en fonction de son épaisseur, qui a servi à déterminer α, et sur la figure 3 celle du cobalt en solution en fonction de sa concentration.

e) Effet des fonctions d'importance

La détermination de la section efficace effective suppose que l'importance des neutrons est identique pour toutes les énergies auxquelles ils sont capturés. Une étude [17] a montré que le rapport des importances des neutrons capturés à l'énergie de résonance E_r et à l'énergie thermique est voisin de l'unité jusqu'à 10 eV et décroît ensuite légèrement pour atteindre 0,96 à 300 eV.

f) Correction de l'effet de la diffusion

Lorsque l'on introduit un échantillon diffusant dans un réacteur, la variation de réactivité produite par les neutrons diffusés est proportionnelle à la section de diffusion et au gradient de flux régnant au point de mesure. Pour un corps absorbant et diffusant on a donc

$$\sigma_m = \sigma_0 - \beta \sigma_d \qquad (22)$$

β est déterminé expérimentalement avec des échantillons de graphite et de magnésium.

g) Précision des mesures

Les erreurs entachant les résultats proviennent des erreurs statistiques des mesures et de l'incertitude sur la valeur de la section efficace thermique à utiliser.

Les erreurs sur les sections efficaces effectives correspondant à la dilution infinie sont estimées en fonction du nombre d'échantillons utilisés et de l'incertitude provenant de l'extrapolation suivant la courbe théorique.

La concentration des échantillons en solution est connue avec une précision suffisante; pour certains d'entre eux, la teneur en impuretés peut introduire une erreur dont on a tenu compte.

Les erreurs dues aux étalonnages sont négligeables, ainsi que l'incertitude sur la correction de diffusion, sauf dans le cas de corps d'absorption faible et de diffusion importante comme le zirconium.

TABLEAU II. ECHANTILLONS SOUS FORME DE SOLUTIONS

Matériau	$\hat{\sigma}$ (b)	σ_0 (b)	I mesurée (b)	I calculée (b)
Indium	469 ±1,5	193,3±1,2	3200±70	3050 ±50
Hafnium	277 ±1	101,4±0,5	2080±50	1900 ±100
Argent	120,4±0,5	64,8±0,2	670±20	730 ±50
Cobalt	41,8±0,2	37,6±0,3	53±5	50,3±5
Césium	65,3±0,1	28 ±1	450±15	380 ±60
Thorium	14,70±0,35	7,5±0,1	87±4	87 ±6

h) Calcul des intégrales de résonance à partir des paramètres

Pour chaque corps mesuré, nous avons calculé l'intégrale de résonance à partir des paramètres publiés en adoptant la formule de Breit-Wigner, qui s'écrit avec les notations habituelles

$$\sigma_a(E) = \pi\lambda_r^2 \, g \sqrt{\frac{E_r}{E}} \, \frac{\Gamma_n \Gamma_\gamma}{(E-E_r)^2 + (\Gamma/2)^2} \qquad (23)$$

en tenant compte de la contribution des résonances non résolues.

5. Résultats

On donne les résultats obtenus avec des solutions dans le tableau II et avec des plaques dans le tableau III. Pour chaque matériau on indique

- la section efficace effective extrapolée à la dilution infinie corrigée des impuretés et éventuellement des effets de diffusion,
- la section efficace d'absorption à 2200 m/s adoptée,
- la valeur mesurée de l'intégrale de résonance d'absorption I correspondant à la teneur naturelle de l'élément pour la dilution infinie, rapportée au spectre de référence en 1/E et ne comprenant que l'excès sur la partie en 1/v,
- la valeur de l'intégrale de résonance calculée à partir des paramètres.

TABLEAU III. ECHANTILLONS SOUS FORME DE PLAQUES

Matériau	$\hat{\sigma}$ (b)	σ_0 (b)	I mesurée (b)	I calculée (b)
Manganèse	14,34 ± 0,06	13,2 ± 0,1	10,5 ± 1	10,2
Fer	2,69 ± 0,02	2,57 ± 0,03	1,1 ± 0,3	-
Cobalt	43,1 ± 0,3	37,6 ± 0,3	50,5 ± 4	50,3 ± 5
Nickel	4,71 ± 0,02	4,60 ± 0,1	1,0 ± 0,4	-
Cuivre	4,00 ± 0,02	3,76 ± 0,03	2,2 ± 0,3	-
Zirconium	0,298 ± 0,015	0,182 ± 0,002	1,10 ± 0,15	1,1 ± 0,1
Molybdène	5,20 ± 0,10	2,65 ± 0,04	23,2 ± 1	23

Pour les matériaux dont les paramètres de résonance sont bien connus, on constate un très bon accord entre les valeurs mesurées et celles calculées à partir des paramètres.

CONCLUSION

La méthode d'oscillation de phase utilisée à ZOE permet de mesurer avec précision les sections efficaces de capture de corps peu capturants et très diffusants.

Grâce à la très grande sensibilité de MINERVE, des mesures très précises d'intégrales de résonance ont pu être effectuées, levant ainsi les désaccords qui existaient entre plusieurs auteurs, et montrant un bon accord avec les valeurs calculées.

REFERENCES

[1] BRETON, D., «Le contrôle des matériaux par la méthode d'oscillation à la pile de Châtillon», Actes Conf. int. util. EAFP 4 (1955) 145.

[2] DEBUS, G.H., The isotopic composition of samples, originating from different stocks of boron standatd, used in laboratories of EANDC-area as bases for neutron measurements, EANDC(E) 36L (1962).

[3] DERUYTER, A., DEBUS, G., LAUER, R., Measurement of the thermal neutron absorption cross section by a time of flight technique, EUR 12e (1962).

[4] WESCOTT, C.H., WALKER, W.H., ALEXANDER, T.K., "Effective cross sections and cadmium ratios for the neutron spectra of thermal reactors", Proc. 2nd UN Int. Conf. PUAE 16 (1958) 70.

[5] AMOUYAL, A., BENOIST, P., HOROWITZ, J., Nouvelle méthode de détermination du facteur d'utilisation thermique d'une cellule, J. nucl. Energy 6 (1957) 79.

[6] CASE, K.M., HOFFMANN, F., de, PLACZEK, G., Introduction to the Theory of Neutron Diffusion 1, Los Alamos Scientific Laboratory (1953) 174 p.

[7] HUGUES, P.S., SCHWARTZ, R.B., Neutron cross section, BNL 325 2nd ed. (1958), Suppl. No. 1 (1960).

[8] ROSE, H., COOPER, W.A., TATTERSALL, R.B., "The use of pile oscillator in thermal reactor problems", Proc. 2nd UN Int. Conf. PUAE 16 (1958) 34.

[9] TATTERSALL, R.B., ROSE, H. et al., Pile oscillator measurements of resonance integrals, J. nucl. Energy, Part A, React. Science 12 (1960) 32-46.
[10] MACKLIN, R.L., POMERANCE, H.S., "Resonance capture integrals", Proc. UN Int. Conf. PUAE 5 (1955) 96.
[11] KLIMENTOV, V.B., GRIAZEV, V.M., Measurement of neutron resonance absorption integrals, J. nucl. Energy 9 (1959) 20.
[12] HOROWITZ, J., TRETIAKOFF, O., Effective cross sections for thermal reactors, Oak Ridge Meeting, EANDC(E) 14 (1960).
[13] NAUDET, R., Calcul des sections efficaces effectives et thermalisation des neutrons, Note CEA n°438 (1963).
[14] TEUTSCH, H., MATEESCU, N., TIMIS, P., Nukleonik 4 4 (1962) 165.
[15] DESJARDINS, J.S., HAVENS, W.W., ROSEN, J.L., RAINWATER, J., Slow neutron resonance spectroscopy II, Ag, Av, Ta, WASH 1029 (1960).
[16] NORDHEIM, L.W., KUNCIR, G.H., A program of research and calculations of resonance absorption, GA 2527 (1961).
[17] BOUCHARD, J., Etude des fonctions d'importance dans un milieu modérateur et dans un élément combustible. Thèse doctorat 3e cycle, Faculté des Sciences d'ORSAY (1964).

DISCUSSION

J.R. SMITH: The manganese resonance integral is very important for corrections to measurements made by the manganese bath technique. Your value of 10.5 b is appreciably higher than values reported previously. It is shown to agree with a calculated value of 10.2 b. What parameters do you use to obtain this calculated value?

R. VIDAL: We used parameters from BNL-325 (1960 edition).

J.R. SMITH: These parameters are from analysis of the Argonne total cross-section measurements. Coté has since reanalysed the data and adjusted his parameters to agree with the measured integral of 8.0 b, considering this value to be more accurate than any he could derive from total cross-section measurements.

R. VIDAL: The average of the three most recent values for manganese - Louwrier (1966) 10.0 ± 1.9 b; Vidal (1966) 10.5 ± 1 b; Baumann (1964) 12.7 ± 1.8 b - lies much nearer to 11 b than to 8 b.

If the uncertainty involved in measuring manganese parameters is such that one can go from 10 b to 8 b, they should not be used as a reference.

G.H. KINCHIN: How confident are you that the epithermal spectrum of the reactor has 1/E dependence?

R. VIDAL: The reactor has enriched uranium as fuel and light water as moderator. The measurements are made at the centre of the core, in a zone where the slowing-down density is not disturbed by leakages or by resonant captures since the fuel is enriched to 90%.

Moreover, we have found no systematic deviation from the values calculated for a 1/E spectrum (taking into account the precision of the measurements) in the case of cobalt, the resonance energy of which is very high (close to 300 eV).

PILE NEUTRON CAPTURE CROSS-SECTIONS OF RARE EARTH ISOTOPES

R. DOBROZEMSKY, E. FORMANN, G. LUGMAIR,
F. PICHLMAYER, F.P. VIEHBÖCK, H. WOTKE
PHYSIKALISCHES INSTITUT,
REAKTORZENTRUM SEIBERSDORF,
SEIBERSDORF, AUSTRIA

Abstract

PILE NEUTRON CAPTURE CROSS-SECTIONS OF RARE EARTH ISOTOPES. Cross-sections were determined by measuring isotopic ratios before and after irradiation. The relative change of the isotopic ratio, and hence the accuracy of the result, is higher the better the enrichment of the isotope in question before irradiation. Since the enrichment of commercially available isotopes is insufficient, separated isotopes were prepared with the Seibersdorf inhomogeneous magnetic field isotope separator. Oxides were used as ion source charge material and vaporized by the chlorination method. To obtain optimum focusing conditions, the positions of the accelerating electrodes are adjustable during operation. The isotopes were collected in water-cooled graphite or aluminium pockets. After chemical processing, the isotopic ratios were determined by mass spectrometry. In a one-step separation, we obtained ^{156}Gd enriched to 99%, ^{154}Gd to 89%, ^{170}Yb to 96% and the heavier Yb isotopes to 99%. The samples were irradiated together with a cobalt flux monitor, with and without Co shielding. Afterwards the isotopic ratios were determined again. Cross-section data are given.

The most commonly used methods for the determination of pile neutron capture cross-sections are activation analysis [1, 2], the pile oscillator method [3, 4] and mass spectrometric analysis. The activation method is restricted to those isotopes which have radioactive daughters of convenient half-life. In the pile oscillator method small isotopic as well as chemical impurities with high cross-sections have

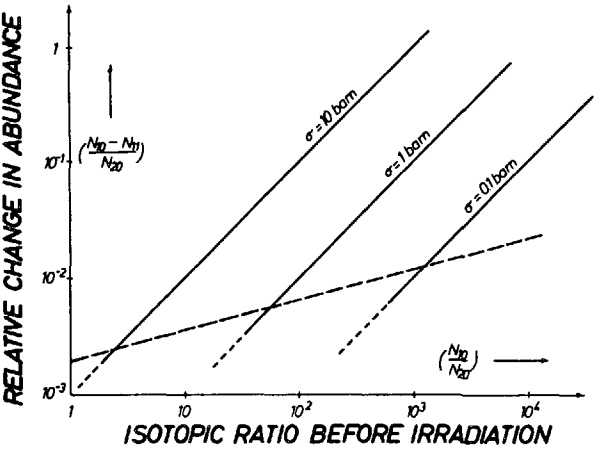

FIG.1. Relative change in abundance of the neighbouring isotope by irradiation

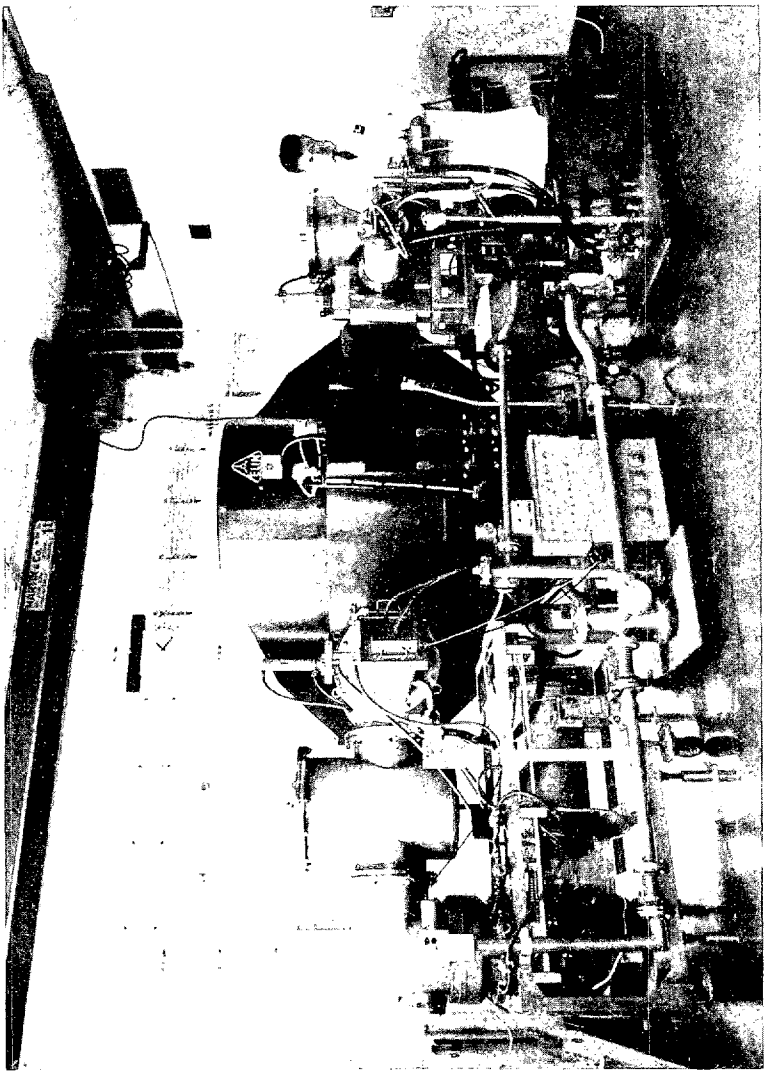

FIG. 2. Seibersdorf-type multi-purpose electromagentic isotope separator

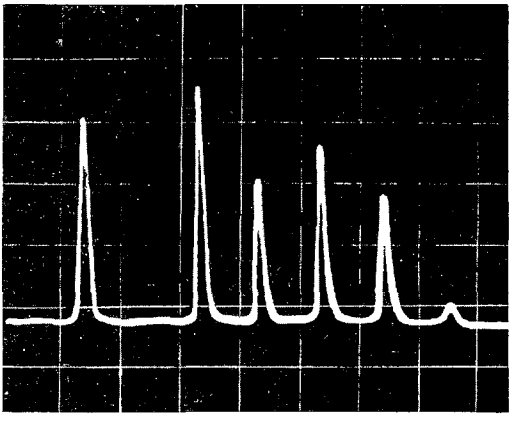

FIG.3. Mass spectrum of gadolinium

a deleterious influence on the reliability of the results. The principle of the mass spectrometric determination [5], which was used in our experiments, is to irradiate samples of known isotopic composition and to measure the change in the isotopic composition after the irradiation.

Since the accuracy of the measurement of an isotopic ratio is limited, it is obvious that an isotope, of which the cross-section has to be determined, should be enriched as highly as possible. For illustration, the change in the isotopic ratio for cross-sections of 10, 1 and 0.1 b and an integrated neutron flux of 10^{20} nvt is shown in Fig. 1. In this figure, for better clearness, only two isotopes (with the mass M and M+1) are considered. N_{10} represents the number of atoms of the isotope to be investigated (mass M) before and N_{11} the number after irradiation. N_{20} is the number of atoms of the neighbouring isotope (mass M+1) before irradiation. Furthermore the cross-section of the isotope with mass M+1 is taken to be zero.

N_{10}/N_{20} is the isotopic ratio before irradiation, N_{11}/N_{21} the isotopic ratio after irradiation and $(N_{10}-N_{11})/N_{20}$ the relative change in abundance

TABLE I. MASS SPECTROMETRIC ANALYSIS OF ENRICHED ^{174}Yb

Ytterbium	168	170	171	172	173	174	176
Natural abundance	0.14	3.03	14.31	21.82	16.13	31.84	12.73
Measurement No.1	-	-	-	0.015 ±0.001	0.054 ±0.003	99.898 ±0.003	0.033 ±0.001
Measurement No.2	-	-	-	0.020 ±0.002	0.060 ±0.004	99.887 ±0.006	0.033 ±0.002
Measurement No.3	-	-	-	0.018 ±0.002	0.052 ±0.002	99.896 ±0.006	0.034 ±0.001

TABLE IIa. ISOTOPIC COMPOSITION OF THE SAMPLES BEFORE AND AFTER IRRADIATION (GADOLINIUM)

Gadolinium	152	154	155	156	157	158	160
Natural abundance	0.20	2.15	14.73	20.47	15.68	24.87	21.90
^{154}Gd							
Before irradiation		91.647 ±0.012	3.601 ±0.006	2.034 ±0.008	0.994 ±0.007	1.041 ±0.003	0.683 ±0.004
Irradiated without Cd shielding		90.812 ±0.015	0.260 ±0.005	6.281 ±0.010	(a)	2.013 ±0.008	0.634 ±0.010
Irradiated with Cd shielding		91.430 ±0.010	3.730 ±0.005	2.108 ±0.003	0.998 ±0.007	1.090 ±0.004	0.644 ±0.007
^{156}Gd							
Before irradiation		0.017 ±0.002	0.148 ±0.004	99.195 ±0.008	0.349 ±0.006	0.209 ±0.002	0.082 ±0.003
Irradiated without Cd shielding		0.015 ±0.001	(a)	99.284 ±0.003	(a)	0.620 ±0.003	0.081 ±0.002
Irradiated with Cd shielding		0.017 ±0.001	0.145 ±0.004	99.153 ±0.008	0.405 ±0.007	0.209 ±0.003	0.071 ±0.004

(a) Below the detection limit of the mass spectrometer (< 0.001).

of the neighbouring isotope caused by irradiation. The limit for our mass spectrometric accuracy is shown by the dotted line, whereby the inaccuracy introduced by the determination of the neutron flux has been neglected. It is evident that the obtainable accuracy of the cross-section measurements is the better the higher the initial isotopic ratio N_{10}/N_{20}, that is, the higher the enrichment of the investigated isotope. Furthermore a high enrichment reduces disturbing effects from other neutron-induced reactions in the neighbouring isotopes. For gadolinium the corrections of the flux depression caused by the high cross-section isotopes can be made small. Since the isotopic enrichment of the commercially available isotopes is insufficient for our purposes, the required isotopes were separated with the Seibersdorf Multi-purpose Isotope Separator. This separator (Fig. 2) is an inhomogeneous magnetic sector field machine with a sector angle of 169°40', a logarithmic field gradient of n = 0.5 and a radius of the medium ion trajectory of r_m = 100 cm [6]. For the central ion beam, stigmatic second order focusing can be achieved. Because

TABLE IIb. ISOTOPIC COMPOSITION OF THE SAMPLES BEFORE AND AFTER IRRADIATION (YTTERBIUM)

Ytterbium	168	170	171	172	173	174	176
^{172}Yb							
Before irradiation			0.072 ±0.005	99.607 ±0.007	90.171 ±0.002	0.127 ±0.003	0.023 ±0.003
Irradiated without Cd shielding			0.071 ±0.002	99.543 ±0.004	0.205 ±0.002	0.148 ±0.003	0.033 ±0.002
Irradiated with Cd shielding			0.078 ±0.004	99.606 ±0.006	0.184 ±0.004	0.114 ±0.002	0.018 ±0.002
^{173}Yb							
Before irradiation			0.107 ±0.002	0.113 ±0.002	99.236 ±0.011	0.506 ±0.008	0.038 ±0.006
Irradiated without Cd shielding			0.103 ±0.002	0.135 ±0.003	98.791 ±0.004	0.931 ±0.002	0.040 ±0.001
Irradiated with Cd shielding			0.114 ±0.007	0.138 ±0.007	98.916 ±0.012	0.789 ±0.004	0.043 ±0.007

the aberrations for masses within ± 5% of the mass of the central beam are small, simultaneous collection of a wide mass range with extremely high isotopic purity is possible. This has been confirmed both by experiments and numerical calculation [7]. In our case the oxides of the rare earth elements were used as charge material for the ion source and the chlorination method [8] was employed. The ions were collected in a water-cooled pocket collector, from which they can easily be recovered. The isotopic purity of the separated isotopes depends essentially on the quality of the focus of the ion beams at the collector. Figure 3 shows the mass spectrum of gadolinium at a collector current of 1 mA.

After recovery and chemical refinement, the isotopic composition of the separated isotopes was measured with a 180° mass spectrometer. The reproducibility of the mass spectrometric results as well as the homogeneity of the enriched substances are demonstrated for ^{174}Yb in Table I, where three different measurements, spread over a period of a few months, are given.

A few milligrams of monoisotopic rare earth oxides ($^{154}Gd_2O_3$, $^{156}Gd_2O_3$, $^{172}Yb_2O_3$, $^{173}Yb_2O_3$) were irradiated in the ASTRA reactor (90% enriched uranium fuel, light-water moderator). To separate the influence of the epithermal neutrons two samples of each isotope were

TABLE III. CROSS-SECTIONS OF GADOLINIUM AND YTTERBIUM ISOTOPES

Work of Walker [12] σ-pile (barn)	This work		
	Preliminary experiment σ-pile (barn)	Present experiment σ-pile (barn)	Σ' (barn)
^{154}Gd 250±120	83 ±17[a]	105 ±11	303±31
^{156}Gd < 14	8.67±0.43 [13]	6.3± 1.0	78±21
^{170}Yb < 18	92 ±11[a]		
^{171}Yb 55±15	69 ± 8[a]		
^{172}Yb < 5	2.7 ± 0.9[a]	3.3± 0.4	18± 7
^{173}Yb 20± 10	40 ± 3[a]	41.4± 2.3	390±42

[a] integrated flux $5 \cdot 10^{19}$ nvt

irradiated under equivalent conditions; one without and one with cadmium shielding (0.5 mm thick). For the flux determination cobalt monitors were irradiated together with the rare earth isotope (with and without Cd shielding). For these monitors small pieces of wire (0.25-mm diameter) of cobalt aluminium alloy with 1.00± 0.03 wt. % Co were used.

The effective neutron capture cross-section of ^{59}Co was calculated [9-11] from the measured Cd ratio (= 7.88) for the given pile neutron spectrum as $\hat{\sigma}$ = 40.8± 1.4 b. All the pile neutron capture cross-sections reported in this paper correspond to this spectrum.

The samples were irradiated in a central position in the core at an integrated thermal neutron flux of 1.03×10^{20} nvt (± 5%). After irradiation, the isotopic composition of the irradiated samples was again analysed. Tables IIa and b show the isotopic composition of the samples before and after irradiation. From a comparison of the isotopic composition before and after irradiation, the cross-sections were computed. In the case of gadolinium the effects of the extremely high cross-sections of ^{155}Gd and ^{157}Gd were taken into consideration. The results are given in Table III. For comparison the values reported by Walker [12] are indicated in the first column. In the second column results of preliminary experiments are given. The pile neutron cross-sections and resonance integrals of the present work are listed in columns three and four. The higher accuracy in the present work is chiefly a result of the higher integrated neutron flux, a more accurate flux determination and, compared to Walker, the use of extremely high enriched isotopes. The uncertainties given in Table III were calculated from:

(a) The mass spectrometric errors (see Table II)
(b) The error in the ^{59}Co cross-section of ± 3.5% [10, 11]
(c) The error in the specific activity measurements of the monitors (± 3.5%)
(d) In the case of ^{154}Gd from the uncertainty in the flux depression correction (10%)

The measurements of cross-sections will be continued with dysprosium and erbium isotopes.

REFERENCES

[1] SEREN, L., FRIEDLANDER, H.N., TURKER, S.H., Phys.Rev. 72(1947) 888.
[2] YAFFE, L., HAWKINGS, R.C., MERRITT, W.F., CRAVEN, J.H., Phys.Rev. 82(1951) 553.
[3] ANDERSON, H.L., FERMI, E., WATTENBERG, A., WEIL, G.L., ZINN, W.H., Phys.Rev. 72 (1947) 16.
[4] POMERANCE, H., HOOVER, J.J., Phys.Rev. 73a (1948) 1265.
[5] DEMPSTER, A.J., Phys.Rev. 71 (1947) 829.
[6] VIEHBÖCK, F.P., Electromagnetic Separation of Radioactive Isotopes (HIGATSBERGER, M.J. and VIEHBÖCK, F.P., Eds.) Springer Verlag, Vienna (1961) 91.
[7] RÜDENAUER, F., VIEHBÖCK, F.P., Nucl.Instrum.Meth. 38 (1965).
[8] SIDENIUS, G., SKILBREID, O. in Electromagnetic Separation of Radioactive Isotopes (HIGATSBERGER, M.J. and VIEHBÖCK, Eds.) Springer Verlag, Vienna (1961).
[9] WESTCOTT, C.H., WALKER, W.H., ALEXANDER, T.K., Proc.2nd UN Int.Conf. PUAE 16 (1958) 70.
[10] BECKURTS, K.H., WIRTZ, K., Neutron Physics, Springer. Berlin (1964) 235.
[11] MEADOWS, J.H., WAHLEN, J.F., Nucl.Sci.Engng 9 (1961) 132.
[12] WALKER, W.H., "The relative abundances and pile neutron capture cross sections of the isotopes of Sm, Gd, Dy and Yb," Thesis, Mc.Master University, Hamilton, Canada.
[13] LUGMAIR, G., Die Bestimmung des Absorptionsquerschnittes von Gd-156 für Reaktorneutronen, Thesis, University of Vienna, Austria.

DISCUSSION

R. BLOCK: I should merely like to draw your attention to the fact that Professor White of the Rensselaer Polytechnic Institute has been carrying out similar thermal cross-section measurements and has, I believe, already measured capture in erbium isotopes.

MEASUREMENTS OF EFFECTIVE (RESONANCE-SHIELDED) NEUTRON CROSS-SECTIONS IN THE keV REGION

H. MIESSNER AND E. ARAI
KERNFORSCHUNGSZENTRUM KARLSRUHE,
FEDERAL REPUBLIC OF GERMANY

Abstract

MEASUREMENTS OF EFFECTIVE (RESONANCE-SHIELDED) NEUTRON CROSS-SECTIONS IN THE keV REGION. Effective capture and transport cross-sections which are fundamental for Doppler coefficient calculations in fast reactor design have been measured on lead, uranium and tantalum in the low keV region. In this energy range the resonances of the cross-sections of fertile and fissile materials and of most structural materials are separated but are still experimentally unresolved.

For the following measurements the pulsed method which has been proved in the thermal energy range for measuring capture and transport cross-sections is extended to the keV region. A short burst (1 or 10 ns) of nearly monoenergetic neutrons with energies below the threshold for inelastic scattering is injected into assemblies of lead, uranium and tantalum (parallelepipeds of 10 to 20 cm side length) and the decay of the neutron field in the block is measured. Moderation effects during the decay are small for materials as heavy as lead, uranium and tantalum and can be eliminated from each decay spectrum by a calculated moderation correction function F(t), which corrects the measured neutron density N(t) in the following way:

$$\frac{N(t)}{F(t)} \sim e^{-\alpha_0 t}$$

The corrected neutron density decays exponentially with a decay constant

$$\alpha_0 = v_0 \Sigma_a^{eff} + \frac{v_0}{3\Sigma_{tr}^{eff}} B^2 + C_T B^4$$

v_0 is the neutron injection velocity, B^2 the buckling of the assembly and C_T a correction term due to transport theory. α_0 is measured as a function of B^2 and in this way Σ_a^{eff} and Σ_{tr}^{eff} are obtained. The effective cross-sections are related to "infinite dilution" average values $\langle\Sigma_a\rangle$ and $\langle\Sigma_{tr}\rangle$ by self-shielding factors f_a and f_t, which have been calculated for many nuclides by Abagjan and others. The measured effective cross-sections are compared with self-shielding factors and $\langle\Sigma\rangle$ values measured by other authors. Further dilution effects in mixtures of a resonance absorber (^{238}U) and a potential scatterer (Pb) are investigated.

AN IMPROVED ANALYSIS OF SPHERE TRANSMISSION EXPERIMENTS FOR AVERAGE CAPTURE CROSS-SECTIONS

D. BOGART
LEWIS RESEARCH CENTER, NATIONAL AERONAUTICS AND SPACE ADMINISTRATION, CLEVELAND, OHIO, UNITED STATES OF AMERICA

Abstract

AN IMPROVED ANALYSIS OF SPHERE TRANSMISSION EXPERIMENTS FOR AVERAGE CAPTURE CROSS-SECTIONS. Sphere transmission experiments for measuring average capture cross-sections $\bar{\sigma}_C$ in the unresolved resonance region have been interpreted in the past by an analysis adapted from that of Bethe, which assumes capture and scattering cross-sections to be energy independent in the keV region. Because of the resonant nature of these cross-sections, relatively large resonance self-protection corrections have been applied to these results.

Monte Carlo calculations that account directly for energy-dependent cross-sections and multiple-scattering processes in the sphere experiments have provided significantly larger values of $\bar{\sigma}_C$ as a result of including effects of resonance scattering. The consequences of this are particularly important for Au, for which interpretation of the same experiments provides a value of $\bar{\sigma}_C$ at 24 keV of 635±50 mb by Monte Carlo analysis compared with 532±60 mb by Bethe analysis with a resonance self-protection correction. This difference can be attributed to the incorrect inclusion of an average resonance scattering cross-section in using the Bethe analysis.

The problem in applying the Bethe method when microscopic cross-sections are energy dependent may be reduced to the determination of an effective scattering cross-section. By comaring values of average capture cross-sections obtained from the Monte Carlo analyses with values obtained from the Bethe analyses for Ag, Sb, I, and Au, a suitable criterion was obtained. The use of the potential scattering cross-section as the effective scattering cross-section in the Bethe analysis was shown to provide results that were in reasonable agreement with the Monte Carlo results without the necessity for applying resonance self-protection corrections.

1. INTRODUCTION

The sphere transmission method has been used with Sb-Be neutron sources to measure absolute values of average capture cross-sections at 24±2 keV for many elements by SCHMITT and COOK [1], and BELANOVA et al. [2]. Average capture cross-sections are obtained from the values of transmission by a method described by BETHE et al. [3]. This calculational method accounts for the neutron multiple scattering processes prior to capture or escape from the sphere. However, a major limitation of the method is that the cross-sections are considered to be independent of neutron energy. At 24 keV, even for medium-weight and some heavy nuclei of interest, the average spacings of resonances far exceed average Doppler-broadened neutron widths so that resonances retain their characteristic shape, and cross-sections vary considerably with energy. For these nuclei, the average spacing of resonances is ~10 eV so that hundreds of levels are encompassed in the 4-keV spread of Sb-Be source neutrons. It is, therefore, necessary to take into account the effects of neutron resonances in interpreting the sphere transmission experiments.

In the Monte Carlo analysis, described by BOGART and SEMLER [4], the resonance cross-sections enter directly into the problem as primary input

data in addition to the assumed values of potential scattering cross-sections. In this way, values of sphere transmission as a function of assumed cross-sections are obtained. The calculations yield values of average p-wave capture and potential scattering cross-sections that preserve published values of total cross-sections and that satisfy the experimental values of sphere transmission.

It is shown that the use of the Bethe method as applied in the past [1,2,5] without the use of resonance self-protection corrections provides values of average capture section that underestimate significantly the values obtained by Monte Carlo analyses of the same sphere transmission

TABLE I. - SPHERICAL-SHELL TRANSMISSION DATA AT 24 keV AND AVERAGE s-WAVE PARAMETERS USED IN MONTE CARLO ANALYSES

Spherical-shell transmission						s-wave parameters				
Shell	Reference	Inner sphere radius (cm)	Outer sphere radius (cm)	Atom density, (atom/cm^3)	Transmission	Strength function, S_0	Average observed level spacing, $\bar{D}_{obs}$ (eV)	Average neutron width, $\bar{\Gamma}_n$ (eV)	Average radiation width, $\bar{\Gamma}_\gamma$ (eV)	Reference
Ag	[1,5][a]	4.30	7.46	0.0561×10^{-24}	0.694±0.004	$0.46\pm0.06\times10^{-4}$	9.4±0.8	0.265	0.150	[8]
Ag	[2][a]	2.05	3.05	.0581	.9222±0.0025	.46±0.06	9.4±0.8	.265	.150	[8]
Ag	[2][a]	2.05	5.05	.0581	.7277±0.0045	.46±0.06	9.4±0.8	.265	.150	[8]
Ag	[2][b]	2.05	5.05	.0561	.7146±0.0050	.46±0.06	9.4±0.8	.265	.150	[8]
Sb	[1,5][a]	2.54	7.62	.0328	.873±0.005	.32±0.03	8.0±0.5	.160	.125	(c)
I	[1,5][a]	4.96	11.21	.01227	.923±0.006	.62±0.09	13.5±0.5	.260	.107	[8]
Au-1	[1,5][a]	5.93	7.62	.0587	.876±0.005	1.50±0.20	16.8±0.5	.780	.170	[9]
Au-2	[1,5][a]	5.08	7.62	.0587	.800±0.004	1.50±0.20	16.8±0.5	.780	.170	[9]
Au	[2][a]	2.05	3.55	.0587	.8955±0.0023	1.50±0.20	16.8±0.5	.780	.170	[9]
Au	[2][b]	2.05	3.55	.0587	.8887±0.0027	1.50±0.20	16.8±0.5	.780	.170	[9]

[a]Transmission determined by long counter.

[b]Transmission determined by water bath.

[c]Private communication from J. B. Garg, Columbia University.

experiments. The application of resonance self-protection corrections [1,5] to the results obtained by the Bethe analysis considerably improves agreement with the Monte Carlo results for Ag, Sb, and I, but not for Au.

Both the Monte Carlo calculations and the Bethe method with resonance self-protection corrections require a priori knowledge of average s-wave resonance parameters as input data. For many isotopes, accurate statistical data are not available. In addition, the direct Monte Carlo analysis is laborious and perhaps is not a working method for general interpretation of sphere transmission experiments. Therefore, a method of interpretation of sphere transmission experiments that uses the Bethe analysis but avoids the necessity for applying resonance self-protection corrections is desirable. By comparing values of average capture cross-section obtained from the Monte Carlo analyses with values from the Bethe analyses for Ag, Sb, I and Au, a suitable criterion is presented.

2. MONTE CARLO ANALYSIS

Sphere transmission experiments have been analyzed by a Monte Carlo method [4] that employs resonance cross-sections that are based on published s-wave statistical data. Spherical shell dimensions and transmission data for spheres of Ag, Sb, I, and Au that have been analyzed [1,2] and the average s-wave resonance parameters at 24 keV that have been obtained from

published statistics from slow-neutron spectroscopy studies are presented in Table I. Cross-sections based on these parameters are employed in the Monte Carlo analysis and are generated from the Porter-Thomas distribution of reduced neutron widths as represented by 10 Doppler-broadened Breit-Wigner resonances and from the Wigner distribution of level spacings as represented by 10 values; each value is the average of a decile of the respective normalized populations. The scattering and capture cross-sections for each resonance are represented by 200 energy values at 1/2-eV intervals. The general operation of the Monte Carlo program is described in reference [4]. An isotropic point source of neutrons is assumed to be centrally located in the shell. For each shell 100 000 case histories are followed either to capture or to transmission. The average energy a neutron may lose in an elastic collision is from 1 to 2 percent of its energy; at 24 keV, this energy loss is very much greater than the average level spacing. Therefore, a collided neutron encounters energy intervals with equal probability. The reaction cross-sections for an energy interval are generated as the sum of the contributions of the scattering and capture cross-sections of two adjacent noninteracting Wigner-spaced Doppler-broadened resonances chosen at random.

The conditions that are satisfied simultaneously by the Monte Carlo analyses are the experimental values of average total cross-section $\bar{\sigma}_T$ and transmission T. The constituent parts of $\bar{\sigma}_T$ are the s-wave and p-wave capture cross-sections $\bar{\sigma}_{C_s}$ and $\bar{\sigma}_{C_p}$, the s-wave resonance scattering component $\bar{\sigma}_{S_s}$, and the potential scattering cross-section σ_{pot}. In the Monte Carlo calculations the p-wave scattering component is assumed to be small and the p-wave capture cross-section is considered to be energy independent and is approximated by an average value. The s-wave resonance parameters used are averages over all isotopes of elemental samples; a spin weight factor g of 1/2 was used.

Some limitations of the Bethe method of sphere analysis were explored by BOGART and SEMLER [4] in performing several idealized sphere transmission problems by the Monte Carlo method. Illustrative calculations were made for Au and I shells using several arbitrary repetitive step scattering and capture cross-sections superimposed on the potential scattering. The spacings and magnitudes of the steps were such that the same average value of capture cross-section was provided as that used for a nucleus possessing constant scattering and capture cross-sections. It was found that all values of $\bar{\sigma}_C$ that satisfy a given value of sphere transmission and that consider the resonance nature of the cross-sections as represented by the steps, are larger than the values of $\bar{\sigma}_C$ for energy-independent cross-sections. These step values of $\bar{\sigma}_C$ are particularly increased by resonance scattering. In the same way, the present Monte Carlo calculations that account directly for energy-dependent cross-sections and multiple scattering processes in the sphere experiments have provided significantly larger values of $\bar{\sigma}_C$ as a result of including the effects of resonance scattering, which are particularly important for Au. Interpretation of Au transmission experiments provides a value of $\bar{\sigma}_C$ at 24 keV of 635 ± 50 mb by Monte Carlo analysis[1] compared with 532 ± 60 mb reported by SCHMITT [5] which includes a resonance

[1] A biasing error in the coding of those Monte Carlo problems of reference [4] that employed the Wigner distribution of level spacings, forced convergence on erroneously high values of s-wave capture and scattering cross-sections for Au and I. As a result, the inferred values of p-wave capture that satisfied observed values of sphere transmission for these nuclei were too low. This coding error has been corrected, and the results presented herein have been corrected for this computational error.

TABLE II. - RESULTS OF SPHERE TRANSMISSION EXPERIMENT ANALYSES BY MONTE CARLO;

COMPARISON OF RESULTS AT 24 keV BY BETHE AND BY MONTE CARLO ANALYSES

Shell	Reference	Average cross sections from Monte Carlo analysis						σ_{pot} [b] (b)	Average capture cross section, $\bar{\sigma}_C$		
									Bethe (mb)		Present Monte Carlo (mb)
		$\bar{\sigma}_{C_S}$ (b)	$\bar{\sigma}_{C_p}$ (b)	$\bar{\sigma}_C$ (b)	$\bar{\sigma}_{S_S}$ (b)	σ_{pot} (b)	$\bar{\sigma}_T$ [a] (b)		Uncorrected for resonance self-protection[c] [1,2,5]	Corrected for resonance self-protection [1,5]	
Ag	[1,5]	0.600±0.060	0.480±0.050	1.080±0.060	1.65±0.3	5.2±0.3	7.9±0.3	6.0±0.5	958±45	1127±80	1080±60
Ag	[2]	0.600±0.060	.360±0.040	.960±0.070	1.65±0.3	5.2±0.3	7.9±0.3	6.0±0.5	960±60	-------	960±70
Ag	[2]	0.600±0.060	.470±0.050	1.070±0.070	1.65±0.3	5.2±0.3	7.9±0.3	6.0±0.5	975±66	-------	1070±70
Ag	[2]	.600±0.060	.540±0.050	1.140±0.070	1.65±0.3	5.2±0.3	7.9±0.3	6.0±0.5	1095±55	-------	1140±70
Sb	[1,5]	.325±0.040	.235±0.025	.560±0.040	1.35±0.2	4.2±0.2	6.0±0.2	4.2±0.5	509±27	578±45	560±40
I	[1,5]	.340±0.040	.455±0.050	.795±0.050	1.46±0.3	4.4±0.4	6.6±0.3	4.8±0.6	653±70	768±90	795±50
Au-1	[1,5]	.485±0.050	.135±0.025	.620±0.050	3.18±0.4	9.9±0.4	13.7±0.3	10.8±0.6	495±52	532±60	620±60
Au-2	[1,5]	.485±0.050	.150±0.015	.635±0.050	3.18±0.4	9.9±0.4	13.7±0.3	10.8±0.6	480±83	518±90	635±50
Au	[2]	.485±0.050	.155±0.030	.640±0.060	3.18±0.4	9.9±0.4	13.7±0.3	10.8±0.6	560±28	-------	640±60
Au	[2]	.485±0.050	.195±0.040	.680±0.060	3.18±0.4	9.9±0.4	13.7±0.3	10.8±0.6	590±30	-------	680±60

[a] Values of $\bar{\sigma}_T$ privately obtained from E. G. Bilpuch, Duke University.

[b] Values of σ_{pot} obtained from effective nuclear radii of Seth et al. [6].

[c] Values have been corrected from Sb - Be spectrum averages to 24 keV values.

self-protection correction; a value of $\bar{\sigma}_C$ for Au of 660 ± 60 mb by Monte Carlo is to be compared with a value of 570 ± 30 mb by BELANOVA [2].

The results of the sphere transmission experiment analyses by Monte Carlo and a comparison of results at 24 keV by Bethe and Monte Carlo analyses are presented in Table II. The internally consistent values of $\bar{\sigma}_{C_s}$, $\bar{\sigma}_{C_p}$, $\bar{\sigma}_C$, $\bar{\sigma}_{S_s}$ and σ_{pot} obtained by the Monte Carlo analyses that satisfy the experimental transmissions and reported values of $\bar{\sigma}_T$ are also listed in Table II. The effects of an estimated 10-percent uncertainty in Γ_γ and the measured uncertainties in Γ_n and D are evaluated by separate calculations and are combined to provide the listed uncertainties in $\bar{\sigma}_{C_s}$ and $\bar{\sigma}_{S_s}$. The uncertainties in $\bar{\sigma}_{C_p}$ result from the uncertainties in the measured values of shell transmission T. Although the values of $\bar{\sigma}_{C_s}$ and $\bar{\sigma}_{C_p}$ are found individually to have the listed uncertainties, their sums $\bar{\sigma}_C$ have been found to vary slowly with relatively larger changes in σ_{pot} and $\bar{\sigma}_T$ because of partial compensation in satisfying experimental transmissions. Therefore, the precision of the Monte Carlo value of $\bar{\sigma}_C$ is not believed to be the sum of the uncertainties in $\bar{\sigma}_{C_s}$ and $\bar{\sigma}_{C_p}$ but has been taken to be of the same order of magnitude as the uncertainty in $\bar{\sigma}_{C_s}$.

The measured values of sphere transmission of SCHMITT [1] had been corrected to monoenergetic values at 24 keV. However, in the experiments of BELANOVA [2], reported values of transmission referred not to 24-keV neutrons but to the various spectra for an Sb-Be source with various thicknesses of beryllium envelope. In order to correct these spectral results to monoenergetic values at 24 keV, the Monte Carlo values of $\bar{\sigma}_C$ were reduced by factors of 0.96 for Ag and 0.92 for Au, as inferred from the final results that were corrected from calculated spectra and reported by BELANOVA [2]. The values of $\bar{\sigma}_{C_p}$ for Belanova spheres listed in Table II have been adjusted so that they are consistent with the corrected values of $\bar{\sigma}_C$ and the spectroscopic value of $\bar{\sigma}_{C_s}$.

Also shown in Table II are values of σ_{pot} obtained from the relation $4\pi(R')^2$, where values for the effective nuclear radii R' were obtained from SETH et al. [6], their values being derived from analysis of total cross-section data in the range from 50 to 150 keV. The values of σ_{pot} obtained in the Monte Carlo analysis are in reasonable agreement with the values reported by SETH.

The Monte Carlo results for $\bar{\sigma}_C$ are compared with the results obtained by the Bethe method in the last three columns of Table II. The Monte Carlo results exceed significantly the results of sphere transmission interpretation by the Bethe method that are uncorrected for resonance self-protection. The values of average total cross-section on which the Bethe method results were based [2,5] are essentially identical with those used in the Monte Carlo method that are listed in Table II. Also shown in Table II are the results of SCHMITT [5] that have been corrected for resonance self-protection so that the Bethe values of $\bar{\sigma}_C$ were increased. These corrected values agree with the Monte Carlo results for all shells except the gold shells. As mentioned previously, the relatively large average neutron width for the levels of Au introduces an average resonance scattering cross-section that is larger for Au than for the other elements.

3. COMPARISON OF RESULTS OF MONTE CARLO AND BETHE ANALYSES

The analytical model that has been used to interpret sphere transmission experiments at 24 keV is the thick-shell theory of BETHE [3] that was developed

to compute average inelastic scattering cross-sections from sphere transmission experiments at neutron energies in the MeV region. The method consists of calculating separate escape probabilities from a spherical shell after isotropic elastic scattering on the first and second collisions. After the second collision, the neutrons are taken to be distributed in random directions and in a spatial normal mode so that the effects on transmission of the third and all subsequent collisions are combined into a single escape probability. Inherent in the method is the energy independence of cross-sections.

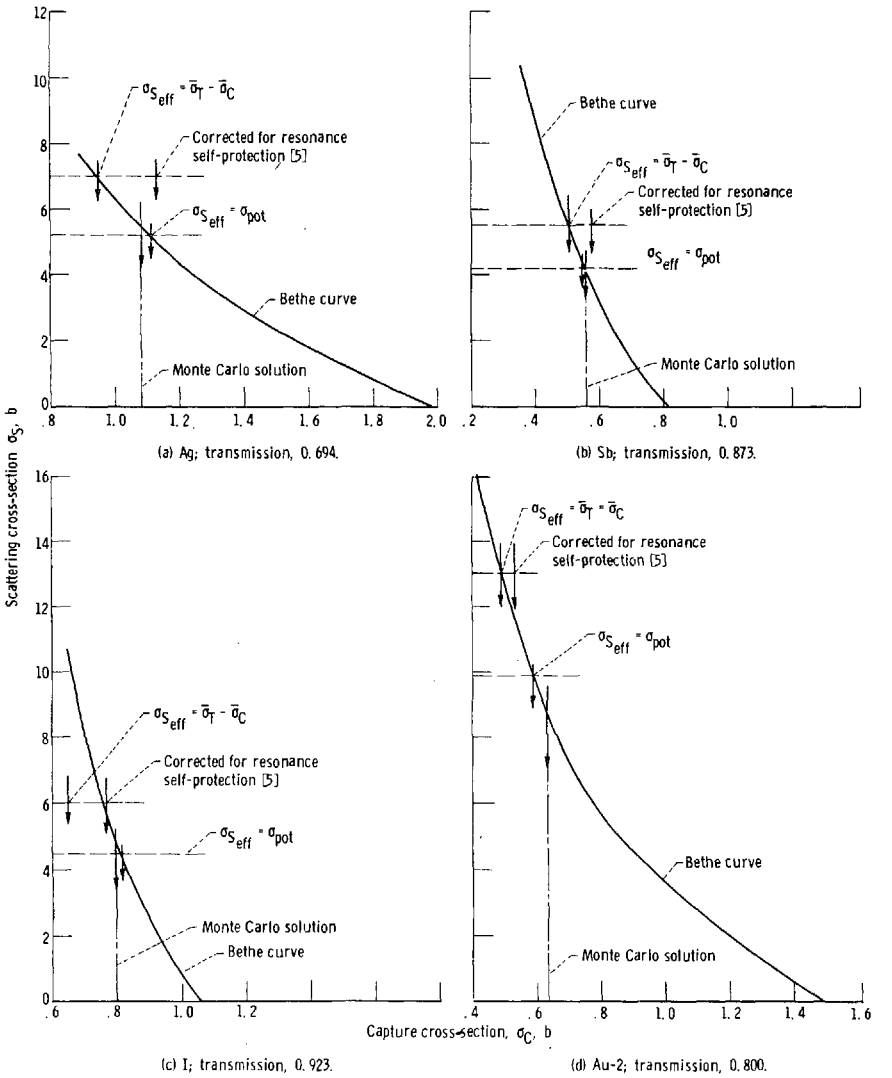

FIG. 1. Loci of Bethe solutions for Ag, Sb, I, and Au-2 shells (SCHMITT [1, 5]).

The Bethe method has been used to compute the values of σ_C that satisfy the experimental values of transmission for several shells for a range of scattering cross-section σ_S. Because the Monte Carlo code employed herein is readily capable of reproducing the Bethe calculations for energy-independent cross-sections, several Monte Carlo calculations were also made as a check. The two methods were found generally to agree quite accurately. Inasmuch as there are many combinations of constant scattering cross-section σ_S and constant capture cross-section σ_C that satisfy a given value of transmission for a shell, the locus of such values has been determined.

The locus curves have been calculated for shells that were measured by SCHMITT [1], namely Ag, Sb, I, and Au-2. The curves are presented in Fig. 1. In each case reduction of σ_S results in an increase in σ_C.

The problem in applying the Bethe method when microscopic cross-sections vary with energy can be reduced to the determination of an effective scattering cross-section $\sigma_{S_{eff}}$. In the past, the measured average total cross-section $\bar{\sigma}_T$ at 24 keV has been used to estimate $\sigma_{S_{eff}}$:

$$\sigma_{S_{eff}} = \bar{\sigma}_T - \bar{\sigma}_C \qquad (1)$$

Since $\bar{\sigma}_C$ is generally much smaller than $\bar{\sigma}_T$, a single iteration results in a good value for $\sigma_{S_{eff}}$. However, since $\bar{\sigma}_T$ consists of the sum of σ_{pot}, $\bar{\sigma}_S$, and $\bar{\sigma}_C$, relation (1) is equivalent to using

$$\sigma_{S_{eff}} = \sigma_{pot} + \bar{\sigma}_S$$

in the Bethe analysis.

The question arises as to what the effective value of energy-independent scattering cross-section is that provides a value of $\bar{\sigma}_C$ that is in reasonable agreement with the results of the present Monte Carlo analysis. Indicated in Fig. 1 are the values of σ_C for values of $\sigma_{S_{eff}}$ that correspond to $\sigma_T - \sigma_C$ and to σ_{pot}. The Monte Carlo values of $\bar{\sigma}_C$ are shown to correspond closely to the values obtained by using $\bar{\sigma}_{pot}$ as the effective scattering cross-section. Values of $\bar{\sigma}_C$ reported by Schmitt that have been corrected for resonance self-protection are also shown. These corrected values increase the values of $\bar{\sigma}_C$ so as to agree reasonably well with Monte Carlo values for Ag, Sb, and I. They disagree, however, for Au. Therefore, it appears that the method of Bethe may be used to interpret sphere transmission experiments; it can provide a good approximation to the average capture cross-section at 24 keV, if the potential scattering cross-section is known with reasonable precision and is used as the effective scattering cross-section.

An analogy to the present finding that a complex multiple scattering resonance capture problem may be treated by simply ignoring the resonance scattering contributions of absorptive nuclei is to be found in the methods evolved to handle the problem of the calculation of heterogeneous effective resonance integrals for absorbers possessing wide resonances (see DRESNER [7]). Dresner discusses the essential expression for the escape probability from spatially uniform volume sources in lumps of the resonance absorber, for which the width of the resonance in lethargy units greatly exceeds the average lethargy increment per collision. He notes that the escape proba-

bility can be expressed accurately over a large range of scattering probability per collision in the lump by a relation that ignores resonance scattering completely.

It would appear that for nuclei having large s-wave strength functions and small average level spacings such as Au, average s-wave resonance scattering contributions are large. These s-wave scattering cross-sections coincide in energy with capture cross-sections with the result that probability of capture is reduced and the probability of scattering is increased. Therefore, inclusion of the average resonance scattering cross-section in estimating the value of $\sigma_{S_{eff}}$ that is to be used in the Bethe method is incorrect. It was shown by BOGART and SEMLER [4] that the s-wave levels with the larger neutron widths in the Porter-Thomas distribution account for the larger share of the resonance capture integral; for example, 50 percent of the resonance capture integral is contributed by about 20 percent of the levels with the larger neutron widths. Therefore, a first order representation of the cross-sections that are effective for capture at 24 keV consists of the potential scattering cross-section with the superposition of cross-sections for relatively widely spaced resonances possessing the larger neutron widths.

4. CONCLUSIONS

A method of interpretation of sphere transmission measurements that uses the Bethe analysis but avoids the necessity for applying resonance self-protection corrections is suggested. By comparing values of average capture cross-sections obtained from Monte Carlo analyses with values obtained from the Bethe analyses for Ag, Sb, I, and Au, a suitable criterion for estimating the value of the effective scattering cross-section to be used in a Bethe analysis was obtained. The use of the potential scattering cross-section as the effective scattering cross-section in the Bethe analysis provides results that are in reasonable agreement with the Monte Carlo results without the necessity of applying resonance self-protection corrections.

REFERENCES

[1] SCHMITT, H. W. and COOK, C. W, Absolute Neutron Cross Sections for Sb-Be Photoneutrons, Nucl. Phys. 20 (1960) 202 -19.

[2] BELANOVA, T. S., VAN'KOV, A. A., MIKHAILUS, F. F., and STAVISSKII, YU. YA., Absolute Measurements of the Absorption Cross Sections of 24 keV Neutrons, J. Nucl. Energy Parts A/B 20 (1966) 411 -17.

[3] BETHE, H. A., BEYSTER, J. R., and CARTER, R. E., Inelastic Cross-Sections for Fission-Spectrum Neutrons, I, J. Nucl. Energy 3 (1956) 207 -23.

[4] BOGART, D. and SEMLER, T. T., Monte Carlo Interpretation of Sphere Transmission Experiments for Average Capture Cross Sections at 24 keV, Rept. No. CONF-660303, Atomic Energy Commission (USA)(1966).

[5] SCHMITT, H. W., Rept. No. EANDC-33U, Atomic Weapons Res. Estab. (Gr. Brit.) (1963) 41-43.

[6] SETH, K. K., TABONY, R. H., BILPUCH, E. G., and NEWSON, H. W., s-, p-, and d-wave Neutron Strength Functions, Phys. Letters 13 (1964) 70-72.

[7] DRESNER, L., Resonance Absorption in Nuclear Reactors, Chap. 6. Pergamon Press (1960) 72-86.

[8] GARG, J. B., RAINWATER, J., and HAVENS, W. W., Neutron Resonance Spectroscopy. V. Nb, Ag, I, and Cs, Phys. Rev. 137 (1965) B547-B575.

[9] DESJARDINS, J. S., ROSEN, J. L., HAVENS, W. W., and RAINWATER, J., Slow Neutron Resonance Spectroscopy. II. Ag, Au, Ta, Phys. Rev. 120 (1960) 2214 – 26.

DISCUSSION

A.I. ABRAMOV: Have you compared, using a single method of calculation (Monte Carlo), results obtained with and without allowance for resonance self-protection, thereby determining directly the size of the correction for this effect?

D. BOGART: For the spheres used by Schmitt, both the monoenergetic and energy-dependent cross-sections were employed in the identical Monte Carlo multiple scattering calculation routine, so that the results for these spheres are direct indications of the consequences of ignoring the energy variation in the statistically present s-wave resonances.

A.I. ABRAMOV: What is your opinion regarding the possibility of experimental verification of the corrections for the resonance self-protection effect?

D. BOGART: Belanova's method, involving spheres of various thicknesses and atom dilution by lead, should in principle indicate self-protection effects if the experimental technique and analytical method are sufficiently sensitive. However, since we have found that the self-protection effect is about 15% for silver and about 20% for gold, it is very difficult to observe such an effect with any precision.

D.K. BUTLER: In a comment on the paper presented by Dr. Abramov (paper CN-23/96), you indicated that the use of lead as a diluent in spherical shell transmission measurements did not adequately eliminate self-shielding of the resonance. If there is sufficient diluent, however, the elastic down-scattering by the diluent into the resonance of the absorber should eliminate the depletion. In other words if the excess potential scattering is high enough, the effect of self-shielding should be negligible. For these reasons I do not understand the physical basis for your criticism of the method used by Dr. Abramov and his colleagues.

D. BOGART: Your argument may well be correct in principle; the only explanation I can offer is that the range of the Belanova experiments was insufficient and the method of analysis too insensitive for detection of a significant self-shielding effect. Dilution reduces absorption and makes the interpretation of transmission more difficult.

CAPTURE CROSS-SECTION MEASUREMENTS FOR SOME MEDIUM- AND HEAVY-WEIGHT NUCLEI USING A LARGE LIQUID SCINTILLATOR*

D. KOMPE
KERNFORSCHUNGSZENTRUM KARLSRUHE,
FEDERAL REPUBLIC OF GERMANY

Abstract

CAPTURE CROSS-SECTION MEASUREMENTS FOR SOME MEDIUM- AND HEAVY-WEIGHT NUCLEI USING A LARGE LIQUID SCINTILLATOR. Radiative neutron capture cross-sections of several elements in the energy range from 10 to 150 keV have been measured at the Karlsruhe 3-MeV pulsed Van de Graaff generator. Neutrons are produced by the ^{7}Li(p, n) reaction in a thick lithium metal target. Neutron energies are determined by time-of-flight. A large liquid scintillator with 3-ns timing resolution is used as a detector for capture events in the sample. Energy resolution is determined by the 10-ns burst width of the accelerator and flight path of 1.5 m. Capture cross-sections of the elements Nb, Mo, Pd, Ag, Cd, In, Cs, Hf, Ta, W and Re were measured relative to the standard capture cross-section of gold which was taken from other experiments.

1. INTRODUCTION

In the past few years many neutron capture cross-sections in the keV region have been measured, since they are of interest for nuclear reaction theory and for the design of fast reactors. But there are still many materials not yet investigated, and there are large discrepancies among existing results; thus further experiments are required.

We have measured neutron capture cross-sections of 12 elements in the energy range from 10 to 150 keV at a pulsed Van de Graaff generator; a large liquid scintillator was used to detect capture events in the sample. Capture cross-sections can be determined in this experiment relative to a known standard cross-section.

In the present work all measurements are based on the capture cross-section of gold as standard. It can be measured absolutely with good accuracy at certain energies by activation methods, as Pönitz points out in his paper [1]. The capture cross-section curve for gold recommended in that paper was used here for normalization of all other capture cross-sections.

2. EXPERIMENTAL METHOD

The experimental arrangement was similar to that described by Gibbons et al. [2]. A broad neutron spectrum is produced by the ^{7}Li(p, n) reaction in a thick lithium metal target. Neutron energies are determined by time-of-flight. The well collimated neutron beam is incident on the sample located in a hole at the centre of a liquid

* Work performed within the association in the field of fast reactors between the European Atomic Energy Community and the Gesellschaft für Kernforschung mbH, Karlsruhe.

scintillator tank of 1.1-m diameter. The two samples used for the relative measurement are interchanged at short time intervals controlled by a current integrator for the proton beam. The timing resolution of the detector was 3 ns, accelerator burst width was 10 ns; thus at a flight path of 1.5 m the overall resolution was 7 ns/m. This resolution is sufficient for the present investigations; but it can be improved for future experiments to 2 ns/m by bunching the proton beam to 1-ns pulse width.

The efficiency of the detector for capture events in the sample is

$$\epsilon = p_{ne} \cdot p_b,$$

where p_{ne} is the probability that not all capture γ-rays of a cascade escape without interaction from the scintillator, and p_b is the probability that a detector signal from a capture event exceeds the discriminator bias level. An exact calculation of p_{ne} would be very complicated and would require detailed knowledge of the γ-ray spectra. However, p_{ne} can be estimated with reasonable accuracy, for a scintillator of this size from a calculated efficiency curve for single γ-rays. Such an estimate suffices because of the high average multiplicities of capture γ-ray cascades from heavy nuclei. We estimate $p_{ne} = 0.96 \pm 0.03$, where the uncertainty applies even to unfavourable cases with an appreciable admixture of high-energy transitions such as gold.

For the determination of p_b one has to evaluate the capture pulse-height spectra. In the present experiment capture pulse-height spectra were taken simultaneously with the time-of-flight spectra. Subtraction of background for the pulse-height spectra was performed by means of a time gate set alternately on time regions of capture events and of background. The high background does not allow an exact determination of the pulse-height spectra below γ-ray energies of 1 MeV. Only extrapolations with an uncertainty of about 5% are possible.

The capture cross-section measured relative to a standard cross-section σ_{st} is

$$\sigma_\gamma = F \frac{N}{N_{st}} \frac{\epsilon_{st}}{\epsilon} S \sigma_{st}$$

where F is a factor which is determined by the two sample thicknesses, N, N_{st} are the two counting rates after subtraction of background, S is the ratio of the multiple scattering corrections [3] made for the two samples. The index st refers to the standard.

For the total error in σ_γ we get the following contributions: The error in ϵ_{st}/ϵ based on the above estimate is 8%. For sample thicknesses of about 1 mm as used here the relative scattering correction [3] given by S is less than 4%; its error is estimated to be less than 1%. Resonance self shielding effects, which are even smaller than the multiple scattering corrections and largely compensate in relative measurements, are neglected here. This may introduce an error of less than 1%.

The statistical error in the ratio of the counting rates N/N_{st} is important only in the low energy tail of the neutron spectrum, where we have a poor signal-to-background ratio. The statistical accuracy below 20 keV was improved by combining channels in the time-of-flight spectra; as a result, the energy resolution is reduced. Then we obtain a statistical

accuracy of about 5% at 15 keV, 2% at 20 keV and better than 1% above 30 keV for typical runs.

The error in the standard capture cross-section of gold σ_{st} quoted by Pönitz [1] is 8% below 40 keV and increases to 12% at higher energies.

To summarize, the total error varied from 12% at low energies to nearly 15% at energies above 40 keV.

3. MEASUREMENTS AND RESULTS

The standard capture cross-section of gold is accurately measured by several methods at certain energies, as reported by Pönitz [1]. The

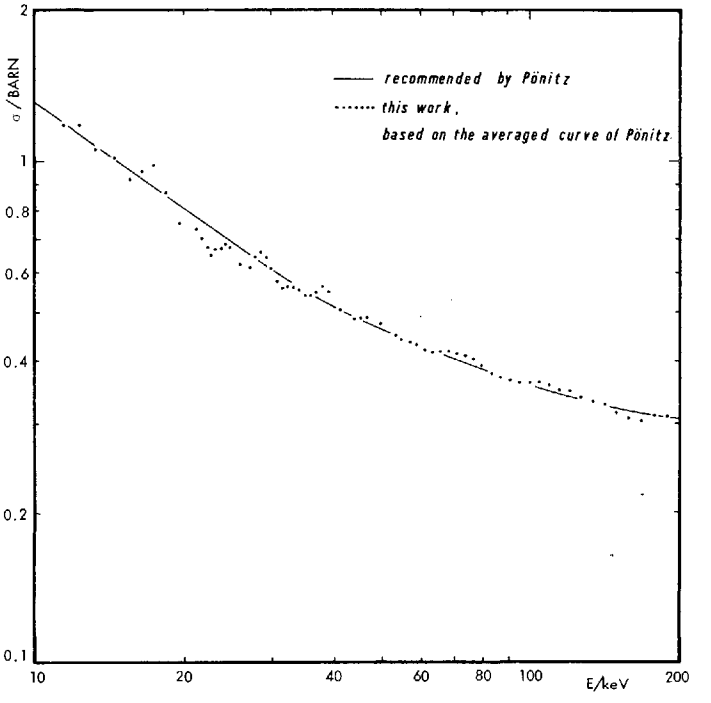

FIG.1. Capture cross-section of Au normalized at 30 keV

shape of this cross-section is known with less accuracy. Therefore an additional time-of-flight measurement for the determination of this shape was performed by comparison with the shape of the cross-section for the $^6Li(n,\alpha)$ reaction given by Schwarz et al. [4]. For this measurement a 1-mm thick glass scintillator with enriched ^6Li was mounted at some distance from the phototube to minimize backscattering effects. The resulting capture cross-section which was normalized at 30 keV to the value given by Pönitz [1] agrees with other measurements renormalized by Pönitz at low and high energies. But there are considerable deviations between 30 and 100 keV. In the region of maximum deviations near 60 keV

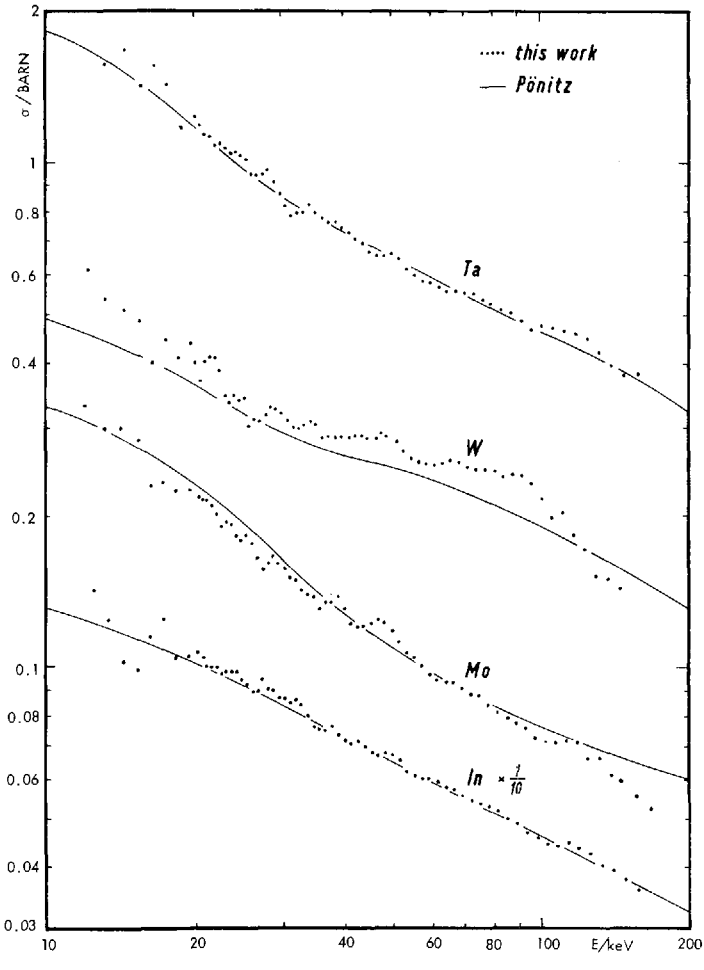

FIG.2. Capture cross-sections of Ta, W, Mo, In

the results of this measurement are about 17% above those of several other experiments.

The reason for these discrepancies is not yet understood. Therefore Pönitz assumes in his evaluation of several gold cross-section measurements (including the present one of the shape) a mean curve with a large error in this energy region which is represented by the solid line in Fig.1. The points in this figure show the results of the experiment described above, normalized to the smooth curve of Pönitz. This cross-section was adopted as a standard for the other cross-section measurements of this work.

The shape of the capture cross-section of gold as observed with the energy resolution of this experiment is not completely smooth but shows an intermediate structure. This structure should be taken into account in comparing various results at different energies, e.g. the measurements at 24 and 30 keV by several authors. A similar structure can be

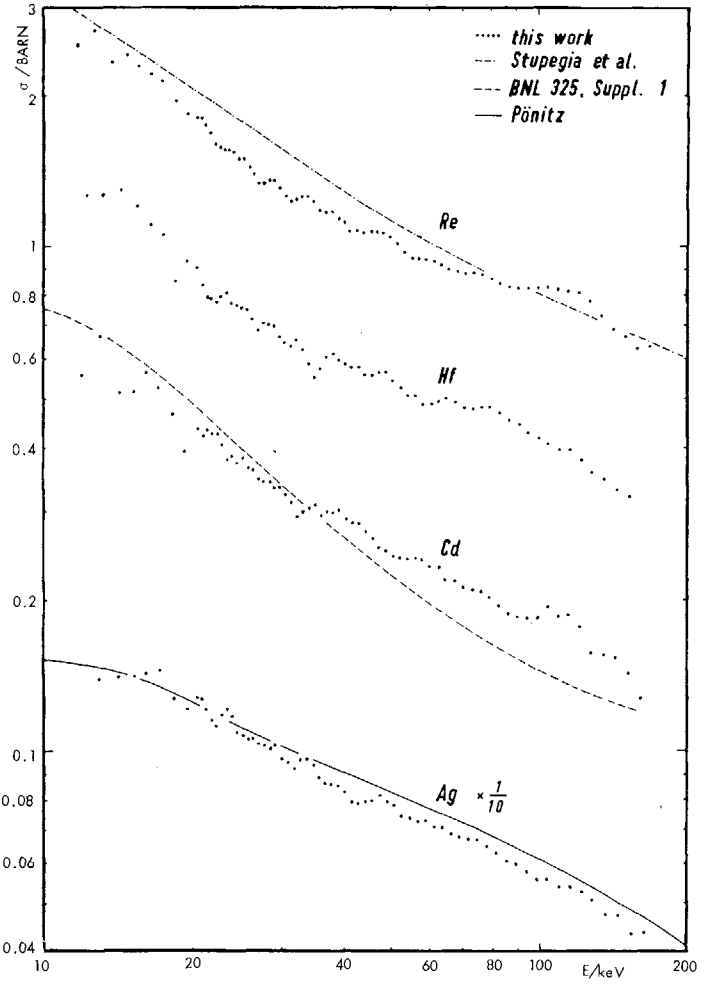

FIG.3. Capture cross-sections of Re, Hf, Cd, Ag

seen in other cross-sections also, but it is most pronounced for elements with a single isotope, such as Au and Nb.

In considering the limits of error, we find that the measured capture cross-sections of Ta, Mo and In (Fig. 2) agree surprisingly well with the recommended curves which Pönitz has extracted from other experiments after renormalization to the recommended Au cross-section. The agreement for W is not quite as good, but is within the limits of error. Ag (Fig. 3) is in rather good agreement with the evaluation of Pönitz. It is interesting to compare Re with the data of Stupegia et al. [5] since they represent an absolute activation measurement. The agreement is not very good for all energies, but in the region where the largest deviations occur (near 30 keV) the errors of the two measurements still overlap. For two energies, 30 and 65 keV, there exist still other data of Macklin et al. [6] which are 40% below the present curve.

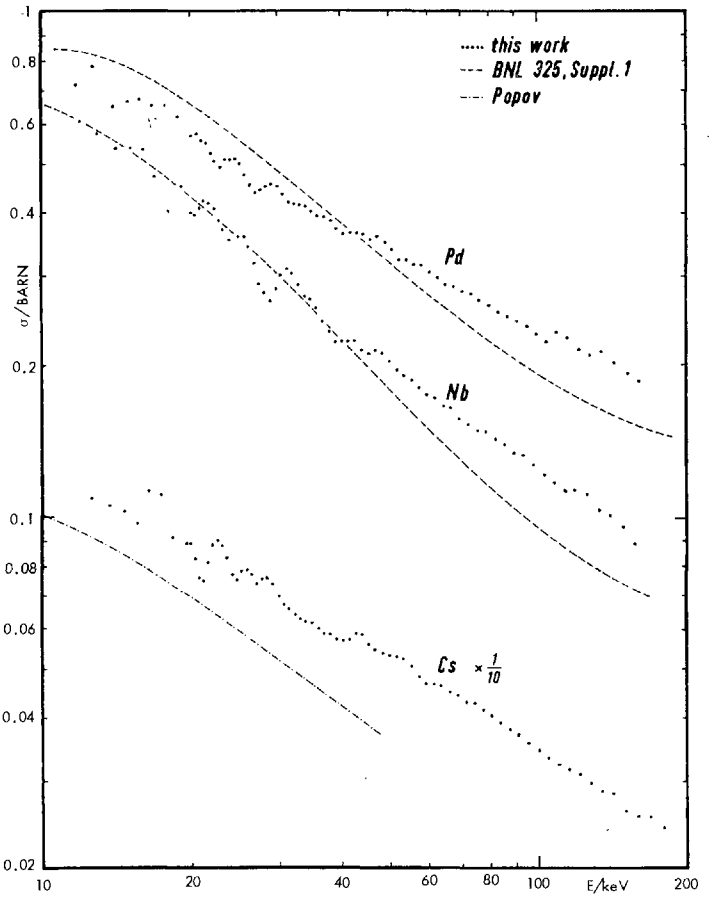

FIG.4. Capture cross-sections of Pd, Nb, Cs

The shape of the Re capture cross-section shows a steep decrease near 130 keV which must be due to inelastic scattering. A similar effect is observed for W (Fig. 2) near 100 keV. For the capture cross-section of Hf given in Fig. 3 no other data in this energy region are known, but the present measurement seems to join well the data of Block et al. up to 8 keV [7]. The present data for Cd, as well as for Pd and Nb (Fig. 4) show systematic deviations from the values quoted in [8]. They agree quite well below 40 keV, but at higher energies the curves of [8] are almost 20% below ours. Obviously these discrepancies show a similar tendency as those for Au and must be ascribed to differences in the standard cross-sections. For Nb there is still another measurement above 175 keV reported by Diven et al. [9] which joins the present curve very well. For Cs only one measurement up to 40 keV, made by Popov and Shapiro [10] at the lead slowing-down time spectrometer, exists and differs by 30% from the present results.

4. CONCLUSIONS

The capture cross-sections given in this work indicate that the accuracy for relative measurements is rather good. This is obvious from the good agreement with most of the curves recommended by Pönitz, which are all renormalized to the same cross-section standard. Nevertheless there are large discrepancies in the absolute cross-section values based on different standard cross-sections which indicate that probably the differences are mostly due to errors in these standard cross-sections. Though the capture cross-section of gold has been previously investigated with considerable effort, its shape is known in some regions only with a large uncertainty. Since we hope that this accuracy can be improved by some future experiments which we plan, the absolute cross-section data given in the present work should be considered as preliminary. There might be slight changes in the shape of the capture cross-section of gold, which would cause a renormalization of the present data.

REFERENCES

[1] PÖNITZ, W.P., paper CN-23/6, these Proceedings, vol. I.
[2] GIBBONS, J.H., MACKLIN, R.L., MILLER, P.D., NEILER, J.H., Phys. Rev. 122 (1960) 182.
[3] SCHMITT, H.W., Rep. ORNL-2883.
[4] SCHWARZ, S., STRÖMBERG, L.G., BERGSTRÖM, A., Nucl. Phys. 63 (1965) 593.
[5] STUPEGIA, D.C., SCHMIDT, M., MADSON, A.A., J. nucl. Engng A/B, 19 (1965) 767.
[6] MACKLIN, R.L., GIBBONS, J.H., INADA, T., Phys. Rev. 129 (1963) 2695.
[7] BLOCK, R.C., VON DER LAGE, F.C., WESTON, L.W., Rep. ORNL-3085 (1961).
[8] Rep. BNL 325, Supplement 1.
[9] DIVEN, B.C., TERREL, J., HEMMENDINGER, A., Phys. Rev. 120 (1960) 556.
[10] POPOV, Y.P., SHAPIRO, F.L., Trudy Fiz. Inst. Akad. Nauk XXIV (1964).

DISCUSSION

A.B. SMITH: You stated that monoisotopic elements display the most prominent structure, and your gold data do indeed indicate such a structure. However, tantalum (monoisotopic) displays very little structure, whereas tungsten (three isotopes) shows perhaps the most prominent structures. Would you care to comment on this?

D. KOMPE: A more or less prominent structure is observed in all the cross-section curves. I agree that the fluctuations for tantalum are weaker than those for tungsten, but with most of the monoisotopic elements (for example, gold, niobium and caesium) particularly large fluctuations occur. Nevertheless, this should not be taken as a general rule; we certainly did not try to draw any conclusions from it.

A. DE VOLPI: Have you considered correcting for the probability of detection or non-detection of a gamma cascade? With a detector of high efficiency, this probability should vary somewhat according to the decay scheme of the capture source.

D. KOMPE: The effect of variations in efficiency according to the decay scheme of the gamma cascade is very small, but we allowed for it in the margin of uncertainty assigned to the detection efficiency.

R. BLOCK: We have also measured neutron capture in tungsten at low energies and, for a given isotope, have observed practically no change in the spectrum fraction (i.e. the scintillator detection efficiency) for different tungsten resonances.

NEUTRON CAPTURE BETWEEN 5 keV AND 3 MeV

D. C. STUPEGIA, C. R. KEEDY, M. SCHMIDT AND A. A. MADSON
ARGONNE NATIONAL LABORATORY, ARGONNE, ILLINOIS
UNITED STATES OF AMERICA

Abstract

NEUTRON CAPTURE BETWEEN 5 keV AND 3 MeV. Neutron capture cross-sections over a wide range of mass number are being measured for neutron energies between about 5 keV and 3 MeV. The nuclei studied to date are ^{41}K, ^{85}Rb, ^{86}Sr, ^{87}Rb, ^{89}Y, ^{98}Mo, ^{139}La, ^{141}Pr, ^{158}Gd, ^{170}Er, ^{175}Lu, and ^{176}Yb. The experimental technique used is the activation method, in which the radioactive capture product formed in the neutron bombardment is measured by beta or gamma counting, and the counters are calibrated against a 4π-beta counter. Monoenergetic neutrons are produced by bombarding lithium or tritium targets with protons from the 4-MeV Van de Graaff accelerator. The neutron intensity is measured with a fission chamber, which counts fissions in a thin deposit of ^{235}U.

The data are compared with calculations based upon the statistical model of uncorrelated and non-interfering compound nuclear states. This model, which yields the energy averages of resonant or fluctuating compound nuclear cross-sections, was first used to calculate capture cross-sections by Lane and Lynn, and has been developed further by Moldauer. The calculations take into account the variation of radiation width and level density with excitation energy and spin of the compound nucleus, and include the competition of compound elastic and inelastic scattering and the variation of neutron widths from level to level (Porter-Thomas distribution). Neutron widths were calculated from optical model transmission coefficients, with the parameters chosen according to the spherical optical model of Moldauer.

Another phenomenon is considered in the calculations. If the compound state, de-exciting through a gamma-ray cascade, ends its de-excitation in a low-lying level of (Z, A + 1), the event is radiative capture, as measured experimentally. If, however, after a gamma-ray decay, the compound system is at an excitation energy above the neutron emission theshold, the gamma-ray cascade may be ended by neutron emission, and the process does not contribute to the capture cross-section. The computations take into account the competition between those two modes of de-excitation.

The experimental results are compared with calculations using the model described above. The agreement is good from a few keV to about 1 MeV for ^{89}Y, ^{98}Mo, ^{139}La, and ^{141}Pr. The agreement is not as good for the distorted nuclei, ^{158}Gd, ^{170}Er, ^{175}Lu, and ^{176}Yb. In all cases, the calculations become uncertain at energies above which the level schemes of the target nuclei are poorly known, since this lack of data introduces uncertainty in the calculation of the competition of inelastic scattering.

In the calculations, the influence of the termination of the gamma-ray cascade by neutron emission begins to be appreciable above about 200 keV. The inclusion of this effect in the computations is an important factor in allowing the radiative capture cross-sections to be calculated accurately above that energy.

FISSION-PRODUCT ABSORPTION IN THERMAL REACTORS

W. H. WALKER
ATOMIC ENERGY OF CANADA LIMITED,
CHALK RIVER NUCLEAR LABORATORIES,
CHALK RIVER, ONTARIO, CANADA

Abstract

FISSION-PRODUCT ABSORPTION IN THERMAL REACTORS. The current status of our knowledge of fission-product yields and cross-sections is outlined and the data now in use at Chalk River is given. This data has been incorporated into a computer programme (FISSPROD) which takes account of accumulation of radioactive nuclides with half-lives > 5 h, and changes in flux, the epithermal component and reactor temperature. Computer results are used to demonstrate the effect on reactivity of uncertainties in the basic nuclear data.

The fission-product absorption in ^{233}U, ^{235}U and ^{239}Pu has recently been determined from reactor oscillator measurements of samples irradiated to 2-3 n/kb (AECL 2510). The results are compared to FISSPROD calculations and the significance of the differences is discussed.

1. INTRODUCTION

In power reactors fission products are unfortunate by-products of the fission process which both absorb neutrons and produce β and γ-radiation. In this review I will be concerned only with neutron absorption, particularly after a long irradiation of the fuel, and for this purpose the term "fission products" includes those nuclides that are formed by neutron capture.

Many surveys of fission-product yields and cross-sections have been published by various laboratories since Dr. K. Way first estimated fission-product poisoning in 1944 [1]. The most recently published Chalk River review [2] is an up-dating of earlier work [3] and was used in a survey of reactivity measurements presented at the 1964 Geneva Conference [4]. Recently the computer program FISSPROD [5] has been used to calculate fission-product poisoning for particular irradiations. In this program the concentrations of approximately 200 fission-product nuclides, with half-lives exceeding approximately 5 hours, are calculated by solving a coupled set of linear differential equations.

FISSPROD has been used with a recent compilation of cross-section, yield and half-life data [6] to determine the fission products which are most important in a well-moderated reactor after an irradiation of 1 neutron/ kilobarn (10^{21}n/ cm^2). These are listed in Table I with relevant nuclear data, and with their effective absorption cross-section in barns per initial fissile atom for ^{233}U, ^{235}U, ^{239}Pu and natural uranium fuel. The arrangement is in order of importance in natural uranium fuel at 1 n/ kb, for which 1 barn per initial fissile atom is equivalent to about 0.9 millik.

Before proceeding to a consideration of recent results I would first like to draw attention to the fission products in the mass range 146 to 154

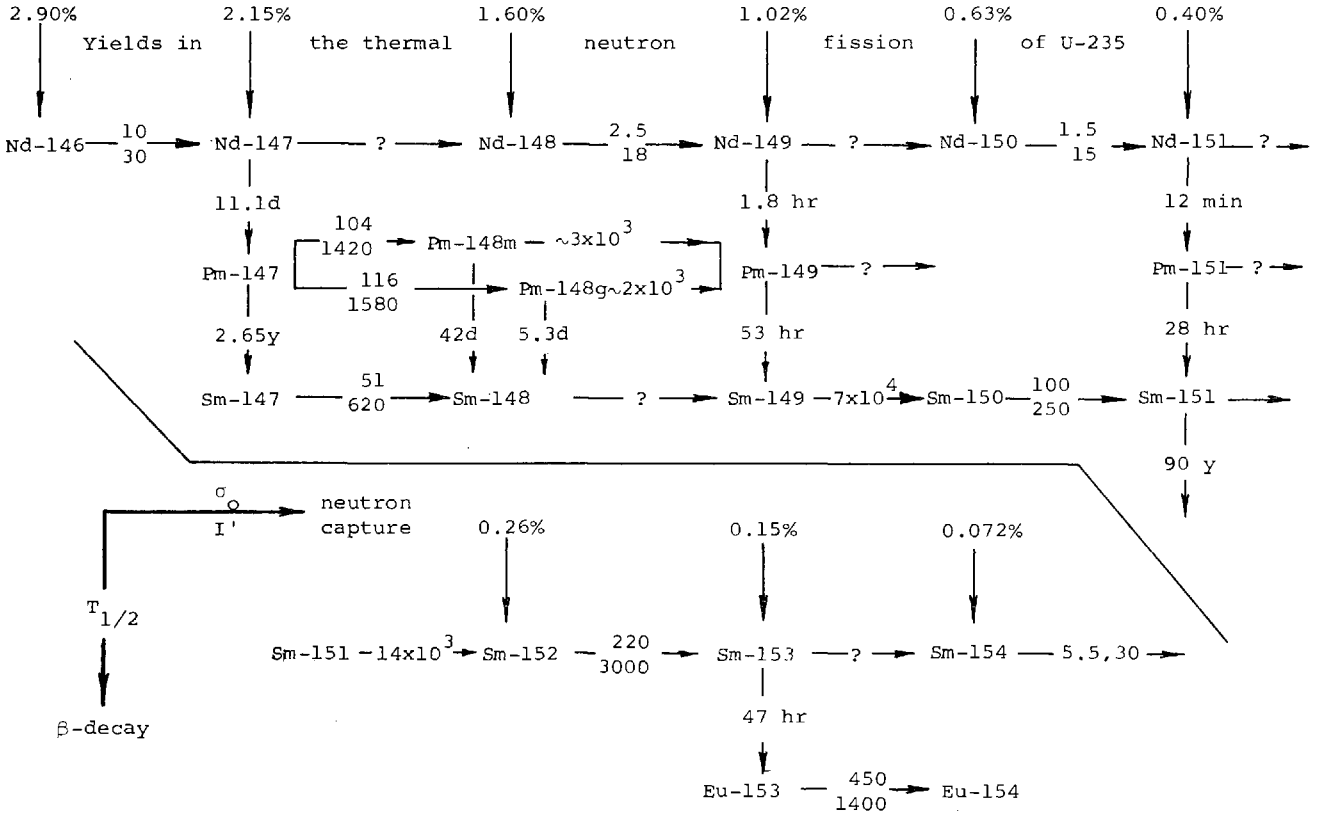

FIG.1. Fission products in the mass range 146-154

TABLE I

MOST IMPORTANT FISSION PRODUCTS
AFTER IRRADIATION OF 1 NEUTRON/KILOBARN

NUCLIDE	HALF-LIFE	THERMAL[a] CROSS-SECTION	RESO-NANCE[a] INTEGRAL	ABSORPTION CROSS-SECTION[b] ^{233}U	^{235}U	^{239}Pu	Nat. U
^{135}Xe	9.16 h	$\sim 3 \times 10^6$		15.67	16.50	16.12	24.29
^{143}Nd	stable	335	48	6.67	6.26	5.96	8.00
^{149}Sm	stable	~ 69000		2.97	3.58	4.06	5.33
^{147}Pm	2.65 y	220	3000	2.14	2.33	2.55	3.09
^{103}Rh	stable	146	1180	0.94	1.74	4.11	2.96
^{151}Sm	90 y	~ 14000		1.33	1.61	2.80	2.77
^{131}Xe	stable	100	800	1.74	1.46	2.28	2.15
^{105}Rh	35 h	~ 25000		0.27	0.46	2.64	1.75
^{133}Cs	stable	29	440	1.07	1.25	1.56	1.72
^{152}Sm	stable	220	3000	0.70	0.85	2.07	1.50
^{148m}Pm	42 d	~ 27000		0.88	0.95	1.05	1.27
^{145}Nd	stable	53	255	0.91	0.98	0.94	1.25
^{99}Tc	2×10^5 y	25	200	0.67	0.85	0.99	1.15
^{150}Sm	stable	100	250	0.39	0.49	0.73	0.71
^{153}Eu	stable	450	1400	0.30	0.39	1.03	0.70
^{155}Eu	1.7 y	~ 14000		0.15	0.25	0.91	0.59
^{83}Kr	stable	200	150	0.91	0.42	0.26	0.49
^{109}Ag	stable	91	1400	0.02	0.02	1.12	0.38
^{154}Eu	16 y	~ 1500		0.14	0.19	0.52	0.33
^{95}Mo	stable	14	100	0.22	0.25	0.24	0.31
All F.P.				41.4	44.4	57.8	67.8

[a] In barns per atom.

[b] In barns per initial fissile atom. Equal to the product of effective cross-section (barns per atom) and fission-product concentration (atoms per initial fissile atom).

(Fig. 1). Interdependence between these nuclides due to neutron capture is so great that they must be treated as a single group. For example, for an irradiation of 1 n/ kb at a flux of 5×10^{13} n/ cm^2sec, about 25% of the ^{149}Sm present will have been formed by capture in ^{147}Pm and ^{148m}Pm. Similarly masses 147-149 contribute to the accumulation of ^{151}Sm and masses 147-151 have appreciable effect at mass 152. The total absorption of nuclides in the mass range 147-154 listed in Table I adds to 15.7 barns per initial fissile atom for natural uranium. This group, together with ^{135}Xe and ^{143}Nd, accounts for about 70% of fission-product absorption for these conditions of irradiation.

2. YIELD MEASUREMENTS

Fission yields are important nuclear data which, like all other measured values, are subject to uncertainties. In the past the spread in reported values has been so great that the unfortunate compiler has been

TABLE II

YIELDS FOR SELECTED NUCLIDES

NUCLIDE	Yield[a]	^{233}U Fission	^{235}U Fission	^{239}Pu Fission	^{241}Pu Fission
^{135}I	C	5.1[10]	5.6, 6.3[10]	5.5[10]	
(6.7 h)	C	4.78±.16[b][20]		5.97±.20[b][20]	7.53±.30[b][20]
	C	4.80±.15[b][25]		6.29±.20[b][25]	7.62±.26[b][25]
^{135}Xe	D	.195±.016[23]	.044±.017[23]	.162±.025[23]	.070±.040[23]
(9.16 h)	D	.218±.005[24]	.0341±.0019[24]	.1512±.0017[24]	.0321±.0012[24]
	C	6.12±.16[c]	5.9[10]	7.22±.20[c]	7.83±.25[c]
^{135}Cs	C	6.02±.18[11]	6.45±.19[15]	7.43±.20[17]	7.08±.35[21]
$3x10^6$y	C			6.95±.19[12]	
^{143}Ce	C	6.99±.35[13]	5.4[10]	5.1[10]	
(33 h)	C	5.77[22]	5.88[22]		
^{143}Nd	C	5.19±.17[12]	5.8±.2[12]	6.10±.15[12]	
(stable)	C	5.87±.10[14]	5.89±.06[14]		
	C		5.71±.18[15]	4.56±.14[18]	4.44±.22[21]
	C		6.16±.18[10]		
^{147}Nd	C		2.6[16]	2.2[19]	
(11.1 d)	C	1.77[22]	2.21[22]		
^{147}Pm	C		2.6[10]		
(2.65 y)	C	1.53±.06[12]	2.9±.4[12]	2.58±.05[12]	
^{147}Sm	C	1.79±.06[14]	2.13±.05[14]		
(10^{11}y)	C		2.16±.06[15]	1.99±.06[18]	

[a] C ≡ percent cumulative yield to this isotope; D ≡ fractional direct (independent) yield to this isotope.

[b] Relative ^{135}I yields normalized to 6.25% for ^{235}U fission. Uncertainty includes 3% uncertainty in this value.

[c] Sum of cumulative yield to ^{135}I (av. of [20] and[25]) and direct yield to ^{135}Xe[24].

forced to use rather dubious methods in arriving at a set useful for reactor calculations.

The spread in cumulative yield values is apparent in recent surveys of data up to 1962 [7, 8, 9]. Fortunately there are signs that the situation is improving. Table II lists measurements of thermal neutron fission yields for masses 135, 143 and 147. More recent values (1962 and later), which are underlined, are quite consistent. For this reason, I have great hope that mass spectrometric and radiometric measurements now in progress will provide the basis for a complete set of thermal fission yields reliable to 2% or better. A comparison of the ^{235}U results from McMaster University and the USAEC National Reactor Testing Station [15, 14] in general differ by less than 3% but even here there are difficulties. For the Kr isotopes the disagreement is approximately 10% and for ^{154}Sm approximately 25%. The radiometric yields of Bunney and Scadden [22] agree with the recent mass spectrometric values within approximately 2% except at masses 149 (^{233}U) and 153 (^{235}U).

The direct or independent yields of fission fragments are of less importance than cumulative yields to long-lived or stable nuclides in calculations of fission-product absorption. The data up to 1962, mainly for ^{235}U, has been reviewed by Wahl et al.[26] and a semi-empirical model of nuclear charge distributions for fission proposed. Additional work is reported by Wolfsberg [27] who has extended the model to include ^{233}U and ^{239}Pu fission.

The results of some recent work diverge markedly from the predictions of this model however. Direct yields of ^{135}Xe (Table II) measured at Chalk River [23, 24] are about twice the predicted values [23] for ^{233}U and ^{239}Pu fission. There is also evidence that the yields of ^{140}La in ^{233}U and ^{239}Pu fission are unexpectedly large [20]. A recent attempt to observe the direct yield of the shielded nuclide ^{148}Pm gave an upper limit of (1/50)th the predicted value [28]. Also, the primary distributions of nuclear charge for ^{235}U fission fragments reported by Konecny et al.[29] and the study of delayed neutron precursors by Herrmann et al.[30] indicate that the width of the primary charge distribution may vary with both mass and the fissioning nucleus. It appears, therefore, that there is some doubt about the applicability of the semi-empirical model of Wahl et al.[26] for predicting direct yields, particularly in ^{233}U and ^{239}Pu fission.

3. CROSS-SECTIONS

For calculating absorption in well-moderated reactors, fission-product cross-sections can be separated into thermal and epithermal components. At Chalk River we use the Westcott treatment of reaction rates and reactor flux [31], in which the effective capture cross-section, $\hat{\sigma}$, is related to the 2200 m/s cross-section, σ_o, and the reduced resonance integral, I' (i.e. with 1/v portion not included), by

$$\hat{\sigma} = g\sigma_o + I' r\sqrt{\frac{4T}{\pi T_o}}$$

Here r, the epithermal index, is approximately equal to the fraction of the total neutron density in the epithermal region, and g, which is a function of neutron temperature, T, is equal to $\hat{\sigma}/\sigma_o$ in a pure Maxwellian flux ($r = 0$). The majority of fission products have cross-sections which vary very nearly as 1/v in the thermal region of interest in well-moderated reactors, and for these $g \simeq 1.0$.

Fission products may be classified as "saturating" and "non-saturating". If $(\hat{\sigma}\phi+\lambda) >> \hat{\sigma}_a$, where ϕ is the flux, λ is the fission-product decay constant and $\hat{\sigma}_a$ is the absorption cross-section of the fissile material, then the fission-product concentration will reach an equilibrium value during an extended irradiation. For these "saturating" fission products neutron capture is proportional to $(1+(\lambda/\hat{\sigma}\phi))^{-1}$. Neutron capture in non-saturating fission products $\left((\hat{\sigma}\phi+\lambda) << \hat{\sigma}_a\right)$ is proportional to $\hat{\sigma}$.

3.1 RESONANCE INTEGRALS

Of the nuclides listed in Table I, the resonance integral of ^{103}Rh had an uncertainty of $\sim$ 50% at the time of the 1964 fission-product review

TABLE III

CROSS-SECTION MEASUREMENTS: ^{105}Rh and ^{148}Pm

^{105}Rh	Experimenter	Method	σ_o (kilobarns)	I' (kilobarns)	$\hat{\sigma}$ (kilobarns)
	Cuninghame et al. [37]	Mass spectrometer, anomaly in fission yields			≥ 18
	Glendenin et al. [38]	Activation[a] - TRIGA reactor (30 sec activity)			14.4 ± 2.0
		CP5 reactor (2.2 h activity)			5.8 ± 1.2
	Lantz et al. [39]	Mass spectrometer, Pd isotopes			25.4 ± 2.5
	Lantz et al. [40]	Mass spectrometer, Pd isotopes	~20	165	

[a] Both ^{106}Rh isomers decay by β-emission only. These cross-sections would be additive except that TRIGA was operated in pulsed mode so that the thermal component is at a high temperature.

^{148}Pm	Experimenter	Method	$\bar{\sigma}(^{148g}Pm)$ (kilobarns)	$\bar{\sigma}(^{148m}Pm)$ (kilobarns)
	Schuman, Berreth [41]	Activation	3 ± 2	29 ± 5
	Tomlinson [42]	Mass spectrometer, Sm isotopes	~1.4	~30
	Fenner, Ridley [43]	Mass spectrometer, Sm isotopes		21 ± 2.5

TABLE IV

CROSS-SECTION MEASUREMENTS: ^{147}Pm

Method	Sample	→ 5d ^{148g}Pm		→ 42d ^{148m}Pm		Both Isomers[d]	
		σ_o barns	I' barns	σ_o barns	I' barns	σ_o barns	I' barns
Activation [44]	^{147}Pm	60 ± 20[a]					
Time-of-flight [45]	^{147}Pm					180 ± 20	2220[b]
Mass spectrometer [46]	^{233}U					200 ± 50[a, c]	
Activation [47]	^{147}Pm	120	900	140	1200	(260)	(2100)
Activation [41]	^{147}Pm	111 ± 11	1520 ± 230	124 ± 13	1700 ± 250	(235)	(3200)
Mass spectrometer [43]	^{147}Pm	83.3 ± 7.8	610 ± 100	73.4 ± 7.4	590 ± 100	(157)	(1200)
Mass spectrometer [48]	^{235}U	54 ± 10[a]		150 ± 15[a]		(204)[a]	
Mass spectrometer [42]	^{147}Pm	105 ± 5	1074 ± 95	12 ± 9	1334 ± 166	(117)	(2408)

[a] Measurement of effective cross-section, $\hat{\sigma}$.

[b] Calculated from resonance parameters of ref. [44] including estimate of contribution from unresolved resonances.

[c] Irradiation at flux of 5.8×10^{13} n/cm^2 sec. No correction for possible neutron capture in ^{148m}Pm

[d] Values in brackets summed from preceding columns.

[2]. This discrepancy has now been resolved [32]. In the case of ^{131}Xe there is an uncertainty of ~ 25%. A recent measurement [43] of the ^{147}Pm resonance integral (Table IV) gives a value appreciably lower than some earlier work, and leaves the correct value to be used for this important fission product in doubt.

3.2 THERMAL CROSS-SECTIONS

On the basis of current knowledge the effective cross-sections of the two most important fission products, ^{135}Xe and ^{143}Nd, can be estimated with sufficient accuracy [33-37]. Although the uncertainty in σ for ^{135}Xe may be as great as 5%, if $(\lambda/\sigma\phi)<0.2$, as in most power reactors, the uncertainty in neutron absorption is less than 1%.

Two radioactive nuclides, 35-h ^{105}Rh and 42-d ^{148m}Pm, are known to have effective cross-sections of about 20 kb (Table III). Since cross-sections of this magnitude are associated with large capture resonances in or very near the thermal region, the effective cross-section is expected to be sensitive to neutron temperature ($g \neq 1.0$). Time-of-flight or crystal spectrometer measurements of $\sigma(E)$ from thermal energies to a few eV would permit the calculation of $g\sigma_0$ over a wide temperature range.

Because of this probable temperature dependence the ^{105}Rh cross-sections yielding the two ^{106}Rh activities [37], which were measured in fluxes with quite different neutron temperatures and epithermal components, cannot be simply added together. Further, the resonance integral listed in Table III is too large, by a factor of 3 or more in comparison with the thermal cross-sections, to be accounted for by a single Breit-Wigner resonance. Since $\lambda/\sigma\phi$ is about 5 for ^{105}Rh in a flux of $5 \times 10^{13} n/cm^2 sec$, neutron absorption, which is proportional to $(1+(\lambda/\sigma\phi))^{-1}$, will be nearly proportional to σ. For this reason the present uncertainty in the ^{105}Rh cross-section is too great and additional integral measurements are needed. For ^{148}Pm on the other hand, $\lambda/\sigma\phi$ is about 0.14, so that neutron absorption in this nuclide will be relatively insensitive to uncertainties in the cross-section.

Table IV shows the current state of ^{147}Pm cross-section measurements. The only cheerful note is that the ratio I'/σ_0 from the published activation measurement [41] and the time-of-flight data are in reasonable agreement, even though the absolute values differ by ~30%. At present the thermal and resonance integral of ^{147}Pm are the greatest single source of uncertainty in fission-product calculations.

Another group of nuclides that introduces a considerable uncertainty into neutron absorption calculations are those radioactive nuclides with half-lives greater than approximately 1 day having unknown cross-sections. For fission yields greater than ~ 0.1%, they will have a significant absorption if the cross-section is large enough. Table V lists these radioactive nuclides together with the hypothetical thermal cross-section each would need to change the reactivity by 0.2 millik in a well-moderated natural uranium reactor at a flux of $5 \times 10^{13} n/cm^2 sec$. I have included these radioactive fission products in the thermal cross-section

group because under these irradiation conditions resonance absorption is expected to be less than thermal absorption.

4. ASSESSMENT OF UNCERTAINTY IN FISSION-PRODUCT ABSORPTION

On the basis of the available data I have attempted to estimate the uncertainties in the yields and cross-sections and the effect on FISSPROD calculations. These are given in Table VI for ^{135}Xe, ^{143}Nd, the main absorbing nuclides in the mass range 147-154, and the more important of the remaining nuclides in Table I. The uncertainties, Δ, refer to the fission-product absorption cross-section in barns per initial fissile atom listed in the last three columns of Table I.

For non-saturating fission products Δ is the square root of the sum of the squares of the uncertainties in yield and cross-section. For saturating fission products the uncertainty in $(1+(\lambda/\sigma\phi))^{-1}$ is used. For the group from mass 147-154 the interdependence is included. Thus for ^{147}Pm a 10% uncertainty in yield or cross-section will be the source of the following uncertainties: 10% in ^{147}Pm, 10% in ^{148m}Pm, and 2.5% (25% of 10%) in ^{149}Sm. These would be summed to obtain Δ for ^{147}Pm.

In addition to the Δ's of Table VI there will be an error in estimating the contribution from the remainder of the fission products. In the case of those with known cross-sections this should be negligible. In FISSPROD calculations nuclides with unknown cross-sections have values assigned that are the average of cross-sections of neighbouring fission products grouped by neutron and proton number (even-even, even-odd, etc.). These estimated cross-sections account for from 2% to 4% of the calculated fission-product absorption. If the uncertainty in this estimate is assumed to be roughly equal to its magnitude, the radioactive "unknowns" might be expected to introduce an uncertainty in fission-product absorption comparable to that due to the major known neutron absorbers listed in Table VI. This is not the case, however, because the main contributors to absorption by the "unknowns" lie in the region of large cross-sections (mass 149 to 157) and are, in fact, mainly precursors of saturating nuclides such as ^{149}Sm and ^{151}Sm, so that total absorption for a given mass will be changed only by secondary effects. There remains the possibility that some of the other nuclides in Table V could have cross-sections larger than the "figure of merit".

5. COMPARISON WITH EXPERIMENT

Two measurements of fission-product absorption have been made by measuring the reactivity of irradiated fuel using a pile oscillator [49, 50]. In Table VII these results are compared with values computed to simulate the irradiation, $1\frac{1}{2}$ year cooling period and pile oscillator conditions of the Chalk River irradiations as closely as possible. The uncertainties in the computed values are the square root of the sum of the squares of a set of Δ values similar to those in Table VI, but referring to the particular irradiation conditions of the experiment. The ^{135}Xe and ^{105}Rh contributions are

TABLE V

RADIOACTIVE FISSION PRODUCT WITH UNKNOWN CROSS-SECTIONS

Nuclide	$T_{\frac{1}{2}}$ (days)	Figure[a] of Merit	Nuclide	$T_{\frac{1}{2}}$ (days)	Figure[a] of Merit	Nuclide	$T_{\frac{1}{2}}$ (days)	Figure[a] of Merit
^{99}Zr	65	15	^{126}Sn	10^7	300	^{147}Nd	11.1	270
^{99}Mo	2.8	370	^{127}Sb	3.7	8 000	^{149}Pm	2.2	3 000
^{103}Ru	40	60	^{129m}Te	33	600	^{151}Pm[c]	1.2	6 600[b]
^{107}Pd	10	20[b]	^{131m}Te[c]	1.2	13 000	^{153}Sn	1.96	11 000[b]
^{111}Ag	7.5	5000[b]	^{132}Te[c]	3.25	450	^{156}Eu	15	700[b]
^{125}Sb	950	1000	^{133}I[c]	0.9	1 120			

[a] Figure of merit is hypothetical cross-section in barns required by a particular nuclide to affect the reactivity of a well-moderated reactor fuelled with natural uranium (except where noted) by 0.2 millik in a flux of 5×10^{13} n/cm^2 sec.

[b] Figure of merit applies to ^{239}Pu fuel.

[c] Differences in mass spectrometric yields from samples of fissile material irradiated in high and low fluxes indicate an upper limit for the cross-section of this nuclide which is less than half the figure of merit.

TABLE VI

EVALUATION OF UNCERTAINTIES IN FISSION-PRODUCT ABSORPTION

Nuclide	Estimated Uncertainties (%) in					Δ[a]		
	$g\sigma_o$	I'	$y(^{233}U)$	$y(^{235}U)$	$y(^{239}Pu)$	^{233}U	^{235}U	^{239}Pu
^{135}Xe	±5	-	±3.5	±3	±3.5	±.55	±.50	±.56
^{143}Nd	±2	±10	±2	±2	±4	±.19	±.18	±.26
^{103}Rh	±4	±10	±10	±10	±4	±.10	±.18	±.25
^{105}Rh	±15	-	±10	±10	±4	±.04	±.08	±.42
^{131}Xe	±10	±25	±2	±2	±2	±.17	±.15	±.23
^{133}Cs	±3	±10	±3	±3	±4	±.05	±.06	±.08
^{147}Pm	+10 -20	+6 -50	±3	±3	±4	+.39 -.93	+.43 -1.03	+.48 -1.15
^{148m}Pm	±15	-	-	-	-	±.02	±.02	±.02
^{149}Sm	±10	-	±3	±2	±4	±.10	±.08	±.14
^{150}Sm	±10	±10	-	-	-	±.04	±.05	±.07
^{151}Sm	±10	-	±3	±3	±4	±.06	±.07	±.18
^{152}Sm	±5	±10	±3	±3	±4	±.04	±.05	±.11
^{153}Eu	±5	±10	±5	±4	±5	±.03	±.04	±.10

[a] Effect on fission-product absorption in barns per initial fissile atom for an irradiation of 1.0 n/kb at a flux of 5×10^{13} n/cm^2 sec.

not included since these nuclides will have decayed away. The radioactive "unknowns", however, increase the uncertainty appreciably in these calculations. For example, the larger the ^{149}Pm cross-section, the smaller will be the equilibrium concentration during irradiation of both ^{149}Pm and ^{149}Sm, and in consequence, after the fuel is removed from the reactor and the ^{149}Pm has decayed, the smaller will be the final amount of ^{149}Sm. The radioactive "unknowns" in the region of large cross-sections are assumed to have cross-sections of 10 ± 10 kilobarns in calculating the values in Table VI. The corresponding uncertainty in absorption is about 1 barn per fission.

The agreement between the calculated cross-section for ^{235}U and the measurements reported by Nisle et al. [49] is satisfactory, although insufficient information is provided concerning the irradiations to decide whether they are reasonably approximated by the conditions assumed in the calculations.

The experimental work of Okazaki et al. is well documented [50]. Each irradiated sample was analyzed for either uranium or plutonium content and the isotopic abundances of these elements were measured mass

TABLE VII

COMPARISON OF MEASURED AND COMPUTED FISSION-PRODUCT ABSORPTION

Experimenter	^{233}U		^{235}U		^{239}Pu	
	σ_o[a]	I'[a]	σ_o[a]	I'[a]	σ_o[a]	I'[a]
Nisle et al. [49]			55 ± 4	160 ± 30[b]	(64% burnup)	
			47 ± 3	148 ± 30[b]	(81% burnup)	
			51 ± 4	124 ± 25[b]	(77% burnup)[c]	
Okazaki et al. [50]	32.0 ± 2.8[d]	208 ± 45[d]	38.6 ± 3.2[f]	259 ± 47[f]	50.7 ± 4.8[h]	214 ± 89[h]
	29.6 ± 2.5[e]	201 ± 41[e]	38.4 ± 3.0[g]	223 ± 44[g]	48.8 ± 5.1[i]	176 ± 89[i]
Calculated Cross-Sections[j]	45.3[d] +1.3 / 42.6[e] -1.5	154[d] +7 / 148[e] -15	48.9[f] +1.5 / 47.6[g] -1.7	179[f] +8 / 175[g] -16	56.8[h] +1.7 / 54.8[i] -1.9	251[h] +11 / 241[i] -17

[a] In barns per fission.

[b] The resonance integral above 0.12 eV was measured. This has been reduced by 0.9 σ_o to obtain the value of I' listed.

[c] This irradiation was done in a harder spectrum.

[d] $\phi = 6.47 \times 10^{13}$ n/cm^2 sec, $\phi t = 2.286$ n/kb, 74% burnup.

[e] $\phi = 8.20 \times 10^{13}$ n/cm^2 sec, $\phi t = 2.899$ n/kb, 82% burnup.

[f] $\phi = 5.75 \times 10^{13}$ n/cm^2 sec, $\phi t = 2.031$ n/kb, 74% burnup.

[g] $\phi = 6.40 \times 10^{13}$ n/cm^2 sec, $\phi t = 2.286$ n/kb, 78% burnup.

[h] $\phi = 6.08 \times 10^{13}$ n/cm^2 sec, $\phi t = 2.150$ n/kb, 92% burnup of ^{239}Pu, 8% of fissions from ^{241}Pu.

[i] $\phi = 7.38 \times 10^{13}$ n/cm^2 sec, $\phi t = 2.609$ n/kb, 95% burnup of ^{239}Pu, 11% of fissions from ^{241}Pu.

[j] Uncertainties are based on the percent uncertainties in yield and cross-sections listed in Table VI, and include a contribution of ±1 barn due to radioactive "unknowns".

spectrometrically. The standard samples, containing various amounts of fuel, boron, or a mixture of the two, had a range of reactivities that included the reactivity range of the irradiated samples. The fission-product absorption was resolved into a thermal and epithermal component on the basis of measurements in two fluxes with different epithermal components. Since the two spectra were not very different, the magnitudes of these components may be open to question. In this case, a comparison of measured and calculated effective cross-sections will be more meaningful. If the four results for each fuel (two spectra, 2 irradiations) are averaged the differences in barns per fission are 9 ± 1 for ^{233}U, 5 ± 1.5 for ^{235}U and 10 ± 2 for ^{239}Pu, where the quoted errors represent the approximate spread in the four values. Calculated values are the greater in each case. This work has been reviewed intensively and a number of auxiliary experiments are planned.

It is difficult to see how the calculated absorption could be reduced by 5-10 barns. Referring to Table I, it appears that only the diversion of a large fraction of the yields of ^{143}Nd, ^{147}Pm and ^{149}Sm could account for this discrepancy. If this were the case high flux irradiations should give very high yields of ^{144}Nd, ^{148}Nd and ^{150}Sm, and this has not been observed [46] (or compare Nd yields of [14] and [15]).

To summarize, uncertainties in yields and measured cross-sections have been shown to introduce an uncertainty of about $2\frac{1}{2}\%$ in calculations of fission-product absorption, mostly attributable to uncertainties in the cross-section of ^{147}Pm and the yields of ^{135}Xe. Radioactive fission products for which the cross-sections are not yet known will increase this uncertainty appreciably during reactor shut-downs. In one case in which calculations were compared to measurements, there was reasonable agreement, but in a second case the measured values are 10-20% lower than calculated. No simple explanation of this discrepancy seems possible.

6. ACKNOWLEDGEMENTS

I am indebted to Dr. C. H. Millar for a critical review of this paper, to Dr. M. F. Duret, Dr. M. J. Halsall and Mr. A. G. Ward for discussions on the reactivity of thermal reactors after long irradiations, and to Dr. A. Okazaki for help in reaching a fuller understanding of the pile oscillator technique. I would like to thank Dr. R. G. Nisle, Dr. R. H. Tomlinson and Dr. R. C. Hawkings for granting the use of unpublished experimental results.

REFERENCES

[1] WAY, K., USAEC publication CP-2465 (1944).

[2] WALKER, W. H., Atomic Energy of Canada report AECL-2111 (1964).

[3] WALKER, W. H. (with appendix by KUSHNERIUK, S. A.) Atomic Energy of Canada report AECL-1054 (1960).

[4] DURET, M. F., DURHAM, R. W., LOUNSBURG, M., OKAZAKI, A., WALKER, W. H., WARD, A. G., PEASE, L., Proc. 3rd ICPUAE 3, 347 (1964).

[5] BAIN, F., KENNEDY, J. M., to be published as Atomic Energy of Canada report.
[6] WALKER, W. H., to be published as Atomic Energy of Canada report.
[7] KATCOFF, S., Nucleonics 18, 201 (Nov., 1960)
[8] FERGUSON, R. L., O'KELLEY, G. D., USAEC report ORNL-3305 (1962).
[9] ZYSIN, Yu. A., LBOV, A. A., SEL'CHENKOV, L. I., "Fission Product Yields and Their Mass Distribution" Consultants Bureau, New York 1964, (Russian original, Moscow, 1963).
[10] STEINBERG, E. P., GLENDENIN, L. E., Proc. 1st ICPUAE 7 3 (1955).
[11] BIDINOSTI, D. R., IRISH, D. E., TOMLINSON, R. H., Can. J. Chem. 39, 628 (1961).
[12] ANIKINA, M. P., ARON, P. M., GORSHKOV, V. K., IVANOV, R. N., KRIZHANSKY, L. M., KUKAVADZE, G. M., MURIN, A. N., REFORMATSKY, I. A., ERSHLER, B. V., Proc. 2nd ICPUAE 15, 446 (1958).
[13] SANTRY, D. C., YAFFE, L., Can. J. Chem. 38, 421 (1960).
[14] MAECK, W., REIN, J. E., (editors) USAEC progress report IDO-14667 (1965). (Other data in IDO-14660, IDO-14663, IDO-14676).
[15] FARRAR, H., TOMLINSON, R. H., Nucl. Phys. 34, 367 (1962). (For yield at light masses see H. Farrar, H. R. Fickel, R. H. Tomlinson, Can. J. Phys. 40, 1017 (1962).
[16] SWIATECKI, W. J., Phys. Rev. 100, 936 (1955).
[17] BAYLY, J. G., DURET, M. F., POULSEN, N. B., TOMLINSON, R. H., Can. J. Phys. 39, 1391 (1961).
[18] FICKEL, H. R., TOMLINSON, R. H., Can. J. Phys. 37, 926 (1959).
[19] BUNNEY, L. R., SCADDEN, E. M., ABRIAM, J. O., BALLOU, N. E., Proc. 2nd ICPUAE 15, 444 (1958).
[20] OKAZAKI, A., WALKER, W. H., Can. J. Phys. 43, 1036 (1965).
[21] FARRAR, H., CLARKE, W. B., TOMLINSON, R. H., THODE, H. G., Can. J. Phys. 42, 2063 (1964).
[22] BUNNEY, L. R., SCADDEN, E. M., J. Inorg. Nucl. Chem. 27, 273 (1965). (^{233}U yields have been re-normalized to their own ^{235}U yields rather than the ^{235}U reference yields used in their paper).
[23] OKAZAKI, A., WALKER, W. H., BIGHAM, C. B., Can. J. Phys. 44, 237 (1966).
[24] HAWKINGS, R. C., EDWARDS, W. J., OLMSTEAD, W. J. (Private communication, 1966).
[25] NISLE, R. G. (Private communication of results to be published in Nucl. Sci. Eng. These supersede values appearing in Nucl. Sci. Eng. 25, 93 (1966).
[26] WAHL, A. C., FERGUSON, R. L., NETHAWAY, R. L., TROUTNER, D. R., WOLFSBERG, K., Phys. Rev. 126, 1112 (1962).
[27] WOLFSBERG, K., Phys. Rev. 137, B929 (1965).
[28] UMEZAWA, H., Japan Atomic Energy Research Inst. report JAERI-1103 (1966).
[29] KONECNY, E., OPOWER, H., GUNTHER, H., GÖBEL, H., Proc. Salzburg Symp. on Phys. and Chem. of Fission I, 401 (1965).

[30] HERMANN, G., FIEDLER, J., BENEDICT, G., ECKHARDT, W., LUTHARDT, G., PATZETT, P., SCHLÜSSER, H. D., Proc. Salzburg Sym. on Phys. and Chem. of Fission II, 197 (1965).
[31] WESTCOTT, C. H., WALKER, W. H., ALEXANDER, T. K., Proc. 2nd ICPUAE 16, 70 (1958).
[32] WALKER, W. H., COPLEY, L. A., Can. J. Phys. 44 (1966) in press.
[33] FICKEL, H. R., TOMLINSON, R. H., Can. J. Phys. 37, 531 (1955).
[34] SMITH, E. C., PAWLICKI, G. S., THURLOW, P. E. F., PARKER, G. W., MARTEN, W. J., CREEK, G. E., LANTZ, P. M., BERSTEIN, S., Phys. Rev. 115, 1693 (1959).
[35] TATTERSALL, R. B., ROSE, H., PATTENDEN, S. K., JOWITT, D., J. Nucl. En. "A" 12, 32 (1960).
[36] BIANCHI, G., COLMIN, J., CORGE, C., HUYHN, V. D., MORGENSTERN, J., JULIEN, J., NETTER, F., VASTEL, M., reported in EANDC (E) 49, p. 52 (1963).
[37] CUNINGHAME, J. G., GLENDENIN, L. E., HARKNESS, A. L., J. Inorg. Nucl. Chem. 24, 1009 (1962).
[38] GLENDENIN, L. E., GRIFFIN, H. C., SCHMITT, R. A., Bull APS II; 9 (No. 2) 179 (1964).
[39] LANTZ, P. M., BALDOCK, C. R., IDOM, L. E., USAEC progress report ORNL-3488 p. 16 (1963).
[40] LANTZ, P. M., STOUGHTON, R. W., BALDOCK, C. R., IDOM, L. E., USAEC progress report ORNL-3679, p. 12 (1964).
[41] SCHUMAN, R. P., BERRETH, J. R., Nucl. Sci. Eng. 12, 519 (1962).
[42] TOMLINSON, R. H. (private communication of preliminary result).
[43] FENNER, N. C., RIDLEY, R. G., et al. Reported in EANDC-47U (1965).
[44] PARKER, G. W., LANTZ, P. M., INGHRAM, M. G., HESS, D. C., HAYDEN, R. J., Phys. Rev. 72, 85 (1947).
[45] HARVEY, J. A., BLOCK, R. C., SLAUGHTER, C. G., MARTEN, W. J., PARKER, G. W., Proc. 2nd ICPUAE 16, 150 (1958).
[46] BIDINOSTI, D. R., FICKEL, H. R., TOMLINSON, R. H., Proc. 2nd ICPUAE 15, 459 (1958).
[47] STOUGHTON, R. W., HALPERIN, J., DRUSCHEL, R. E., JOHNSTON, F. J., LANTZ, P. M., OLIVER, J. H., PARKER, G. W., USAEC report WASH-1031, p. 43 (1960).
[48] Reported in USAEC progress report ORNL-TM-889, p. 6 (1964).
[49] NISLE, R. G., deBOISBLANC, D. R., FAST, E., CONNOR, J. C., GUNST, S. B., Proc. 3rd ICPUAE 3, 398 (1964).
[50] OKAZAKI, A., DURHAM, R. W., LOUNSBURY, M., Atomic Energy of Canada reports AECL-2510 (1966) and AECL-2506 (1966).

DISCUSSION

R. VIDAL: Does your value for total capture of ^{235}U fission products agree with the Okazaki measurements on the Pool Test Reactor at Chalk River, or is it higher? Measurements now being carried out in France on natural uranium give results considerably higher than the Okazaki ones.

W.H. WALKER: The calculations give a cross-section approximately 5 b higher than the Okazaki result for ^{235}U fission.

FISSION-PRODUCT NEUTRON-CAPTURE CROSS-SECTIONS IN THE ENERGY RANGE 1 keV - 10 MeV*

V. BENZI AND M.V. BORTOLANI
CENTRO DI CALCOLO DEL COMITATO NAZIONALE PER L'ENERGIA NUCLEARE, BOLOGNA, ITALY

Abstract

FISSION-PRODUCT NEUTRON-CAPTURE CROSS-SECTIONS IN THE ENERGY RANGE 1 keV-10 MeV. In this work the radiative capture cross-sections of nuclei produced in the fission process are evaluated in the energy range 1 keV-10 MeV by means of the statistical model formulae. Competition between capture and inelastic scattering is considered. In addition, the contribution due to the direct capture process is roughly estimated. Whenever possible theoretical values are compared with the experimental ones.

1. INTRODUCTION

To solve the problem of the poisoning of a reactor by fission products, it is necessary to know the capture cross-sections of more than sixty nuclei. Such a requirement is rather well fulfilled at low energies, since the thermal absorption cross-sections of most of the important fission products have been measured.

As far as the higher energies are concerned, the data available are quite scarce, so that theoretical estimates are required. For this purpose, the statistical model methods have been used in the past by several authors, under various simplifying assumptions [1-4]. This paper gives some results of an evaluation of radiative capture cross-sections of fission products in the energy range 1 keV - 10 MeV, which have been obtained on the basis of the available experimental data and statistical model calculations, taking into account the competition between capture and inelastic scattering processes.

2. THE MODEL

The radiative capture cross-section for a neutron of kinetic energy E captured by a target nucleus of spin I can be written in terms of neutron penetrabilities $T_\ell(E)$ as

$$\sigma_{n\gamma}(E) = \frac{\pi \lambda^2}{2(2I+1)} \sum_{\ell} T_\ell(E) \sum_{J} \frac{\varepsilon^J_{j\ell} (2J+1) f(E;E)}{1+\xi_J f(E;0) \sum_{\ell'} \sum_{n} \varepsilon^J_{j_n \ell'} T_{\ell'}(E-E_n)} \quad (1)$$

where J is the compound nucleus spin; ℓ and ℓ' are orbital momenta of the incident and the emitted neutrons; E_n is the energy of the n-th ex-

* Work performed under CNEN-EURATOM contract.

cited residual level. Factors $\epsilon^J_{J\ell}$ and $\epsilon^J_{J_n\ell'}$ are the accessible reaction channel numbers; moreover

$$\xi_J = D^J(B_n)/2\pi\Gamma^J_\gamma(B_n)$$

$$f(E;\omega) = \int_\omega^{B_n+\omega} \varepsilon^{2\varphi+1}\,\rho_{oc}(U-\varepsilon)d\varepsilon \Big/ \int_0^{B_n+E} \varepsilon^{2\varphi+1}\,\rho_{oc}(U'-\varepsilon)d\varepsilon$$

with B_n the neutron binding energy, U and U' excitation energy, 2φ the multipole type of the radiation emitted in the γ-decay of the compound nucleus (index c), and ρ_{oc} (U) density of states at excitation energy U. The inelastic scattering by target nucleus levels with unknown characteristics can be taken into account approximately by putting

$$\sum_{\ell'}\sum_n \varepsilon^J_{j_n\ell'}\,T_{\ell'}(E-E_n) \approx \sum_{\ell'}\sum_{n\le p} \varepsilon^J_{j_n\ell'}\,T_{\ell'}(E-E_n) + \int_{E_p}^{E} (2J+1)\rho_{ot}(E-\varepsilon)\sum_{\ell'} T_{\ell'}(\varepsilon)d\varepsilon$$

where E_p is the energy of the highest known level and ρ_{ot} (U) is the density of states of the target nucleus at excitation energy U. Under the hypothesis of high level density and the assumption of an equal distribution of levels between the two parities, Eq. (1) reduces to [5]

$$\sigma_{n\gamma}(E) \approx \frac{\pi^2\hbar^2}{2m}\left(\mu+\frac{\nu}{E}\right)\bar{\Gamma}_\gamma(B_n)\rho_{oc}(B_n)\cdot \frac{g(E)}{\int_0^E (\mu\varepsilon+\nu)\rho_{ot}(U-\varepsilon)d\varepsilon} \qquad (2)$$

with $\bar{\Gamma}_\gamma$ (B_n) average radiation width at neutron binding excitation energy (assumed to be parity and J-independent) and

$$g(E) = \int_E^{E+B_n} \varepsilon^{2\varphi+1}\,\rho_{oc}(U'-\varepsilon)d\varepsilon \Big/ \int_0^{B_n} \varepsilon^{2\varphi+1}\,\rho_{oc}(U''-\varepsilon)d\varepsilon$$

The quantities μ and ν are empirical A-dependent parameters defined by

$$\sigma_c(E) \approx \sigma_g(\mu+\nu/\varepsilon)$$

where σ_c (E) and σ_g are the compound and geometrical cross-sections respectively of a nucleus of mass number A. Eq. (1) provides a method for estimating neutron radiative capture cross-sections which represents an average over resonances in the low energy region and which approximates the actual cross-sections in the smoothly varying region if only neutron and γ-ray emission are allowed. It must be noted that in Eq. (1) the fluctuations of the neutron widths around the average value are

neglected. In addition, direct and cascade capture are not taken into account, two processes which can play an important role at energies of several MeV [6, 7]. The direct capture cross-section can be estimated very roughly by means of the following formula [6]

$$\left[\sigma_{n\gamma}(E)\right]_d \approx K \frac{Z^2}{A} \left[(E+4)/E^{\frac{1}{2}}\right]^3 \qquad (3)$$

where E is in MeV, K is constant and Z is the atomic number.

3. THE LEVEL DENSITY FORMULA

To compute $\sigma_{n\gamma}(E)$ by means of Eqs. (1) and (2), it is necessary to specify the dependence of the level density $\rho_0(U)$ on the excitation energy U. It is well known that the number of levels as a function of the excitation energy for neighbouring nuclei mainly depends on the odd-even character of the nucleus considered. This effect manifests itself as a shift on the excitation energy U of the order of the pairing energy of the nuclei considered.

This means that the level density $\rho_0(U)$ of a nucleus is independent of the odd-even character of the nucleus itself, if an effective excitation energy $\bar{U}$ is defined in a suitable manner. If U is the excitation energy evaluated from the ground state and 2δ a positive quantity of the order of the pairing energy, one has

$$\left[\rho_0(U)\right]_{\text{odd-A}} \approx \left[\rho_0(U+\delta)\right]_{\text{even-even}}$$

$$\left[\rho_0(U)\right]_{\text{odd-odd}} \approx \left[\rho_0(U+2\delta)\right]_{\text{even-even}}$$

so that the effective excitation energy is

$$\bar{U} = U + \Delta$$

with

$$\Delta = \begin{cases} 0 & \text{for even-even nuclei} \\ \delta & \text{for odd-A nuclei} \\ 2\delta & \text{for odd-odd nuclei} \end{cases}$$

It can be noted that 2δ is more frequently assumed to be a negative quantity. In this case the definition of Δ must be reversed, i.e. $\Delta = 2\delta$ for even-even nuclei and $\Delta = 0$ for odd-odd nuclei.

The choice of 2δ as a positive quantity gives some advantages in performing the integrations in Eqs. (1) and (2). For the dependence of ρ_0 on $\bar{U}$ there are several formulae. A very simple one, based on the gas-like model [8], is

$$\rho_o(\bar{U}) = C\left[A(\bar{U}+t)\right]^{-2} \exp\left[2(b\bar{U})^{\frac{1}{2}}\right] \qquad (4)$$

where C is a constant for all nuclei, A the mass number of the nucleus considered, b is a parameter and t is defined by

$$\bar{U} = bt^2 - t$$

Eq. (4) contains three parameters, namely C, b and Δ (or δ). This last quantity can be estimated as a function of A by means of an empirical relationship given by Newton [9]

$$2\delta \approx 0.82(4-A/100)\text{MeV} \quad ; \quad A > 40 \qquad (5)$$

As far as the parameters b are concerned, they can be obtained from the analysis of the observed low-energy resonance spacings. If $\bar{D}_{obs}$ is the observed mean spacing for $\ell = 0$ neutron resonances for a target nucleus of spin I, one has

$$\rho_o(B_n) \approx \left[(2I+1)\bar{D}_{obs}\right]^{-1} \approx \frac{n-1}{(2I+1)(E_H - E_L)}$$

where n is the total number of observed resonances, and E_H and E_L are the energies of the observed higher and lower resonances, respectively. From the values of $\rho_o(B_n)$ obtained in this way the b-values can be estimated by means of Eq. (4) and by assuming [5]

$$C = 1 \text{ MeV}$$

when $\bar{U}$ and t are expressed in MeV and ρ_o in $(\text{MeV})^{-1}$. In Fig. 1 the dependence of b on the neutron number N of the nucleus is shown. There is a reasonably good behaviour of b as a function of N, and it seems that the full line drawn through the points can be used with some confidence for an estimate of b when experimental values of $\bar{D}_{obs}$ are lacking. There are some b-values which strongly deviate from the general behaviour. They correspond to the level densities of ^{98}Mo, ^{100}Mo and Tl isotopes. The anomalous behaviour of Tl isotopes has been pointed out also by other authors [10].

For the Mo isotopes, the high value of the parameter b (which corresponds to a low value of $\bar{D}_{obs}$) may be due to the presence of p-resonances at low energies, which have been considered as s-resonances.

4. CROSS-SECTION CALCULATIONS

To evaluate the radiative capture cross-sections of the fission product nuclei in the energy range 1 keV - 10 MeV, the following procedure was adopted. First, the experimental data available on $\sigma_{n\gamma}$ were renormalized, whenever possible, to the same standard value. The main source of these data was Ref. [11]. Then computations were performed starting with the average experimental values of $\bar{D}_{obs}$ and $\bar{\Gamma}_\gamma$ obtained from the

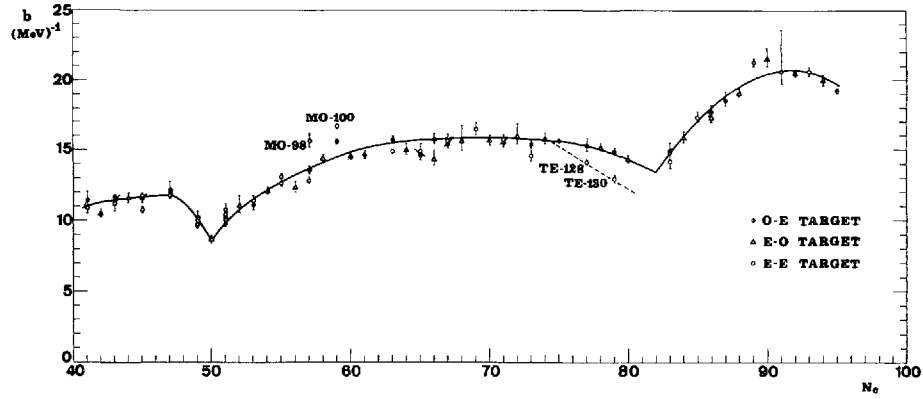

FIG.1. b-values from the analysis of $\bar{D}_{obs}$ as a function of neutron number N_C.

analysis of low-energy resonances. The radiation widths $\bar{\Gamma}_\gamma$ were assumed to be J- and π-independent whereas the J-dependence of D^J was assumed to be given by $D^J = [(2J+1)\,\rho_o\,]^{-1}$.

When $\bar{D}_{obs}$ and $\bar{\Gamma}_\gamma$ were lacking, an estimate was obtained by means of Eq. (4) and the full line curves of Figs. 1 and 2. The penetrabilities

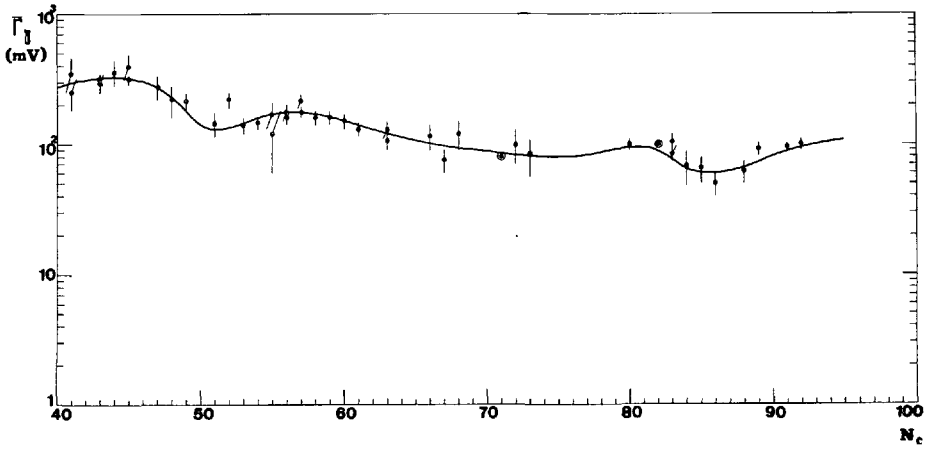

FIG.2. Values of average radiation widths as a function of the neutron number in the compound nucleus.

T_ℓ (E) were computed according to the "black nucleus" model, with a nuclear radius given by $R = 1.25\ A^{\frac{1}{3}} \times 10^{-13}$ cm. The maximum ℓ-value considered was $\ell = 4$, and the number of excited levels allowed was up to 10.

It can be noted that Eq. (1) is not very sensitive to the values of T_ℓ (E). It has been shown [12] that if one increases or decreases all the T_ℓ (E) by a factor of about 10, the cross-section does not vary more than by a factor of about 2, except at very low energies where $\sigma_{n\gamma}$ is proportional to T_o only. For this reason, and to reduce considerably the computer time required for the calculations, the "black nucleus" model has been adopted. The validity of Eq. (2) was assumed above 2 MeV, whenever a

detailed level scheme was not available up to or above this energy. For μ and ν parameters, the following A-dependences were adopted [13]

$$\mu = 0.76 + 2.2\ A^{-1/3}$$

$$\nu = 2.12\ A^{-2/3} - 0.05$$

Only dipole γ-ray emission was assumed both in Eqs.(1) and (2). The validity of Eq.(3), whose values were added to those obtained by compound nucleus calculations, was assumed above 4 MeV. The value of the

TABLE I. DATA FOR FISSION PRODUCT CROSS-SECTIONS

Target Nucleus		y x 10^2	$\bar{\Gamma}_\gamma$ (mV)	$\bar{D}_{obs}$ (eV)	$\sigma_{n\gamma}$(mb) 10^3eV	10^4eV	10^5eV	10^6eV	10^7eV
Kr-83	*	0.544	230	35	7916	1253	278	51.7	1.4
Kr-84	*	1.000	180	6868	175	56	16	4.3	1.4
Kr-85	*	0.293	140	1009	356	77	14	1.4	1.3
Rb-85		1.007	185	127	2738	467	109	10.7	1.4
Kr-86	*	2.020	130	36600	52	9	3	2.7	1.3
Rb-87		2.490	130	1422	265	60	12	2.0	0.03
Sr-88	*	3.570	130	17400	82	19	6	4.7	1.5
Y -89		4.790	105	2509	170	44	11	4.5	1.5
Sr-90	*	5.770	150	7440	150	45	13	3.5	1.4
Zr-91		5.840	160	572	656	142	28	15.0	1.5
Zr-92		6.030	150	3286	262	88	24	10.6	1.5
Zr-93	*	6.450	160	249	1362	266	57	16.7	1.5
Zr-94		6.400	160	2000	406	134	36	17.0	1.5
Mo-95		6.270	205	95	3761	629	157	69.8	1.6
Zr-96		6.330	150	3328	262	88	25	10.5	1.5
Mo-97		6.090	190	75	4250	706	180	72.7	1.6
Mo-98		5.780	160	1156	642	193	55	20.8	1.6
Tc-99	*	6.060	180	21	9170	1633	454	177.8	1.6
Mo-100		6.300	170	1560	526	167	47	12.4	1.5
Ru-101	*	5.000	170	22	8668	1525	427	40.0	1.7
Ru-102		4.100	170	229	2733	524	198	73.5	1.7
Rh-103		3.000	195	33	8095	1444	472	83.8	10.6
Ru-104		1.800	130	498	1114	287	90	20.9	10.3
Pd-105	*	0.900	150	9.6	11763	2358	689	72.7	1.8
Pd-106	*	0.380	140	339	1661	375	128	42.3	1.8
Pd-107	*	0.190	130	9.4	11247	2202	642	71.4	1.7
Pd-108		0.090	140	382	1500	352	118	33.9	1.7

Table I Cont.

Target Nucleus		y x 10^2	$\bar{\Gamma}_\gamma$ (mV)	$\bar{D}_{obs}$ (eV)	$\sigma_{n\gamma}$(mb) 10^3eV	10^4eV	10^5eV	10^6eV	10^7eV
Ag-109		0.030	170	18	10094	1939	645	143.3	1.8
Cd-111	*	0.019	110	20	7820	1396	468	72.8	1.8
Cd-112	*	0.010	105	250	1686	384	131	50.2	1.8
Cd-113	*	0.012	100	26	6340	1104	370	87.3	1.8
In-115		0.0104	70	11	7754	1346	370	185.6	1.8
Sb-121		0.015	88	9.6	9444	1736	285	99.5	1.9
Sb-123		0.0013	80	19	6054	1033	276	27.7	1.8
Sb-125	*	0.021	80	21	5614	959	254	128.1	1.8
Te-126		0.020	65	740	452	151	44	12.8	1.9
Sn-126	*	0.080	82	1316	347	118	35	40.2	1.7
I -127		0.139	100	14	8308	1482	333	82.3	1.9
Te-128		0.411	65	2704	182	54	17	4.1	1.8
I -129	*	0.800	85	18	6512	1123	248	33.3	1.9
Te-130		2.000	65	6313	110	26	8	2.7	1.8
Xe-131	*	2.650	85	36	4070	713	182	25.5	1.9
Xe-132	*	4.380	90	795	557	182	53	15.9	1.9
Cs-133		6.900	90	24	5582	961	234	28.1	2.0
Xe-134	*	8.060	95	1430	368	125	37	14.8	1.9
Cs-135	*	6.410	95	55	3141	567	135	11.7	2.0
Xe-136	*	6.460	78	9802	96	20	7	8.6	1.9
Cs-137	*	6.150	78	392	503	111	22	3.3	1.9
Ba-138		5.740	46	14940	52	9	3	3.7	0.5
La-139		6.550	60	484	345	74	15	7.2	1.2
Ce-140		6.440	80	3340	186	55	18	19.4	2.1
Pr-141		6.000	60	103	1269	266	57	16.2	2.2
Ce-142		6.010	50	1155	274	90	29	8	2.1
Nd-143	*	6.030	65	36	3243	589	142	35.7	2.2

constant K was estimated, assuming that for neutrons of about 14 MeV the radiative capture process is practically due to the direct mechanism only. With such an hypothesis one obtains an average value of $\bar{K} \approx 10^{-3}$, if in Eq.(3) E is given in MeV. The results of the computations were compared, whenever possible, with the experimental values and, if necessary, $\bar{\Gamma}_\gamma$ and $\bar{D}_{obs}$ were adjusted until a reasonably good fit was reached.

5. RESULTS

Calculations have been performed at energy points $E_{r,s} = r \cdot 10^s$ keV, with r = 1, 2..., 9 and s = 1, 2, 3, 4. The nuclei considered are those shown

Table I Cont.

Target Nucleus		y x 10^2	$\bar{\Gamma}_\gamma$ (mv)	$\bar{D}_{obs}$ (eV)	$\sigma_{n\gamma}$(mb) 10^3eV	10^4eV	10^5eV	10^6eV	10^7eV
Nd-144	*	5.620	60	541	553	183	55	20.5	2.2
Nd-145	*	3.980	60	13	6311	1105	267	58.4	2.2
Nd-146	*	3.070	62	349	816	250	78	26.4	2.1
Pm-147	*	2.360	62	5	11020	2190	633	107.7	2.2
Nd-148		1.710	80	190	1705	417	147	47.4	2.1
Sm-149		1.130	70	3	13164	2916	880	111.1	2.2
Nd-150		0.670	85	113	2774	582	225	49.0	2.1
Sm-151	*	0.440	80	2.6	14231	2651	666	106.9	2.2
Sm-152		0.281	80	58	4433	833	344	95	2.2
Eu-153		0.169	95	1	16589	4682	1598	400	2.3
Sm-154		0.077	80	140	2209	501	138	48.5	4.3
Eu-155	*	0.033	100	1.4	16177	4415	1472	454.4	2.2
Gd-156		0.014	100	32	7615	1394	548	245.3	2.3
Gd-157	*	0.0078	105	4.4	13371	3025	818	120.4	2.3
Gd-158		0.002	110	90	4074	785	261	102.1	2.3
Tb-159		0.00107	110	3.7	14096	3331	938	220.5	2.3
Dy-161	*	7.6×10^{-5}	115	4.6	13467	3056	585	76.6	2.4

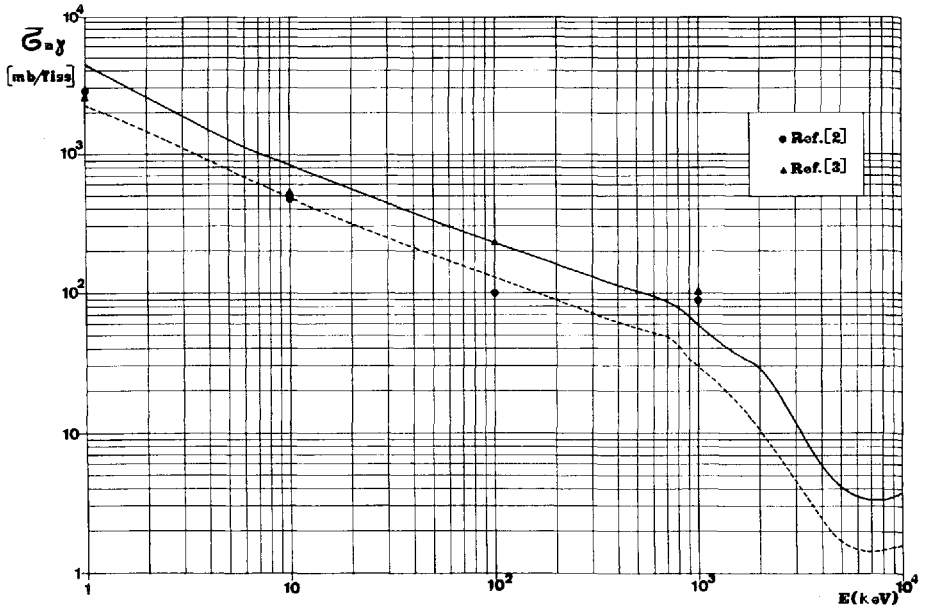

FIG.3. Energy dependence of the average radiative capture cross-section of a pair of ^{235}U fission fragments. The dashed line represents the contribution of all those nuclei for which no experimental measurements exist.

in Table I, in which the values of the cross-sections obtained at energies 10^3, 10^4, 10^5 and 10^6 eV are given.

An asterisk indicates those nuclei for which no experimental measurements in the energy range considered were found in Ref. [11]. In the same table the adopted values of $\bar{\Gamma}_\gamma$ and $\bar{D}_{obs}$ are reported, as well as the yields for thermal fission of ^{235}U taken from Ref. [14]. Figure 3 shows the energy dependence of the average capture cross-section $\bar{\sigma}_{n\gamma}$ obtained by summing the cross-sections of all the nuclei considered, weighted by the yield fraction. The dashed line represents the contribution of those nuclei for which no experimental measurements are available, whereas the points are the values of $\bar{\sigma}_{n\gamma}$ given in Refs. [2] and [3].

It is very probable that at low energies, below 10 keV say, our results

TABLE II. MEASURED AND THEORETICAL ISOTOPIC CROSS-SECTIONS FOR FISSION NEUTRONS

Target Nucleus	$\sigma_{therm.}$ (b)	$\bar{\sigma}$ (exp.) fiss. (mb)	$\bar{\sigma}$ (theor.) fiss. (mb)
Kr-84	0.1 ±0.03	< 10	6
Kr-86	0.06±0.02	2.4±0.8	1.9
Rb-85	0.91±0.08	29.2±2.6	17
Rb-87	0.12±0.03	1.8±0.5	2.8
Sr-88	0.0065	2.7	3.9
Y -89	1.0 ±0.2	5.0±1	4.0
Mo-98	0.2 ±0.02	16±2	23
Mo-100	0.2 ±0.05	13.6±3.4	15
Ru-102	1.44±0.16	36±4	70
Ru-104	0.7 ±0.2	31±10	26
Rh-103	152±32	109±20	84
Pd-108	9.3 ±0.7	130±10	36
Ag-109	86.2	178	137
In-115	202±16	234±18	154
Sb-121	6.0	79	65
I -127	6.12±0.20	96±3	68
Xe-136	0.28±0.028	1.9±0.2	5.4
Ba-138	0.5 ±0.1	2.3±0.4	1.9
La-139	8.2 ±0.8	4.9±0.5	6.1
Ce-140	0.59±0.06	11.8±1.2	13
Ce-142	0.94±0.05	4.6±0.3	11
Pr-141	11.3 ±0.6	11.0±0.6	12
Nd-146	1.8 ±0.6	40±12	28
Nd-148	3.4 ±1.0	73±21	43

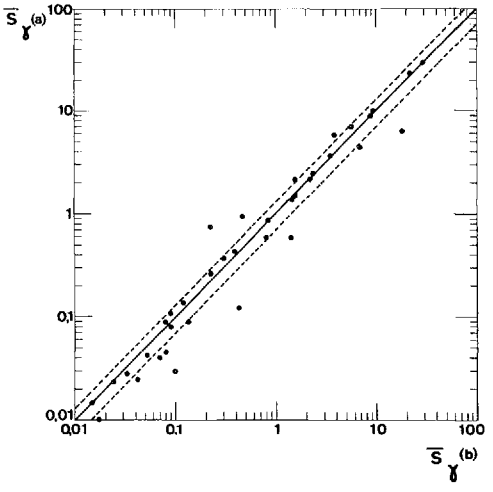

FIG. 4. Values of $\bar{S}_\gamma(a) = \bar{\Gamma}_\gamma/\bar{D}_{obs}$ obtained from fits of $\sigma_{n\gamma}$ versus $\bar{S}_\gamma(b)$ obtained from the full line curves of Figs. 1 and 2.

are overestimated, due to the fact that fluctuations around the average neutron width have been neglected.

In addition, our results are probably underestimated above 2 MeV, where only very rough calculations have been performed. As regards the energy range between 10 keV and 1 MeV, approximately, it can be noted that for not too low energies one has

$$\frac{|\delta\sigma_{n\gamma}|}{\sigma_{n\gamma}} \approx \frac{|\delta\bar{S}_\gamma|}{\bar{S}_\gamma}$$

where $\bar{S}_\gamma = \bar{\Gamma}_\gamma / \bar{D}_{obs}$. In Fig. 4 are plotted the values of $\bar{S}_\gamma$ obtained from the fit of the experimental measurements versus those obtained using the full line curves of Figs. 1 and 2 (quoted as $\bar{S}_\gamma(a)$ and $\bar{S}_\gamma(b)$ respectively).

Points falling in the region bounded by the two dashed lines indicate a difference between corresponding values less than 30%. As one can see, the agreement is in general rather good, and it seems reasonable to assume that the estimated cross-sections for those nuclei for which no experimental measurements exist are not in error by more than 50% on the average. Now, the contribution of these nuclei to the total cross-section is about 50%, so that the inaccuracy due to the "unknown" component is estimated to be about 25% at worst, i.e. when all the estimated cross-sections are systematically higher or lower.

For the "known" component the overall inaccuracy is expected to be appreciably lower, even if in some cases the cross-sections for single nuclei are subject to large uncertainties. To have an additional check, the theoretical cross-sections of some nuclei have been averaged over the fission spectrum. These average cross-sections have been compared with the experimental ones obtained by Hughes et al. [15], renormalized to more recent values of thermal activation cross-sections. The results are given in Table II, together with the values of the thermal cross-sections adopted. A rather good agreement is obtained for 20 nuclei out of 24.

ACKNOWLEDGEMENTS

Our grateful thanks are due to Mr. G. Panini who wrote the programme for the IBM 7094 computer and assisted with the numerical calculations.

REFERENCES

[1] BUSINARO, U.L. et al., J. nucl. Energy I 4 (1957) 319.
[2] GREEBLER, P. et al., Nucl. Sci. Engng 2 (1957) 334.
[3] GORDEEV, I.V., PUPKO, V.Y., Proc. 2nd UN Int. Conf. PUAE 6 (1958) 141.
[4] BENZI, V., SARUIS, A.M., Physics of Fast and Intermediate Reactors I IAEA, Vienna (1962) 179.
[5] BENZI, V., BORTOLANI, M.V., Nuovo Cim. 38 (1965) 216.
[6] LANE, A.M., LYNN, J.E., Nucl. Phys. 11 (1959) 646.
[7] ZAKHAROVA, S.M., MALYSHEV, A.V., Proc. Antwerp Int. Conf. on Study Nucl. Structure (1965) P/201.
[8] LANG, J.M.B., Le COUTEUR, K.J., Proc. phys. Soc., A 67 (1954) 586.
[9] NEWTON, T.D., Can. J. Phys. 34 (1956) 804.
[10] BERGMAN, A.A. et al., Proc. Antwerp Int. Conf. on Study Nucl. Structure (1965) P/182.
[11] CINDA - An Index to the Literature on Microscopic Neutron Data - (EANDC 46 "U" - NYO-GEN-72-27), (1965) and Suppl. No.2 (1966).
[12] CAMERON, A.G.W. et al., "Fast Neutron Physics - Part II", Ch. V. M., Fast Neutron Capture Cross Sections (MARION, J.B. and FOWLER, J.L., Eds.), Intersci. Publ., New York (1963).
[13] DOSTROVSKY, I., FRAENKEL, Z., Phys. Rev. 116 (1959) 683.
[14] KATCOFF, S., Nucleonics 18 11 (1960).
[15] HUGHES, D.J. et al., Phys. Rev. 91 (1953) 1423.

STATISTICAL CALCULATION OF FISSION-PRODUCT CROSS-SECTIONS

J. L. COOK
AUSTRALIAN ATOMIC ENERGY COMMISSION
RESEARCH ESTABLISHMENT, LUCAS HEIGHTS,
N. S. W., AUSTRALIA

Abstract

STATISTICAL CALCULATIONS OF FISSION-PRODUCT CROSS-SECTIONS. Theoretical methods are outlined for estimating average resonance parameters and group cross-sections of fission products where experimental measurements are unavailable. The GUNYA sequence of programmes, designed to generate group cross-sections for use in reactor burn-up calculations, is described.

1. INTRODUCTION

Fission products are responsible for about 10% of neutron absorptions in the average thermal reactor. They have a critical effect upon the stability of a reactor over both small and large operating time intervals. Although there are important quickly saturating nuclides, the accumulation of many slowly saturating nuclides over a period of years causes a marked deterioration in a reactor's performance.

In carrying out burnup calculations using the code GYMEA (1), it has been found essential to treat at least 78 nuclides, and for 33 of them no detailed cross-section measurements have been carried out. For almost all of these nuclides, however, the thermal cross-section, and less frequently the resonance integral, have been measured. This paper deals with various attempts to achieve a realistic representation of the detailed multi-group cross-section, bearing in mind that the above two experimental quantities should be reproduced by the derived data.

There is quite comprehensive theoretical support for estimating the cross features of cross-sections, though it is impossible to predict fluctuations of individual resonance heights. Accordingly resort must be made to the concept of an average resonance, with averaged parameters, to generate cross-sections. This technique is acceptable if there are more than several resonances to a group, or alternatively, no resonances at all. Since the most unpredictable region of one or two resonances per group usually occurs just above thermal energies, the resonance energies one can use may be fixed by the criterion that the tails of such resonances must yield the correct thermal cross-section.

2. FISSION-PRODUCT NUCLIDES

The important fission-product nuclides range from mass numbers A = 80 to 160. Theoretical burnup studies, first conducted using the 45 nuclide set considered by Nephew (2), indicated a contribution of 9% to the multiplication factor of a Be-moderated, Pu239-fuelled reactor. It was ascertained that a number of significant poisons, such as Pm148, were left out of the Nephew scheme; a list of nuclides was prepared, ordered in terms of the magnitude of the product $y\sigma_a$, where y is the yield from thermal fission, and σ_a the thermal absorption cross-section. A maximum of 78 locations were available in the GYMEA library NDXC (3), and the first 78 were taken from this nuclide list. These are:-
Br81, Se82, Kr83, Kr84, Kr85, Kr86, Rb85, Rb87, Sr88, Sr89, Sr90, Y89, Y90, Y91, Zr91, Zr92, Zr93, Zr94, Zr96, Mo95, Mo97, Mo98, Mo100, Tc99, Ru101, Ru102, Rh103, Ru104, Rh105, Pd105, Pd106, Pd107, Pd108, Ag109, Cd113, In115, Sb125, Te128, I127, I129, Te130, I131, Xe131, Xe132, Xe133, Cs133, Xe134, Cs134, I135, Xe135, Cs135, Xe136, Cs137, Ba138, La139, Ce140, Pr141, Ce142, Nd143, Nd144, Nd145, Nd146, Pm147, Pm148, Pm148m, Nd148, Sm149, Nd150, Sm150, Sm151, Sm152, Eu153, Eu154, Sm154, Eu155, Gd155, Gd156, Gd157.

For the 33 underlined nuclei, no measurements in the resonance region are known to the author, while for the others, at least one set of resonance parameters has been determined. After estimating theoretically the resonance cross-sections where they were unmeasured, the net contribution to the absorption reaction rate was found to be 14%, to which the 33 marked nuclides contributed about one fifth. Even though the paucity of data hampers a more accurate determination of detailed poisoning effects, it is expected that the overall estimates are fairly reliable.

3. GENERAL DESCRIPTION OF THE GUNYA PROGRAMMES

The GUNYA programmes (4) for prediction of multigroup cross-sections assume that the (n,γ) reaction can everywhere be represented by a simple sum over many unbroadened Breit-Wigner energy levels (5).

To treat all data on an equal basis, the following scheme of calculation was used. Firstly, the statistically averaged resonance parameters were estimated. These consist of the average radiation width Γ_γ, average level spacing D, and the s and p wave strength functions, S_o and S_1 respectively.

The programme GUNYA 1 computes and prepares this data in a standard format, and employs two alternative methods for estimating D. GUNYA 2 is the main cross-section generating programme which computes multigroup cross-sections for an arbitrary set of lethargy groups. It deals with nuclides where no resonance parameters are known and all cases where up to three hundred resonances per nuclide have been resolved.

Where no parameters are available the theory uses standard (6) statistical cross-section formulae, when there are more than ten resonances per group, and the Breit-Wigner equation when there are less than ten resonances per group. Analytical integrals given by Doherty (7) are used over resolved regions. The output is specially arranged to be compatible with the GYMEA loading programme EDITOR (8). Other GUNYA programmes adjust the low energy data to give the experimental thermal cross-sections as the tail contribution from adjacent resonances.

4. STATISTICAL DATA

4.1 Calculation of Average Level Spacings

The current version of the code employs two methods of interpolating $\bar{D}$ throughout the periodic table. A purely empirical but simple interpolation procedure was devised by assuming that:

$$\log \bar{D} = f_s(A) + P(Z) + P(N) ,$$

in which $f_s(A)$ = a background, mass-dependent function determined empirically for the four separate cases of even-even, even-odd, odd-even, and odd-odd nuclei and $P(Z)$ and $P(N)$ are peaking functions which take account of shell corrections brought about by the influence of magic numbers in Z and N that designate closed proton and neutron shells respectively.

The second method uses an improved version of the level spacing formula given by Cameron and Gilbert (9) which is a sophisticated version of the Bethe (10) free gas formula. At an energy E above the ground state, the density of states of spin J is given by:

$$\rho(E,J) = \frac{\sqrt{\pi}}{12} \frac{\exp\left(2\sqrt{aU}\right)}{a^{1/4}U^{5/4}} \frac{(2J+1)\exp\left[-(J+1/2)^2/2\sigma^2\right]}{2\sqrt{2\pi}\sigma^3} \text{MeV}^{-1}$$

U is the effective excitation energy defined by $U = E - \Delta E$, where ΔE is a correction due to nucleon pairing, and is further decomposed into separate contributions from neutrons and protons, $\Delta E = P(Z) + P(N)$.

The variable σ is the spin cut-off parameter related to the nuclear moment of inertia. In Cameron's treatment:

$$\sigma^2 = 0.0888\,(aU)^{1/2}\,A^{2/3}.$$

For Cameron's semi-empirical mass formula (11), corrections are also made for shell effects in which the contribution to the mass comes from a term $S = S(Z) + S(N)$. Cameron found a rough linear correlation between a/A and S, fitting almost all experimental data to within a factor of 3. This was not

sufficiently exact for our application and the values of 'a' were recalculated (12). For undeformed nuclei, it was found that:

$$a/A = 0.00972S + 0.147,$$

while deformed nuclei line on the parallel line:

$$a/A = 0.00972S + 0.120.$$

The deformed region is

$$54 \leq Z \leq 78; \quad 86 \leq N \leq 122, \text{ and}$$

$$86 \leq Z \leq 122; \quad 130 \leq N \leq 182.$$

Cameron's values of P(Z), P(N), S(Z) and S(N) were least-squares adjusted to give the best possible fit to experimental values, subject to the conditions imposed by the semi-empirical mass formula, namely that P(Z) + S(Z) and P(N) + S(N) should remain unaltered. Weights were assigned to each experimental level spacing according to the number of levels used in its determination, and a least-squares fit carried out. Table I shows a section of the new values for shell and pairing corrections, and Cameron's values are given for comparison. Values for Z or N equal to 35-96 inclusive are available.

TABLE I

SHELL AND PAIRING CORRECTIONS

Z or N	PZ	PZ Cameron	PN	PN Cameron	SZ	SN
54	1.12	1.12	1.73	1.12	-16.54	14.55
55	-0.25		-0.04		-15.43	15.93
56	0.53	1.58	1.79	1.29	-13.70	15.93
57	-0.46		-1.04		-13.25	18.01
58	1.17	1.17	0.34	0.94	-12.87	18.19
59	0.38		0.07		-12.56	18.01
60	0.99	1.18	1.71	1.24	-11.42	18.25
61	0.00		-1.50		-11.09	20.72
62	1.17	1.22	1.25	1.25	-10.73	19.51
63	0.18		-1.20		-10.71	20.93
64	0.97	0.97	2.05	1.14	-10.41	19.00

It was subsequently found that calculated group cross-sections depend upon the estimated value of $\bar{D}$ in a very sensitive way, and it is the errors in this parameter which reflect most strongly errors in the determination of reactor physics data.

4.2 Average Reduced Neutron Widths

The average reduced neutron widths for s and p partial waves were calculated by assuming that the strength functions are systematic functions of the mass number A. The values quoted by Garrison and Roos (13) were employed in initial calculations, although revisions using references from the CINDA (14) compilation are under way. Only s and p states were considered, because higher orbital angular momentum states become important only above 1 MeV, where the cross-section is very small, and should not affect reactor physics calculations appreciably. After estimating $\bar{D}$, the widths Γ_n^o and Γ_n^1 were determined from the strength functions using either experimental or interpolated values of S_o and S_1.

4.3 Radiation Widths

The radiation widths were also taken to be systematic functions of mass number. The available data from Hughes and Schwartz (15), the Nuclear Data Sheets (16) and measurements for the zirconium isotopes by Block (17) indicate that there are no appreciable deviations from this simplifying rule. It was further assumed that fluctuations in Γ_γ from resonance to resonance could be neglected.

5. COMPARISON WITH EXPERIMENT

The experimental values of thermal cross-sections for the 33 nuclides where no resonance data are available may be found in Table II. These are taken from the article by Garrison and Roos and the compilation by England (18). The energy of the lowest resonance which reproduces the thermal cross-section for the given data is shown in the last column. Also shown is the comparison between the Garrison and Roos level spacings and those obtained from the two methods in GUNYA. The computed resonance integral using the first set of GUNYA spacings is shown and compared with experimental values. When actually generating the final group cross-sections, some alterations to $\bar{D}$ and Γ_n^o were made to bring the calculated resonance integral into better agreement with experiments tabulated by Garrison et al. and England.

In some cases, as indicated in the table, the resonance integrals have been determined as the integral over the tail contribution from the thermal 1/v cross-section. It is in agreement with observation and theory that such a practice invariably leads to an underestimate of the resonance integral, which explains why the GUNYA results are much larger in these cases.

TABLE II

RESULTS OF GUNYA CALCULATIONS

Nuclide	$\bar{D}$ eV			Thermal Cross-Section	Resonance Integral		E (eV) (Lowest)
	G.R.	Empirical	FGM		Experiment	GUNYA	
34 Se 82	4,000	4,000	6,800	2.1 ± 1.5	1.4 ± 1.4	1.2	2,055
36 Kr 85	250	43	806	7.0 ± 7.0	29	81	21.5
36 Kr 86	10^4	10^4	5×10^4	0.06 ± 0.02	0.04 ± 0.04	0.07	5,000
37 Rb 88	-	810	1,460	1.0			405
38 Sr 89	-	900	900	0.5 ± 0.1	0.2 (1/v)	0.8	450
38 Sr 90	10^4	850	2,000	1.0 ± 0.06	1.8 ± 1.8	2	193
39 Y 90	-	350	280	3.5 ± 3.5	1.4 (1/v)	17	64
39 Y 91	-	1,500	90	1.07 ± 0.09	0.42 (1/v)	1.4	226
44 Ru 104	600	78	62	0.7 ± 0.2	8.0 ± 8.0	25	34
45 Rh 105	-	0.8	0.1	15,000	5936 (1/v)	56,000	0.4
46 Pd 107	20	34	2	10	40	36	17
51 Sb 125	-	142	50	1.56	0.65 (1/v)	23	71
52 Te 128	700	930	2,000	0.3 ± 0.3	2.0 ± 2.0	0.6	465

TABLE II (Cont.)

Nuclide	$\bar{D}$ eV			Thermal Cross-Section	Resonance Integral		E(eV) (Lowest)
	G.R.	Empirical	FGM		Experiment	GUNYA	
52 Te 130	1,000	650	16,000	0.5 ± 0.3	2.5 ± 2.5	1.5	325
53 I 131	-	20	120	50 ± 40	20 (1/v)	68	4
54 Xe 132	400	1,900	1,300	0.2 ± 0.1	1.8 ± 1.8	0.2	955
54 Ex 133	-	28	150	190 ± 90	75 (1/v)	1,700	1.8
54 Xe 134	2,000	2,500	2,900	0.2 ± 0.1	0.6 ± 0.5	0.2	1,250
55 Cs 134	-	7.4	7.5	134 ± 12	53 (1/v)	1,150	3.7
53 I 135	-	4,700	6,700	-	-	0.17	1,800
55 Cs 135	90	70	200	8.7 ± 0.5	62 ± 5	53	35
54 Xe 136	15,000	9,000	20,000	0.15 ± 0.08	0.1 ± 0.1	0.4	2,350
55 Cs 137	300	8,000	5,000	0.11 ± 0.03	0.3 ± 0.3	0.08	4,000
58 Ce 140	7,000	6,000	3,000	0.66 ± 0.06	0.5 ± 0.2	0.5	1,280
58 Ce 142	2,000	1,400	1,000	1.0 ± 0.2	1.3 ± 0.8	1.0	700
60 Nd 144	500	280	80	5.0 ± 0.6	12.0 ± 12.0	817	140

TABLE II (Cont.)

Nuclide	$\bar{D}$ eV			Thermal Cross-Section	Resonance Integral		E(eV) (Lowest)
	G.R.	Empirical	FGM		Experiment	GUNYA	
60 Nd 146	500	140	1,000	10 ± 1	25 ± 25	25	38
60 Nd 148	100	300	180	3.4 ± 1.0	48 ± 48	11	150
61 Pm 148	-	0.45	2	1500 ± 1500	44,000	39,000	0.162
61 Pm 148m	-	-	-		32,000	28,000	-
60 Nd 150	100	300	190	3.0 ± 1.5	14 ± 13	5	150
62 Sm 154	200	200	1,000	5.5 ± 1.1	25 ± 23	16	64
63 Eu 154	-	1.0	1.0	1500 ± 400	994 (1/v)	7,900	0.5
63 Eu 155	-	2.5	4.2	$14,000 \pm 100\%$	5540 (1/v)	7,060	0.13
64 Gd 156	100	180	35	4	44	79	90

Figure 1 illustrates an example of the reaction rates per 1,000 source neutrons in the main chains for a typical BeO-moderated Pu239-fuelled reactor, as computed by GYMEA from the 120 group library NDXC (19). Other chains are also available with similar information. The elements for which no resonance data are available, and for which crude measurements only have been made of resonance integrals and thermal cross-sections, are shown with dotted lines for their (n,γ) reaction. Clearly, they form important links in the reaction chain and must be included for reliable estimates of long-term build-up of poisons. The need for more accurate and more comprehensive measurements of cross-sections is self-evident.

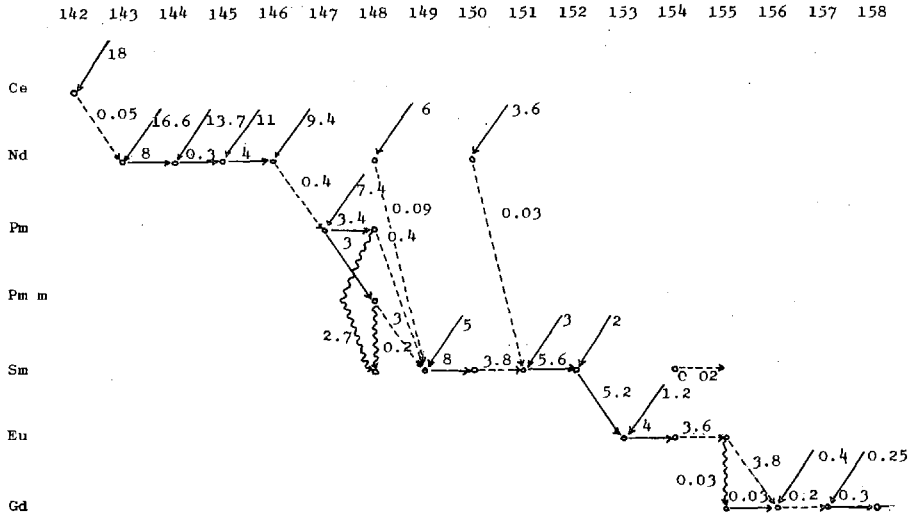

FIG.1. A fission-product chain

6. CONCLUSIONS

In a full treatment of fission products for multigroup calculations of reactor performance, it has proved necessary to supplement experimental information with extensive statistical theory calculations of unknown cross-sections for 78 nuclides. These calculated cross-sections were adjusted to yield the measured thermal cross-section and resonance integral, with encouraging results. Clearly, it is necessary to obtain level spacings and strength functions. Further measurements on (n,γ) cross-sections would be of great assistance.

REFERENCES

(1) POLLARD, J.P., ROBINSON, G.S., "GYMEA", AAEC/E147 (1966).

(2) NEPHEW, E.A., ORNL-2869 (1960).

(3) COOK, J.L., "Preparation and bibliography of the GYMEA library NDXC", AAEC/TM report (in press) (1966).

(4) COOK, J.L., "GUNYA", AAEC/E report (in press) (1966).

(5) BREIT, G., WIGNER, E., Phys. Rev. 49 (1936) 519.

(6) "Reactor physics constants", ANL 5800, USAEC Rep. p. 162 (1963).

(7) DOHERTY, G., AAEC/TM270 (1963).

(8) FORD, G., "EDITOR", AAEC/E150 (1966).

(9) CAMERON, A.G.W., GILBERT, A., Can. J. Physics 43 (1965) 1446.

(10) BETHE, H.A. Phys. Rev. 50 (1963) 332.

(11) CAMERON, A.G.W., Can. J. Phys. 36 (1958) 1040.

(12) COOK, J.L., MUSGROVE, A.R., AAEC/TM report (in press) (1966).

(13) GARRISON, J.D., ROOS, B.W., Nucl. Sci. and Engng. 12 (1962) 115.

(14) CINDA - An index to the literature on microscopic neutron data. EANDC 46 "U" NYO-GEN-72-27 (1965).

(15) HUGHES, D.J., SCHWARTZ, R.B., BNL 325 (1958).

(16) Nuclear Data Sheets, NAS-NRC publication (1960)

(17) BLOCK, R.C., ORNL-3425 (1963).

(18) ENGLAND, T.R., WAPD-TM-333 (1965).

(19) POLLARD, J.P., ROBERTSON, J., AAEC/E report (to be published) (1966).

VALEUR DES LARGEURS RADIATIVES TOTALES Γ_γ EN FONCTION DU NOMBRE DE MASSE A

V.-D. HUYNH, S. DE BARROS*, P.L. CHEVILLON
J. JULIEN, G. LE POITTEVIN,
J. MORGENSTERN ET C. SAMOUR
CEA, CENTRE D'ETUDES NUCLEAIRES DE SACLAY,
FRANCE

Abstract — Résumé

TOTAL RADIATIVE WIDTH (Γ_γ) AS A FUNCTION OF MASS NUMBER A. The total radiative width Γ_γ was measured accurately for a large number of nuclei. These values, which are important for reactor calculations, are difficult to determine. The fluctuations in Γ_γ from resonance to resonance in the same nucleus are discussed in terms of level parity and the de-excitation scheme. The authors compare the experimental values with those predicted by theory.

VALEUR DES LARGEURS RADIATIVES TOTALES Γ_γ EN FONCTION DU NOMBRE DE MASSE A. Les auteurs ont mesuré les valeurs de la largeur radiative totale Γ_γ pour un grand nombre de noyaux avec précision; ces valeurs utiles dans le calcul des réacteurs sont difficiles à déterminer. Ils discutent les fluctuations de Γ_γ de résonance à résonance pour un même noyau en fonction de la parité des niveaux ou du schéma de désexcitation et comparent les valeurs expérimentales aux prévisions.

Les valeurs de la largeur radiative totale Γ_γ ont été systématiquement mesurées avec précision pour un grand nombre de noyaux cibles ayant des nombres de masse A variant entre 50 et 201, à l'aide d'expériences de transmission effectuées par la méthode du temps de vol près de l'accélérateur linéaire de Saclay [1, 2]. Les données ont été analysées par une méthode des formes [3] sur la calculatrice IBM 7094 de Saclay.

Le tableau I donne, pour chaque noyau cible, la valeur moyenne $\langle\Gamma_\gamma\rangle$ calculée à partir des largeurs Γ_γ des résonances individuelles. Si l'on ne tient compte que des transitions dipolaires électriques, la largeur radiative totale s'écrit [4]

$$\Gamma_\gamma = \text{cte}\, A^{2/3}\ D(U) \int_0^U \frac{E^3\, dE}{D(U-E)} \qquad (1)$$

où U désigne l'énergie d'excitation effective du niveau initial, D(U) désigne l'espacement des niveaux de même spin et parité que ce dernier et D(U - E) l'espacement des niveaux vers lesquels la transition peut aboutir. Cameron [5] a obtenu une estimation théorique de Γ_γ en incluant dans l'équation (1) la formule de Newton [6] sur l'espacement des niveaux qui tient compte des effets de structure en couches. La figure 1 présente, pour des neutrons d'onde s, la

* En congé du Centre brésilien des recherches physiques, Rio de Janeiro, Brésil

TABLEAU I. VALEURS EXPERIMENTALES DES LARGEURS RADIATIVES OBTENUES A SACLAY

Noyau cible	J	$\langle\Gamma_\gamma\rangle$	Nombre de niveaux	Noyau cible	J	$\langle\Gamma_\gamma\rangle$	Nombre de niveaux
^{56}Fe		600 ± 100	1	^{112}Sn	1/2	110 ± 21	1
^{63}Cu	2	550 ± 65	1	^{116}Sn	1/2	42 ± 15	2
^{65}Cu	1 ou 2	240 ± 20	1	^{117}Sn	0 et 1	82 ± 20	4
^{64}Zn	1/2	300 ± 15	1	^{124}Sn(ℓ=1)		240 ± 25	1
^{68}Zn	1/2	160 ± 10	1	^{135}Ba	1 et 2	106 ± 6	3
^{69}Ga	2	210 ± 50	1	^{136}Ba	1/2	180 ± 20	1
^{71}Ga	2	350 ± 110	1	^{139}La	3 ou 4	105 ± 15	1
^{75}As	1 et 2	320 ± 30	9	^{141}Pr	2 et 3	85 ± 10	3
^{76}Se	1/2	300 ± 50	1	^{143}Nd	3 et 4	70 ± 20	3
^{77}Se	0	280 ± 100	1	^{145}Nd	3 et 4	65 ± 15	4
	1	440 ± 60	1	^{155}Gd	1 et 2	115 ± 20	7
^{78}Se	1/2	300 ± 70	1	^{157}Gd	1 et 2	105 ± 20	2
^{79,81}Br	1 et 2	300 ± 30	6	^{169}Tm	0 et 1	90 ± 30	6
^{93}Nb ℓ=0	4 et 5	150 ± 30	6	^{192}Pt	1/2	55 ± 8	4
^{93}Nb ℓ=1		230 ± 50	8	^{194}Pt	1/2	60 ± 10	3
^{95}Mo	2 et 3	145 ± 15	2	^{195}Pt	0	93 ± 5	7
^{96}Mo	1/2	40 ± 15	1		1	102 ± 5	15
^{97}Mo	2 ou 3	150 ± 10	1	^{196}Pt	1/2	130 ± 25	2
^{107}Ag	0 et 1	130 ± 15	5	^{198}Pt	1/2	150 ± 25	1
^{109}Ag	0 et 1	135 ± 15	7	^{197}Au	1 et 2	125 ± 10	12
^{111}Cd	0 et 1	150 ± 20	6	^{198}Hg	1/2	140 ± 25	4
^{113}Cd	0 et 1	160 ± 20	5	^{199}Hg	1	320 ± 50	4
					0	200 ± 50	3
				^{201}Hg	1	460 ± 50	4
					2	300 ± 40	3

variation de $\langle\Gamma_\gamma\rangle$ avec A, pour des noyaux cibles de masse A impaire, ainsi que la courbe théorique de Cameron. Expérimentalement, nous observons une décroissance de Γ_γ avec A pour des nombres de masse compris entre 60 ($\langle\Gamma_\gamma\rangle \sim 600$ meV) et 180 ($\langle\Gamma_\gamma\rangle \sim 80$ meV), ainsi qu'une forte croissance de $\langle\Gamma_\gamma\rangle$ pour des valeurs de A voisines de 200. Mais nous n'observons pas le pic très intense aux environs de A = 140 que prévoit la théorie: les valeurs de $\langle\Gamma_\gamma\rangle$ pour ^{135}Ba et ^{139}La sont de l'ordre de 100 meV.

Les paramètres obtenus pour ^{197}Au confirment la non-dépendance de F du spin pour un système complètement statistique [7] pour lequel la densité des niveaux est proportionnelle à (2J + 1) et un grand nombre de niveaux contribuent à Γ_γ. Ainsi, nous trouvons $\langle\Gamma_\gamma\rangle$ = 1 27 ± 1 0 meV pour J = 1 et $\langle\Gamma_\gamma\rangle$ = 125 ± 10 meV pour J = 2 [8].

Pour un système non statistique, lorsque la densité des niveaux est faible et que certaines transitions prédominent pour l'une des deux valeurs du spin et sont interdites pour l'autre, Γ_γ peut être différent

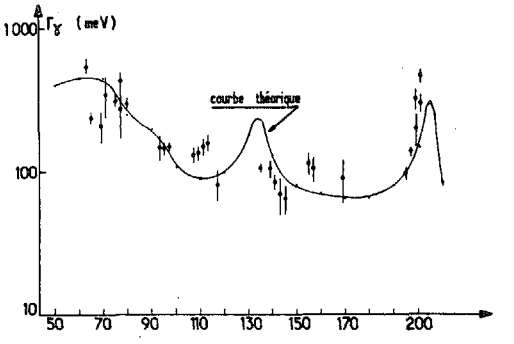

FIG.1. Comparaison des valeurs expérimentales de Γ_γ obtenues à Saclay pour les noyaux cibles de A impair avec la courbe théorique de Cameron

selon la valeur du spin. Pour la résonance de ^{77}Se, située à 339 eV, nous avons observé des rayonnements gamma E1 intenses de l'ordre de 10 MeV, correspondant à des transitions entre l'état de capture 1- et l'état fondamental 0+ ou le premier état excité 2+; pour cette résonance Γ_γ = 440 ± 65 meV tandis que Γ_γ = 280 ± 110 meV pour la résonance J = 0 située à 209 eV. Dans le cas de ^{195}Pt, les transitions aboutissant à l'état fondamental et aux deux premiers états excités de ^{196}Pt sont négligeables pour les résonances J = 0. Nous n'avons cependant trouvé [9] aucune différence dans les valeurs de $\langle\Gamma_\gamma\rangle$, pour J = 1 ($\langle\Gamma_\gamma\rangle$ = 102 ± 5 meV) et J = 0 ($\langle\Gamma_\gamma\rangle$ = 93 ± 5 meV).

Généralement, les largeurs radiatives totales sont presque constantes de résonance en résonance pour un noyau et un spin donnés. Ce résultat paraît logique, Γ_γ étant la somme d'un grand nombre de largeurs radiatives partielles [10]. Cependant, si un petit nombre de largeurs partielles contribue pour une part importante à Γ_γ, une grande fluctuation de Γ_γ devient possible. ^{56}Fe, ^{63}Cu et ^{77}Se devraient être des exemples typiques; malheureusement, le nombre de résonances pour chacun de ces noyaux est trop faible. Le cas le plus net est trouvé dans le mercure (^{198}Hg, ^{199}Hg et ^{201}Hg) et peut être expliqué par plusieurs transitions de haute énergie allant vers l'état fondamental et les premiers états excités [11]. Un autre exemple est fourni par le platine [9], comme le montre le tableau II, mais les fluctuations de la somme des trois premières transitions [12] n'expliquent pas cette anomalie.

Il est intéressant de remarquer la dépendance de Γ_γ de l'énergie de liaison pour un même élément. Généralement, Γ_γ est plus grand pour les isotopes cibles de A impair que pour les isotopes cibles pair-

TABLEAU II. VALEURS DE Γ_γ DE $^{195}Pt + n$

Résonances J = 1			Résonances J = 0	
E(eV)	Γ_γ(meV)	$\Sigma\ \Gamma_{\gamma_i}$ (unité arbitraire)	E(eV)	Γ_γ(meV)
11,8	112 ± 7	332	67,1	130 ± 30
19,4	100 ± 8	122	119,25	70 ± 20
67,5	137 ± 20	306	154,7	152 ± 20
111,7	127 ± 15	182	204,8	100 ± 10
120,5	140 ± 15	286	261,7	64 ± 15
139,5	110 ± 13	463	309,6	64 ± 25
150,4	90 ± 15	53	453,2	82 ± 50
188,5	117 ± 10	262	515,2	72 ± 30
222,2	130 ± 13	511		
256,6	103 ± 15	94	706	105 ± 50
280	98 ± 25	245		
285,6	105 ± 15	283		
302,3	89 ± 20	314		
382,8	100 ± 20	65		
410,1	88 ± 10	90		
484,8	108 ± 15			
529,3	182 ± 32	717		
548,8	144 ± 26	606		
558,7	142 ± 31	369		
659,8	168 ± 25	99		
680	118 ± 25	21		

pair, ainsi que le montre le calcul de Cameron. Citons par exemple le sélénium, le molybdène, le mercure et les isotopes 195, 192 et 194 du platine (tableau I). Nous trouvons cependant le résultat inverse pour les isotopes 195, 196 et 198 du platine [9]. On notera la croissance uniforme de Γ_γ avec A pour les cinq isotopes du platine. Nous avons également trouvé le résultat inverse pour ^{135}Ba ($<\Gamma_\gamma> = 105 \pm 5$ meV) et ^{136}Ba ($\Gamma_\gamma = 180 \pm 20$ meV pour la résonance à 101 eV)[13] et aussi pour les isotopes 112 et 117 de l'étain. Enfin, nous obtenons deux valeurs très différentes pour les isotopes 63 et 65 du cuivre [13].

Nous avons également étudié [14] des résonances p dans ^{93}Nb et trouvé des valeurs de Γ_γ différentes pour les ondes s ($<\Gamma_\gamma> \sim 150$ meV)

et les ondes p ($<\Gamma_\gamma> \sim 230$ meV), qui peuvent être expliquées par les schémas des niveaux [15, 16]. Nous obtenons par ailleurs une largeur radiative totale du même ordre de grandeur (240 meV) pour la résonance p de ^{124}Sn, située à 62 eV; par contre la résonance p située à 46 eV de ^{118}Sn a une largeur Γ_γ analogue à celles obtenues pour les résonances s des autres isotopes.

La difficulté, dans de telles expériences, est de trouver, pour chaque isotope, un nombre suffisant de résonances isolées. D'autre part, une valeur précise de Γ_γ ($\Gamma_\gamma = \Gamma - \Gamma_n$) implique que la largeur de neutron Γ_n soit faible et que la largeur totale de réaction Γ soit connue avec précision.

L'incertitude de la valeur Γ_γ pour certains noyaux, figurant dans le tableau I, est due à l'ignorance de la valeur du spin de certaines résonances. Si la valeur I du spin du noyau cible est faible (1/2 ou 3/2), il devient nécessaire de déterminer la valeur $J = I \pm 1/2$ des résonances même si la valeur de $g\Gamma_n$ n'est pas élevée.

L'emploi de détecteurs Ge-Li pour une étude détaillée des spectres des rayonnements γ des résonances devrait permettre une interprétation de ces valeurs Γ_γ.

REFERENCES

[1] SAMOUR, C. et al., BAPS II 10 4 (1965) 514.
[2] HUYNH, V.-D. et al., Int.Conf. on the Study of Nuclear Structure with Neutrons, Antwerp (July 1965) No.73.
[3] CORGE, C., Rapports CEA nos 1998 (1961) et 2780 (1965).
[4] BLATT, J.M., WEISSKOPF, V.F., Theoret.nucl.Phys., John Wiley and sons, New York (1952).
[5] CAMERON, A.G.W., Can.J.Phys. 35 (1957) 666.
[6] NEWTON, T.D., Can.J.Phys. 34 (1956) 804.
[7] BRINK, D.M., cité par KINSEY, B.B., Handbuch der Physik XL (1957) 316.
[8] JULIEN, J. et al., Nucl.Phys. 76 (1966) 391.
[9] DE BARROS, S., Thèse, Paris (1966).
[10] PORTER, C.E., THOMAS, R.G., Phys.Rev. 104 (1956) 483.
[11] HUYNH, V.-D., Thèse, Paris (1965).
[12] SAMOUR, C. et al., ces comptes rendus, CN-23/60.
[13] CHEVILLON, P.L., Thèse, Paris (1966).
[14] LE POITTEVIN, G. et al., Nucl.Phys. 70 (1965) 497.
[15] SHELINE, R.K. et al., Nucl. Phys. 61 (1965) 342.
[16] BHATT, K.H. et al., Nucl.Phys. 63 (1965) 286.

DISCUSSION

R. BLOCK: I am delighted that you agree with my Harwell data, published in 1962, showing that the 1150-eV resonance in ^{56}Fe is symmetrical and hence not an s-wave resonance. I would point out, however, that in 1963 we measured the capture spectra from this resonance, using the Oak Ridge fast chopper, and concluded that it could be a p-wave resonance and that the observed gamma-ray transitions were M1 transitions. The strength of these M1 transitions was not excessively large when compared with similar values measured in thermal neutron capture.

We also considered the possibility that the resonance was a d-wave resonance, but concluded that, if one assumed $\ell = 2$ (as you do at Saclay), then the reduced neutron width computed for a d-wave level would exceed the Wigner limit.

J. JULIEN: It is true that M1 transitions are very strong in the case of some nuclei; in the level scheme for ^{57}Fe there is a $7^-/2^-$ level. If we could find a transition to this level, it would be safe to conclude that this resonance of $^{56}Fe + n$ was a d-wave resonance, and the spin would also be determined ($S = 5^+/2$). For the resonance to be of the p-wave type the transitions would have to be of the E_2 type, which is most unlikely. Moreover, if the resonance is of the d-wave type, the value S_2 of the strength function ($\ell = 2$) will be of the order of 4×10^{-4} for the energy range 0-50 keV, this resonance being the strongest for $\ell = 2$. This value would be in suitable agreement with the maximum predicted by the optical model for a mass number $A \sim 50$.

ETUDE DES SPECTRES DE RAYONNEMENT GAMMA DE CAPTURE A L'AIDE DE DETECTEURS AU GERMANIUM

H. JACKSON, C. SAMOUR, A. BLOCH, J. JULIEN
C. LOPATA ET J. MORGENSTERN
CEA, CENTRE D'ETUDES NUCLEAIRES DE SACLAY, FRANCE

Abstract — Résumé

GERMANIUM-DETECTOR STUDY OF GAMMA CAPTURE SPECTRA. Using germanium detectors, and working in the energy range between a few eV and a few hundred eV, the authors measured the spectra of gamma rays emitted after the capture of neutrons. They discuss the advantages, resolution effects and efficiency of these detectors. They also present curves for such spectra along with new de-excitation schemes for several nuclei.

ETUDE DES SPECTRES DE RAYONNEMENT GAMMA DE CAPTURE A L'AIDE DE DETECTEURS AU GERMANIUM. Des mesures de spectres de rayonnement gamma émis après capture des neutrons ont été réalisées à l'aide de détecteurs au germanium dans le domaine d'énergie compris entre quelques électrons-volts et quelques centaines d'électrons-volts. Les mérites, les effets de résolution et l'efficacité de ces détecteurs sont discutés. Les auteurs présentent des courbes de tels spectres et les nouveaux schémas de désexcitation obtenus pour de nombreux noyaux.

NEUTRON RADIATIVE CAPTURE MEASUREMENTS AT THE RENSSELAER POLYTECHNIC INSTITUTE'S ELECTRON LINAC*

R. C. BLOCK**, R. W. HOCKENBURY, Z. BARTOLOME
AND R. R. FULLWOOD
RENSSELAER POLYTECHNIC INSTITUTE,
TROY, NEW YORK,
UNITED STATES OF AMERICA

Abstract

NEUTRON RADIATIVE CAPTURE MEASUREMENTS AT THE RENSSELAER POLYTECHNIC INSTITUTE'S ELECTRON LINAC. Until recently the capture cross-section measurements with the 1.25-m diamter liquid scintillator detector had been limited to neutron energies below ~10 keV. Improvements in the experimental geometry and electronics have now enabled measurements to be carried out to energies of hundreds of keV. Measurements have been made with elemental samples of Na, Al, Fe, and Ni, and with isotopically enriched samples of Fe and Ni. Time-of-flight resolutions of 1.3, 2.5, or 5, 0 ns/m were used in these measurements, corresponding to neutron energy spreads of 0.4, 0.8, or 1.6 keV at 50 keV. Resonance structure is observed in Al up to a neutron energy of 1.1 MeV, demonstrating the recent improvements in this capture experiment. The data are characterized by many neutron resonances previously undetected in transmission measurements, e.g. a new resonance is observed in Na at 7.6 keV; 36 resonances are observed in elemental Fe below 100 keV, compared to 16 resonances reported from transmission measurements; and about 30 resonances are observed in elemental Ni below 50 keV, compared to only 8 reported from transmission measurements. These capture measurements provide a powerful tool for detecting weak p-wave or d-wave resonances in the presence of strong s-wave scattering. The capture in the resolved resonances can be determined to an accuracy of ~15%.

INTRODUCTION

The measurement of neutron radiative capture cross-sections in the keV energy range is of significant interest to both reactor designers and to nuclear structure physicists. Capture measurements have been carried out over the past few years at many laboratories but the interesting region in light and medium weight nuclei over the energy range from ~10 keV to several hundreds of keV has in general suffered from either low neutron intensity or poor energy resolution; thus only average capture cross-sections or the capture in a few isolated resonances could be determined. By combining an efficient capture detector with an intense pulsed electron linear accelerator, capture measurements have been carried out at R.P.I. on Na, Al, Fe, ^{56}Fe, ^{57}Fe, ^{58}Fe, Ni, ^{58}Ni, ^{60}Ni ^{61}Ni and ^{64}Ni with sufficient resolution to resolve resonance structure up to a few hundred keV.

* Research sponsored jointly by the United States Atomic Energy Commission under contract with the Union Carbide Corporation and by Rensselaer Polytechnic Institute.

** Formerly at Oak Ridge National Laboratory, Tenn.

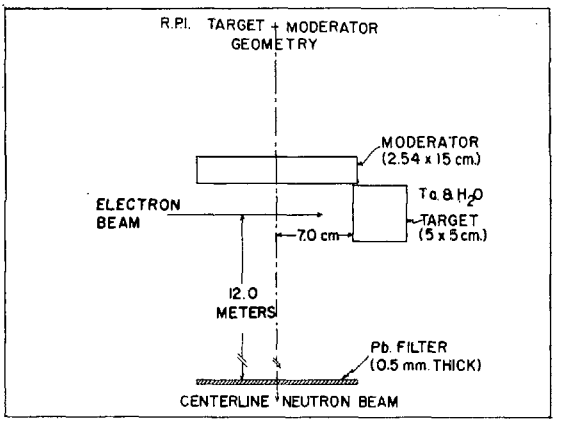

FIG.1. Photonuclear target and moderator

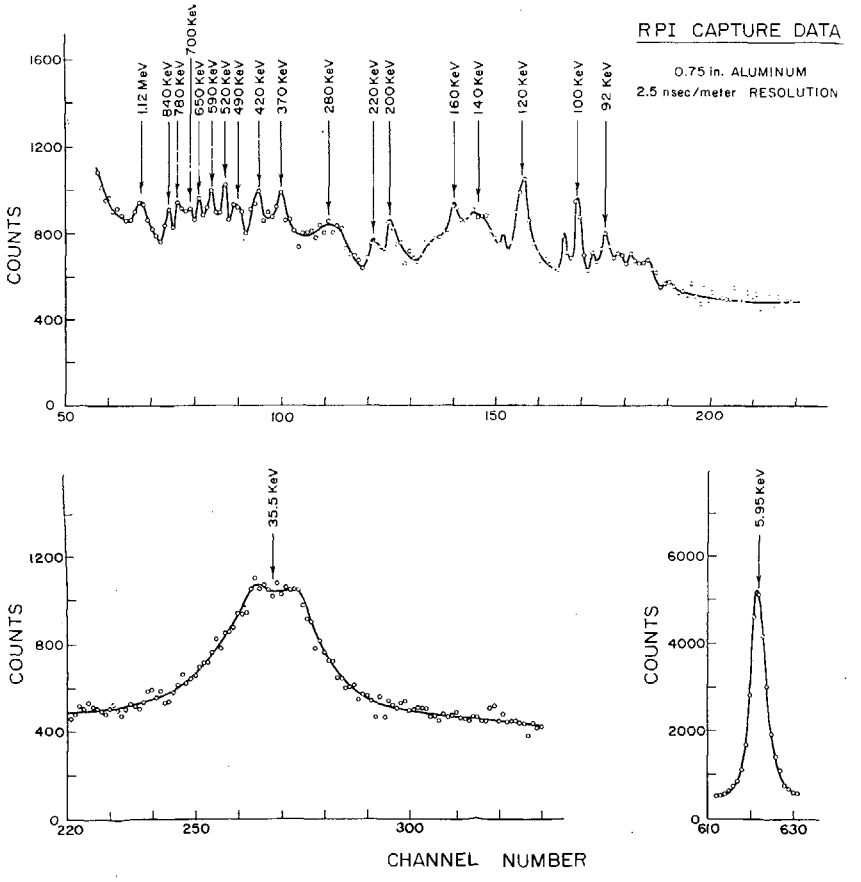

FIG.2. Neutron capture in Al - 2.5 nsec/m resolution

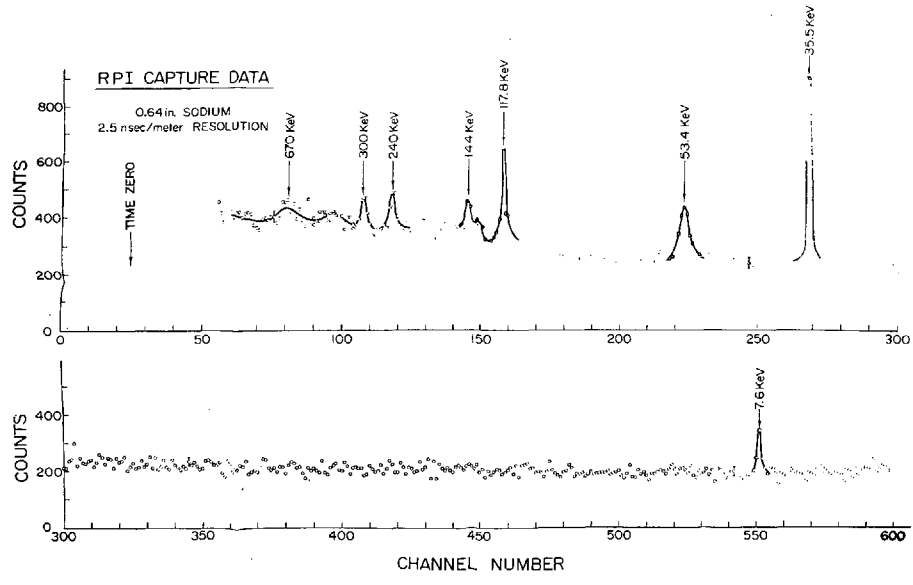

FIG.3. Neutron capture in Na - 2.5 nsec/m resolution

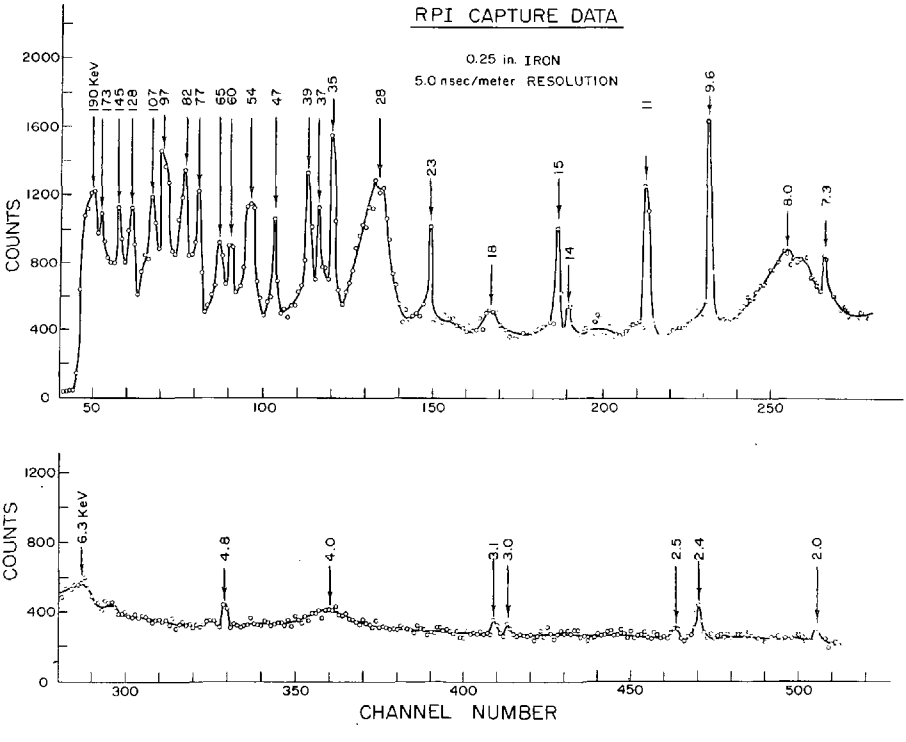

FIG.4. Neutron capture in Fe - 5.0 nsec/m resolution

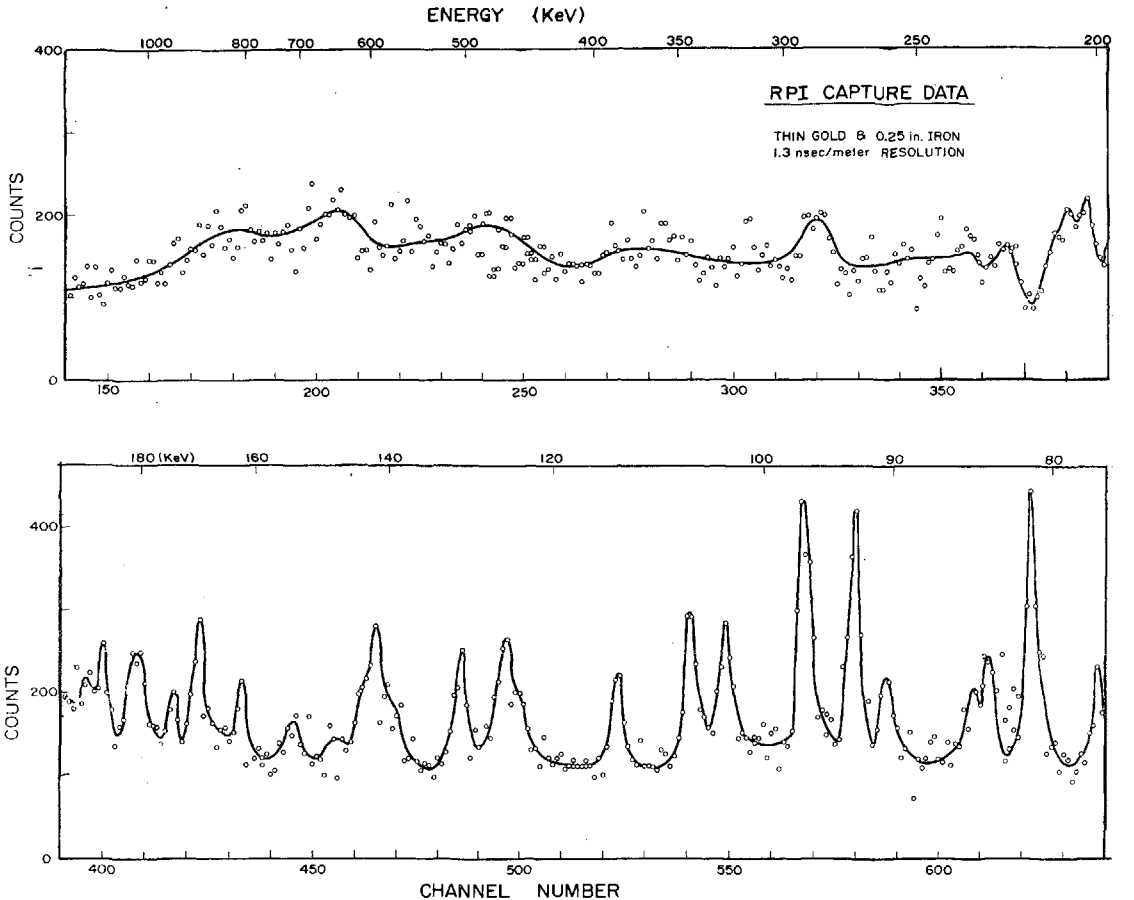

FIG.5. Neutron capture in Fe - 1.3 nsec/m resolution

EXPERIMENTAL APPARATUS

The ORNL 1.25-meter diameter capture detector used in this experiment has been described in detail elsewhere [1], but certain modifications have been made to adapt this detector for use at the R.P.I. Linac. The original rectangular hole passing through the detector has been replaced by an 18-cm diameter cylindrical hole, and a 4.5-cm thick ^{6}LiH shield has been placed in this hole to shield the scintillator from scattered neutrons. Capture samples up to 8-cm diameter are placed at the center of the detector, and the detector has a capture efficiency of approximately 60% when biased at a gamma ray energy of 3 MeV. This detector has a timing uncertainty of $\lesssim$ 25 nanoseconds, and measurements have been carried out at the 25-meter flight station with a resolution of 1.3, 2.5, or 5.0 nanosecond/meter, corresponding respectively to an energy spread of 0.4, 0.8 or 1.6 keV at 50 keV.

Until recently this experiment suffered from intense overloading from the accelerator beam flash, but recent improvements in target geometry have drastically reduced this problem. The present target geometry is illustrated in Figure 1. The polyethylene moderator is placed at an angle of 135^{o} to the 70-MeV electron beam. Most of the bremsstrahlung is emitted in the forward direction, so that only a small number of relatively low energy gamma rays reach the moderator. By placing the neutron flight path at an additional angle of 135^{o} to the gamma rays striking the moderator, the gamma rays which are again scattered by the moderator are so degraded in energy that a 0.3-mm sheet of Pb removes most of them from the neutron beam. This technique has been so successful that the gamma flash in the scintillator is within the linear range of the amplifier and that complete recovery is obtained in 6 $\sim$ 600 nanoseconds without pulsing off the phototubes. Effects due to resonance scattering of neutrons from the carbon in the polyethylene moderator and inelastic scattering of neutrons in the capture samples are now clearly observed with this apparatus over the neutron energy range from about 3 MeV to $\sim$20 MeV.

RESULTS

The capture data for elemental Na, Al, Fe, and Ni have been reduced to deadtime-corrected capture counts vs. time-of-flight (and energy) and are presented in Figs. 2-8. (An 11-mg/cm^{2} sample of Au was placed inside the detector to serve as a flux monitor. Some of the resonances below 3 keV in the figures are resonances in Au.)

The data have not yet been corrected for background but the results clearly show such strong resonance structure that it is relatively easy to estimate the background from the counts in the wings of the resonances. These data are in the state of being reduced to capture cross-sections and analyzed for resonance parameters. However, these final results are not ready in time for this conference and shall be published at a later date.

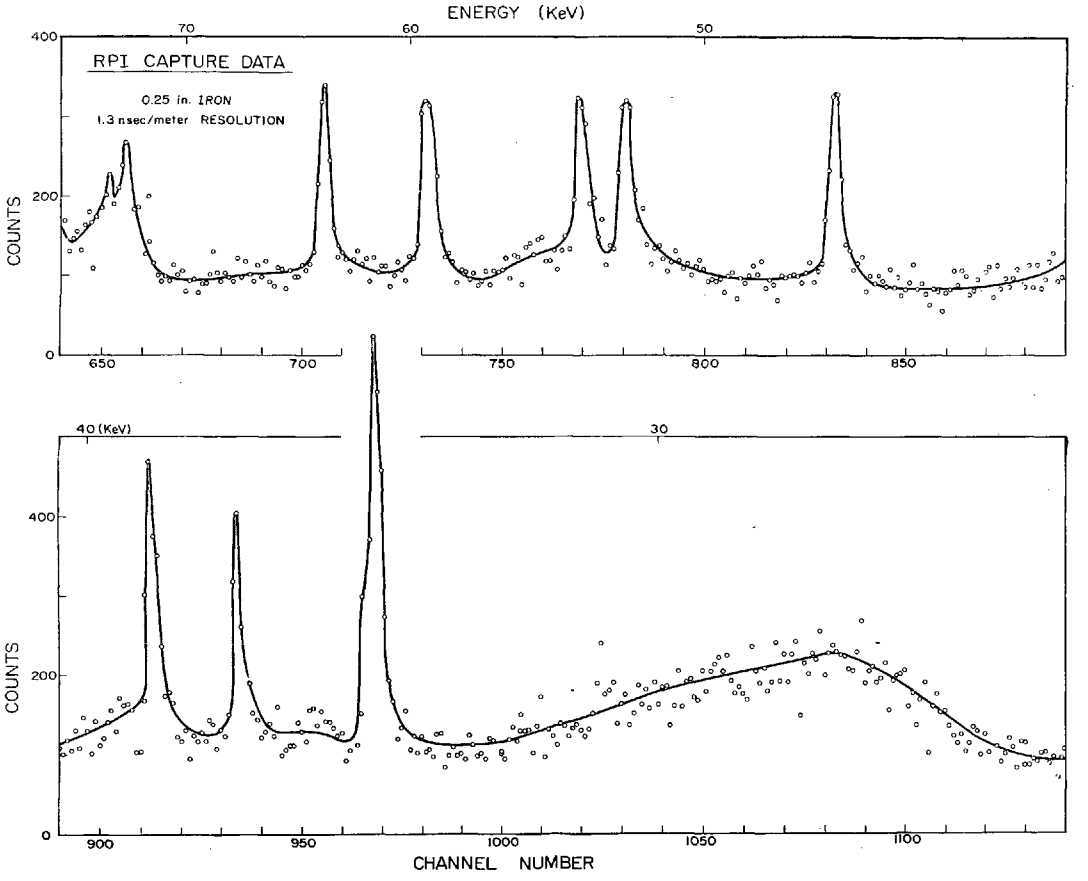

FIG. 6. Neutron capture in Fe - 1.3 nsec/m resolution

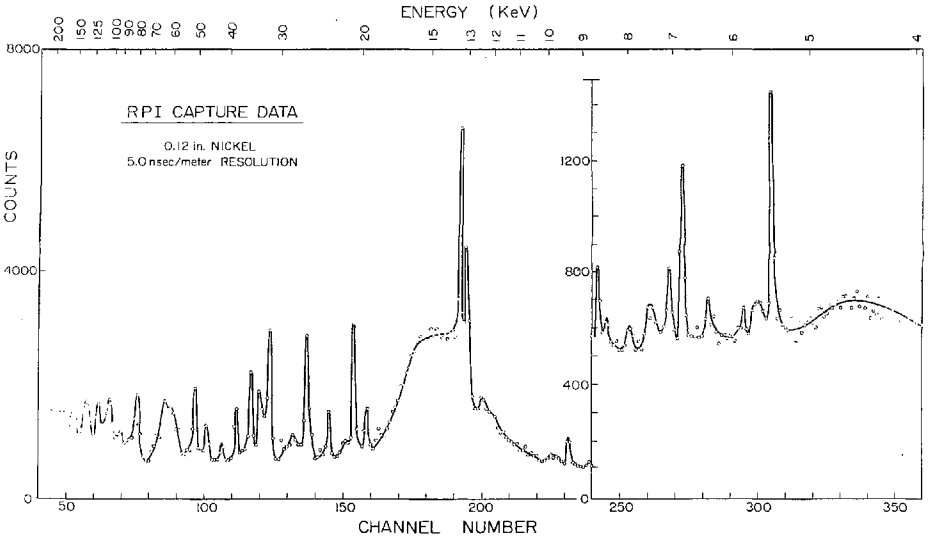

FIG.7. Neutron capture in Ni - 5.0 nsec/m resolution

In the Al data of Figure 3 it is clearly shown that this experiment is capable of observing resonance structure up to ~ 1 MeV, and the higher energy structure is in agreement with the structure observed in activation measurements [2]. A new resonance is observed in Al at 100 keV, with possibly another weak resonance occurring at 92 keV. The Na capture data in Figure 2 show the presence of a previously undetected resonance at 7.6 keV along with the resonances previously observed at higher energies (the 2.85 keV resonance is not plotted here). The Fe and Ni data are illustrated in Figures 4 through 8, and the resonance energies and isotopic assignments based on separated isotopic measurements* are listed in Tables I and II. There again, the capture data are characterized by many more resonances than have been observed in high-resolution transmission measurements. The Fe data from this experiment exhibit the same resonance structure as has been observed in capture at Harwell [3] below 30 keV.

In comparing the number of resonances observed in capture to those observed in transmission, about 3-4 times as many appear in Fe below 100 keV and about three times as many appear in Ni below 50 keV. This large number of resonances with such small neutron widths is in disagreement with a Porter-Thomas distribution for s-wave resonances in either Fe or Ni. Thus it is reasonable to expect that many of these small resonances are p-wave or perhaps even d-wave resonances. It is interesting at this point to emphasize the vital effect that weak

* The isotopic assignment here is based on observing a resonance in the isotopically enriched sample at the same energy as the elemental sample. The assignments must be regarded as only tentative until the resonance strengths are compared in the elemental and isotopic samples.

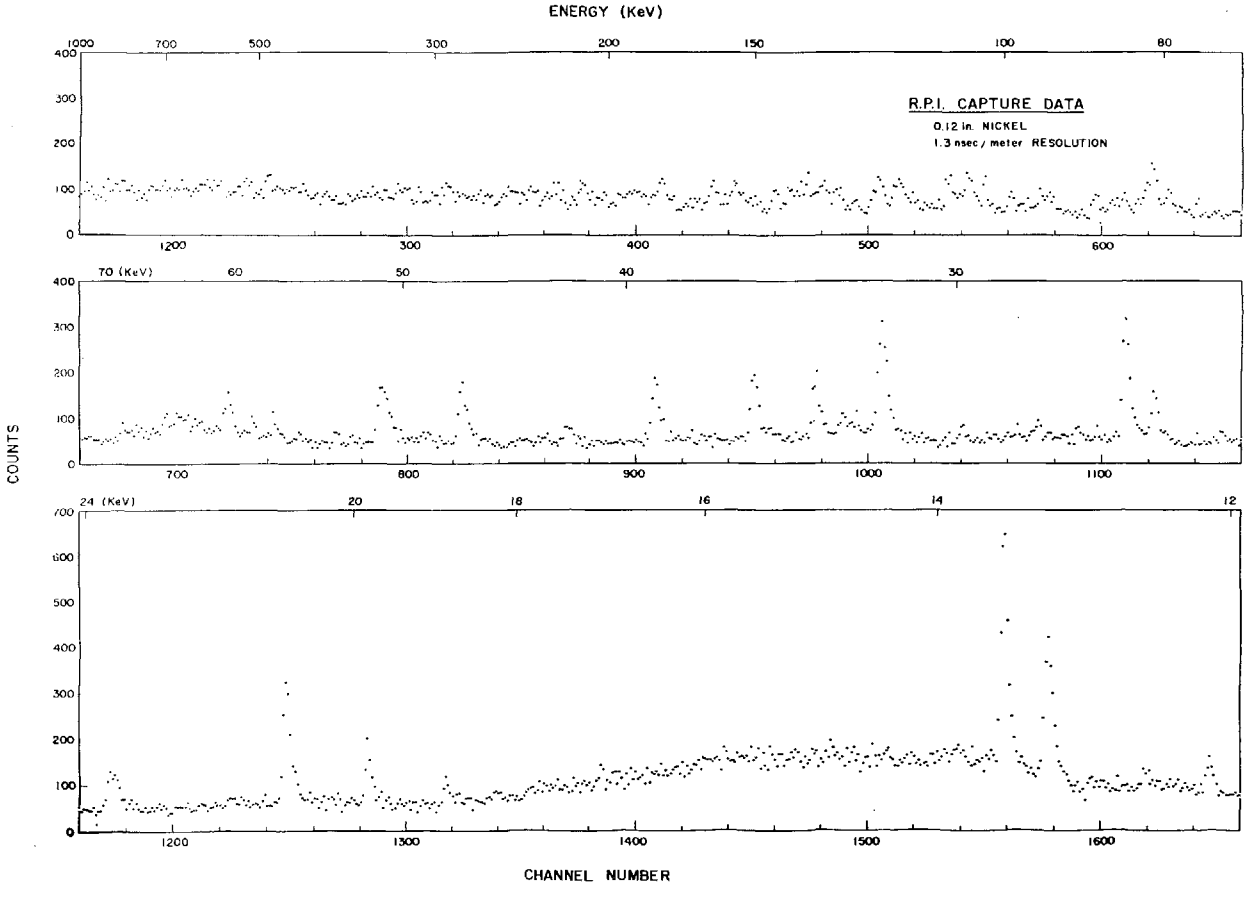

FIG. 8. Neutron capture in Ni - 1.3 nsec/m resolution

TABLE I

Fe Resonance Energies

E_o(keV)	Isotope*
0.230	Fe, 58
0.359	Fe, 58
1.150	Fe, 56
1.63	Fe, 57
2.35	Fe, 56
2.82	Fe, 58
3.96	Fe, 57
4.75	Fe, 57
4.96	Fe, 58
6.16	Fe, 58
6.24	Fe, 57
7.22	Fe, 57
7.82	Fe, (Assigned 54)
7.94	Fe, 57
9.29	58
9.49	Fe, 56
10.4	58
11.2	Fe, 56
12.9	Fe, 57
14.0	Fe, 57
14.5	Fe, (Assigned 54)
18.2	Fe, 57
21.3	Fe, 57
22.8	Fe, 56
28.5	Fe, 56
34.2	Fe, 56
37.1	Fe, 56
38.3	Fe, 56
46.1	Fe, 56
52.2	Fe, 56
53.8	Fe, 56
59.4	Fe, 56
63.6	Fe, 56
73.1	Fe, 56
77.3	Fe
81.1	Fe, 56
83.7	Fe
90.5	Fe
92.8	Fe
96.6	Fe

*Fe in this column means that the resonance was observed in the elemental Fe sample.

TABLE II

Nickel Resonance Energies

E_o (keV)	Isotope*
1.294	60
1.354	Ni,61
2.26	Ni,60
2.34	Ni(assigned to 62)
2.35	61
3.15	Ni,61
3.31	Ni,61
≈4.6	Ni(assigned to 62)
5.54	Ni,60
6.49	Ni,61
6.91	Ni,58
7.12	Ni,61
7.53	Ni,61
8.73	Ni,61
9.54	Ni(64)
9.90	61
10.2	61
12.2	Ni,60
12.6	Ni,58,61
13.3	Ni,58
13.6	Ni,58
13.8	60
14.0	61
12-14	60
14.3	61
14-16	Ni,58
14-15	64
15.3	61
16.5	58
16.7	61
17.2	58
17.8	61
19.0	Ni,58,61
20.0	Ni,58
20.4	61
20.5	60
21.1	Ni,58
21.4	61
23.8	Ni,60
24.8	Ni,61
26.0	Ni,64
26.6	Ni,58
27.6	Ni,61
28.5	Ni,60

*Ni in this column means that the resonance was observed in the elemental Ni sample.

TABLE II (cont'd.)

E_o (keV)	Isotope
(29.0)	61
30.2	Ni, 60
30.8	61
(31.7)	61
32.2	64
32.4	Ni, 58
33.4	Ni, 60
33.8	61
34.2	Ni, 58
36.1	Ni, 58
37.3	61
39.2	64
39.5	Ni, 58,60
41.3	61
42.9	Ni, 60
46.1	61, 64
47.9	Ni, 58
49.7	Ni
(50.7)	61
51.8	60
52.1	Ni, 58
53.9	Ni, 64
54.8	Ni (58)
57.0	Ni, 60
58.7	Ni, 61
60.1	Ni
61.8	Ni, 58
64.0	Ni, 64
65.2	Ni, 60
66.4	Ni, 58
70.0	Ni, 61
72.8	Ni, 60
78.2	Ni
81.3	Ni
83.0	Ni, 58
83.4	64
87.0	Ni, 60
89.6	Ni, 61
95.9	Ni (58)
97.2	Ni, 60

resonances (i.e., resonances with small neutron widths) play in determining neutron capture in the resonance region. In Figure 3, the sodium resonance at 53.4 keV shows up quite strongly in transmission measurements and has a rather large neutron width. On the other hand the resonance at 35.5 keV has a very small neutron width and only just recently has been observed at Saclay [4] in transmission measurements with thick sodium samples. Yet the areas under the 53.4 and 35.5 keV resonances in Figure 2 are comparable, so that it

is quite obvious that the 'weak' 35.5 keV resonance contributes as strongly to capture as the 53.4 keV resonance.** Thus, it is demonstrated that resonances which are so small as to be frequently missed in transmission measurements do show up in capture measurements and can contribute strongly to resonance capture.

SUMMARY

This high-resolution capture experiment clearly shows the extreme sensitivity for detecting resonances with small neutron widths which are frequently missed in transmission measurements. It is further demonstrated that these 'small' resonances contribute significantly to capture in the neutron energy range of fast reactors. The rather large number of resonances with such small neutron widths suggests that p-wave, or perhaps even d-wave, neutrons are responsible for many of the observed resonances. These data are now being reduced to capture cross-sections and analyzed for resonance parameters; an accuracy of ~15% is estimated for this measurement.

REFERENCES

1 BLOCK, R. C., SLAUGHTER, G. G., WESTON, L. W., AND VONDERLAGE, F. C., pg. 203, Neutron Time of Flight Methods, European Atomic Energy Community (Euratom), Brussels 1961.

2 HENKEL, R. L. and BARSCHALL, H. H., Phys. Rev. 80, 145 (1950).

3 MOXON, M. C., "The Neutron Capture Cross Section of Iron and Cobalt", paper 88, Int'l Conference on the Study of Nuclear Structure With Neutrons, Antwerp, Belgium, July 19-23, 1965.

4 MICHAUDON, A., (private communication).

** Actually, the areas must be corrected for the neutron flux incident on the samples, but this effect is only ~25% between the two areas.

CONFERENCE ON NUCLEAR DATA MICROSCOPIC CROSS-SECTIONS AND OTHER DATA BASIC FOR REACTORS

HELD IN PARIS, 17-21 OCTOBER 1966

CHAIRMEN OF SESSIONS

Session I	P. W. MUMMERY	United Kingdom Atomic Energy Authority, Reactor Group Headquarters, Risley, Warrington
Session II	R. JOLY	Centre d'études nucléaires de Saclay, Gif-sur-Yvette
Session III	J. JULIEN	Centre d'études nucléaires de Saclay, Gif-sur-Yvette
Session IV	J. SPAEPEN	EURATOM, Geel
Session V	R. BATCHELOR	United Kingdom Atomic Energy Authority, Atomic Weapons Research Establishment, Aldermaston, Berks
Session VI	K. H. BECKURTS	Kernforschungszentrum Karlsruhe
Session VII	N. STARFELT	AB Atomenergi, Studsvik
Session VIII	J. RYABOV	Joint Institute of Nuclear Research, Moscow
	M. NEVE DE MEVERGNIES	Centre d'étude de l'énergie nucléaire, Mol
Session IX	S. I. SUKHORUCHKIN	Institute of Theoretical and Experimental Physics, Moscow
Session X	G. C. HANNA	Atomic Energy of Canada Limited, Chalk River, Ontario
Session XI	A. DIVATIA	Atomic Energy Establishment Trombay, Bombay

SECRETARIAT OF THE CONFERENCE

Scientific Secretaries:	K. EKBERG	Division of Research and Laboratories, IAEA
	P. OTSTAVNOV	Division of Research and Laboratories, IAEA
Administrative Secretary:	P. GHELARDONI	Division of Scientific and Technical Information, IAEA
Editor:	P. SMIRNOV	Division of Scientific and Technical Information, IAEA
Records Officer:	D.J. MITCHELL	Division of Languages, IAEA

IAEA SALES AGENTS

Orders for Agency publications can be placed with your bookseller or any of our sales agents listed below:

ARGENTINA
Comisión Nacional de
Energía Atómica
Avenida del Libertador
General San Martin 8250
Buenos Aires - Suc. 29

AUSTRALIA
Hunter Publications,
23 McKillop Street
Melbourne, C.1

AUSTRIA
Georg Fromme & Co.
Spengergasse 39
A-1050, Vienna V

BELGIUM
Office international de librairie
30, avenue Marnix
Brussels 5

BRAZIL
Livraria Kosmos Editora
Rua do Rosario, 135-137
Rio de Janeiro

Agencia Expoente Oscar M. Silva
Rua Xavier de Toledo, 140-1° Andar
(Caixa Postal No. 5.614)
São Paulo

BYELORUSSIAN SOVIET SOCIALIST REPUBLIC
See under USSR

CANADA
The Queen's Printer
Ottawa, Ontario

CHINA (Taiwan)
Books and Scientific Supplies
Service, Ltd.,
P.O. Box 83
Taipei

CZECHOSLOVAK SOCIALIST REPUBLIC
S.N.T.L.
Spolena 51
Nové Město
Prague 1

DENMARK
Ejnar Munksgaard Ltd.
6 Nörregade
Copenhagen K

FINLAND
Akateeminen Kirjakauppa
Keskuskatu 2
Helsinki

FRANCE
Office international de
documentation et librairie
48, rue Gay-Lussac
F-75, Paris 5e

GERMANY, Federal Republic of
R. Oldenbourg
Rosenheimer Strasse 145
8 Munich 8

HUNGARY
Kultura
Hungarian Trading Co. for Books
and Newspapers
P.O.B. 149
Budapest 62

ISRAEL
Heiliger and Co.
3 Nathan Strauss Street
Jerusalem

ITALY
Agenzia Editoriale Internazionale
Organizzazioni Universali (A.E.I.O.U.)
Via Meravigli 16
Milan

JAPAN
Maruzen Company Ltd.
6, Tori Nichome
Nihonbashi
(P.O. Box 605)
Tokyo Central

MEXICO
Librería Internacional
Av. Sonora 206
Mexico 11, D.F.

NETHERLANDS
N.V. Martinus Nijhoff
Lange Voorhout 9
The Hague

NEW ZEALAND
Whitcombe & Tombs, Ltd.
G.P.O. Box 1894
Wellington, C.1

NORWAY
Johan Grundt Tanum
Karl Johans gate 43
Oslo

PAKISTAN
Karachi Education Society
Haroon Chambers
South Napier Road
(P.O. Box No. 4866)
Karachi 2

POLAND
Ośrodek Rozpowszechniana
Wydawnictw Naukowych
Polska Akademia Nauk
Pałac Kultury i Nauki
Warsaw

ROMANIA
Cartimex
Rue A. Briand 14-18
Bucarest

SOUTH AFRICA
Van Schaik's Bookstore (Pty) Ltd.
Libri Building
Church Street
(P.O. Box 724)
Pretoria

SPAIN
Librería Bosch
Ronda de la Universidad 11
Barcelona

SWEDEN
C.E. Fritzes Kungl. Hovbokhandel
Fredsgatan 2
Stockholm 16

SWITZERLAND
Librairie Payot
Rue Grenus 6
1211 Geneva 11

TURKEY
Librairie Hachette
469, Istiklâl Caddesi
Beyoğlu, Istanbul

UKRAINIAN SOVIET SOCIALIST REPUBLIC
See under USSR

UNION OF SOVIET SOCIALIST REPUBLICS
Mezhdunarodnaya Kniga
Smolenskaya-Sennaya 32-34
Moscow G-200

UNITED KINGDOM OF GREAT BRITAIN AND NORTHERN IRELAND
Her Majesty's Stationery Office
P.O. Box 569
London, S.E.1

UNITED STATES OF AMERICA
National Agency for
International Publications, Inc.
317 East 34th Street
New York, N.Y. 10016

VENEZUELA
Sr. Braulio Gabriel Chacares
Gobernador a Candilito 37
Santa Rosalía
(Apartado Postal 8092)
Caracas D.F.

YUGOSLAVIA
Jugoslovenska Knjiga
Terazije 27
Belgrade

IAEA publications can also be purchased retail at the United Nations Bookshop at United Nations Headquarters, New York, at the news-stand at the Agency's Headquarters, Vienna, and at most conferences, symposia and seminars organized by the Agency.

In order to facilitate the distribution of its publications, the Agency is prepared to accept payment in UNESCO coupons or in local currencies.

Orders and inquiries from countries where sales agents have not yet been appointed may be sent to:

Distribution and Sales Group, International Atomic Energy Agency,
Kärntner Ring 11, A-1010, Vienna I, Austria

INTERNATIONAL
ATOMIC ENERGY AGENCY
VIENNA, 1967

PRICE: US $12.00
Austrian Schillings 310,-
(£4.4.8; F.Fr.58,80; DM 48,-)